https://ntrs.nasa.gov/search.jsp?R=19940010718 2020-06-16T19:51:54+00:00Z

LMSC-HSV TR P037989
26 Feb 1993

Final Report

SPACE STATION THERMAL STORAGE/REFRIGERATION SYSTEM RESEARCH AND DEVELOPMENT

Contract: NAS8-36401

Prepared for

National Aeronautics and Space Administration
George C. Marshall Space Flight Center
Marshall Space Flight Center, Alabama 35812

Lockheed
Missiles & Space Company, Inc.
4800 Bradford Blvd., Huntsville, AL 35807

FOREWORD

This document is the final report for the work performed for NASA's George C. Marshall Space Flight Center under Contract NAS8-36401, "Space Station Thermal Storage/Refrigeration System Research and Development." The contract was awarded in May 1985 for an initial period of performance of two years and nine months. Subsequent contract modifications extended the period of performance to 1 March 1993. This report reviews all the technical tasks performed by Lockheed Missiles & Space Co., Inc., during this period. The NASA Contracting Officer's Technical Representative (COTR) at the time of award of the contract was Mr. J. W. Owen, EP44. Subsequently, Mr. J. B. McConnell became the COTR for this work.

The people at Lockheed-Huntsville who contributed to this program are William G. Dean (Program Manager), Zain Karu, Jeff E. McCracken, Billie Joe Osmer, Dave Pettie, Gene Sims, Sydne Anderson, and Erik West.

PRECEDING PAGE BLANK NOT FILMED

CONTENTS

Section		Page
	Foreword	ii
	Contents	iii
	Figures	iv
	Tables	ix
	Summary	x
1	INTRODUCTION	1
2	TECHNICAL DISCUSSION	2
	2.1 Thermal Storage Development	2
	2.1.1 Demonstration Unit for -20 °F Food Freezer	12
	2.1.2 Demonstration Unit for -94 °F Bio-Sample Freezer	17
	2.1.3 Getter Pump Testing	38
	2.2 Refrigeration Systems Development	45
	2.2.1 Design Requirements	45
	2.2.2 Definition of Cryogenic Requirements	50
	2.2.3 Assessment of Feasible Cycles	50
	2.2.4 Design and Fabrication of Prototype Hardware and Component Testing	51
3	REFERENCES	109
	Appendix A Summary of the Work in Progress on the Design and Fabrication of the -20 °F Food Freezer and the -94 °F Bio-Sample Freezer	A-1
	Appendix B Biofreezer Test Configuration/Design Updates and Results of Testing at Lower Temperatures	B-1
	Appendix C Evaluation and Comparison of Refrigerants for the Vapor Compression Cycles and Comparison Between Single and Cascade Cycles	C-1
	Appendix D Bibliography	D-1
	Appendix E Description of Various Compressor Types for Application to Space Station Refrigeration	E-1

ILLUSTRATIONS

Figure		Page
1	Space Station Thermal Storage Unit Concept	4
2	Logistics Module Thermal Storage Unit Concept	5
3	Cross Section of the Passive Thermal Storage Container Showing the Components and Their Nodal Breakdown as Modeled	7
4	Latest Concept Design for -94 °F Bio-samples Thermal Storage Unit	8
5	Alternate Concept for Logistics Module Frozen Food Thermal Storage Unit	9
6	Two-Halves Thermal Storage Unit Concept for Frozen Food at -20 °F	11
7	Preliminary Drawing of New Inner Tank Design for -20 °F Food Storage Demonstration Unit	14
8	Preliminary Drawing of Modified Outer Tank for -20 °F Thermal Storage Demonstration Unit	15
9	Preliminary Design of New Fiberglass Support Struts for Positioning the Inner Tank Inside the Outer Tank	16
10	Epoxy/Glass Cylinder with 0.010 in. Thick Neck and 0.005 in. Stainless Steel Liner for Use in -94 °F Thermal Storage Unit	19
11	Inner and Outer Cylinder Honeycomb Bottom Panel in the Process of Fabrication for Bio-sample Freezer	19
12	Inner and Outer Cylinder Honeycomb Bottom Panels for Bio-sample Freezer after Insertion of Adhesive to Bond Core to Outer Rings	20
13	Two Inner Cylinders and Two Outer Cylinders during Fabrication Process	20
14	Two Inner Cylinders and Two Outer Cylinders Showing Honeycomb Bottom Panels in Place	21
15	Outer Cylinder Ready for Bonding in Place of NW-25 Flange Vacuum Connection	22
16	Outer Cylinder after Bonding in Place of the NW-25 Flange Vacuum Connection	22
17	Outer Cylinder Showing Aluminum Reinforcing Ring Bonded in Place	23
18	Leak Test Being Performed on Inner Cylinder	23
19	Leak Test in Progress for Outer Cylinder	24
20	Leak Test in Progress for Outer Cylinder with Plastic Film Hood Filled with Helium	24
21	MLI Being Laid up onto the Inner Cylinders of Bio-sample Freezer	26
22	Bio-sample Freezer Inner Cylinder with MLI After Bottom was Trimmed	26
23	Top End of MLI Applied to Inner Cylinder of Bio-sample Freezer	27
24	Open End of Inner Cylinder of Bio-sample Freezer after MLI was Trimmed	27
25	Completed MLI Showing Thickness of 0.6 in. for 30 Layers on Bio-sample Freezer Inner Cylinder	28
26	Bio-sample Freezer Inner Cylinder with MLI in the Process of Being Bonded to the Annular Closeout	28

ILLUSTRATIONS (CONT.)

Figure		Page
27	Completed Bio-sample Freezer Halves and Heat Sinks/Cold Blocks Ready for Testing	30
28	Bio-sample Freezer Attached to Vacuum Pumping Station, Ready to Undergo Testing	31
29	Turbomolecular Vacuum Pumping Station	32
30	Bio-sample Freezer and Turbopumping Station During Test	33
31	Temperature vs Time for Bio-sample Freezer Test on 23 May 1990	35
32	Temperature vs Time for Bio-sample Freezer Test on 25 May 1990	36
33	Temperature vs Time for Bio-sample Freezer Test on 29 May 1990	37
34	Original Getter Pump Tested for Food Thermal Storage Unit	38
35	Setup for Testing Getter Pump Attached to the Thermal Food Storage Demonstration Unit	39
36	Temperature-Time Histories for Two Positions on Getter Material and on Pump Flange During First Activation Test	41
37	Pressure vs. Time for First Getter Pump Test	41
38	Temperature-Time Histories for Two Positions on Getter Material and on Pump Flange During Second Activation Test	42
39	Pressure vs. Time for Second Getter Pump Test	42
40	Temperature-Time Histories for Two Positions on Getter Materials and on Pump Flange During Third Activation Test	43
41	Pressure vs. Time for Third Getter Pump Test	43
42	Pressure Versus Time for Getter Pump Test	44
43	Assumptions for Cooling Load Calculations	47
44	Detailed Analysis of Cooling Loads in the Habitation Module Refrigeration System	47
45	Detailed Summary of Cooling Loads for the Logistics Module	48
46	Detailed Summary of Cooling Loads for the Life Sciences Lab Module	49
47	Thermal Control Test Bed with Temperature Controller Installed	53
48	Data System and Control Panel for Thermal Control Test Bed	54
49	Temperatures, Flow Rates, and Controller Set Points vs Time for the Thermal Control Test Bed Data	55
50	Temperatures, Flow Rates, and Controller Set Points vs Time for the Thermal Control Test Bed Data	56
51	Temperatures, Flow Rates, and Controller Set Points vs Time for the Thermal Control Test Bed Data	57
52	Temperatures, Flow Rates, and Controller Set Points vs Time for the Thermal Control Test Bed Data	58
53	Temperatures, Flow Rates, and Controller Set Points vs Time for the Thermal Control Test Bed Data	59

ILLUSTRATIONS (CONT.)

Figure		Page
54	Temperatures, Flow Rates, and Controller Set Points vs Time for the Thermal Control Test Bed Data	60
55	Temperatures, Flow Rates, and Controller Set Points vs Time for the Thermal Control Test Bed Data	61
56	Temperatures, Flow Rates, and Controller Set Points vs Time for the Thermal Control Test Bed Data After Modifications to the Controller Electronics/Control System	62
57	Outlet Temperatures vs Set Point for the Modified Test Bed Mixing Valve Controller	63
58	Comparisons of Various Refrigeration Cycle Efficiencies Over a Range of Temperatures	65
59	Magnavox Stirling Cycle Refrigeration Unit Under Test at Lockheed-Huntsville	66
60	Stirling Cold Head Heater Adapter	67
61	Carnot COP vs Cold Head Temperature for Each Operating Point During Three Stirling Unit Tests	70
62	Typical Magnavox Model MX-7043-10 Stirling Unit Test Results for Input Power Levels of 70, 55, and 50 W	70
63	Measured COP for the Magnavox Model MX-7043-10 Stirling Unit for Input Power Levels of 70, 55, and 50 W	71
64	Ratio of Measured Carnot COP vs Cold Head Temperature for Input Power Levels of 70, 55 and 50 W for the Magnavox MOdel MX-7043-10 Stirling Unit	71
65	Disassembled Diaphragm Compressor for Vapor Compression Unit	72
66	Inside View of Diaphragm Compressor Head-Vapor Compression Unit	73
67	Diaphragm and O-Ring from Vapor Compression Unit	73
68	Intake and Exhaust (Reed) Valves from Vapor Compression Unit	74
69	Cam Bearing from Vapor Compression Unit (Diaphragm Compressor)	74
70	Insulated Cabinet to be Used for Zero-g Refrigeration Demonstration Unit	76
71	Schematic for Zero-g Vapor Compression Cycle Refrigeration Demonstration Unit	77
72	Functional Block Diagram for Zero-g Vapor Compression Cycle Refrigeration Demonstration Unit	78
73	Diaphragm Compressor to be Used in the Zero-g Vapor Compression Cycle Demonstration Unit	86
74	Diaphragm Compressor to be Used in the Zero-g Vapor Compression Cycle Demonstration Unit	86
75	Zero-g Vapor Compressor Freezer Demonstration Unit Condenser During Construction, Before Preliminary Bonding	87

ILLUSTRATIONS (CONT.)

Figure		Page
76	Zero-g Vapor Compressor Freezer Demonstration Unit Condenser During Construction, After Preliminary Bonding	87
77	Zero-g Vapor Compressor Freezer Demonstration Unit Condenser During Construction, Before Final Bonding	88
78	Zero-g Vapor Compressor Freezer Demonstration Unit Condenser During Construction, After Final Bonding	88
79	Zero-g Vapor Compressor Freezer Demonstration Unit Condenser During Construction, BX-402 Foam Being Added	89
80	Zero-g Vapor Compressor Freezer Demonstration Unit Condenser During Construction, Construction Completed	89
81	Zero-g Vapor Compressor Freezer Demonstration Unit Condenser, Installed in Refrigeration Unit	90
82	Zero-g Vapor Compressor Freezer Demonstration Unit Evaporator Under Construction, Double Coil	90
83	Zero-g Vapor Compressor Freezer Demonstration Unit Evaporator Under Construction, Preliminary Bonding	91
84	Zero-g Vapor Compressor Freezer Demonstration Unit Evaporator Under Construction, Bonded to Evaporator Fins	91
85	Zero-g Vapor Compressor Freezer Demonstration Unit Evaporator Blower	92
86	Zero-g Vapor Compressor Freezer Demonstration Unit Evaporator with Blower Installed	92
87	Schematic for Zero-g Vapor Compression Refrigeration/Freezer Demonstration Unit	93
88	Front View of the Compressor Compartment for the Zero-g, Vapor Compression Refrigerator/Freezer Demonstration Unit under Construction	95
89	Rear View of the Compressor Compartment for the Zero-g, Vapor Compression Refrigerator/Freezer Demonstration Unit under Construction	95
90	Front View of the Entire Zero-g, Vapor Compressor Unit Refrigerator/Freezer under Construction	96
91	Rear View of the Entire Zero-g, Vapor Compressor Unit Refrigerator/Freezer under Construction	96
92	Absorption Isotherm for Freon 12 onto Activated Charcoal	97
93	Bottom View of Typical Reciprocating Freon Compressor Body	98
94	TopView of Typical Reciprocating Freon Compressor	98
95	Typical Freon Compressor Crankshaft with the Motor Armature and Oil Slinger Removed	99
96	Centrifugal Oil Slinger Removed from the Lower End of the Crankshaft	100
97	Crankshaft, Piston, Rod, Rod Bearings, Compressor Head, and Valve Body	100
98	Design Detail for Lip Seal (or Spring Energized Seal) and Wear Ring Concept	103

ILLUSTRATIONS (CONT.)

Figure		Page
99	Detail Dimensions for Spring Energized Lip Seal Design	104
100	Detail Design of Step Cut Seal Concept Energized by Expander	105
101	Photomicrograph of DU Self-Lubricating Bearing Material Cross-Section	106
102	Photomicrograph of DX Prelubricated Bearing Material	106
103	Needle Bearing Fatigue Life Nomogram	108

TABLES

Table		Page
1	Refrigeration Cycle for R-12 with Evaporator Temp, = -20 °F, Condenser Temp. = 90 °F	79
2	Refrigeration Cycle for R-12 with Evaporator Temp, = 20 °F, Condenser Temp. = 90 °F	79
3	Refrigeration Cycle for R-12 with Evaporator Temp, = 35 °F, Condenser Temp. = 90 °F	80
4	Refrigeration Cycle for R-502 with Evaporator Temp, = -20 °F, Condenser Temp. = 90 °F	80
5	Refrigeration Cycle for R-502 with Evaporator Temp, = 20 °F, Condenser Temp. = 90 °F	81
6	Refrigeration Cycle for R-502 with Evaporator Temp, = 35 °F, Condenser Temp. = 90 °F	79
7	Comparison of Performance and Design Parameters for Refrigerants R-12 and R-502	82

SUMMARY

During the contract, the following tasks were accomplished.

1. A -20 °F passive thermal storage food freezer was designed, analyzed, fabricated, tested, and delivered to NASA. This freezer consisted of an inner container supported by low heat leak struts inside an outer container and insulated with MLI. Special strut designs were developed. The unit was instrumented and tested extensively. The design goal was to maintain the food in a frozen state for 90 days. Test results showed the final design was good for approximately 48 days.

   The results of this task are presented herein on pages 12 through 16 and in Appendix A. These efforts resulted in obtaining the following patent:

   U.S. Patent No. 4, 821, 914, 18 April 1989, "Low Temperature Storage Container for Transporting Perishables to Space Station," issued to J. Owen (NASA) and W.G. Dean (Lockheed).

2. A -70 °C (-94 °F) bio-sample freezer was designed, analyzed, tested, and delivered to NASA. This design consisted of a "two halves" concept which was based on the use of either an onboard spacecraft vacuum subsystem or a vent directly to space to maintain the vacuum level of 10^{-4} Torr or less on the MLI insulation. A minimum volume design was developed which used epoxy glass honeycomb ends to eliminate the need for domes usually found in vacuum/MLI designs. The "two halves" concept resulted in each half being 22.9 cm (9 in.) O.D. by 30.5 cm (12 in.) outside length with a 17.8 cm (7 in.) I.D. by 26.7 cm (10.5 in.) inner container. A special diaphragm was designed to minimize the heat leak from outer to inner container while maintaining the required internal MLI vacuum space environment.

   Numerous tests of this freezer were performed down to a temperature of -188 °C (-370 °F) and indicated a heat leak of approximately 3 W at that internal temperature level. The analysis of this freezer is documented in Ref 3. Test results are presented on pages 17 through 37 and in Appendices A and B.

3. A vapor compression cycle refrigerator for operation in zero-g was designed, analyzed, tested, and delivered to NASA. This refrigerator used a dual loop design for redundancy with two compressors, two evaporators, and two condensors. It utilized "double containment" in that all freon carrying components were installed inside a sealed, self-contained compartment. The design operating conditions for this refrigerator were

   - Cooling load — 250 W
   - Condenser operating temperature — 32 °C
   - Evaporator operating temperatures — -29 °C (-20 °F) and 2 °C (35 °F).

   Both condenser and evaporator designs were based on centrifugal phase separation. This design used a commercially available diaphragm compressor and refrigerant 502. This

refrigerator was tested down to a temperature of -24 °C (-11 °F), where problems were encountered with the overheating of the compressor/motor, precluding further testing.

Results of this task are presented in paragraph 2.2.4.2.2, pages 69 through 108.

4. A production model Stirling refrigeration unit was obtained and tested extensively over a range of temperatures to determine its performance outside its design range, i.e., at higher temperatures. Results indicated that the unit met the cooling capacity specified by the manufacturer at the specified design temperature of -196 °C (-320 °F). It also continued to operate and produce cooling up to approximately -80 °C (-112 °F).

   Results of this task are presented in Ref 14.

5. A study and review were performed to determine the applicability of various compressor concepts to zero-g operation. Various types of reciprocating, rotary, and continuous flow compressors were reviewed and evaluated based on liquid carryover, tolerance to lubricaton, efficiency, maintenance, and typical flow rate, i.e., size. These results are presented in Appendix E.

6. Several getter pump concepts were designed, fabricated, and tested for potential use in maintaining low pressures in the MLI insulation space. These results are discussed in paragraph 2.1.3.

7. A Spacecraft Refrigeration Development study was performed by SRS Technologies under a subcontract as a part of this total effort. This subcontract consisted of the following subtasks:
   - Definition of design requirements
   - Assessment of feasible cycles
   - Definition of cryogenic refrigeration requirements
   - Assessment of heat pump applications.

   The results of this work flowed into the subsequent design, fabrication, and testing during the remainder of the contract period.

8. A fluid loop test bed flow control valve controller was modified, assembled, and tested. The original controller was used on the Skylab/ATM thermal control system to control radiator bypass flow. It had a fixed temperature setpoint. The controller was modified so that a range of temperature setpoints could be selected. This unit was delivered to NASA as a part of the NASA/MSFC thermal/fluid loop test bed which was assembled under a separate contract (see Ref 8). The controller work and tests are described in paragraph 2.2.4.1.

Section 1. INTRODUCTION

Space Station thermal loading conditions represent an order of magnitude increase over current and previous spacecraft such as (1) Skylab, (2) Apollo, (3) Pegasus III, (4) Lunar Rover Vehicle, and (5) Lockheed TRIDENT missiles. Thermal storage units (TSUs) were successfully used on these, as well as many applications for ground based solar energy storage applications. It is desirable to store thermal energy during peak loading conditions as an alternative to providing increased radiator surface area which adds to the weight of the system. Basically, TSUs store heat by melting a phase change material (PCM) such as a paraffin. The physical property data for the PCMs used in the design of these TSUs is well defined in the literature. Design techniques are generally well established for the TSUs. However, the Space Station provides a new challenge in the application of these data and techniques because of three factors: (1) the large size of the TSU required, (2) the integration of the TSU for the Space Station thermal management concept with its diverse opportunities for storage application, and (3) the TSU's interface with a two-phase (liquid/vapor) thermal bus/central heat rejection system. The objective in the thermal storage research and development task was to design, fabricate, and test a demonstration unit. One test article was to be a passive thermal storage unit capable of storing frozen food at -20 °F for a minimum of 90 days. A second unit was to be capable of storing frozen biological samples at -94 °F, again for a minimum of 90 days. The articles developed were compatible with shuttle mission conditions, including safety and handling by astronauts. Further, storage rack concepts were presented so that these units can be integrated into Space Station logistics module storage racks.

The extreme sensitivity of spacecraft radiator systems design-to-heat rejection temperature requirements is well known. A large radiator area penalty is incurred if low temperatures are accommodated via a single centralized radiator system. As per the scope of work of this task, the applicability of refrigeration system tailored to meet the specialized requirements of storage of food and biological samples was investigated. The issues addressed were the anticipated power consumption and feasible designs and cycles for meeting specific storage requirements. Further,development issues were assessed related to the operation of vapor compression systems in micro-gravity addressing separation of vapor and liquid phases (via capillary systems).

Section 2. TECHNICAL DISCUSSION

The task was kicked off by defining requirements for both thermal storage and refrigeration units for the Space Station common module and the logistics module. Storage for the frozen and refrigerated food supplies and experiment specimens must be provided in the logistics module during prelaunch, launch, on-orbit prior to linkup with Space Station, on-orbit attached to the station, and during reentry and landing. A novel idea was proposed in which NH_3 is encapsulated in small metal capsules, and MSFC concurred that this concept was worth investigation. In the capsules, the liquid volume of NH_3, as it evaporates, would raise the vapor pressure and saturation temperature, resulting in variable temperature "sink" or thermal storage concept. This concept had its drawbacks: manufacturing the capsules, developing a method for charging the capsules, and determining the amount the capsules should be charged.

As the Space Station work progressed, preliminary thermal requirements for the logistics and habitation modules, the materials lab module, and the life sciences lab module were formulated and converted to thermal storage volumes at required temperatures. Cooling loads for the habitation module are relatively low because the food stored in the habitation refrigeration system will be maintained at the required low temperatures by the logistic module refrigeration system, prior to transfer to the habitation module. The cooling loads in the life sciences lab module will be high because of the large number of biological samples to be frozen and stored and because of the low temperatures required. To obtain a more accurate estimate of the cooling loads in the life sciences lab, the rate at which biological samples are stored needs to be determined from an experiment manifest. It is important that a baseline experiment manifest be developed to identify experiments requiring refrigeration for each 90-day period. As of now, the logistics module presents the greatest challenge for designing refrigeration systems to meet all cooling requirements. Refrigeration systems must be designed to cover the entire spectrum of mission phases from prelaunch through return and landing. The logistics module must maintain food temperatures until the food is transferred to the habitation module, and must also provide a means of returning to Earth the frozen life sciences biological samples in a -94 °F freezer.

2.1 THERMAL STORAGE DEVELOPMENT

The concept of thermal storage for the -20 °F frozen food for the logistics module food/freezer and for the -94 °F biological sample storage requirement of the life sciences module was conceived as a super insulated container with a PCM liner. The container would have a double wall vacuum jacketed shell with multilayer insulation (MLI) and "getter" materials inside. Also, the PCM liner would have imbedded within the PCM itself (or in good thermal contact with it) a refrigerant coil for charging the capacitor, i.e., freezing the PCM.

Conceptually, this thermal storage unit would be used as follows. While on the launch pad the unit would be connected to GSE to keep it charged. Before liftoff the GSE would be disconnected and the PCM would hold the required temperature through launch, orbit, and docking of the

logistics module with the Space Station. After docking, the unit would be connected to an on-board refrigeration system for the mission duration and for recharging the PCM for the return trip. Alternately, the -94 °F unit and conceivably even the -20 °F and +35 °F requirements could be met by providing enough PCM mass for the entire 90-day mission.

Unknowns in the design of this type unit included the effect of opening of the container lid and the number of times the container lid would typically be opened per mission. Estimates were made of these factors. Also, it may be desirable to vent the container inside storage volume overboard after each use to minimize PCM melting. Another facet of this concept is to use an ammonia boiler as a heat sink rather than a liquid/solid PCM such as lithium chloride. *Figures 1* and *2* illustrate these thermal storage concepts.

The -94 °F biological sample freezer was the subject of an indepth analysis. The biological samples are to be stored at -94 °F, and a total storage capacity of 3.6 ft^3 is required. A passive thermal storage container has advantages over an active vapor compression system because it requires no electrical power and uses no toxic refrigerant. In view of the available storage volume, such as the arrangement/size of the racks inside the module, three storage containers of 1.2 ft^3 each in internal volume were selected to yield the required 3.6 ft^3. The passive thermal storage system selected uses composite materials, multilayer insulation, and a PCM. The PCM must provide an effective thermal barrier at -94 °F for the frozen bio-samples and have a large enough heat of fusion to absorb all heat leaks into the storage container for the required mission duration of 90 days. The PCM chosen for this purpose is a 30 percent solution of lithium chloride and water, which melts at -95 °F and has heat fusion of 109 Btu/lbm. Its density is 73.4 lbm/ft^3 – slightly higher than water.

The PCM in the selected system is surrounded by 160 layers of MLI in an encapsulated composite material jacket lined with a stainless steel foil and evacuated to obtain a high vacuum on the order of 10^{-5} torr. The PCM container is supported on the inside by standoffs that go through the MLI blankets. With this basic concept, several configurations were thermally modeled and analyzed, leading to a final concept which consisted of two identical freezer halves joined together at the center with a seal to prevent cryo pumping of air. A preliminary structural analysis on this configuration showed that it would be acceptable. Work on building the test article was started to prove the concept of the passive freezer. Problems such as achieving a high vacuum and maintaining it for long periods due to leaks in joints/sealants, material outgassing, etc., and other problems such as MLI layup were encountered.

Computer analysis of the thermal storage freezer concept was started concurrently by first thermally modeling the container without the lid. This was performed to see if the 1 in. jacket of LiCl PCM would last for 90 days. A 3 in. jacket around the PCM was provided to contain 160 layers of double aluminized Mylar multilayer insulation. The modified MLI jacket was considered to be evacuated to a high level of vacuum, 10^{-5} torr or better. MLI effective conductivity and layer density were obtain from Ref 1. The walls of the PCM and MLI jackets were modeled as 0.060 in. thick phenolic glass to minimize heat conduction to the PCM. The internal container was 10 in. in diameter by 26.4 in. long to render a storage volume of 1.2 ft^3.

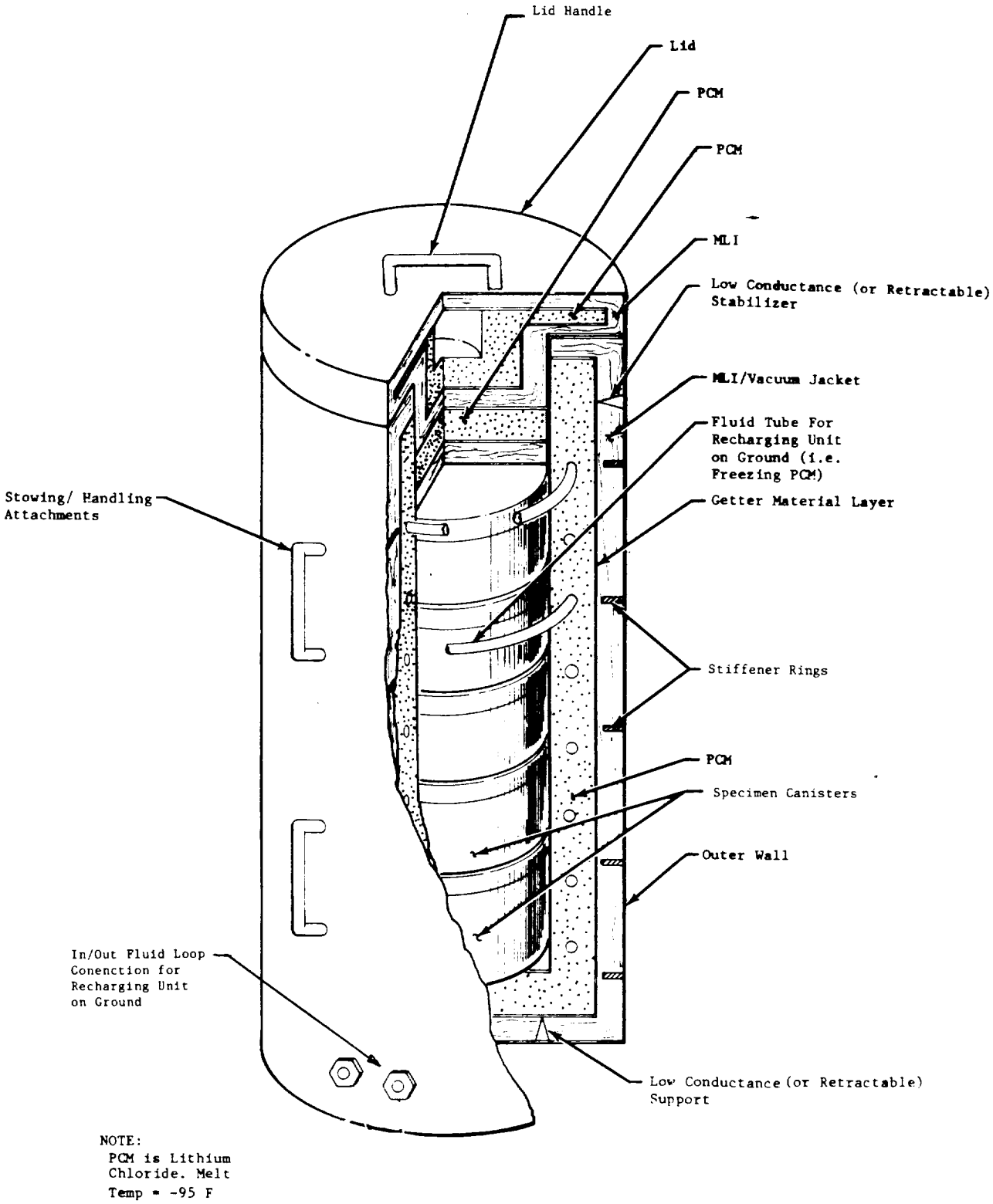

Figure 1. Space Station Thermal Storage Unit Concept

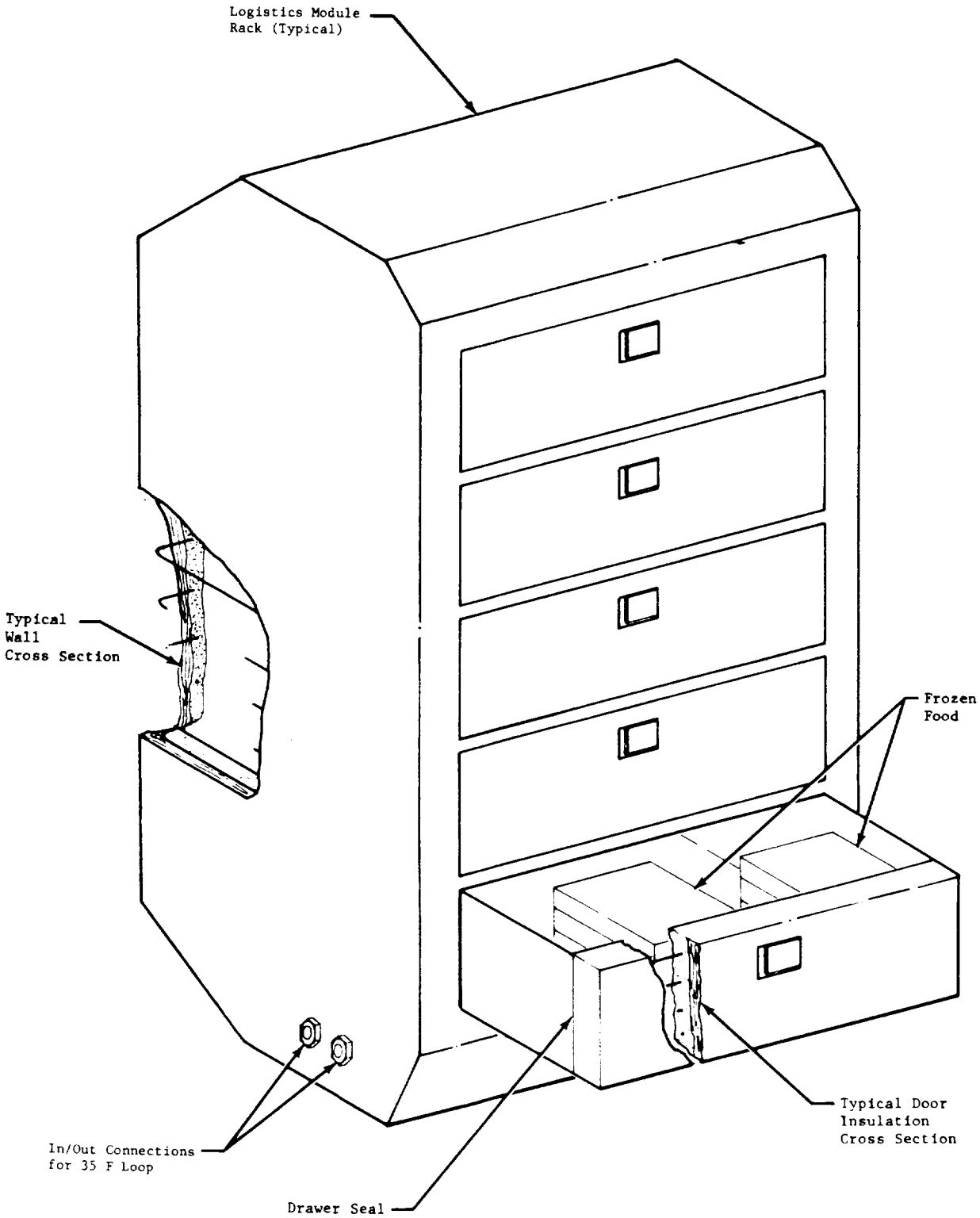

Figure 2. Logistics Module Thermal Storage Unit Concept

A partial cross section of the container as modeled is shown in *Figure 3* with the node number designations for the different components and their dimensions. Analysis was performed using SINDA (Ref 2) with and without the phenolic standoffs shown in this concept.

It is well known that phenolic resin outgasses in a vacuum environment. Therefore, to sustain a high vacuum in the MLI jacket to obtain minimum effective conductivity as measured in the work of Ref 1, and as modeled, the phenolic walls inside the vacuum area were lined with a metallic foil. Initially, a 3-mil thick foil was modeled on the phenolic glass. This was performed by effectively changing the conductivity of phenolic to include the conductance provided by 0.003 in. thick stainless steel. The results directed that the liner thickness be reduced to 0.0005 in., which was acceptable for heat transfer reduction.

The next task was to design and analyze the lid for the containers. Merely providing a plug type cover to the container did not prove thermally acceptable. The problem was providing a sufficient length for the heat path to the PCM in the lid. Manufacturing difficulties, PCM charging, and structural integrity of the lid/container also needed to be considered.

Since the storage container bottom itself is thermally acceptable and structurally feasible, it was conceived that the lid could be made identically; in other words, the freezer could be made in two identical halves joined by a common flange with an O-ring type seal. This freezer half was analyzed with appropriate dimensions as shown in the sketch of *Figure 4*. The freezer half with these dimensions was first checked structurally, then thermally. Structural changes included use of 0.25 in. thick honeycomb sandwich panel with 0.25 in cells of 0.004 in. thick phenolic material walls and 0.020 in. thick face sheets of G-10 epoxy glass. This panel is used at the top and bottom of the container for strength required to hold the vacuum inside the MLI jacket. The bottom standoffs are replaced with a 10 in. diameter by 0.030 wall by 3 in. high phenolic glass cylinder lined with 0.0005 in. stainless steel foil to carry the g-loads of the inner PCM jacket and PCM material.

The analytical effort as described above is documented in detail in Ref 3. It was concluded from this work that the -94 °F passive bio-sample storage concept was marginally feasible for the 90-day mission. It was assumed that the units could be fabricated to meet the idealized thermal conductances and MLI effective conductivities. This proved to be correct in the manufacture and test phases of the food freezer unit described below.

The superinsulated container/thermal storage concept was considered for the -20 °F frozen food requirements for the logistics module. The

The superinsulated container/thermal storage concept was considered for the -20 °F frozen food requirements for the logistics module. The earlier concept shown in *Figure 2* was replaced with the concept shown in *Figure 5* since the cylindrical shape is much better structurally for containing the double wall vacuum jacket than the flat wall conventional freezer concept. Detailed thermal models were made; results were promising, except for the neck plug heat leak which required very thin walls made from low conductivity materials such as phenolic glass. Structural analysis revealed a problem of buckling of these thin walls for the required 10 in. diameter. To

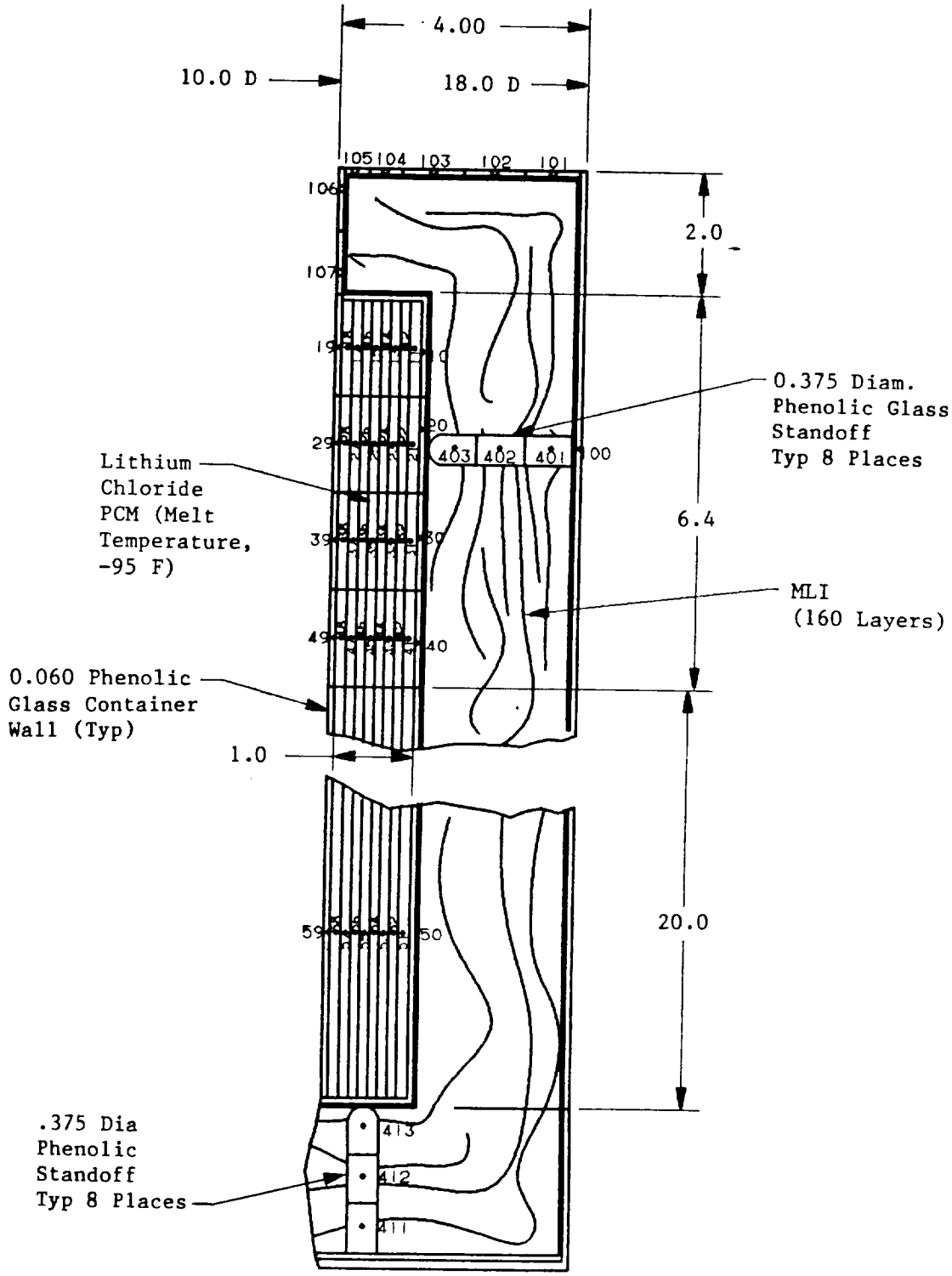

Figure 3. Cross Section of the Passive Thermal Storage Container Showing the Components and Their Nodal Breakdown as Modeled

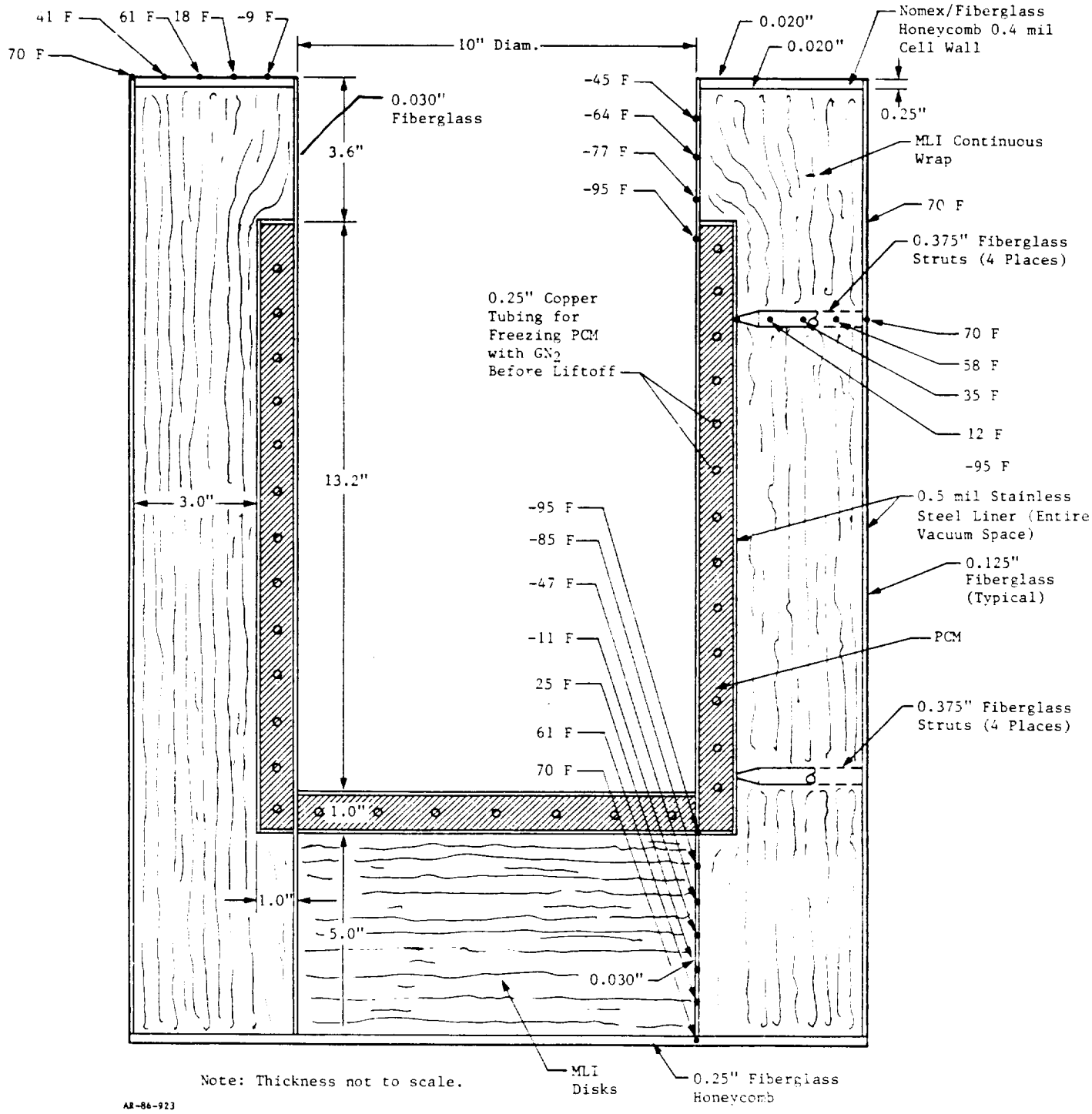

Figure 4. Latest Concept Design for -94 °F Bio-Samples Thermal Storage Unit (Only one-half of "two halves" is shown; other half is mirror image.)

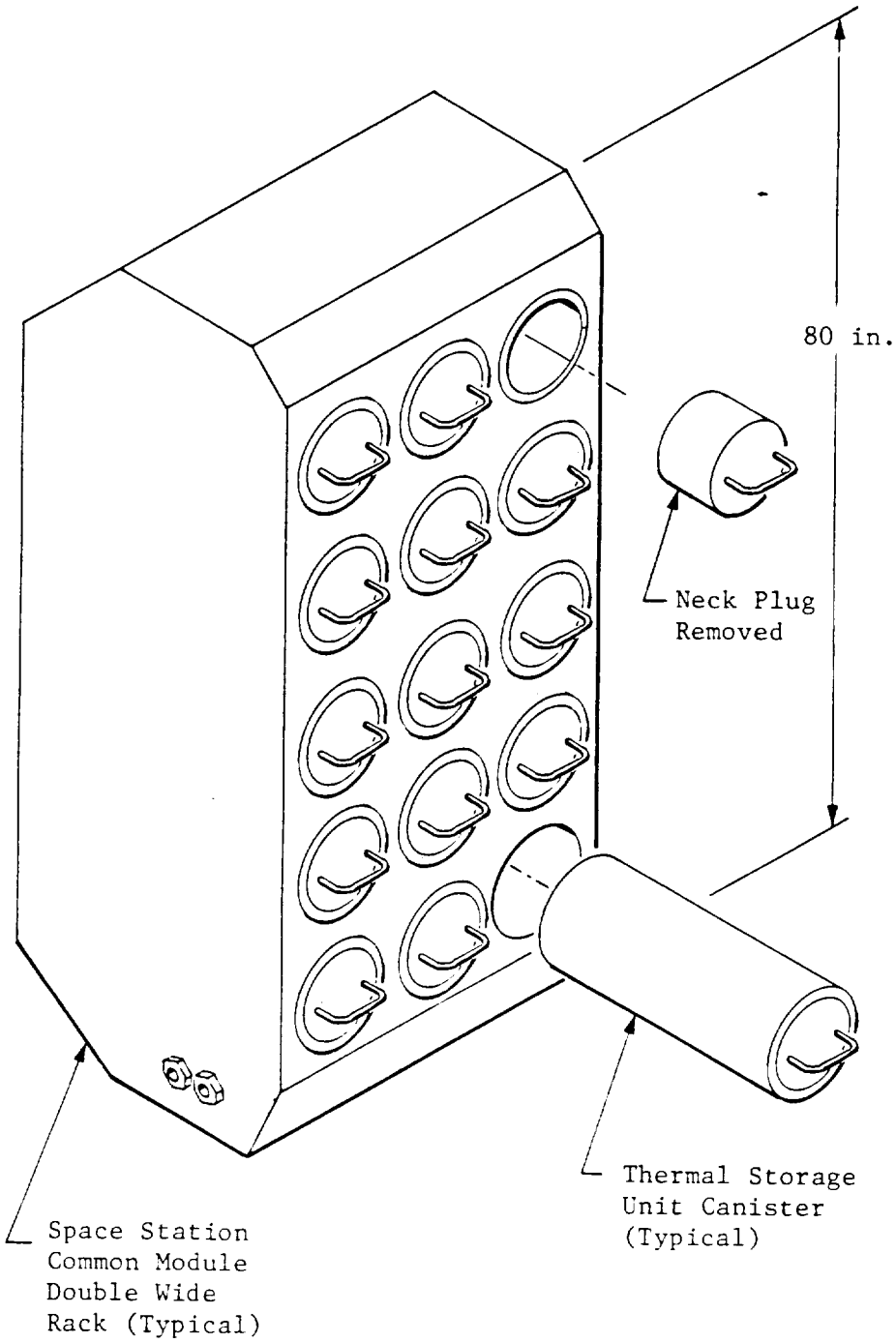

Figure 5. Alternate Concept for Logistics Module Frozen Food Thermal Storage Unit

meet the conflicting requirements for thin walls thermally and thick walls structurally, a capsule was conceived with two mirror image halves, shown in *Figure 6*. In this concept, the entire internal volume is evacuated (including the MLI space) rather than having a separate MLI with a double wall vacuum jacket as in the original design. The joint between the two capsule halves has an O-ring seal. This design, although preliminary when first conceived, required improvements in the areas of MLI closeouts at the joint where the tank halves came together; closeouts at the hemispherical ends; MLI penetrations for the support wires and instrumentation cables; and weight. However, the design formed the basis for manufacturing and testing the thermal storage demonstration unit.

The purposes of the thermal storage demonstration unit are (1) to check out some of the practical aspects of the design, such as strut wire attachment and MLI layup and (2) to verify the thermal model of the -20 °F thermal storage unit. This test unit was designed with a PCM container (CaCl and water for a melt temperature of -20 °F) to simulate the frozen food volume and dimensions. The mass of PCM was calculated to yield a test time (i.e., melt time) of the order of one week to expedite testing. The PCM container was mounted inside a wire "basket" supported by 0.030 in diameter strut wires mentioned earlier.

Operation of this thermal storage unit design is now changed from the original design operation because there is no separate neck plug that can be taken out, food removed, and then the neck plug replaced. In the new design, once the capsule is opened by the Space Station astronaut, all the food should be removed and placed in the refrigerator since after the vacuum is lost on the container MLI, the insulation ceases to be effective and any remaining food starts to thaw. This mode of operation seems to be acceptable. Each capsule is being designed for about 100 pounds of frozen food. This could be compared to going "shopping" in the logistics module, opening a single capsule from the freezer area, and then taking this frozen food, at approximately -20 °F, back to the habitation module for temporary storage in the +35 °F refrigerator until the food is consumed.

The efforts that followed soon afterward were concentrated on making the demonstration units for the -20 °F food freezer thermal storage and the -94 °F bio-samples thermal storage. As with any hardware development program, this program had its share of problems. These were resolved when encountered in the process of development to achieve the final goal. All events that occurred, steps taken to improve on the design, and efforts spent to alleviate problems were categorically described in the monthly progress reports and discussed firsthand with the COTR.

The practical aspects of the design of the -20 °F thermal storage unit were several. These were the strut wire attachment techniques, layup of MLI layers, cutout and "goring" of MLI near ends of the inner basket, penetrations through MLI for the support wires, instrumentation feed-throughs for penetrating the tank wall, outgassing of materials inside the tank, use of proper netting materials between MLI layers, getter materials, and, very importantly, maintaining an ideal vacuum for proper MLI function. The impact on the design and desired results in each of these areas and the alternatives and solutions proposed and tried, as the development and testing of the thermal storage unit progressed, were documented and reported on a regular monthly basis. Photographs describing pertinent changes to the design and showing test and laboratory setups were included in these regular reports.

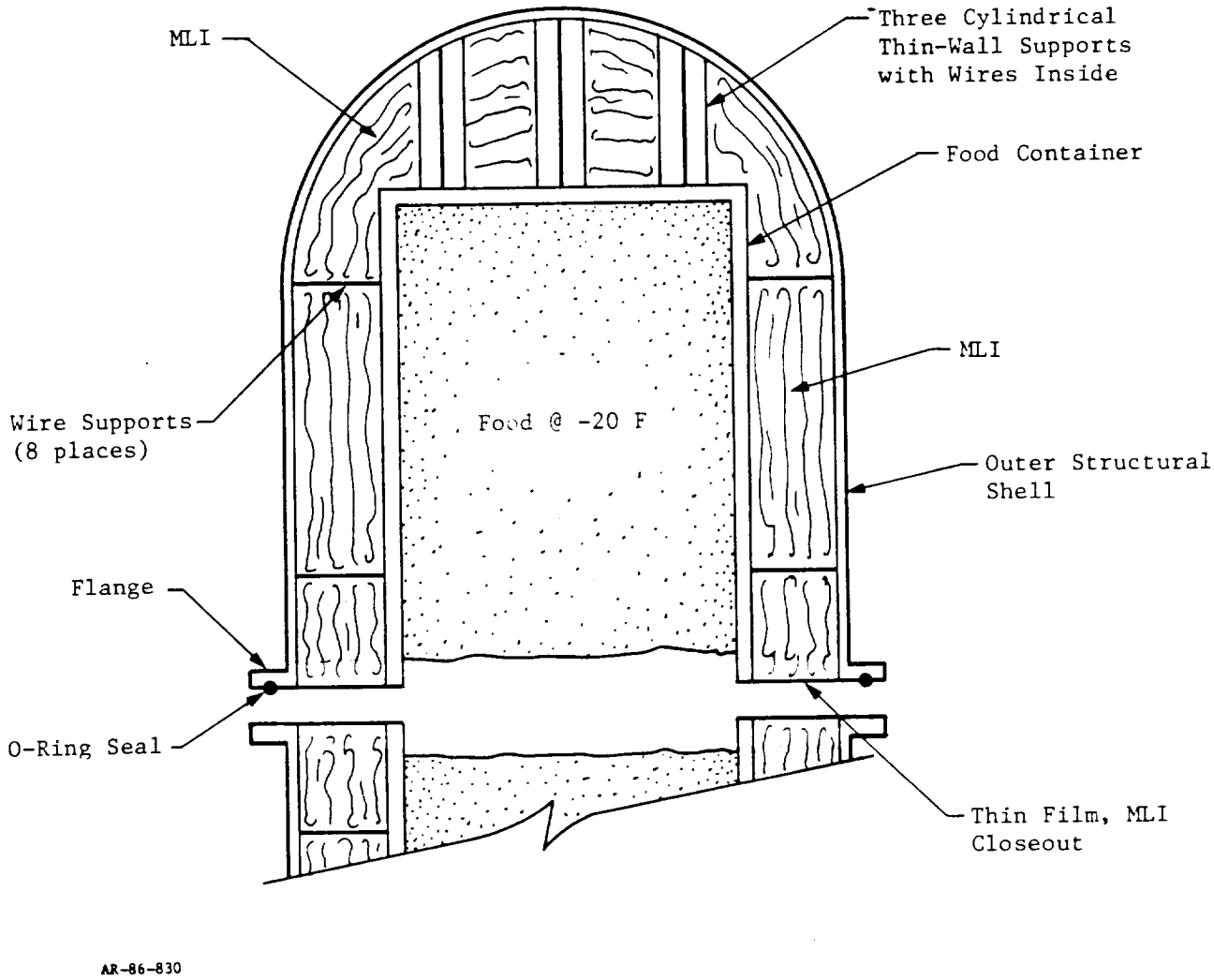

Figure 6. Two-Halves Thermal Storage Unit Concept for Frozen Food at -20 °F

In the area of -94 °F bio-sample thermal storage demonstration unit, efforts were directed towards the design, manufacture, and test of thermally and structurally acceptable honeycomb panels mounted on top of each half of the tank. This area is thermally critical since it is the shortest length of heat leak path. Efforts were also spent in the area of achieving proper joint/closeout of the two halves, lining and bonding the fiberglass wall with a thin stainless steel sheet to prevent outgassing, and creating a vacuum vessel of fiberglass approximately 10 in. diameter x 30 in. long for testing outgassing rates and permeability effects.

Thermal and structural design, manufacturing techniques and difficulties, use of materials, achievement of required vacuum qualities, and interfaces with relevant organizations were areas of concern in the fabrication and test of the demonstration thermal storage unit. An excerpt from the June 1987 Progress Report, LMSC-HEC PR D066068, is included in Appendix A to provide background information and illustrate the fabrication activities that took place toward development and test of the thermal storage units.

2.1.1 Demonstration Unit for -20 °F Food Freezer

As discussed in the progress report excerpt included in Appendix A, the test results showed that MLI performance was at first considerably below that expected and used in the analysis. The continuous winding of the double aluminized Mylar and dacron netting, the slitting of this MLI for penetration of the strut wires, and the "goring" and taping of the MLI at the tank ends were not ideal. These factors may have caused some "thermal shorting" between MLI layers, and the slits allowed radiation heat leaks.

After discussing this problem with NASA-MSFC personnel (Dave Clark and Joe Lawrence), it was decided to change the MLI design/fabrication procedure. In the new design, the MLI was applied in sub-blankets of 10 layers each. Each individual layer within the sub-blankets was held together using 1/2 in. lengths of double back (or adhesive transfer) tape (3M-Y966). These sub-blankets were then applied to the cylinder with 2 in. overlaps. The joints were staggered around the circumference. Each strut wire was threaded through the sub-blankets as they were assembled.

The test article inner basket (tank) shape was changed from a flat end to a hemispherical dome to better represent the flight hardware shape/design. The new ends were made by forming heavy aluminum foil over a 9 1/2 in. hemispherical mandrel. The cylindrical part of each basket was shortened so that it would still fit inside the same outer test tank.

The MLI which covers the dome is now continuous with the cylindrical side sub-blankets, thereby eliminating the joint between the dome and cylinder MLI. The dome MLI is then formed by cutting pie-shaped sections out, leaving "gores." These gores are then butt-jointed to form the hemispherical shape. The tip ends of the gores are sewn together across the tip of the dome to hold them in place. The joints are then taped over with reflective tape for closeout. The butt joints in the gores are alternated from one sub-blanket to another so that consecutive joints do not fall on top of each other. The gores are purposely sewn and taped to prevent thermal shorting between layers.

Drawings for each of the 16 individual sub-blankets were made on the Lockheed CADAM system. These were then cut out and used as full scale patterns for cutting the MLI.

The redesigned MLI fabrication/assembly was installed inside the test article and testing began. Several tests were conducted with a sufficiently low pressure of -10^{-4} torr for good MLI performance. The MLI performance is determined by assuming that the hand calculated thermal conductances/heat leaks for the strut wires and copper instrumentation wires are correct. This was a reasonable assumption since their lengths, diameters, and properties are well defined. These calculated heat leaks were then subtracted from the total heat leak, yielding the net heat leak through the MLI. When this MLI heat leak was compared to that calculated using the idealized data from Ref 1, we found that our MLI performance was lower by a factor of 8.4 to 9.7. However, the data of Ref 1 were taken with a "guarded tank" approach and without any joints or penetrations in the MLI.

A calculation was made, using results of these tests to date, to estimate the flight performance of this concept for food storage. Using the inner tank dimensions and the measured MLI/strut wire heat leaks, a 48-day storage time capability was calculated. Hence, an improvement in overall performance by a factor of approximately 2 was needed to get through the typical 90-day Space Station mission plus prelaunch stay time.

In order to make this improvement, further changes in the MLI design were made by removing the middle joint and bellyband and wrapping the entire tank except the top dome. The gores for this dome were to be left loose until after the food was loaded; then these gores were to be sewn and taped after closing the dome/lid. A design for an upgraded storage demonstration unit was started. A new inner tank was made to replace the existing "baskets" and aluminum foil domes. *Figure 7* shows a reduced copy of the preliminary shop drawing for this inner tank. This tank was designed to accommodate the new "one-piece" MLI blanket concept. It has one dome welded permanently in place. The other dome is attached to the cylindrical part of the tank with threads and has an O-ring seal.

Figure 8 shows the modification made to the outer tank. The changes allowed the outer tank to be opened at one end rather that at the middle to accommodate the new one-piece MLI blanket concept. Two new flanges with an O-ring seal were added. Two new larger instrumentation feed-through ports were also added. Receptacles were added to the sides of the tank for the new fiberglass support strut design, shown in *Figure 9*. This strut is installed through the MLI as follows. As each individual blanket is applied to the inner tank, a cloth "sock" is threaded through the blanket at the proper position along the diagonal path of the strut. After all blankets are in place and the inner tank/blankets are placed inside the outer tank, the strut is threaded through the inside of the sock to its position on the surface of the inner tank. It is then threaded into its fitting. Next, the sock is removed, leaving the strut end exposed through the outer tank wall. Finally, the outer strut end position/tensioner is put in place with its O-ring seal.

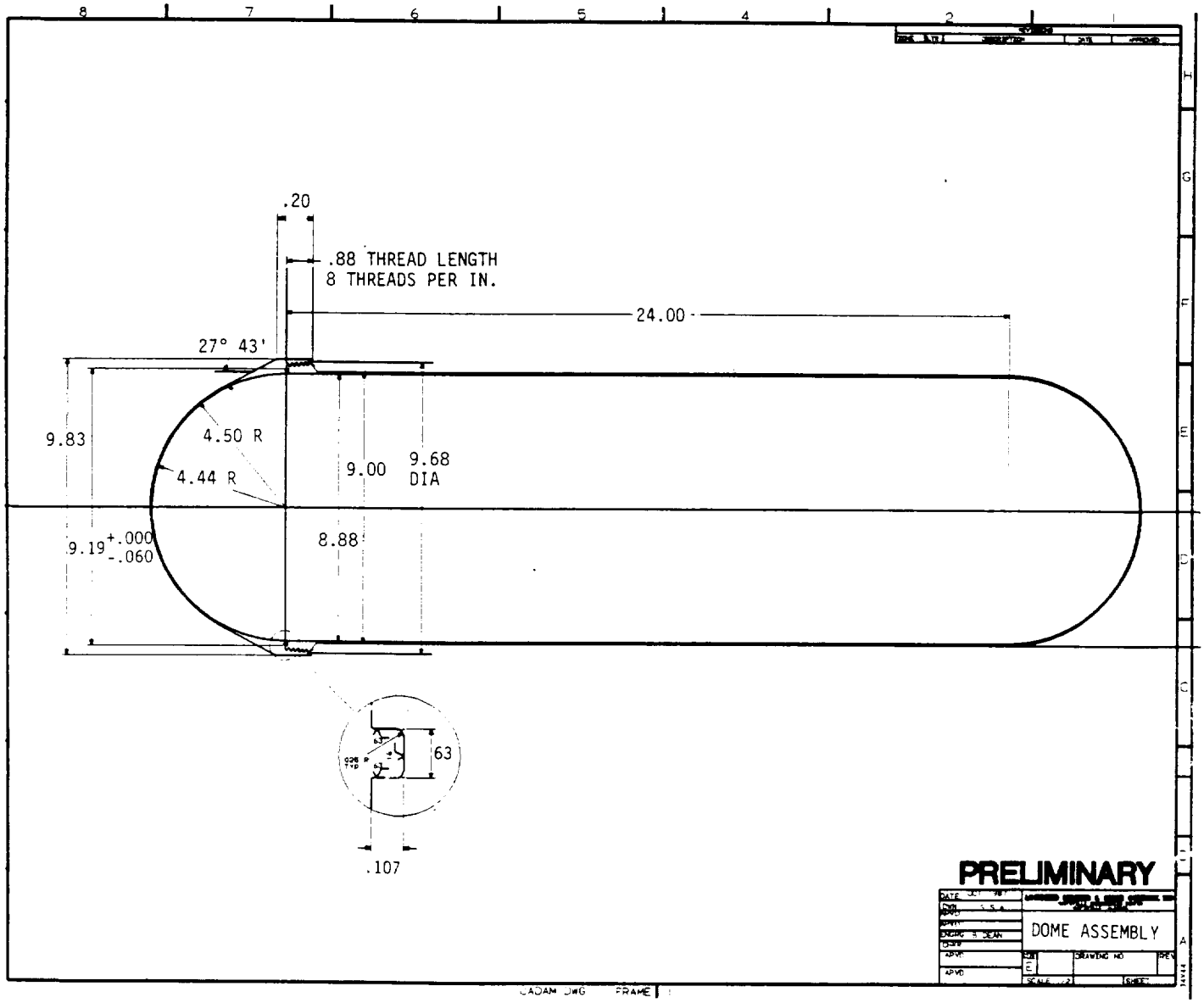

Figure 7. Preliminary Drawing of New Inner Tank Design for -20 °F Food Storage Demonstration Unit

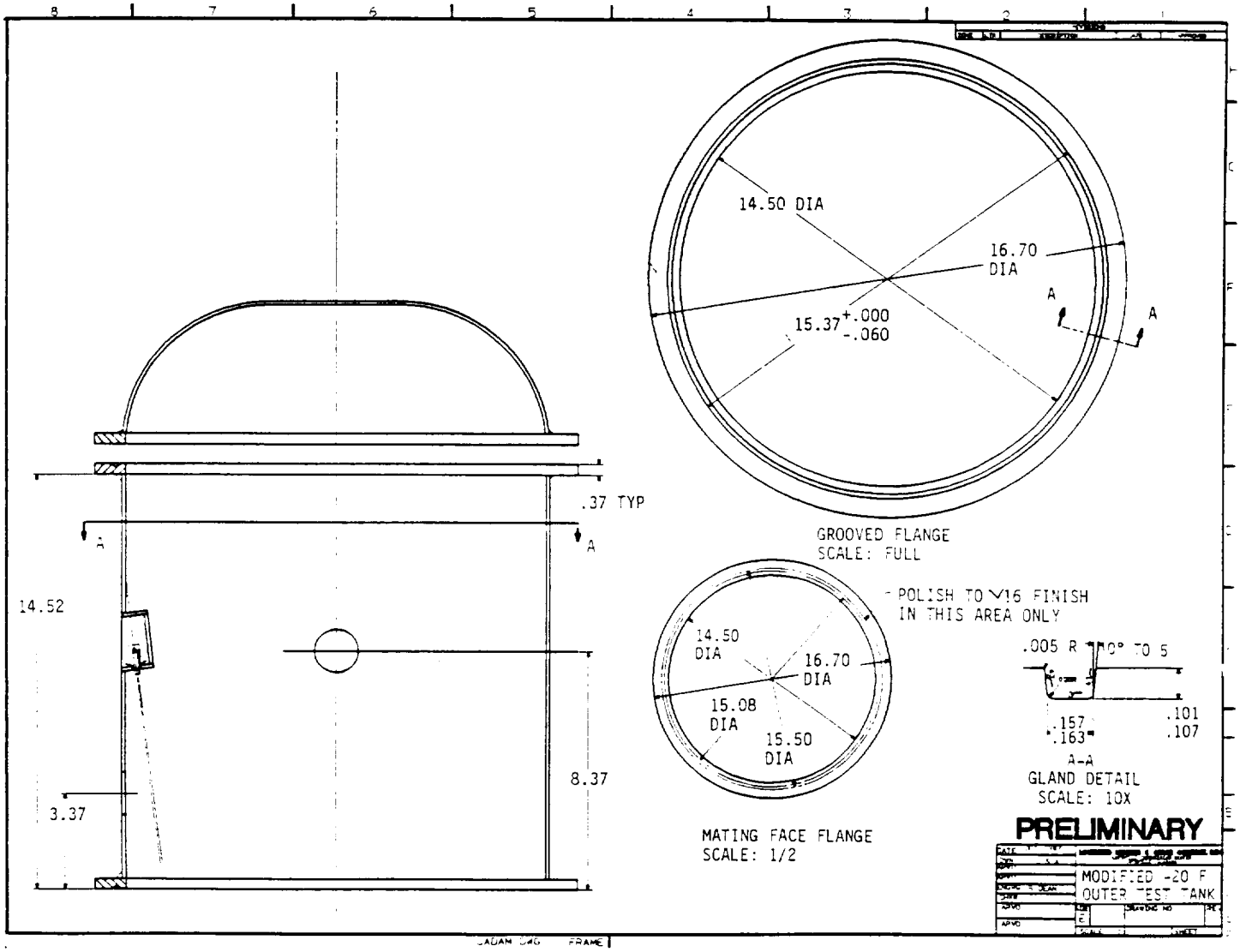

Figure 8. Preliminary Drawing of Modified Outer Tank for -20 °F Thermal Storage Demonstration Unit

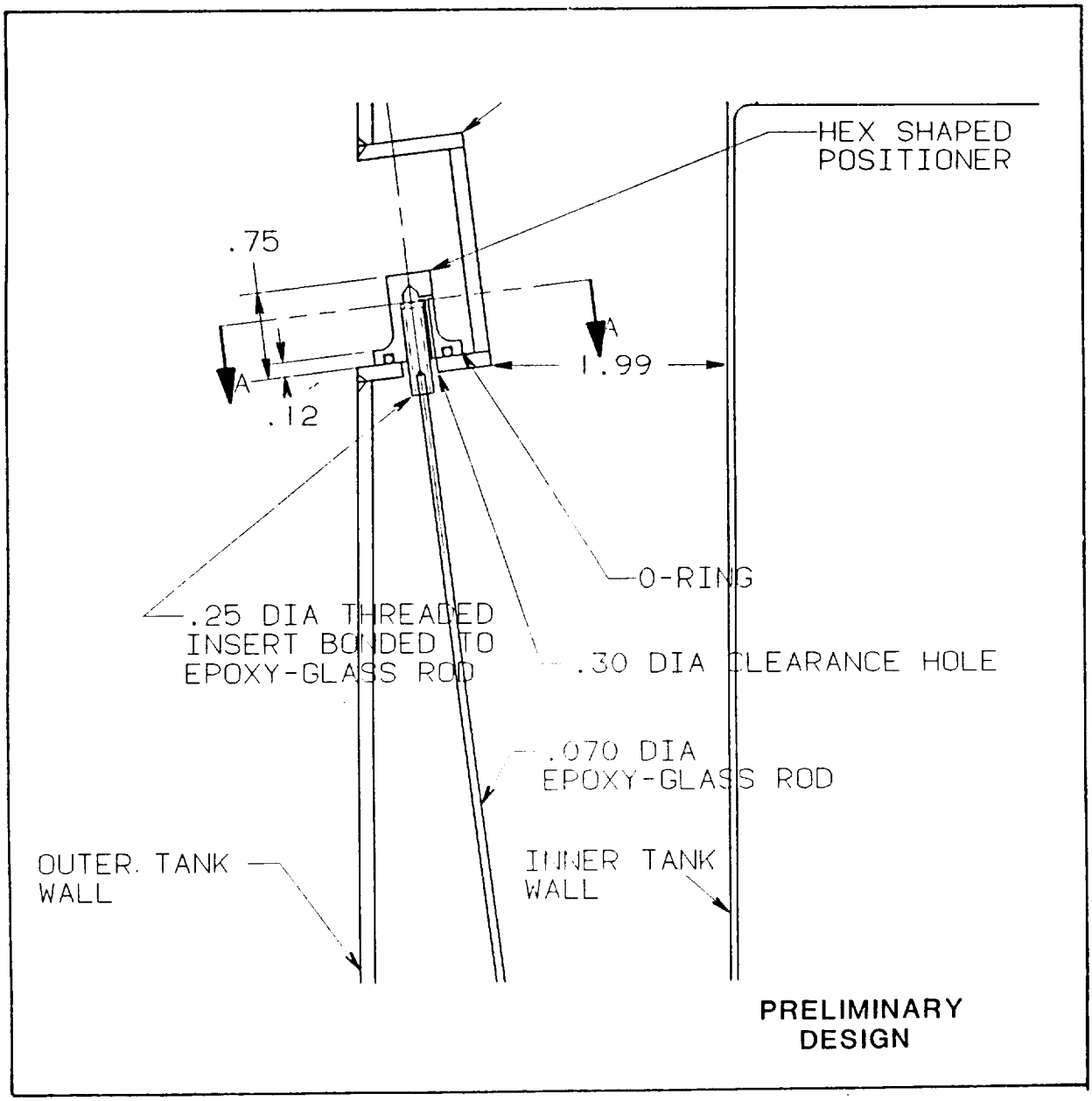

Figure 9. Preliminary Design of New Fiberglass Support Struts for Positioning the Inner Tank Inside the Outer Tank

2.1.2 Demonstration Unit for -94 °F Bio-Sample Freezer

The following design goals/requirements were established for the final freezer design to be delivered to MSFC.

- Minimize heat leaks.
- Design for operation in orbit only (i.e., this is not a logistics function design).
- Design for utilization of Space Station on-board vacuum utility system (i.e., there is no requirement to send the unit back to Earth for repumping of the MLI insulation/vacuum jacket volume).
- Assume that the unit can be provided internal cooling either by (1) an active refrigeration unit such as a Stirling Unit, (2) a PCM canister which is precooled before being inserted inside this freezer, or (3) a porous matrix filled with a cryogen before being installed inside this freezer.

Two sizes of freezer outside diameter were studied, 15 in. and 9 in., both with a 7 in. inside container/cold space. Honeycomb panel bottom plates were analyzed for both cases. It was decided that the 9 in. cylinder would be large enough. This allows an approximately 1 in. space for the MLI. The results of the analysis for the 15 in. and the 9 in. cylinder design were presented in the February 1990 monthly progress report. As a result of these analyses, face sheet thicknesses of 0.040 in. and a core depth of 0.50 in. were selected. This selection provided a deflection of 0.0579 in. of the honeycomb, which was acceptable.

A stress analysis was also conducted to determine the cylinder wall thickness requirements for the 9 in. diameter cylinder design. This analysis resulted in a 0.075 in. thick wall for a 12 in. long cylinder made of G-10 epoxy glass material.

A new concept was developed for the overall freezer configuration. This concept consisted of two cylindrical parts which were mated end-to-end. Each cylinder was 12 in. long with 9 in. O.D. To minimize volume, these cylinders had honeycomb bottom plates. The honeycomb bottom plates used thin wall face sheets consisting of 0.040 in. epoxy glass with a 0.001 in. thick stainless steel liner to prevent vacuum leaks and outgassing. A diaphragm closed out the annular space between the inner and outer cylinders. This diaphragm disk was made extremely thin in order to reduce the heat leak from the outer cylinder to the inner cylinder. This diaphragm is not strong enough to withstand a full one atmosphere pressure difference. This limitation was overcome in our design by pulling a vacuum between the two mated-cylinder top ends before evacuating the MLI insulation space. This vacuum between the cylinders pulled the two diaphragms tightly together and produced no net stress on them. Then the MLI space was evacuated, and the pressure difference across each diaphragm was zero.

Heat leak calculations were made for the 15 in. diameter design, with the following results:

- MLI = 0.17 W
- Donut (diaphragm) = 0.20 W

Total = 0.37 W

This design condition was near optimum because the MLI and other heat leaks were equal.

The progress report excerpt in Appendix A includes discussion of various aspects of developing the demonstration unit. These topics include tooling, fabricating, machining, testing, and venting honeycomb samples, bonding techniques, method needed for closeouts, joint designs, etching of stainless steel liner sheets, etc. Success was shown in the area of bonding the 0.0005 stainless steel liner to the composite material cylinders. A typical part, shown in *Figure 10*, was later load-tested.

Two inner cylinder and two outer cylinder bottom panels were fabricated. These four parts are shown in *Figure 11*, with the honeycomb core and outer rings bonded to the bottom face sheets. The inner cylinder bottom panels are approximately 7 in. in diameter and the outer cylinder bottom panels are 9 in. in diameter. The core is 0.5 in. thick, Hexcell HR H-10/F35-(5)-3.5. This core has a density of 3.5 lb/ft^3, a cell wall thickness of 0.005 in., a cell size of 0.375 in., a compressive strength of 350 psi, a shear strength of 150 psi, and a compressive modulus of 24 ksi. The HR H-10 designates the material composition, which is a Nomex Aramid fiber reinforced with phenolic resin. The face sheets of honeycomb panel skins are 0.040 in. thick and made from Hexell fiberglass Prepreg with 1581 glass fabric and F155 epoxy resin.

Figure 12 shows the same four panels after insertion of the paste type adhesive (Hysol 960) which bonds the core to the outer ring. This bond is required in order to carry the shear load from the core into the support ring. The load is then carried from the ring into the bottom end of the freezer cylinder outer wall.

Figure 13 shows the two inner cylinders and the two outer cylinders under construction. In *Figure 13*, the two outer cylinders have been lined with a 0.001 in. thick stainless steel foil. This foil is required to make the composite (i.e., epoxy glass) material impervious and to eliminate outgassing, which would destroy the vacuum in the vacuum jacketed insulation space. One of the inner cylinders has been covered with the first layers of MLI.

Figure 14 shows these same cylinders after the honeycomb bottom plates have been placed on one of the outer cylinders and both of the inner cylinders. The honeycomb cells' imprint can be seen through the bottom stainless steel face sheet of the honeycomb panel.

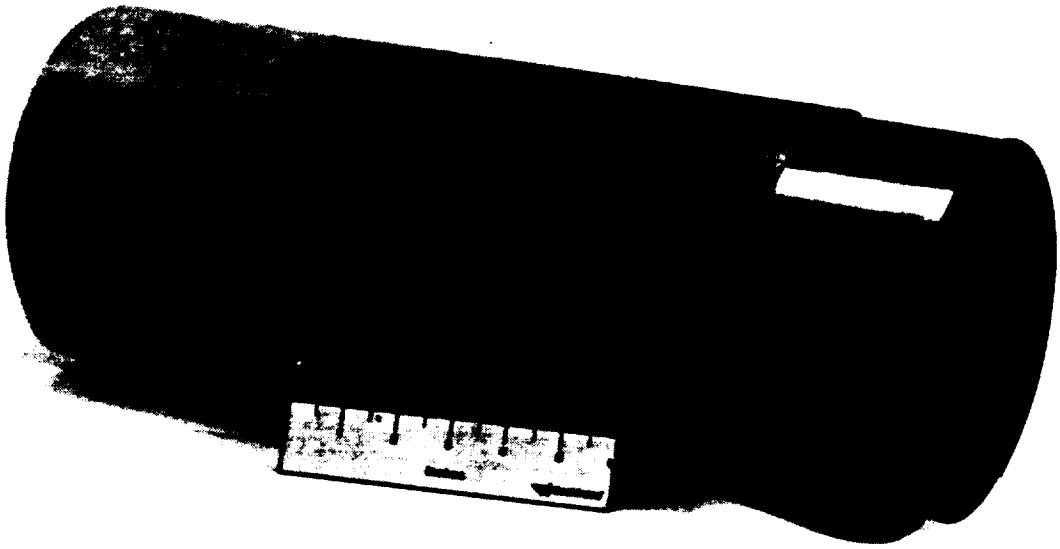

Figure 10. Epoxy/Glass Cylinder with 0.010 in. Thick Neck and 0.005 in. Stainless Steel Liner for Use in -94 °F Thermal Storage Unit

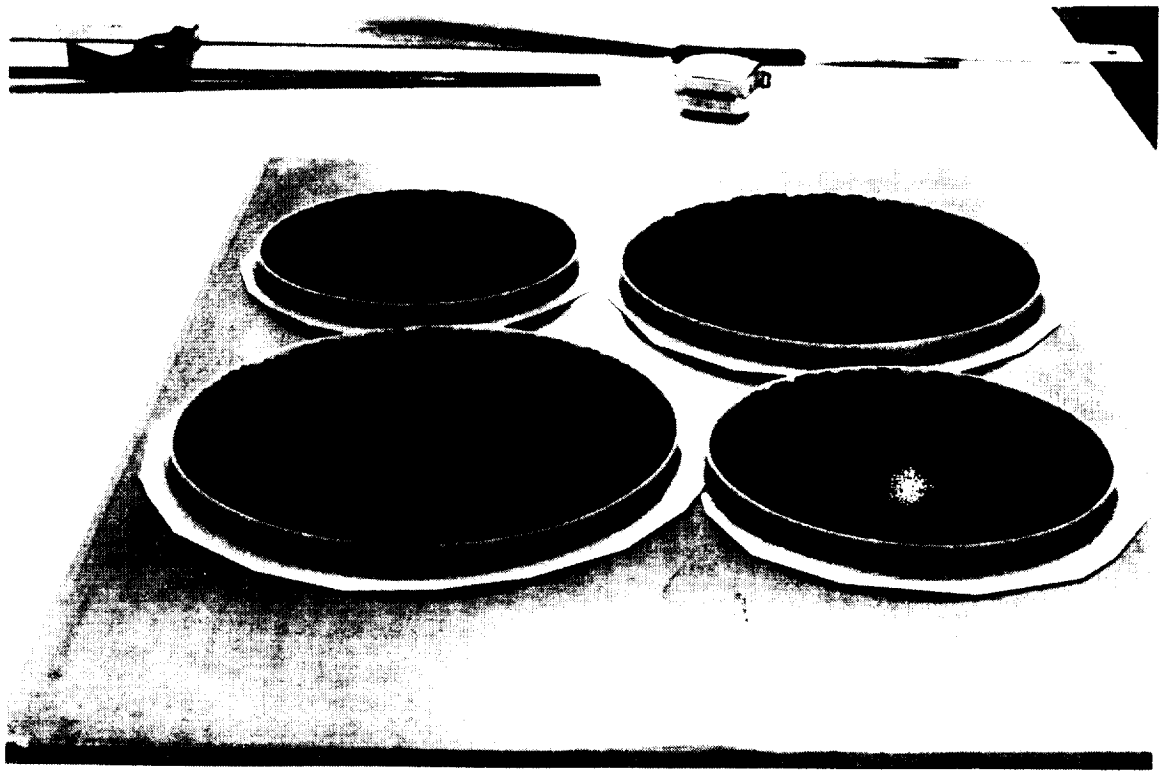

Figure 11. Inner and Outer Cylinder Honeycomb Bottom Panel in the Process of Fabrication for Bio-Sample Freezer

Figure 12. Inner and Outer Cylinder Honeycomb Bottom Panels for Bio-Sample Freezer after Insertion of Adhesive to Bond Core to Outer Rings

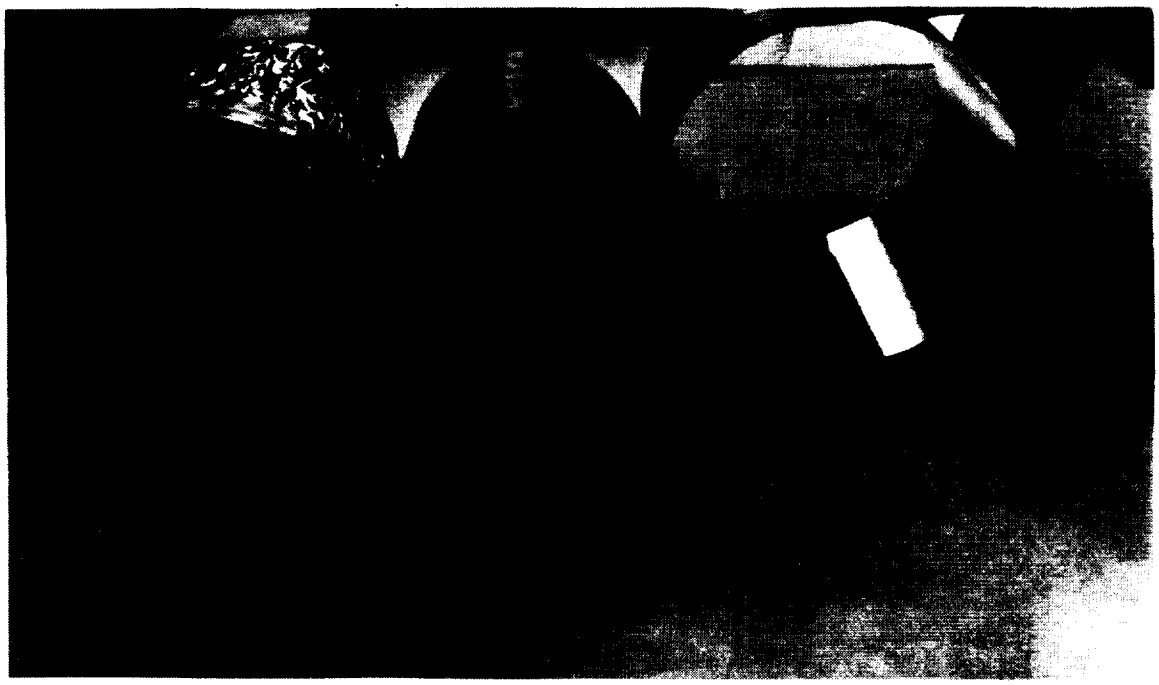

Figure 13. Two Inner Cylinders and Two Outer Cylinders during Fabrication Process

Figure 14. Two Inner Cylinders and Two Outer Cylinders Showing Honeycomb Bottom Panels in Place

Figure 15 shows one of the outer cylinders ready for bonding in place of the NW-25 flange vacuum connection and its reinforcing doubler. The brown covering material seen on the outside of this cylinder is a protective teflon cover used to protect the stainless steel outer liner.

Figure 16 shows one of the outer cylinders after the NW-25 flange vacuum connection has been bonded in place. *Figure 17* shows one of the outer cylinders after bonding in place of the aluminum reinforcing ring. This ring is required to beef up the joint between the thin outer cylinder wall (0.070 in.) and the thin (0.010 in.) annular diaphragm closeout sheet between the inner and outer cylinders.

Figure 18 shows the leak test in progress on one of the inner cylinders. These cylinders were pressurized to 16 psig with helium gas and leak checked with a helium detector. No leaks were found in either cylinder. *Figure 19* shows the leak test in progress on one of the outer cylinders. In this test a vacuum was drawn on the inside of the cylinders, and helium gas was sprayed around the outside of the cylinder. The inside space was connected to a helium leak detector for the tests. No leaks were found even on the instrument's lowest scale, i.e., 10^{-9} SCC per second.

Figure 20 shows an additional leak test which was performed on the outer cylinders. In this test a plastic film "hood" was placed over the end of the cylinder. This hood was then filled with helium gas while a vacuum was drawn on the internal volume. This is a more severe test since the helium is maintained around the outside of the joint for an extended period of time. Again, no leaks were detected in either cylinder, even on the leak detector's lowest scale, 10^{-9} SCC per second.

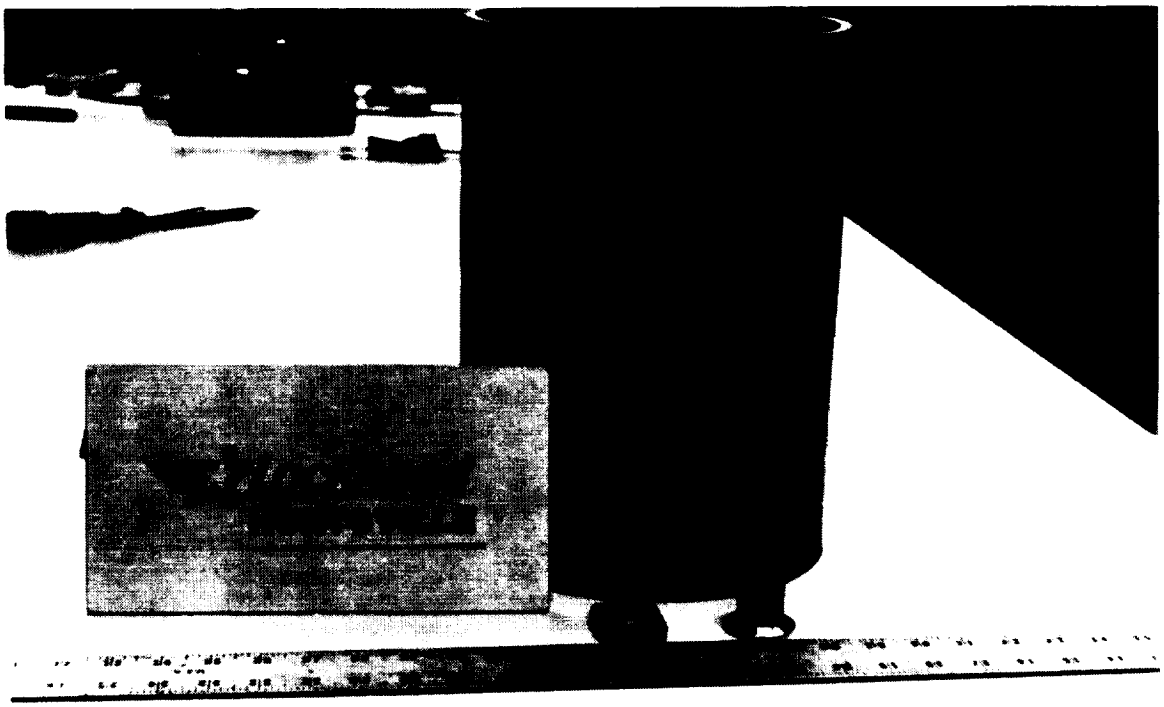

Figure 15. Outer Cylinder Ready for Bonding in Place of NW-25 Flange Vacuum Connection

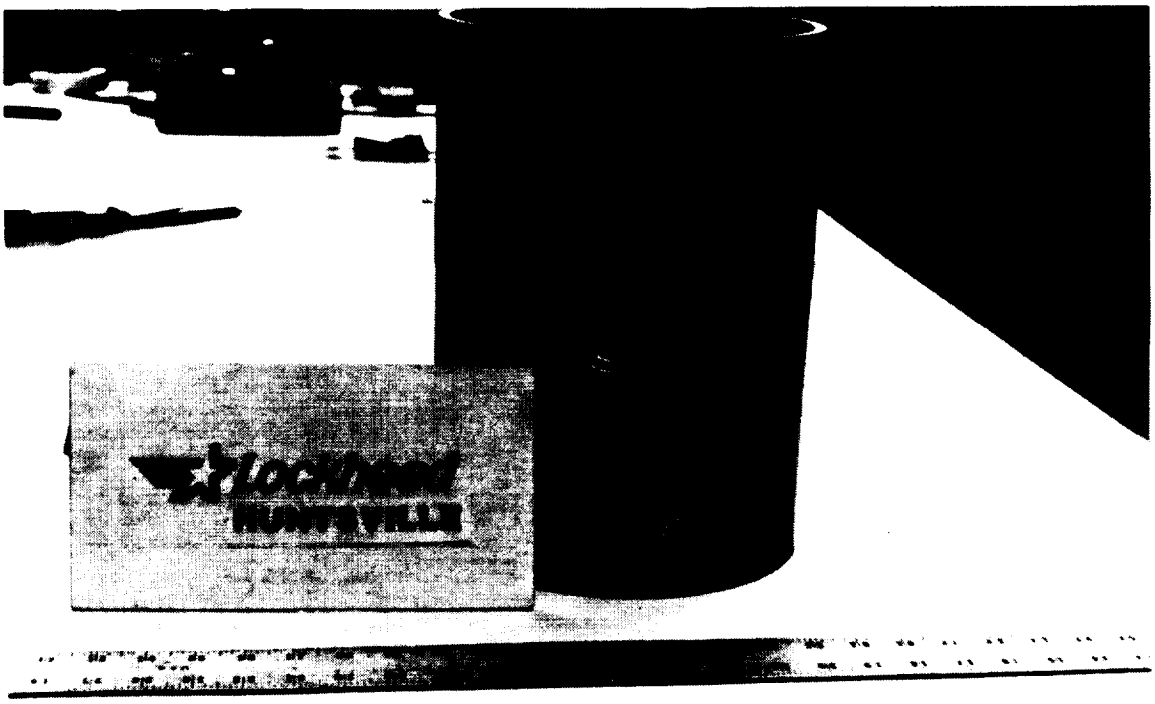

Figure 16. Outer Cylinder after Bonding in Place of the NW-25 Flange Vacuum Connection

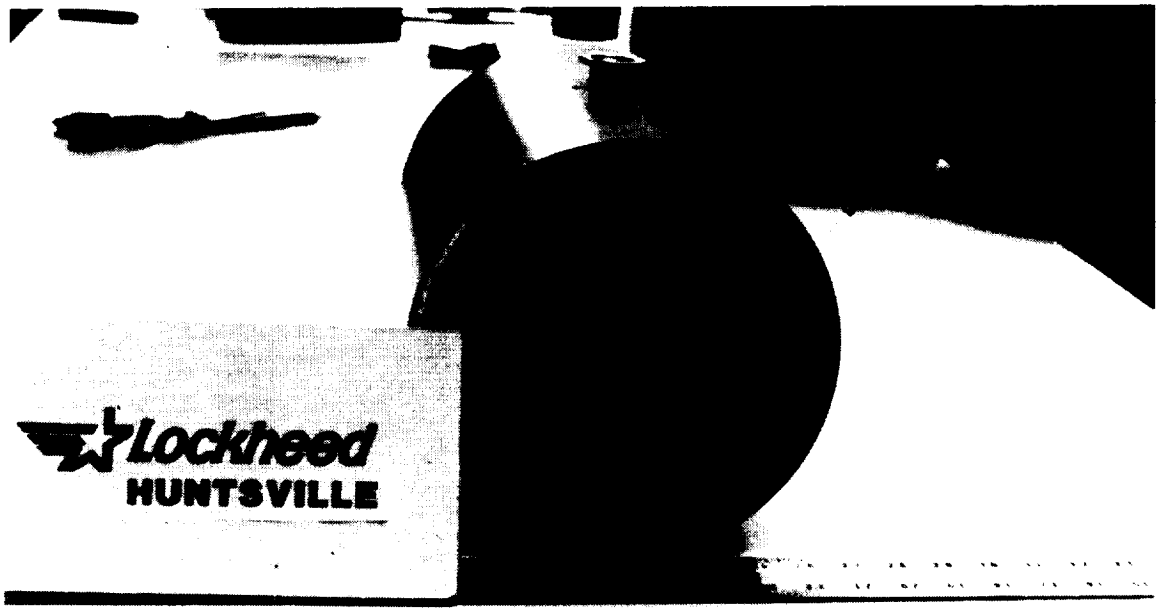

Figure 17. Outer Cylinder Showing Aluminum Reinforcing Ring Bonded in Place

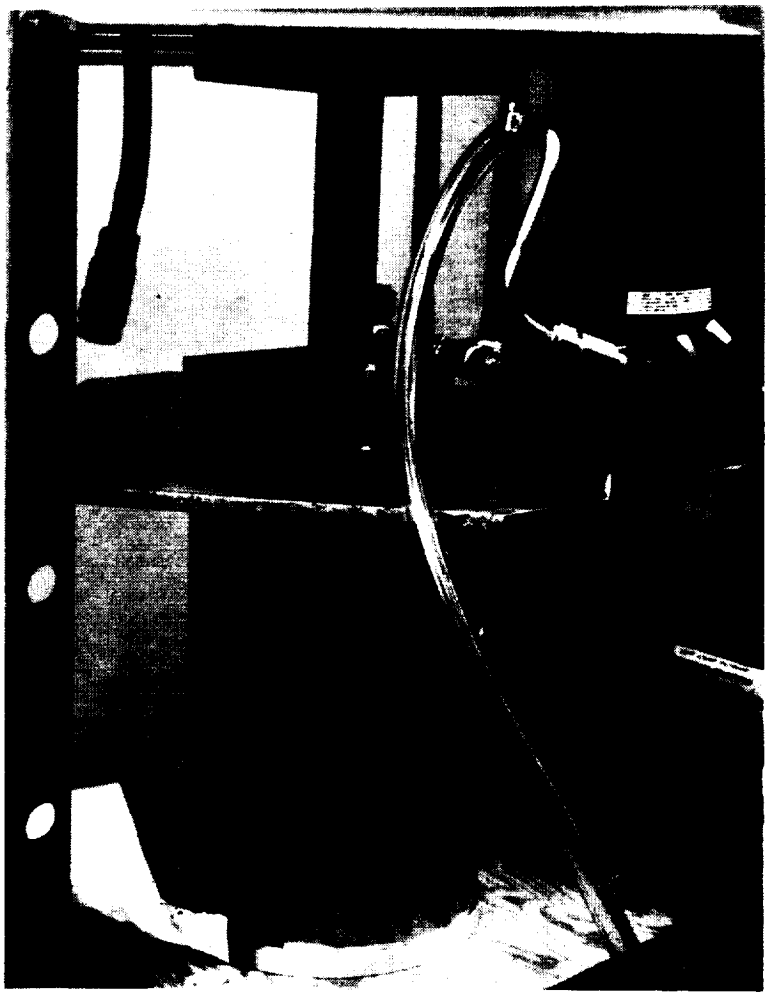

Figure 18. Leak Test Being Performed on Inner Cylinder

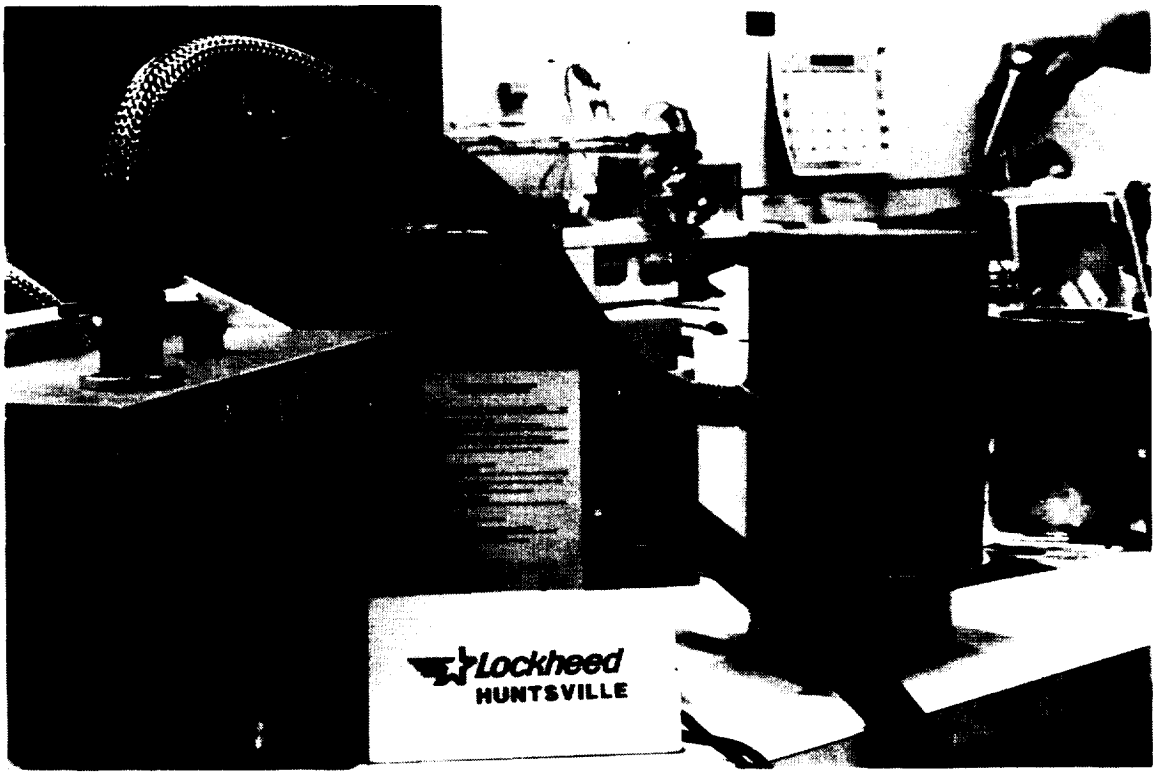

Figure 19. Leak Test in Progress for Outer Cylinder

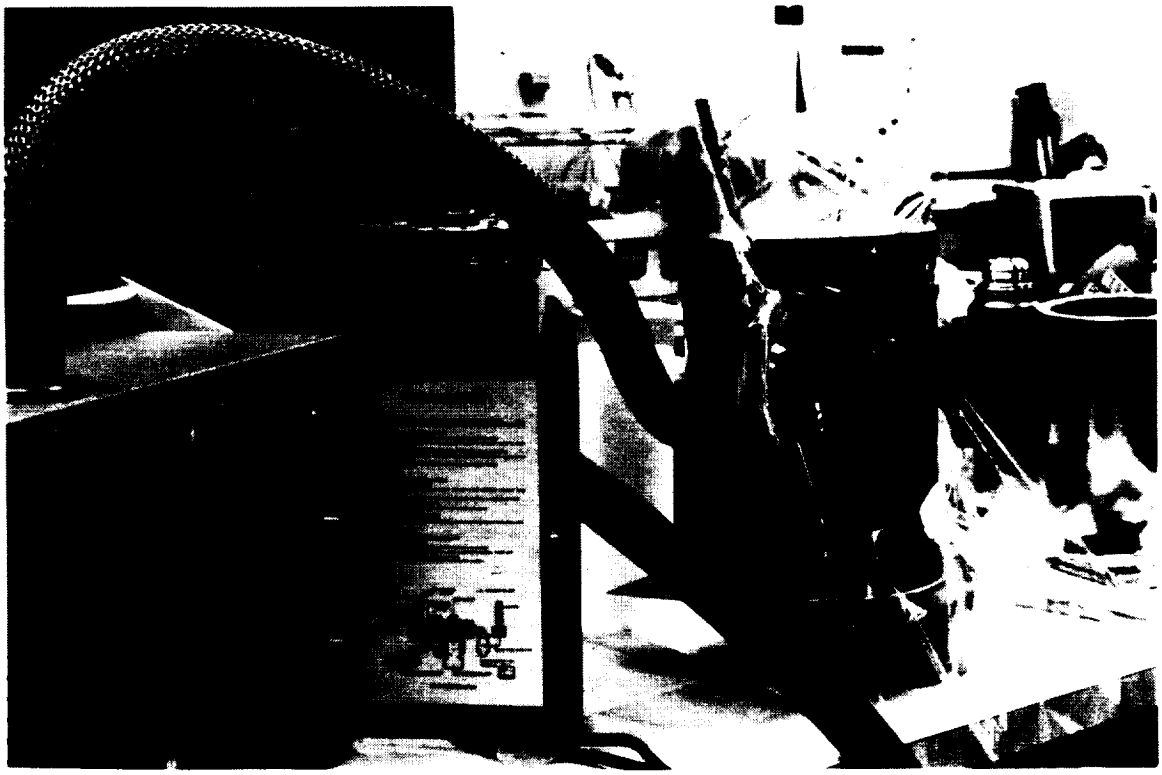

Figure 20. Leak Test in Progress for Outer Cylinder with Plastic Film Hood Filled with Helium

It is noted that the pressure loading on both the inner and outer cylinder tests was in the same direction as in these cylinders when they are assembled into the freezer. That is, the inner cylinder was under a burst-pressure load, while the outer cylinder was under a crushing-pressure load.

A problem was encountered in the procedure for cleaning these completed parts. We cleaned them with 111 trichloroethane, then a stainless steel polishing compound, then detergent and water, and then we rinsed with running tap water. Normally this should provide a good oil-free surface. However, these parts would not pass the "water-break free" test. Later it was discovered that the paper towels used to dry these parts apparently changed the surface chemistry enough to cause the water to break. After several analytical tests, it was decided that the parts were indeed oil-free and clean enough for this application. (The parts have to be as clean as possible in order to not outgas and destroy the internal vacuum.)

A method was developed for wrapping the MLI around the inner cylinder without having any joint at the junction between the flat cylindrical end and the round outer cylindrical barrel section. Layup of the MLI on both inner cylinders was completed. This MLI consisted of 30 layers of double aluminized mylar and 30 layers of dacron netting. The mylar was perforated with 0.062 in. holes, with 0.5 in. between holes in rows which were 0.25 in. apart. The netting mesh size was approximately 0.070 x 0.070 in. square with openings. Silk thread was used to hold some of the layers in place. A minimum of aluminized tape was also used (3-M Scotch Brand No. YR84373624579).

Figure 21 shows a photo of the MLI during fabrication. A layer of netting can be seen on the outside in this view. *Figure 22* shows the MLI after being trimmed at the bottom. *Figure 23* shows the top end of a completed MLI layup. *Figure 24* shows the completed MLI at the open end of the cylinder. *Figure 25* shows a closeup of the completed MLI with a total thickness of 0.6 in. for the 30 layers, for an average thickness per layer of 0.020 in.

After the MLI layup was completed, the inner cylinders with MLI were bonded to the 0.010 in. thick annular closeout skins. *Figure 26* shows this step in progress. The outer cylinders were then bonded in place over the MLI/inner cylinder and onto the annular closeout skins. This completed the fabrication of the two cylindrical halves of the freezer.

Next a vacuum seal was designed and fabricated to close out the joint between the two halves. This consisted of a 2 1/2 in. wide by 0.050 in. thick natural rubber band with a butt joint. The butt joint was made using "super glue." An NW-25 vacuum flange connection was placed through a 1 in. hole in the center of this band. This design was tested and found to provide a seal with an acceptable leak rate.

The final assembly of the bio-sample freezer was completed. Parts were leak checked and no leaks were found. The vacuum pumping station was set up and checked out. The flex hoses, valves, connections, etc., were all taken to MSFC for cleaning with Freon 113 (trichlorotrifluoroethane) in their cleanroom area. Heaters were attached to the hoses and they were baked out under vacuum. The entire system was then leak checked. The residual gas analyzer (RGA) unit was installed and checked out for use in monitoring the freezer MLI space gas constituents during and after pumpdown.

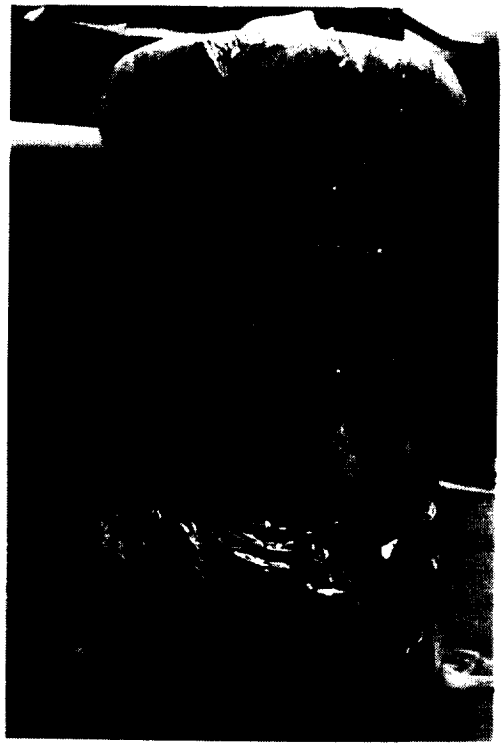

Figure 21. MLI Being Laid up onto the Inner Cylinders of Bio-sample Freezer

Figure 22. Bio-sample Freezer Inner Cylinder with MLI After Bottom was Trimmed

Figure 23. Top End of MLI Applied to Inner Cylinder of Bio-sample Freezer

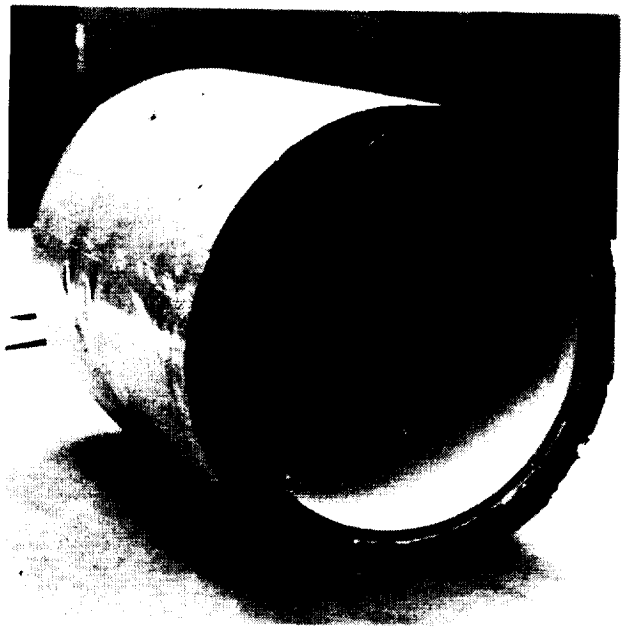

Figure 24. Open End of Inner Cylinder of Bio-sample Freezer after MLI was Trimmed

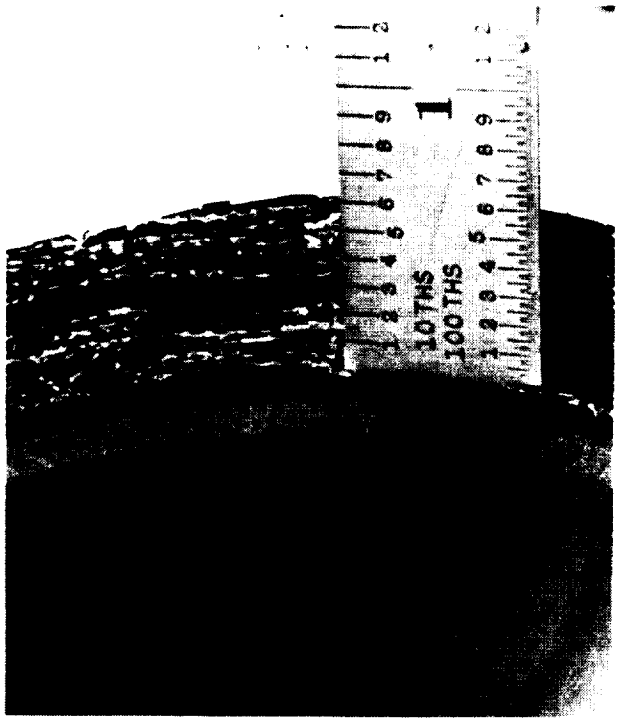

Figure 25. Completed MLI Showing Thickness of 0.6 in. for 30 Layers on Bio-sample Freezer Inner Cylinder

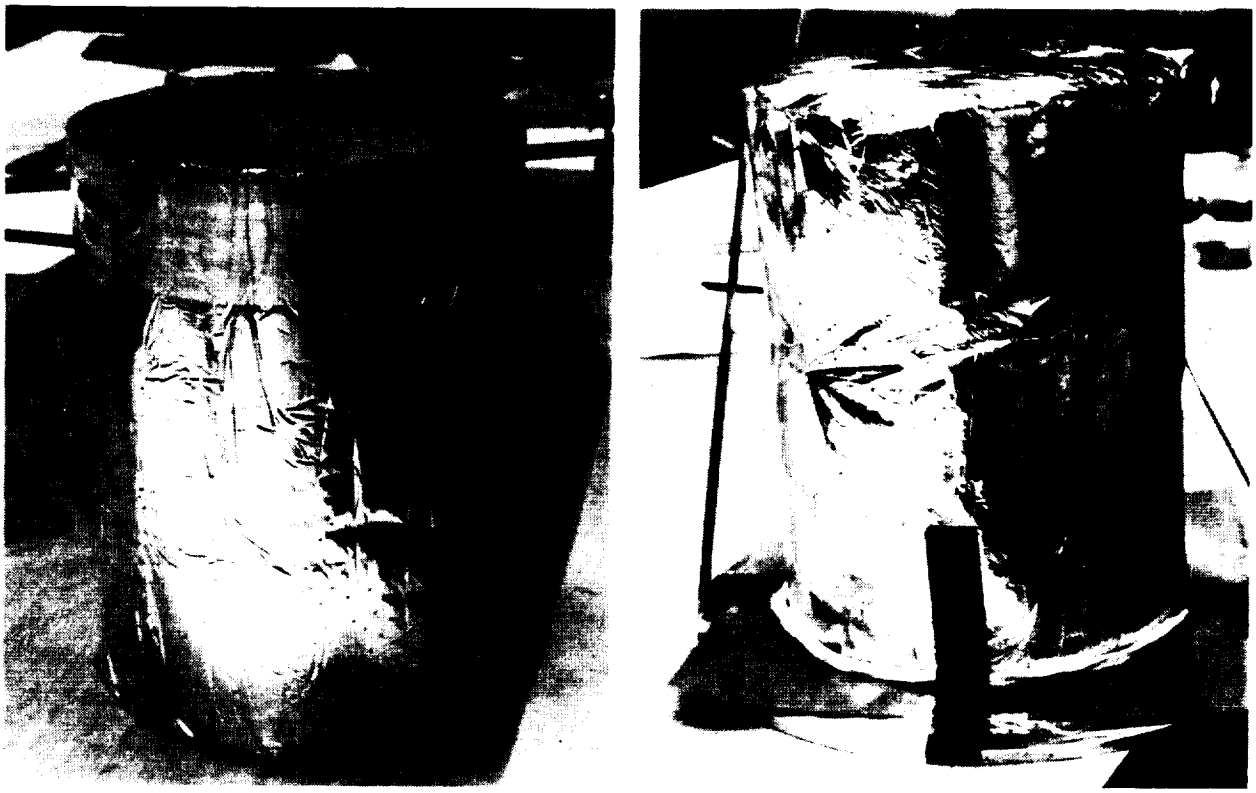

Figure 26. Bio-sample Freezer Inner Cylinder with MLI in the Process of Being Bonded to the Annular Closeout

The next step was to set up the freezer for testing. The data system, consisting of the 60-channel Acurex Autocalc and a PC, was hooked up and checked out. Two aluminum cold block/heat sinks were machined and instrumented. They were both 6 in. in diameter and 1 in. thick; one weighed 1465 g and the other weighed 1390 g. They were instrumented with 0.003 in. diameter Chromel/Alumel thermocouples. These thermocouples were bonded on with Furane 1210 epoxy. Thermocouples were also installed on the two inside cylinders of the bio-sample freezer. The heat sinks were installed inside the freezer inner cylinder for testing. They were chilled down with LN_2, and then the temperature was allowed to rise due to the heat leaking through the MLI. The temperature rise rate was used together with the thermal mass of the heat sinks to compute the net heat leak rate of the freezer. The bio-sample freezer and test setup are shown in *Figures 27 through 30.*

The first preliminary test was run on 23 May 1990. In this test, the temperature was taken down only to about 0 °F. As a safety precaution, we did not want to go below this value during this checkout run. The insides of the two halves of the freezer were chilled down separately using LN_2 boiloff. The two halves were then joined with the natural rubber seal, and the internal space was evacuated using a mechanical vacuum pump. The MLI volumes of both halves were then evacuated using the turbomolecular vacuum pumping station. The temperature rise of the heat sinks was recorded and plotted. The resulting slope was used to calculate the heat leak into the bio-sample freezer. Preliminary tests were also run on 25 May and 29 May 1990.

During these checkout tests it was found that the freezer needed about one hour of cold soak time before starting the steady state temperature slope evaluation. This period was needed for the mass of the MLI to get cold. During one of these tests, frost formed on the mating ends of the inner cylinder/outer cylinder diaphragm closeout. When the halves were mated, they stuck together. This did not allow proper evacuation of the inner space when the mechanical pump was turned on. However, this was not known because there was no pressure measurement on the inner space. When the turbopump was turned on to evacuate the MLI space, the resulting ΔP cracked one of the freezer bond joints. This was repaired and testing was resumed. A GN_2 purge bag was designed and used to prevent this frost buildup. GN_2 purge bags were also used over the NW-25 flange pumping ports during chilldown to prevent aspiration or cryopumping of atmospheric air and water vapor into the MLI space.

The procedure for chilldown was later changed. The two halves of the freezer were chilled simultaneously with LN_2 boiloff using a "tee" nozzle arrangement. The halves were mounted on two separate cradles so that they could be moved together or apart without disconnecting from the turbovacuum pumping station hoses. The minimum MLI vacuum space pressure obtained to date with this test setup and procedure is approximately 2×10^{-4} torr.

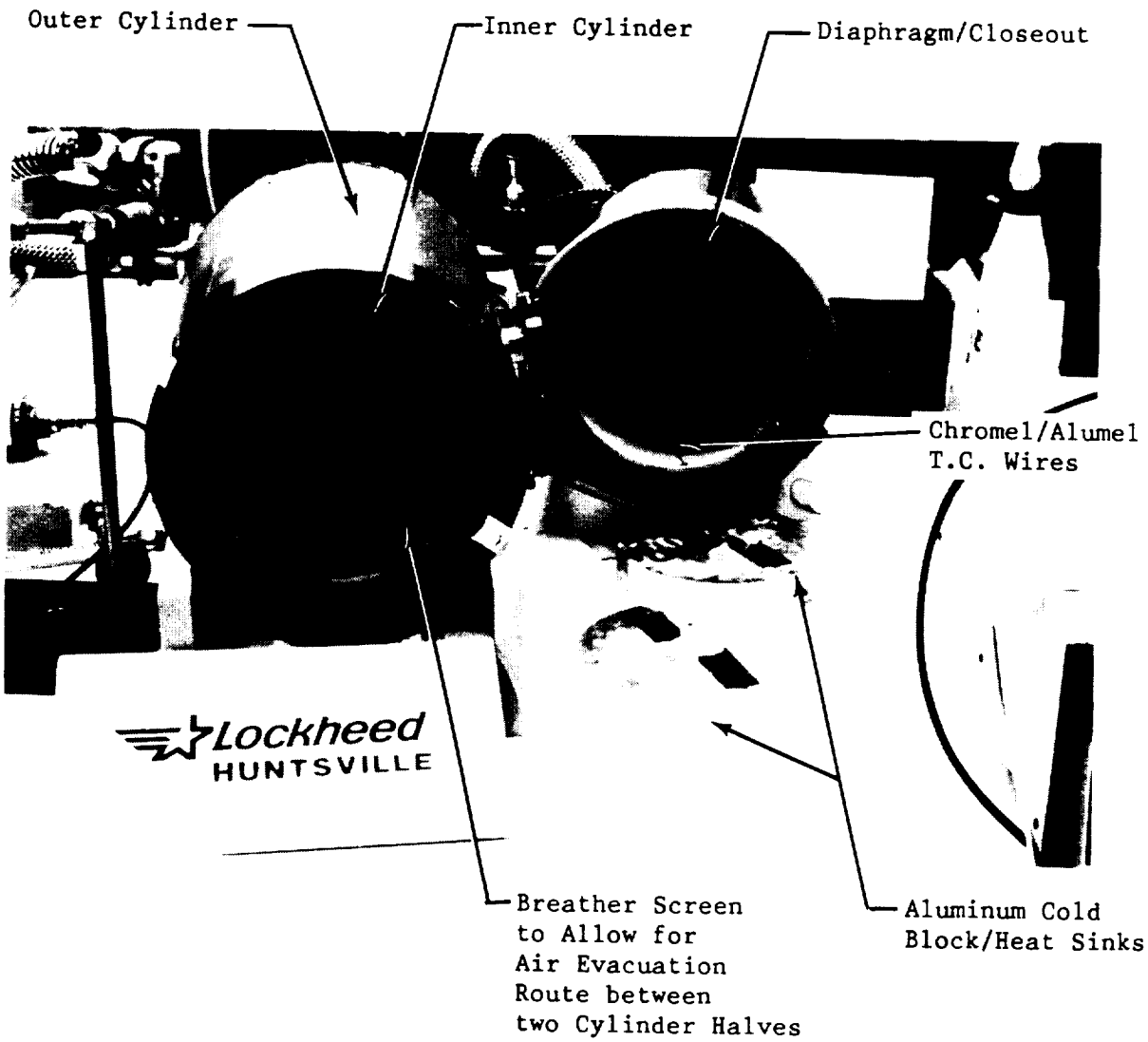

Figure 27. Completed Bio-sample Freezer Halves and Heat Sinks/Cold Blocks Ready for Testing

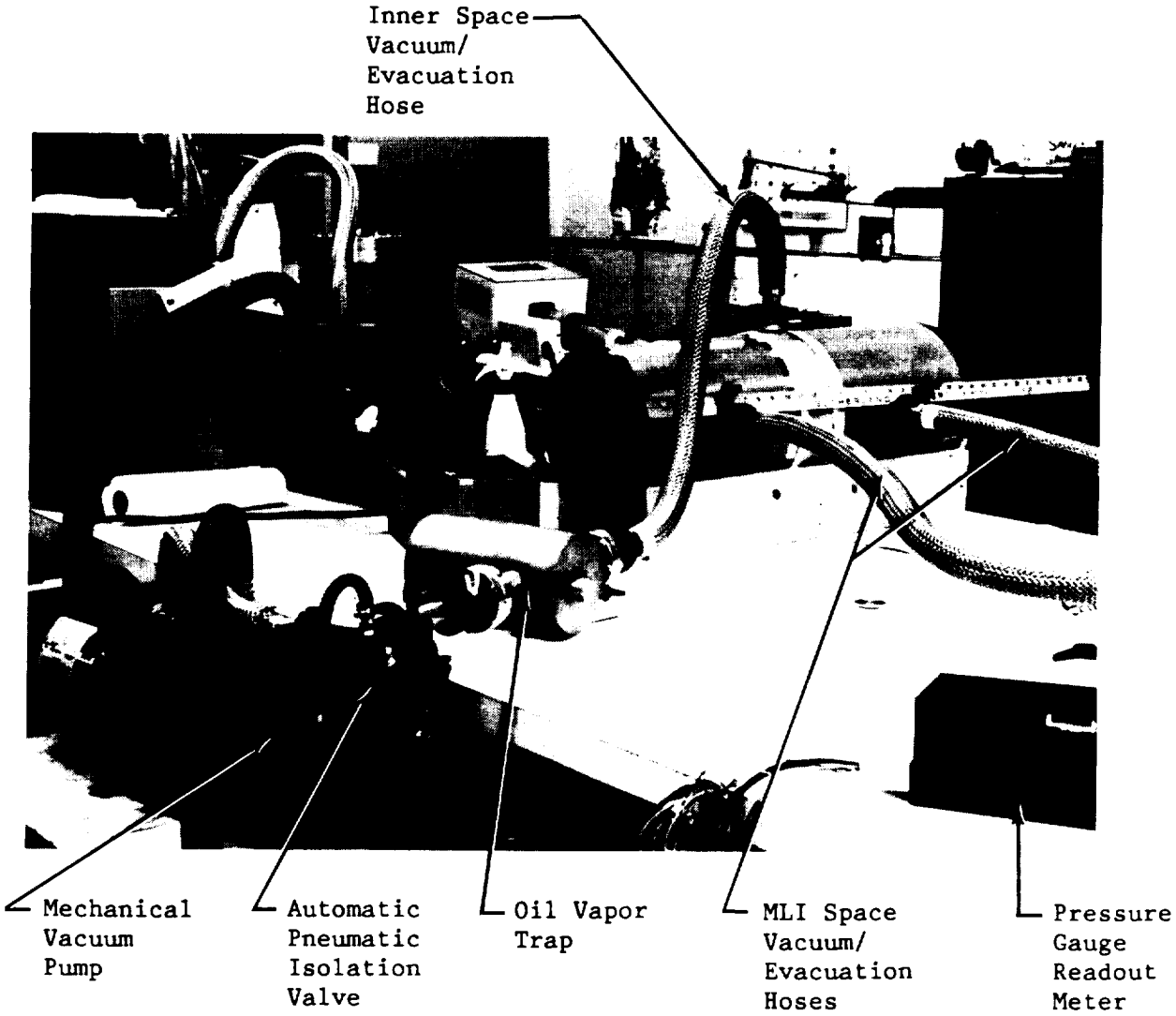

Figure 28. Bio-sample Freezer Attached to Vacuum Pumping Station, Ready to Undergo Testing

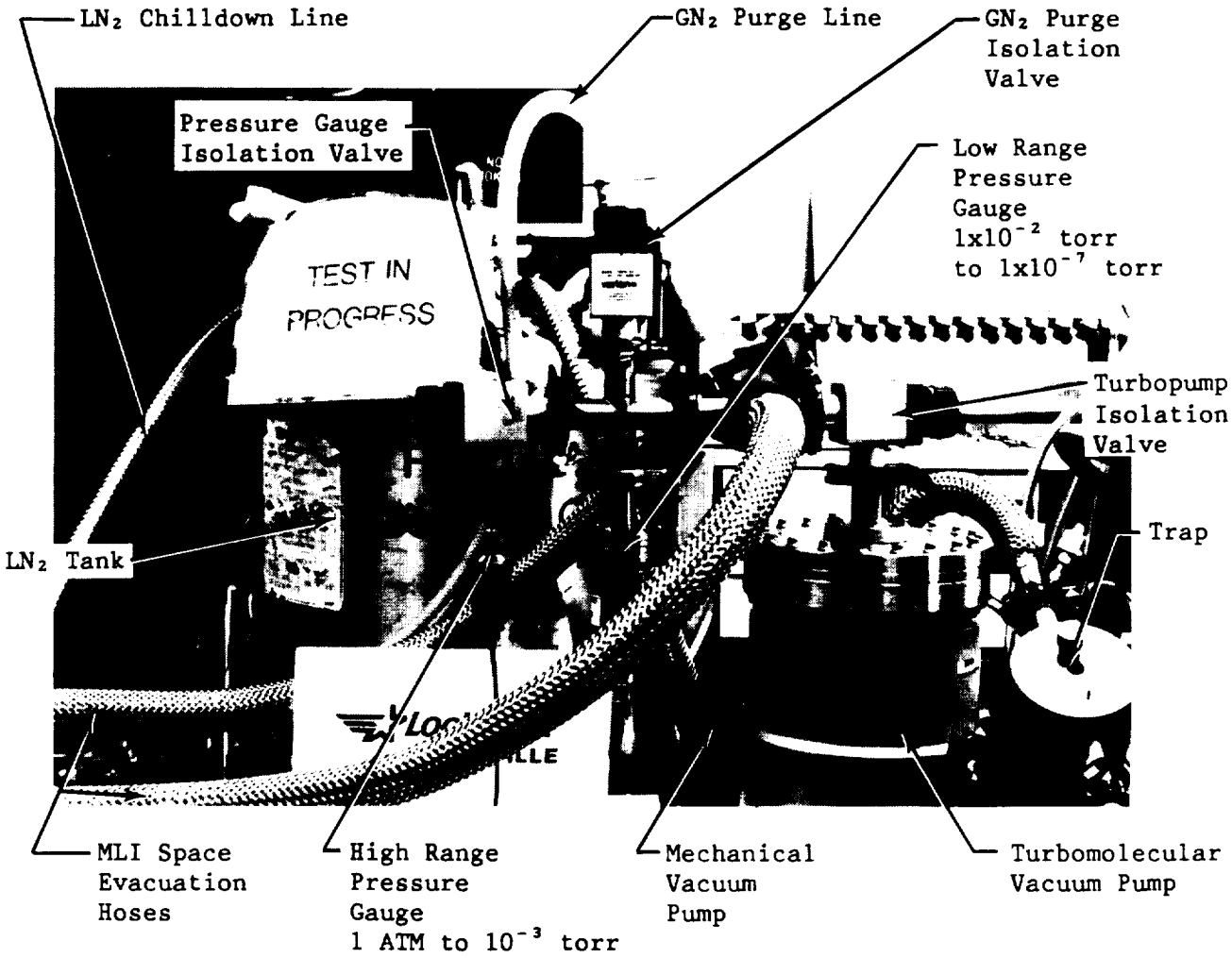

Figure 29. Turbomolecular Vacuum Pumping Station

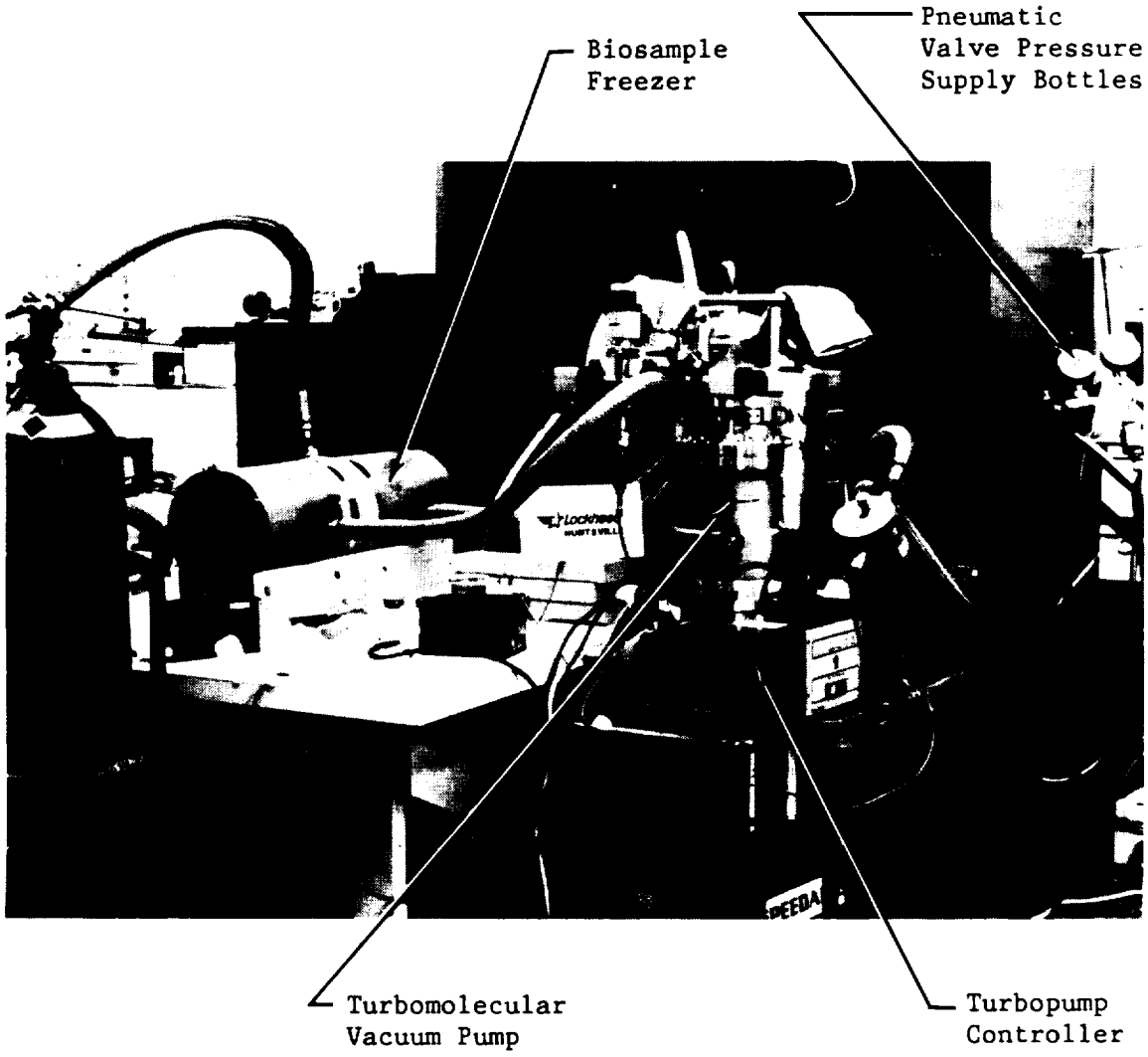

Figure 30. Bio-sample Freezer and Turbopumping Station During Test

Figures 31 through 33 show typical temperatures obtained from the preliminary tests. Testing was continued with gradual lowering of the heat sink temperature to -240 °F. This was the practical lower limit for the present configuration because of difficulties with the rubber band center joint seal and frost problems at the joint. The rubber band became so brittle that we were unable to move it onto the joint in any reasonable time without thawing it out with a heat gun, even though it was located outside the GN_2/LN_2 purge bag. During this thawing time, the exposed freezer ends frosted up considerably, causing difficulty in mating the two halves. Again, the purge bag was being used, but it had to be removed while the rubber band seal was being put into place. Also, the rubber band cracked on some occasions due to its brittleness, causing it to leak.

After proceeding to this point in the testing (i.e., -240 °F), it was decided to temporarily suspend testing and modify the test configuration in order to get to lower temperatures. Two fill and vent access ports were added through the MLI. The instrumentation leads were replaced and vacuum sealed where they penetrated the walls of the freezer. The fill line configuration was modified. The rubber band center seal was replaced with the O-ring. This was done so that the freezer could be chilled down after being joined together at the center joint.

When testing was resumed, we were able to reach a low temperature of -370 °F inside the freezer. This was attained as a result of two factors: (1) we modified the biofreezer test configuration/design, and (2) with this modified design we were able to get liquid nitrogen into the inner cylinder and then subcool it by lowering the vapor pressure over the liquid. This caused the temperature to drop below the melting point and freeze the nitrogen. (The boiling point of nitrogen is -320.4 °F at 1 atmosphere pressure; the melting point of nitrogen is -346.0 °F. When the vapor pressure is reduced to 1 mm Hg, the solid temperature drops to -375.0 °F.) The various hardware changes are enumerated and pictorially depicted in the August 1990 monthly progress report, an excerpt from which is presented in Appendix B.

Beginning during the August 1990 reporting period and continuing through January 1991, twenty-eight tests were performed at low sink temperatures starting at -310 °F and gradually dropping to -370 °F. Tests included chilldown runs in preparation for subsequent testing. Some minor problems were encountered and resolved along the way. Heat leak calculations were performed using data from tests that did not exhibit apparent problems. The results from these tests, heat leak evaluations, and descriptions of problems encountered and their solutions are included in Appendix B as excerpts from reports detailing monthly progress from August 1990 through January 1991 for this contract.

One typical bio-sample freezer test was observed by NASA-MSFC personnel at the Lockheed-Huntsville lab facility on 28 November 1990.

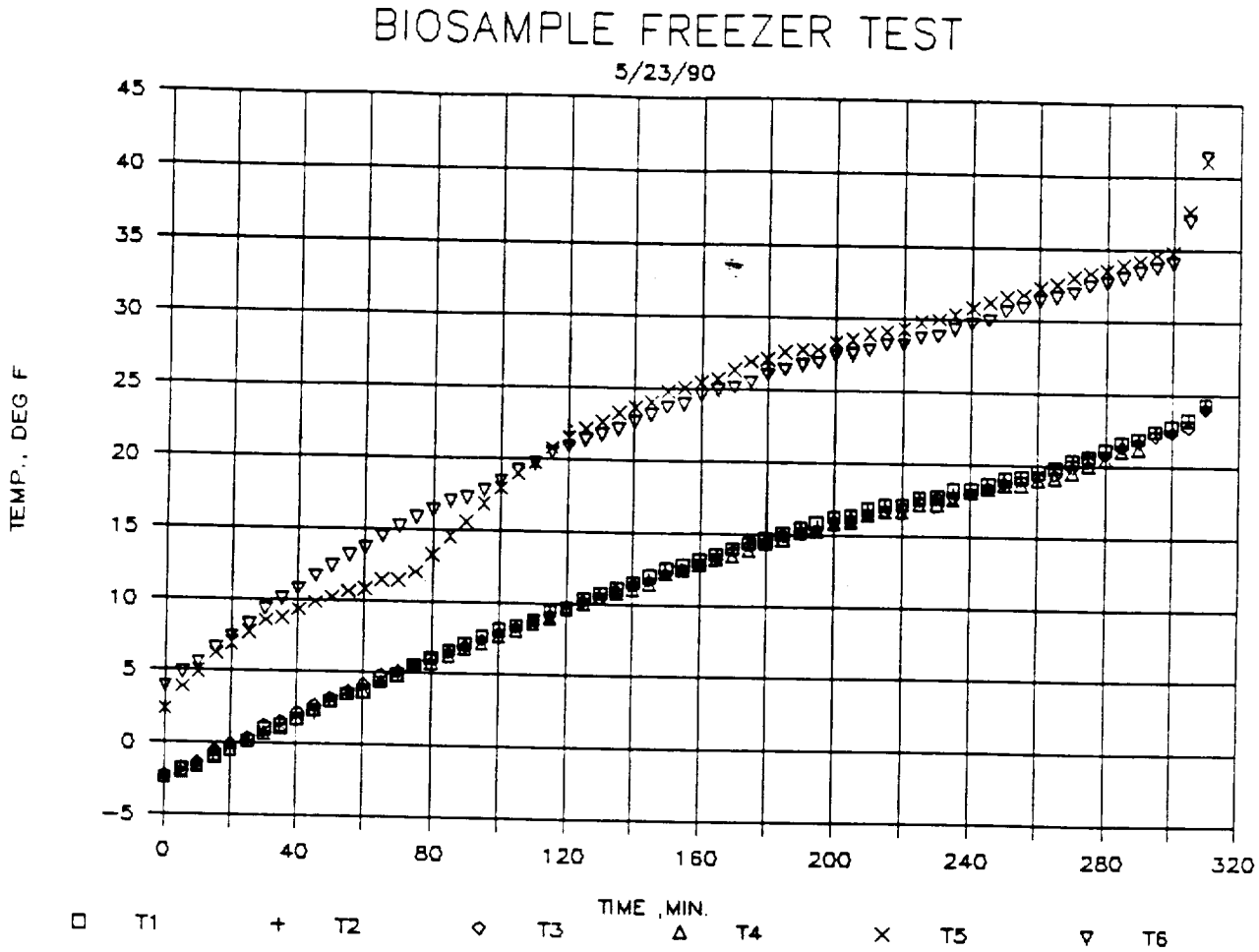

Figure 31. Temperature vs Time for Bio-sample Freezer Test on 23 May 1990 (Thermocouples 1 through 4 are on heat sinks; 5 and 6 are on inner cylinder wall. Lag in T5 is apparently due to not allowing enough time for all parts to come to equilibrium before start of test.)

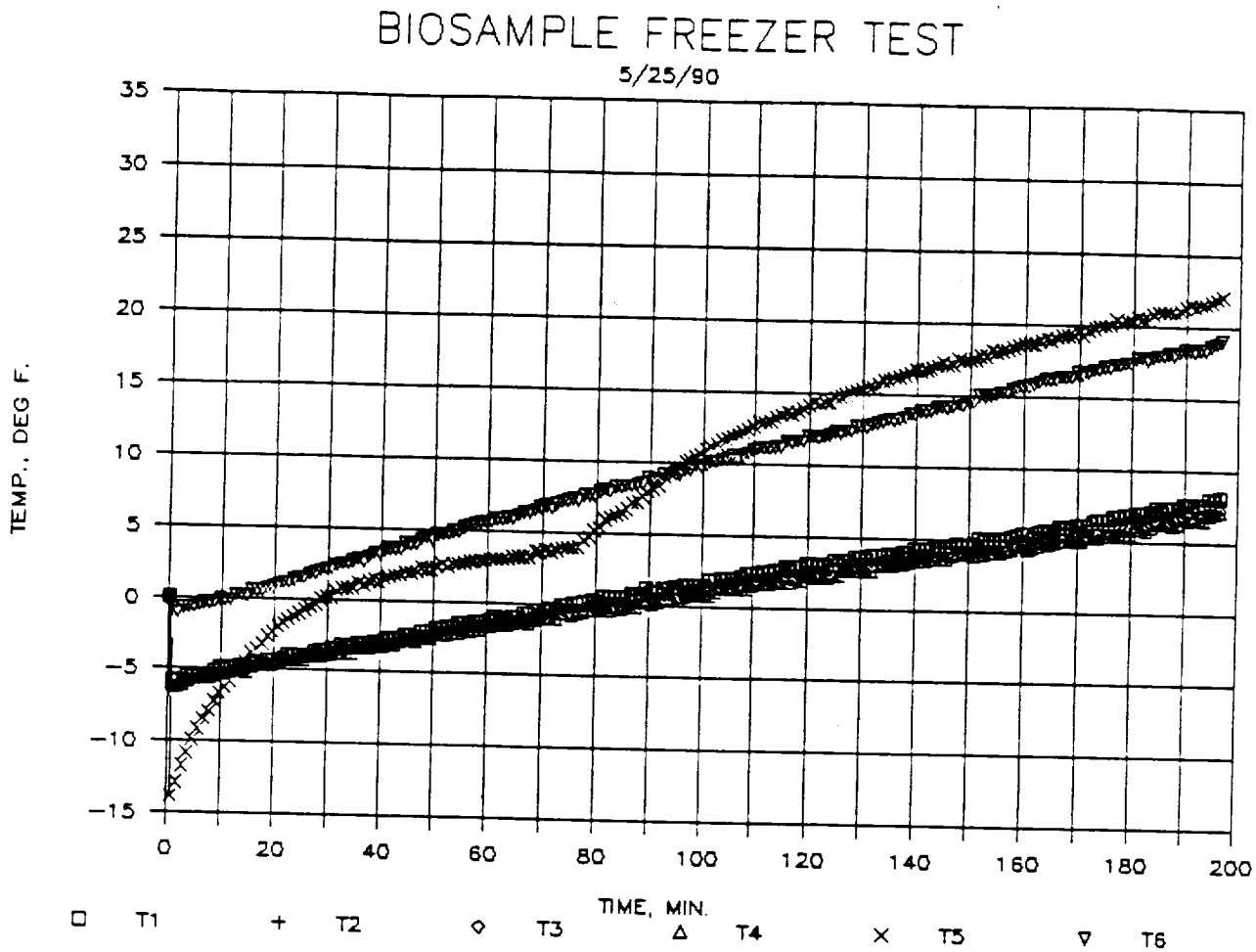

Figure 32. Temperature vs Time for Bio-sample Freezer Test on 25 May 1990 (Thermocouples 1 through 4 are on heat sinks; 5 and 6 are on inner cylinder wall. Lag in T5 is apparently due to not allowing enough time for all parts to come to equilibrium before start of test.)

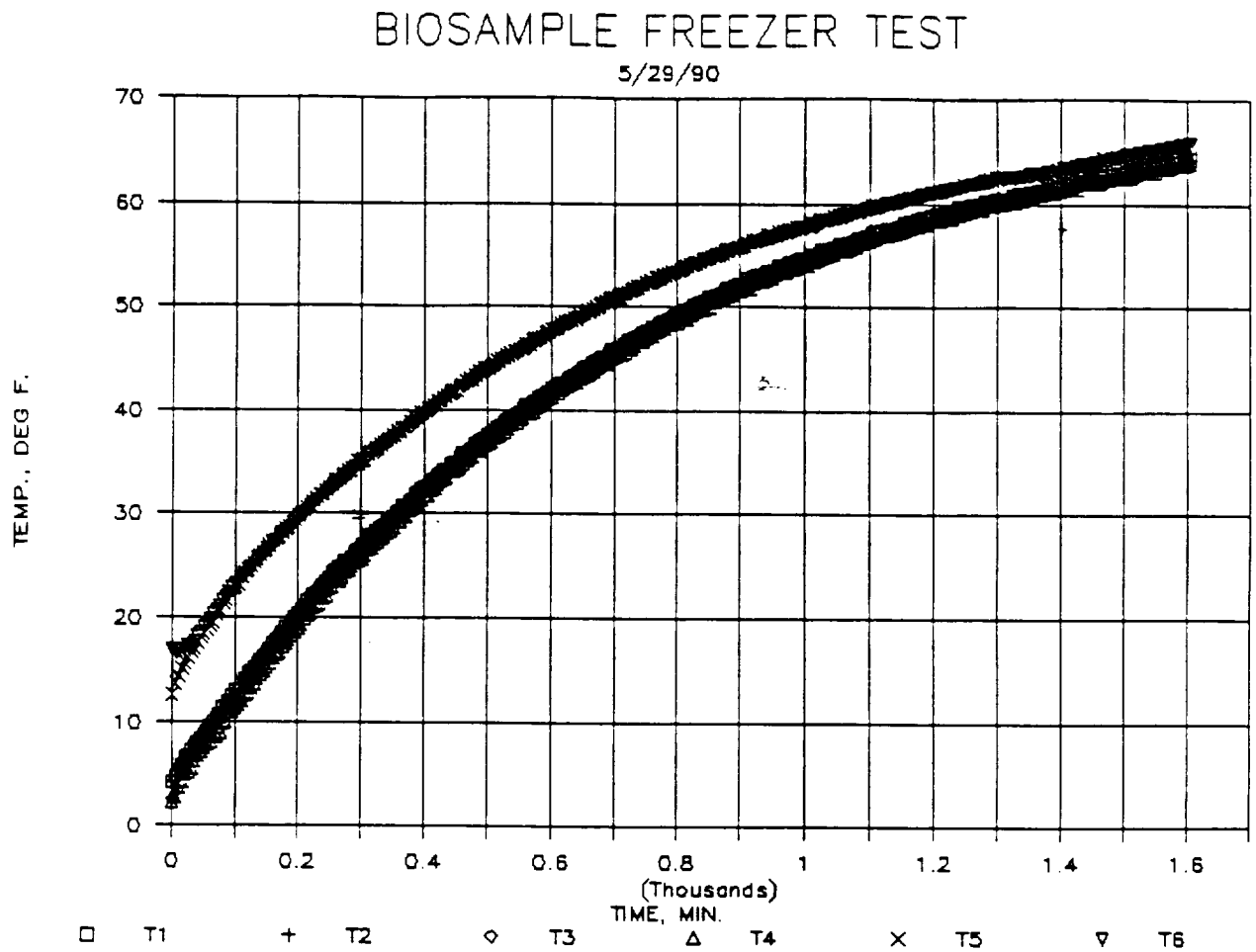

Figure 33. Temperature vs Time for Bio-sample Freezer Test on 29 May 1990 (Thermocouples 1 through 4 are on heat sinks; 5 and 6 are on inner cylinder wall. Lag in T5 is apparently due to not allowing enough time for all parts to come to equilibrium before start of test.)

2.1.3 Getter Pump Testing

For MLI to perform efficiently, its pressure must be maintained below about 10^{-4} Torr. Any outgassing from MLI materials or container surfaces will increase this pressure. Every effort must be made to reduce outgassing through cleaning and vacuum bakeout. However, it is impossible to reduce the outgassing rate to absolute zero. Therefore, over a period of time the pressure inside the MLI space will gradually rise, thus increasing the effective thermal conductivity of the MLI and the heat leak rate. To overcome this problem, we developed and tested several getter pump concepts.

Figure 34 shows a photograph of the first pump tested. This pump was activated by raising the heater jacket to 750 °F for a period of time which should have been adequate for activation; however, pump performance was limited. The pumping speed was small – barely measurable. This was attributed mostly to the pump configuration. Also, the flow to the pump was restricted by a 90 deg vacuum valve in series with the pump.

A new pump was designed and tested. A 6 in. pump mouth was used instead of the original 1 1/2 in. size. The pump valve was eliminated and the outlet of the pump mouth was coupled directly to the vacuum tank/food storage unit. The getter pump was then connected directly to the turbomolecular vacuum pump. The shutoff valve was next, followed by the mechanical vacuum roughing pump. This configuration did not allow the getter pump to be turned on and off as in the previous design. Therefore, the testing was performed by comparing the "with and without" getter pump operation. First the vacuum tank pressure due to outgassing of the MLI was monitored. Then the getter pump was activated and the pumping action observed. *Figure 35* shows the getter pump under test.

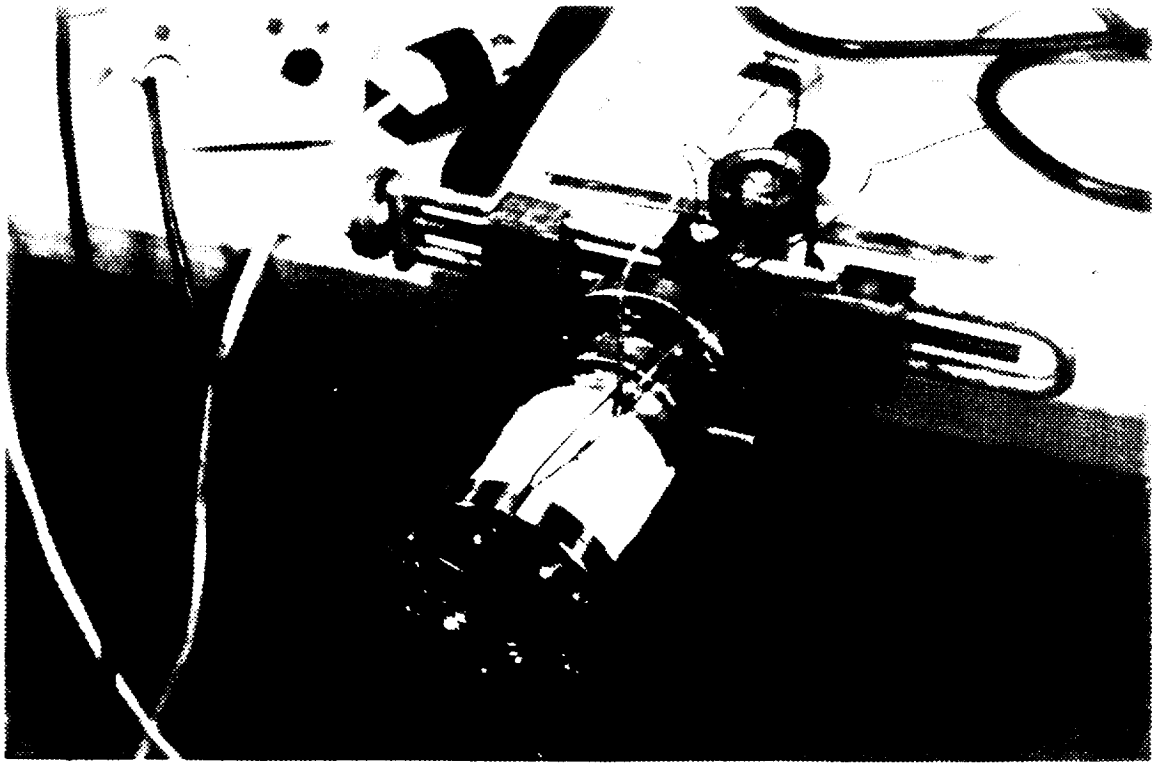

Figure 34. Original Getter Pump Tested for Food Thermal Storage Unit (This pump proved to be too small for this application.)

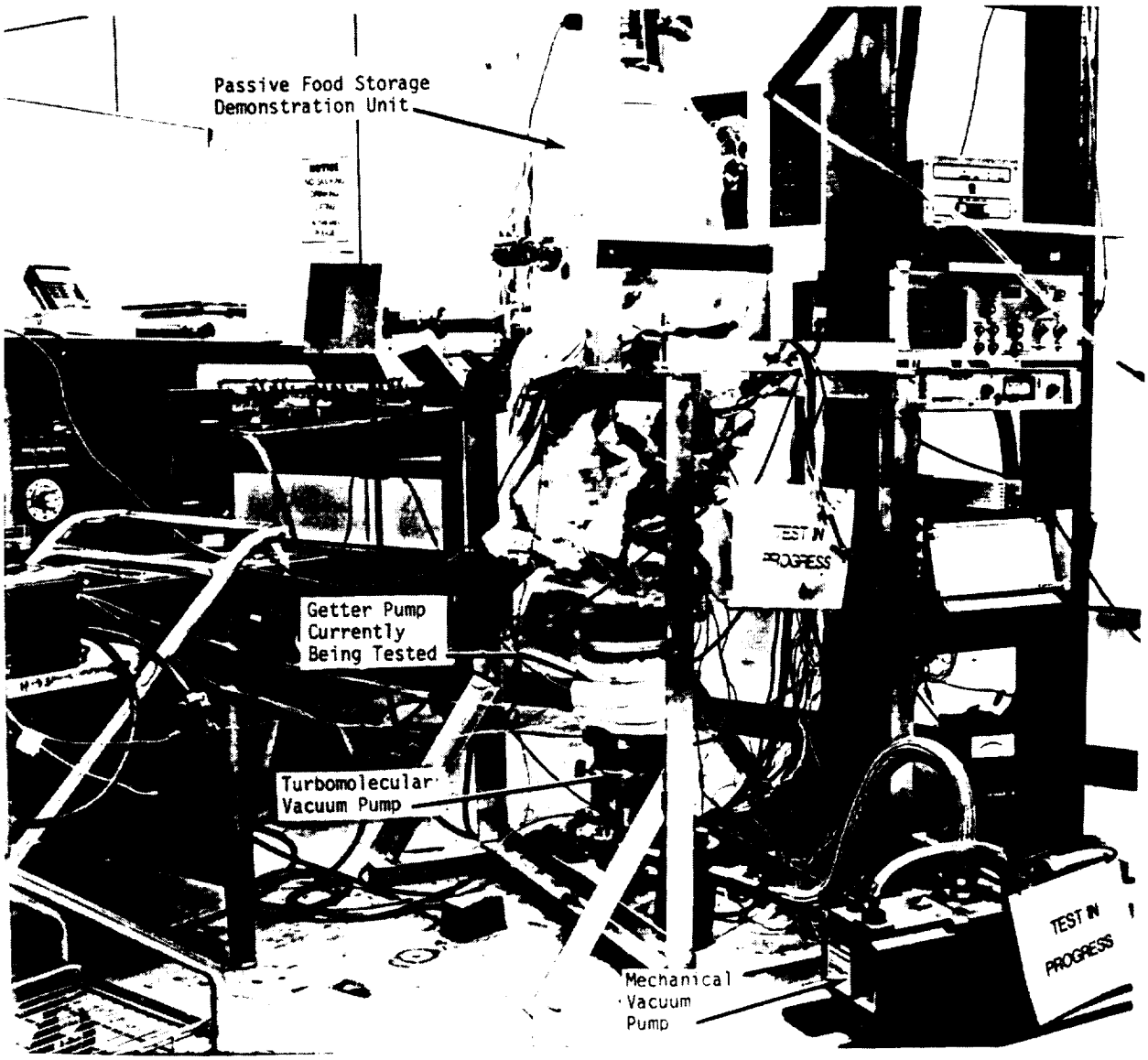

Figure 35. Setup for Testing Getter Pump Attached to the Thermal Food Storage Demonstration Unit

Three tests of this new getter pump were made. *Figures 36* through *41* show the results. Some difficulty was encountered in activating the getter material. Activation normally requires a temperature of approximately 750 °F for 10 minutes. This getter pump temperature was difficult to obtain without exceeding the turbo-pump top flange allowable temperature of 250 °F. *Figure 36* shows the results of the initial attempt to achieve the activation temperature. *Figure 37* shows the resulting getter pump test results after activation of the getter at these temperatures. *Figures 38* and *39* show results of the second test. *Figures 40* and *41* present results of the third test. As seen, each test showed improvement in the getter pump performance.

Additional efforts were made at developing a getter pump. The quantities of getter material were not sufficient to hold the pressure at an acceptable level. The following quantities of materials were used:

- Activated charcoal 77.5 g
- 13X Mole Sieve 100 g
- 4A Mole Sieve 100 g
- 3A Mole Sieve 100 g.

These materials were placed inside the food storage demonstration unit and the pressure pumped down to 3×10^{-6} torr. The tank was then valved off and the getter test started. The results are shown in *Figure 42,* where pressure rise versus time is plotted. As is evident in this figure, the getter's performance was not sufficient to hold the pressure at a low level. This indicates that these getters are not very efficient at room temperature. The adsorption data for nitrogen and carbon dioxide for 13X Mole Sieve, 4A Mole Sieve, and activated charcoal obtained from Union Carbide, manufacturer of Mole Sieve materials, show a marked decrease in adsorption with pressure, as expected. Temperature has a significant effect on the performance of these materials. Our application at near room temperature made the gettering more difficult.

We also contacted a manufacturer of commercial getter pumps. These pumps are applicable to certain vacuum container designs but have the problem of requiring an activation temperature of either 400 or 750 °C, depending on the type of pellet used. These high temperatures are not compatible with our MLI temperature limits. The pumps would have to be activated "offline," valved off, and then transferred to our container for use. Quoted pumping speeds for one of these pumps were as follows:

- 500 L/s at 400 °C and 3×10^{-6} torr for CO_2
- 250 L/s at 400 °C and 3×10^{-6} torr for N_2.

No pumping speeds were quoted for 25 °C, which is our desired operating temperature. A power of 300 W is required to keep the pump operating at 400 °C. The sorption capacity of this pump is quoted at 280 torr-L before reactivation is required. This would give us a time of

$$\frac{280 \text{ torr - L}}{300 \times 10^{-7} \text{ torr - L/s}} = 108 \text{ days}$$

before reactivation for an assumed throughput of 300×10^{-7} torr - L/s, which is approximately what was experienced on the food storage demonstration unit.

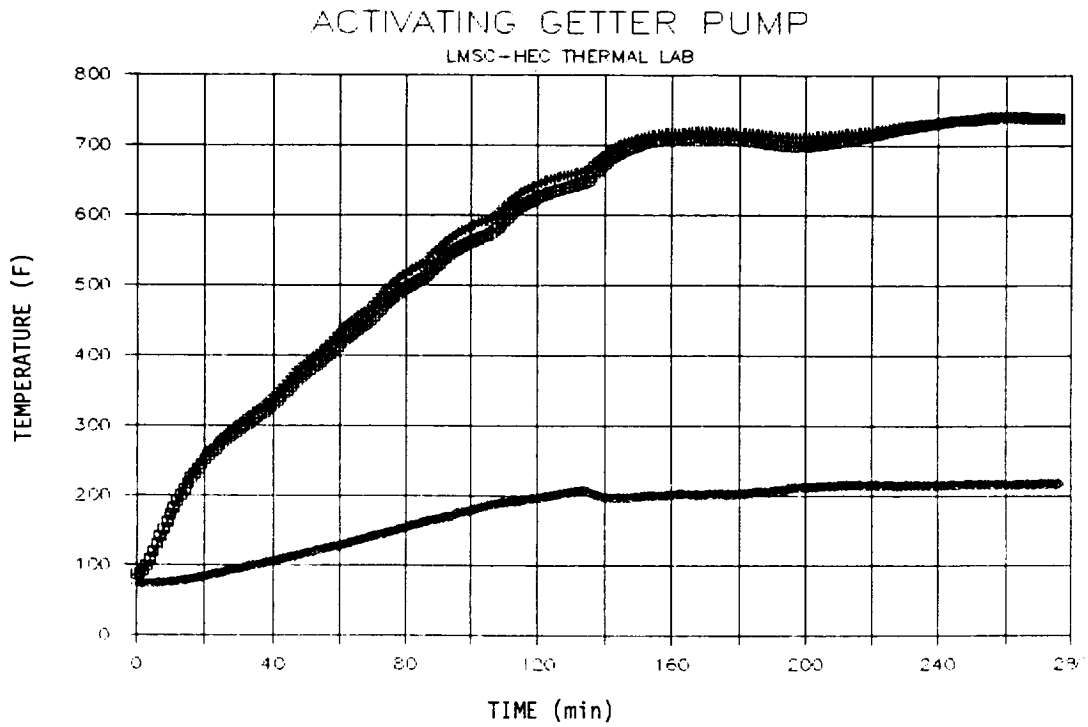

Figure 36. Temperature-Time Histories for Two Positions on Getter Material and on Pump Flange During First Activation Test

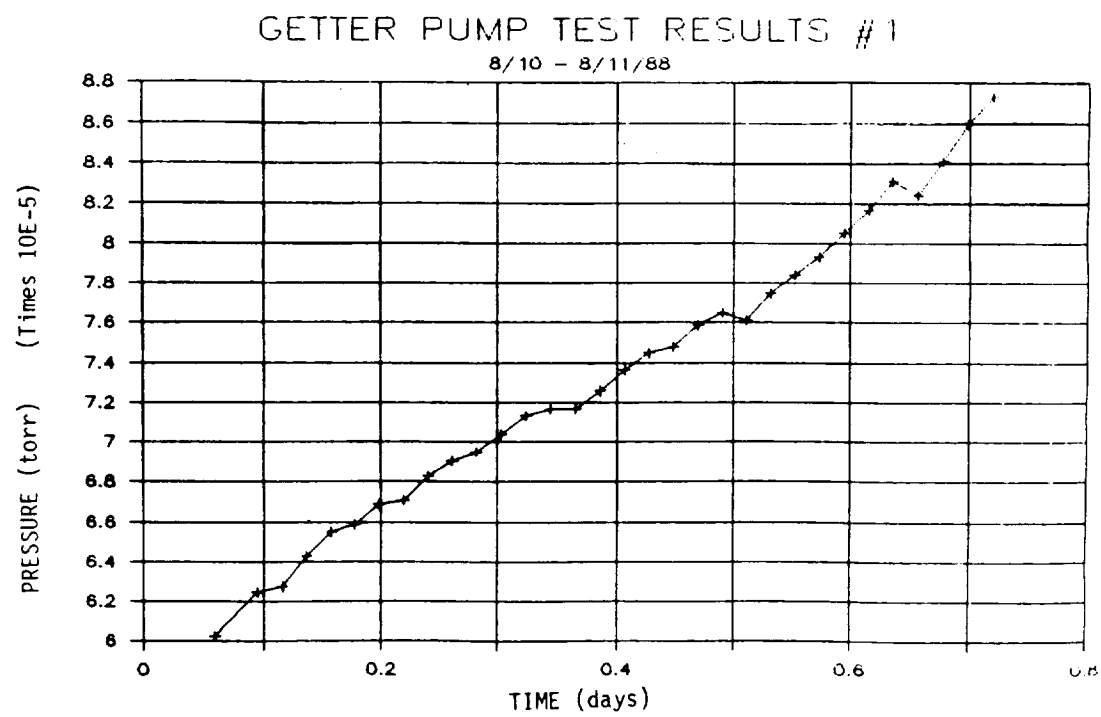

Figure 37. Pressure vs. Time for First Getter Pump Test (Getter pumping speed was insufficient to hold the pressure, i.e., outgassing rate plus minor leaks were greater than pumping speed.)

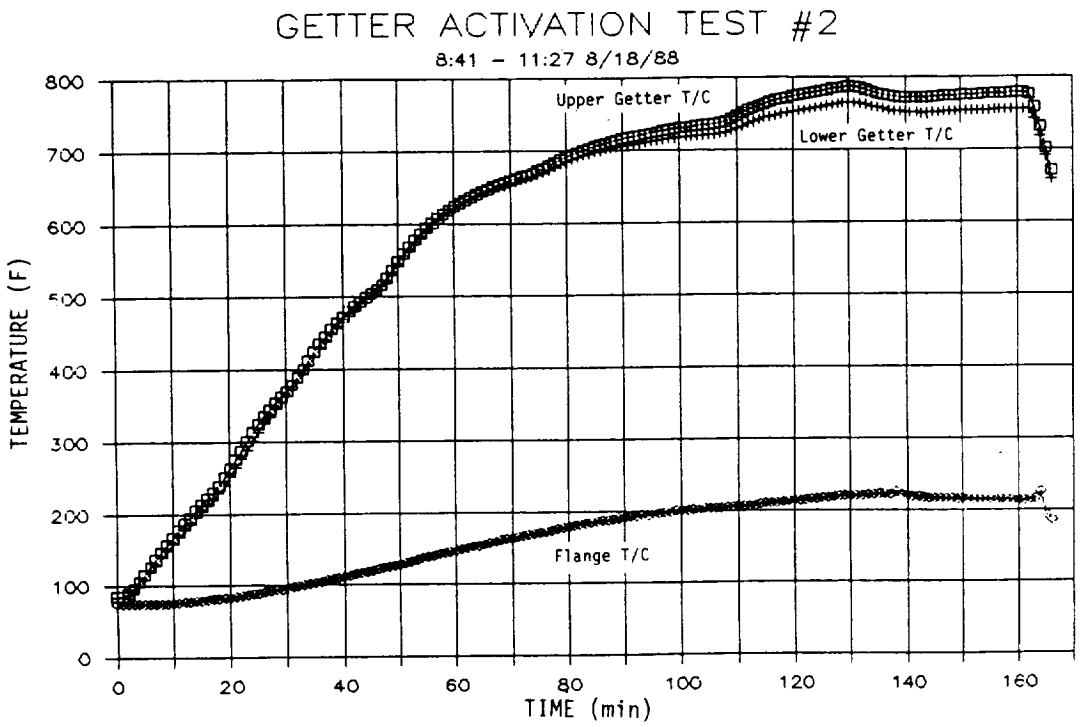

Figure 38. Temperature-Time Histories for Two Positions on Getter Material and on Pump Flange During Second Activation Test

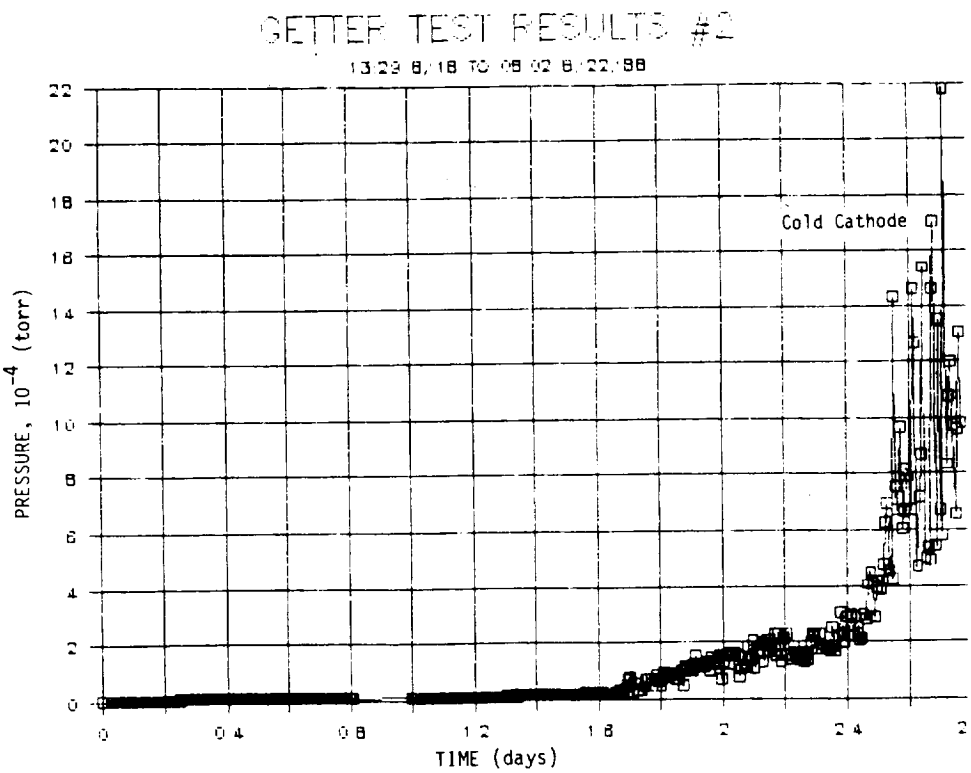

Figure 39. Pressure vs. Time for Second Getter Pump Test (Getter pumping speed was improved over first test, but still less than outgassing plus minor leaks.)

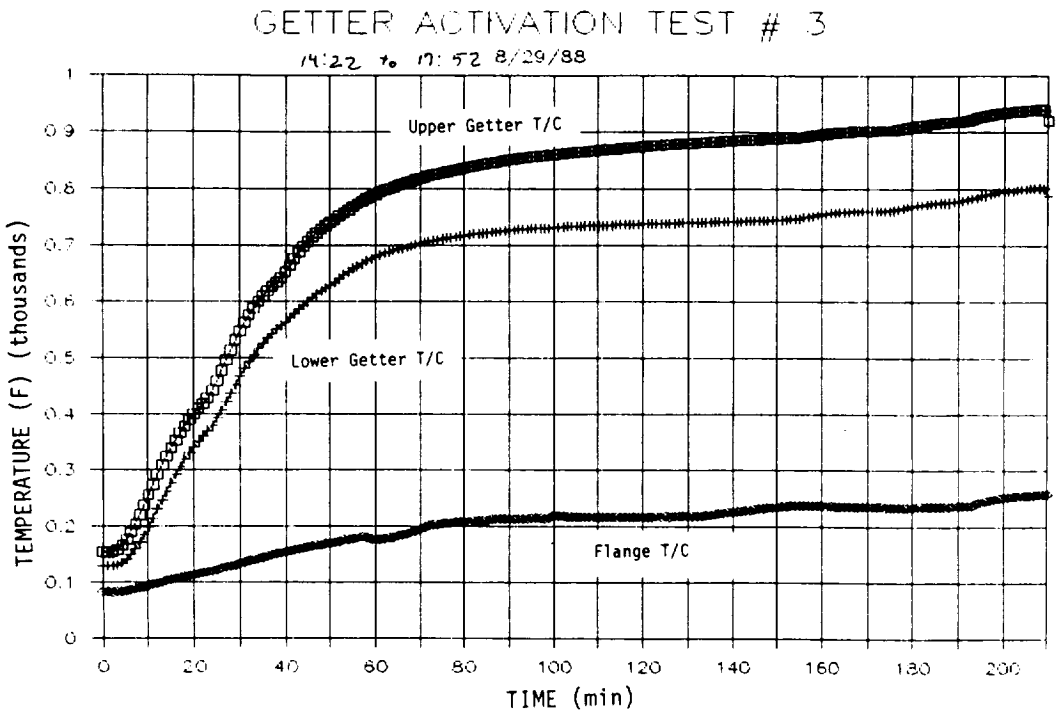

Figure 40. Temperature-Time Histories for Two Positions on Getter Materials and on Pump Flange During Third Activation Test

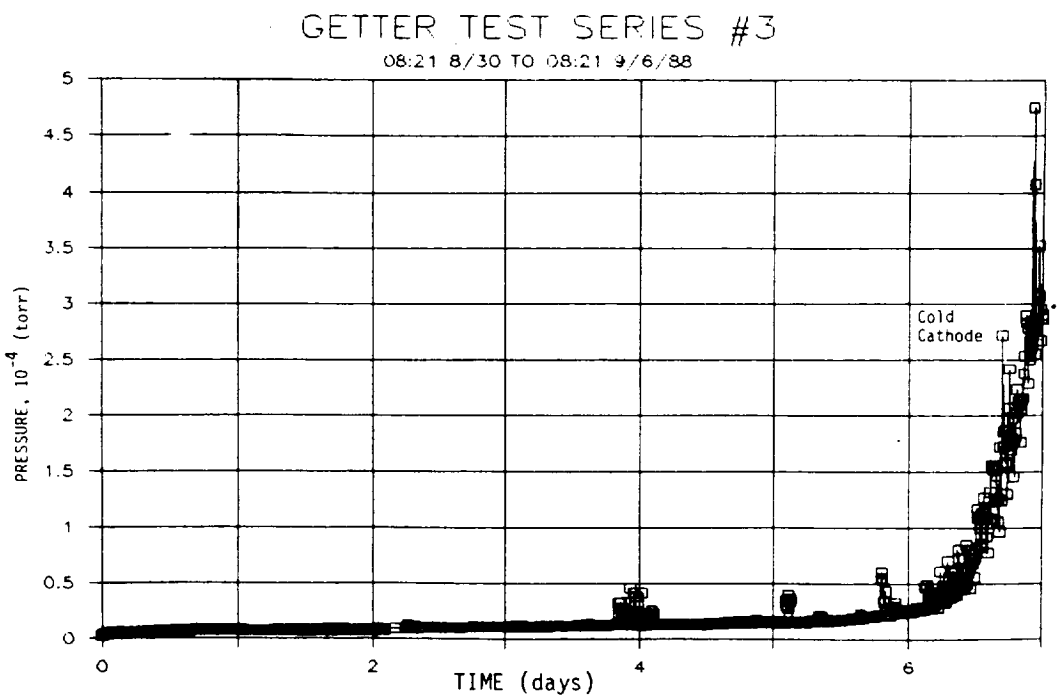

Figure 41. Pressure vs. Time for Third Getter Pump Test (Getter pumping speed increased but still was not sufficient to hold pressure with present outgassing plus minor leaks rate.)

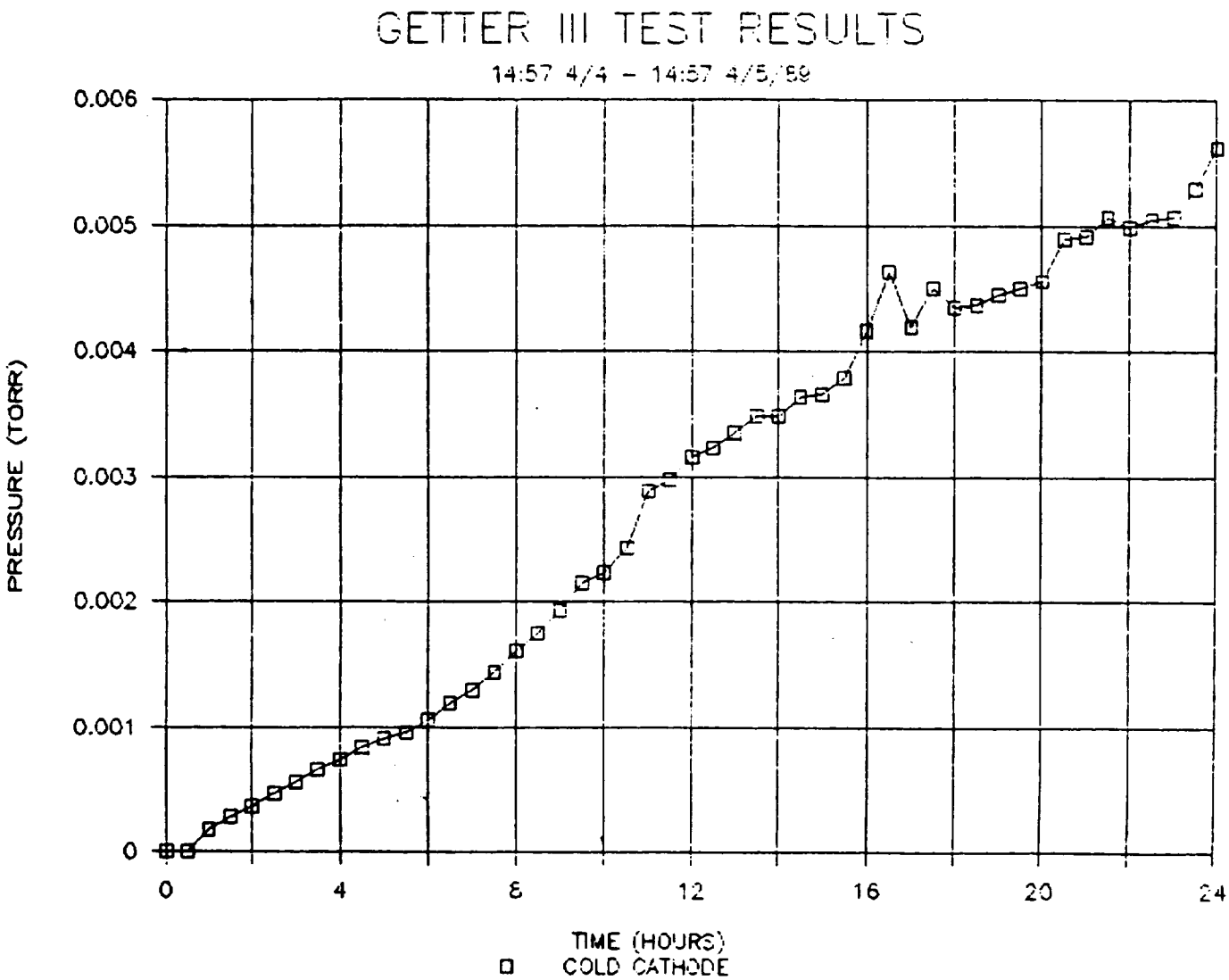

Figure 42. Pressure Versus Time for Getter Pump Test

2.2 REFRIGERATION SYSTEMS DEVELOPMENT

The extreme sensitivity of spacecraft radiator systems design-to-heat rejection temperature dictates separating heat sources based on temperature requirements. For example, a large Space Station may require 80 percent of the total load to be rejected at 70 °F (294 K), 15 percent at 30 °F (272 K), and the remaining 5 percent at -10 °F (250 K) or lower. It is not practical to penalize the radiator cost and weight to provide for the lowest temperature for the total cooling load. A viable alternative would be to group load and temperature requirements and provide radiator systems for each group and/or provide mechanical or other refrigeration methods to remove the heat at low temperatures and reject heat at a high temperature compatible with more efficient radiator rejection temperatures. The need for this alternative method prompted the refrigeration system development study as described herein.

The refrigeration systems development task was divided into several subtasks:

1. Definition of design requirements
2. Assessment of feasible cycles
3. Definition of cryogenic requirements
4. Assessment of heat pump applications
5. Definition of flight test requirements and development of implementation plans
6. Design and fabrication of prototype hardware
7. Testing of components.

All of these subtasks formed the basis of the overall effort under refrigeration systems development and are covered in the following sections. The first four subtasks were subcontracted to SRS Technologies, Huntsville, Alabama, and are discussed as follows. These results are also documented in Ref 7.

2.2.1 Design Requirements

The efforts in the area of refrigeration were started by establishing the requirements. Contacts were made, data bases such as "Langley Space Station Data Base" documentation were screened for requirements definition, and meetings were held with MSFC and Boeing personnel. This served as a starting point for collecting refrigeration/freezer requirements and cooling loads for the Space Station.

During the performance of this task, the emphasis was on updating the refrigeration requirements and providing more comprehensive estimates of cooling loads required. Cooling loads for the habitation module are relatively low because the food stored in the habitation refrigeration system will be maintained at the required low temperatures by the logistic module refrigeration system, prior to transfer to the habitation module. The cooling loads in the life sciences lab module will be high because of the larger number of biological samples to be frozen and stored and because of the low temperatures required. To obtain a more accurate estimate of the cooling loads in the life sciences lab, the rate at which biological samples are stored needs to be

determined from an experiment manifest. It is important that a baseline experiment manifest be developed to identify experiments requiring refrigeration for each 90-day period.

The logistics module presented the greatest challenge for designing refrigeration systems to meet all cooling requirements. Refrigeration systems must be designed to cover the entire spectrum of mission phases from prelaunch through return and landing. The logistics module must maintain food temperatures until the food is transferred to the habitation module, and must also provide a means of returning to Earth the frozen life sciences biological samples in a -94 °F freezer.

The refrigeration requirements for the habitation module include a refrigerator and a freezer for the storage of a 14-day supply of food in the galley area. According to the Space Station Reference Configuration document (Ref 4), the refrigerator and freezer will be restocked every 14 days from food stored in the logistics module refrigerator and freezer. There is no requirement to refrigerate or freeze thawed food in the habitation module because the food is already frozen or chilled when transferred from the logistics module.

To estimate the cooling loads for the refrigerator and freezer in the habitation module, the assumptions in *Figure 43* were made. The internal volume required for refrigerated and frozen food was estimated based on average food weights and average usage rates. The habitation freezer needed 6 ft^3 internal volume, while the habitation refrigerator only required 2 ft^3. The maximum thickness of insulation was used to allow room for accessories and the required internal volume and still stay within the total volume of 12 ft^3. From these calculations, it was decided to use 3 in. thick insulation for estimating the heat leaks. *Figure 44* contains a breakdown of the individual heat loads for the habitation module refrigeration system.

The refrigeration requirements for the logistics module include a refrigerator and a freezer. The refrigerator and freezer are used for transporting refrigerated and frozen food and medicine to the Space Station, storing food during the 90-day mission, and for returning frozen and refrigerated items to Earth. The logistics module freezer must have the capability to match the -94 °F temperature requirement of the life sciences lab freezer to be able to return lab samples to Earth. Another requirement of the logistics module is to be able to maintain proper temperatures through all phases of the logistics module operation. The different phases for which the logistics module must maintain refrigeration are prelaunch, launch, on-orbit, docking, docked configuration, retrieval, on-orbit, landing, and post-landing.

The refrigerator in the logistics module has a total volume of 20 ft^3. Using assumptions in *Figure 43,* an internal volume was estimated as 13 ft^3. The logistics module freezer has a total volume of 60 ft^3 and an estimated internal volume of 34 ft^3. Using the estimated internal volumes, cooling loads for the logistics module refrigerator and freezer were calculated. Even though the logistics module will be stocked with prefrozen and prechilled food during the prelaunch phase, an additional food load was estimated to design for the possibility of freezing or refrigerating room temperature food. The additional food load for the refrigerator is based on cooling 25 pounds of food with 80 percent water content in six hours. For the freezer, the additional food load is based on freezing 250 lb of food with 80 percent water content in 24 hours. These loads will not normally be imposed on the refrigeration system and thus only serve in defining a design point.

- Thermal Conductance = 0.0162 Btu/hr-F-ft
- Average Food Weight = 30.08 lb/ft^3 (Frozen)
  29.76 lb/ft^3 (Refrigerated)
- Average Usage Rate = 1.88 lb/man/day (Frozen)
  0.62 lb/man/day (Refrigerated)
- Number of Crew = 6
- Thickness of Insulation = 3 in.
- Safety Factor of 1.5 is Assumed for Heat Leak Through Walls
- 70 Percent Air Exchange When Door Is Opened
- Water Content in Food is 80 Percent

Figure 43. Assumptions for Cooling Load Calculations

HABITATION MODULE COOLING LOAD (WATTS)		
	REFRIGERATOR +35°F	FREEZER -20°F
HEAT LEAK THROUGH WALLS	13.4	64.7
FAN LOAD	0.5	1.75
DOOR OPENING	0.3	4.9
FOOD LOAD	0.0	0.0
TOTAL LOAD	14.2	71.35

Figure 44. Detailed Analysis of Cooling Loads in the Habitation Module Refrigeration System

Another consideration in determining the refrigeration requirements of the logistics module is the possibility of needing to preserve a deceased crew member. Although the death of a crew member might set a refrigeration requirement, it was not used to drive the requirements.

The cooling loads for the -94 °F freezer only include the heat leak through the walls and a fan. *Figure 45* contains an analysis of the cooling loads for the logistics module refrigeration system. The -94 °F requirement precludes using the -20 °F freezer to store biological samples as the food is transferred to the habitation module. A relaxation of the biological requirements to -20 °F would allow utilization of otherwise unused space.

The refrigeration requirements for the life sciences lab module include a variable temperature refrigerator, a -94 °F freezer, and a -319 °F freezer. The variable temperature refrigerator must be able to operate in a range from -7.6 to +50 °F. The purpose of the variable temperature refrigerator is to be able to cool blood, body fluids, and fluids intended for injection as well as have the capability to house small animals and incubate amphibian zygotes. A usable volume of 2.5 ft^3 and a cooling load of approximately 200 W for the variable temperature refrigerator are given in Ref 5.

LOGISTICS MODULE COOLING LOADS (WATTS)			
	REFRIGERATOR 35°F	FREEZER -20°F	FREEZER -94°F
HEAT LEAK THROUGH WALLS	52.4	199.4	85.4
FAN LOAD	2.3	16.7	2.2
DOOR OPENING	2.1	14.3	3.9
FOOD LOAD	39.1	455.5	---
BIOLOGICAL LOAD	---	---	0.0
TOTAL LOAD	95.9	685.90	91.5

Figure 45. Detailed Summary of Cooling Loads for the Logistics Module

The -94 °F freezer is intended for the freezing and long term storage and preservation of biological samples such as blood, tissue, and whole rats. Bone samples, tissue samples, and even some whole rats will be prefrozen in the -319 °F freezer prior to storage in the -94 °F freezer. Since all experiments in Ref 5 will not be done at the same time, a proposed timeline of experiments for the first year of operation was obtained from Ref 6. The cooling loads for the -94 °F and the -319 °F freezers were estimated based on the experiments to be done in the first year of operation of the Space Station. From Ref 5, experiments (A) BLla, (A) MLla, and (W) CV2 were used to determine cooling requirements. The cooling loads calculated were based on a freezing time of 24 hours. Dr. John Hilchey (MSFC) indicated that an increased cooling rate may be required, and suggested contacting Dr. Adrian Mandel (ARC) for specific requirements. According to Dr. Mandel, the cooling rate should be adequate, provided the freezer is chilled to -94 °F prior to insertion of the samples. If a faster cooling time is required, the cooling loads will go up proportionally.

The -319 °F cryogenic freezer in the Life Sciences Lab is for quick freezing biological samples before the samples deteriorate. Biological samples will be stored in the -94 °F freezer after freezing in the -319 °F freezer. To calculate the cooling requirements for the -319 °F freezer, the same experiments were considered as with the -94 °F freezer. With a cryogenic freezer, it is more important to know the total cooling required than the cooling rate because the total cooling sets the requirement for the amount of coolant (i.e., LN_2) needed. *Figure 46* gives a detailed summary of the cooling requirements for the life sciences lab module.

LIFE SCIENCES LAB			
	REFRIGERATOR -7.6, +50°F	FREEZER -94°F	FREEZER -319°F
HEAT LEAK THROUGH WALLS	33.1 watts	85.4 watts	----
FAN LOAD	4.1 watts	3.4 watts	----
DOOR OPENING	1.9 watts	3.9 watts	----
BIOLOGICAL LOAD	160.9 watts	47.30 watts	1034 watt-hr
TOTAL LOAD	200.0 watts	140.0 watts	1034 watt-hr

Figure 46. Detailed Summary of Cooling Loads for the Life Sciences Lab Module

The refrigeration requirements for the materials lab module consist of a refrigerator and a freezer for storing biological samples such as protein solutions. The operating temperature of the freezer will be -20 °F and the temperature of the refrigerator will be 35 °F. To calculate cooling loads for the refrigerator and freezer, a coefficient of performance of 2.0 was assumed. From approximations for peak power obtained from Ref 6, the cooling loads were calculated. It is estimated that the freezer will require approximately 250 W of cooling power and the refrigerator will require 150 W of cooling power.

2.2.2 Definition of Cryogenic Requirements

Under this subtask, several candidate fluids for a low temperature radiator system to meet Space Station low temperature refrigeration requirements were evaluated. The following criteria were used to assess the candidate fluids:

- Ratio of fluid properties that determine the pumping power to heat transfer capability
- Density
- Vapor pressure
- Stability
- Inertness
- Toxicity.

While not extensive, this initial evaluation addresses some of the more promising fluids. Additional evaluation may be necessary as a low temperature radiator system becomes better defined and/or additional candidate fluids are identified. The above criteria were fully investigated and the analysis and the recommendations for Coolanol and fluorinert fluids are documented in SRS Technologies' report of Ref 7.

2.2.3 Assessment of Feasible Cycles

Ten refrigeration cycles have been considered to assess the feasibility of meeting refrigeration requirements in the Space Station. These cycles are

- Absorption
- Claude
- Low temperature radiator
- Stirling
- Vapor compression
- Adsorption
- Joule-Thomson
- Reversed Brayton
- Thermoelectric
- Vuilleumier.

Detailed performance evaluations and trades were conducted for the most promising candidates: thermoelectric, vapor compression, Stirling, and low temperature radiator systems. Less detailed evaluation of the other systems was adequate to eliminate them as candidates. Considerable effort was made to define the best configuration for each of the two prime candidates: vapor compression and low temperature radiator systems. This effort included investigation of candidate coolant and working fluids in terms of their performance and potential toxicity characteristics. For the vapor compression systems, various combinations of cascading and/or combining the cycles were investigated. An evaluation procedure to determine the relative performance of different systems was developed. This was used as an initial screening technique to narrow the list of candidates. The candidate refrigeration systems were initially evaluated on the basis of weight penalties associated with the combined radiator and power requirements. This screening procedure narrowed the choice between the low temperature radiators and the vapor compression systems.

Further detailed trades and evaluations resulted in the recommendation of vapor compression as the best approach for meeting the Space Station low temperature requirements. This recommendation was strongly driven by the ability of the vapor compression systems to utilize the shuttle heat transport loop during the logistic module launch, rendezvous, and docking phases, thus not requiring thermal capicitance during these times. The various trade studies performed for the refrigeration cycles are described in Ref 7.

An evaluation and comparison of refrigerants for the vapor compression cycle was performed. Candidate refrigerants were evaluated to select the most promising working fluid for a Space Station vapor compression refrigeration cycle. Ten representative refrigerants were initially evaluated based on an evaporator temperature of -40 °F and condenser temperature of 50 °F. For a cold space temperature of -20 °F this allows 20 °F for interface heat exchanger delta temperatures. For these conditions, the interfacing Space Station cabin coolant loop was assumed to be 35 °F, providing a 15 °F delta temperature for an interfacing heat exchanger. These temperature differences can probably be reduced, but they should be realistic for comparison of refrigerant characteristics. Single and cascade cycles were also compared for selected refrigerants, and the effects of condenser temperature on cycle performance were evaluated. A computer program was developed to rapidly evaluate various parameters and their effects on cycle efficiency.

The work done to evaluate several refrigerants and compare single and cascade cycle analysis of a vapor compression refrigeration system using selected refrigerants is described in Ref 7 and in an excerpt from the November 1985 monthly progress report presented in Appendix C.

2.2.4 Design and Fabrication of Prototype Hardware and Component Testing

Under these subtasks, a laboratory effort was undertaken to integrate a flow controller mixing valve into an existing thermal/fluid loop test bed, and an investigation was begun for a refrigeration demonstration unit to be tested.

2.2.4.1 Application of Flow Controller Mixing Valve

The flow controller mixing valve would be to mix the flows from the radiator and the radiator bypass in proper proportions to obtain a given coolant temperature as it enters the part of the loop where heat is to be picked up. In June 1987, we received from MSFC a flow controller mixing valve along with the following surplus Skylab hardware items:

- One Coolanol pump package
- One Coolanol pump package power supply
- Four coldplates
- One mixing valve controller.

The purpose was to incorporate and test the flow controller mixing valve on an existing thermal control fluid loop test bed built under a separate NASA-MSFC Contract NAS8-36199 (Ref 8). The original controller was used on the Skylab/ATM and had only one temperature set point (at 50.5 °F). After the controller and mixing valves were set up and checked on the bench, a control circuit was designed and assembled which allowed dialing a range of temperature set points from -20 to +100 °F. This system was then installed in the test bed and tested.

The purpose of the coldplates was for adding an additional 1500 W of heat to the test bed Coolanol loop so that this part of the loop could be operated independently from the water loop if desired. Foil heaters were sized and installed on the coldplates.

The new Coolanol pump was added in parallel with the existing identical pump in order to increase the flowrate needed for testing of an ammonia heat pipe radiator built by LTV. The surplused pump had to be disassembled and all O-rings replaced for it to function properly. New flow meter bearings were also required. Also, a printed circuit board for the Autocalc was made up to convert Vrms to Vdc for measuring the power input to the 1500 W heaters.

As testing with the mixing valve on the test bed progressed, the Skylab flight unit controller was found to have a very large time constant, which allowed the temperature to drift gradually toward the set point. Also the RTD being used for the temperature measurements and control feedback had a different ohm/degree characteristic because it had to span a large range of temperatures. The circuits were modified to correct for these problems. *Figures 47* and *48* show the test bed under operation. *Figures 49* through *55* are typical test results showing the "mixed" temperature drift. *Figure 56* shows the results of a typical plot after the problem was corrected. It can be seen that the controller is holding the outlet temperature over a wide range of input values. *Figure 57* shows the set point versus temperature calibration for this controller.

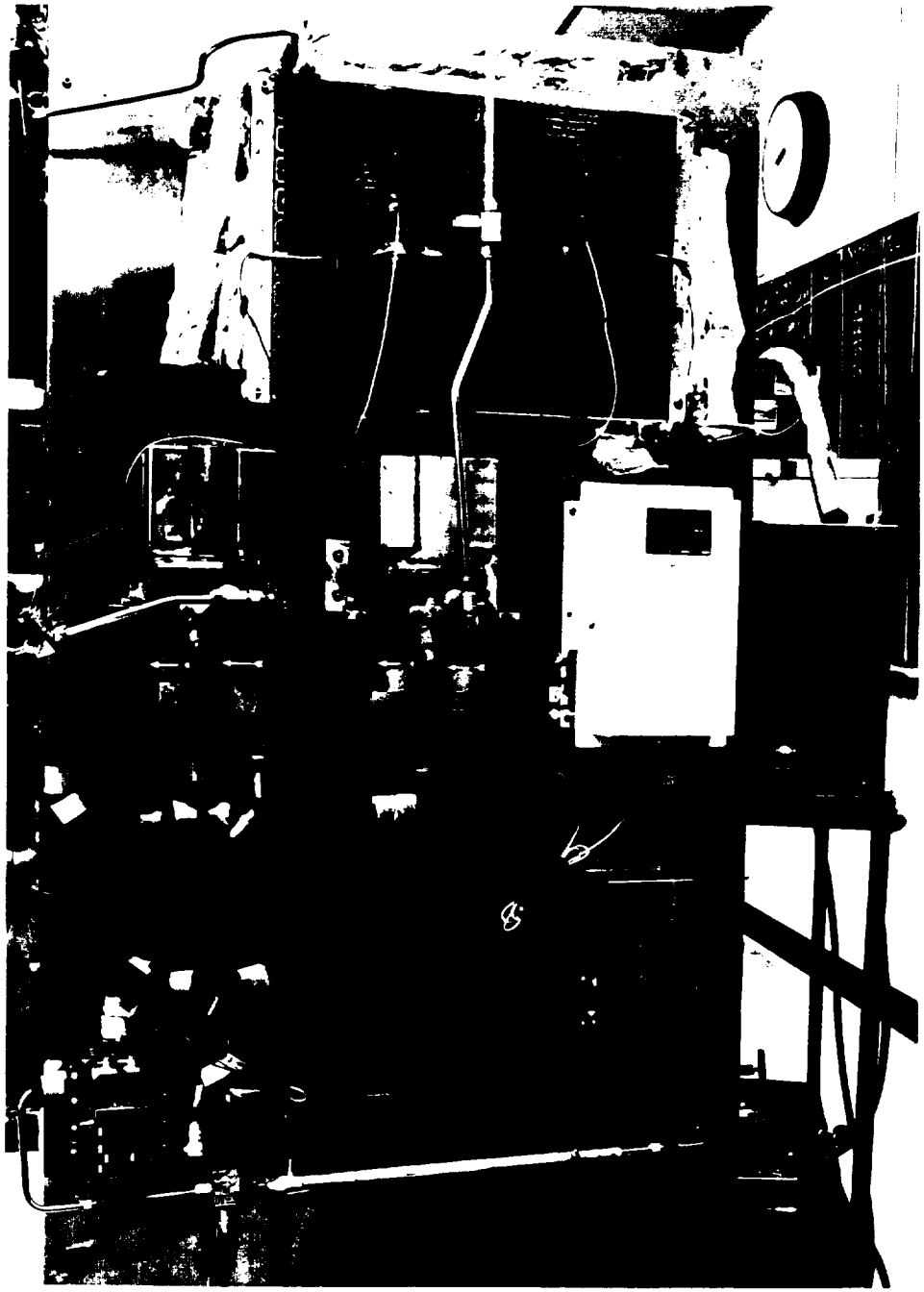

Figure 47. Thermal Control Test Bed with Temperature Controller Installed

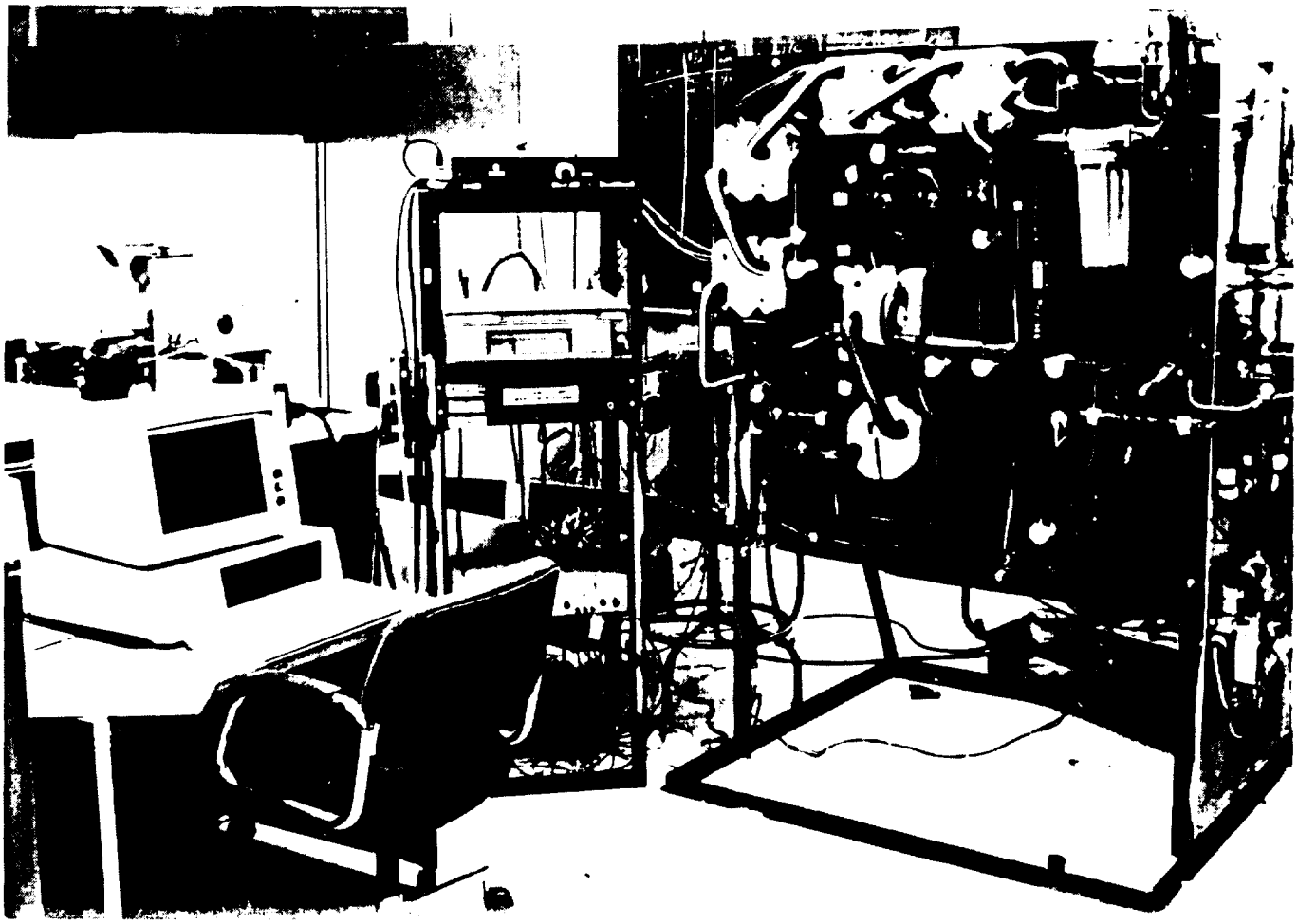

Figure 48. Data System and Control Panel for Thermal Control Test Bed

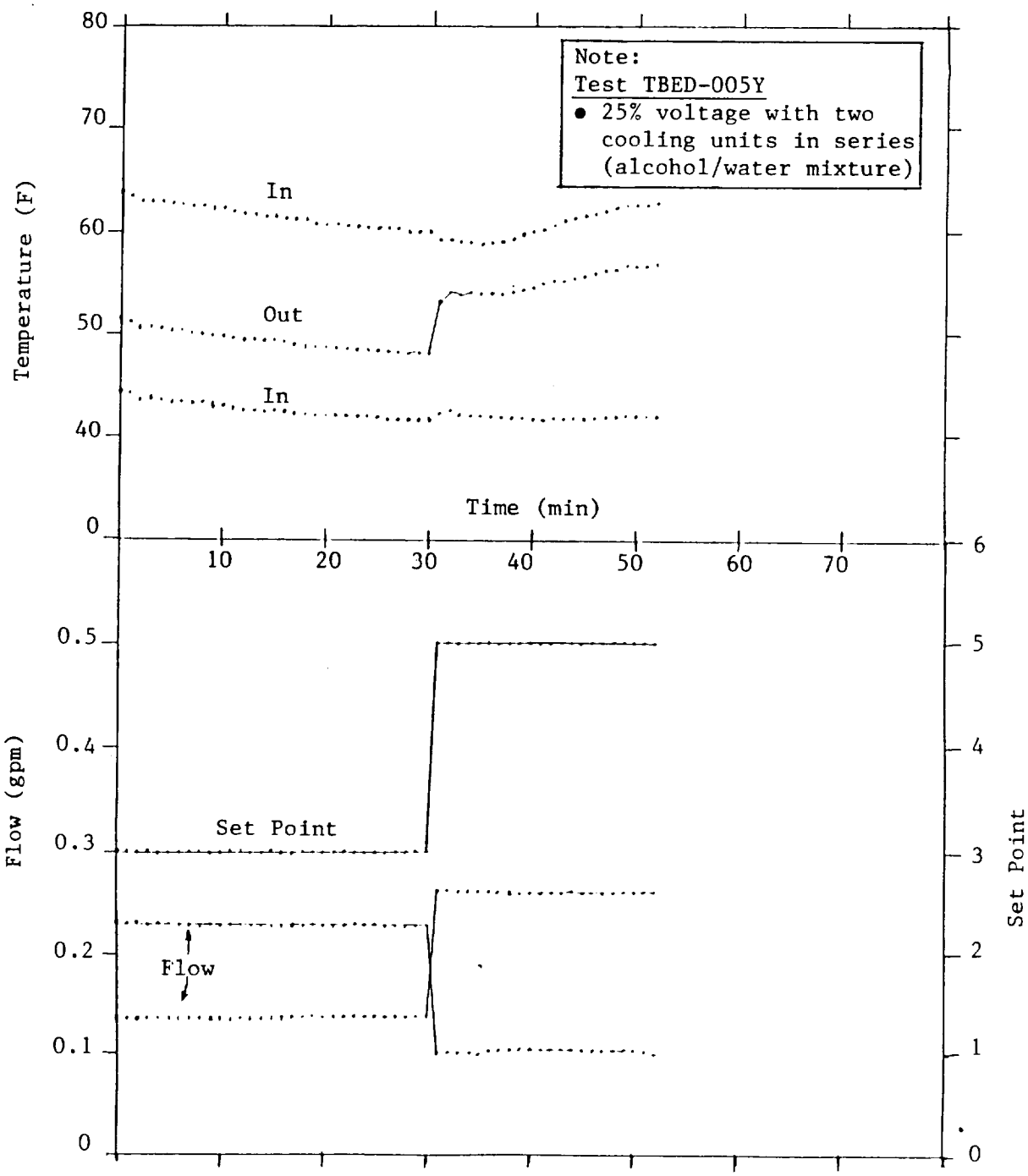

Figure 49. Temperatures, Flow Rates, and Controller Set Points vs Time for the Thermal Control Test Bed Data (See "Notes" box for test conditions.)

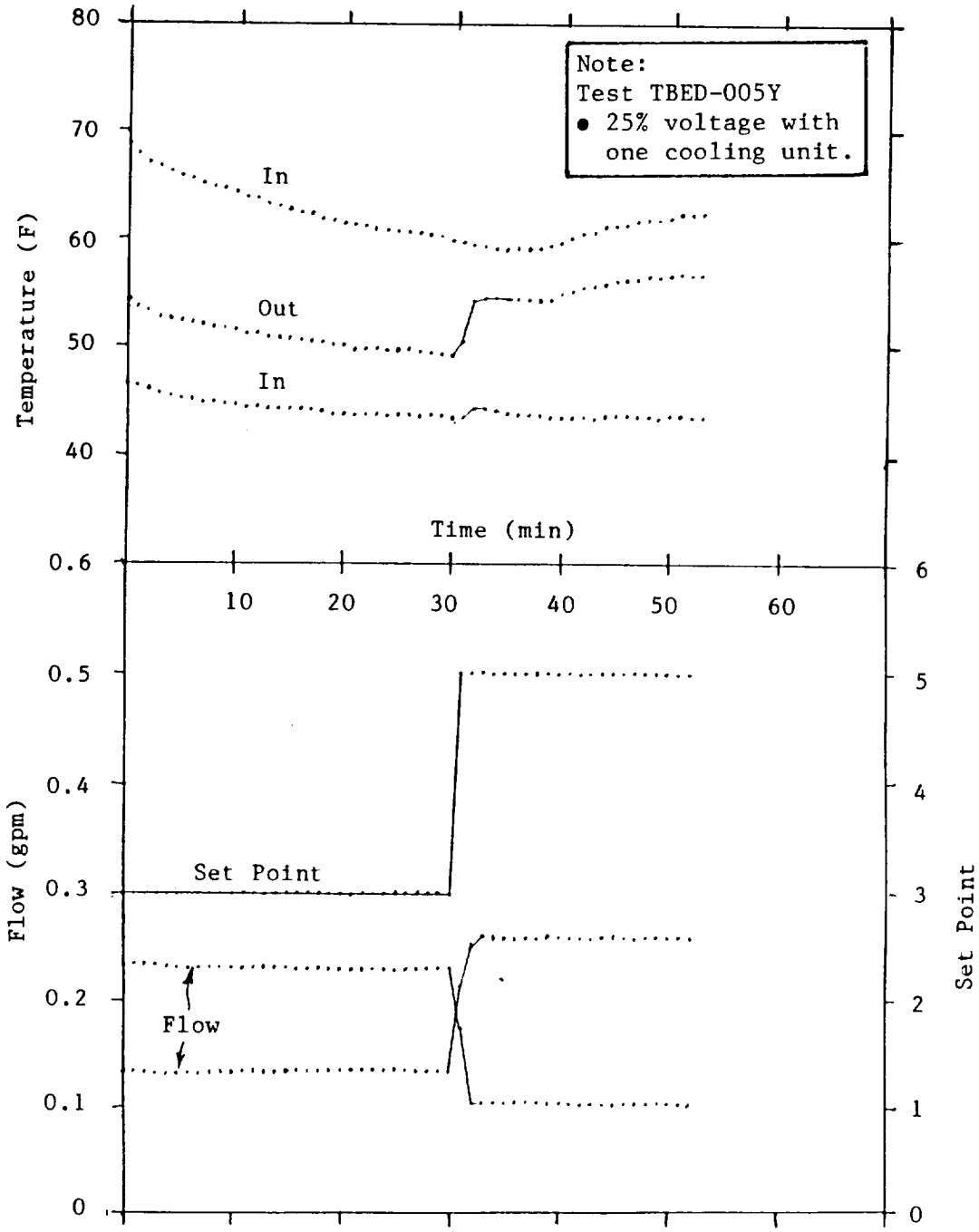

Figure 50. Temperatures, Flow Rates, and Controller Set Points vs Time for the Thermal Control Test Bed Data (See "Notes" box for test conditions.)

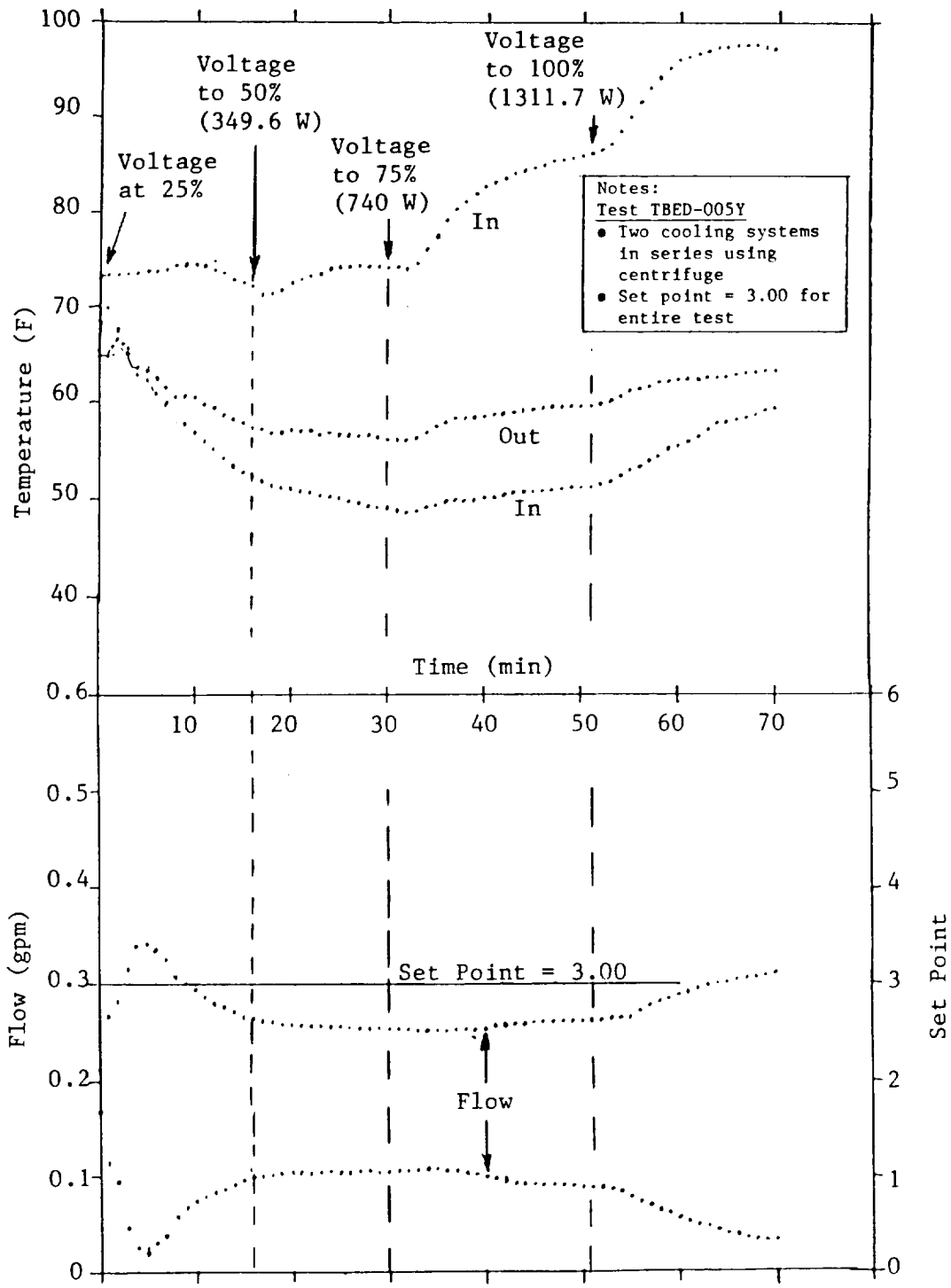

Figure 51. Temperatures, Flow Rates, and Controller Set Points vs Time for the Thermal Control Test Bed Data (See "Notes" box for test conditions.)

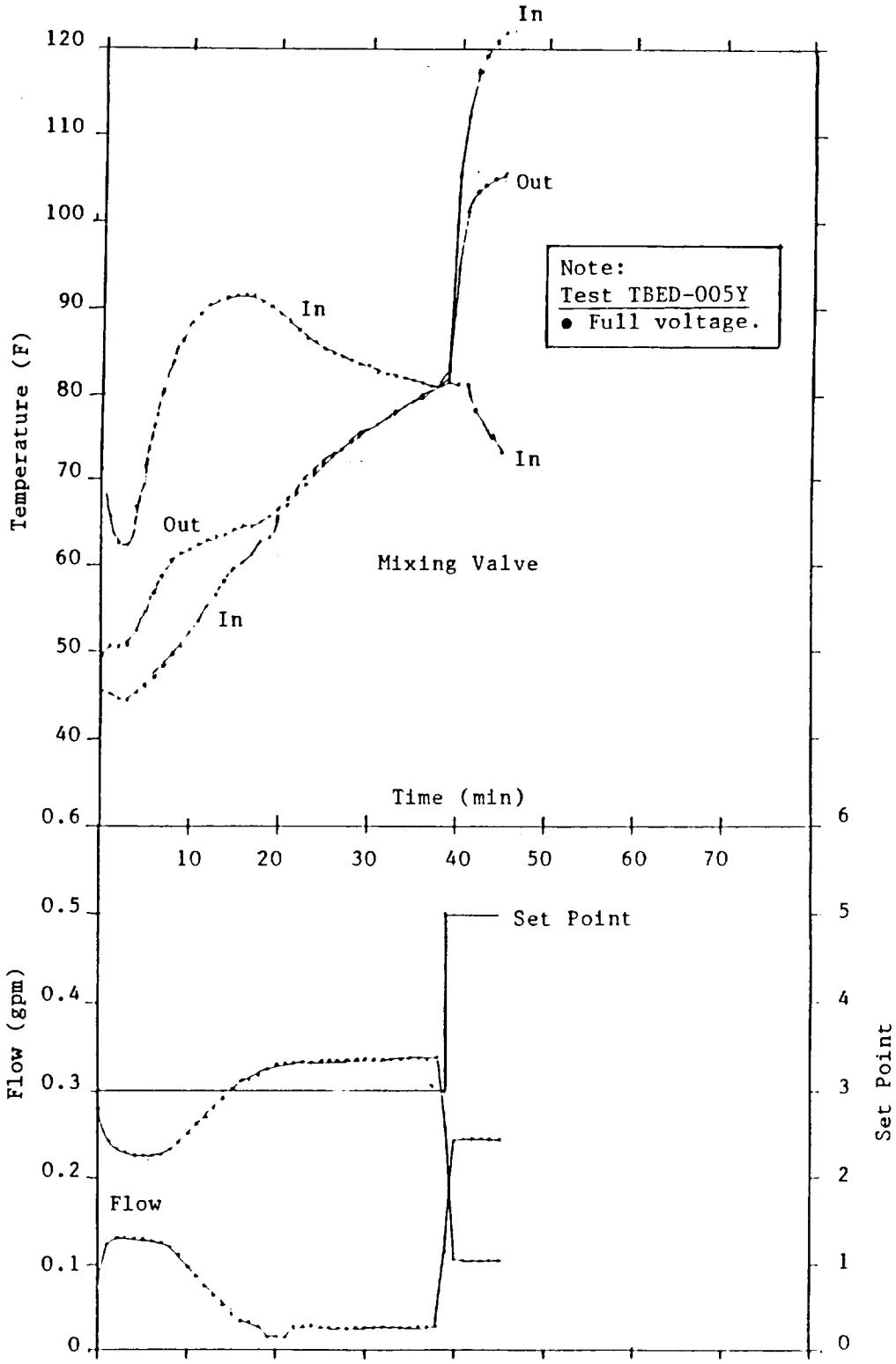

Figure 52. Temperatures, Flow Rates, and Controller Set Points vs Time for the Thermal Control Test Bed Data (See "Notes" box for test conditions.)

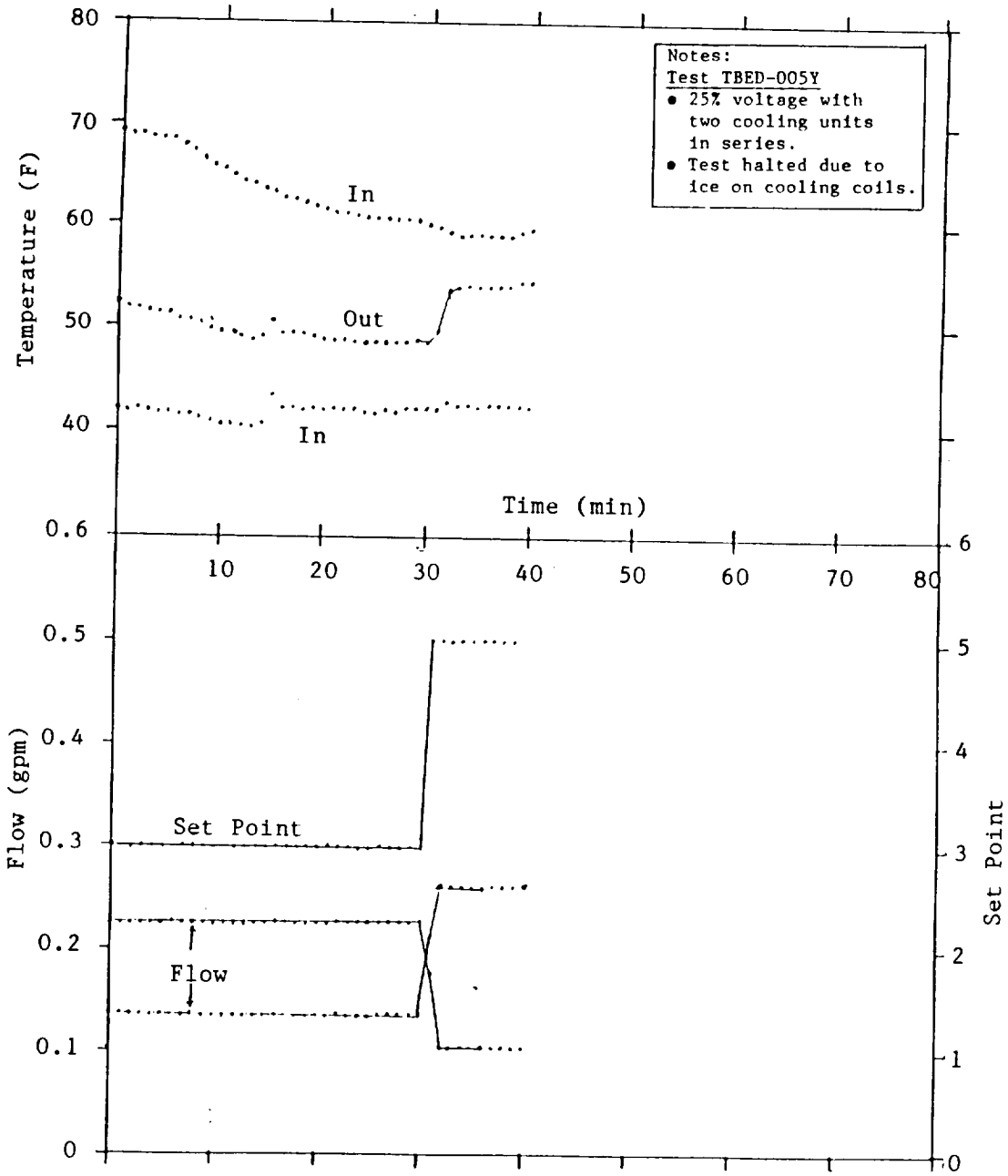

Figure 53. Temperatures, Flow Rates, and Controller Set Points vs Time for the Thermal Control Test Bed Data (See "Notes" box for test conditions.)

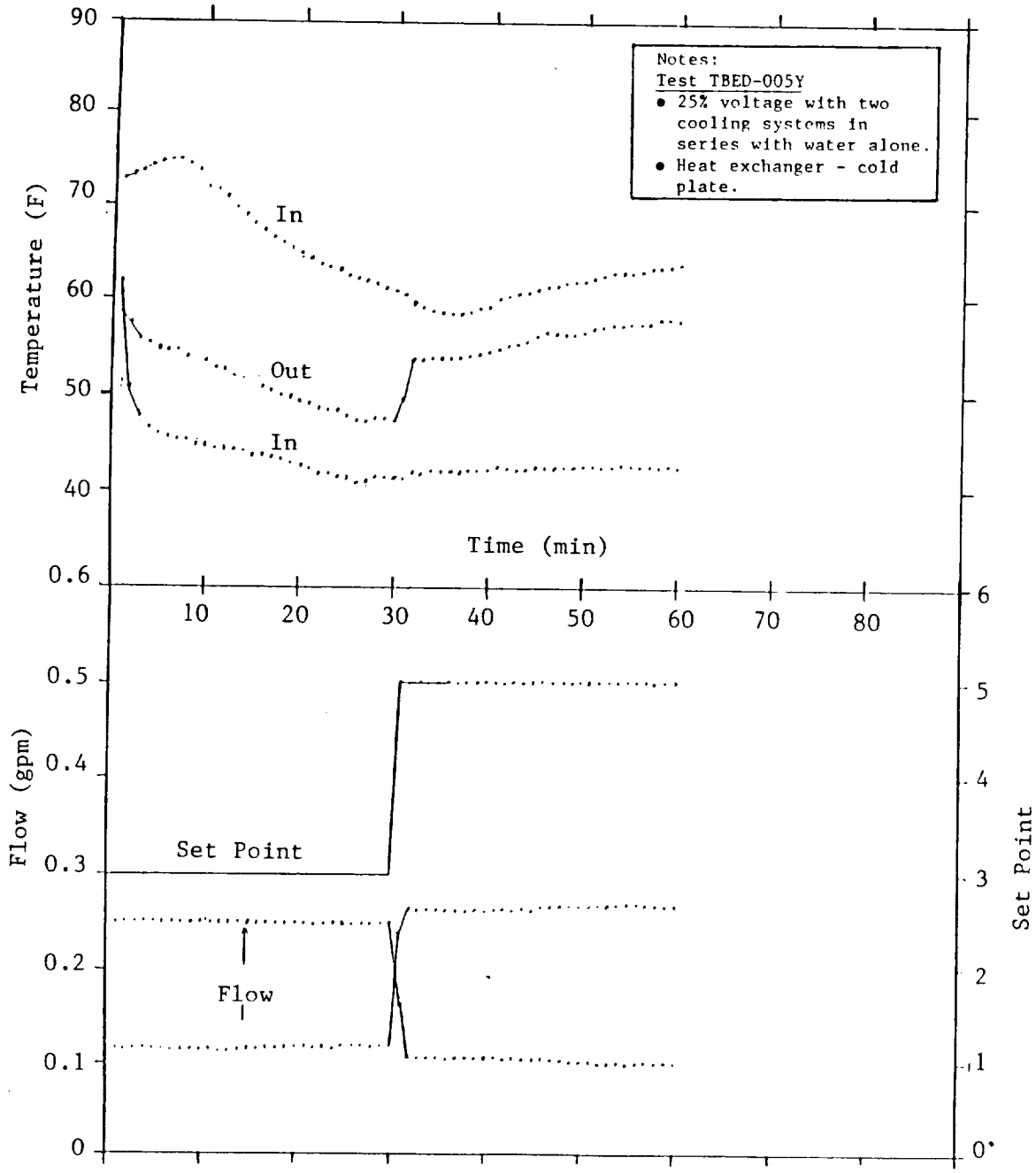

Figure 54. Temperatures, Flow Rates, and Controller Set Points vs Time for the Thermal Control Test Bed Data (See "Notes" box for test conditions.)

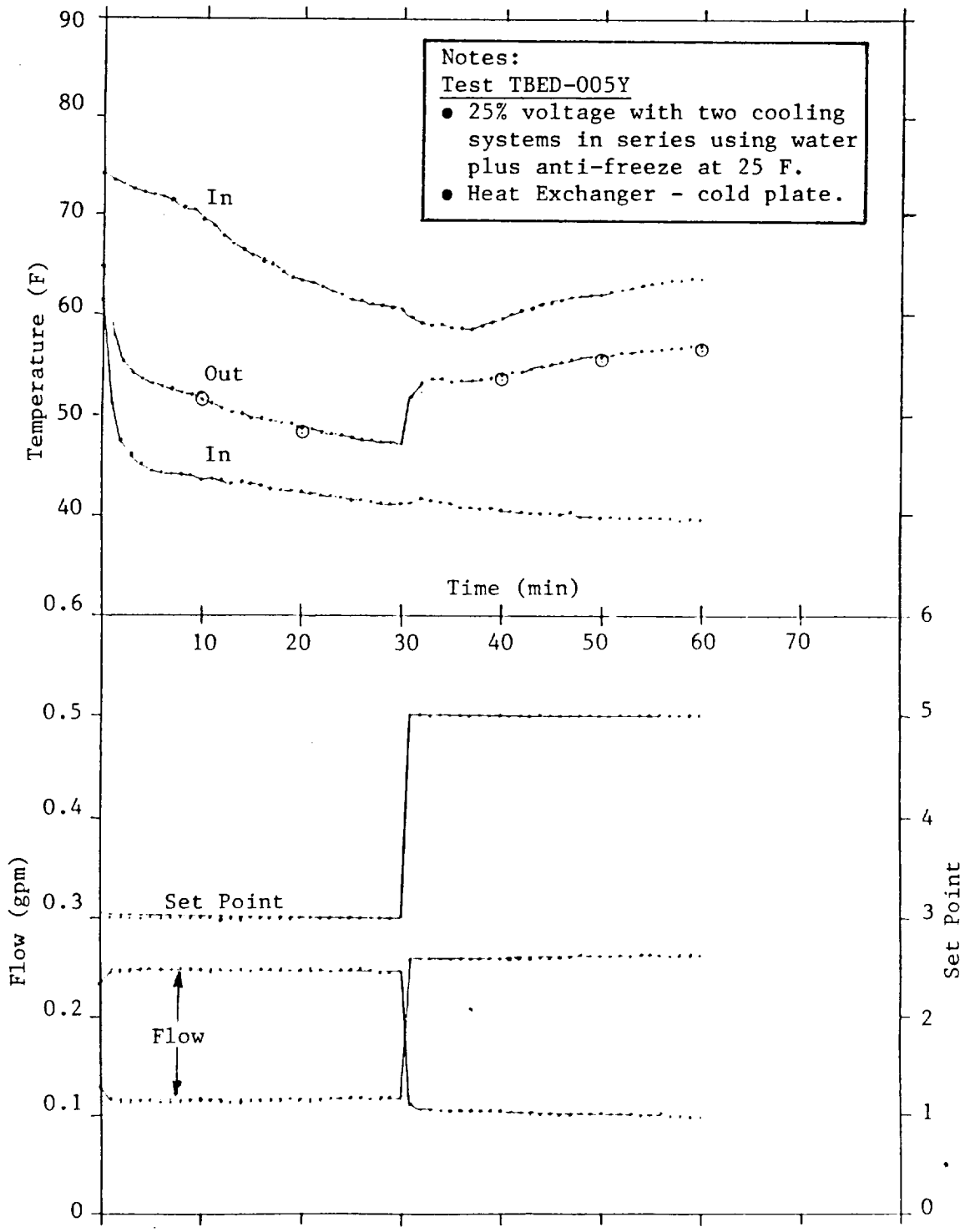

Figure 55. Temperatures, Flow Rates, and Controller Set Points vs Time for the Thermal Control Test Bed Data (See "Notes" box for test conditions.)

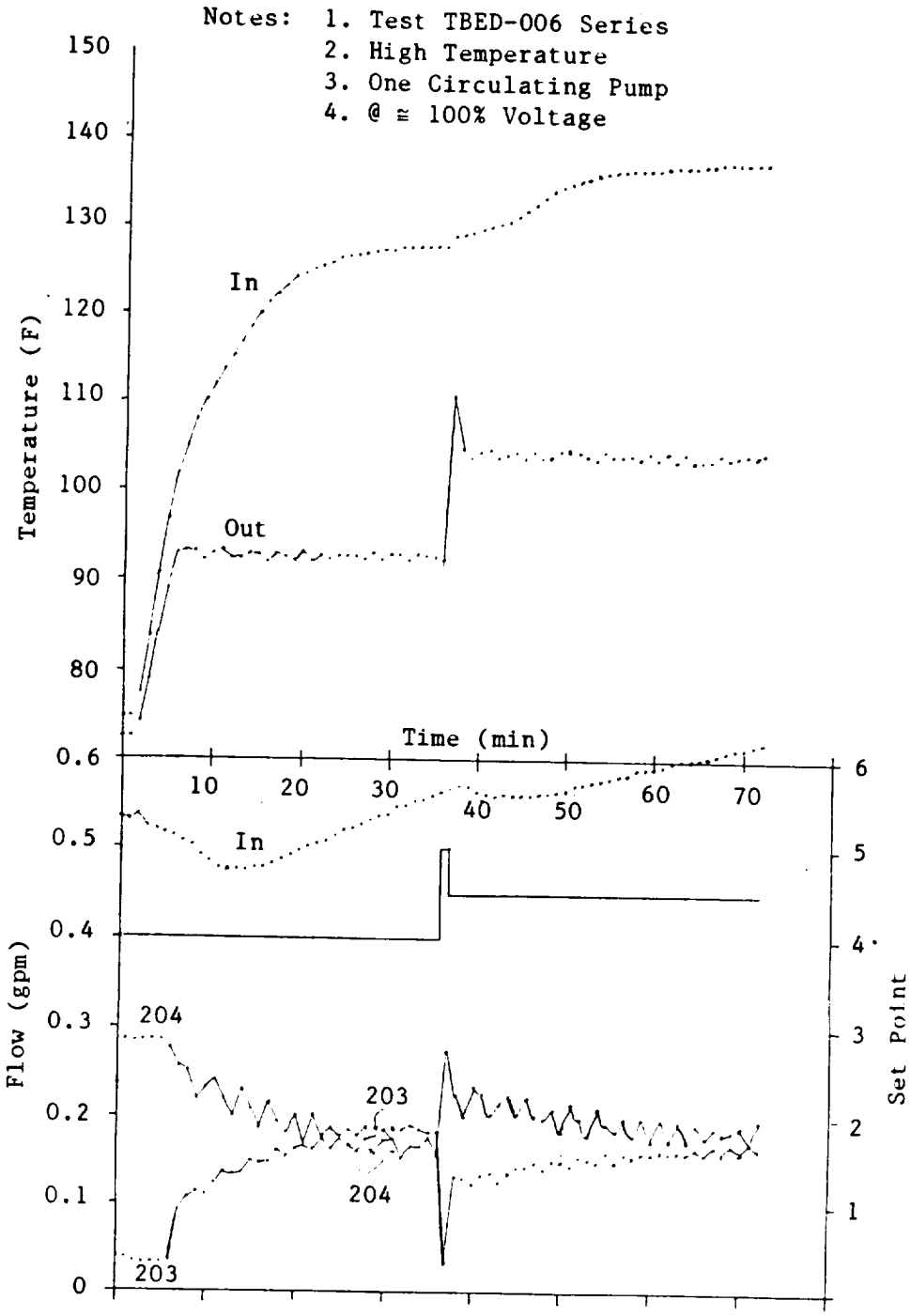

Figure 56. Temperatures, Flow Rates, and Controller Set Points vs Time for the Thermal Control Test Bed Data After Modifications to the Controller Electronics/Control System

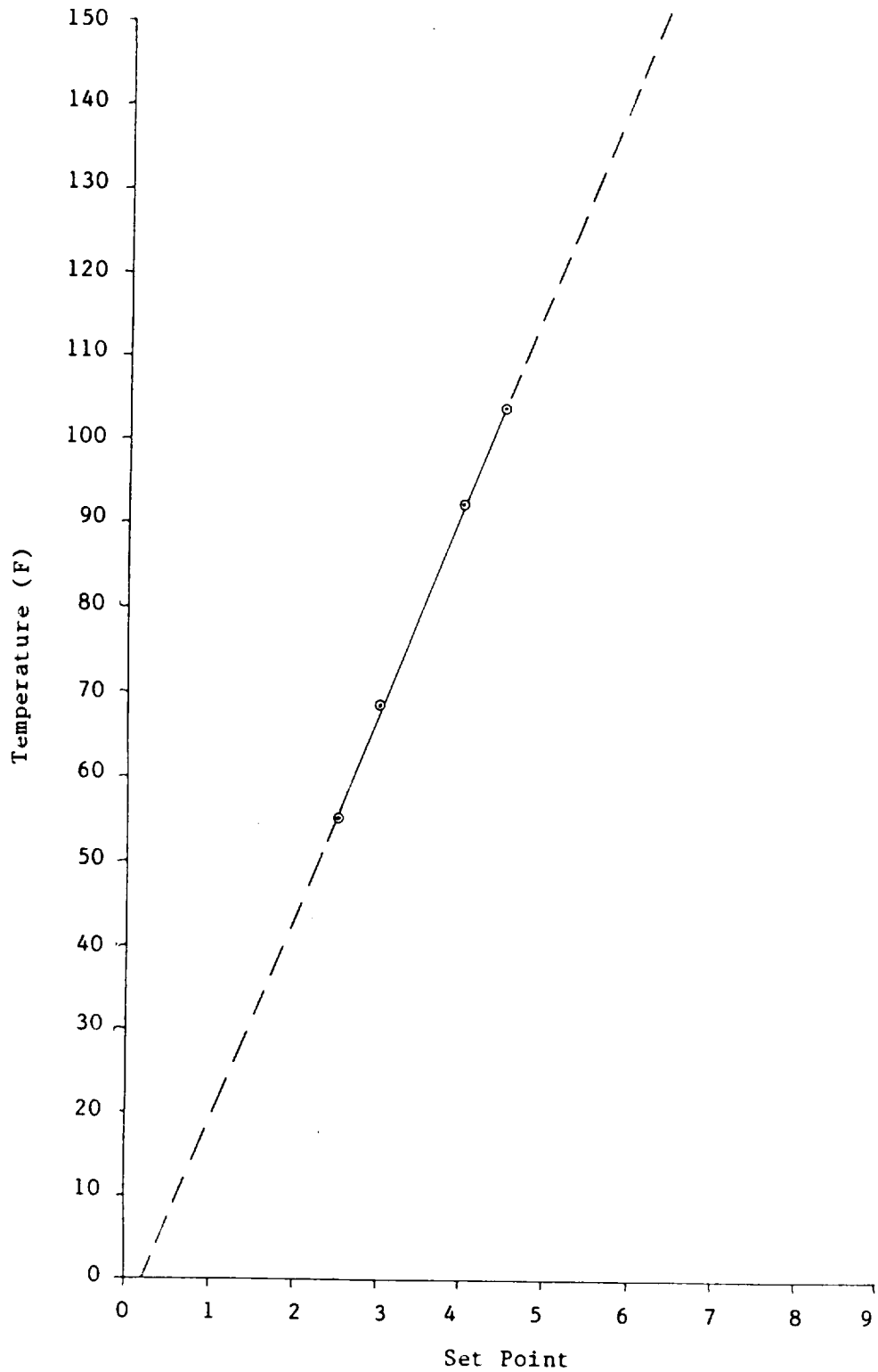

Figure 57. Outlet Temperatures vs Set Point for the Modified Test Bed Mixing Valve Controller

2.2.4.2 Refrigeration Demonstration Units Testing

Efforts in the area of design, fabrication, and testing of refrigeration systems protoype flight hardware were directed towards two types of systems: the vapor compression and the Stirling cycle refrigerator/freezer units.

2.2.4.2.1 Stirling Cycle Refrigeration Unit Investigation and Testing

These types of units are commonly used in IR detector applications. They have been used frequently on Army tanks and flown on numerous military satellites as well as on the Space Shuttle. A vast literature review was conducted to get an insight into the Stirling cycles units.

References 9 through 12 are examples of the type of literature reviewed. A set of curves comparing Stirling, vapor compression, Claude and Joule-Thomson cycles was found in Ref 13. These curves are shown in *Figure 58*. The "efficiency" presented in this figure is the ratio of indicated cycle coefficient of performance (COP) to the Carnot COP and shows clearly that the Phillips-Stirling process has superior efficiencies at extremely low temperatures. Findings of this nature provided a greater resolve in the Stirling cycle refrigeration system investigation.

A production model Stirling unit was obtained on loan from Magnavox Electro-Optical Systems of Mahwah, New Jersey, for evaluation and testing. It was set up in our lab and a demonstration of this unit under test was given to NASA-MSFC personnel. *Figure 59* shows a photo of the unit under test.

The Magnavox Model MX-7043-10 1 W Linear Stirling unit under test is driven by a unique "voice-coil" (i.e., moving coil or opposed to moving magnet) linear drive motor. It operates on 50 Hz ac power. The motor drive operates at 50 Hz in phase with the input frequency. Its output can be varied by reducing the input voltage while holding the input frequency constant. These type motors are very efficient, reportedly up to 80 percent as compared to about 35 percent for common rotating electric motors. This linear "voice coil" or moving coil gets its name from the design used to drive typical home stereo speakers. This design also has the advantage of inducing very small side loads onto the driver (compressor) piston. This contributes to the reduced wear and long life of these units. We know of one Magnavox Stirling unit that Lockheed operated in orbit for over 9,000 hours.

Testing of the Stirling refrigeration unit was continued through approximately five months. During the period improvements were made to the test setup. The power module originally used to measure heater input power was replaced with a more accurate method of measurement. This method involved measuring the heater power by the voltage drop across a 50 ohm precision power resistor mounted on a heat sink to maintain its temperature and eliminate resistance variation due to temperature. This voltage was then used to calculate the current through the cold head heater (which is in series with the externally mounted precision resistor). The voltage across the cold head heater was also measured. The heater voltage and current were then used to determine the heater power independently of the heater resistance. This new method eliminated the unknown effects of varying resistance of the cold head heater with temperature, which can be significant at cryogenic temperatures.

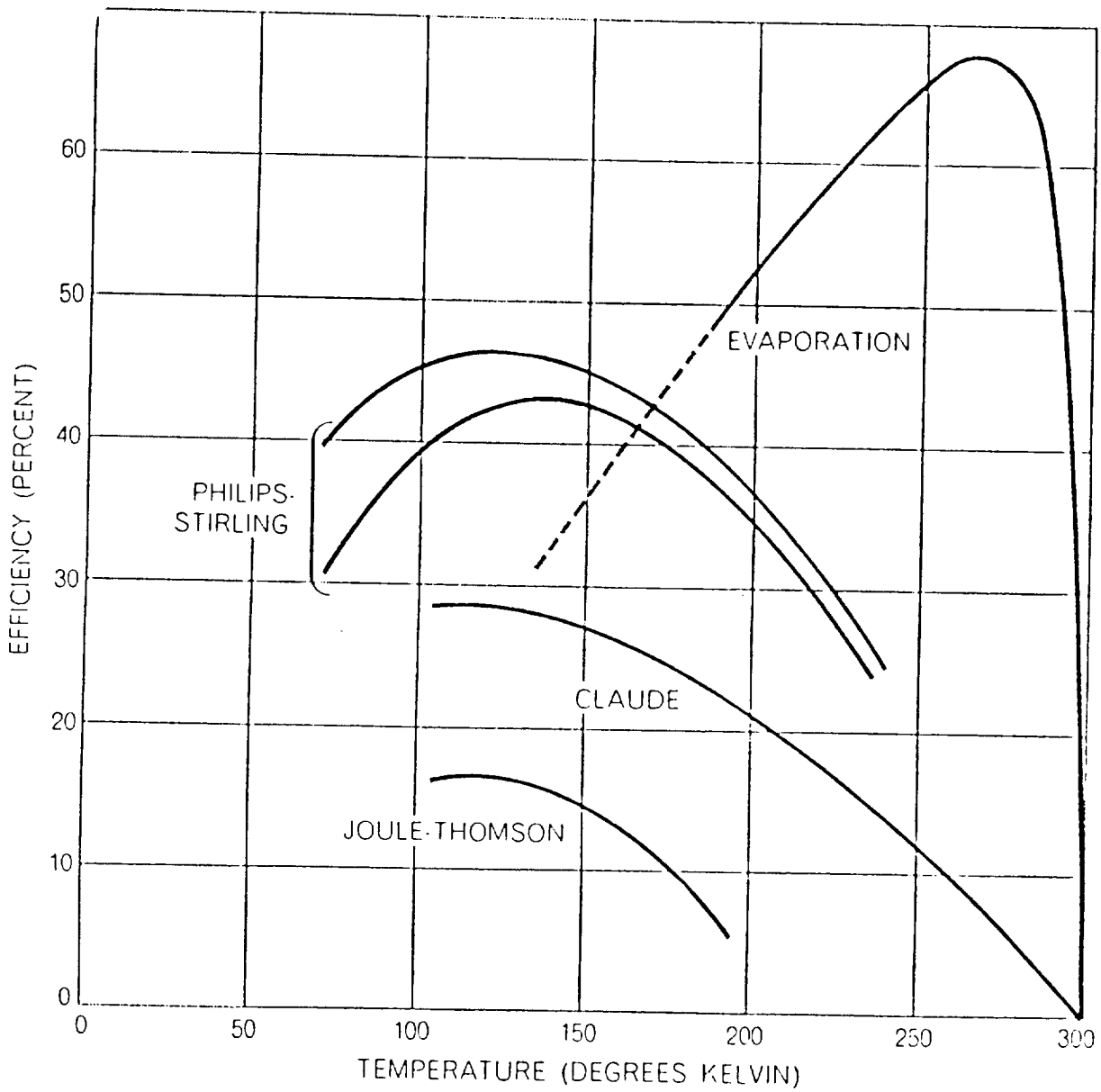

Figure 58. Comparisons of Various Refrigeration Cycle Efficiencies Over a Range of Temperatures (from Ref. 13)

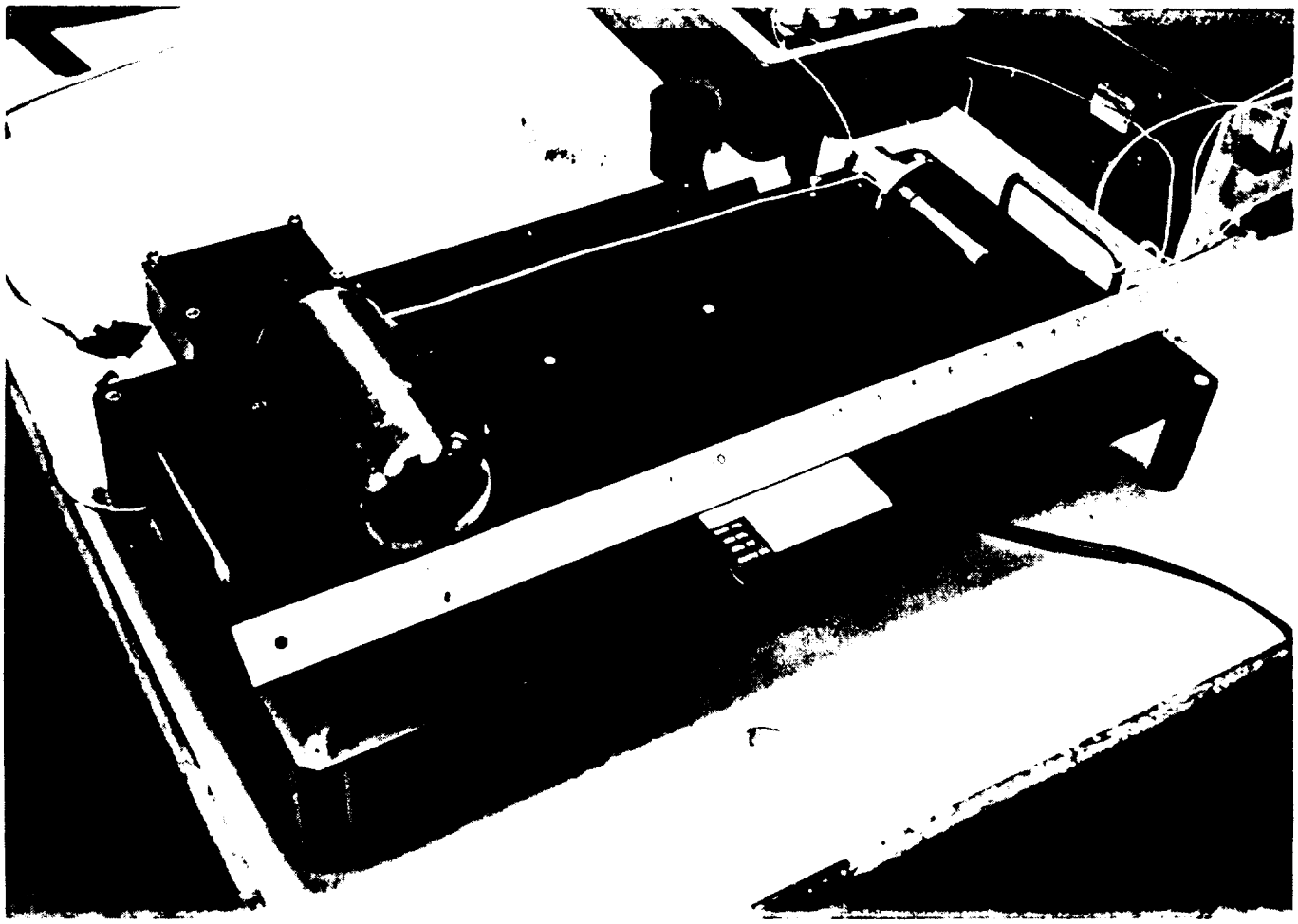

Figure 59. Magnavox Stirling Cycle Refrigeration Unit Under Test at Lockheed-Huntsville (This unit produces 1 W of refrigeration at 77 K and approximately 7 W at 200 K with 55 W input power.)

A problem was encountered in bonding the cold head heater to the Stirling cold head end. Initially a thermally conductive epoxy was used to ensure good thermal contact between the cold head and the heater. However, the severe thermal gradient between the cold head and the heater caused this epoxy to debond, and the heater overheated. We proceeded to design and fabricate a copper heater/cold head adapter. This adapter has a hole in which the heater/ resistor is bonded in place using "torr seal" epoxy. The adapter also had a through hole for the thermocouple, which was added to help secure the thermocouple to the cold head and prevent debonding at cryogenic temperatures. *Figure 60* shows the drawing of this copper adapter. This adapter was then soft-soldered to the Stirling cold head using low temperature solder (244 °F) to prevent damage to the cold head and to ensure good thermal contact.

The instrumentation was also improved. The original RTD was replaced with a Chromel/Constantan thermocoupled with 0.005 in. diameter wire. This was done to replace the RTD copper leads with materials of lower thermal conductivity. Copper conductivity increases dramatically at cryogenic temperatures--by a factor of about 8 over room temperature values. This reduction is needed to reduce the "parasitic" heat load to the cold head in addition to the input heater power. Also, the heater leads were changed from copper to 0.010 in. diameter Constantan wire.

We continued testing of the Magnavox Model MX-7043-10 Stirling refrigeration unit. Tests were run at a constant input power of 70 W. The unit was turned on, allowed to cool down to about -200 °C, and then power was added to the cold head heater in steps of 0.5 W. The temperature was allowed to reach equilibrium between each step change of heater input power.

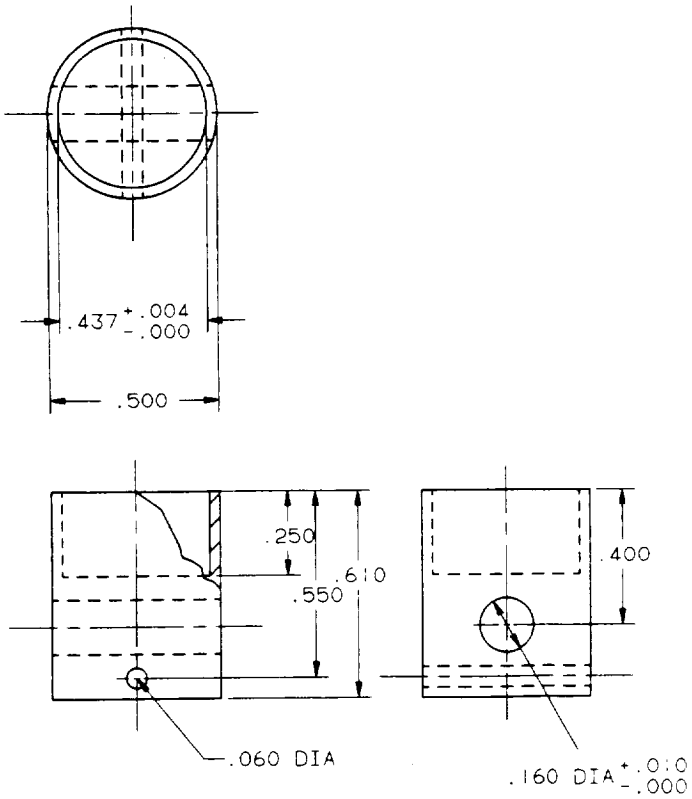

Figure 60. Stirling Cold Head Heater Adapter

Net refrigeration produced at each temperature level was calculated by making corrections for the following terms: (1) power loss in the small diameter wires that feed the cold head heater; (2) heat gain to the cold head by conduction through the lead wires both to the thermocouple and to the cold head heater; and (3) heat gain to the cold head due to radiation from the vacuum container walls to the cold head. Heat gain by convection was assumed to be negligible because we held a vacuum of about 1×10^{-4} torr around the cold head during testing. Conduction down the cold head body to its flange was not considered because this is a parasitic heat loss inherent in the design and has nothing to do with the instrumentation/testing.

We ran several tests by increasing the power in steps. We were interested in finding the maximum operating temperatures for this unit. This was found when the cold head temperature reached about -60 °C with a power input of 10.5 W and a net refrigeration of about 7.8 W. At this point, the unit started to "knock" and the temperature had to be lowered.

As testing continued, improvements were constantly made. (1) The Chromel/Constantan thermocouple was replaced with Medtherm Model No. PRT-100-60-10830 RTD with 0.003 in. diameter Constantan lead wires with polyamide enamel insulation. (The thermocouple lead wires were uninsulated, which made it difficult to prevent shorting of the wires inside the vacuum chamber.) (2) The inside of the vacuum chamber and the outside of the cold head were both taped with a highly reflective (E = 0.03 to 0.06) tape. This was done to reduce the radiation from the walls to the cold head which contributes to the cold head heat load and has to be calculated. This calculation introduced an unknown into the net refrigeration term. (3) A new resistor and resistor adapter were used with shorter lead wires.

New test results tend to confirm the previous testing done before the test setup improvements were made. The performance was somewhat below that expected from the data previously received from Magnavox. Tests were all conducted with the Stirling unit expander base bolted to an aluminum heat sink. Some tests were repeated using an acively cooled coldplate clamped to the expander base. This was done to see if the performance would improve. The coldplate was cooled using a methanol/water solution circulated through a cooling cart with an active refrigeration unit. The net result of this effort was that the base cooling did not significantly improve the unit's performance.

As discussed above, several tests were performed on the Stirling refrigeration unit. A comprehensive report describing (1) the test unit, (2) test setups and interfaces, (3) instrumentations for temperature, power, and vacuum, and (4) observations and test results, was prepared (Ref 14). The report covers the undesirable effects of external heat gain by conduction through wires, radiation heat gain on the cold head surface, and power losses in heater lead wires.

Some of the typical results were compared to the ideal (Carnot) efficiency. *Figure 61* shows a plot of Carnot COP versus cold head temperature for three tests. The Carnot COP was calculated for each individual test point on each of these curves for its particular test condition, using the relationship

$$COP_{Carnot} = \frac{T_C}{T_H - T_C}$$

where

T_C = cold head temperature

T_H = expander base temperature.

Figure 62 shows plots of net refrigeration produced versus cold head temperature for four test conditions. *Figure 63* shows the measured COP versus cold head temperature for three tests. *Figure 64* compares measured COP and Carnot COP versus cold head temperature. From this it can be seen that the Magnavox unit reaches a maximum of about 9 percent of Carnot efficiency at about -140 °C. It is also seen that the performance is better at 55 W than at either 70 W or at 50 W. This is consistent with Magnavox's literature. The Model MX-7043-10 is quoted as being a "55 W input" unit, and that is the power that they recommend for operation. It does indeed seem to be optimized at 55 W.

All results of this testing are presented in Ref 14.

2.2.4.2.2 Vapor Compression Cycle Refrigeration Demonstration Unit Activities

A vapor compression refrigerator/freezer unit was flown on an early Shuttle flight (STS-4), and later it was qualified for Space Lab flights. This unit was a modified, commercially available unit made by Amfridge Co. of Elkhart, Indiana. The description, tests, flight results, etc. for this unit were obtained from Refs 15 through 20. After studying this unit, it was decided to purchase one for our evaluation and test. An investigation of zero-g effects on vapor compression unit operation, condensation, evaporation, etc., was also performed. Some of the references used are listed in Appendix D, "Bibliography."

The Amfridge vapor compression (Freon) diaphragm-type compressor unit was set up in the lab and checked out for proper operation. This commercially available unit was later disassembled to examine its construction, valves, lubrication, etc. *Figures 65 through 69* show photos of the disassembled unit. The STS flight units were similar but with upgrades to the diaphragm compressor unit technology. A "delta CDR" on this unit was held at JSC in which technology was discussed related to reducing leak rates, various diaphragm materials tested, and modifications to cam bearings, along with many other details such as double containment and effects of refrigerant charge weight on system performance.

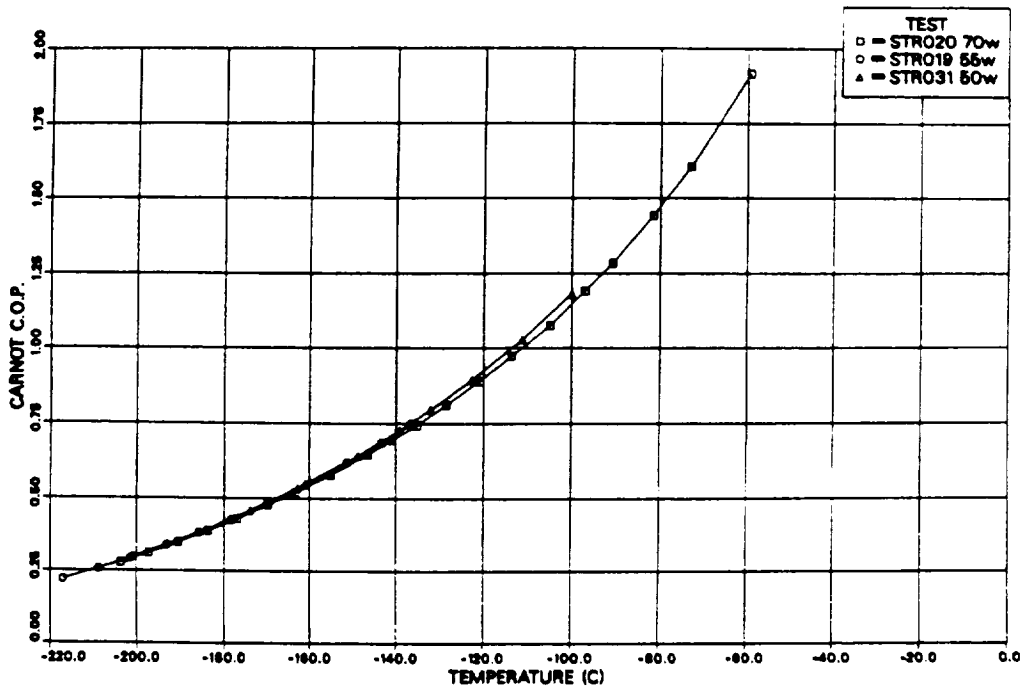

Figure 61. Carnot COP vs Cold Head Temperature for Each Operating Point During Three Stirling Unit Tests

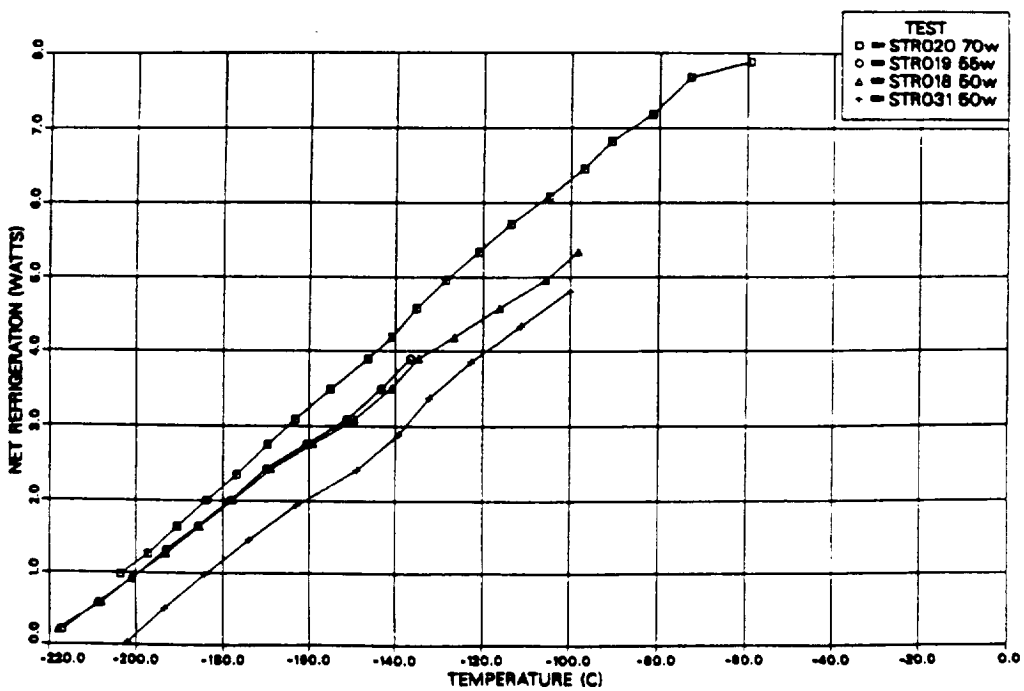

Figure 62. Typical Magnavox Model MX-7043-10 Stirling Unit Test Results for Input Power Levels of 70, 55, and 50 W

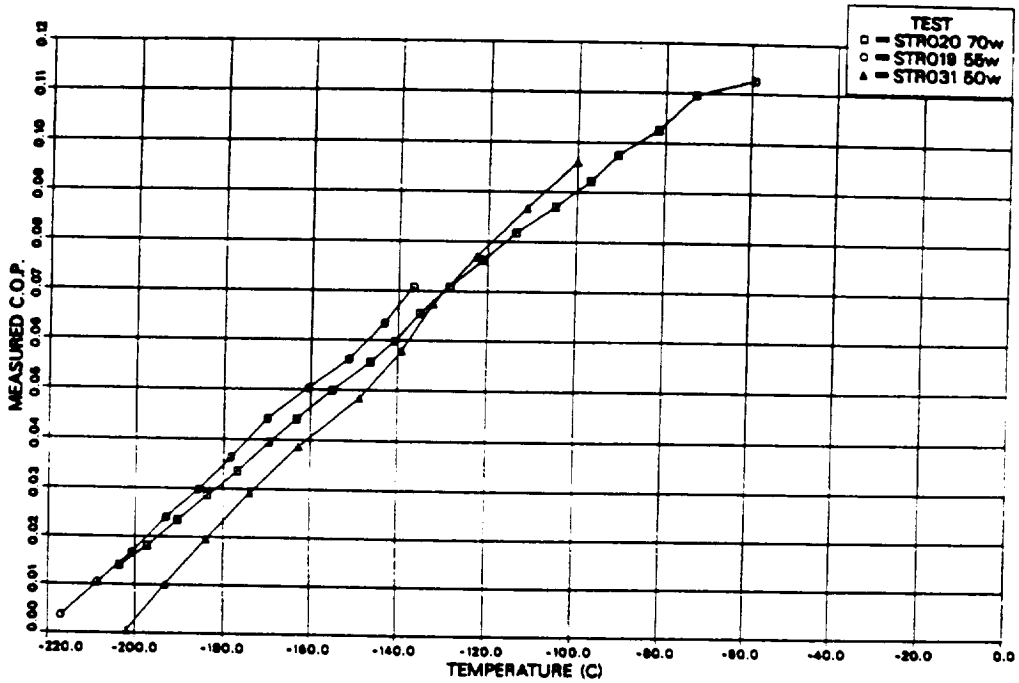

Figure 63. Measured COP for the Magnavox Model MX-7043-10 Stirling Unit for Input Power Levels of 70, 55, and 50 W

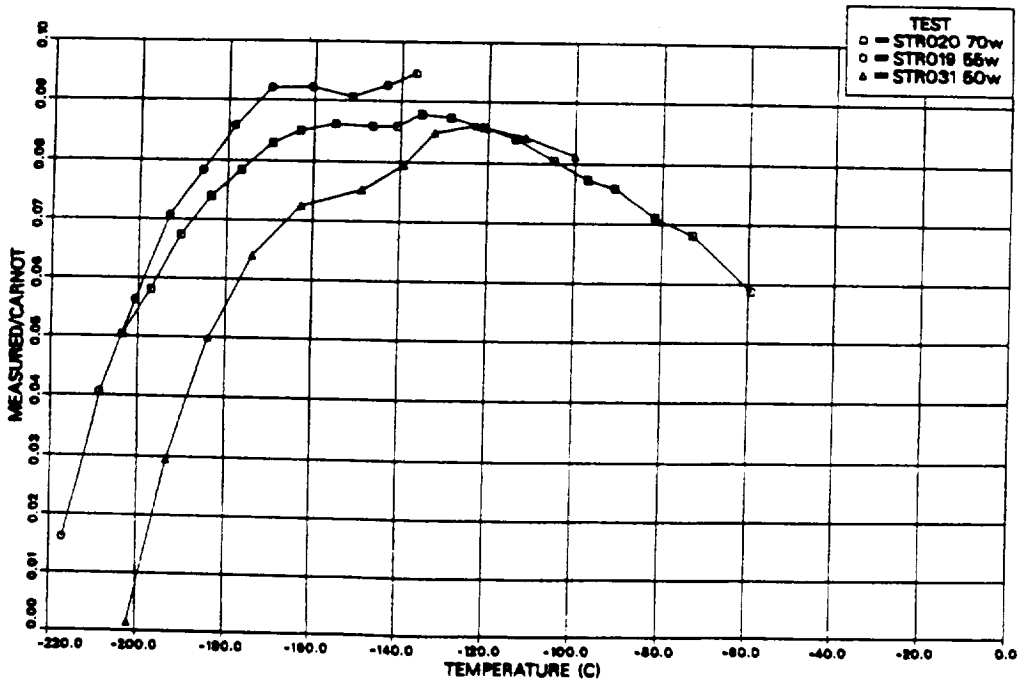

Figure 64. Ratio of Measured Carnot COP vs Cold Head Temperature for Input Power Levels of 70, 55, and 50 W for the Magnavox Model MX-7043-10 Stirling Unit

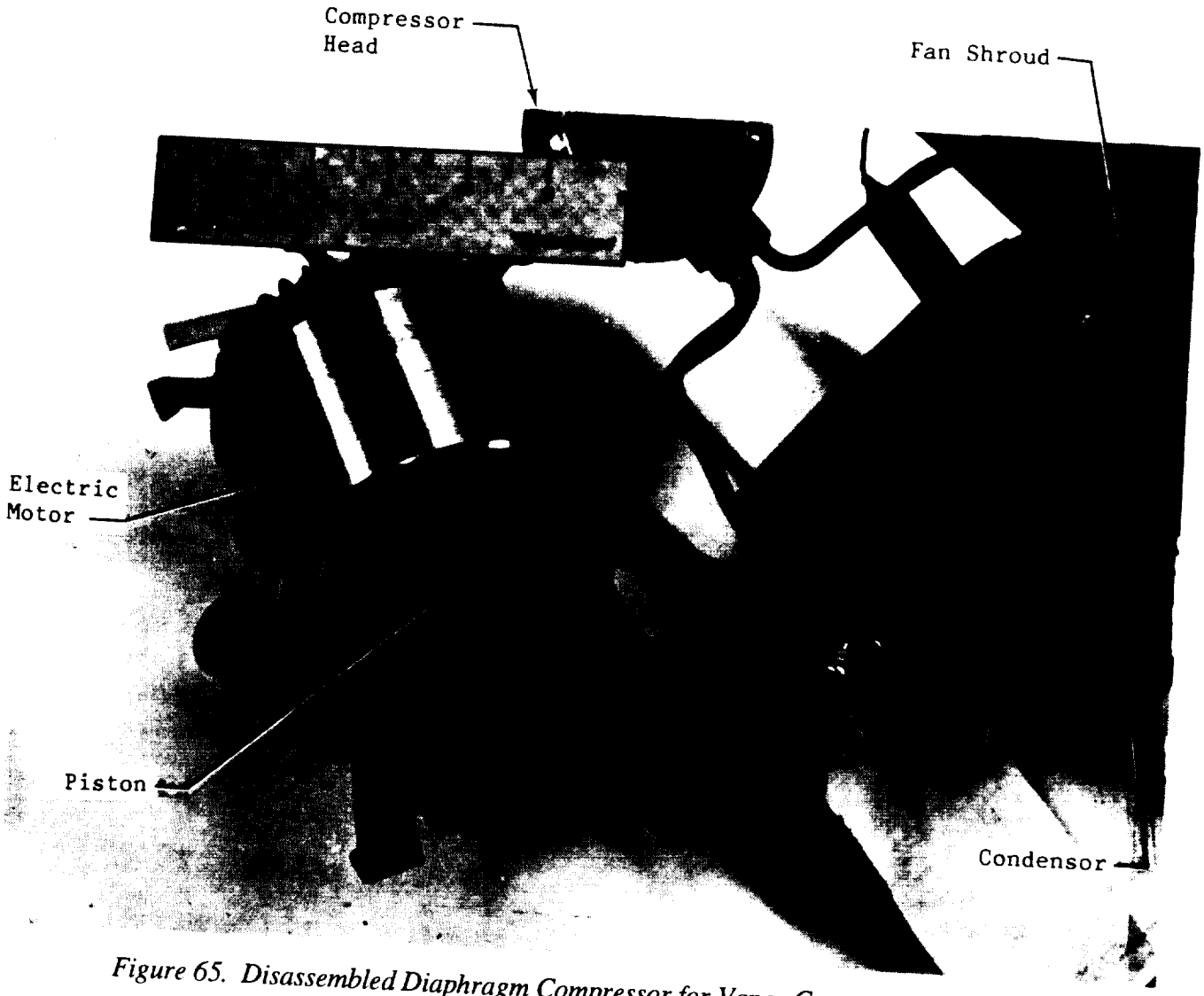

Figure 65. Disassembled Diaphragm Compressor for Vapor Compression Unit

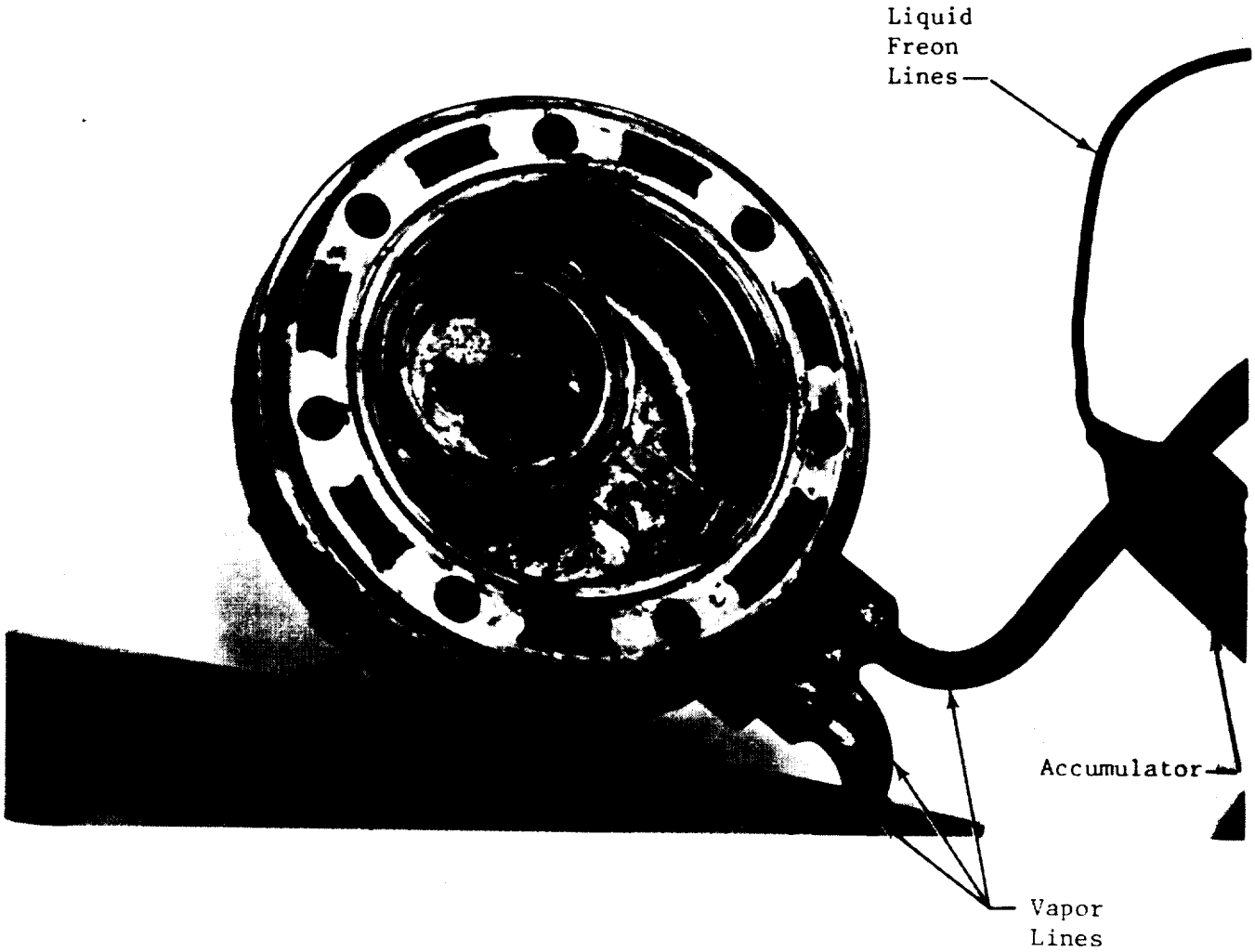

Figure 66. Inside View of Diaphragm Compressor Head-Vapor Compression Unit

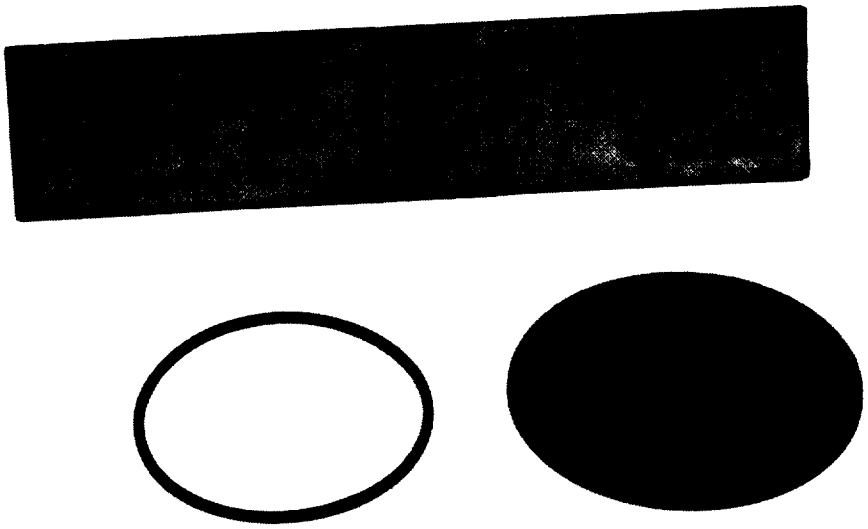

Figure 67. Diaphragm and O-Ring from Vapor Compression Unit

Figure 68. Intake and Exhaust (Reed) Valves from Vapor Compression Unit

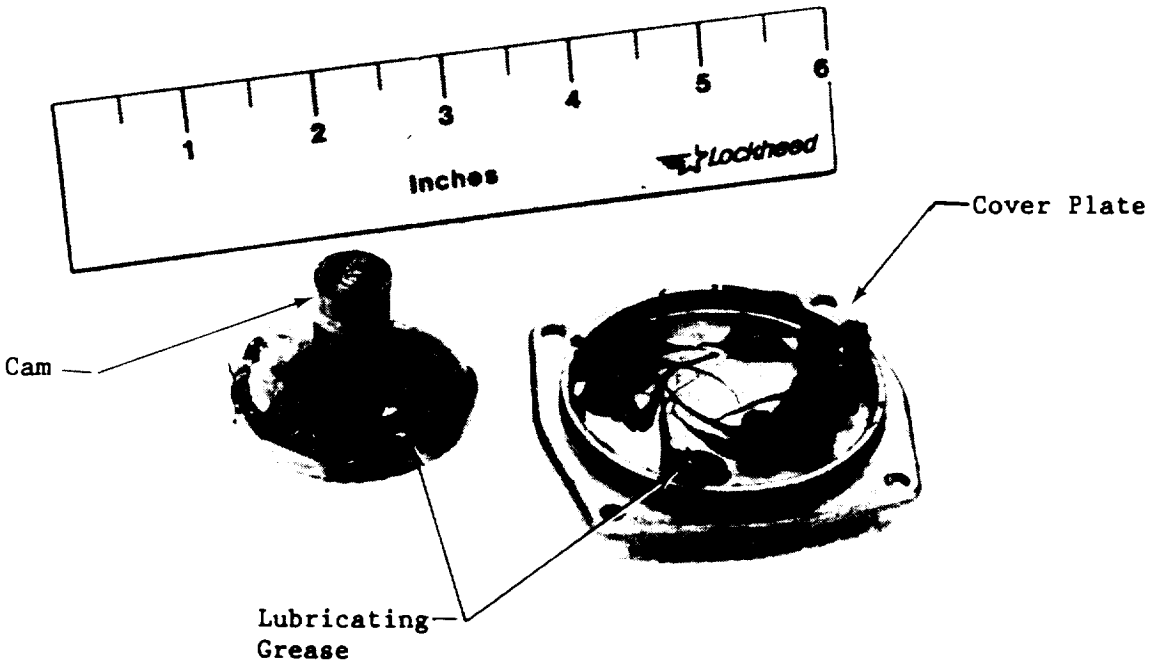

Figure 69. Cam Bearing from Vapor Compression Unit (Diaphragm Compressor)

As work progressed under this subtask, certain backup refrigerator/freezer compressor concept subtasks were identified and added as a contract modification towards the overall efort. These subtasks are listed below.

1. Define design requirements for refrigeration system.
2. Research various compression systems relative to zero-g.
3. Define lubrication concepts and proof of concept.
4. Design system relative to refrigerant phase separation in zero-g.
5. Complete preliminary design of a unit with component testing.

In order to begin testing with the lab demonstration unit, a commercially made cabinet (*Figure 70*) with an internal volume of approximately 5 ft^3 and a heat leak no greater than 100 W was purchased. It was constructed of stainless steel and could be modified to demonstrate operation in zero-g condition by installing a diaphragm freon compressor and an evaporator and condenser designed to operate at zero-g conditions. The diaphragm compressor was selected because it requires no oil in contact with the freon refrigerant; hence, no liquid/vapor separation device is required. Also, this compressor could operate at any orientation. The compressor required a maximum input of about 420 W. A schematic and functional block diagram are shown in *Figures 71 and 72*, respectively.

Analyses were performed to support the modified design. From Ref 19 it is shown that a vapor Reynolds number of at least 3,000 is required (at a quality of 0.2) for the evaporator and a vapor Reynolds number of greater than 15,000 is required for the condenser to operate properly in zero-g conditions. The Froud number, which is the ratio of momentum forces to gravity forces, needs to be large. These inputs were used to size the evaporator and condenser tubing diameters and lengths.

An analysis was also performed to determine which refrigerant to use in this application. The performances of R-12 and R-502 were calculated and compared. Three design operating points were analyzed for each refrigerant. These operating points are as follows:

1. Evaporator temperature = -20 °F
   Condenser temperature = 90 °F
2. Evaporator temperature = 20 °F
   Condenser temperature = 90 °F
3. Evaporator temperature = 35 °F
   Condenser temperature = 90 °F

A cooling load of 250 W (854 Btu/hr), a compressor efficiency of 50 percent, and 10° of superheat were assumed in all cases. All freon state properties were calculated for all locations in the loop as well as coefficients of performance (COPs) and the mass flow rates.

Figure 70. Insulated Cabinet to be Used for Zero-g Refrigeration Demonstration Unit

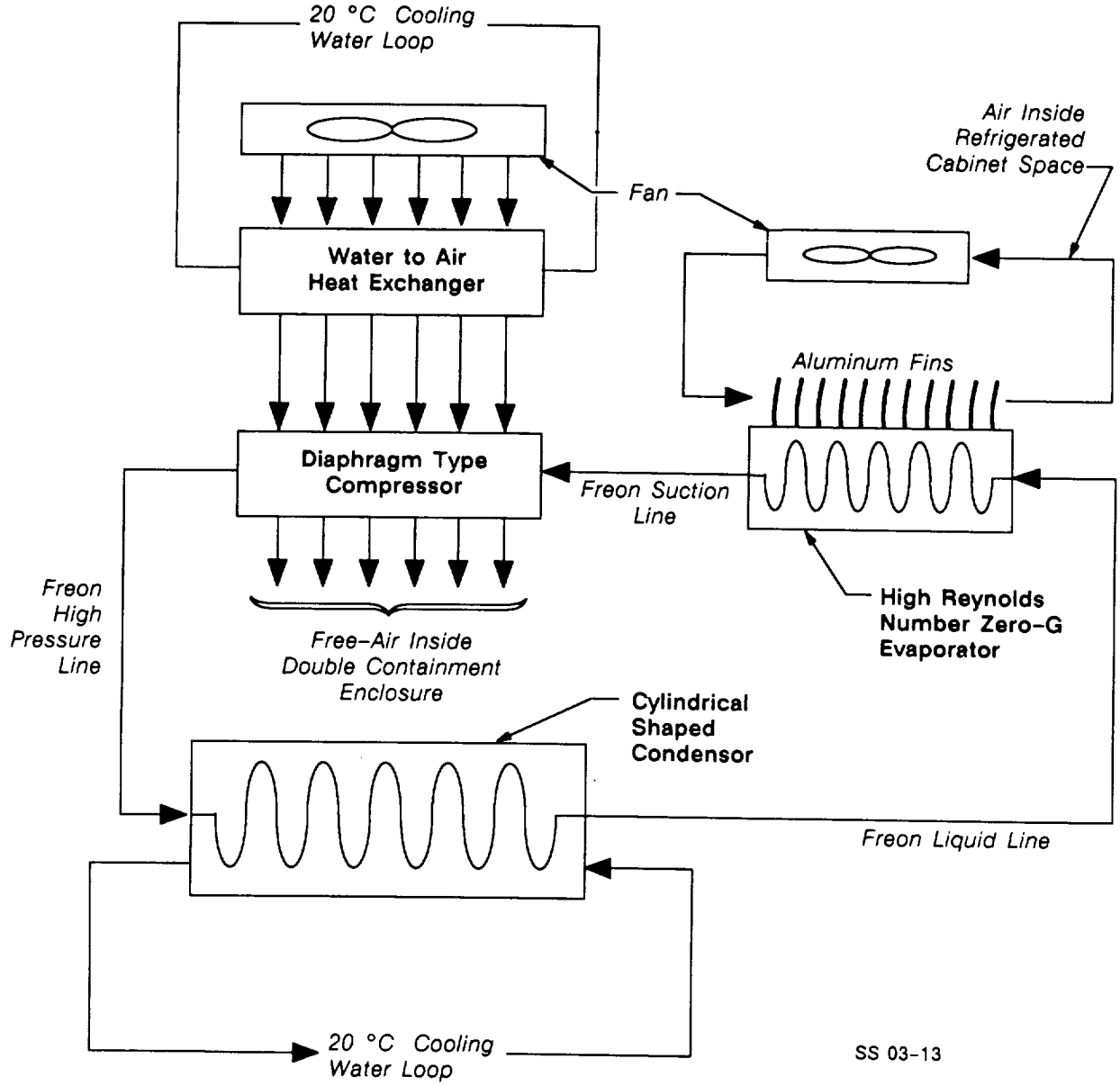

Figure 71. Schematic for Zero-g Vapor Compression Cycle Refrigeration Demonstration Unit

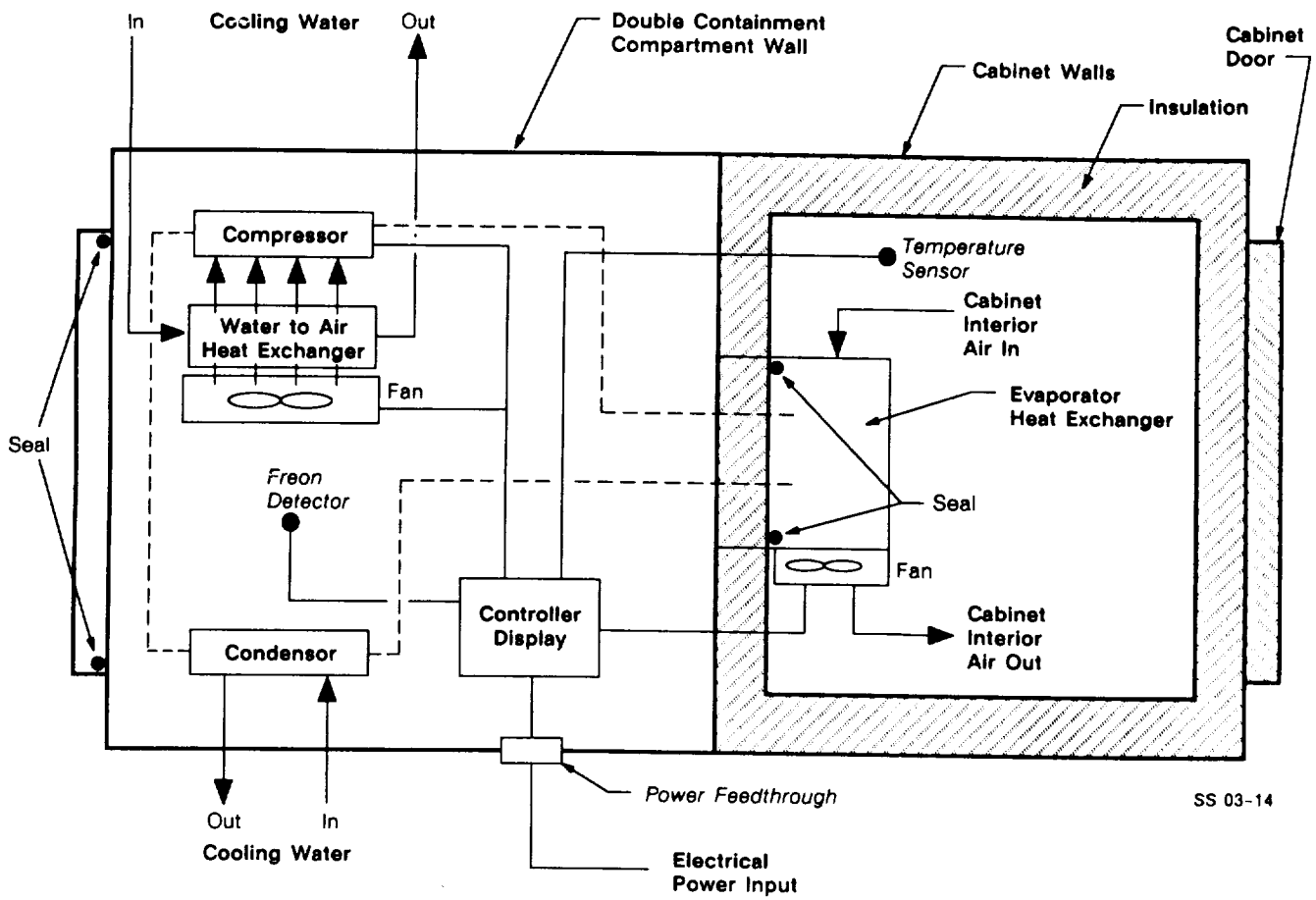

Figure 72. Functional Block Diagram for Zero-g Vapor Compression Cycle Refrigeration Demonstration Unit

The refrigeration COP is defined as

$$COP_{REFRIG} = \frac{\text{Heat Adsorbed}}{\text{Compressor Work}}$$

Also shown for reference purposes is the heat pump COP, defined as

$$COP_{H.P.} = \frac{\text{Heat Rejected + Compressor Work}}{\text{Compressor Work}}$$

The compressor efficiency is defined as

$$CE = \frac{\text{Ideal Energy to Compress}}{\text{Actual Energy to Compress}}$$

and commonly called the adiabatic efficiency.

The COP is not necessarily linear with compressor efficiency because the Cp is not constant with temperature; hence, the enthalpy versus temperature curve is not linear.

Both compressor shaft input power and motor input power were also calculated. A motor efficiency of 70 percent was assumed. This motor efficiency is typical of small electric motors; however, special "high energy efficiency" motors, such as brushless DC or special AC squirrel cage motors, may achieve 80 to 82 percent efficiency.

Results for each case are shown in *Tables 1 through 6*. A summary of results is shown in *Table 7*. From these results it appears that R-12 is better from a performance standpoint. Its COPs are higher, and it operates at lower evaporator and condenser pressures. However, its mass flow rate is lower, which will affect the Reynolds number in the evaporator/condenser, which needs to be kept high. The evaporator Reynolds number needs to be at least 3,000 (at a quality of 0.2) and the condenser Reynolds number needs to be at least 15,000 for proper zero-g operation.

Table 1. Refrigeration Cycle for R-12 with Evaporator Temp. = -20 °F, Condenser Temp.= 90 °F

REFRIGERATION CYCLE ANALYSIS - R12	CONDENSER (114.49 psia)		EVAPORATOR (15.17 psia)		COMPRESSOR
	INLET	OUTLET	INLET	OUTLET	INLET
TEMPERATURE (deg.F)	214.15	90.00	-20.00	-20.00	-10.00
VOLUME (cu.ft/lbm)	0.48	.01249	0.81	2.463	2.509
ENTHALPY (Btu/lbm)	107.66	28.77	27.39	75.11	75.49
ENTROPY (Btu/lbm-deg.F)	0.1990	0.0592	0.0625	0.1711	0.1742

CYCLE PERFORMANCE

COMPRESSOR EFFICIENCY (%) = 50
DEGREES SUPERHEAT (deg.F) = 10
REFRIGERATION C.O.P.= 1.53
HEAT PUMP C.O.P.= 2.53

LOAD AND POWER REQUIREMENTS

COOLING LOAD (Btu/hr) = 854
HEATING LOAD (Btu/hr) = 1411
MASS FLOW RATE (lbm/hr) = 17.596
COMPRESSOR POWER (kW) = .16

Table 2. Refrigeration Cycle for R-12 with Evaporator Temp. = 20 °F, Condenser Temp.= 90 °F

REFRIGERATION CYCLE ANALYSIS - R12	CONDENSER (114.49 psia)		EVAPORATOR (35.74 psia)		COMPRESSOR
	INLET	OUTLET	INLET	OUTLET	INLET
TEMPERATURE (deg.F)	162.77	90.00	20.00	20.00	30.00
VOLUME (cu.ft/lbm)	0.43	.01248	0.25	1.099	1.123
ENTHALPY (Btu/lbm)	98.84	28.77	27.27	74.34	82.92
ENTROPY (Btu/lbm-deg.F	0.1855	0.0593	0.0686	0.1672	0.1704

CYCLE PERFORMANCE

COMPRESSOR EFFICIENCY (%) = 50
DEGREES SUPERHEAT (deg.F) = 10
REFRIGERATION C.O.P.= 2.42
HEAT PUMP C.O.P.= 3.90

LOAD AND POWER REQUIREMENTS

COOLING LOAD (Btu/hr) = 854
HEATING LOAD (Btu/hr) = 1149
MASS FLOW RATE (lbm/hr) = 15.382
COMPRESSOR POWER (kW) =

ORIGINAL PAGE IS
OF POOR QUALITY

Table 3. Refrigeration Cycle for R-12 with Evaporator Temp. = 35 °F, Condenser Temp.= 90 °F

REFRIGERATION CYCLE ANALYSIS - R12	CONDENSER (114.49 psia) INLET	CONDENSER (114.49 psia) OUTLET	EVAPORATOR (47.26 psia) INLET	EVAPORATOR (47.26 psia) OUTLET	COMPRESSOR INLET
TEMPERATURE (deg.F)	146.86	90.00	35.00	35.00	45.00
VOLUME (cu.ft/lbm)	0.42	.01243	0.15	0.843	0.866
ENTHALPY (Btu/lbm)	96.17	28.77	27.22	80.95	82.50
ENTROPY (Btu/lbm-deg.F)	0.1811	0.0593	0.0577	0.1663	0.1694

CYCLE PERFORMANCE

COMPRESSOR EFFICIENCY (%) = 50
DEGREES SUPERHEAT (deg.F) = 10
REFRIGERATION C.O.P.= 3.93
HEAT PUMP C.O.P.= 4.93

LOAD AND POWER REQUIREMENTS

COOLING LOAD (Btu/hr) = 854
HEATING LOAD (Btu/hr) = 1071
MASS FLOW RATE (lbm/hr) = 15.195
COMPRESSOR POWER (kW) = .06

Table 4. Refrigeration Cycle for R-502 with Evaporator Temp. = -20 °F, Condenser Temp.= 90 °F

REFRIGERATION CYCLE ANALYSIS - R502	CONDENSER (202.06 psia) INLET	CONDENSER (202.06 psia) OUTLET	EVAPORATOR (30.01 psia) INLET	EVAPORATOR (30.01 psia) OUTLET	COMPRESSOR INLET
TEMPERATURE (deg.F)	195.24	90.00	-20.00	-20.00	-10.00
VOLUME (cu.ft/lbm)	0.27	.01356	0.52	1.317	1.354
ENTHALPY (Btu/lbm)	107.75	34.72	33.15	75.54	77.14
ENTROPY (Btu/lbm-deg.F)	0.2203	0.0707	0.0754	0.1722	0.1755

CYCLE PERFORMANCE

COMPRESSOR EFFICIENCY (%) = 50
DEGREES SUPERHEAT (deg.F) = 10
REFRIGERATION C.O.P.= 1.39
HEAT PUMP C.O.P.= 2.39

LOAD AND POWER REQUIREMENTS

COOLING LOAD (Btu/hr) = 854
HEATING LOAD (Btu/hr) = 1,2[illegible]
MASS FLOW RATE (lbm/hr) = 20.124
COMPRESSOR POWER (kW) = .18

ORIGINAL PAGE IS
OF POOR QUALITY

Table 5. Refrigeration Cycle for R-502 with Evaporator Temp. = 20 °F, Condenser Temp.= 90 °F

REFRIGERATION CYCLE ANALYSIS - R502	CONDENSER (202.06 psia) INLET	CONDENSER (202.06 psia) OUTLET	EVAPORATOR (57.16 psia) INLET	EVAPORATOR (57.16 psia) OUTLET	COMPRESSOR INLET
TEMPERATURE (deg.F)	152.59	90.00	20.00	20.00	30.00
VOLUME (cu.ft/lbm)	0.25	.01356	0.18	0.609	0.627
ENTHALPY (Btu/lbm)	99.21	34.70	32.99	79.98	81.69
ENTROPY (Btu/lbm-deg.F)	0.1868	0.0707	0.0705	0.1635	0.1720

CYCLE PERFORMANCE

COMPRESSOR EFFICIENCY (%) = 50
DEGREES SUPERHEAT (deg.F) = 10
REFRIGERATION C.O.P.= 3.68
HEAT PUMP C.O.P.= 3.68

LOAD AND POWER REQUIREMENTS

COOLING LOAD (Btu/hr) = 354
HEATING LOAD (Btu/hr) = 1173
MASS FLOW RATE (lbm/hr) = 18.177
COMPRESSOR POWER (kW) =

Table 6. Refrigeration Cycle for R-502 with Evaporator Temp. = 35 °F, Condenser Temp.= 90 °F

REFRIGERATION CYCLE ANALYSIS - R502	CONDENSER (202.06 psia) INLET	CONDENSER (202.06 psia) OUTLET	EVAPORATOR (87.52 psia) INLET	EVAPORATOR (87.52 psia) OUTLET	COMPRESSOR INLET
TEMPERATURE (deg.F)	139.35	90.00	35.00	35.00	45.00
VOLUME (cu.ft/lbm)	0.24	.01356	0.11	0.469	0.485
ENTHALPY (Btu/lbm)	96.52	34.70	33.90	81.50	83.03
ENTROPY (Btu/lbm-deg.F)	0.1824	0.0707	0.0693	0.1675	0.1710

CYCLE PERFORMANCE

COMPRESSOR EFFICIENCY (%) = 50
DEGREES SUPERHEAT (deg.F) = 10
REFRIGERATION C.O.P.= 3.67
HEAT PUMP C.O.P.= 4.67

LOAD AND POWER REQUIREMENTS

COOLING LOAD (Btu/hr) = 354
HEATING LOAD (Btu/hr) = 1653
MASS FLOW RATE (lbm/hr) = 17.579
COMPRESSOR POWER (kW) = .07

ORIGINAL PAGE IS
OF POOR QUALITY

Table 7. Comparison of Performance and Design Parameters for Refrigerants R-12 and R-502

	Case	R-12	R-502
1	Evaporator Temperature = -20 °F		
	Condenser Temperature = 90°F		
	Evaporator Pressure (psia)	15.27	30.01
	Condenser Pressure (psia)	114.49	202.06
	Mass Flow Rate (lbm/hr)	17.89	20.12
	Compressor Power (W)	163.4	179.8
	Motor Input Power (W)	233.4	256.8
	C.O.P. Based on Compressor Power	1.53	1.39
	C.O.P. Based on Motor Input Power	1.06	0.96
2	Evaporator Temperature = +20 °F		
	Condenser Temperature = 90 °F		
	Evaporator Pressure (psia)	35.74	67.16
	Condenser Pressure (psia)	114.49	202.06
	Mass Flow Rate (lbm/hr)	16.38	18.18
	Compressor Power (W)	86.2	93.3
	Motor Input Power (W)	123.1	233.3
	C.O.P. Based on Compressor Power	2.90	2.68
	C.O.P. Based on Motor Input Power	1.96	1.86
3	Evaporator Temperature = +35 °F		
	Condenser Temperature = 90 °F		
	Evaporator Pressure (psia)	47.26	87.52
	Condenser Pressure (psia)	114.49	202.06
	Mass Flow Rate (lbm/hr)	15.89	17.58
	Compressor Power (W)	63.6	68.1
	Motor Input Power (W)	90.8	97.3
	C.O.P. Based on Compressor Power	3.93	3.67
	C.O.P. Based on Motor Input Power	2.74	2.56

Using the condenser inlet conditions for the worst case (i.e., -20 °F evaporator) and the corresponding mass flow rate of 17.9 lbm/hr for R-12, and a minimum required Reynolds number of 15,000, a maximum condenser tube ID of 0.42 in. was calculated. Assuming a 0.25-in. diameter tube ID yields a Reynolds number of 25,300, which allows a good margin. Therefore, 0.25 was chosen as the condenser tubing ID.

Using the evaporator outlet conditions (at -20 °F) and the vapor mass flow rate of 3.18 (i.e., 15.9 with a quality of 0.2), and a minimum Reynolds number of 3,000, a maximum tubing ID of

0.0187 was calculated. If a tubing ID of 0.015 is used, a Reynolds number of 3,740 is obtained, which gives a reasonable margin.

A design effort was undertaken to integrate the compressor and the cabinet. Plans included locating the compressor under the cabinet with the evaporator and its fan located in the bottom (floor) of the cabinet. The fin areas required and the fan CFM to transfer the heat from the evaporator directly into the air inside the cabinet were determined. The evaporator tubing was bonded directly to the bottom side of the finned bottom plate. No evaporator (freon) tubing penetrated the cabinet walls. Heat was transferred by conduction from the fins/plate into the evaporator tubing. The compressor, evaporator, and condensor were doubly contained in an enclosure at the bottom of the unit where an access panel was provided for repairs, installation, etc. The condensor was water-cooled and the motor and compressor were air-cooled by a fan (see *Figures 71 and 72*).

As work continued on the sizing and design of the freon evaporator and the zero-g condensor, the design concept was changed. Initially, as discussed above, the concept was to use a small diameter, long length, high Reynolds number design. In this design concept it was necessary to ensure highly turbulent flow in zero-g to maintain contact between the liquid freon and the inner walls of the tubing. The objective was to prevent vapor lock where a layer of vapor forms on the inner walls of the tube, thus isolating the liquid stream from the tube walls and reducing the heat transfer rate. The problem with this high Reynolds number concept is the high pressure drop.

The revised concept used a spiral-wrapped tubing design and R-502 refrigerant. In this design, liquid is forced to remain in contact with the tube walls by centrifugal force. If the liquid velocity is kept high enough to produce a tangential acceleration equal to or greater than one g, then the standard Earth-based heat transfer calculation techniques can be applied directly to the zero-g design.

The zero-g condenser design for the vapor compression refrigerator/freezer demonstration unit was also based on use of centrifugal flow pattern to maintain contact between the freon and the inner tubing walls. Here the freon and water tubes were wrapped side by side around a copper cylinder 7 1/4 in. in diameter and 4 1/3 in. long.

An analysis was performed to determine the details of this design. The groundrules for this analysis were as follows:

Evaporator temperature = -30 °F
Condenser temperature = 60 °F
Heat load at -30 °F = 650 Btu/hr (190 W)
Condenser cooling water inlet temp. = 50 °F
Refrigerant = R - 502.

The freon loop was divided into two circuits. This provides redundancy for increased reliability. The diaphragm compressor purchased earlier has two separate cylinders and pistons which make it readily adaptable to this two loop design. The total freon flow rate for both loops is 13 lb/hr.

The following detailed results were obtained from the analysis:

- Evaporator tube length: 24 ft (each loop)
- Evaporator freon tube o.d. = 1/4 in.
- Evaporator freon tube wall thickness = 0.035 in.
- Evaporator freon tube material = copper
- Evaporator water tube length = 24 ft (each loop)
- Evaporator water tube o.d. = 1/4 in.
- Evaporator water tube wall thickness = 0.035 in.
- Evaporator water tube material = copper
- Condenser freon tube length = 12 ft (each loop)
- Condenser freon tube o.d. = 1/4 in.
- Condenser freon tube wall thickness = 0.035 in.
- Condenser freon tube material = copper
- Condenser water tube length = 12 ft (each loop)
- Condenser water tube o.d. = 1/4 in.
- Condenser water tube wall thickness = 0.035 in.
- Condenser water tube material = copper
- Compressor outlet temperature = 161.4 °F
- Compressor outlet pressure = 131.1 psi
- Condenser outlet temperature = 60 °F
- Condenser outlet pressure - 130.1 psi
- Evaporator inlet temperature = -30 °F
- Evaporator inlet temperature = 23.9 psi
- Evaporator outlet temperature = -21.6 °F
- Evaporator outlet pressure = 21.6 psi
- Evaporator inlet quality = 0.326
- Evaporator outlet quality = 1.0
- Degrees of superheat = 10 °F
- Evaporator fin spacing = 4 per inch
- Evaporator fin height = 0.5 in.
- Evaporator fin material = copper
- Evaporator projected area = 15 x 15 in.
- Condenser tube bundle diameter = 7 1/4 in.
- Condenser tube bundle length = 4 1/2 in.

It was also decided to cool the compressor and motor within the double containment compartment using the existing compressor/motor fan. The air moved by this fan was in turn cooled by an existing fin tube heat exchanger that came with the diaphragm compressor unit shown in photos of *Figures 73 and 74.*

Fabrication was begun on the zero-g condenser and evaporator. *Figure 75* shows the condenser coil wrapped around and partially bonded to the 1/4 in. thick aluminum cylinder. *Figure 76* shows this same condenser as it is being taken out of the vacuum bag used during a partial bonding. *Figures 77 and 78* show the condenser after final bonding. *Figure 79* shows the condenser during the process of adding BX-402 foam insulation, and *Figure 80* shows the completed condenser with insulation, ready for installation in the refrigeration unit. *Figure 81* shows the condenser and compressor being fit-checked in the refrigeration unit.

The evaporator construction is illustrated starting with *Figure 82*, which shows the copper coils. Two parallel coils are being used, one for each freon loop. The evaporator coil is being bonded to the fin plate in *Figure 83. Figure 84* shows the evaporator coil partially bonded to the fin plate with the outer seal spacers welded in place around the outer edges. The evaporator fan is shown in *Figure 85*, and *Figure 86* shows the evaporator fin plate, coil, and fin after further assembly.

The next step was to assemble all of these hardware components of the zero-g vapor compression refrigerator /freezer demonstration unit and prepare it for testing. *Figure 87* shows the schematic for the unit. As seen from this figure, there are two separate, independent freon loops driven by two separate compressors. This arrangement provides redundancy in the design. These two compressors are diametrically opposed and are driven by a single 12 Vdc electric motor. There is a single cooling water loop which cools the compressor compartment air, which is in turn blown over the compressors and motor. Heat is transferred from the internal freezer air to the two freon loops in the evaporator via fins and a squirrel cage blower inside the freezer. The evaporator shown in *Figure 82* is designed with a flat spiral loop to provide operation in zero-g conditions, i.e., centrifugal force provides the acceleration level to replace gravity effects. The evaporator tubes are mounted in the bottom of the freezer, and a second level of containment is provided by a seal between the evaporator plate and the bottom/inside of the freezer. Any freon leak in the evaporator tubing or fittings would be vented into the sealed compressor compartment below the cold box volume.

Heat is transferred from the freon into the cooling water in the condenser. This condenser is constructed with a helical loop design in order to perform in zero-g, with centrifugal force providing the acceleration level to replace gravity effects (see *Figure 75*). The second level of containment for any leaks from the condenser, compressor, or other freon lines is also within the sealed compressor compartment underneath the cold box.

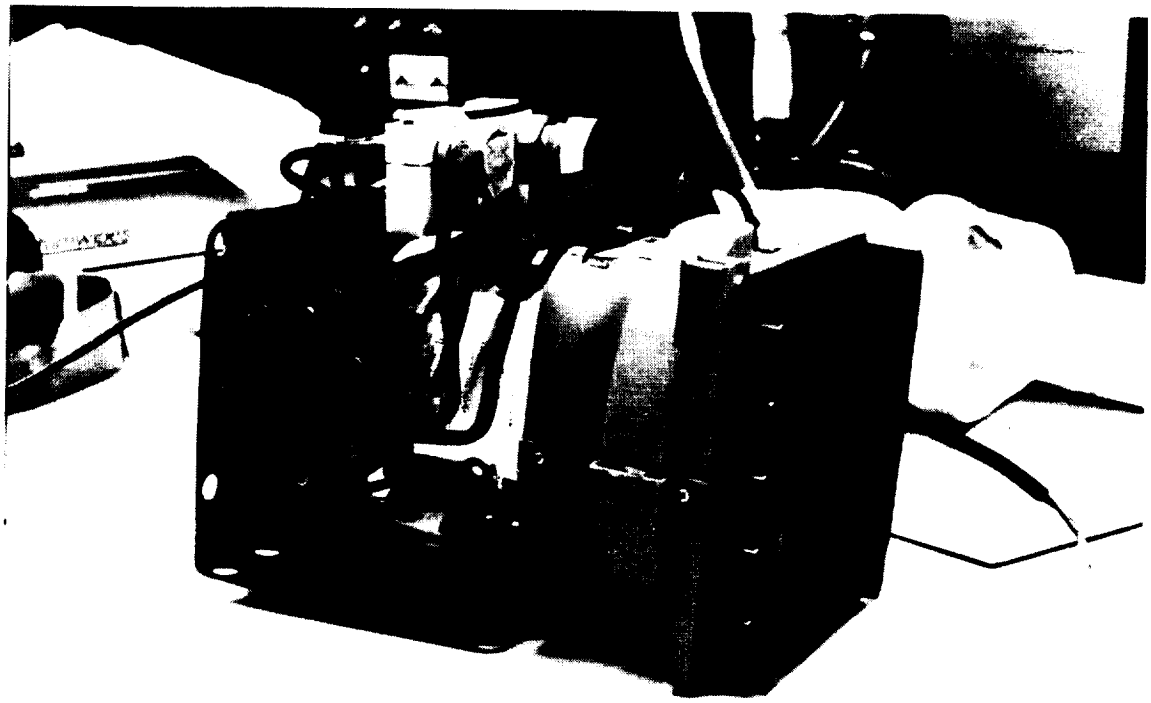

Figure 73. Diaphragm Compressor to be Used in the Zero-g Vapor Compression Cycle Demonstration Unit (with Existing Condenser and Shroud in Place)

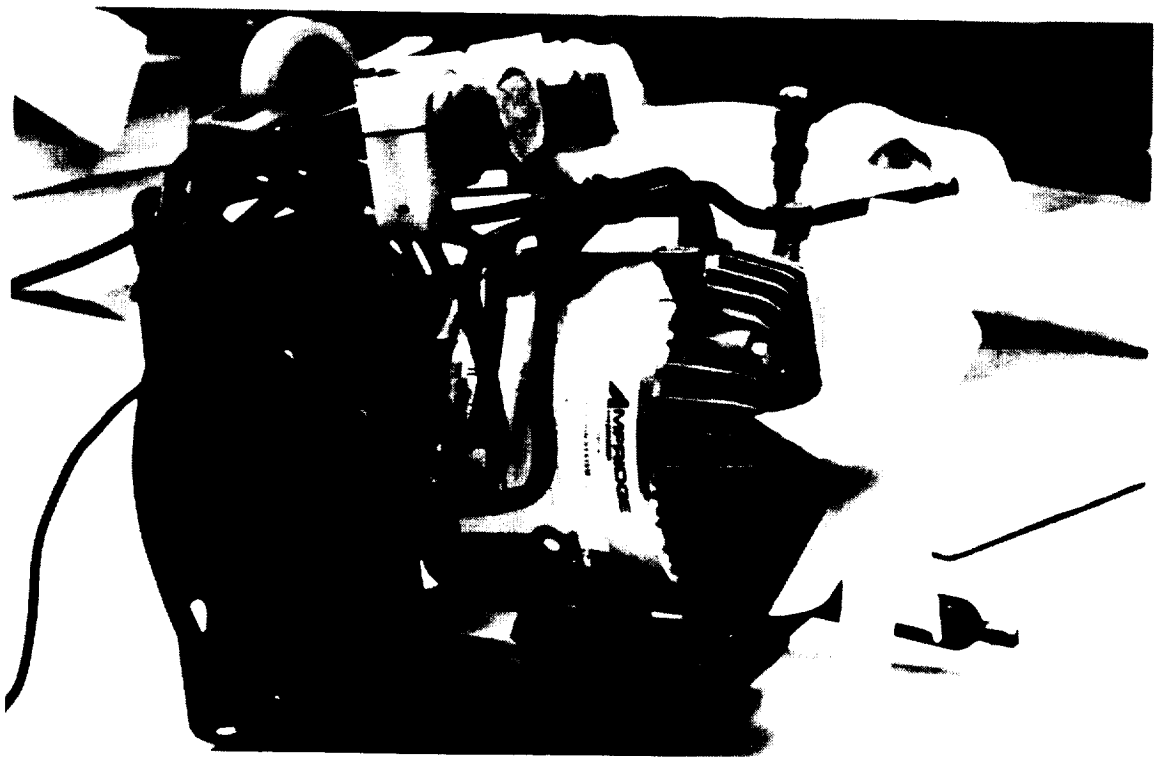

Figure 74. Diaphragm Compressor to be Used in the Zero-g Vapor Compression Cycle Demonstration Unit (after Removal of Condenser Shroud)

ORIGINAL PAGE
BLACK AND WHITE PHOTOGRAPH

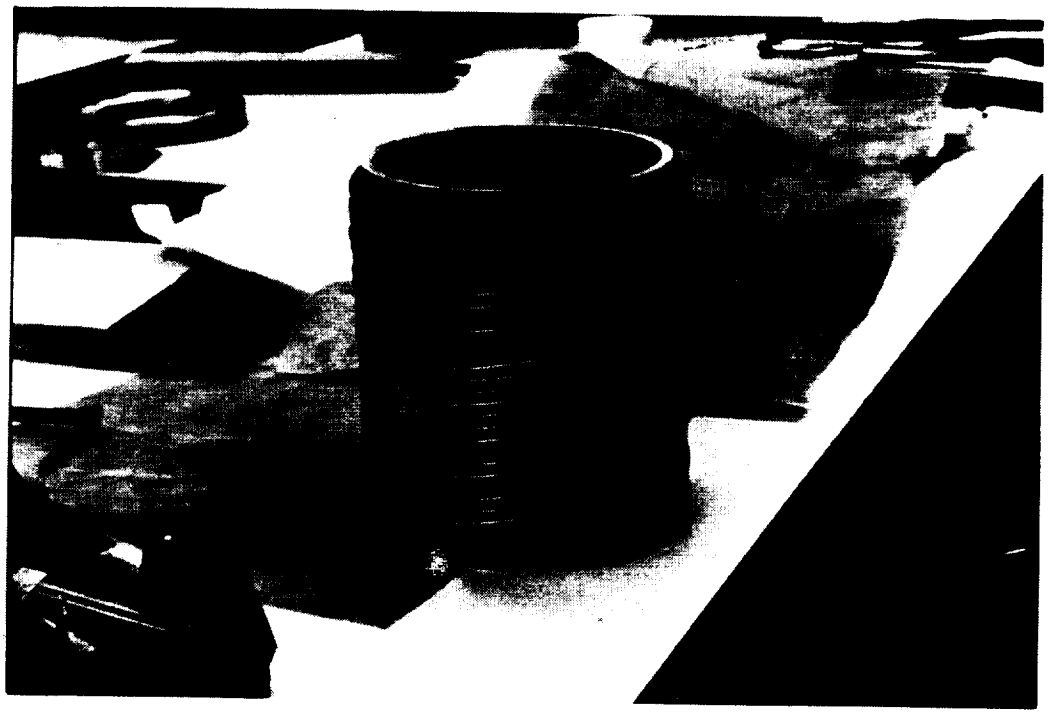

Figure 75. Zero-g Vapor Compressor Freezer Demonstration Unit Condenser During Construction, Before Preliminary Bonding

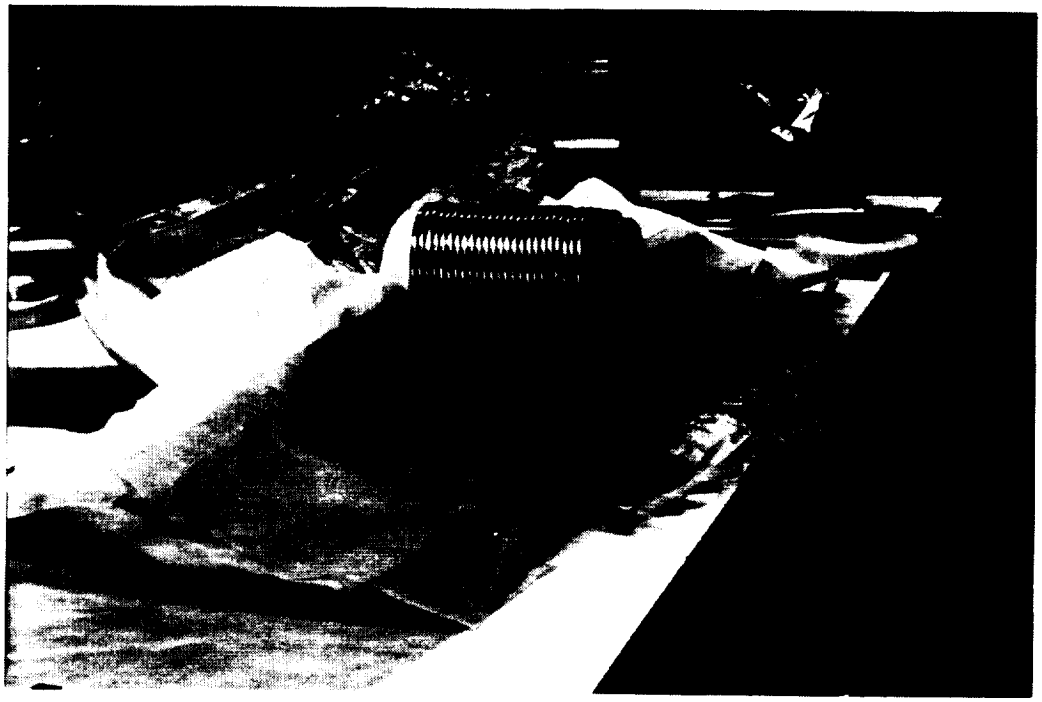

Figure 76. Zero-g Vapor Compressor Freezer Demonstration Unit Condenser During Construction, After Preliminary Bonding

ORIGINAL PAGE
BLACK AND WHITE PHOTOGRAPH

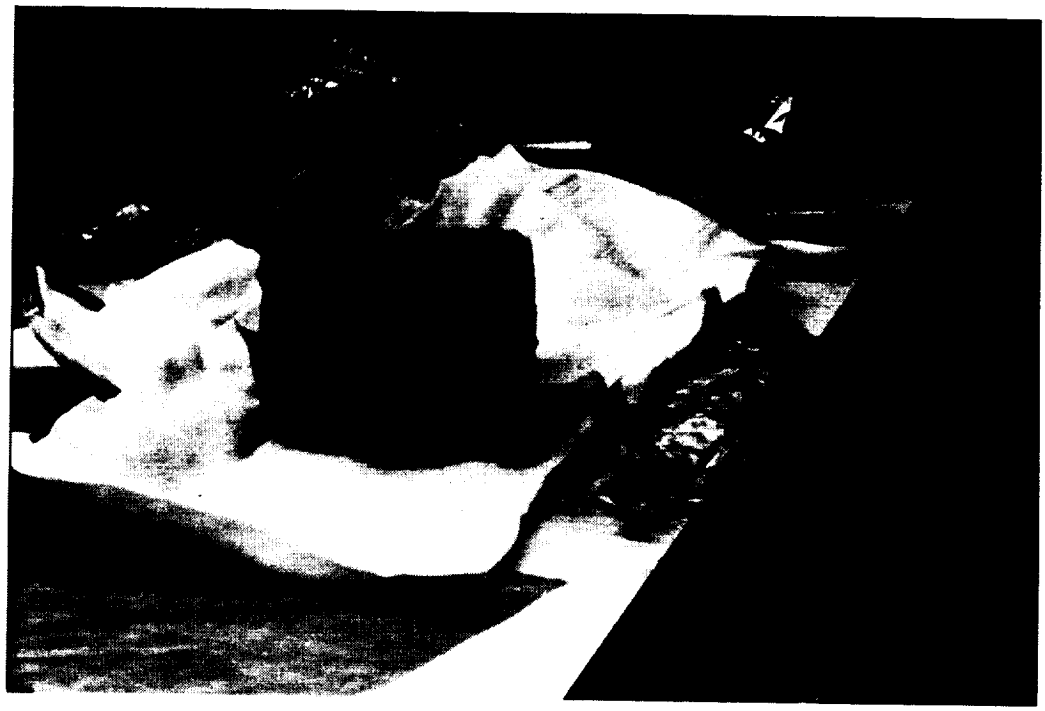

Figure 77. Zero-g Vapor Compressor Freezer Demonstration Unit Condenser During Construction, Before Final Bonding

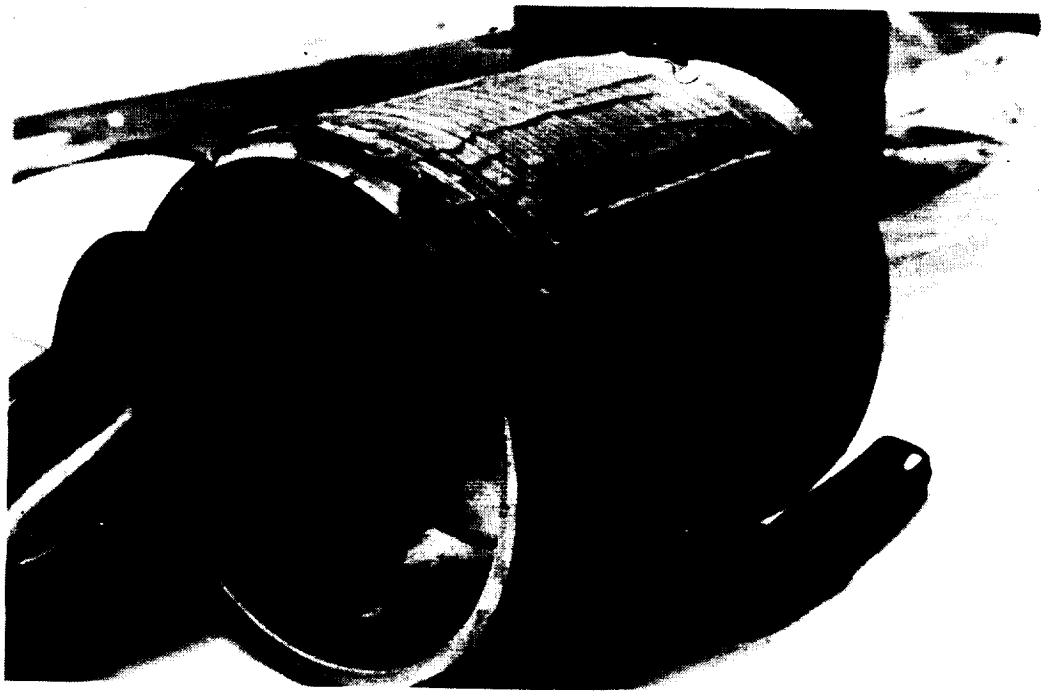

Figure 78. Zero-g Vapor Compressor Freezer Demonstration Unit Condenser During Construction, After Final Bonding

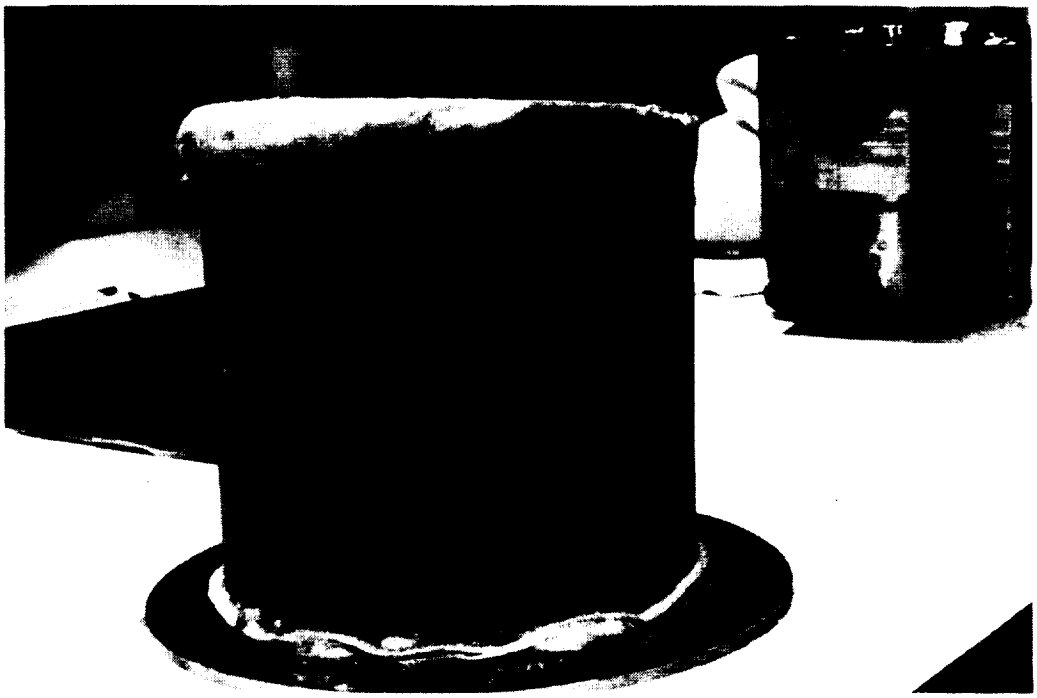

Figure 79. Zero-g Vapor Compressor Freezer Demonstration Unit Condenser During Construction, BX-402 Foam Being Added

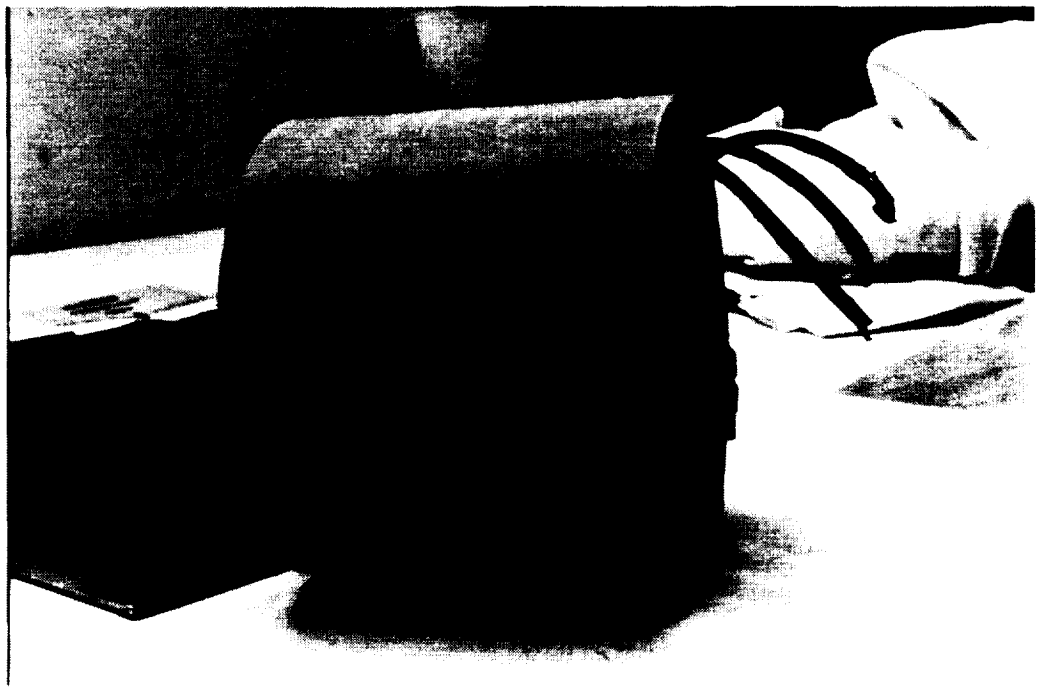

Figure 80. Zero-g Vapor Compressor Freezer Demonstration Unit Condenser, Construction Completed

ORIGINAL PAGE
BLACK AND WHITE PHOTOGRAPH

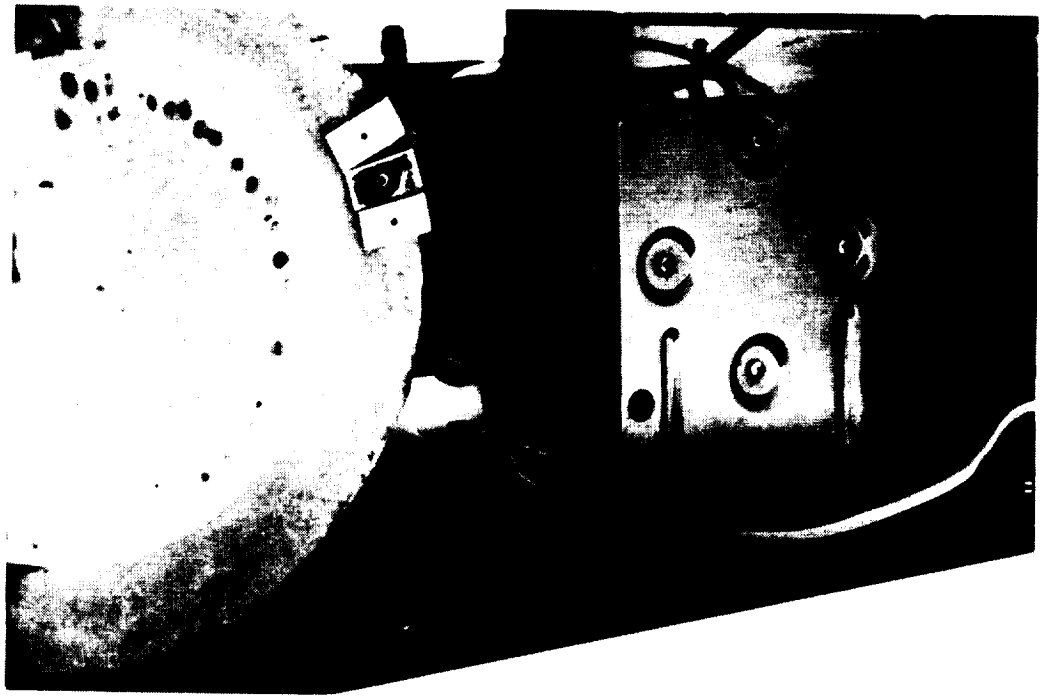

Figure 81. Zero-g Vapor Compressor Freezer Demonstration Unit Condenser, Installed in Refrigeration Unit

Figure 82. Zero-g Vapor Compressor Freezer Demonstration Unit Evaporator Under Construction, Double Coil

ORIGINAL PAGE
BLACK AND WHITE PHOTOGRAPH

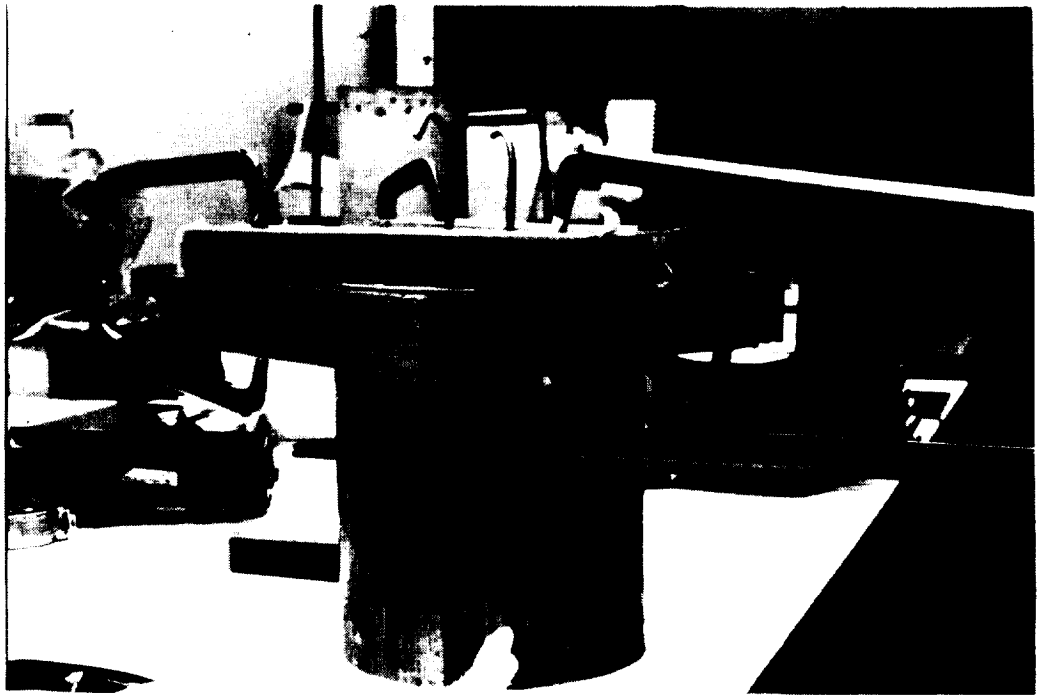

Figure 83. Zero-g Vapor Compressor Freezer Demonstration Unit Evaporator Under Construction, Preliminary Bonding

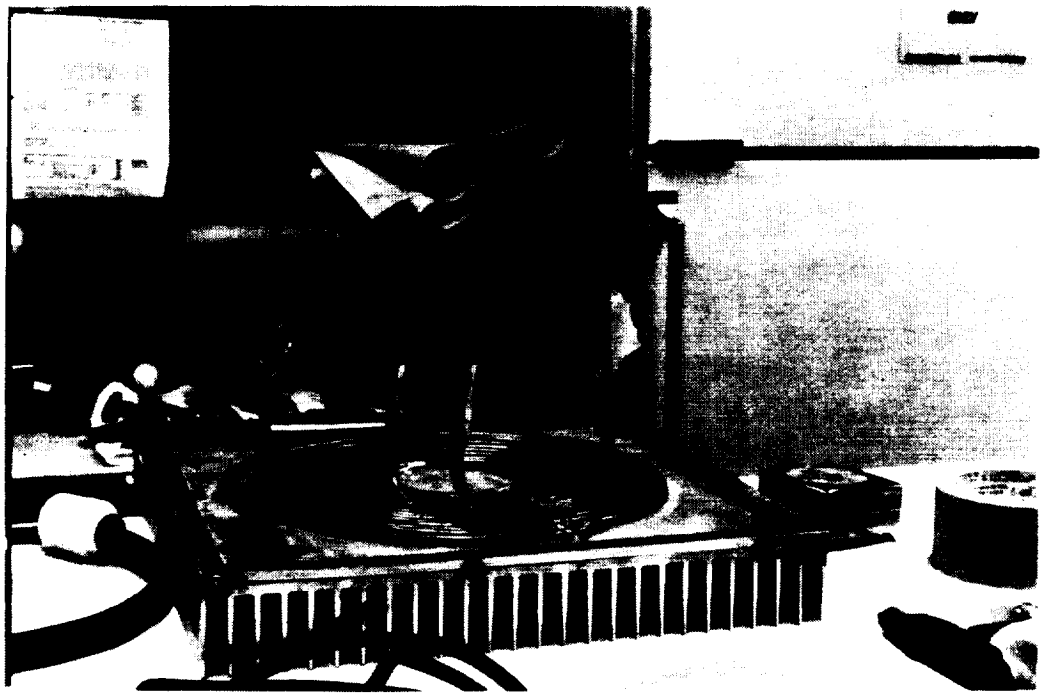

Figure 84. Zero-g Vapor Compressor Freezer Demonstration Unit Evaporator Under Construction, Bonded to Evaporator Fins

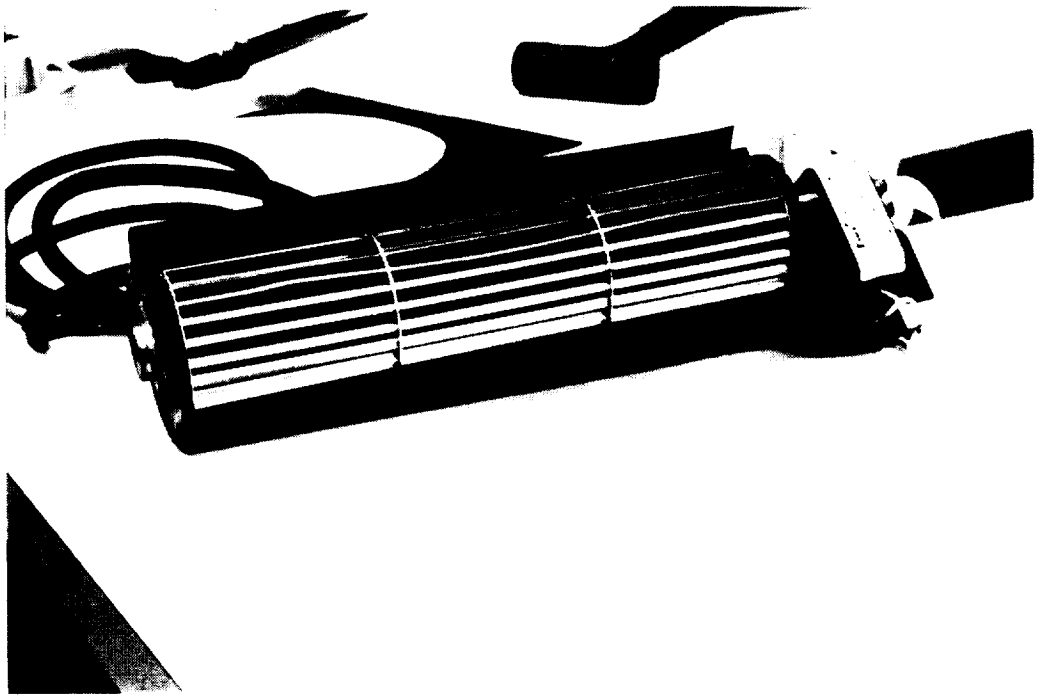

Figure 85. Zero-g Vapor Compressor Freezer Demonstration Unit Evaporator Blower

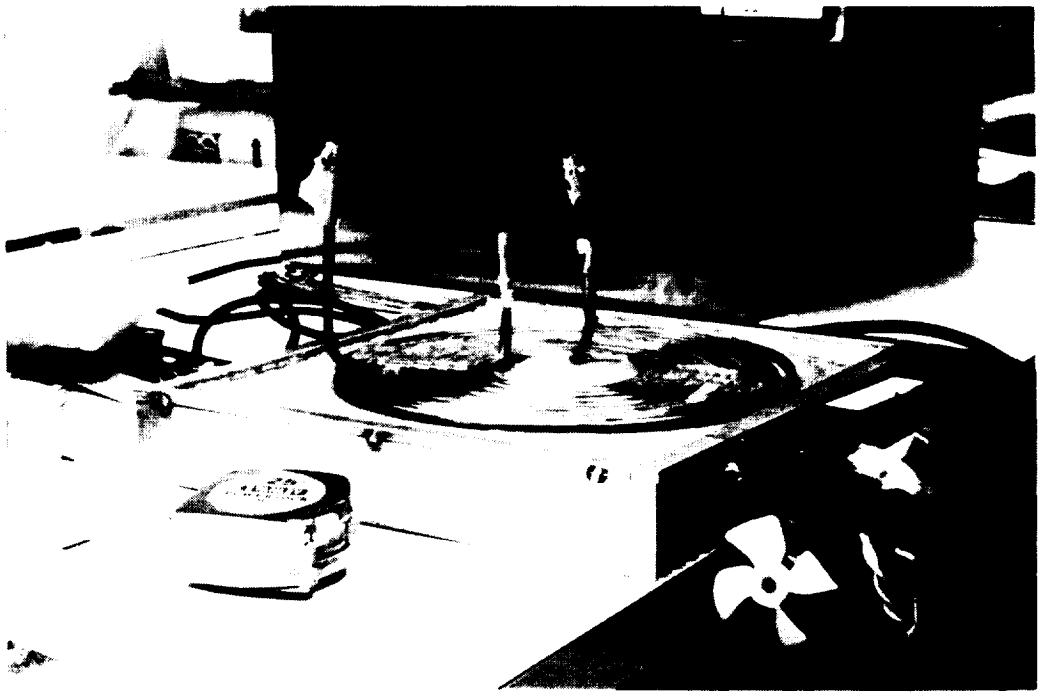

Figure 86. Zero-g Vapor Compressor Freezer Demonstration Unit Evaporator with Blower Installed

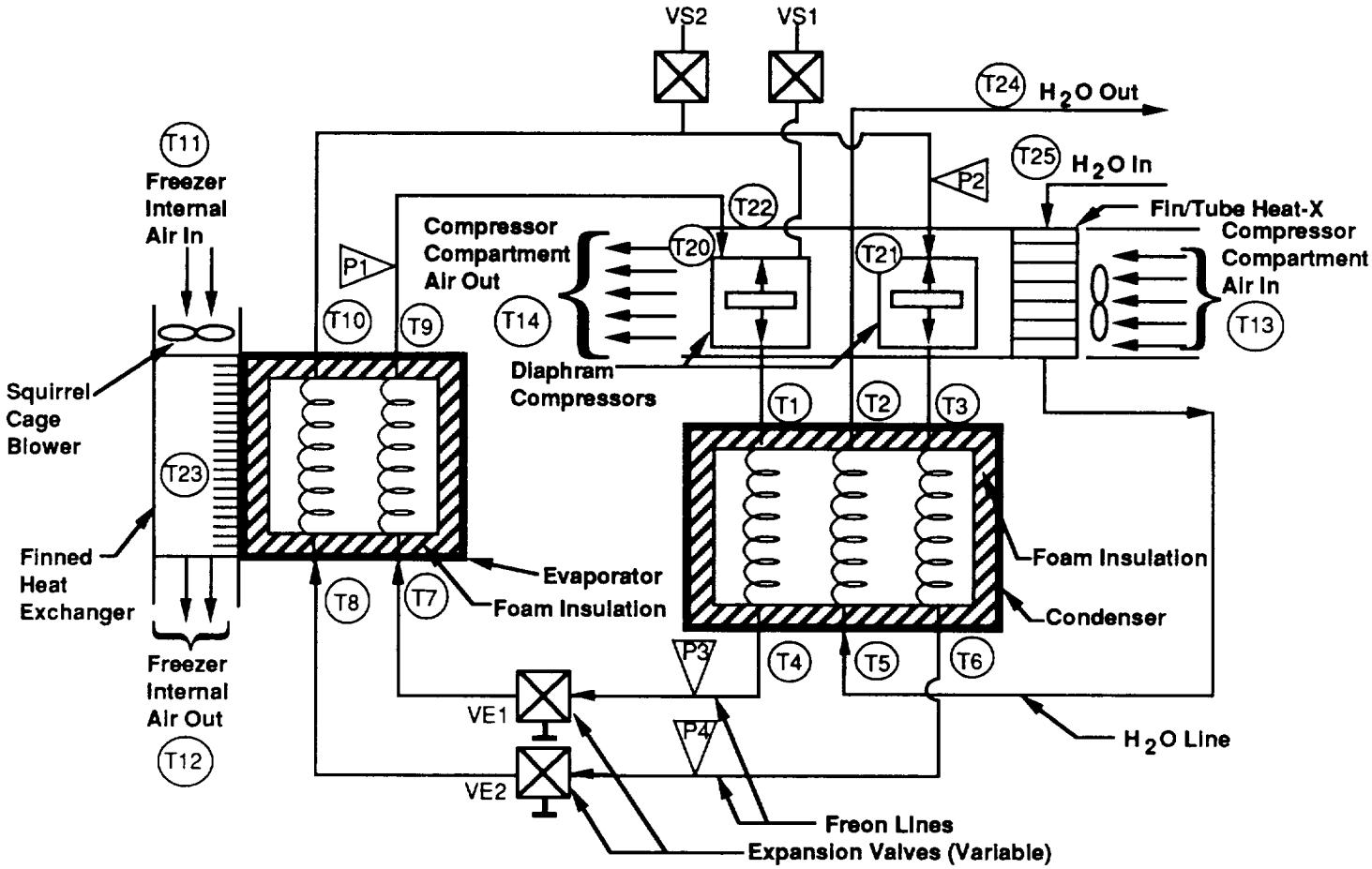

Notes:
1. T1 - T14 Fluids Temps
2. T15, T16 Inside Freezer Walls
3. T17, T18 Outside Freezer Walls
4. T19 Ambient Air
5. VS1, VS2 Schrader Valves
6. P1, P2 Pressures, Range 0 to 100 psia
7. P3, P4 Pressures Range 0 to 200 psia
8. VE1, VE2 Expansion Valves, Variable
9. T20, T21 Compressor Temps
10. T22 Motor Temp
11. T23 Evaporator Fin Temp
12. T24, T25 Water In/out Temps

Figure 87. Schematic for Zero-g Vapor Compression Refrigeration/Freezer Demonstration Unit

The compressors, condenser, evaporator, and two freon loops were connected and leaks checked with GHe and R-502 refrigerant at 100 psia and 150 psia, respectively. Leaks were repaired, and the system was evacuated on a vacuum pump and charged with R-502. Water lines were completed and connected to a portable water chiller lab unit.

Instrumentation was installed consisting of 24 chromel alumel thermocouples and 4 pressure transducers as shown in *Figure 87*. The 120 Vac to 12 Vdc power supply converter was installed on the back/outside of the freezer cold box. A cover/guard for the internal squirrel cage blower was designed and fabricated. Installation of on-off switches for the fan and compressor motors was completed. A used commercial refrigerator thermostat was obtained for use in controlling the

internal temperature level. The two expansion valves, depicted in the circuit diagram of *Figure 87*, are variable flow coefficient valves (tapered stem metering valves) to allow variation of the flow rates and pressure drops. This permits control of the evaporator pressure level and evaporator operating temperature, and balancing of the operation of the two separate loops. *Figures 88 through 91* show photos of the zero-g vapor compression refrigerator/freezer unit during the assembly process.

This unit was tested and achieved an evaporator temperature as low as -11 °F. Problems were encountered with the motor/compressor which did not allow completion of all planned testing. The motor/compressor could only be run for a limited length of time due to overheating of the motor and cutoff by a built-in temperature limiting thermostat.

Progress was made toward the solution of the double contaminant problem for this type design. Data were found that show that activated charcoal will absorb significant amounts of refrigerant Freon 12, even at room temperatures. No data were found for other refrigerants, but there is no reason to suspect that they would not also be absorbed. This absorption means that the double contaminant volume can be kept purged of leaking Freon and will not have to be designed to withstand a significant pressure buildup, allowing an important weight reduction. *Figure 92* shows that approximately 38 grams of Freon 12 can be absorbed onto each 100 grams of charcoal at 70 °F and 1.0 psia partial pressure. Therefore, 2 or 3 pounds of charcoal should solve this problem very easily, assuming a Freon capacity of 344 to 517 gms.

Under the compressor concepts subtask to research various compression systems relative to zero-g, a small commercial typical freon compressor was purchased and disassembled. The puspose of this disassembly was to look at the method used for lubricating the moving parts and wear surfaces. In this design the motor and compressor unit are made integrally. The motor armature is permanently heat shrunk onto the end of the crankshaft. The motor/compressor assembly is mounted on vibration isolation springs inside a hermetically sealed (brazed or welded) heavy sheet metal case. The bottom of this metal case forms an oil sump. The end of the crankshaft extends below the oil level. As the motor/crankshaft spins, a "slinger" centrifugal device sends oil up through the oil chamber inside the crankshaft. This oil then exits at each of the main bearing/bushings and the rod bearing, and flows through the chambers inside the piston rod, the wrist pin and bearing, and the holes around the circumference of the piston. The oil also exits at the upper end of the crankshaft and flows down, by gravity, over the upper main bearing and rod bearing outer surfaces.

Figure 93 shows the bottom view of this unit. The centrifugal oil slinger is shown at the bottom end of the crankshaft.

Figure 94 shows the top view of this unit. Note the hole in the upper end of the crankshaft where oil exits and flows down by gravity over the main bearing. Oil also exits the oil chamber inside the crankshaft via a hole in the side of the crankshaft where it runs inside the main bearing.

Figure 95 shows the crankshaft with the oil exit holes for the rod bearing and the two main bearings and with the spiral oil groove on the outside surface of the crankshaft.

The "slinger" is a "Vee" shaped clip of sheet metal, about 1/2 in. along the sides, 1 in. long, and 0.030 in. thick. This is installed inside a 1/2 in. diameter steel tube which is necked down to 3/8 in. on the end that sits below the oil surface.

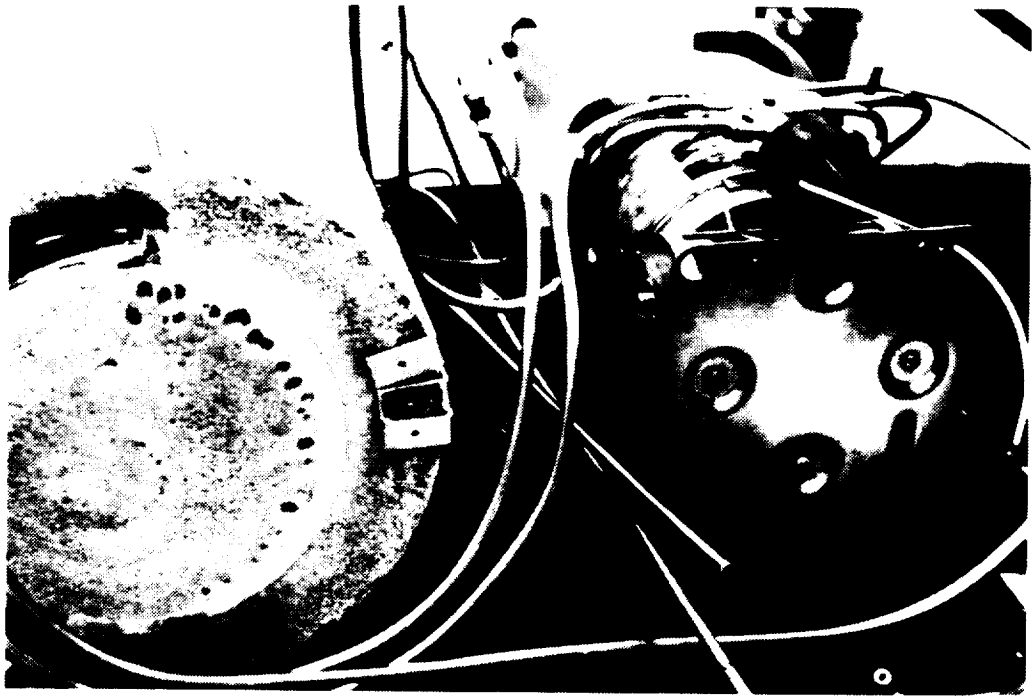

Figure 88. Front View of the Compressor Compartment for the Zero-g, Vapor Compression Refrigerator/Freezer Demonstration Unit under Construction

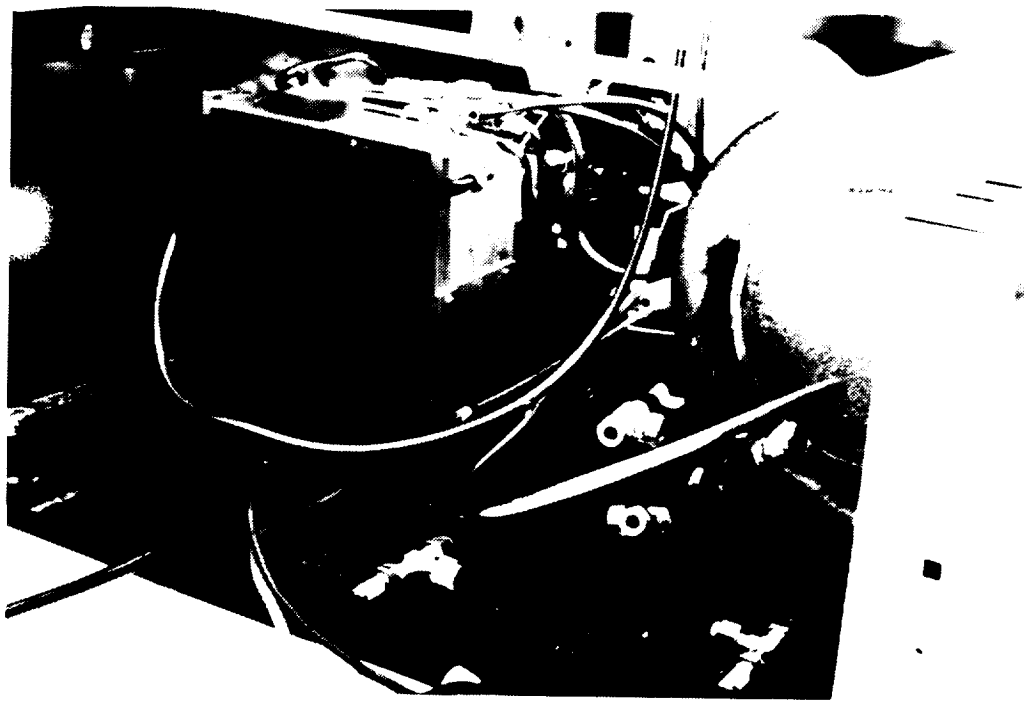

Figure 89. Rear View of the Compressor Compartment for the Zero-g, Vapor Compression Refrigerator/Freezer Demonstration Unit under Construction

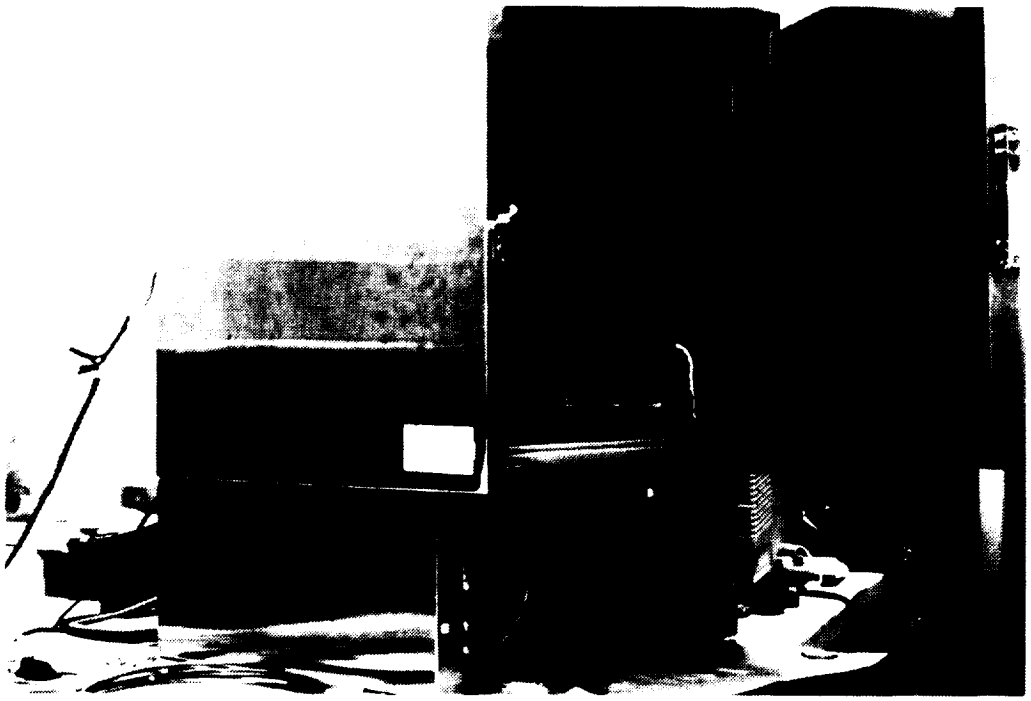

Figure 90. Front View of the Entire Zero-g, Vapor Compressor Unit Refrigerator/Freezer under Construction

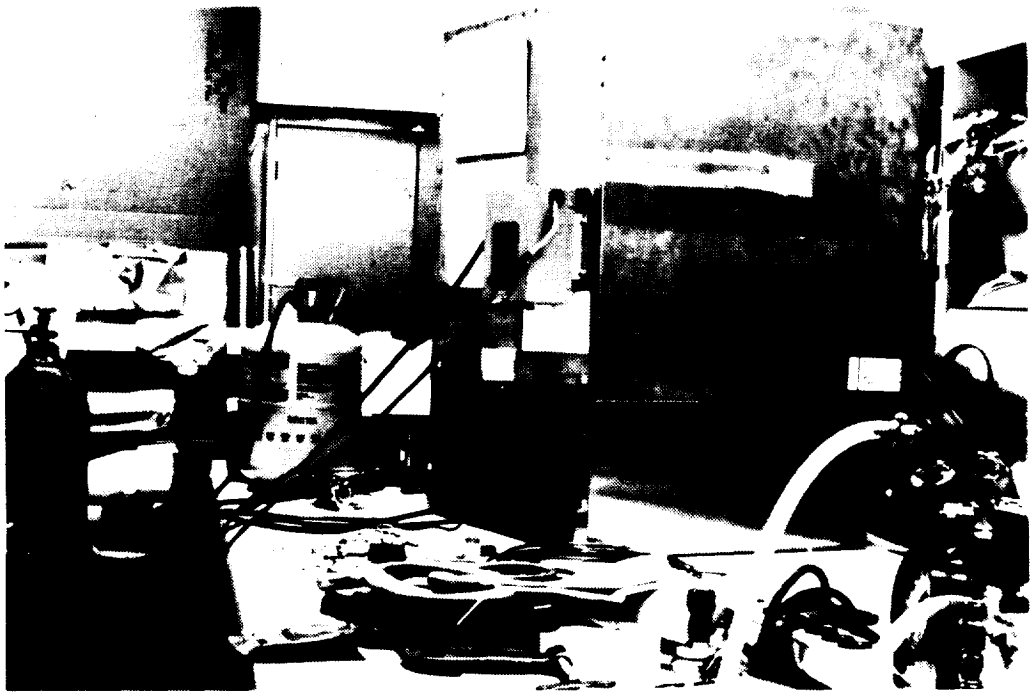

Figure 91. Rear View of the Entire Zero-g, Vapor Compressor Unit Refrigerator/Freezer under Construction

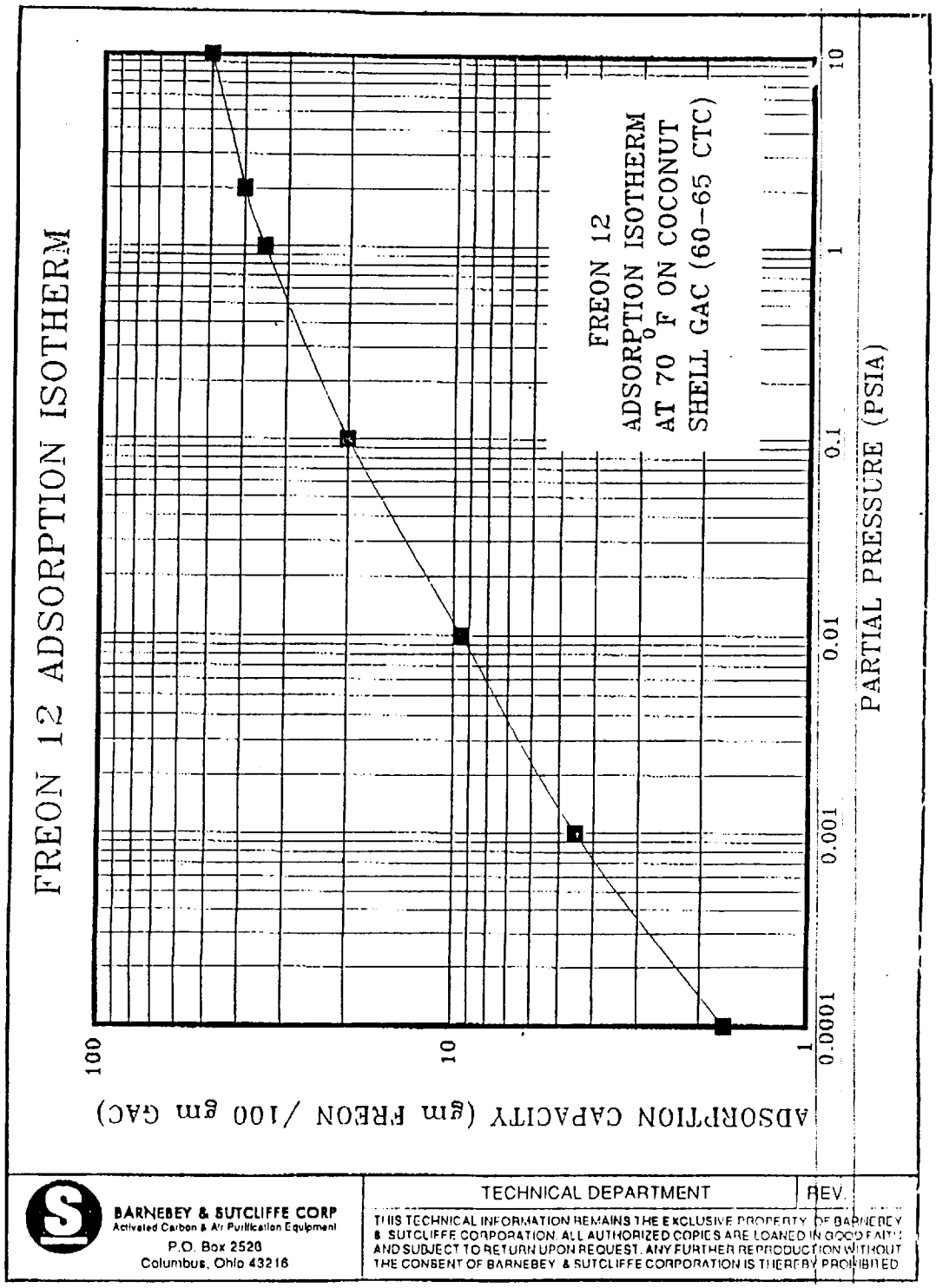

Figure 92. Absorption Isotherm for Freon 12 onto Activated Charcoal (Barnebey and Sutcliffe Corp., Columbus, OH)

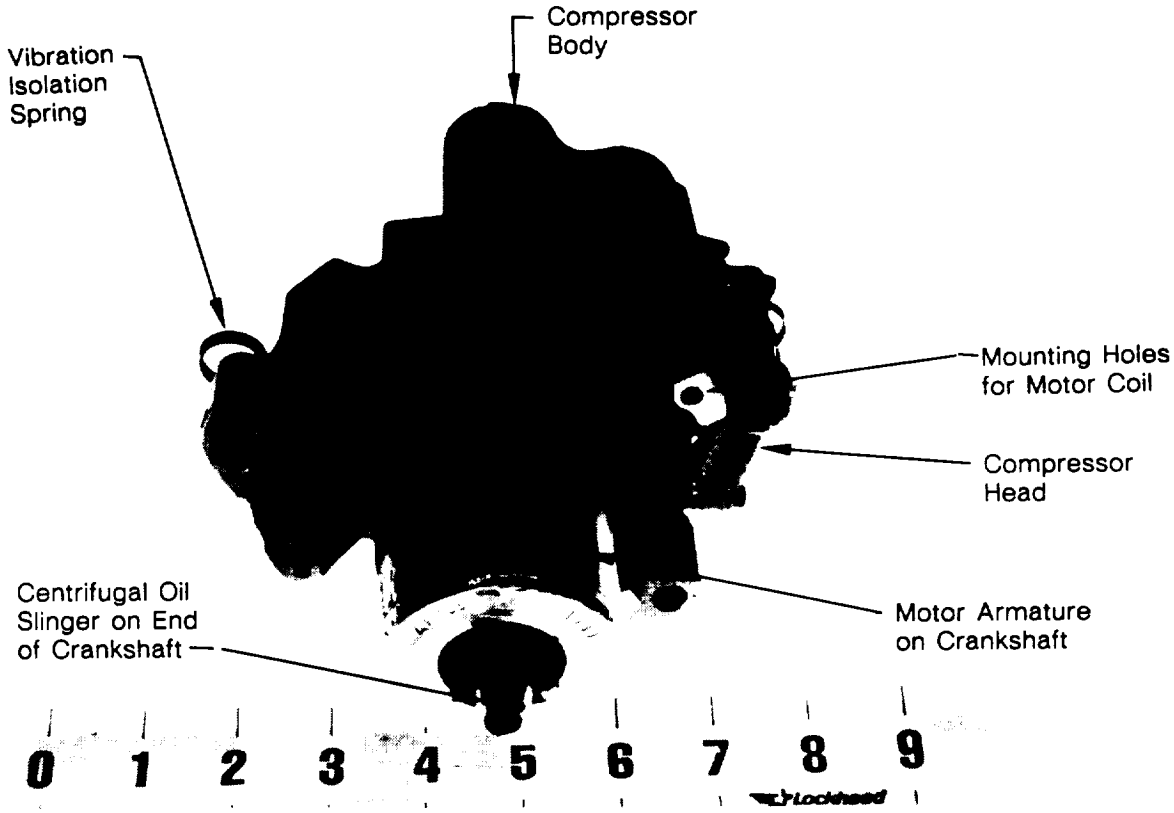

Figure 93. Bottom View of Typical Reciprocating Freon Compressor Body (Scale = in.)

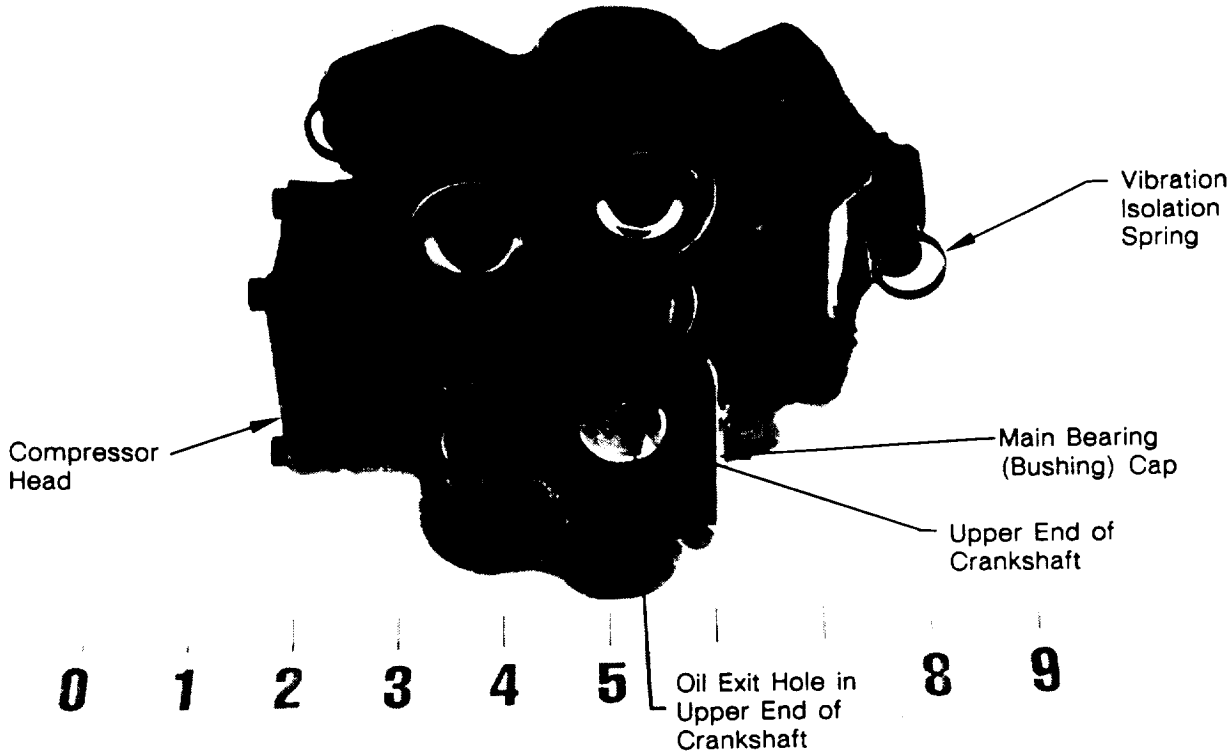

Figure 94. Top View of Typical Reciprocating Freon Compressor (Scale = in.)

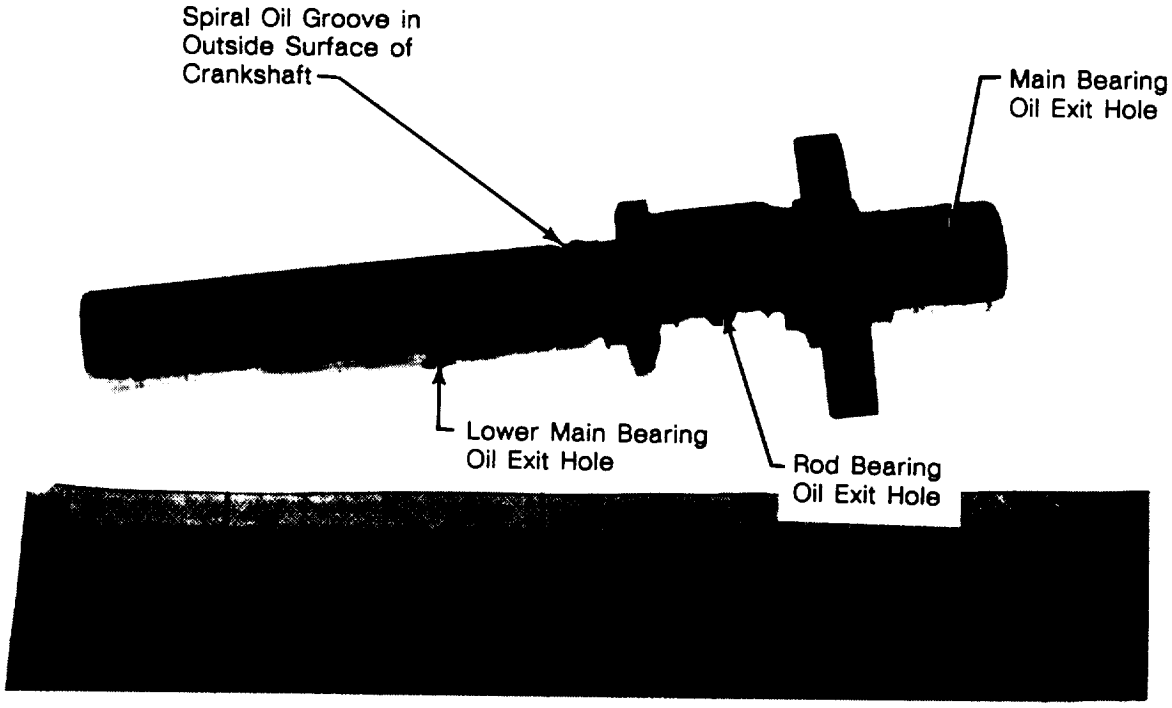

Figure 95. Typical Freon Compressor Crankshaft with the Motor Armature and Oil Slinger Removed (Scale = in.)

Figure 96 shows the centrifugal oil slinger which fits on the bottom of the crankshaft. The oil flows up from this unit into the oil chambers inside the crankshaft and bearings.

This compressor uses reed-type valves. These valves are not oiled directly by the slinger/pump device, but by the entrainment of oil by the freon as it passes through the cylinder. This method indicates that the reed valves need no oil for friction/wear, but only for sealing purposes.

Figure 97 shows the reed valve body, compressor head, crankshaft, piston, and rod. Oil flows up through a hole in the center of the rod to lubricate the side walls of the piston and cylinder.

The oil is not separated from the freon in this design. The oil is freely entrained in the flow throughout the system, and is returned to the bottom of the sump by gravity only.

Under the compressor concepts subtask to define lubrication concepts for the compressor and proof of concept, Refs 21 and 22 were obtained from the NASA COTR. These documents provided valuable information on the lubrication methods used on large commercial reciprocating type freon compressors. These units use an oil pump for maintaining lubrication. However, Refs 21 and 22 do not provide any information on lubrication of other type compressors such as centrifugal or scroll type. An investigation was made to identify the manufacturer of various types of compressors.

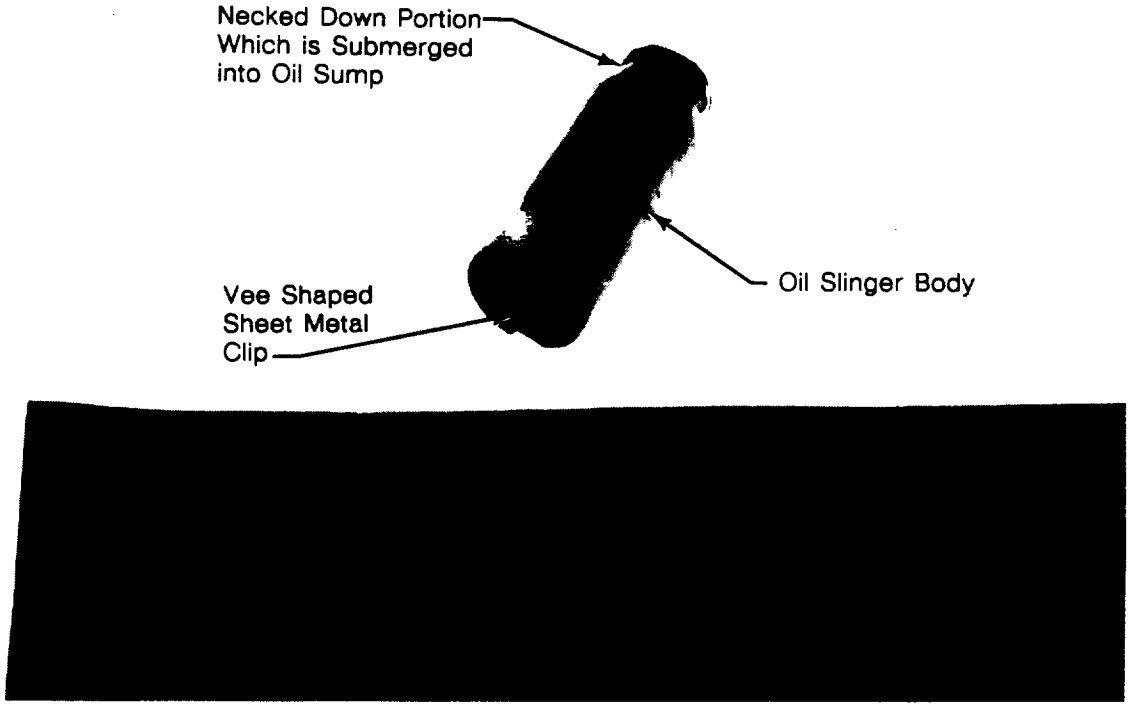

Figure 96. Centrifugal Oil Slinger Removed from the Lower End of the Crankshaft (Scale = in.)

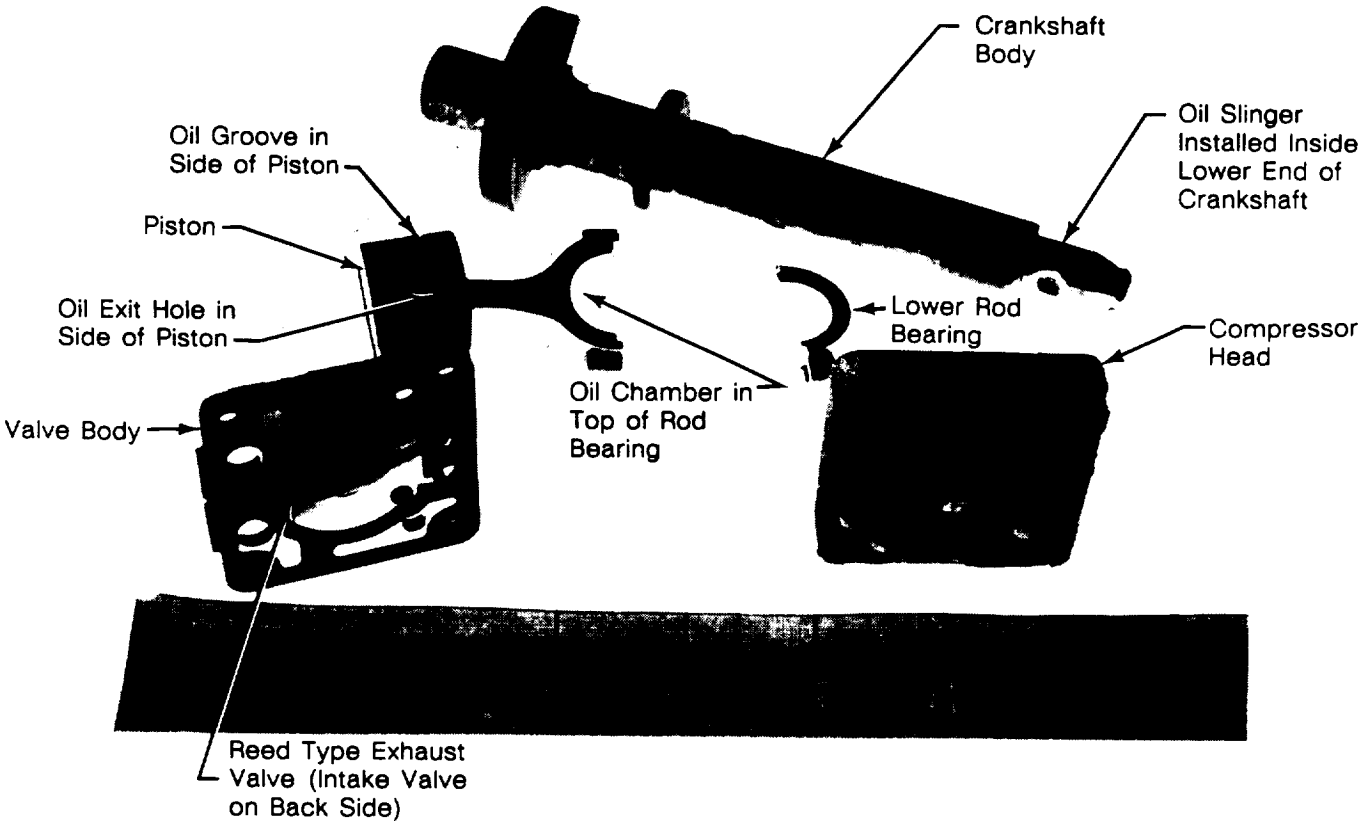

Figure 97. Crankshaft, Piston, Rod, Rod Bearings, Compressor Head, and Valve Body (Scale = in.)

A list as provided in the monthly progress report (Ref 23) of March 1990 was compiled for compressor manufacturers, their addresses and phone numbers, and the types of compressors they built. These manufacturers were contacted to obtain information pertinent to compressor design and lubrication methods and to learn in particular how these methods might be adapted to operation in microgravity. A search was also performed on the following types of compressor designs: (1) rotary, (2) scroll, (3) bellows, (4) diaphragm and (5) rolling piston.

Information on operating principles and lubrication methods was obtained for the following types of compressors:

- Reciprocating Piston
- Reciprocating Diaphragm
- Rotary Sliding Vane
- Rotary Liquid Piston
- Rotary Lobe (Roots)
- Rotary Helical Screw
- Centrifugal
- Axial.

Each of the above types of compressors was described in detail in the February 1991 monthly progress report. An excerpt from this report pertaining to this subject is presented in Appendix E.

A task was instigated to look into an oil-free compressor design. A bearing design software package was obtained from one vendor to help select oil-free, self-lubricated bearings, wear rings and seals. A meeting was held with Mr. Fred Dolan, EH11, MSFC, to discuss the self-lubricating bearing concept and to obtain test results of MSFC sponsored work at Battelle.

The objective of the oil-free compressor design was to eliminate the need for the liquid oil normally used as the lubricant in ground based, one-g design. In these designs, gravity returns the oil to the compressor sump where it is picked up by a centrifugal oil pump and forced through the bearings and around the piston to reduce friction, heat, and wear. The oil also serves to cool the internal parts and motor of the compressor. Elimination of the liquid oil lubrication would simplify a zero-g design because no phase separator (liquid oil from gaseous freon) would be required. It would also eliminate possible compressor damage or failure if liquid oil collected on top of the piston. Since the liquid is uncompressible, the compressor would either lock up or fail on attempted restart. This is a common problem even in ground based compressors if the system is overcharged with refrigerant.

The concept used in this preliminary design of an oil-free freon compressor is to modify an existing oil lubricated commercial compressor. The compressor chosen was a Tecumseh Model No. AE 121AL-014, TB1589CK, 183776, AE 3414A, 1 phase, 115 V, 60 Hz. This compressor was purchased and disassembled. The parts were found to have the following dimensions:

- Bore Diameter = 0.8665 in.
- Bore Length = 1.3 in.
- Bore Finish = 8
- Piston Stroke = 0.48 in.
- Piston Diameter = 0.8661 in.
- Piston Length = 0.853 in.
- Crank Diameter at Rod bearing = 0.6243 in.
- Crank Diameter at Main bearing = 0.751 in.
- Wrist Pin Diameter = 0.275 in.
- Piston Wall Thickness = 0.10 in.

The first step in the preliminary design was to look at the piston to cylinder wall seal. The existing compressor did not have oil or compression rings, but made the seal with pumped oil that came up through the connecting rod and wrist pin and oil grooves in the outside surface of the piston. Two concepts were investigated for modifying the existing design. The first was to use two self-lubricating lip seals and a heavy wear ring. The lip seals are spring-loaded and contact is maintained between the seal and the inner cylinder wall by "u-shaped" spring clips. As the seal wears, the clearance is taken up by the spring pushing the seal out to a larger diamter. The wear ring is designed to take up the side loads transmitted to the piston walls through the connecting rod. This concept is shown in *Figures 98 and 99* . These type seals are available from various sources, including EGC Corporation, Houston, TX, and Furon Corporation, Los Alamitos, CA. Typical materials used are "Alloy 50-F" from EGC, and "Fluorology E-1" from Furon (Ref 24).

A second design concept is illustrated in *Figure 100.* Here the two lip seals are replaced with heavier spring-loaded rings. This choice turned out to be a better design for this application because it is more rugged and provides longer life.

The second step in this preliminary design was to select replacement bearings for the connecting rod, crankshaft main bushings, and the wrist pin bearing. The rod bearing was the most critical from a life/loading standpoint. The PV (pressure, sliding velocity) product was initially calculated to be abut 44,000 Psi - ft/min. Two materials were considered (Refs 25, 26 and 27) to meet this requirement: Garlock DU self-lubricating bearing material and (2) Garlock DX prelubricated bearing material. The DU material, shown in Figure *101*, consists of a PTFE-lead overlay at the surface with a porous bronze inner structure for optimum heat dissipation plus a reservoir of PTFE-lead. This material has a steel backing for structural rigidity. The surface layer provides a transfer film which coats the mating surface. The PTFE-lead then continues to migrate from the porous bronze to the surface as required. The DX prelubricated material, shown in *Figure 102,* consists of an acetal resin layer overlay on a porous bronze inner structure and a steel backing. This material is designed to retain minute quantities of a grease lubricant at the surface and provide long life where only a trace amount of lubricant is allowed.

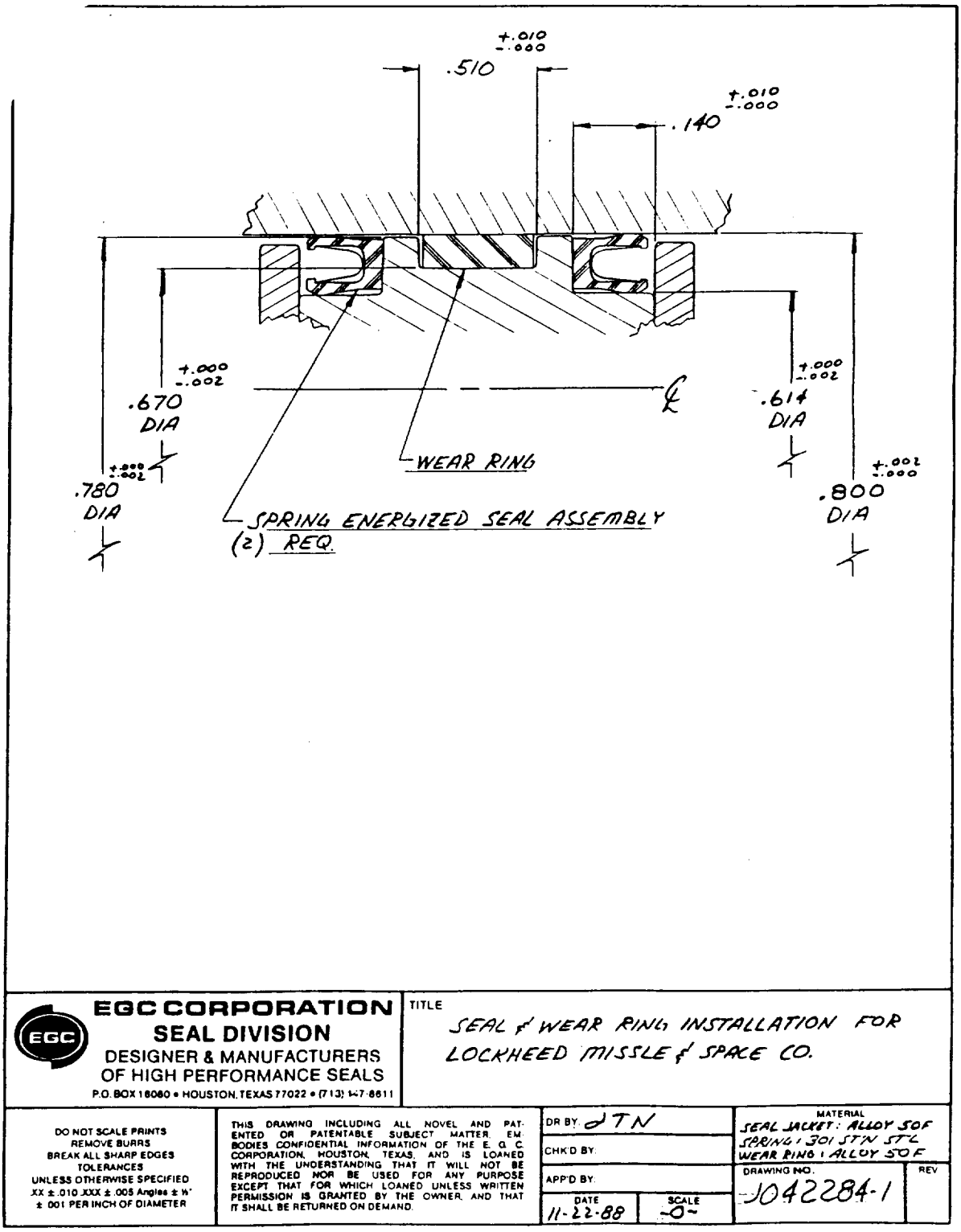

Figure 98. Design Detail for Lip Seal (or Spring Energized Seal) and Wear Ring Concept (EGC Corp., Houston, TX)

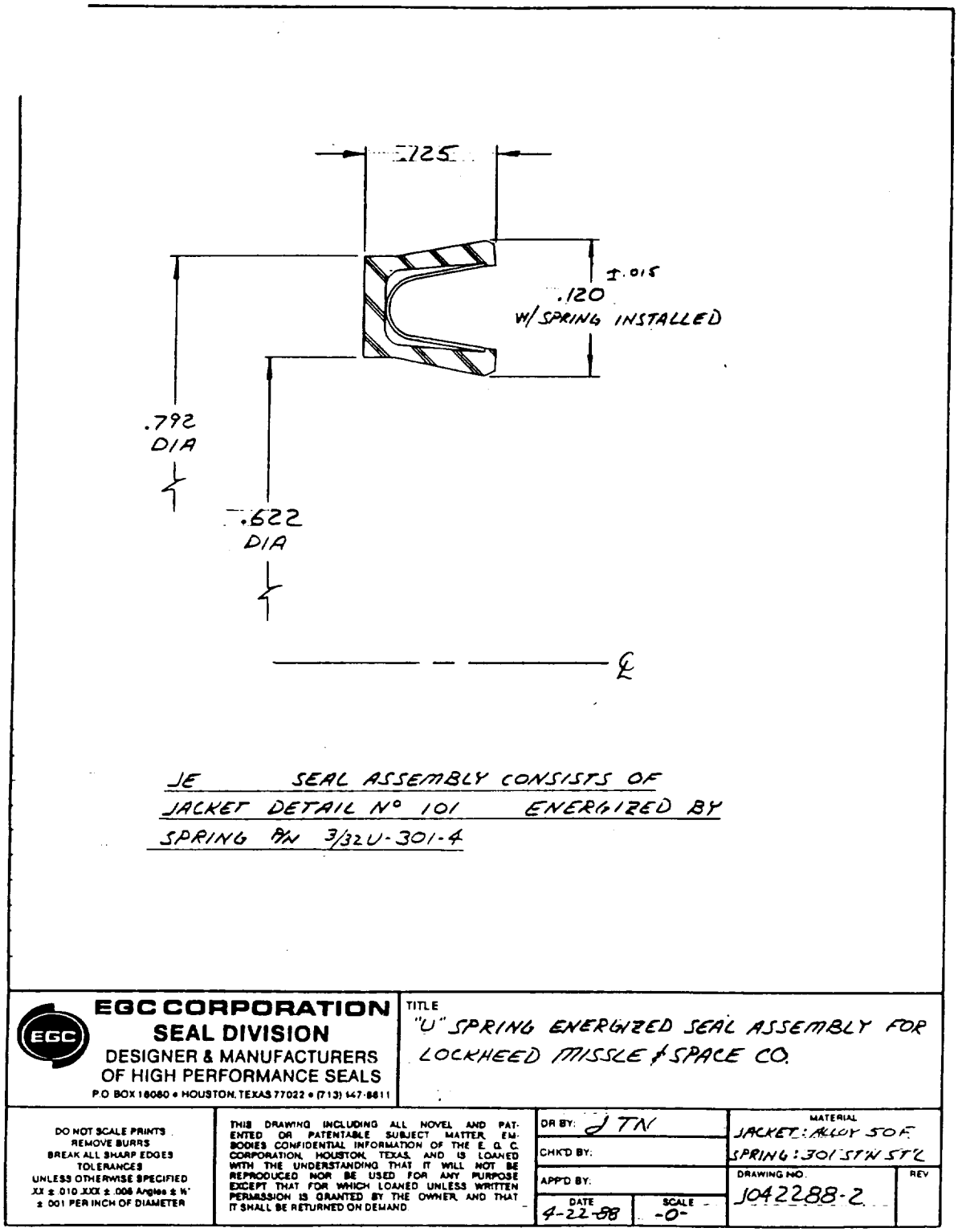

Figure 99. Detail Dimensions for Spring Energized Lip Seal Design (EGC Corp., Houston, TX)

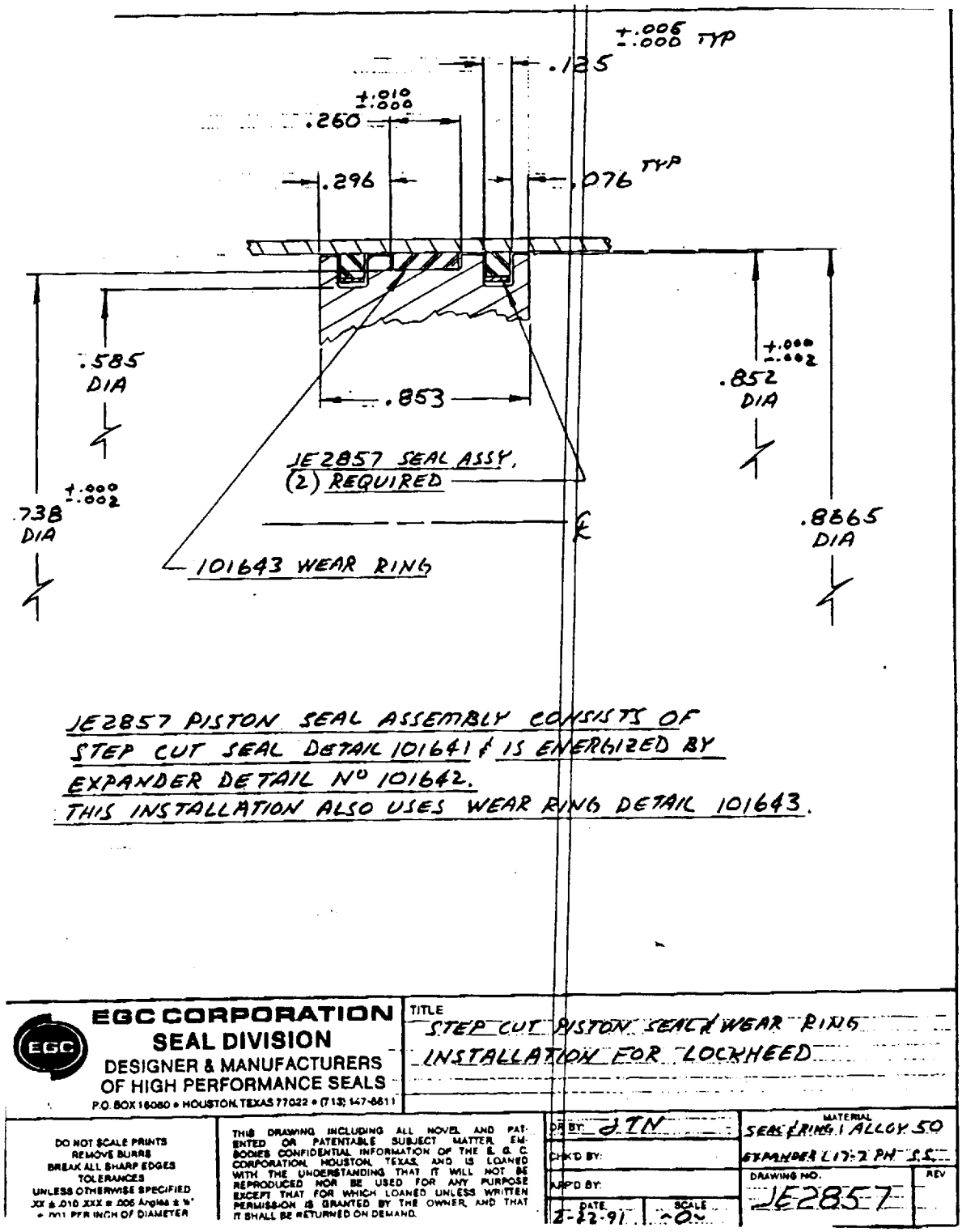

Figure 100. Detail Design of Step Cut Seal Concept Energized by Expander

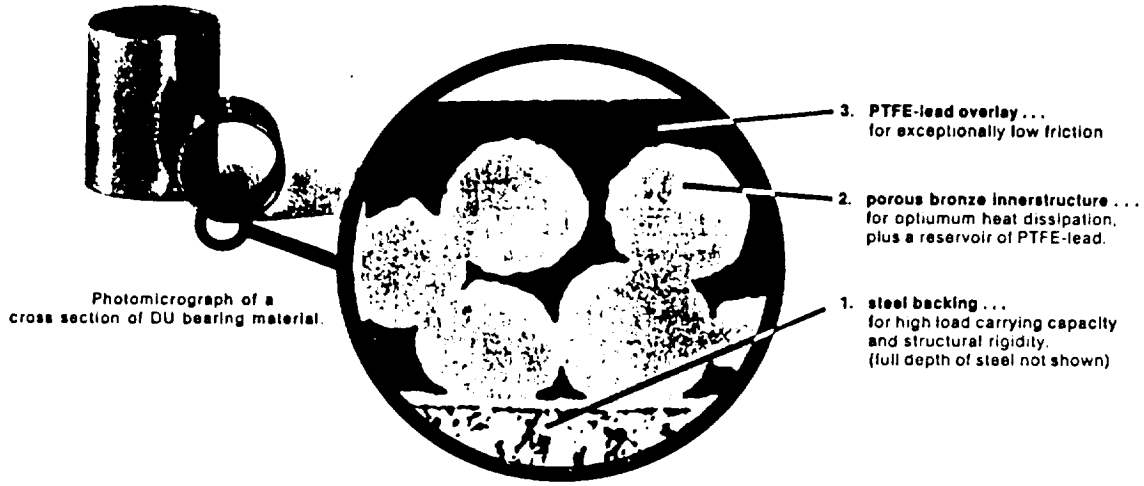

Figure 101. Photomicrograph of DU Self-Lubricating Bearing Material Cross-Section (Garlock Bearing Co., Thorofare, NJ)

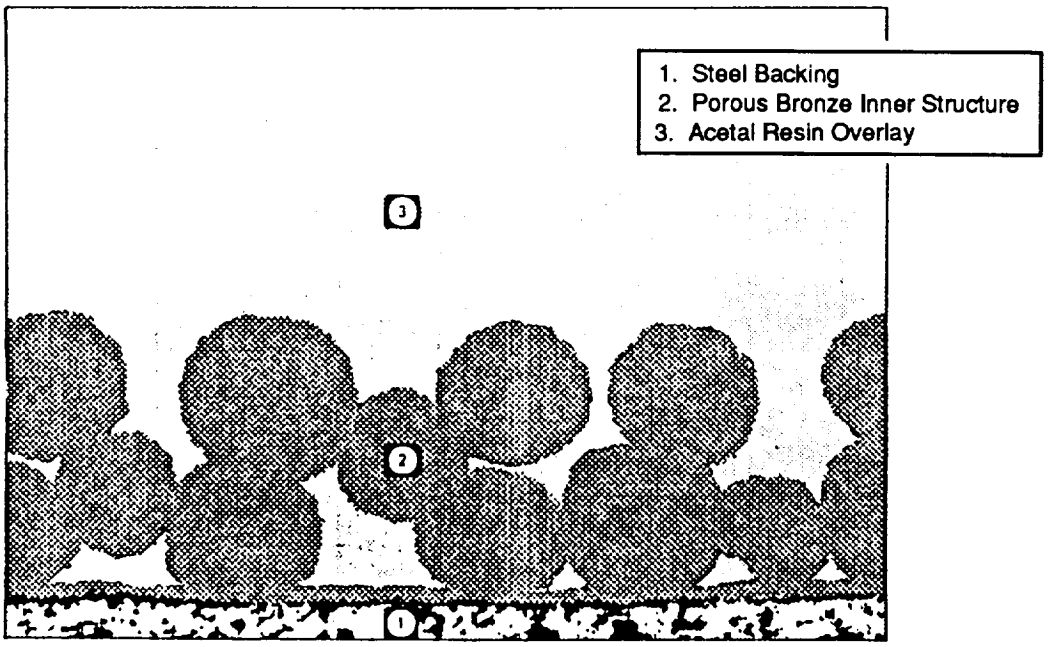

Figure 102. Photomicrograph of DX Prelubricated Bearing Material (Garlock Bearing Co., Thorofare, NJ)

The allowable PV product for both of these materials is approximately 100,000 psi - ft/min, which would give a good margin over our initially calculated value of 44,000. However, we later discovered that the commercial compressor which we were modifying had an rpm value of 3600 rather than the 1750 originally assumed. This pushed the PV product to 90,500, which was too near the limit of 100,000. We therefore had to look for a higher performance material.

We next investigated the DuPont material "VESPEL" (Refs 28 and 29). This material is actually a series of materials consisting of polyimide resin in conjunction with various fillers such as graphite, MoS_2, PTFE and fibers of glass and carbon. These materials have an allowable PV limit of up to 300,000 and were through to be good candidates for this application. However, when the life of these bearings was calculated for our high speed requirements (3600 rpm), it turned out to be less then 100 hours.

The next step was to go to sealed needle/roller bearings (Ref 30). The selected bearings have inward facing lips to help keep the lubricating grease inside the bearings for longer periods of time. The bearing finally selected was an INA brand bearing number SCE89PP sealed-shell needle bearing with a dynamic load capability of 1150 lb. The fatigue life of this bearing in this application was calculated to be 19 years by the manufacturer's method shown in *Figure 103* (Ref 27). This calculation, of course, is based only on load consideration and assumes that the lubricant could be retained for that period of time, or that the bearing could be relubricated from time to time.

In conclusion, no self-lubricating or prelubricated bearing materials were found that would meet the high speed requirements of this design. However, a sealed standard roller type bearing meets the requirement quite readily and is recommended.

Another useful reference for designing PTFE seals which is worth noting here is identified in Ref 31.

TECHNICAL DATA

LOAD CAPACITY AND LIFE

1.0 LOAD CAPACITY AND LIFE

The dynamic and static load capacities C and C_0 listed in this catalog are based on standard R 281 of the International Standards Organization (ISO). These capacities are also in accordance with AFBMA and ANSI Standards.

1.1 DYNAMIC CAPACITY C AND FATIGUE LIFE L_h

The dynamic load carrying capacity C is used to calculate the theoretical fatigue life of a bearing. This so called B-10 life is reached by 90% of all bearings provided proper mounting lubrication and cleanliness. The following diagram is a graphic representation of the empirically established life formula:

$$L_h = \frac{16667}{n}\left(\frac{C_e}{P}\right)^{\frac{10}{3}} \quad \text{or} \quad L_h = \frac{16667}{n}\left(\frac{C_{ae}}{P_a}\right)^{\frac{10}{3}}$$

L_h = B-10 life [hrs].

C_e, C_{ae} = effective radial or axial dynamic capacity [lbs] . . . see Section 2, page 43.

P, P_a = equivalent radial or axial load [lbs] . . . see Section 3, page 44.

The diagram can be used to find either L_h or $\frac{C_e}{P}$, $\frac{C_{ae}}{P_a}$

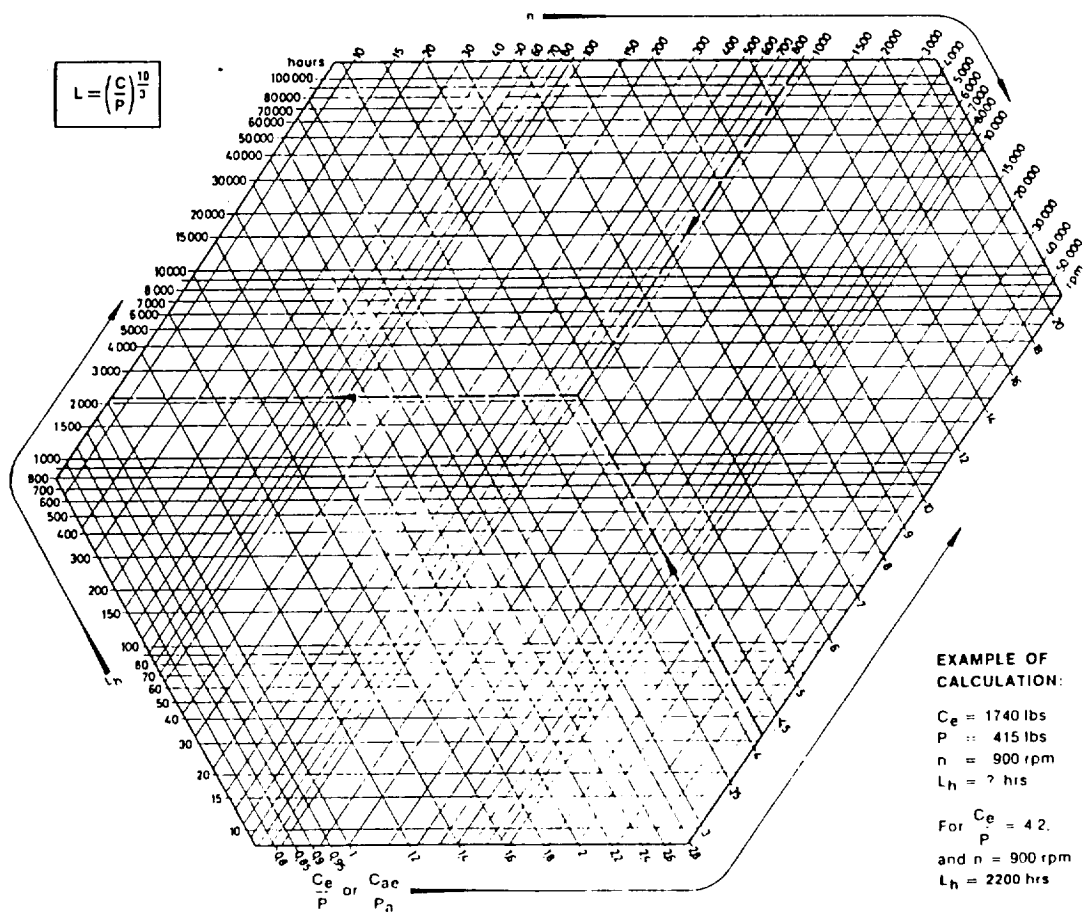

EXAMPLE OF CALCULATION:

C_e = 1740 lbs
P = 415 lbs
n = 900 rpm
L_h = ? hrs

For $\frac{C_e}{P}$ = 4.2,
and n = 900 rpm
L_h = 2200 hrs

Figure 103. Needle Bearing Fatigue Life Nomogram (INA Bearing Co., Fort Mill, SC)

Section 3. REFERENCES

1. Stochl, Robert J., "Base Performance of Multilayered Insulation System Containing 20 to 160 Layers," NASA TND 7659, April 1974.
2. Smith, James P., "SINDA User's Manual – Rev 2," TRW 14690-H001-R0-00, 27 August 1973.
3. Karu, Z. S. and Dean, W. G., "Thermal Analysis for the Development of Space Station Logistics Module Bio-Sample Freezer," Lockheed Missiles and Space Co., Inc., Huntsville, Engineering Center, Huntsville, AL, 35807, 9 January 1987.
4. "Space Station Reference Configuration Description," JSC-19989, August 1984.
5. "Space Station Life Sciences, Research Facility Technology Assessment and Technology Development Plan," NAS2-11539, September 1983.
6. Meetings with Dr. John Hilchy, NASA-MSFC, 26 September 1985.
7. "Space Station Thermal Storage/Refrigeration Systems Research and Development," Final Task Report, SRS Techologies, Systems Technology Division, Huntsville, AL, 35805, SRS/STD-TR86-037, PR-6250/13, July 1986.
8. Hammett, J.C., "Design, Fabrication, Check-out and Operation of the NASA-MSFG Thermal Control System Technology Test Bed," Contract NAS8-36199, Lockheed Missiles and Space Company, Inc., Huntsville Engineering Center, Huntsville, AL, 35807, December 1986.
9. Walker, Graham, "Cryocoolers," University of Calgary, Canada, 1983.
10. Walker, Graham, "Stirling Engines," University of Calgary, Canada, 1980.
11. "Refrigeration for Cryogenic Sensors," NASA Conference Publication 2287, Proceedings of 2nd Biannual Conference on Refrigeration for Cryogenic Sensors and Electrical Systems, Goddard Space Flight Center, Md., 7 December 1982.
12. Proposal for X-Ray Spectrometer/AXAF Telescope, NASA Goddard Space Flight Center, pages 8-15.
13. Kohler, J.W.L., "The Stirling Refrigeration Cycle," *Scientific American*, No. 212 (4), 1965, pages 119-127.
14. McGracken, J.E., "Stirling Cycle Cooling Unit Test Results," Contract NAS8-36401, Technical Memorandum LMSC-HEC TM F268774, Lockheed Missiles and Space Company, Inc., Huntsville Engineering Center, July 1989.
15. Hye, Abdul, "The Freon Loop Double Containment Design for Spacelab Refrigerator/Freezer to Protect Environment," Proceedings of the Conference of Society of Manufacturing Engineers, September 1985.

16. Hye, Abudl, "The Design and Development of an Oil-Free Compressor for Spacelab Refrigerator/Freezer," SAE Technical Paper Series, Fourteenth Intersociety Conference on Environmental Systems, San Diego, CA, July 1984.

17. Hye, Abdul, "The Design and Development of a Vapor Compression Refrigerator/Freezer for Spacelab," SAE Technical Paper Series, Thirteenth Intersociety Conference on Environmental System, San Francisco, CA, July 1983.

18. Hye, Abdul, "Design and Development of Evaporator for Spacelab Refrigerator/Freezer," MATSCO, Houston, TX, 1985.

19. Hye, Abdul, "Safety Considerations in the Design of Spacelab Refrigerator/Freezer," SAE Technical Paper Series, Fifteenth Intersociety Conference on Environmental Systems, San Francisco, CA, July 1985.

20. Hye, Abdul, "Spacecraft Heat Transfer by Two-Phase Flow Method," 36th International Astronautical Congress, Stockholm, Sweden, October 1985.

21. "Service Manual – Installation and Service Data for Copeland Motor Compressors," The Copeland Company, Sidney, Ohio, 1970.

22. "Copeland Refrigeration Manual," Parts 1 through 5, The Copeland Company, Sidney, Ohio, 1966.

23. Dean, W.G., "Space Station Thermal Storage/Refrigeration Systems Research and Development," Monthly Progress Report, Contract NAS8-36401, LMSC-HEC PR F312261, 15 March 1990.

24. "Omniseal Design Handbook," Fluorocarbon Company Publication FC 5367, 1989, Mechanical Seal Division, Fluorocarbon Co., Los Alamitos, CA.

25. "Self-Lubricating Bearings," Bulletin 801-D, GB11346-25M-288-SP, Garlock Bearings, Inc., Thorofare, NJ.

26. "DU-Self Lubricating Bearings," Catalog 781-C, GB1348-388-15M-SP, Garlock Bearings, Inc., Thorofare, NJ.

27. "DX Prelubricated Bearings," Catalog 811-B, GB1391-7M-689-SP, Garlock Bearings, Inc., Thorofare, NJ.

28. "VESPEL: Design and Technical Data," Report E-61500-5-88, DuPont Co., Wilmington, DE.

29. "Bearing Design with Polyimides," Report E-73920-7/86 - Reprint from Richard Von Ryper, "Power Transmission Design," June 1986.

30. "Rolling Bearings Design Data," INA Publication No. 305, INA Bearing Co., Inc., Fort Mill, SC.

31. "PTFE Seals in Reciprocating Compressors - An ASME Design Manual," 1975, Library of Congress Card Number 74-32657, ASME, New York, NY.

APPENDIX A

Summary of the Work in Progress on the Design and Fabrication
of the -20 °F Food Freezer and the -94 °F Bio-Sample Freezer
(Excerpt from the June 1987 Monthly Progress Report, LMSC-HEC PR D066068)

PRECEDING PAGE BLANK NOT FILMED

Preliminary Demonstration Unit for -20 F Thermal Storage (Background): Work was performed on the design and fabrication of a preliminary thermal storage demonstration and test unit. The purposes of this unit are: (1) to check out some of the practical aspects of the design such as strut wire attachment and MLI layup, and (2) to verify the thermal model of the -20 F thermal storage unit. A mild steel cylindrical tank with dome ends (15-in. diameter x 39-in. long) was purchased and modified for this test unit. It was leak checked, then cut in half and flanges welded in place to form an outer container. O-ring grooves were cut and polished in the flanges. Some 16 cable attaching brackets were designed, fabricated, and welded inside each of the two halves of the tank. Pumping ports and pressure measurement ports (ion gauge) were added. The tank was reassembled and leak checked again. Instrumentation (RTDs) were obtained and installed. Extremely small (40 gauge) wire was used to make these measurements in order to reduce the heat leak. Instrumentation feed-throughs for penetrating the tank wall have now been made up and leak checked. This test unit will have a tank with a PCM material inside to simulate the frozen food container volume and dimensions. The mass of PCM will be adjusted to yield a test time (i.e., melt time) of the order of one week to expedite testing. The PCM container will be mounted inside a wire "basket" supported by the 0.030-in. diameter strut wires mentioned earlier. Photos of this unit and test were shown in previous progress reports. The wire strut concept was used to mount the basket inside the pressure vessel and found to be quite rigid - even better than expected.

The following additional efforts were expended on the design, fabrication/build up of the -20 F demonstration unit.

- The 15-in. tank was cleaned, chrome plated inside, and painted outside.
- A getter pump was designed and fabricated. Getter materials have been researched and ordered and will be screened for our application. No final selection of getter material has been made.
- Racks for mounting and fabricating the MLI for the test article were made.
- Various methods were pursued for putting holes at a shallow angle through the MLI blankets for the diagonal strut/wires.
- Our vacuum lab ion pump, titanium sublimation pump, and Vacsorb roughing pumps were refurbished and put back into operation. The pumping rate capability was significantly improved.
- Feed-through ports and getter pump ports were added to the tank.
- The 0.030-in. diameter stranded steel wire was sent out for cleaning. This wire consists of 20 separate wires twisted together. There was some noticeable shop oil or lube on these wires when purchased from the vendor. An effort was made to clean these by going through three cycles of electro-cleaning plus nitric acid washing. However, this did not fully remove the oil/lube. Further examination indicated that this might be a silicone which is known to be very difficult to remove. The wire was then put through a four-day vacuum bakeout at 400 F and approximately 10^{-8} torr.
- Efforts were made to develop a satisfactory method to put holes in the MLI blankets at a shallow (approximately 10 deg) angle for the diagonal strut wires. Various methods were tried, including: (1) small (a few thousandths of an inch) diameter drill bits at high speed; (2) burning through with a laser; (3) various Xacto blade configurations; (4) diamond tipped drill bits; (5) hypodermic needles, rotating and non-rotating; (6) beveled steel tubing with a "burr" at 90 deg to nip the Mylar and start a hole; (7) a 0.020-in. blade on the end of a solid rod, etc. None of these methods proved to be fully satisfactory. It was decided to slit the MLI all the way through and insert the wire rather than put them through discrete holes. The MLI must be vented with slits anyway because it is not perforated. We elected not to have it perforated when purchased rather than risk the possibility of contamination with oil or other hydrocarbons during the punching process as has happened in the past. Any oil inside our vacuum jacket would be disastrous for this application where it is necessary to turn off the pump and hold the vacuum for 90 days.
- The PCM was changed from 25 percent CaCl solution to N-decane wax because it gives a more distinct melting point and about the same temperature, i.e. -27 F versus -20 F.
- The MLI basket and PCM tanks were sent out for cleaning, then instrumented. MLI application was completed on the baskets. At the ends of the basket, the MLI was "gored and taped" and folded down rather than making 160 separate circular end disks and mating the joint with the side wall MLI layers.

- The 160 layers of MLI were wrapped at about 50 layers per inch on the side walls for a total thickness of approximately three inches. The end/dome area had more layers due to "tucking." Here, there are approximately 200 layers with a thickness of approximately 4.5 or 5 in. We are quite pleased with the way the ends turned out.
- Additional research was put into getter material selection; still no final selection has been made. We plan to test several of these when the tank test gets under way.
- Additional research was put into the cleaning and final surface treatment of the inner walls of vacuum vessels and their effects on outgassing quantities and products.
- An attempt was made to calculate the outgassing quantities and products for our system. For example it appears that the largest quantity for the first pumpdown will be water vapor from the MLI, a total of approximately 2 grams. The Mylar also outgasses considerable amounts of N_2 and CO_2.
- Additional getter materials were ordered and delivered, and the molecular sieve trap was baked out.
- The two PCM tank baskets were installed inside each of the two outer container walls using the 0.030-in. strut wires. The PCM tanks were charged with PCM and installed inside their baskets/containers. Instrumentation was completed, and test was begun on 23 December 1986. Dry ice was used to cool down before vacuum pumping was begun.
- The MLI cavity was pumped during the Christmas holidays, but problems were encountered. The pressure fell to 60 microns, then rose to approximately 100 microns and never went any lower. The container was opened, and some liquid water was found inside. This was apparently left over from the frost that had accumulated in the dry ice before installation in the inner container. Apparently, since the MLI did not reach the pressure level required to become effective, the heat leak was such that after the dry ice evaporated the temperature rose to above 32 F and the frost turned to liquid. With this liquid water present, pumping speed was too slow for the pressure to drop below 100 microns. We assume that the 60-micron value was reached while the water was still frozen on the dry ice.
- The tank then was dried out and a second pumpdown (at room temperature) was started. During this pumpdown the pressure dropped to the 10^{-5} torr range, but we were not able to maintain this low pressure. Therefore, a bakeout of the system was planned.
- This bakeout of the 160 layers of MLI proved to be somewhat difficult. For example, problems were encountered on the third pumpdown as follows: The pressure in the tank dropped into the 10^{-4} range but after a period of time, it began to rise again. This was determined to be due to the drop off in the pumping speed of our titanium sublimation pumps. This is a characteristic of this type pump. As the element thicknesses wear down with usage, their resistance increases, the power consumption rate drops and the pumping speed is an exponential function of power. These elements were replaced for the next pumpdown but their practical useful life is only about 8 to 10 hours. Also, in order to decrease the cleanup/outgassing time for the MLI, we added heaters to the outer tank surface and ran it at 250 to 300 F to expedite the process.

- Also, a larger roughing pump was obtained GFE from MSFC to speed up the process, and larger sublimation pumps have been requested.
- The Varian Vacuum Company technical representative was contacted; he agreed to bring in a new 200 liter/sec turbomolecular turbine demonstration pump for our evaluation in this application. This pump is capable of pumping the entire range from atmospheric pressure to below our required 10^{-6} torr range.
- Additional efforts were made to expedite the bakeout/cleanup process. For example, the tank-to-vacuum pump connections were reconfigured with larger fittings, etc. in order to reduce the molecular flow conductance.
- The Acurex Autocalc and IBM PC-XT were hooked up to the pressure and temperature instrumentation to expedite data acquisition/reduction. The data can now be plotted immediately using Lotus 123 software.
- A report has been written on the thermal analysis of this unit and is in the review cycle.
- An unfortunate problem occurred which resulted in contamination of the MLI. The larger (21 cfm) mechanical roughing pump which was obtained GFE from NASA-MSFC was being used to evacuate the tank during a bakeout/cleanup pumpdown when the power failure occurred on Sunday, 15 February, at 9 p.m. Because this pump did not have an "anti-suckback" valve, it allowed oil to be pulled back into the test tank/MLI when the pump ceased working. According to the manufacturer of this pump oil, its vapor pressure is 2×10^{-5} torr at room temperature. Therefore, we cannot expect to get our tank pressure below this level without a complete cleanup of the oil inside and/or replacement of the MLI.
- Shortly after this contamination problem occurred we were able to obtain on loan a turbomolecular demonstration pump for a limited time from the Varian Vacuum Company. Rather than lose the opportunity to try this pump for our application, we decided to use it to pump on the tank even with the oil and contaminants inside. This pump proved to be quite helpful to this effort and we plan to purchase a similar, but larger, pump of this type. This procurement is expected to take about 45 days, so we should have the new pump in operation by mid-April or early May 1987. The demonstration pump is a 200 liter/sec capacity, while the pump being purchased is 300 liter/sec. The 200 liter/sec pump has consistently held the tank pressure in the low 10^{-5} range with the oil inside as expected.
- We plan to go ahead and take some preliminary thermal performance data with this tank "as is" while holding the pressure with the pump running continuously. This may or may not be successful depending on the effect of the oil on the MLI effective emissivity/performance. Depending on the results, this tank will be refurbished or continued in use "as is." We will, of course, not be able to do any "gettering" tests with this particular tank until the hydrocarbons are removed.
- The IBM PC-XT computer and Acurex Autocalc unit have been used extensively to record, reduce, and plot test data. This is a great help in speeding up our testing. Calibration runs were made on both the ion gauge and thermocouple gauge pressure measurement instruments to use in these data reductions so that the PC-XT will now record both pressures and temperatures. Macros were written to sort, reduce, and plot the tank temperature data automatically.

- Since the Varian demonstration turbopump was available and the tank was assembled and instrumented, a decision was made to go ahead and make a preliminary "dry run" test of the storage unit, even with the oil-contaminated multilayer insulation. A six-day test was made from 19 March 1987 through 24 March 1987. Results in the form of temperature plots are shown in Figs. 11 through 14. Figures 11 and 12 show typical outer tank wall temperatures. These values oscillated approximately ± 3 F each day with the daily air temperature fluctuations in the test lab area. These oscillation are not considered to be detrimental to our overall test results. Figure 13 shows three internal temperatures. Temperatures T 120 and T 121 are on one of the aluminum "baskets" which support the PCM tanks. Temperature T 127 is on one of the PCM tanks. Figure 14 superimposes external and internal temperatures. Gaps in the data are due to the times when no data were being taken because the IBM PC-XT computer was being used to reduce data taken up until that time. Data were generated for most of the test duration at 10-minute intervals. The internal PCM tank and basket temperatures in Figs. 13 and 14 have not been corrected for the additional resistance in the leads caused by the use of approximately 6 in. of super small (40 gauge, 0.003-in. diameter) wire. This was used to reduce the thermal heat short across the MLI. This causes a temperature error of approximately -4.5 F. That is, the values are approximately 4.5 F too high as presented. The outer tank wall temperatures do not have this problem because they used ordinary size lead wires.

  The internal PCM tanks and baskets were initially cooled down well below the planned thermal storage design temperature of -20 F. This was done purposely because it was not known how much the temperature would rise before the internal pressure could be reduced to the MLI operating value of 10^{-4} torr. As it turned out, the -65 F temperature was lower than required. Nevertheless, useful heat leak data were obtained.

  A cursory analysis of these test conditions was made, and hand calculated heat leak rates are shown in Table 1.

  These calculated heat leak rates were compared with the measured values as follows. Knowing the MC_p of the internal tanks and baskets and the average temperature rise rate the average measured heat leak rate was calculated to be 2.98 Btu/hr or 0.87 W. This is considerably higher than the calculated value. This, of course, was attributed to the MLI being contaminated by the oil vapor from the vacuum pump as discussed in the March progress report.

  If it is assumed that the heat leak calculated for the strut wires and the instrumentation leads are correct, then the effective thermal conductivity of the MLI would be 4.6×10^{-4} rather than the 1.4×10^{-5} value expected from the literature and used in our original design.

- A new 300 liter/sec tubomolecular pump was purchased and put into operation. New larger tank fittings are being made to accommodate the new pump.
- An MLI "bellyband" was designed and fabricated to use to close out the MLI joint between the two halves of our demonstration test unit.
- A review of our concepts and results to data was given to the NASA-MSFC COR and Boeing Space Station people on 17 March 1987 and to the SRS subcontractor people on 18 March 1987.
- The MLI which was contaminated with vacuum pump oil was discarded. The baskets and PCM baskets were cleaned. New MLI was made using 160 layers of double aluminized Mylar and 160 layers of Dacron netting. The MLI thickness is approximately 1-5/8-in. thick whereas the previously used MLI was approximately 2 to 2-1/2 in. thick. All instrumentation was refurbished and improved.
- A new 300 liters/sec turbomolecular pump was purchased. The tank pumping port was opened up to an 8-in. diameter flange to fit the new, larger pump. A MLI "bellyband" was designed and fabricated to close out the gaps between the two tank halves. The refurbished tank without MLI was pumped down with the new pump and leak checked. The tank pressure reached 1×10^{-4} torr in approximately 5 minutes and 1×10^{-5} in approximately 20 minutes on the first pumpdown. The MLI, baskets, PCM tanks and bellyband were then installed and a vacuum bakeout at a temperature of approximately 200 F was begun on 23 April. This bakeout is still in progress and is expected to take at least two weeks. The pressure is presently in the 10^{-6} torr range. Once the bakeout is completed, the PCM tanks will be chilled down, and a thermal test will be conducted.
- Work was resumed on getter material selection. The Varian Vacuum Company was contacted and they supplied information on getter materials which they are using in their vacuum systems. Also, in connection with this getter selection, the need was established for a Residual Gas Analyzer (RGA). This instrument is essentially a mass spectrometer and will be used to identify the gases present in our vacuum jacket volume due to outgassing of MLI, tank walls, O-rings, instrumentation, air leaks, residual gases, cleaning solvents, etc. Once these molecules are identified, the getter selection should be considerably simplified. The availability and capability of various RGA models were investigated. Various manufacturers were contacted and their literature reviewed. Requirements and capabilities were discussed with MSFC Test Lab personnel, and we looked at some of their present equipment. A specification was written for our RGA requirements. (We are going for a simple basic version RGA rather than the "Cadillac" version, and expect it to meet our present needs.) We are now in the process of purchasing this RGA, and expect delivery around 15 May 1987.
- A new cold cathode pressure gage and controller were purchased and installed on the tank. This gives us a continuous pressure monitoring capability from 1×10^{-3} torr to 10^{-7} torr, which we did not have previously with the combination of thermocouple and ion gages.
- An investigation was made of the effect of the power dissipated by the RTDs inside our inner tank. Since our predicted heat leak is so small

(on the order of 0.13 W) we were concerned about the RTD power effecting the data. However, this was found to be negligible, on the order of 10 milli Watts per RTD. We have 12 internal RTDs.

- Other ideas were investigated to improve the instrumentation such as use of Constantan rather than copper ead wires across the MLI space. Constantan has a thermal conductivity of approximately 9 Btu/ft-hr-F as compared to approximately 220 for copper. Another consideration was to use 1000-ohm RTDs rather than 100 ohm so that the small lead wire resistance would be insignificant in comparison to the RTD resistance. However, these 1000-ohm units are not compatible with the Acurex Autocalc data system we are using. Another concern is the effect of the rosin solder flux outgassing. This effect is still unkown at the present time. Some effort was also put into the design of a flight weight valve design. Since the pumping port is quite large (8-in. diameter) any off-the-shelf vacuum value would be quite heavy. We are designing a value body which would be removable after placing a diaphram closeout over the pumping port. This diaphram may also be combined with the getter pump.
- A report was published on the preliminary thermal analysis of this concept (Ref. 1). Photos of the reconfigured demonstration unit tank are shown in Figs. 15 through 19.

<u>Effort on the -95 F Bio-Samples Thermal Storage Unit (Background)</u>: During previous performance periods, the following accomplishments were made on the -95 F unit:

- A report has been written on the thermal analyses of this unit, and is in publication.
- We obtained access to the MSFC Materials Lab Data Base for materials properties.
- A 10-in. diameter by 3-ft long aluminum tooling mandrel was made for holding the fiberglass cylinders during machining.
- Several fiberglass cylinders and miscellaneous parts were machined.
- A supply of Hexcell prepreg fiberglass material was obtained and used to make several honeycomb samples.
- Honeycomb samples were tested and results analyzed. These samples are adequate structurally, but additional efforts are needed to reduce their thermal conductance. Various bonding techniques are being tried. Methods for closing out the honeycomb edges and bonding these to the fiberglass cylinders were developed. These problems and efforts have been discussed with various MSFC M&P people. They have been very helpful.
- Efforts were made to bond the 0.0005-in. stainless steel foil to the fiberglass without much success.
- Several honeycomb panels were made up and tested structurally. Two different test methods were used as shown in the January progress report. The first method which consisted of a "4 point" loading arrangement using a hydraulic press. This method was later abandoned in favor of a direct vacuum application method. This latter method simply applies a vacuum to a sample over a 4-in. by 8-in. area. The 4 in. is the same span as the honeycomb in our thermal storage unit

design. The 8-in. length was chosen as adequate to minimize end effects. Deflections were measured as a function of applied vacuum (or delta-pressure) across the panel and compared to analytical results. The agreement was reasonably good.

- Another analytical tradeoff was made on honeycomb using face sheet thickness, core depth, core wall thickness, and thermal conductance as parameters. As a result of this, it was decided to increase the core depth from 0.125 in. to 0.50 in. with 0.002 cell wall thickness, and to reduce the face sheet thickness from 0.020 in. to 0.010 in. This gives a stronger panel with less thermal conductance. The 0.50-in. core was ordered from Hexcell. We made the fiberglass face sheets in-house. A report will be written documenting this trade study.
- A technique was developed for making the joint between the "doughnut" honeycomb top and the inner and outer cylinder fiberglass walls. We screened several candidate honeycomb edge closeout materials, and one was selected which will make the closeout and the joint/bond to the cylinder walls simulataneously. A "trial-part" joint was made up and was tested with a one atmosphere pressure load (full vacuum) without joint failure.
- Various methods were investigated and experimented with for bonding the honeycomb core to the face sheets. The objective here is to obtain an adequate structural bond with minimum thermal conductance along the face sheet direction. The normal method to make the bond is with a film adhesive. The fabricated and tested panels using two types of film adhesives and both are acceptable structurally. However, they increase the face sheet thickness, hence conductance significantly. For example, the Normco 329 film adhesive increased the face sheet thickness from 0.020 in. to approximately 0.036 in. i.e., nearly doubling the conductance. Other bonding methods were tried, such as dipping the core in wet resin and then transferring the core to the face sheet and curing it out. This was not very successful because we were unable to maintain a uniform amount of resin onto the core ends. Another method was tried, i.e., placing the film adhesive over the open end core and melting it into place with a heat gun. This has not been successful to date. Another method to be tried again consists of laying up the face sheet prepreg (i.e., B-stage) directly onto the core and curing out in place.
- The problem of bonding the 0.0005-in. stainless steel foil to the fiberglass was pursued with partial success. We still need to work out an acceptable method for etching the steel before bonding. It is very smooth when received from the mill.
- Work was continued on the documentation of the Thermal Analysis/Design Iteration for this unit.
- A "vacuum vessel" of fiberglass approximately 10-in. diameter x 30-in. long was made up for testing to determine the outgassing rates, and permeability effect. It has not been tested yet.
- A meeting was held with the Hexcell Honeycomb Company technical representative concerning some of our problems. He was quite helpful.
- Several additional honeycomb panels were fabricated and tested. These included both 0.25-in. and the new Hexcell 0.5-in. depth core. Face

sheets of 0.010-in. and 0.020-in. thicknesses were used. Three different core-to-face sheet bonding methods were tried. Also the methods of venting the core cells to the vacuum side of the panel were tried. (The cells must be evacuated to prevent natural convection heat transfer while not at zero-g and conductive heat transfer by any trapped air in the cells while the unit is operating in orbit.) The air conductivity and cross-sectional area product is large compared to that of the honeycomb panel values.

- Analytical methods were programmed on the VAX for predicting deflections and stresses in the honeycomb panels. Calculated values were compared with measured values. Thermal conductance value calculations were also added to the program. Figure 5 shows a typical honeycomb test sample with 0.040-in. size vent holes drilled in the bottom face sheet. (Note the separation of the bond between the face sheet and the inner 0.0005-in. stainless steel liner around each vent hole.) This sample failed before reaching full vacuum load due to weakening of the face sheet with the vent holes. Because of this failure it was decided to make a similar panel with a different fabrication technique. The original panel was made by laying up both face sheets onto the core, curing out the adhesive, and then drilling the vent holes. Since these holes were drilled "blind," some of the cell walls were damaged. The second panel was made by bonding only one face sheet, then drilling the vent holes from the open core cells, then bonding on the second face sheet. This second panel was tested with slightly better results. However, it still failed at less than a full vacuum load.
- Another venting method was also tried. Here, each of the core cell walls were "snipped" with a pair of shears for a distance of about 0.125 in. This was to allow the cells to "breathe" between rows. A single vent hole was then provided to allow evacuation of the cells during the test. This sample also failed before reaching full vacuum due to reduction of the core shear strength.
- Hexcell was contacted to determine if they manufacture a vented cell core of this material. They agreed to send us a sample with "vent slits" provided in each node. However, this is not normal practice for them and they do not have any strength data for this product. We will have to do our own testing for these values.
- Testing was begun to measure the thermal conductance of candidate honeycomb panel designs. A test setup was fabricated, and preliminary results were obtained (see Fig. 6). However, results to date have not been satisfactory, apparently because the pressure in our tank was not low enough for the MLI to be effective. This is still being investigated.
- A test was made of the method which was used to make the honeycomb closeout and joint to the two (inner/outer) cylinders. This concept worked quite well. The joint failed at 39 psid giving us a margin of 39/14.7 = 2.65. This test setup is shown in Fig. 7. Pretest sample photos are shown on Figs. 8 and 9, and a post-test photo is shown in Fig. 10.
- The possibility of using a unidirectional tape prepreg for fabrication of the inner cylinder was investigated. This type material has the advantage of having a thermal conductivity value in one direction which

is approximately 70 percent less than the normal bi-directional type materials. This is because the reinforcing fibers are "combed" out in one direction before being saturated with the epoxy resin. Since the reinforcing materials have a significantly higher conductivity than the resin, the composite has a highly directional conductivity value. In our case we would orient the fibers in the circumferential direction so that the conductivity value would be high in this direction and low in the length direction (i.e., down the cylinder) which is the direction in which we want to minimize the heat leak. Hexcell has agreed to supply a free sample of this type material for our evaluation. This is expected at our facility on about 6 April 1987.

- Since we have not been able to purchase off-the-shelf cylinders at the thickness we require (0.030 in.) we have started fabricating these in-house. Some four items have been made to date with varying success. The prepreg tends to wrinkle during the cure cycle causing weak spots in the finished unit. We are continuing to work this problem.
- Honeycomb samples were fabricated using a new concept which would form the vent holes in the face sheets while they are being cured. This would eliminate the post-cure drilling which breaks the reinforcing fibers and reduces the strength of the material. This new concept would form the holes around "pins" in the tooling, hopefully allowing the fibers to be continuous around the individual holes. A tooling board was made up with pins (approximately 0.030-in. diameter) corresponding to each core all location, and a honeycomb sample panel was laid up and cured. This first try was only marginally successful. The fibers did not properly orient around the pins and damage occurred. This venting problem is still being pursued.
- The search for a "cell-edge" adhesive continued, so that the full area film adhesive would not have to be used thereby increasing the face sheet thickness/conductance. Data and literature were received from American Cyanamid Corporation on one of their products which looks promising. They have agreed to furnish a free sample of this for our evaluation.
- Our layup procedures, techniques, bagging materials, etc, were reviewed by the Airtech Technical Representative at Lockheed-Huntsville. This meeting was quite helpful.
- The thermal conductance test tank is being refurbished and refitted for the new turbomolecular pump. An O-ring seal lid is being added to allow us to get down to lower pressures and better performance of the MLI.

<u>Efforts on Fabrication of -95 F Bio-Sample Thermal Storage Demonstration Unit (This Performance Period)</u>: Only a minimum of effort was expended on the -95 F unit during this performance period because we were concentrating on getting the -20 F unit test. The American Cyanamid cell edge adhesive was received and will be tried soon. We are still awaiting the delivery of the unidirectional tape prepeg and vented epoxy glass honeycomb core from Hexcell. Other vacuum bagging materials and shrink tapes were ordered to improve our layup procedures/ results. Some G-10 (epoxy glass) cylinders were received for the purpose of making a smaller diameter bio-sample mockup/model.

Work on the -95 F unit will resume during the June performance period now that we have the -20 F unit under test.

Preliminary Demonstration Unit for -20 F (Food) Storage Unit (This Performance Period): The -20 F thermal storage (food) demonstration unit test was begun and is still in progress. Figures 20, 21, and 22 present preliminary plots of the results to date. The inside aluminum PCM tanks and wire-supported baskets were initially chilled down to below -70 F using LN_2. The test tank is now mounted in a vertical position as shown in Fig. 19. This allowed the LN_2 to fall into the bottom half of the tank thus causing it to be at a lower temperature than the top half. However, as the test progressed these temperatures came together. The temperatures were allowed to rise through the -20 F design point, and the rise rate at that temperature was used to calculate the heat leak into the task. The measured temperature rise rate was approximately 0.193 F/hr at -20 F. This yields a heat-leak rate of 2.3 Btu/hr or 0.67 W with an MC_p value of 12 Btu/F. Table 1 presents hand calculated heat-leak values for the configuration of this test. As Table 1 shows, the total heat leak is calculated to be only 0.122 W. This is a factor of 5.5 or less than that presently being measured. We feel that this discrepancy is in the MLI conductance. From Table 1 it is seen that the strut wire Q is 0.054 W, and the copper instrumentation wire Q is 0.034 W. The length, diameters, and thermal conductivities of these are all well known. This indicates that the MLI conductance of the test article must be higher than that used in the analysis. The conductivity value we used was taken from Ref. 2 as 1.4×10^{-5} Btu/ft^2-hr-F. This was the lowest value presented in Ref. 2, and is for 160 layers which is the number of layers in our test article. After further consideration of this problem it appears that the most likely source of discrepancy is in the method used to form the MLI around the basket ends (inside the tank ends/domes). The cylinders were wrapped by winding continu- ously and a length of MLI was left hanging over the end. This length was then "gored" by cutting out "pie-shaped" section. These MLI layers were laid or folded down into place and taped down. It is possible that these layers were pulled down too tightly before taping, thus compressing the layers and thermally "shorting" the blanket. This is further complicated by the MLI shrinkage at low temperatures.

To avoid this potential problem, we plan to disassemble the tank and reconfigure the MLI design. The "gored and taped" ends will be replaced with blankets made of individual disks/layers laid up in the direction perpendicular to the tank longitudinal axis. Hopefully this will bring the measured results closer to the theoretical values.

The turbopump was left on during the duration of this test to ensure proper pressure levels and worked well. The pressures were in the 10^{-7} torr range for most of the test.

References:

1. Karu, Z.S., "Thermal Analyses for Development of Test Article for Space Station Logistics Module Food Freezer," LMSC-HEC TM D065551, Lockheed Missiles & Space Company, Huntsville, Ala., December 1986.

2. Stochl, Robert J., "Basic Performance of a Multilayer Insulation System Containing 20 to 160 Layers," NASA TN D-7659, April 1974.

Table 1 HAND CALCULATED HEAT LEAK RATES FOR -20 F STORAGE UNIT TESTS OF 27 MAY 1987 THROUGH 8 JUNE 1987

Heat Leak Source	Conductance (Btu/hr-F)	ΔT (F)	$\dot{Q}$ (Btu/hr)	$\dot{Q}$ (watts)	Percent of Total
Stainless Steel Strut Wires	19.5×10^{-4}	75-(-20)	.185	.054	44
Multilayer Insulation (1.5-in. Thick)	12.2×10^{-4}	75-(-20)	.116	.034	28
Copper Instrumentation Wires (24 Wires)	12.24×10^{-4}	75-(-20)	.116	.034	28
Totals			.417	.122	100

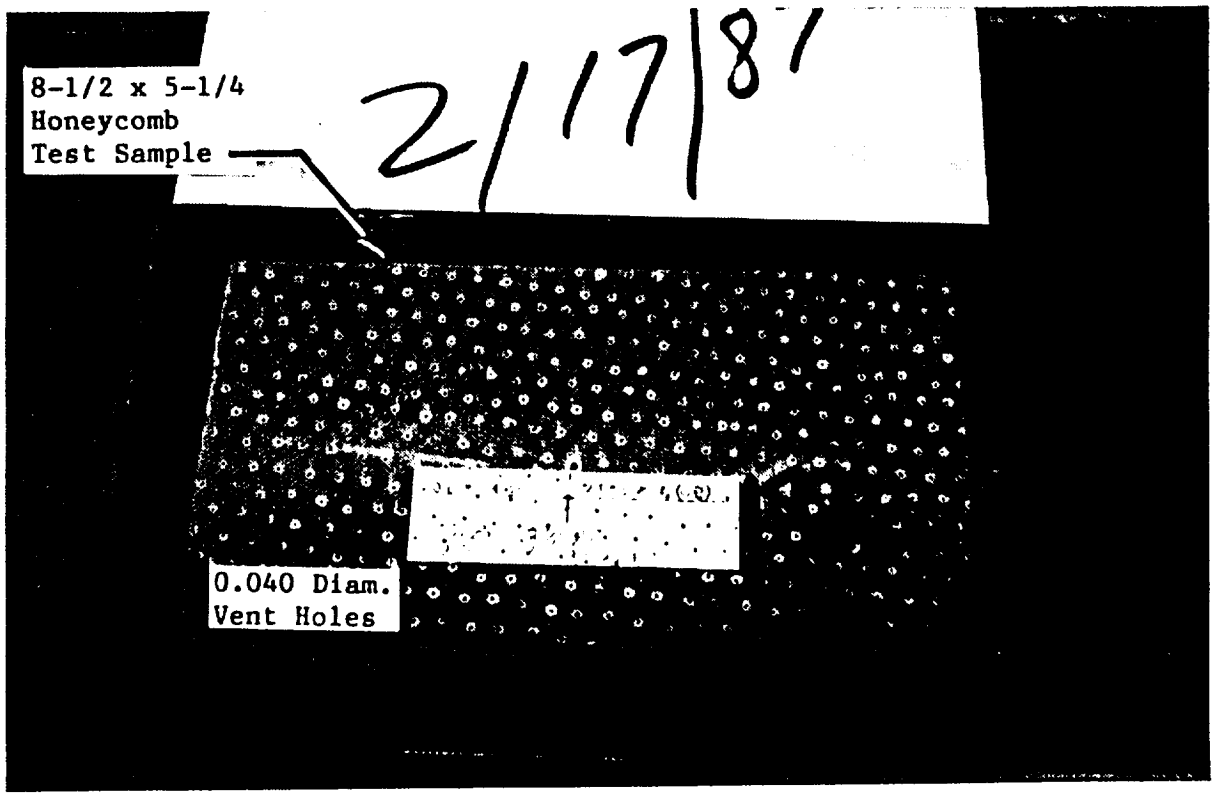

Fig. 5 Honeycomb Panel Sample with Vented Cell Face Sheets, 0.5-in. Core Depth, 0.010 Face Sheets

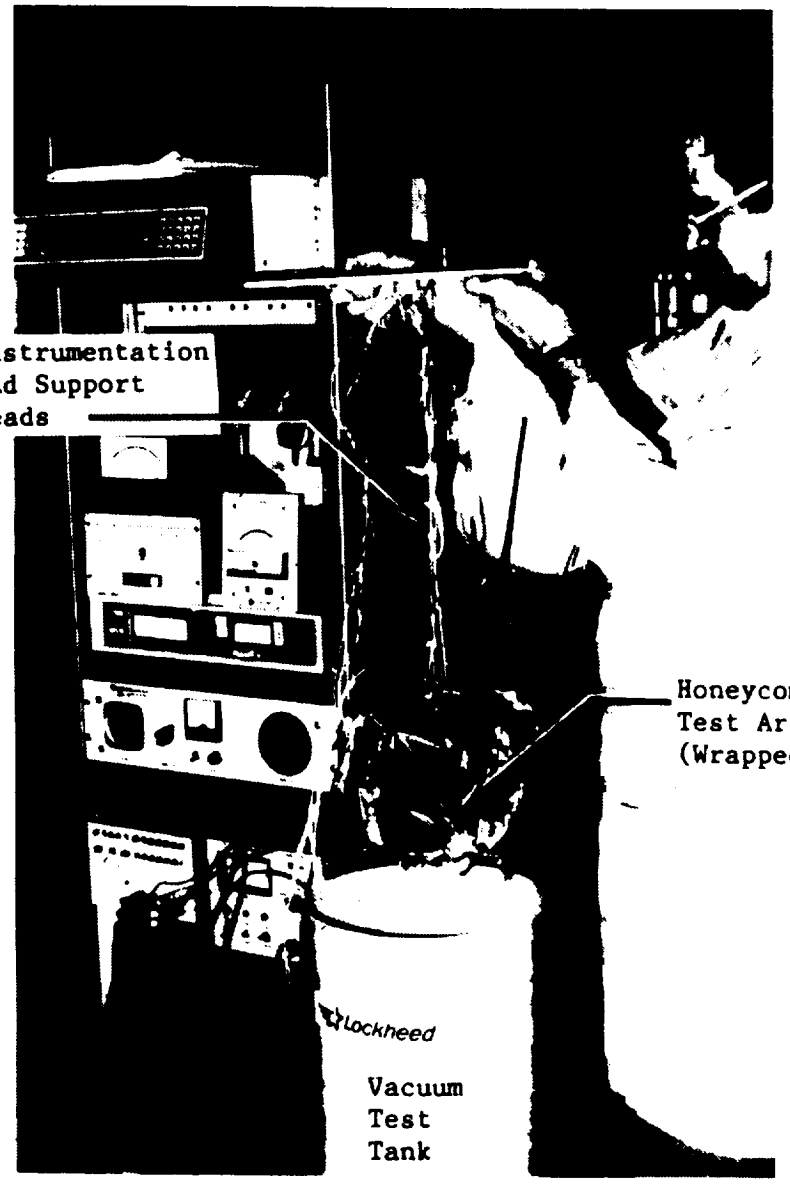

Fig. 6 Thermal Conductance Test Article Being Placed into Test Tank

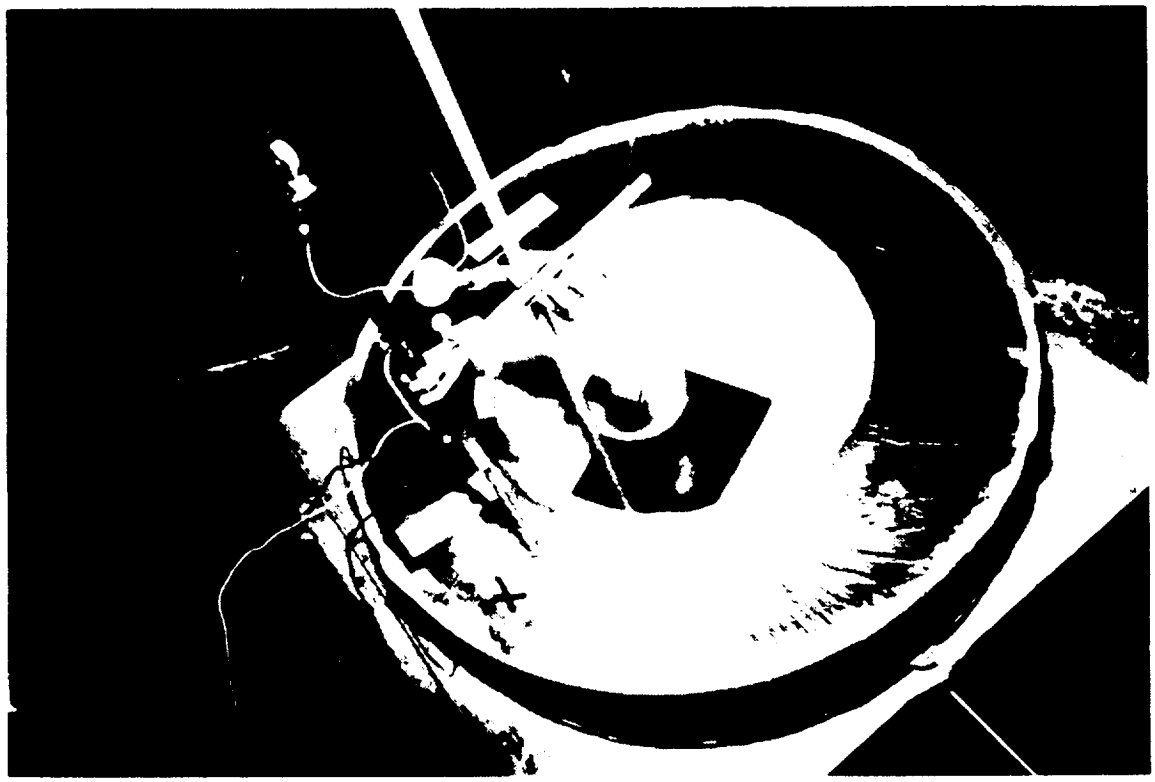

Fig. 7 Setup for Testing Between Honeycomb and Inner and Outer Cylinders Joint

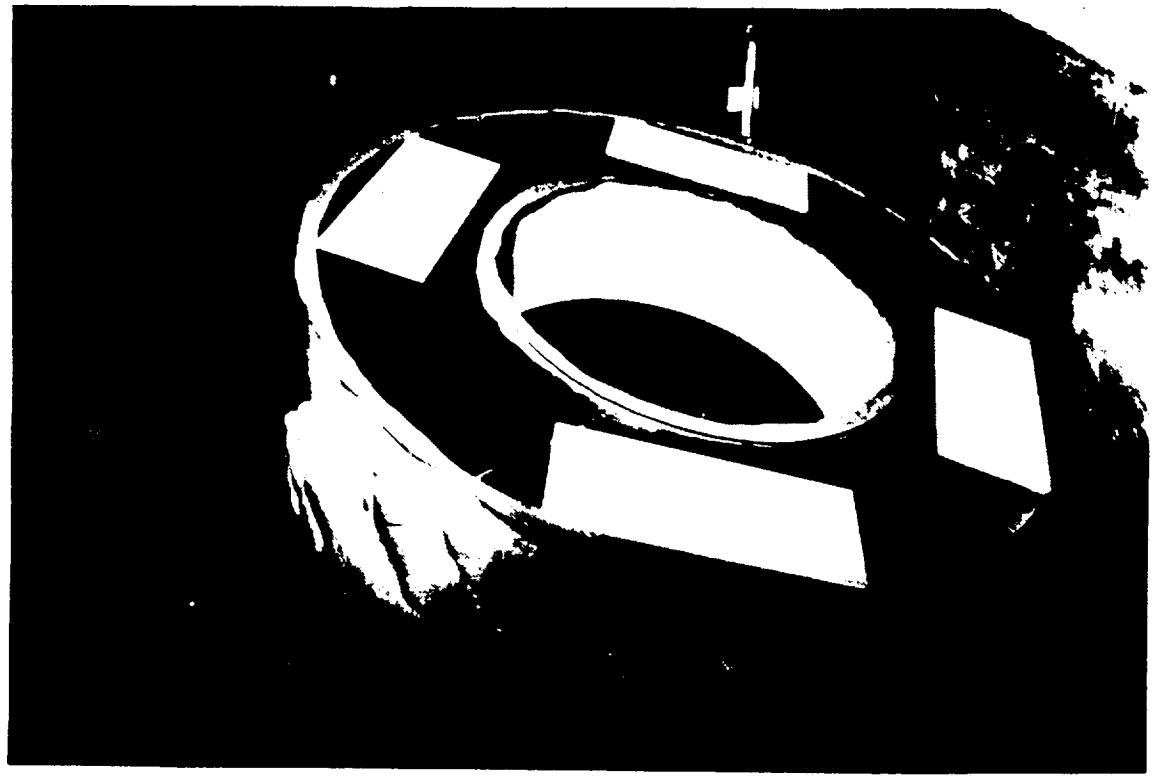

Fig. 8 Pretest Photograph of Joint Test Sample

Fig. 9 Pretest Photograph of Joint Test Sample

Fig. 10 Post-Test Photograph of Joint Test Sample
(Failure Occurred at 39 psia)

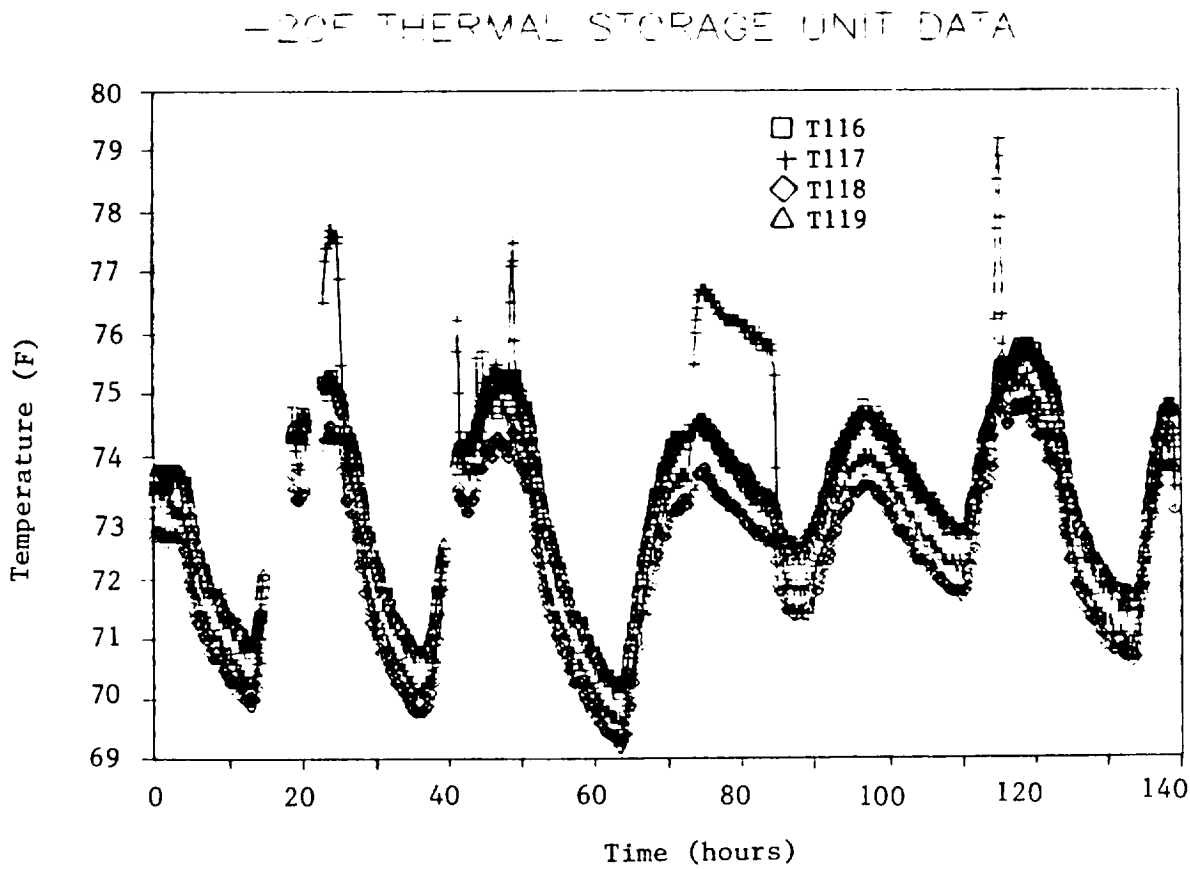

Fig. 11 Typical Outer Wall Temperatures vs Time for -20 F Thermal Storage Unit Test (Tests: 18 Mar 87 Through 24 Mar 87)

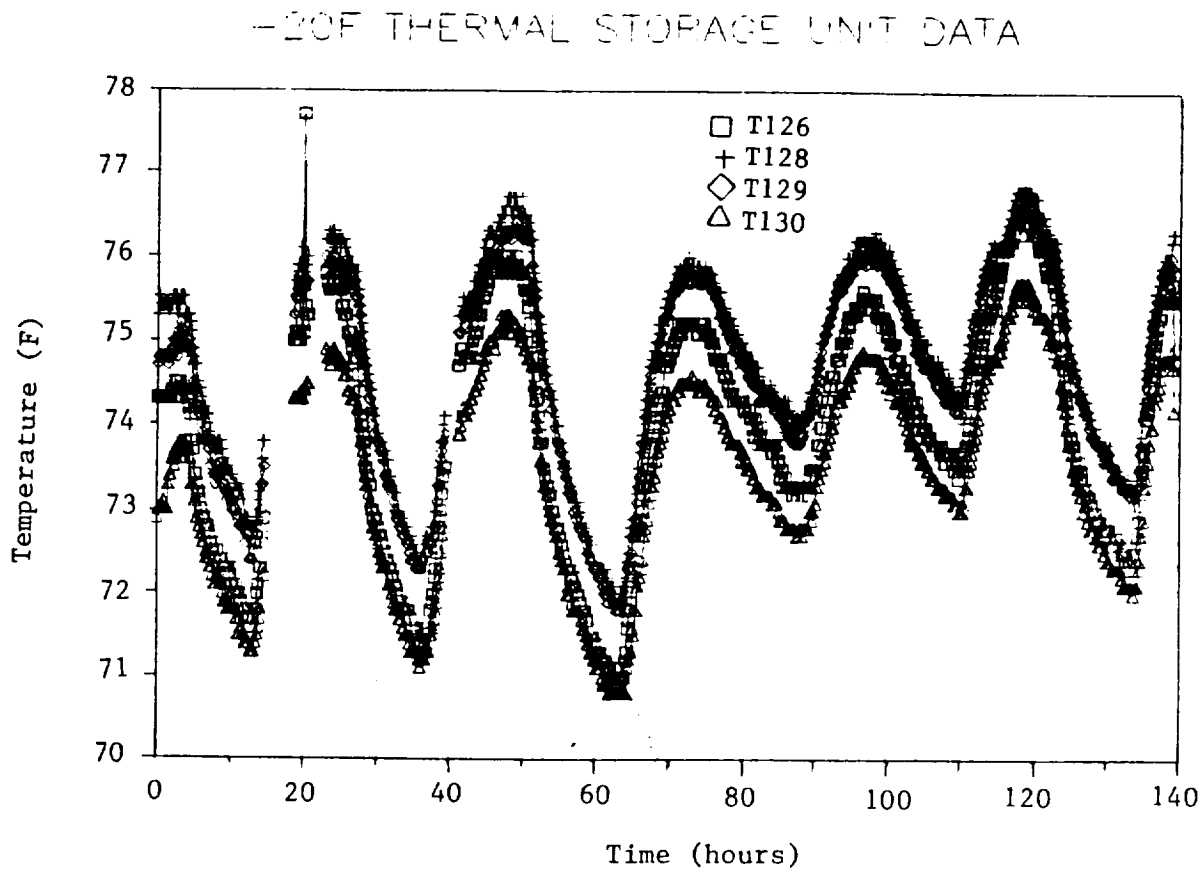

Fig. 12 Typical Outer Wall Temperature vs Time for -20 F Thermal (Food) Storage Unit Test (Tests: 18 Mar 87 Through 24 Mar 87)

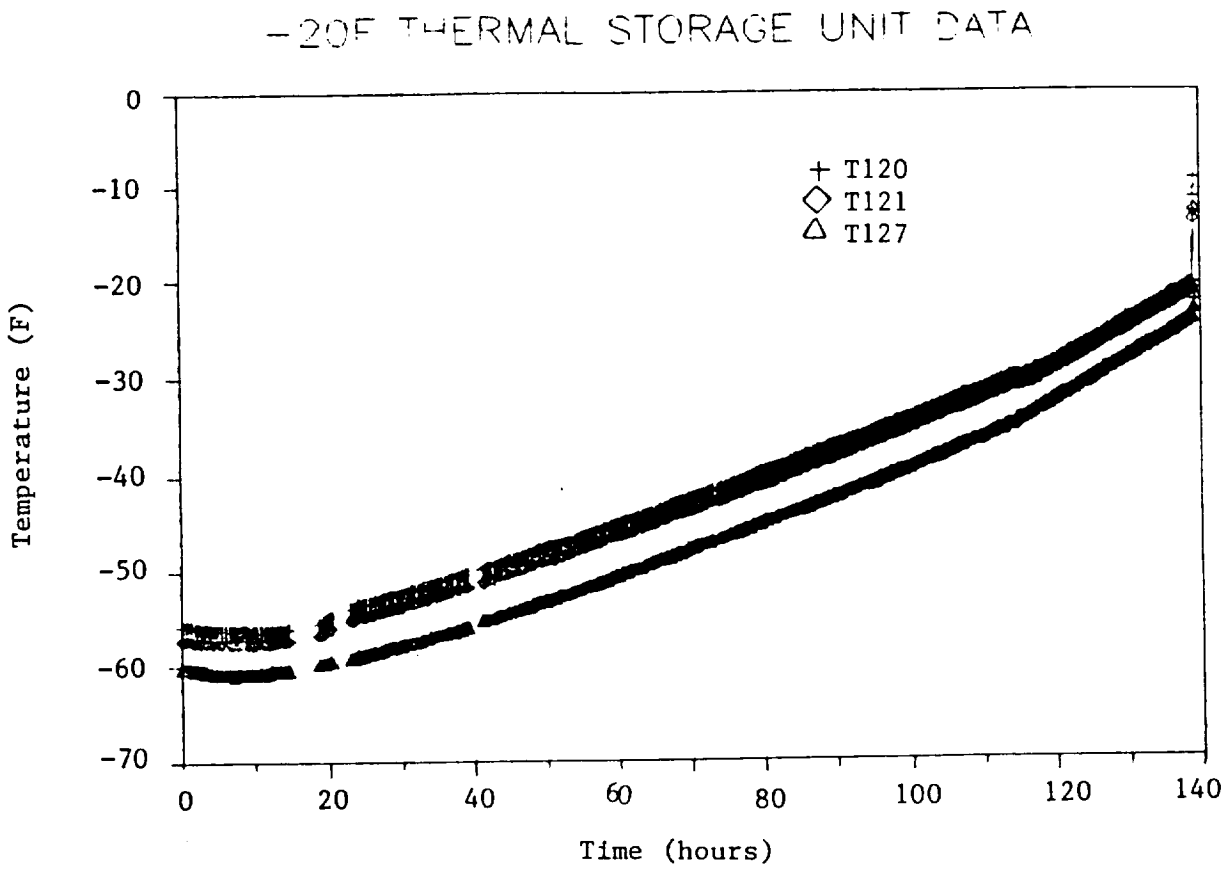

Fig. 13 Temperature vs Time for Three Internal Temperature Measurements for -20 F Thermal (Food) Storage Unit Test (Tests: 18 Mar 87 Through 24 Mar 87)

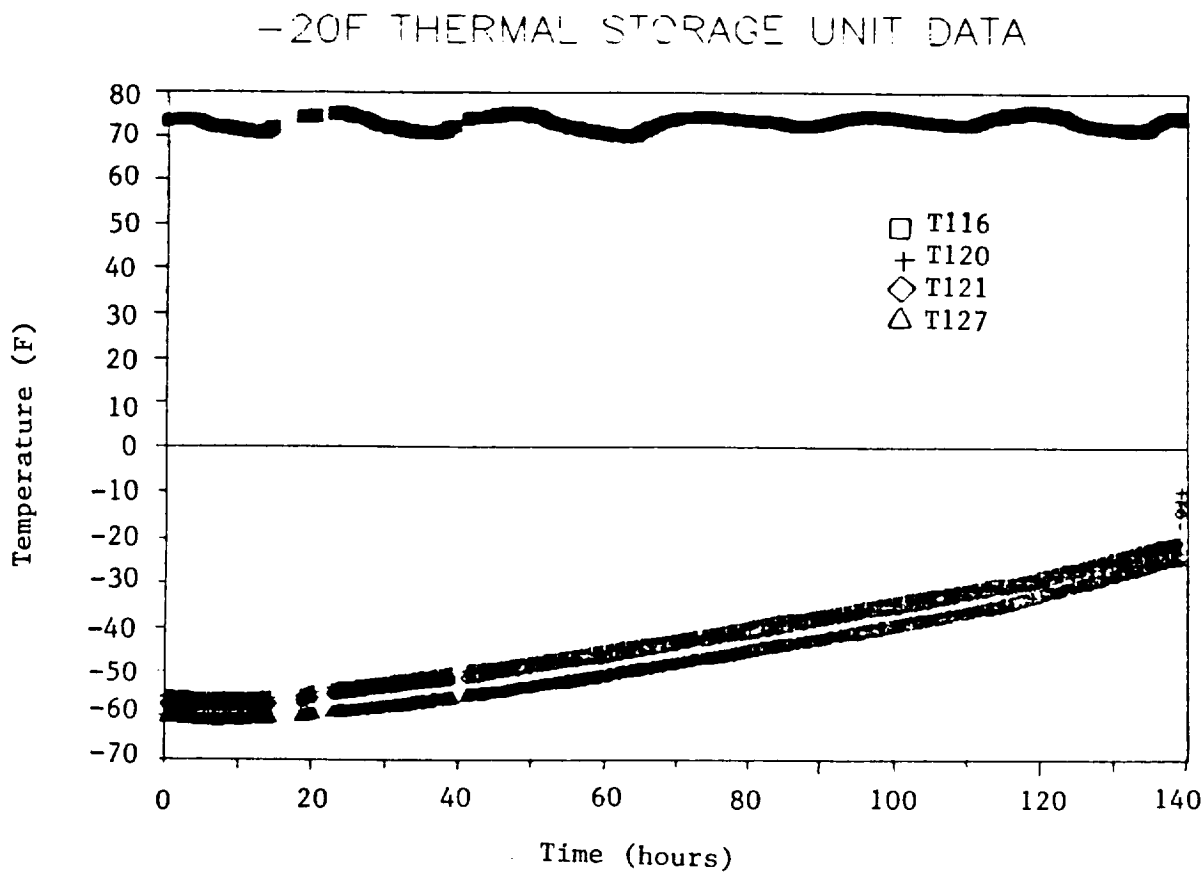

Fig. 14 External and Internal Temperatures Superimposed, for -20 F Thermal (Food) Storage Unit Test (Tests: 18 Mar 87 Through 24 Mar 87)

Fig. 15 Inner Bracket from -20 F Demonstration Unit Wrapped with New MLI

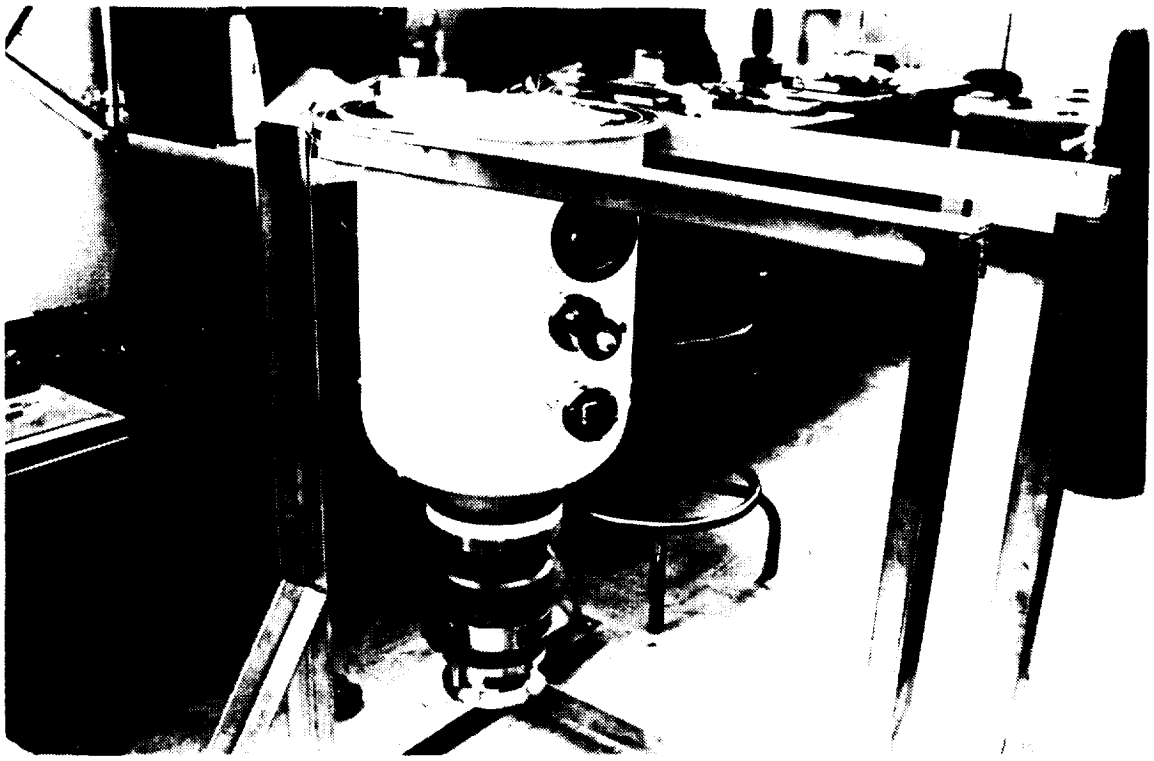

Fig. 16 Lower Tank Half Attached to Turbomolecular Vacuum Pump (-20 F Demonstration Unit)

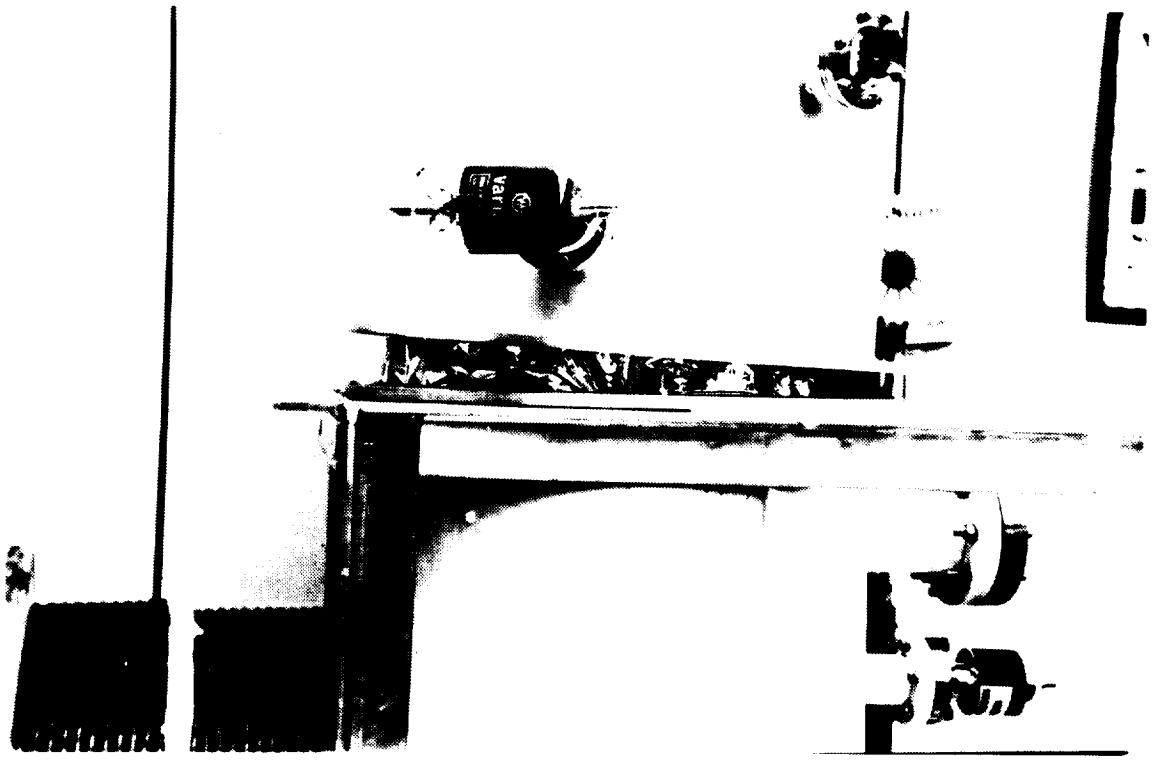

Fig. 17 Two Tank Halves Being Assembled for -20 F Demonstration Unit

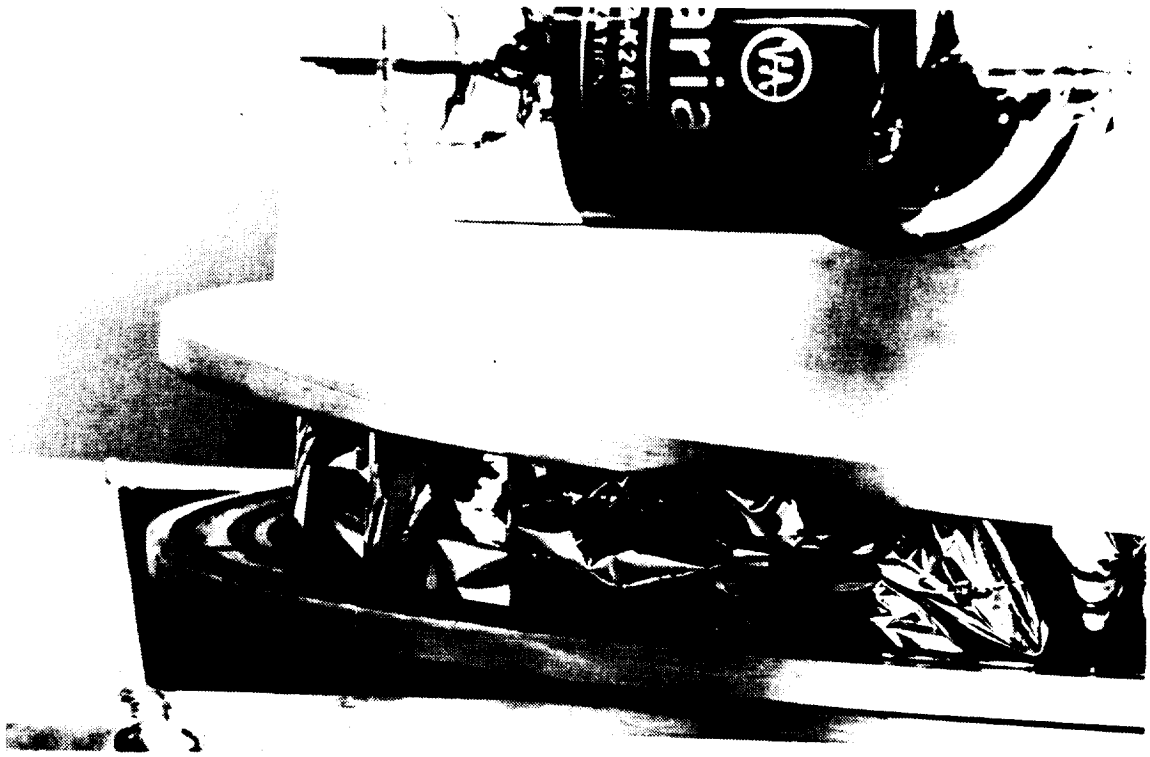

Fig. 18 Closeup of Two Tank Halves During Assembly Showing MLI Bellyband/Closeout

Fig. 19 Minus 20 F Demonstration Unit Tank Under Vacuum Bakeout

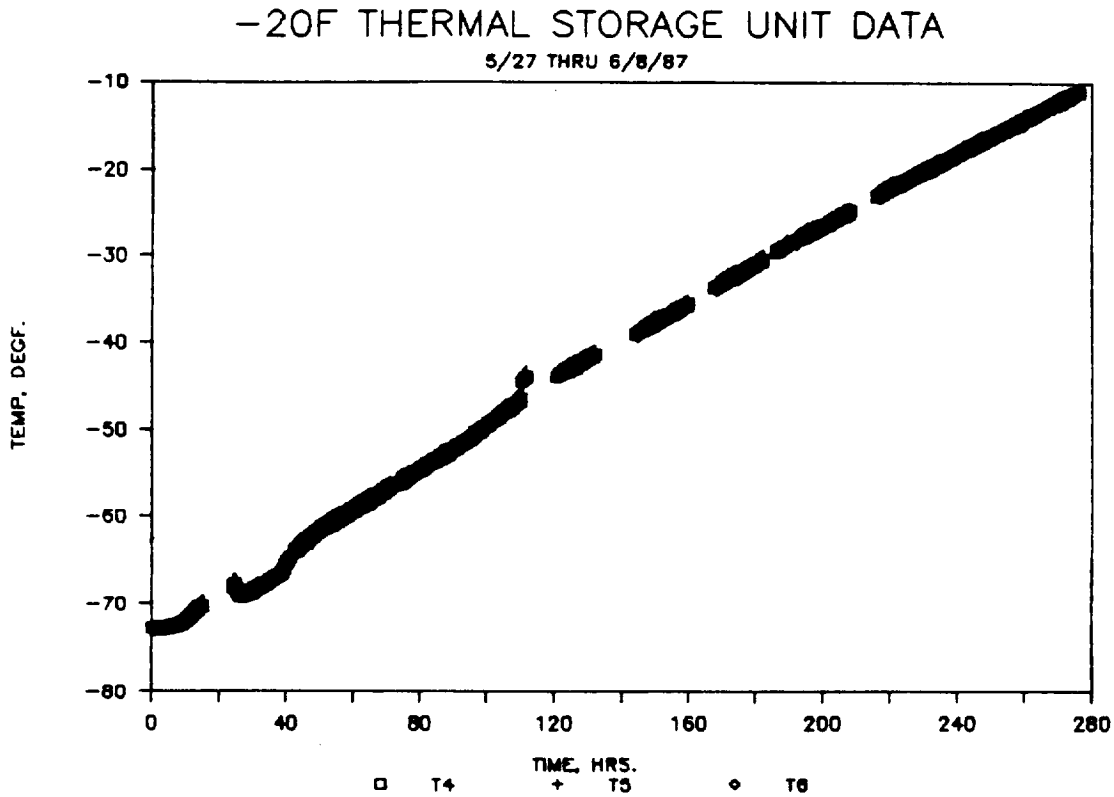

Fig. 20 Temperature vs Time for Three Measurements on Inner Tank During Demonstration Testing 27 May 87 Through 8 Jun 87 (T4, T5, and T6 Are Also on Upper Half of Tank.)

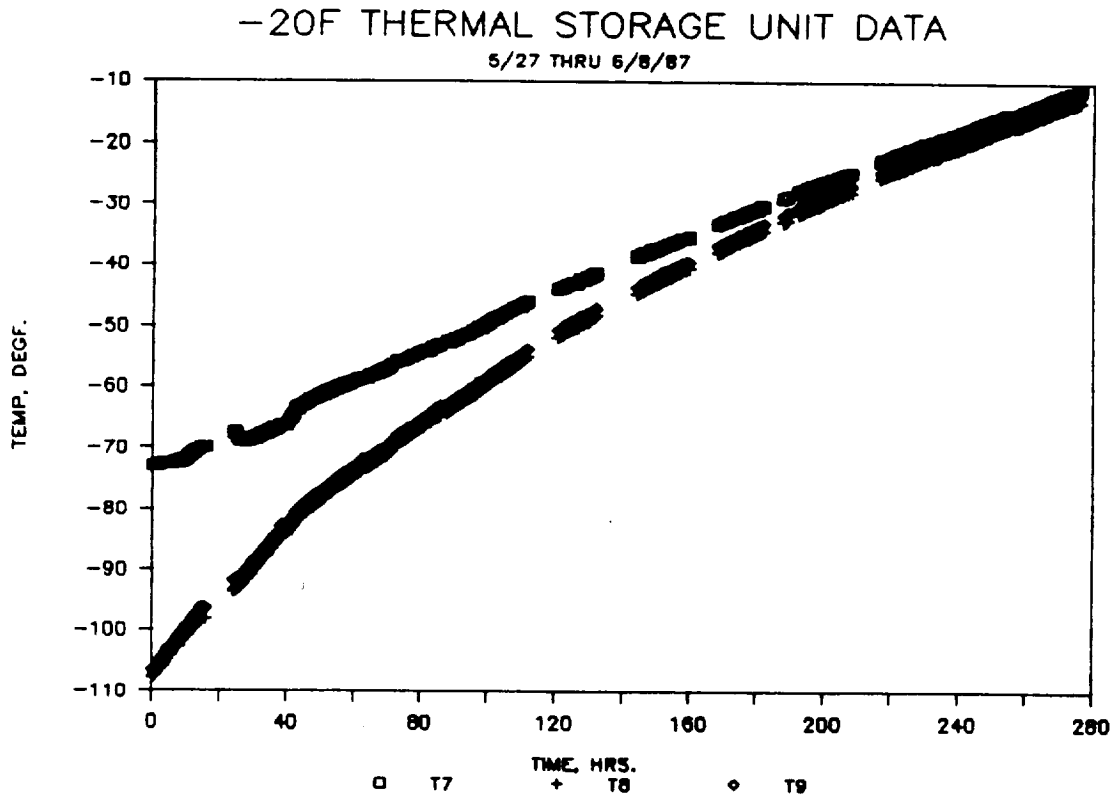

Fig. 21 Temperature vs Time for Three Measurements on Inner Tank During Demonstration Testing 27 May 87 Through 8 Jun 87 (T7 is on Upper Half; T8 and T9 Are on Lower Half.)

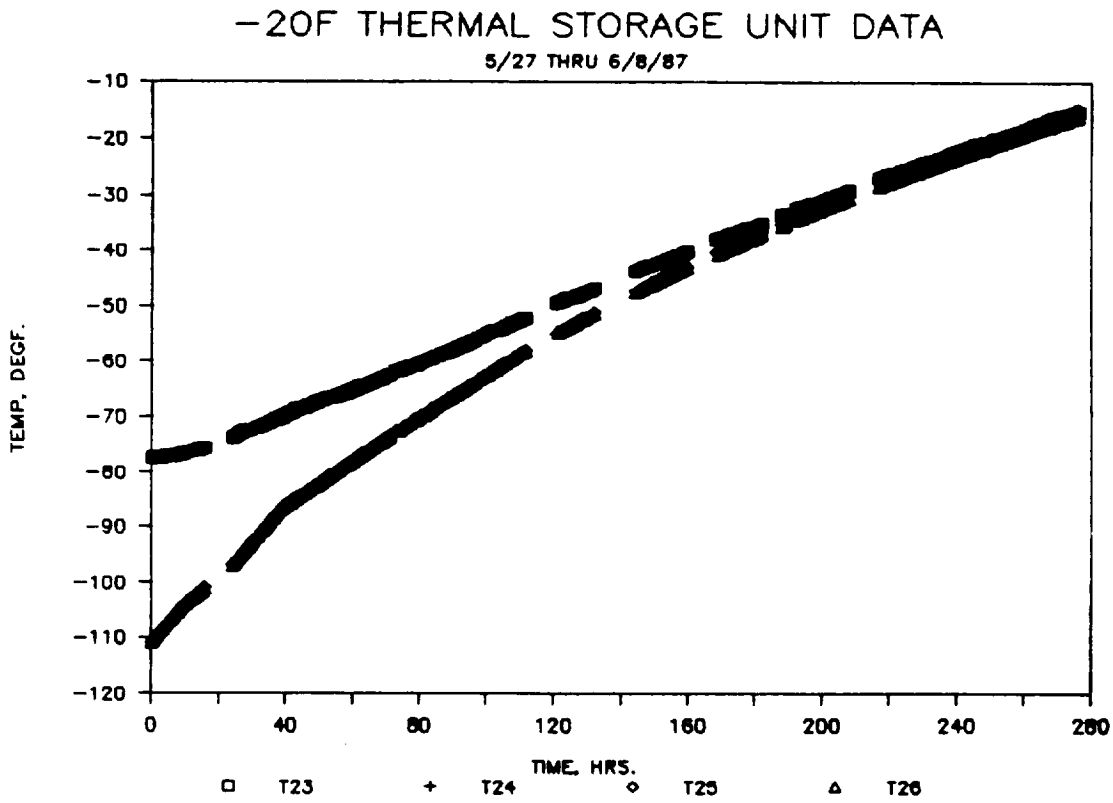

Fig. 22 Temperature vs Time for Three Measurements on Inner Tank During Demonstration Testing 27 May 87 Through 8 Jun 87 (T23 and T24 are on Upper Half of Tank; T25 and T26 Are on Lower Half.)

APPENDIX B

Biofreezer Test Configuration/Design Updates and Results of Testing at Lower Temperatures

(Excerpts from August 1990 through January 1991 Monthly Progress Reports)

Excerpt from August 1990 Monthly Progress Report LMSC-HSV PR F312333

PROGRESS DURING THE CURRENT REPORTING PERIOD

PRECEDING PAGE BLANK NOT FILMED

Testing of Biosample Freezer

A breakthrough was made during this reporting period. As mentioned in last month's progress report, the lowest temperature obtainable at that time was approximately -240 °F. However, we have now been able to reach a temperature of approximately -370 °F. This was attained as a result of two factors: (1) we modified the Biofreezer test configuration/design, and (2) with this modified design we were able to get liquid nitrogen into the inner cylinder and then subcool it by lowering the vapor pressure over the liquid. This caused the temperature to drop below the melting point and freeze the nitrogen. (The boiling point of nitrogen is -320.4 °F at 1 atmosphere pressure and its melting point is -346.0 °F. When the vapor pressure is reduced to 1 mm Hg, the solid temperature drops to -375.0 °F.)

In order to achieve testing at these lower temperatures, the following changes were made to the Biosample Freezer:

1. The rubber band center joint seal was replaced with two mating rings and an O-ring.

2. New aluminum joint seals were made for the joint between the diaphragm and the inner cylinder and bonded in place (see Figure 1).

3. New 0.001 in. thick titanium seals were made and bonded in place at the joint between the outer cylinder and the diaphragm (see Figure 2).

4. A fill tube and a vent tube were made and installed through the MLI. This entailed making a 3/8 in. hole through the MLI and the inner and outer cylinders. The fill/vent tubes were made of 0.010 in. thick epoxy-glass and lined inside and outside with 0.001 in. thick titanium foil (see Figure 3). These tubes were then bonded to a support base and NW-25 flange vacuum connection (see Figures 4 and 5). This assembly was the tested by chilling with LN_2 to check the integrity of the design (see Figure 6). Then it was leak tested under full vacuum load while immersed in LN_2 (see Figure 7). This assembly was then bonded in place through the freezer walls with the RTD leads alongside the tube. This provided a minimum heat-leak penetration through the MLI insulation, which would withstand the vacuum pressure loads (see Figures 8 and 9). The entire freezer assembly was then leak tested with helium gas.

5. The aluminum heat sinks were modified so that they would be stable, i.e., not roll around, or fall over, inside the inner cylinder without being bonded. Two wire-wound platinum RTDs were bonded to each heat sink, with 0.003 in. diameter constantan leads. These were 3-wire configurations to eliminate the effects of the high lead wire resistance. The small diameter is needed in order to minimize heat leaks. Note: the minimum temperature that can be measured with these RTDs is -328 °F.

One annular thin film foil heater was bonded to each heat sink. These were for future use in calibrating the heat capacity of the heat sinks at low (≃ 320 °F) temperatures, since satisfactory test values have not been found in the literature (see Figure 10).

6. A Mylar blanket was made up and installed in the lower part of the inner cylinder to avoid having LN_2 impinge directly on the thin wall of the inner cylinder.

7. Three 0.005 in. diameter Chromel/Alumel thermocouples were made up and installed inside the inner cylinder. These were for the purpose of directly measuring the temperature of the LN_2/SN_2. They were first installed on top of the Mylar blanket and later moved under the blanket.

8. The entire freezer was mounted on a set of lab balances in order to measure the rate of change in weight, i.e., LN_2 boiloff rate, during a given test.

Testing was continued as these changes were being added. Figures 11, 12, and 13 show the Biosample Freezer being filled with LN_2, after being charged with LN_2, and after beginning of pumpdown, respectively.

Table 1 summarizes the tests run to date.

Figures 14 through 45 show preliminary results from these latest tests. For most of the tests, the data are shown for varying time spans starting at the beginning of the test and proceeding to longer and longer times as the test progresses. This is done so that the data in the early part of the test is readable. If only the total time plots were shown, the initial transient temperature details would not be readable.

Figure 25, which shows some of the data from the initial times of the test on 8/2/90, is used to illustrate what is happening during this early transient time. The first phase of the test is the chilldown phase with the temperature dropping from -280 °F to the liquid nitrogen temperature of -320 °F. This temperature levels out while additional LN_2 is being added. Then the next phase starts when the freezer is sealed off and the vapor pressure is lowered using two vacuum pumps. This causes the temperature tc drop below -320 °F and then below -328 °F which is the lower limit of the RTDs being used. (The thermocouples had not yet been added when this test was conducted.) The RTDs go off scale until about 0.8 hours when they start to warm up above -328 °F again. The temperature then increases to about -320 °F where it remains nearly constant for a period of "steady-state" testing while the heat leak is determined from LN_2 boiloff rates.

PRECEDING PAGE BLANK NOT FILMED

Table 1. SUMMARY OF TESTS RUN TO DATE ON BIOSAMPLE FREEZER

Test Date	Heat Sink Temp. at Start of Test (°F)	Miminum Pressure Obtained (torr)	Test Duration (hr)
5/23/90	-2	1×10^{-3}	5
5/25/90	-6	5×10^{-5}	5
5/29/90	4	6×10^{-4}	27
6/11/90	-52	2×10^{-5}	46
6/15/90	-60	1×10^{-5}	64
6/22/90	-100	1×10^{-5}	66
6/25/90	-150	4×10^{-5}	46
6/28/90	-200	7×10^{-5}	24
6/29/90	-240	3×10^{-5}	48
7/25/90	Room temperature pump-down to check O-ring seal		
7/27/90	-310	**	68
7/30/90	< -328	**	22
7/31/90	< -328	**	23
8/1/90	Data not reduced due to problem with cryopumping air into MLI space		
8/2/90	< -328	**	96
8/7/90	< -328 (-340)*	**	24
8/8/90	< -238 (-370)*	**	44

* Temperatures in LN_2/SN_2.

** Data not yet reduced.

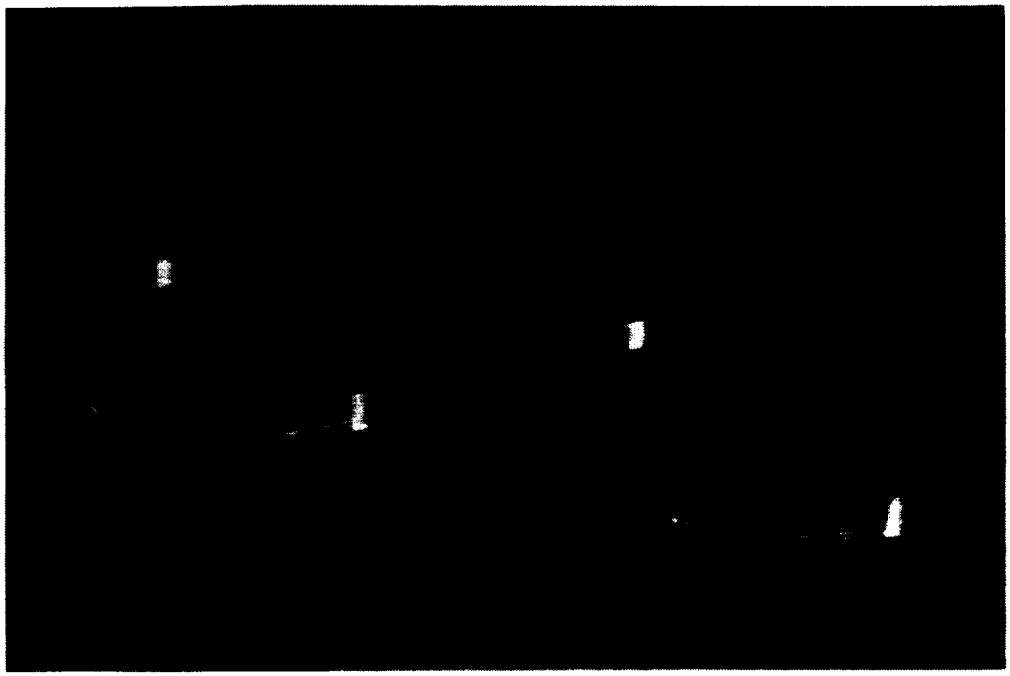

Figure 1. New Aluminum Joint Seals for Inner Cylinder for Diaphragm Joint

Figure 2. New 0.001 in. Thick Titanium Seals for Outer Cylinder to Diaphragm Joint

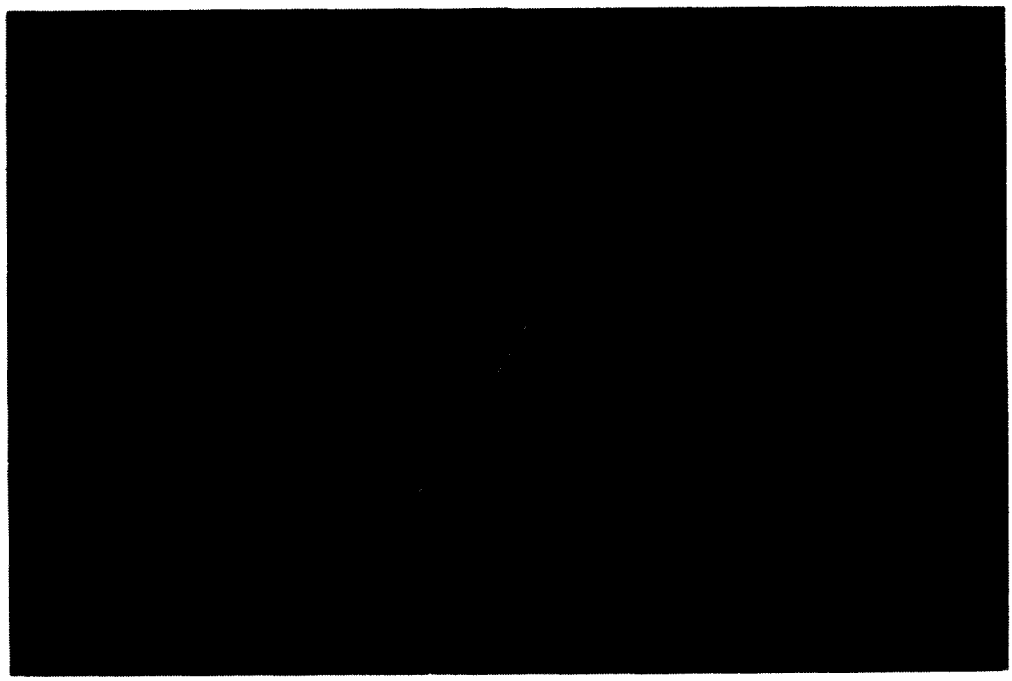

Figure 3. Typical Fill/Vent Tube (0.010 in. Epoxy-Glass with 0.001 in. Titanium Foil Inside and Outside) 3/8 in. Diameter

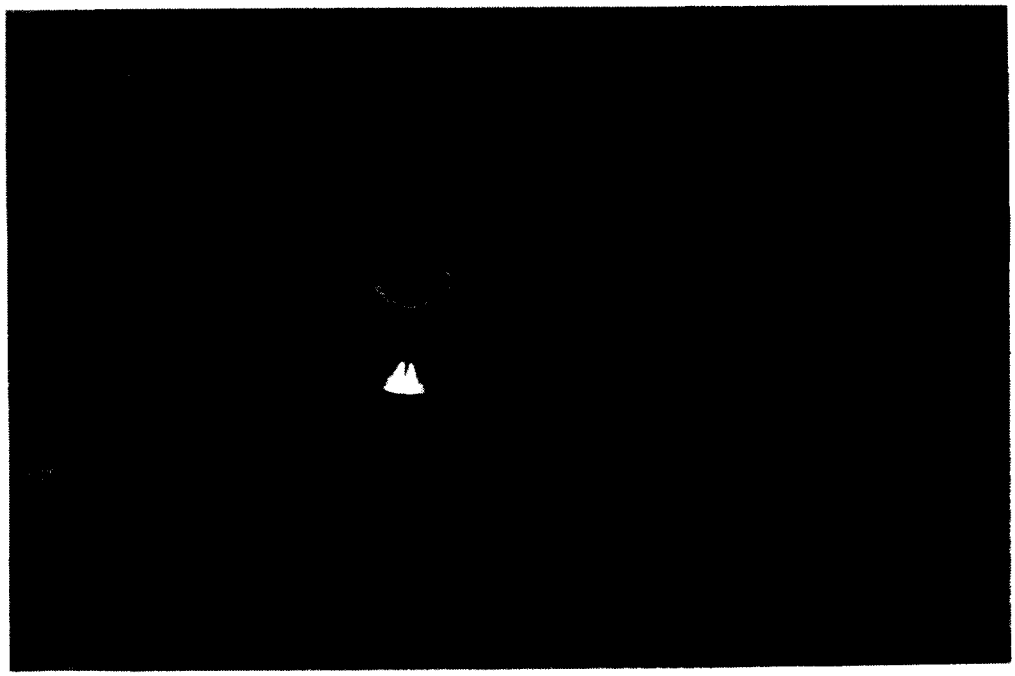

Figure 4. Typical Fill/Vent NW-25 Flange Vacuum Connection

Figure 5. Partially Assembled Fill/Vent Tubes

Figure 6. LN_2 Test of Fill/Vent Tube before Installation

ORIGINAL PAGE
BLACK AND WHITE PHOTOGRAPH

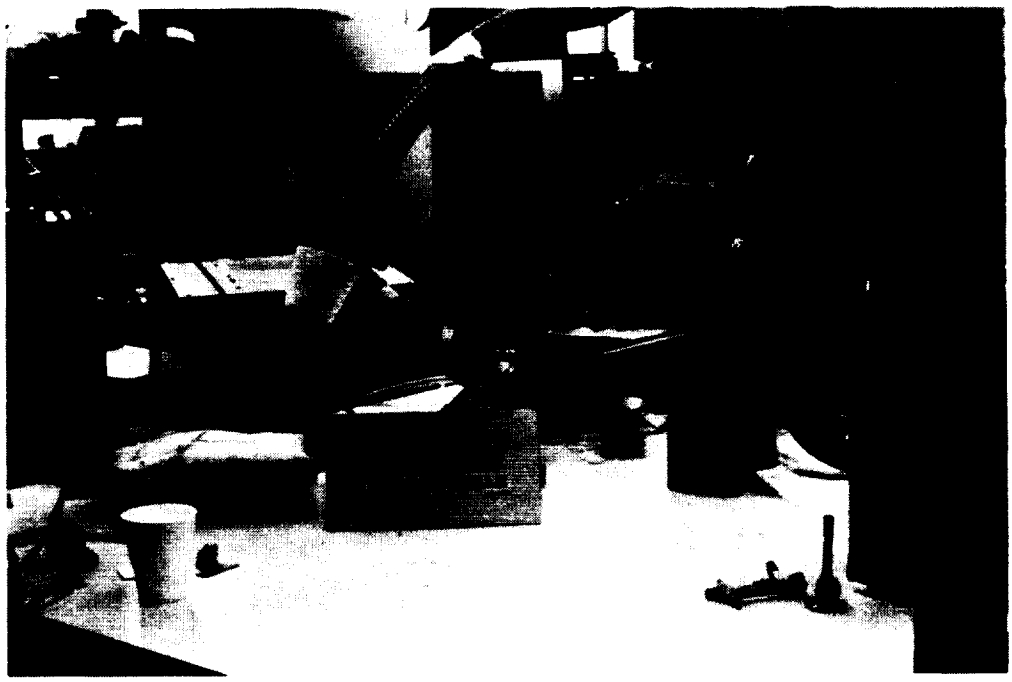

Figure 7. Vacuum Leak Test of Fill/Vent Tube while immersed in LN_2

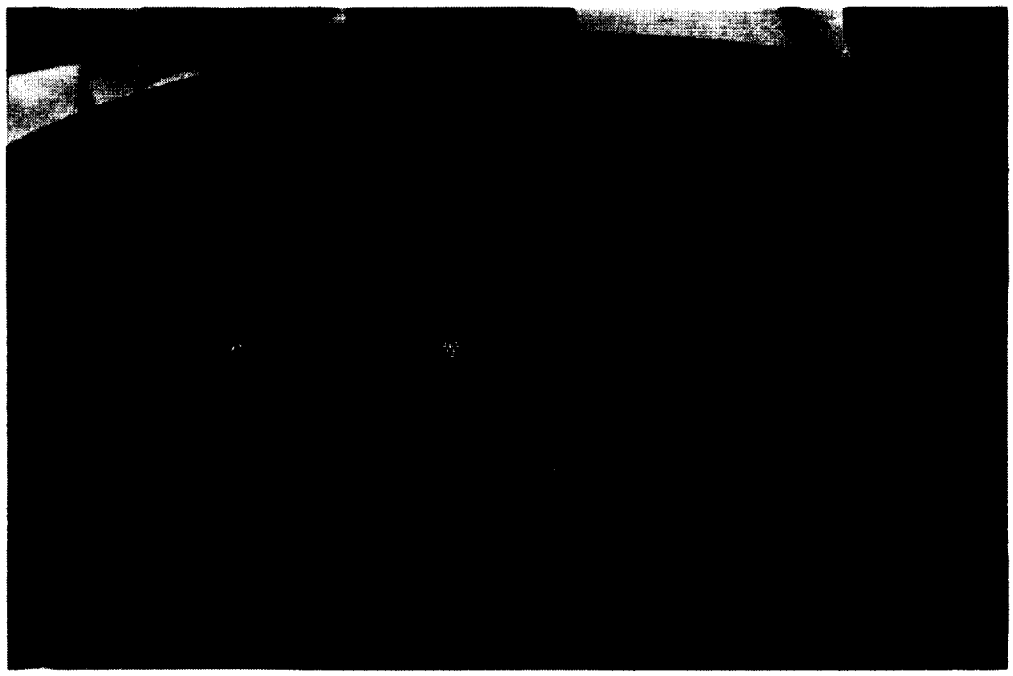

Figure 8. Typical Fill/Vent Tube View after Installation Inside of Freezer Inner Cylinder

ORIGINAL PAGE
BLACK AND WHITE PHOTOGRAPH

Figure 9. Typical Fill/Vent Tube View after Installation with RTD Lead Wires in Place

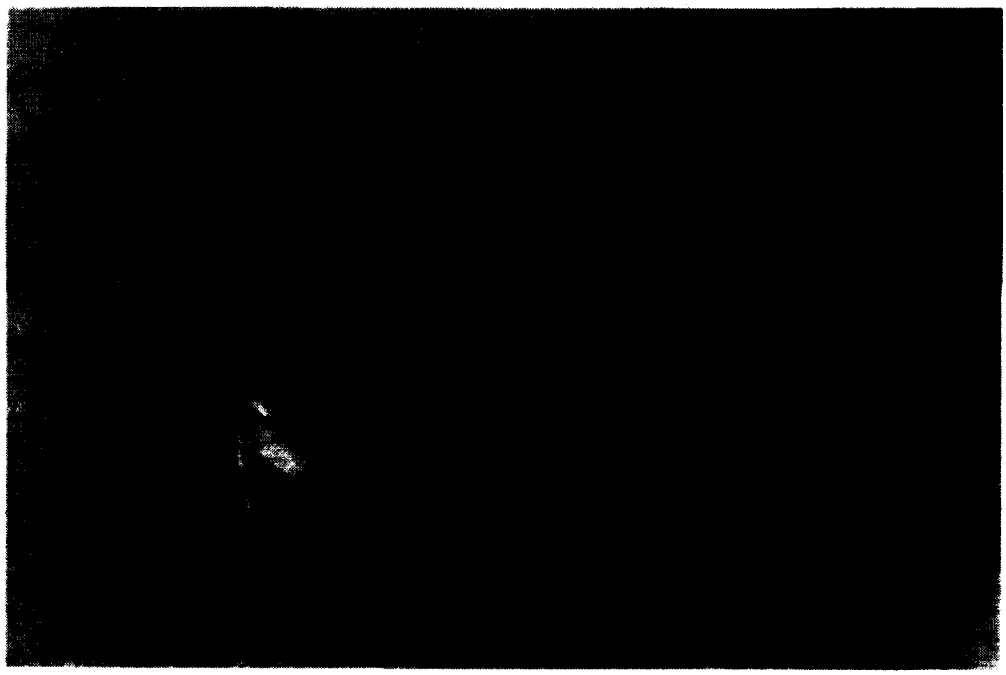

Figure 10. Annular Foil Heater Installed on Aluminum Heat Sink

Figure 11. Biosample Freezer Being Filled with LN_2 Before Start of Test

Figure 12. Biosample Freezer after Being Charged with LN_2

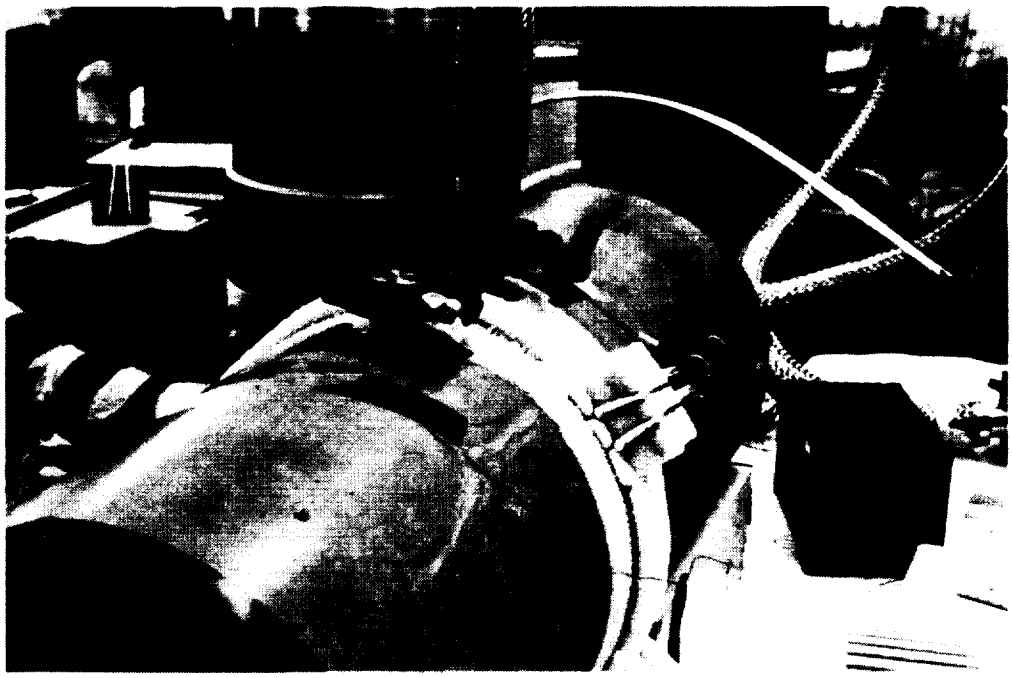

Figure 13. Biosample Freezer at Startup of Test

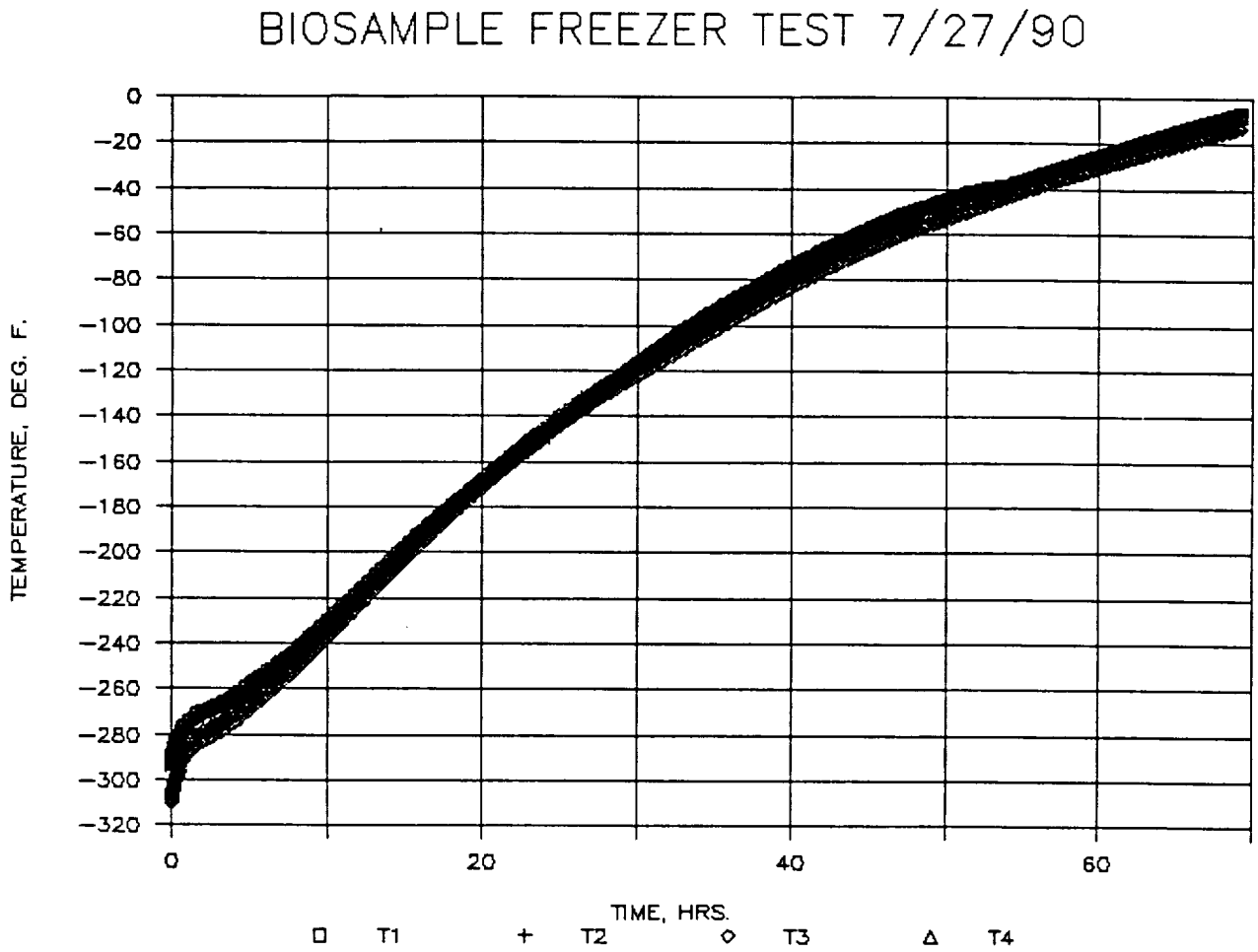

Figure 14. Temperature vs Time for 4 RTDs on Heat Sinks during Biosample Freezer Test on 7/27/90

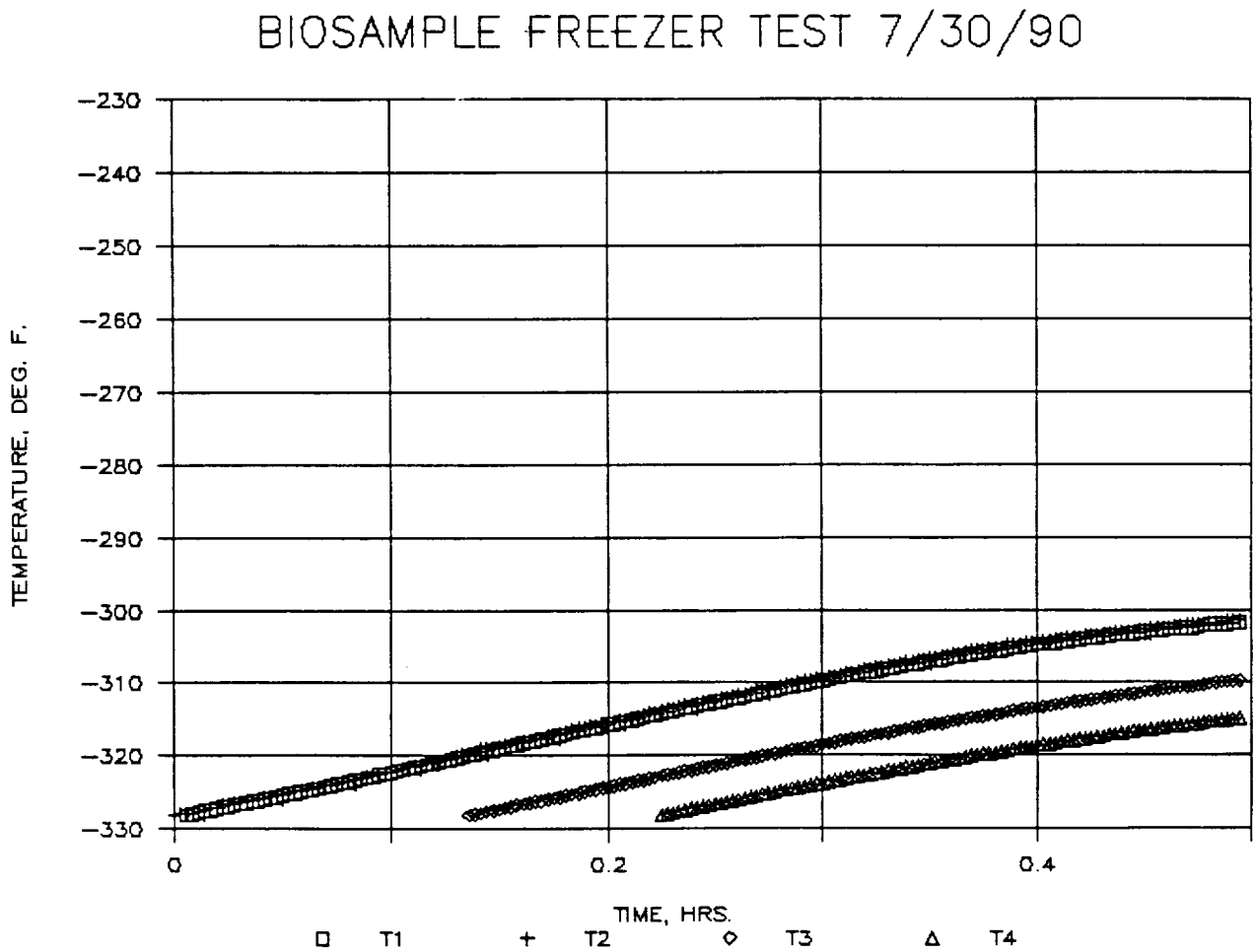

Figure 15. Temperature vs Time for 3 RTDs on Heat Sinks during Initial 0.5 Hour of Biosample Freezer Test on 7/30/90

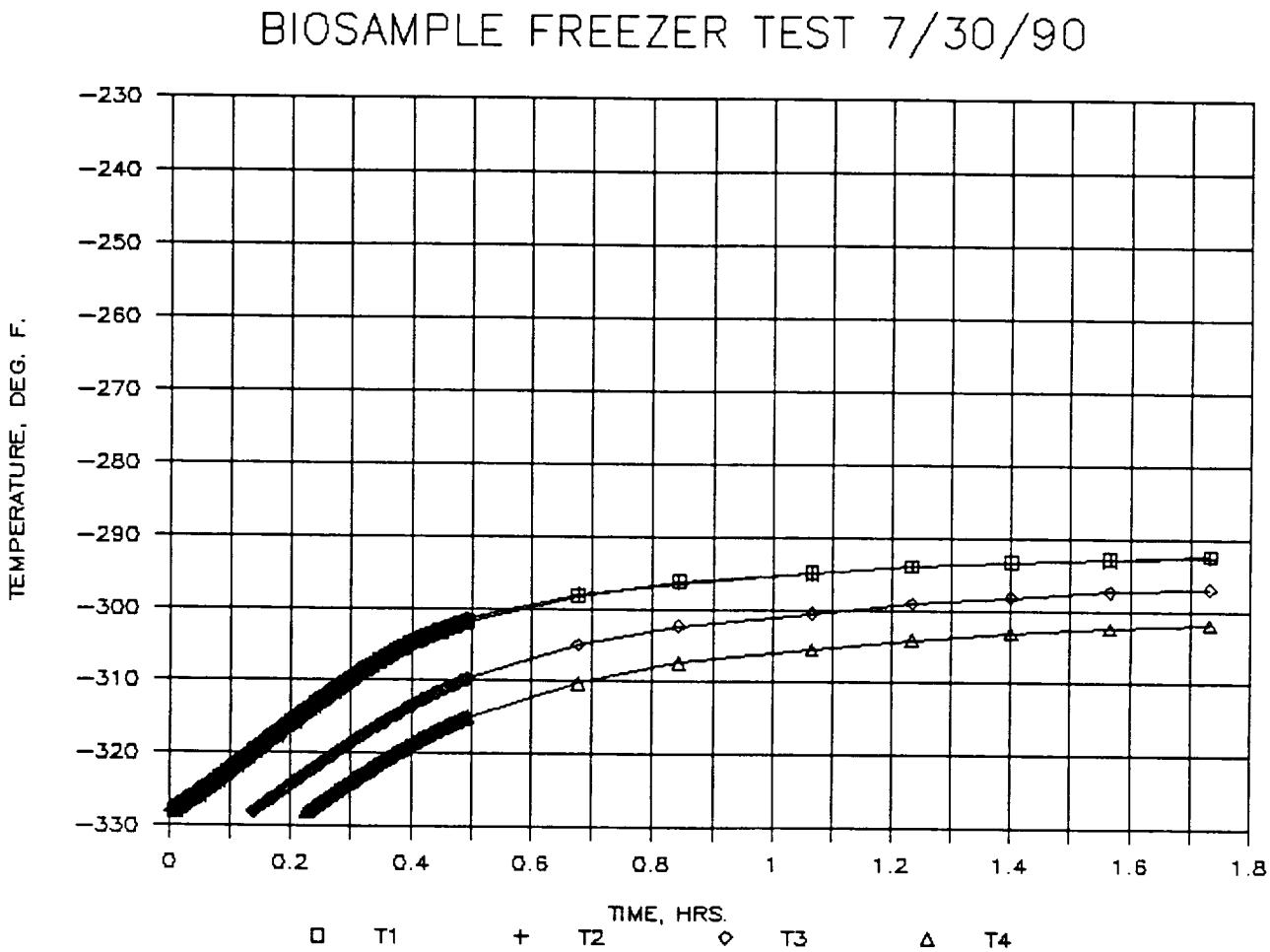

Figure 16. Temperature vs Time for 3 RTDs on Heat Sinks during Initial 1.8 Hours of Biosample Freezer Test on 7/30/90

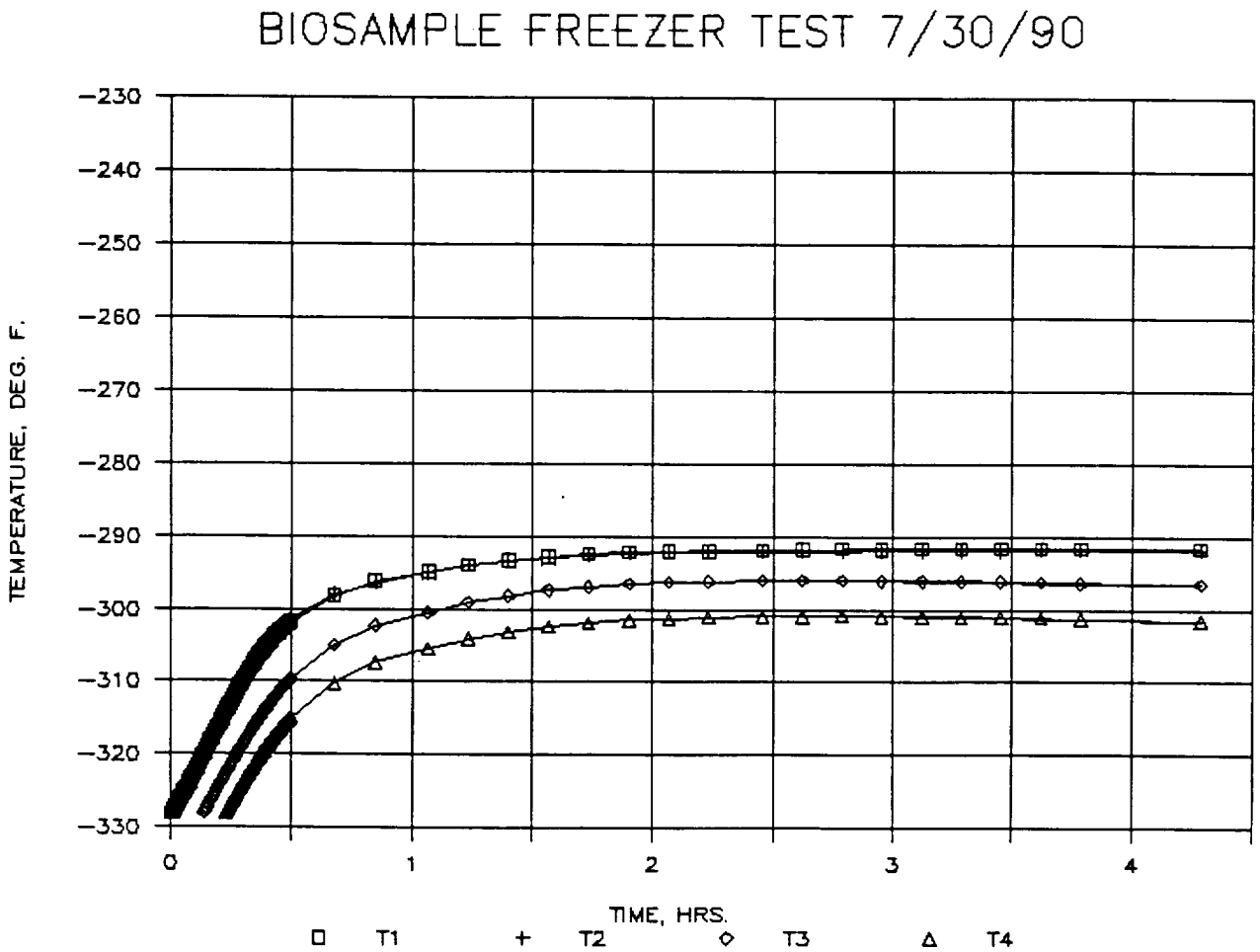

Figure 17. Temperature vs Time for 3 RTDs on Heat Sinks during Initial 5 Hours of Biosample Freezer Test on 7/30/90

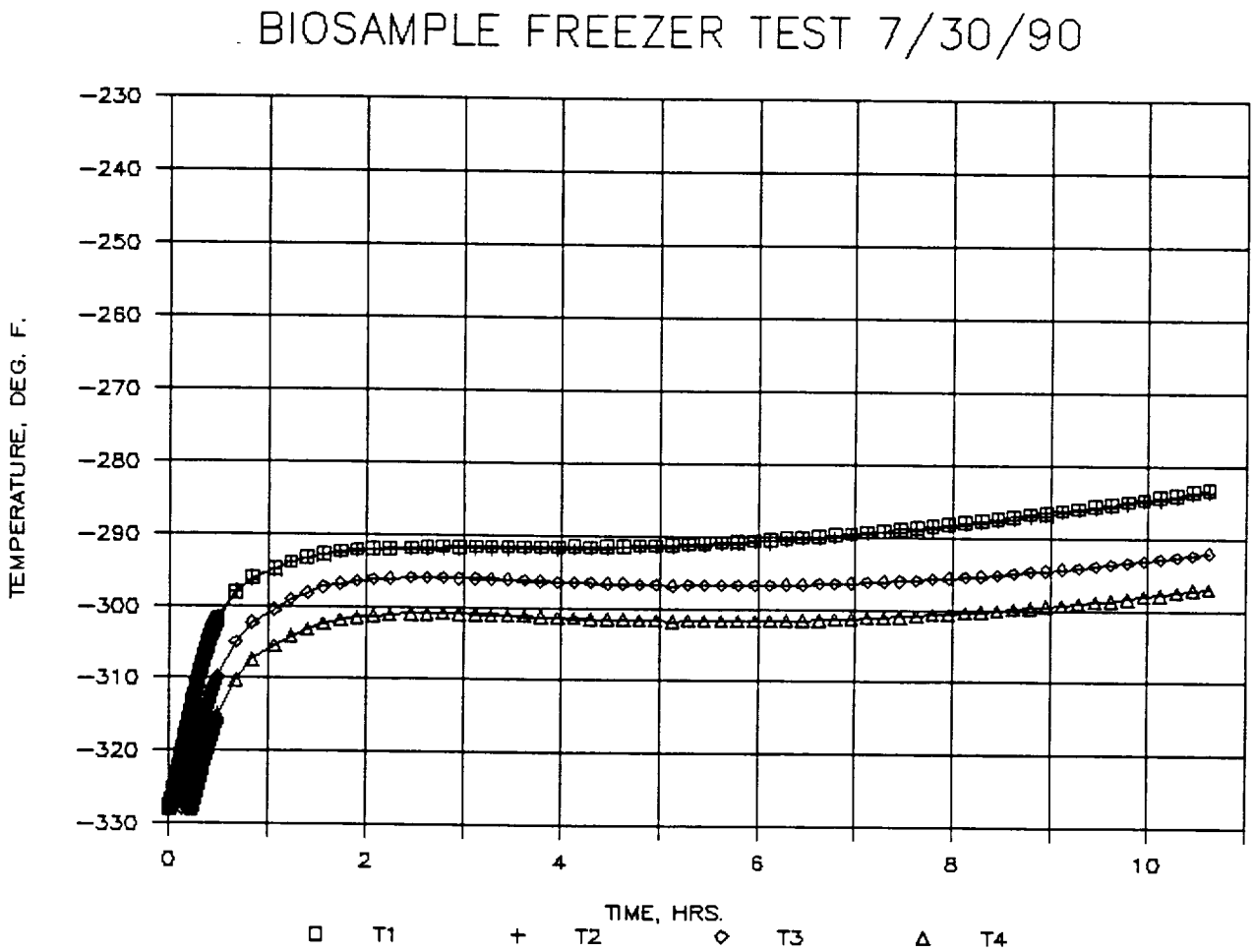

Figure 18. Temperature vs Time for 3 RTDs on Heat Sinks during Initial 11 Hours of Biosample Freezer Test on 7/30/90

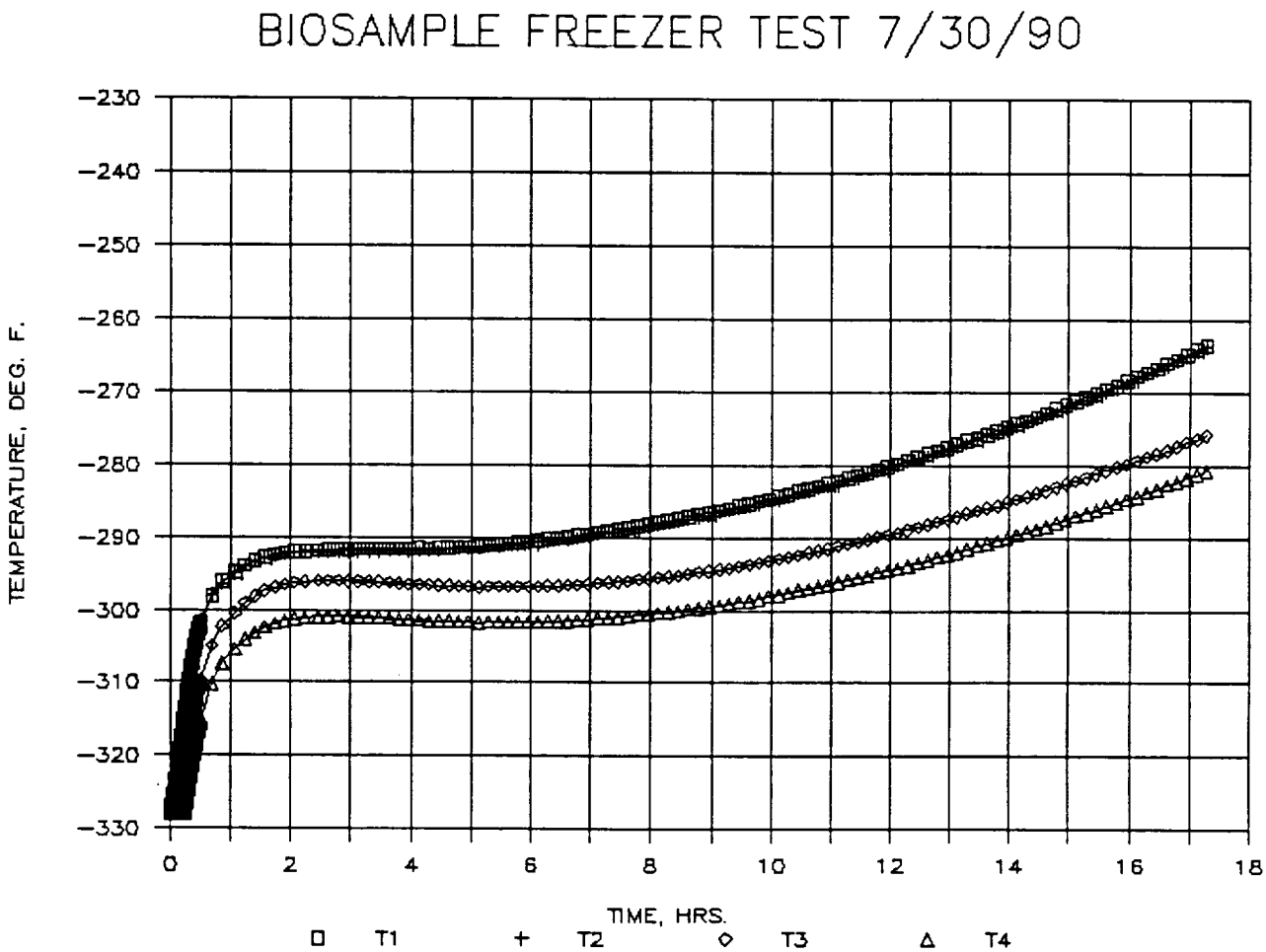

Figure 19. Temperature vs Time for 3 RTDs on Heat Sinks during Initial 17 Hours of Biosample Freezer Test on 7/30/90

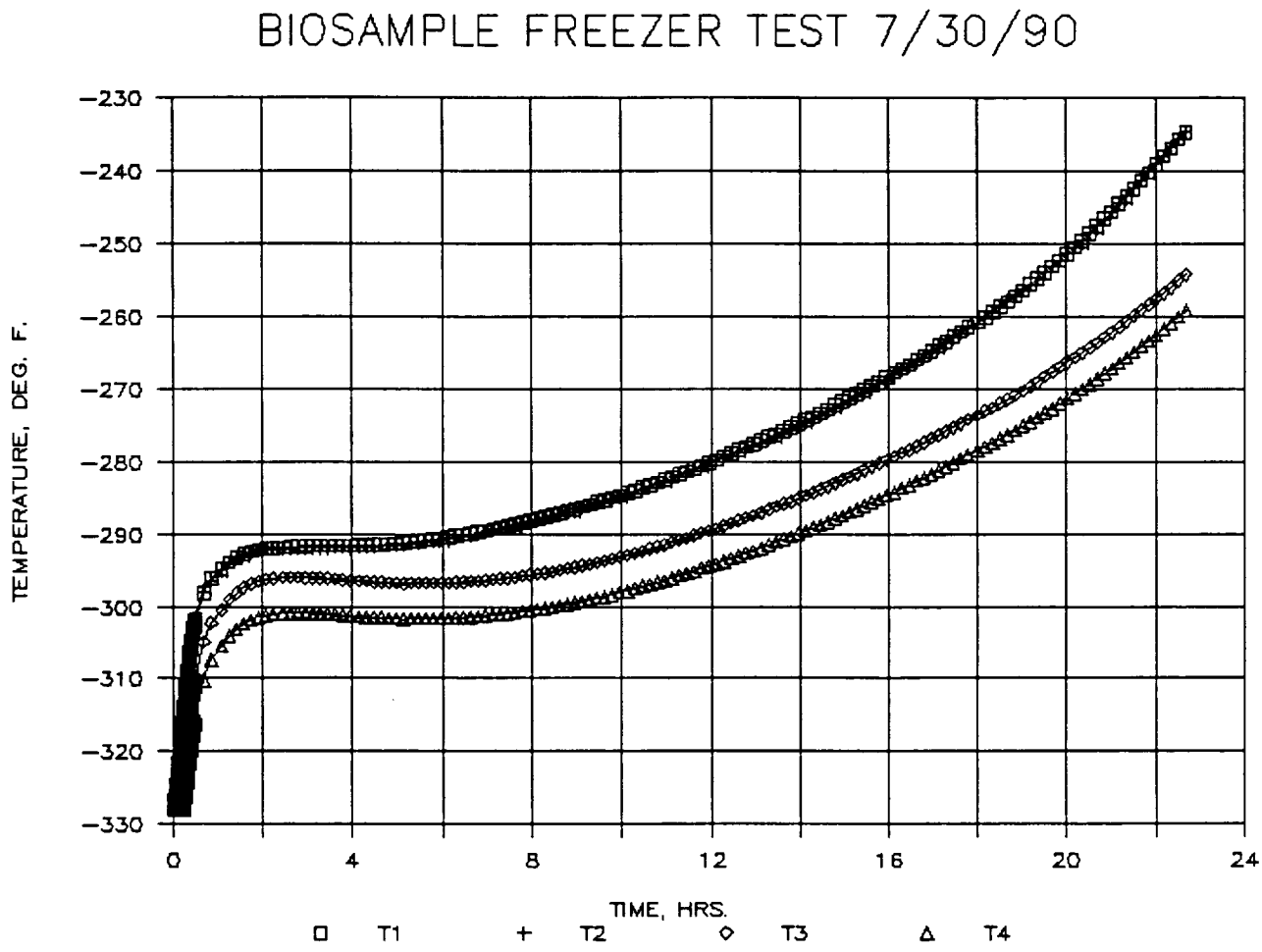

Figure 20. Temperature vs Time for 3 RTDs on Heat Sinks during Initial 22 Hours of Biosample Freezer Test on 7/30/90

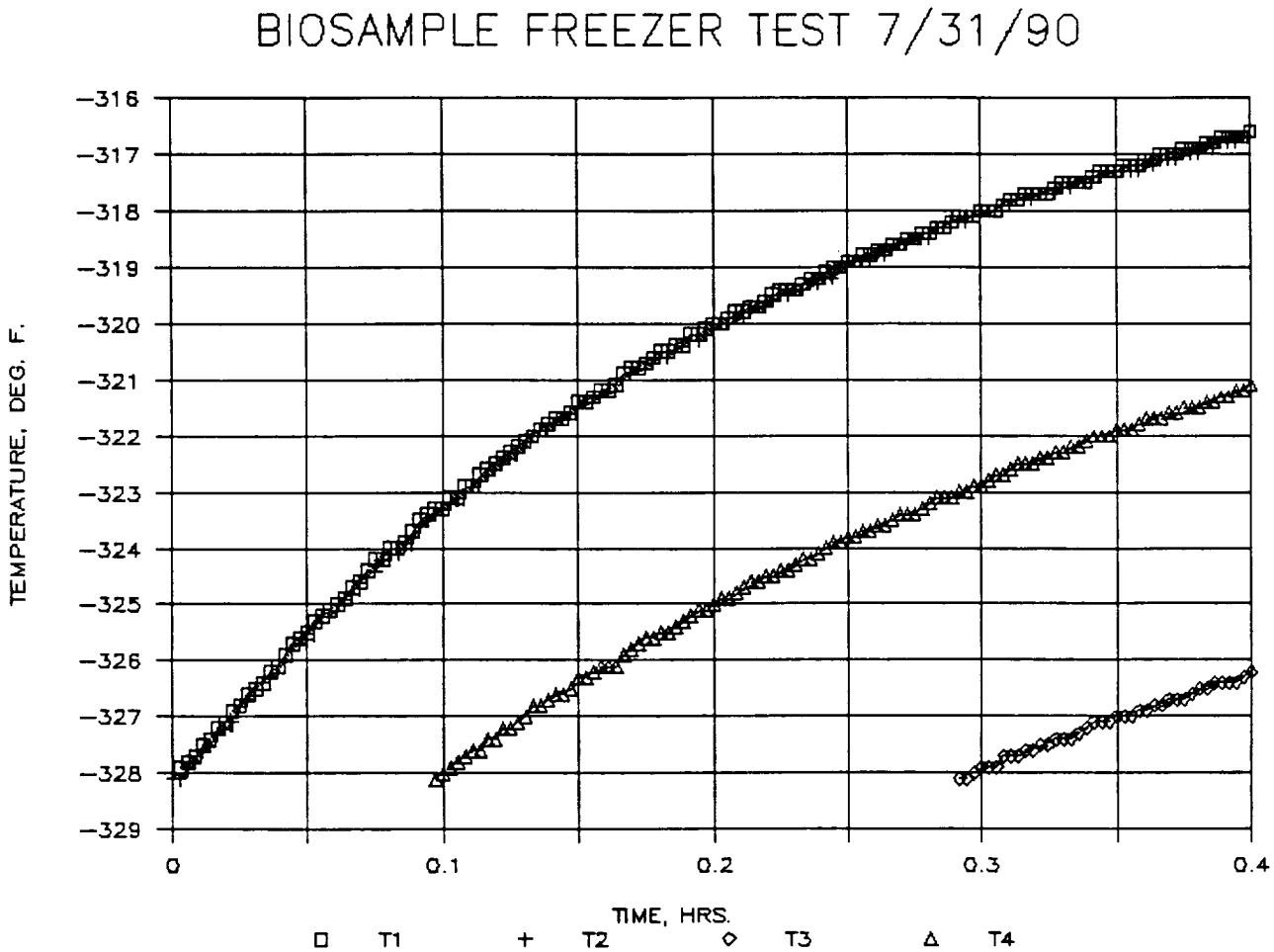

Figure 21. Temperature vs Time for 3 RTDs on Heat Sinks during Initial 0.4 Hour of Biosample Freezer Test on 7/31/90

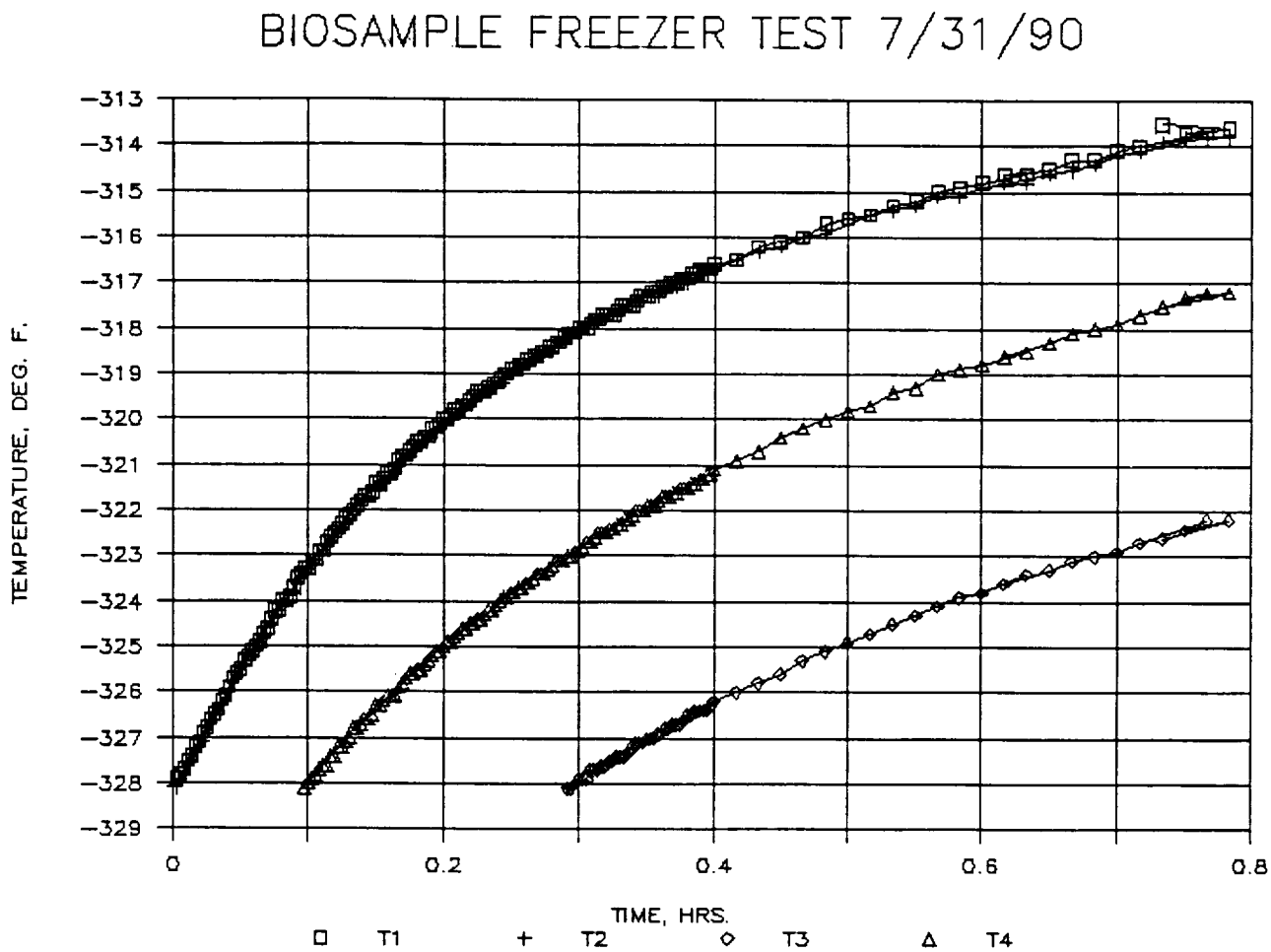

Figure 22. Temperature vs Time for 3 RTDs on Heat Sinks during Initial 0.8 Hour of Biosample Freezer Test on 7/31/90

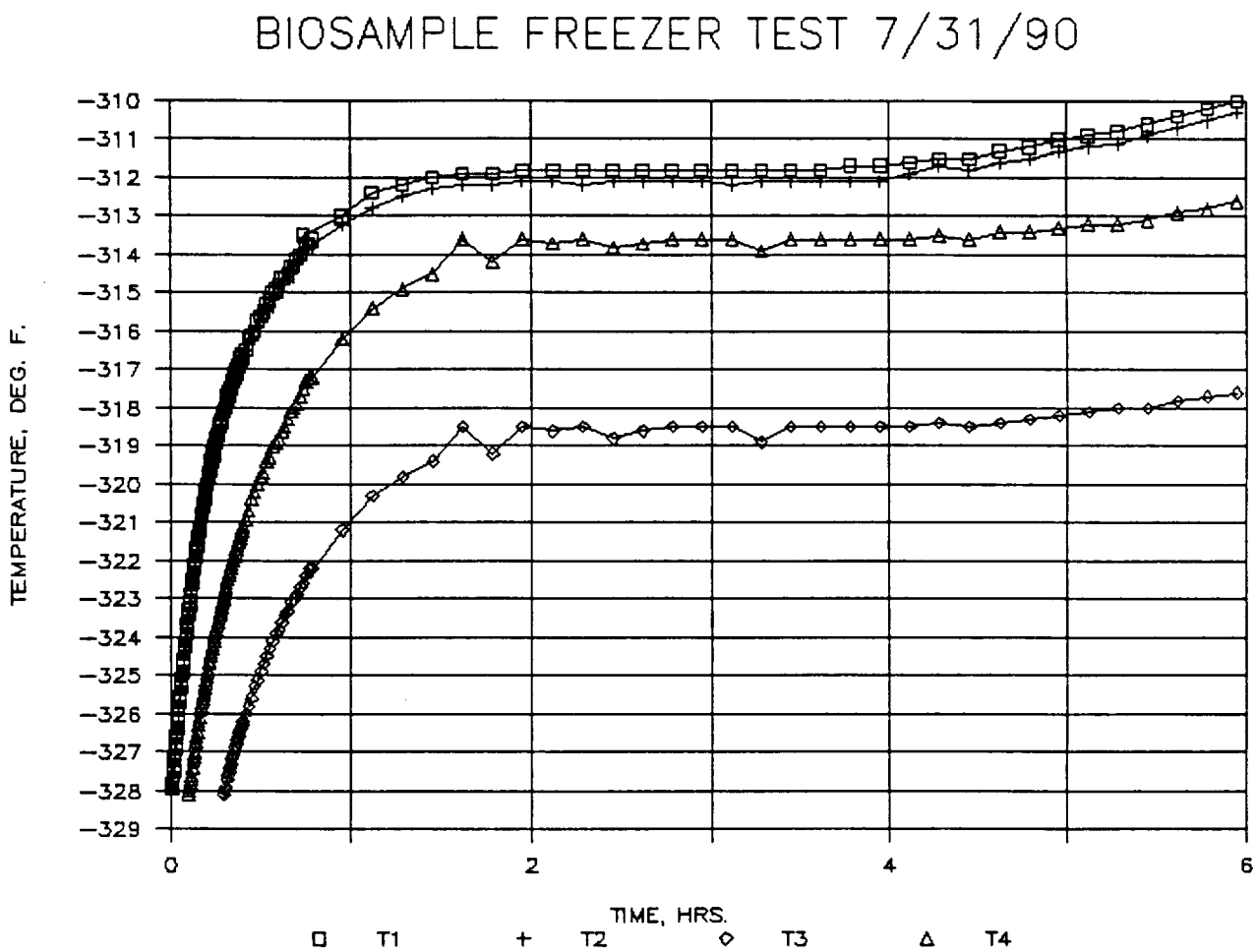

Figure 23. Temperature vs Time for 3 RTDs on Heat Sinks during Initial 6 Hours of Biosample Freezer Test on 7/31/90

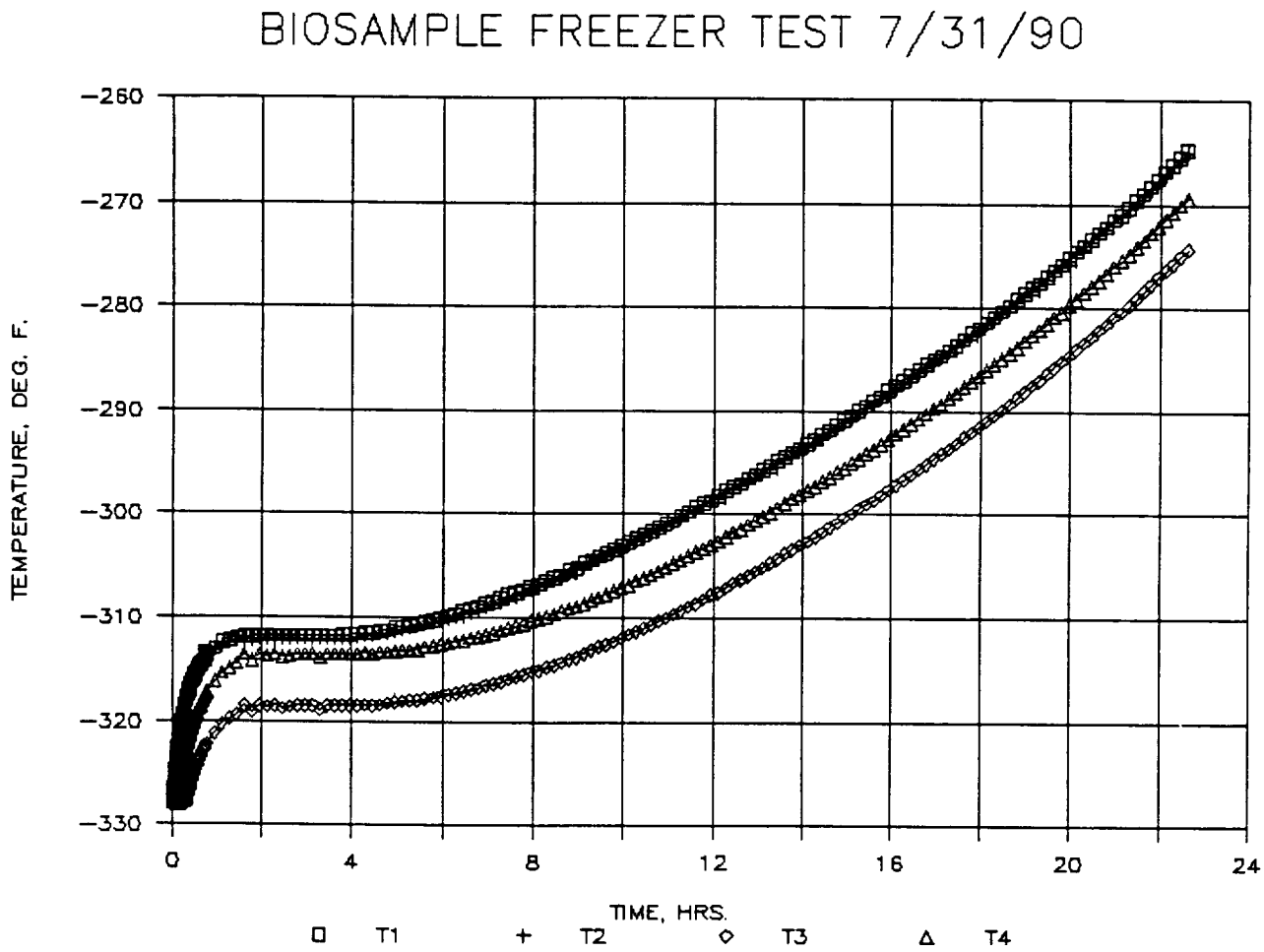

Figure 24. Temperature vs Time for 3 RTDs on Heat Sinks during Initial 23 Hours of Biosample Freezer Test on 7/31/90

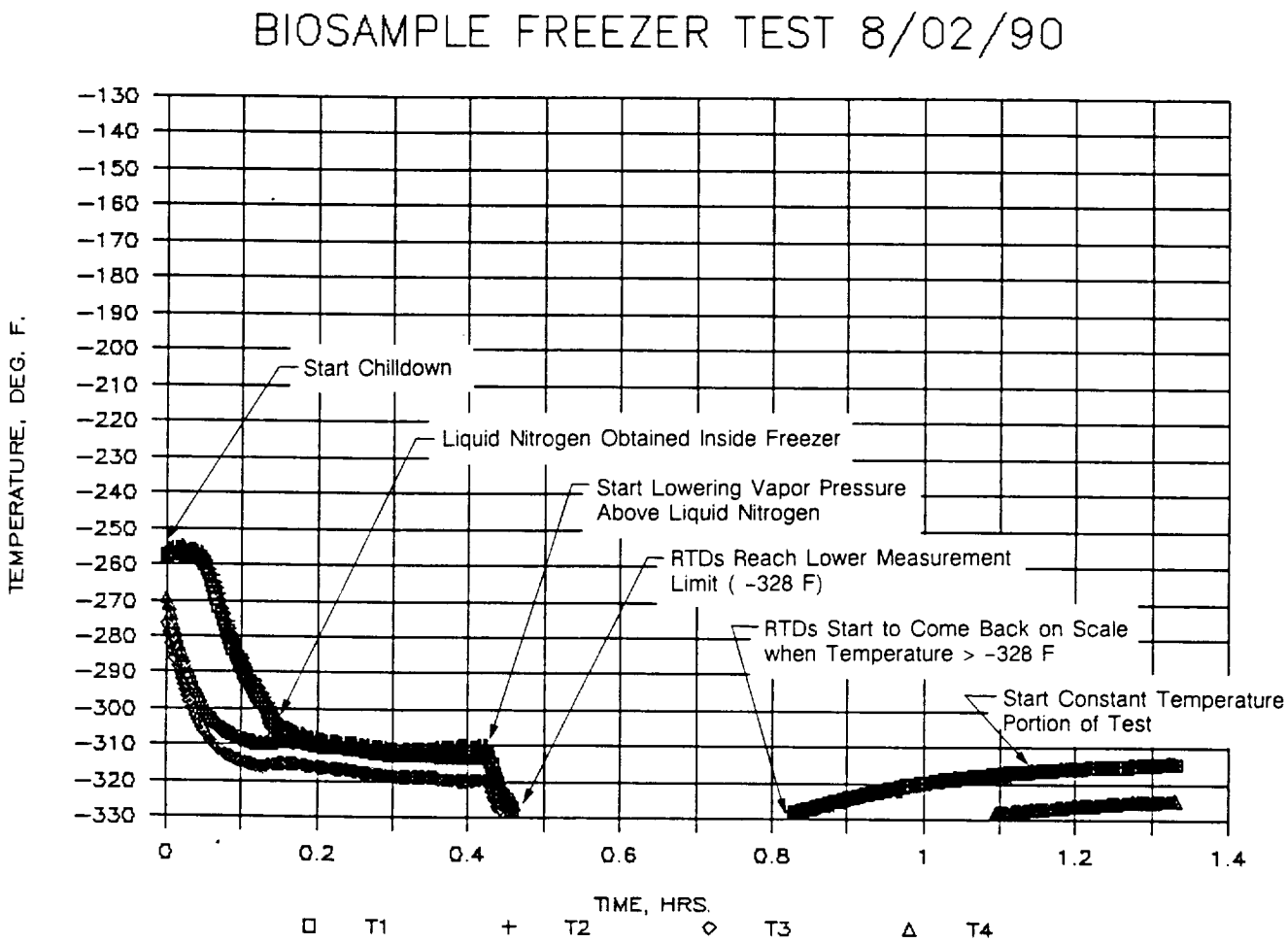

Figure 25. Temperature vs Time for 3 RTDs on Heat Sinks during Initial 1.4 Hours of Biosample Freezer Test on 8/2/90

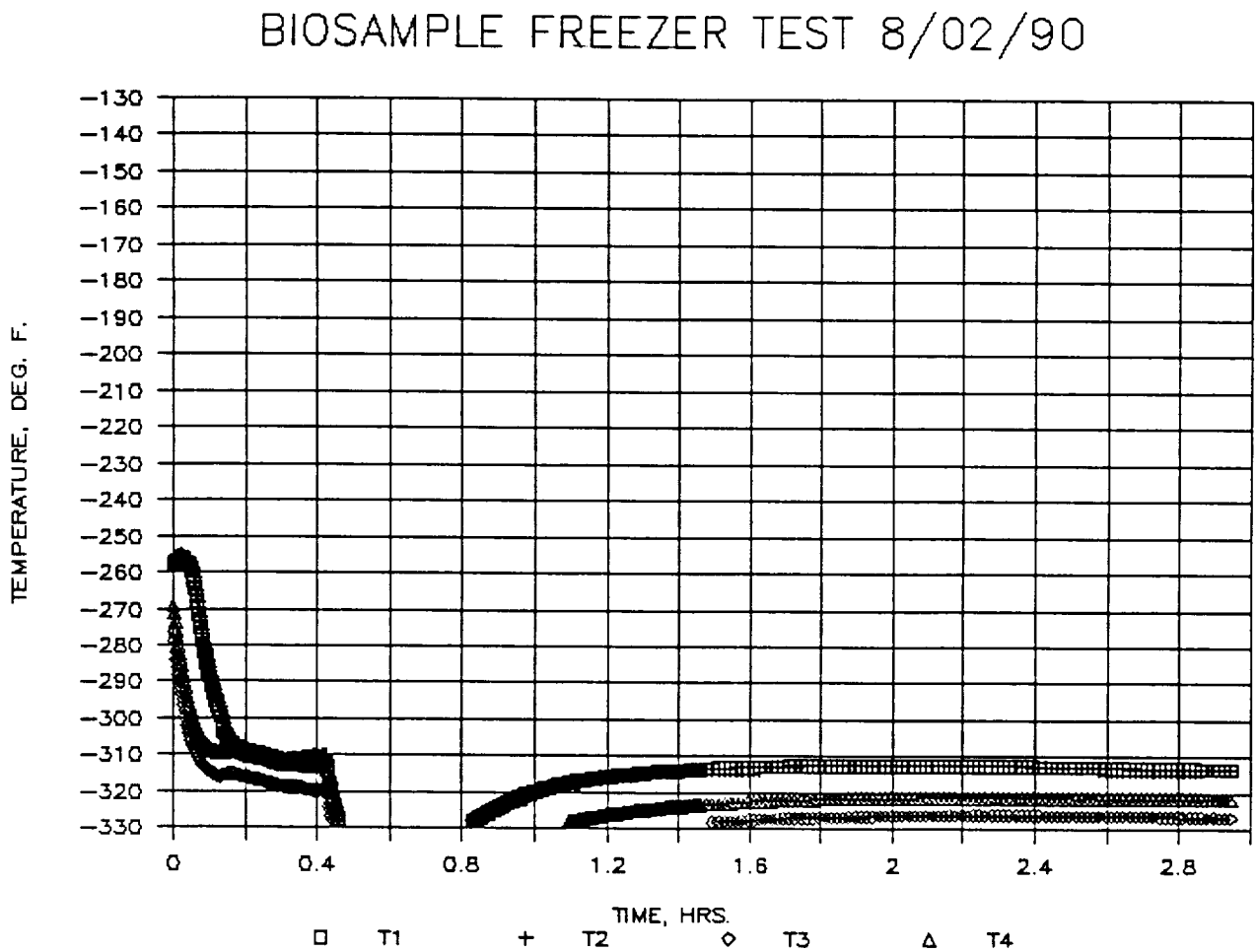

Figure 26. Temperature vs Time for 3 RTDs on Heat Sinks during Initial 3 Hours of Biosample Freezer Test on 8/2/90

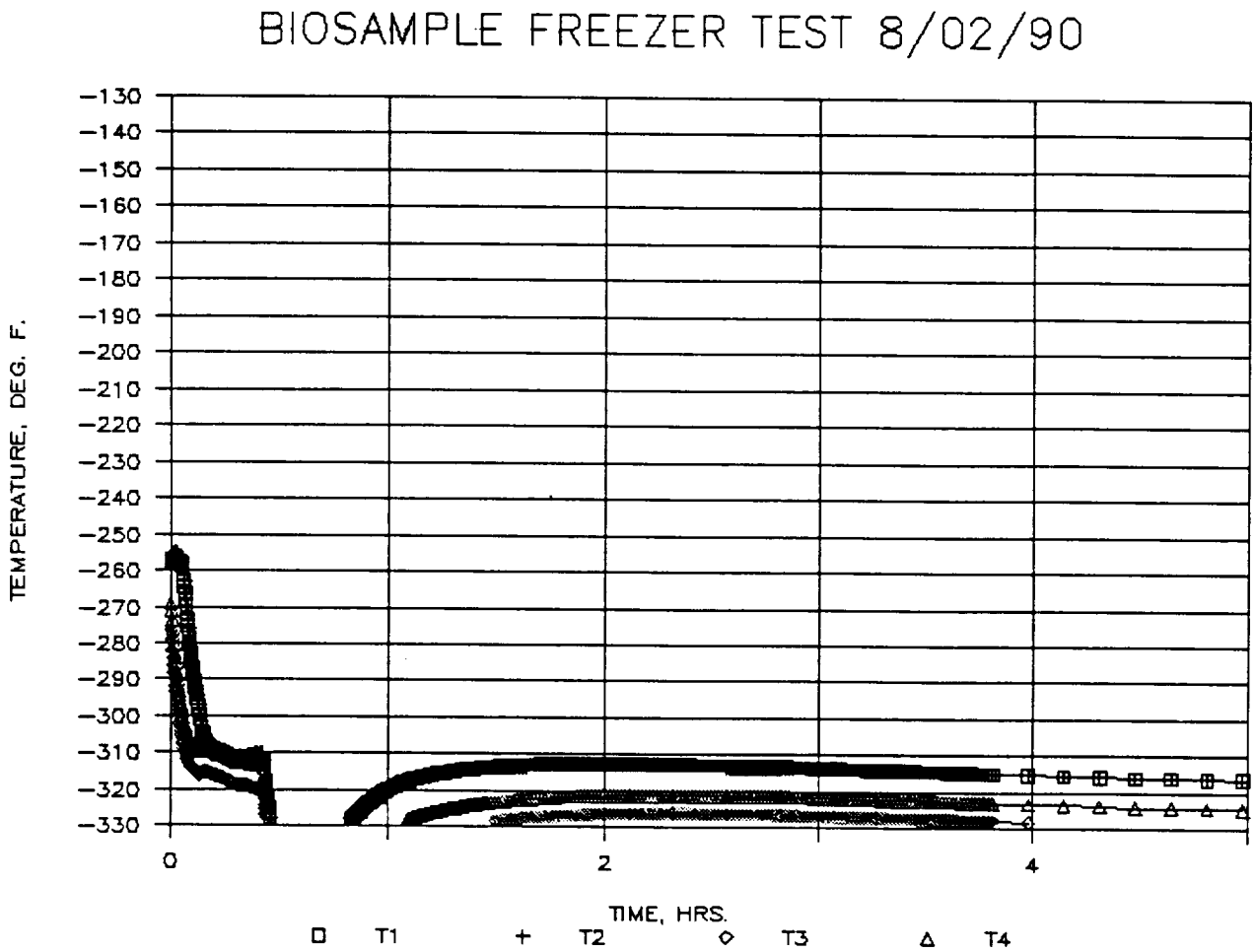

Figure 27. Temperature vs Time for 3 RTDs on Heat Sinks during Initial 5 Hours of Biosample Freezer Test on 8/2/90

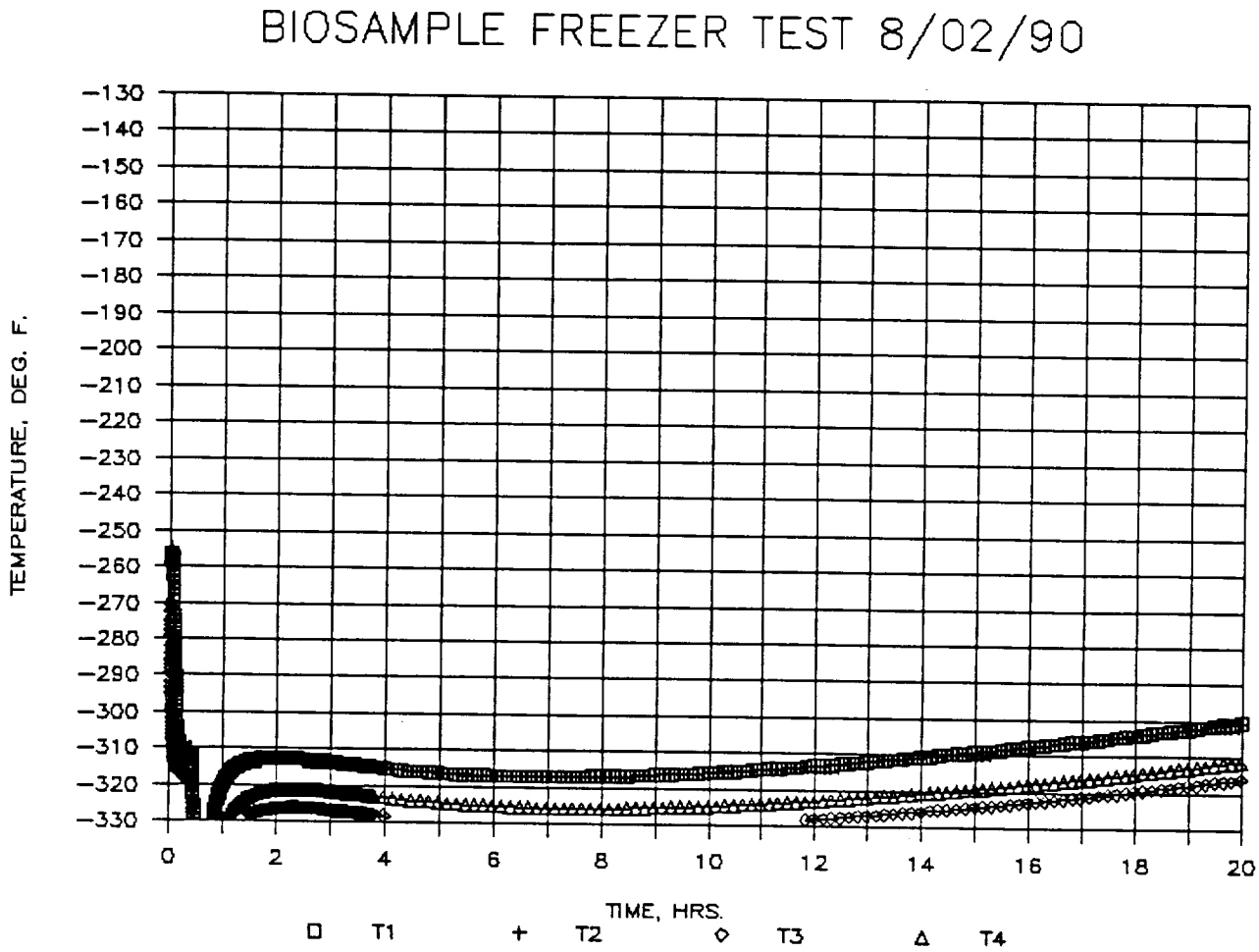

Figure 28. Temperature vs Time for 3 RTDs on Heat Sinks during Initial 20 Hours of Biosample Freezer Test on 8/2/90

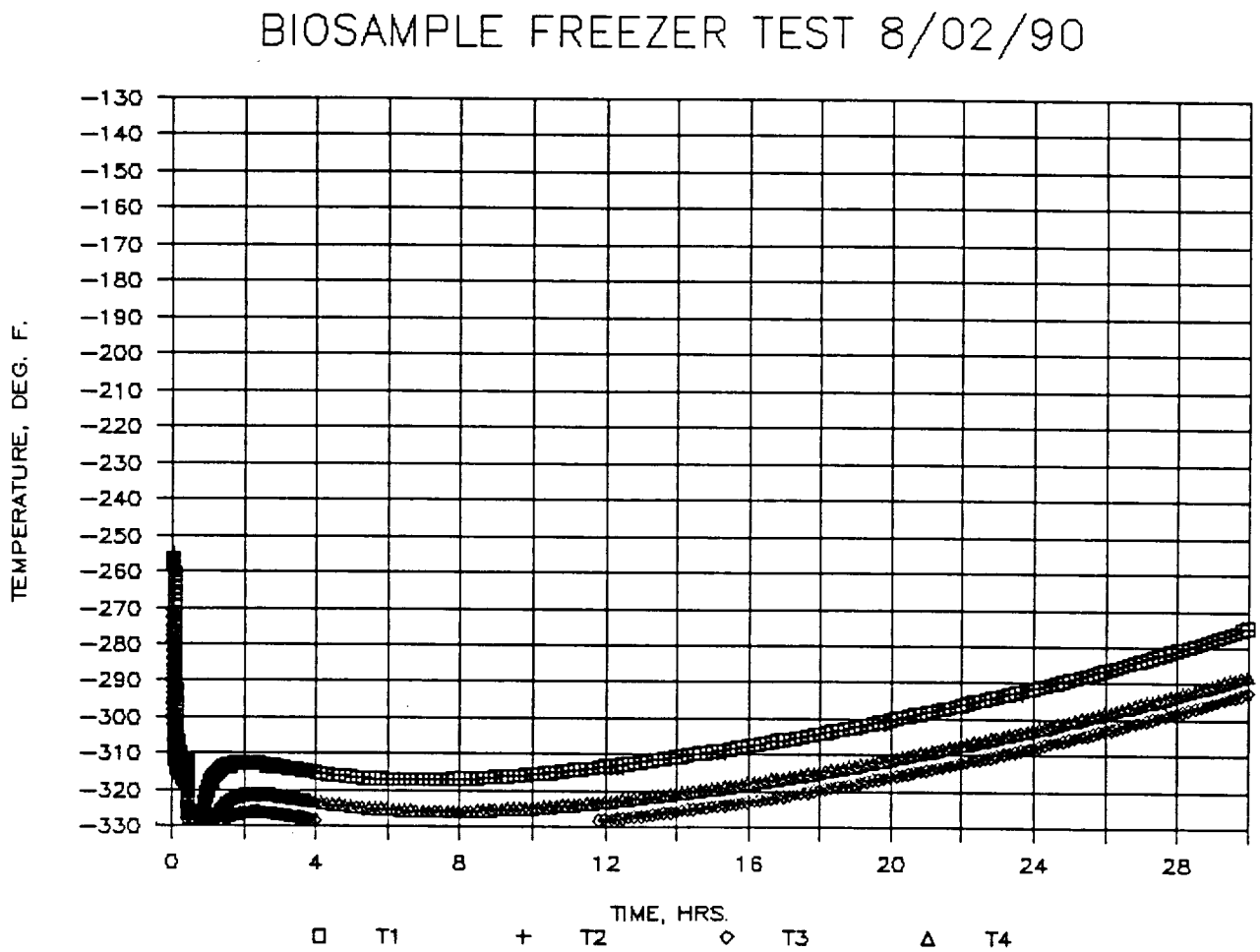

Figure 29. Temperature vs Time for 3 RTDs on Heat Sinks during Initial 30 Hours of Biosample Freezer Test on 8/2/90

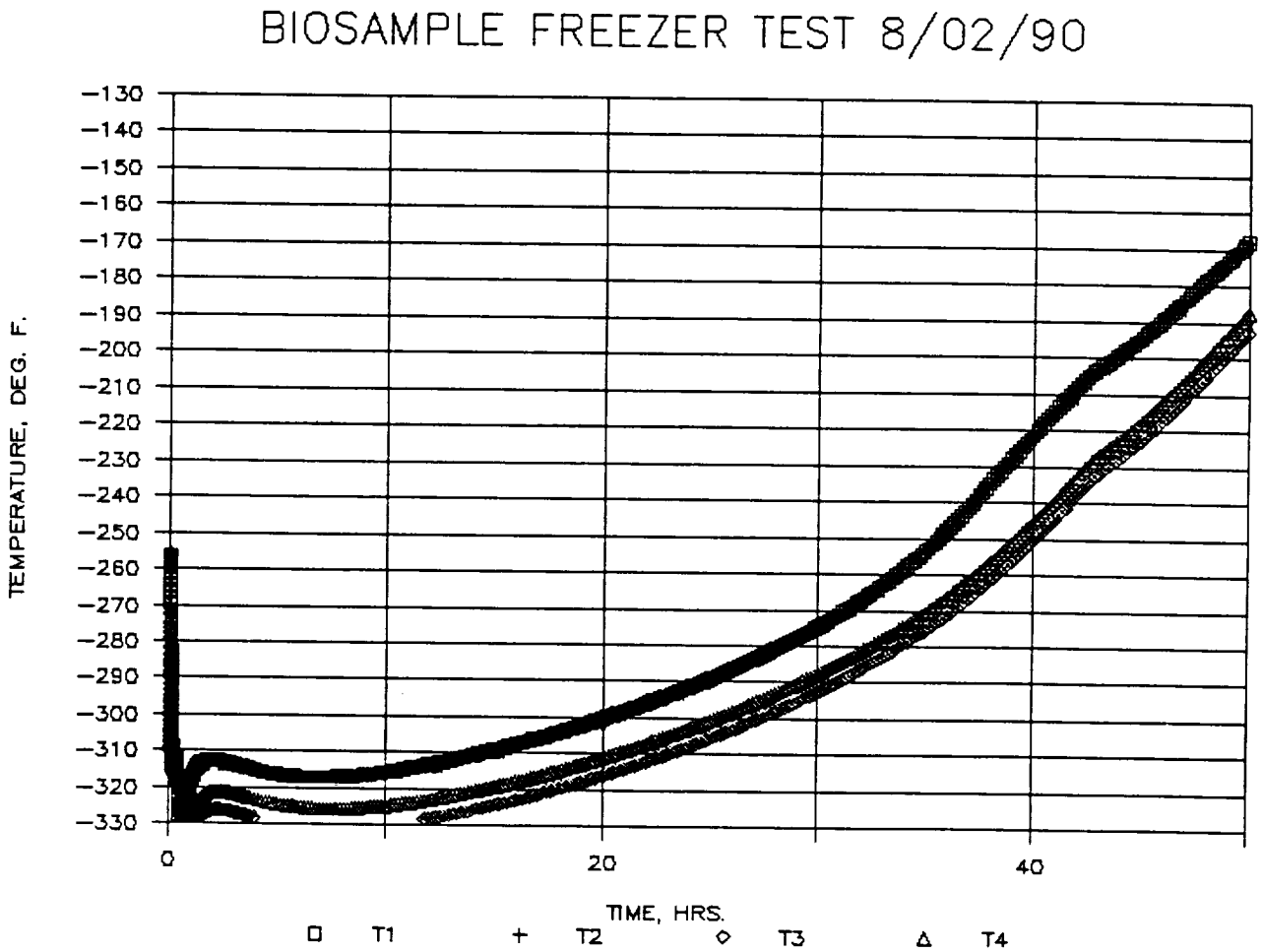

Figure 30. Temperature vs Time for 3 RTDs on Heat Sinks during Initial 50 Hours of Biosample Freezer Test on 8/2/90

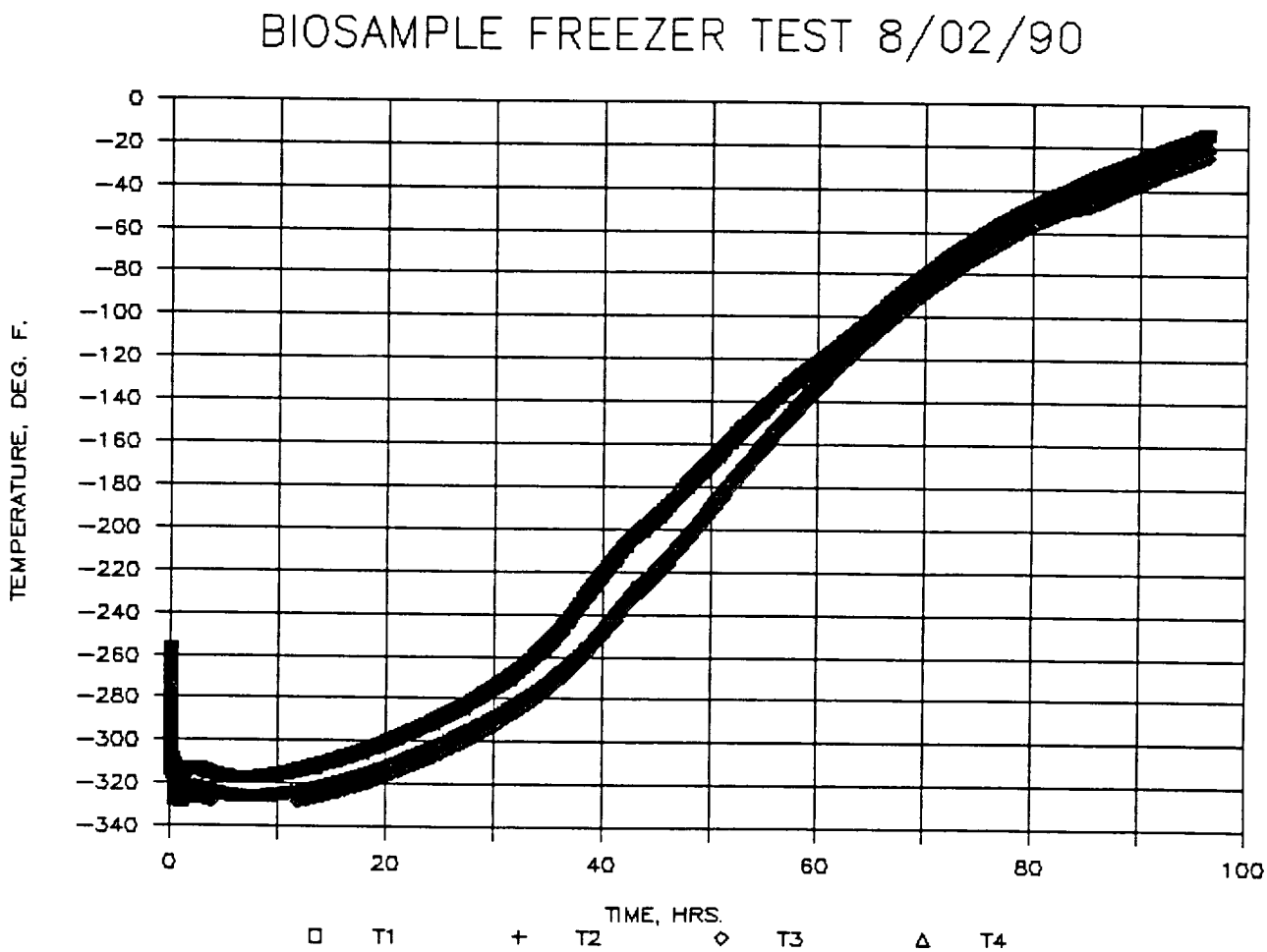

Figure 31. Temperature vs Time for 3 RTDs on Heat Sinks during Initial 96 Hours of Biosample Freezer Test on 8/2/90

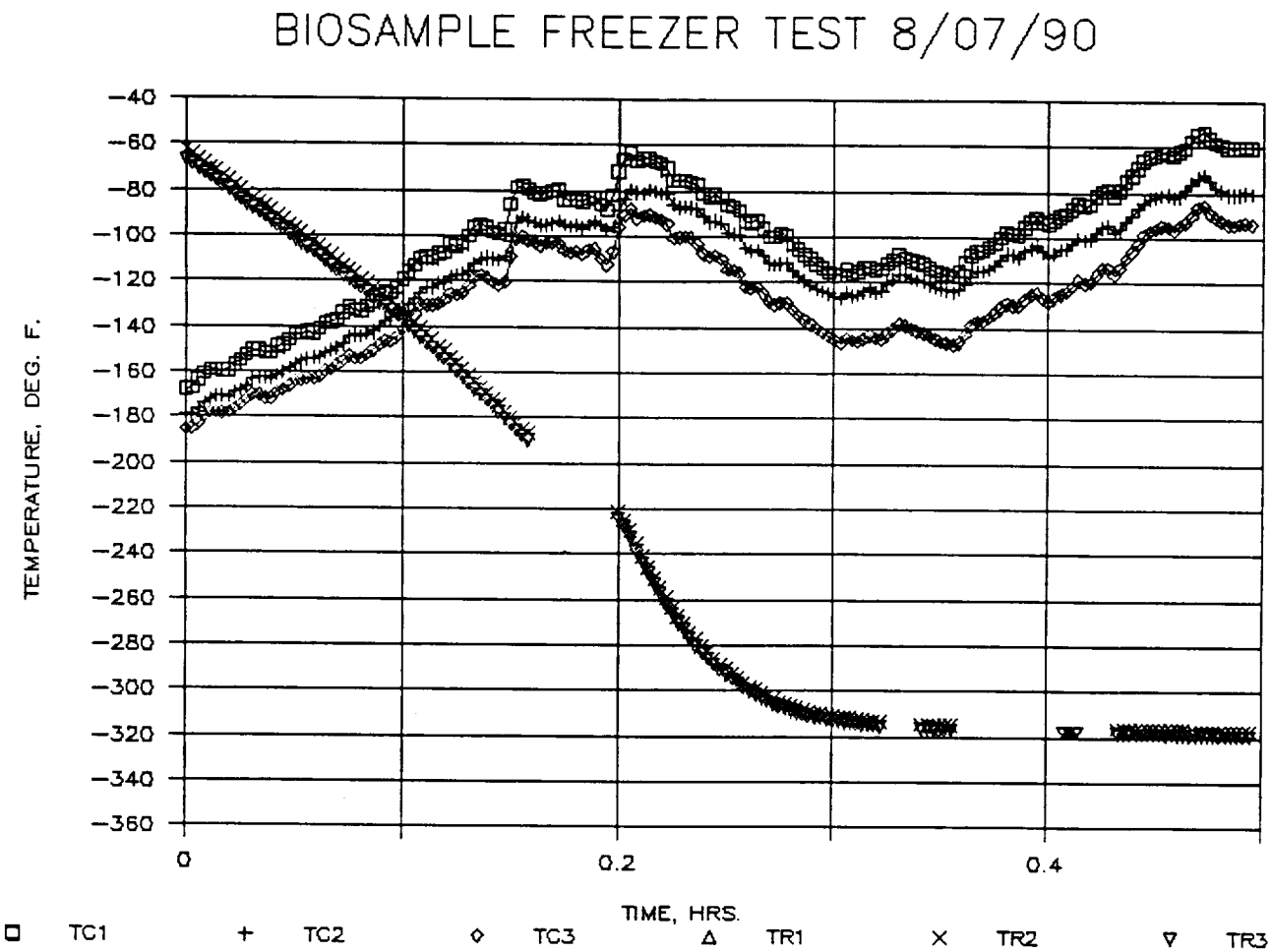

Figure 32. Temperature vs Time for 3 RTDs on Heat Sinks and 3 Thermocouples Inside Freezer on Mylar Blanket during Initial 0.5 Hour of Biosample Freezer Test on 8/7/90

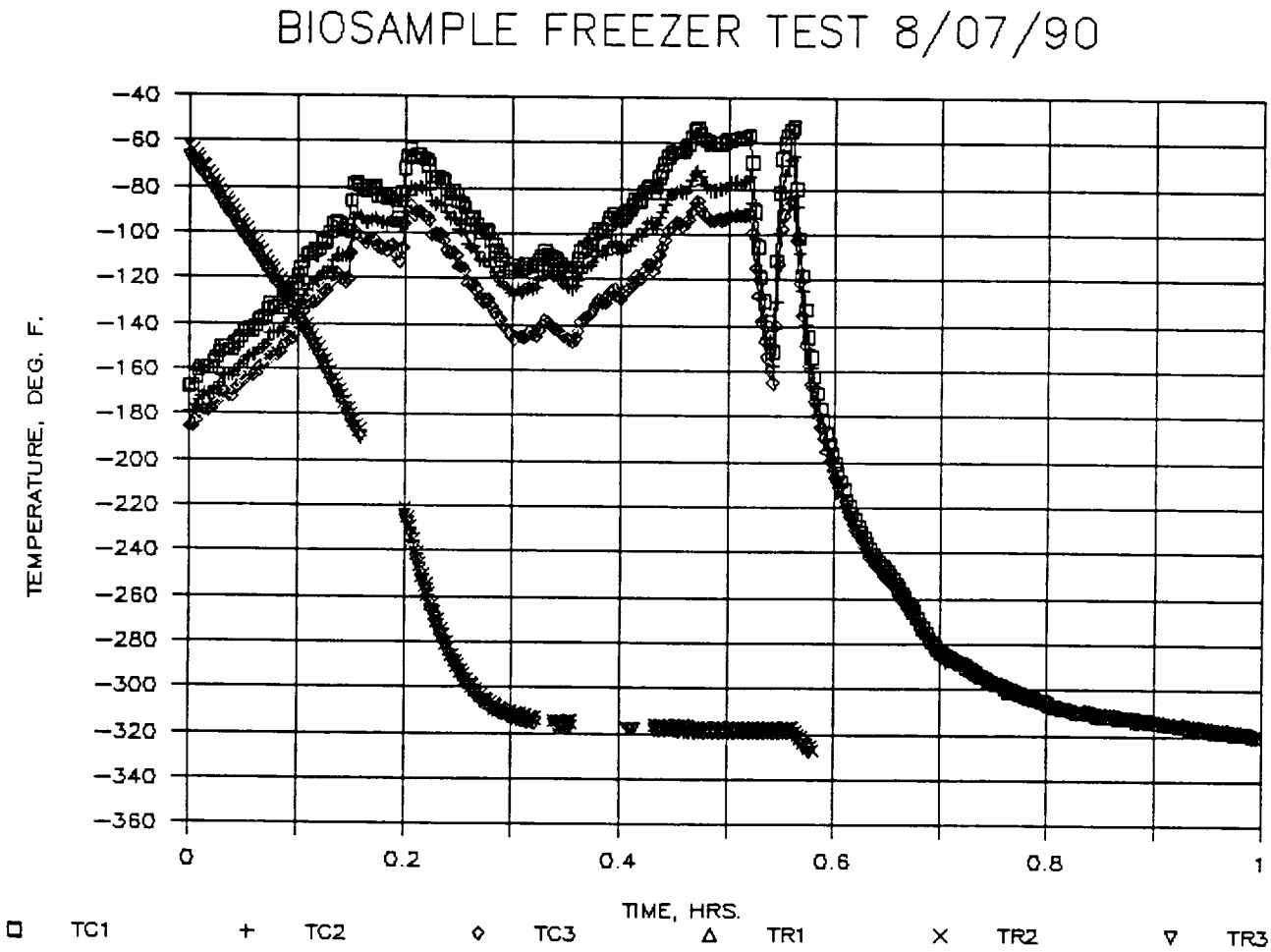

Figure 33. Temperature vs Time for 3 RTDs on Heat Sinks and 3 Thermocouples Inside Freezer on Mylar Blanket during Initial 1 Hour of Biosample Freezer Test on 8/7/90

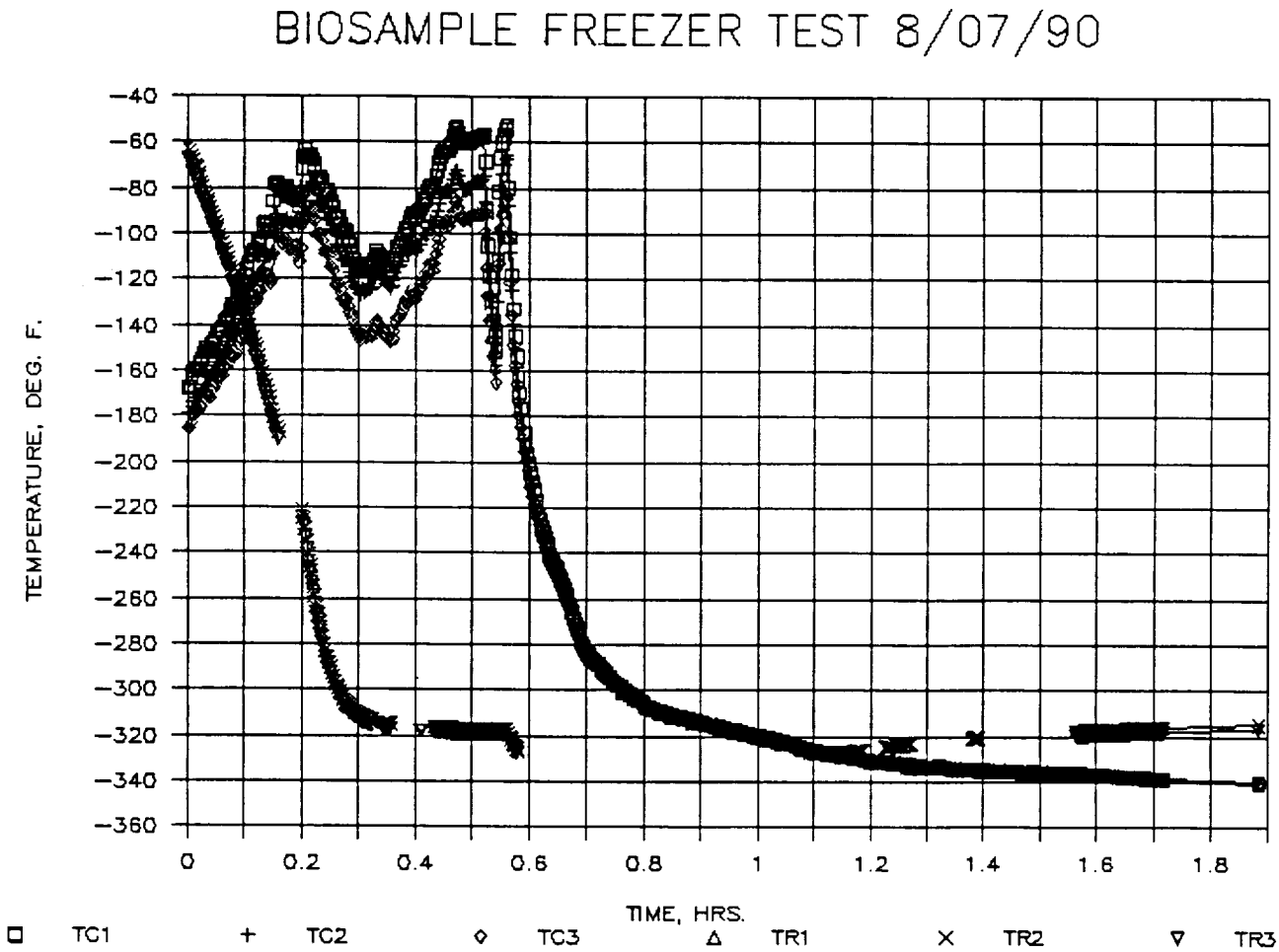

Figure 34. Temperature vs Time for 3 RTDs on Heat Sinks and 3 Thermocouples Inside Freezer on Mylar Blanket during Initial 2 Hours of Biosample Freezer Test on 8/7/90

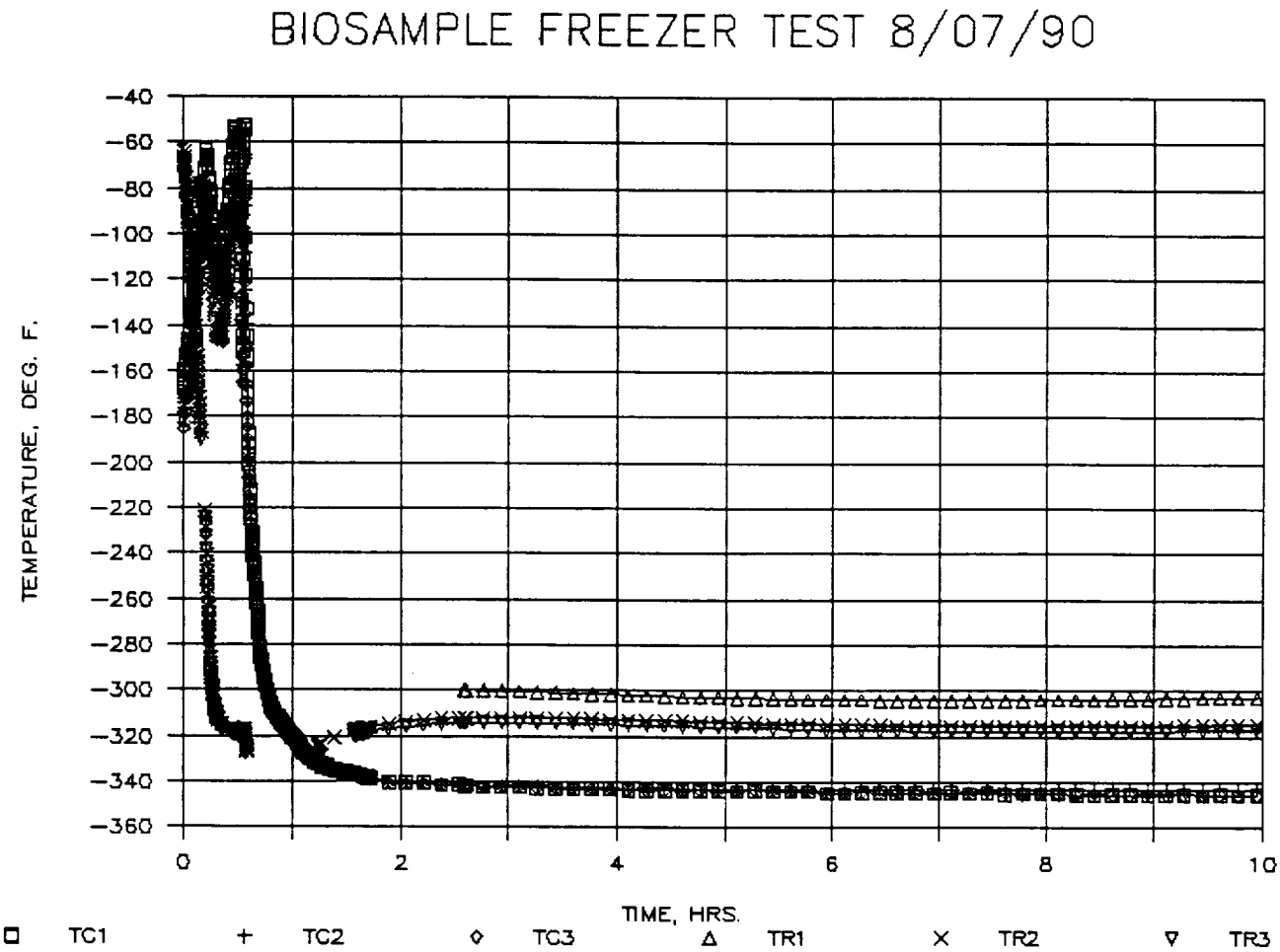

Figure 35. Temperature vs Time for 3 RTDs on Heat Sinks and 3 Thermocouples Inside Freezer on Mylar Blanket during Initial 10 Hours of Biosample Freezer Test on 8/7/90

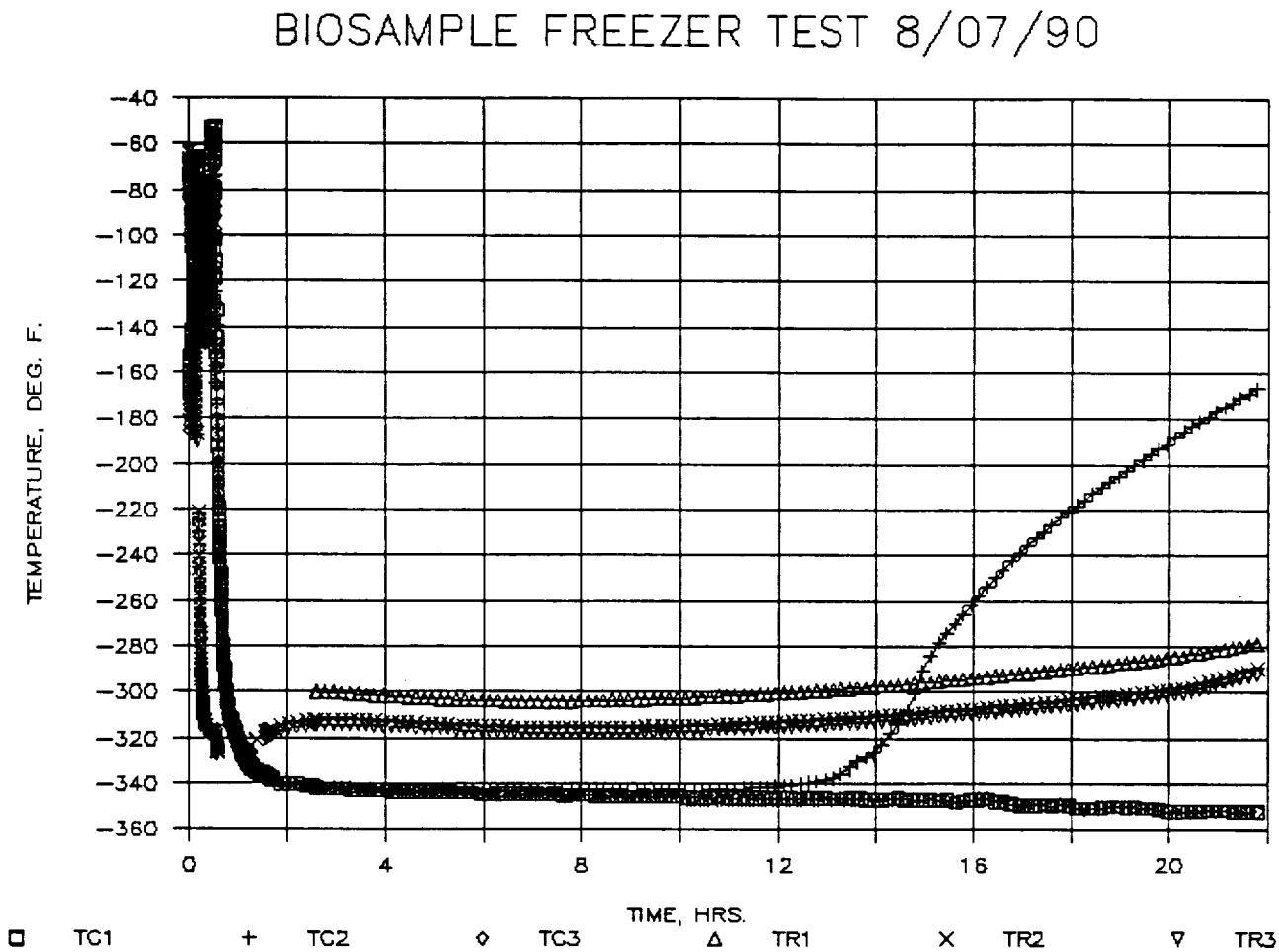

Figure 36. Temperature vs Time for 3 RTDs on Heat Sinks and 3 Thermocouples Inside Freezer on Mylar Blanket during Initial 22 Hours of Biosample Freezer Test on 8/7/90

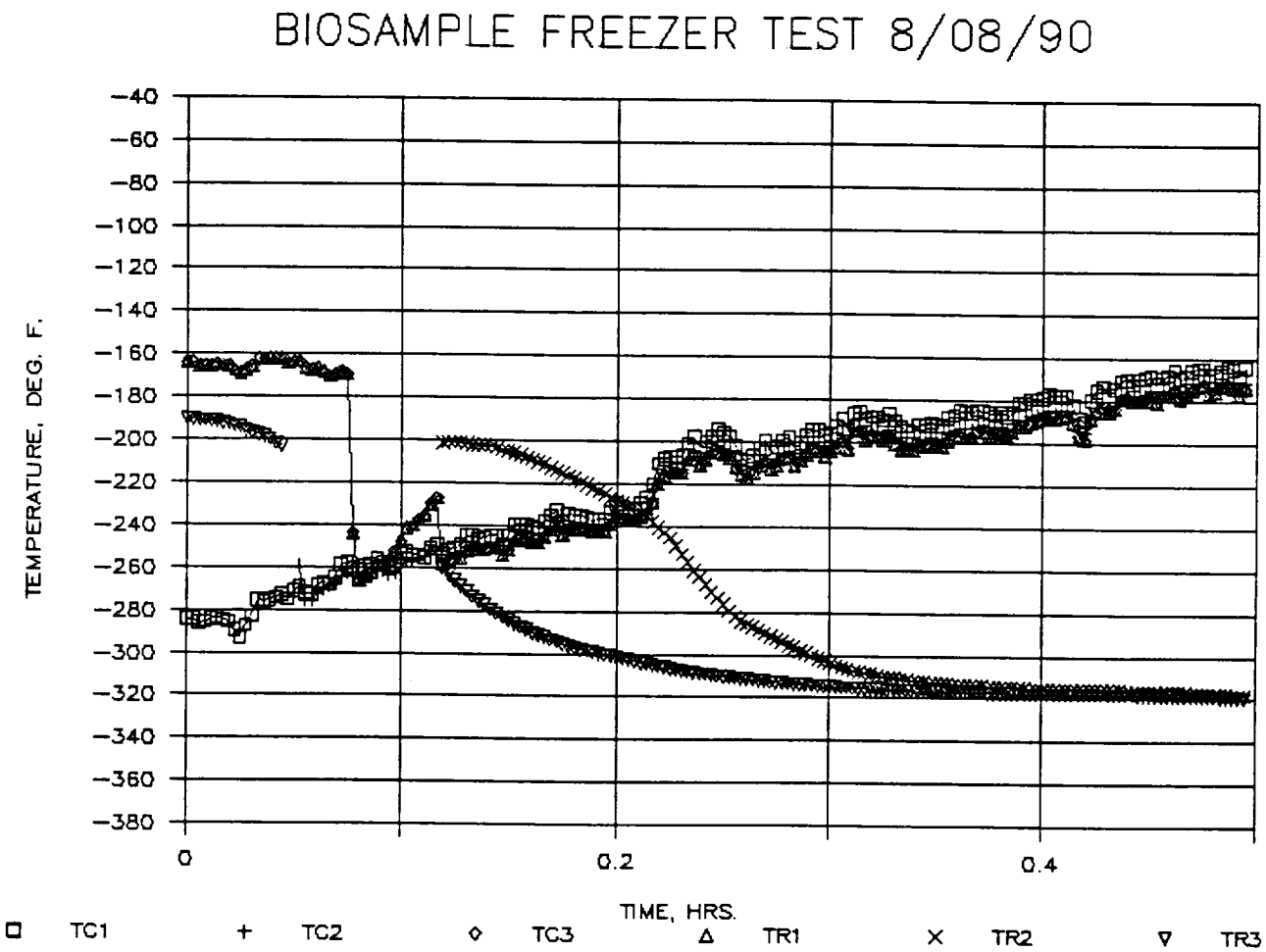

Figure 37. Temperature vs Time for 3 RTDs on Heat Sinks and 3 Thermocouples Inside Freezer on Mylar Blanket during Initial 0.5 Hour of Biosample Freezer Test on 8/8/90

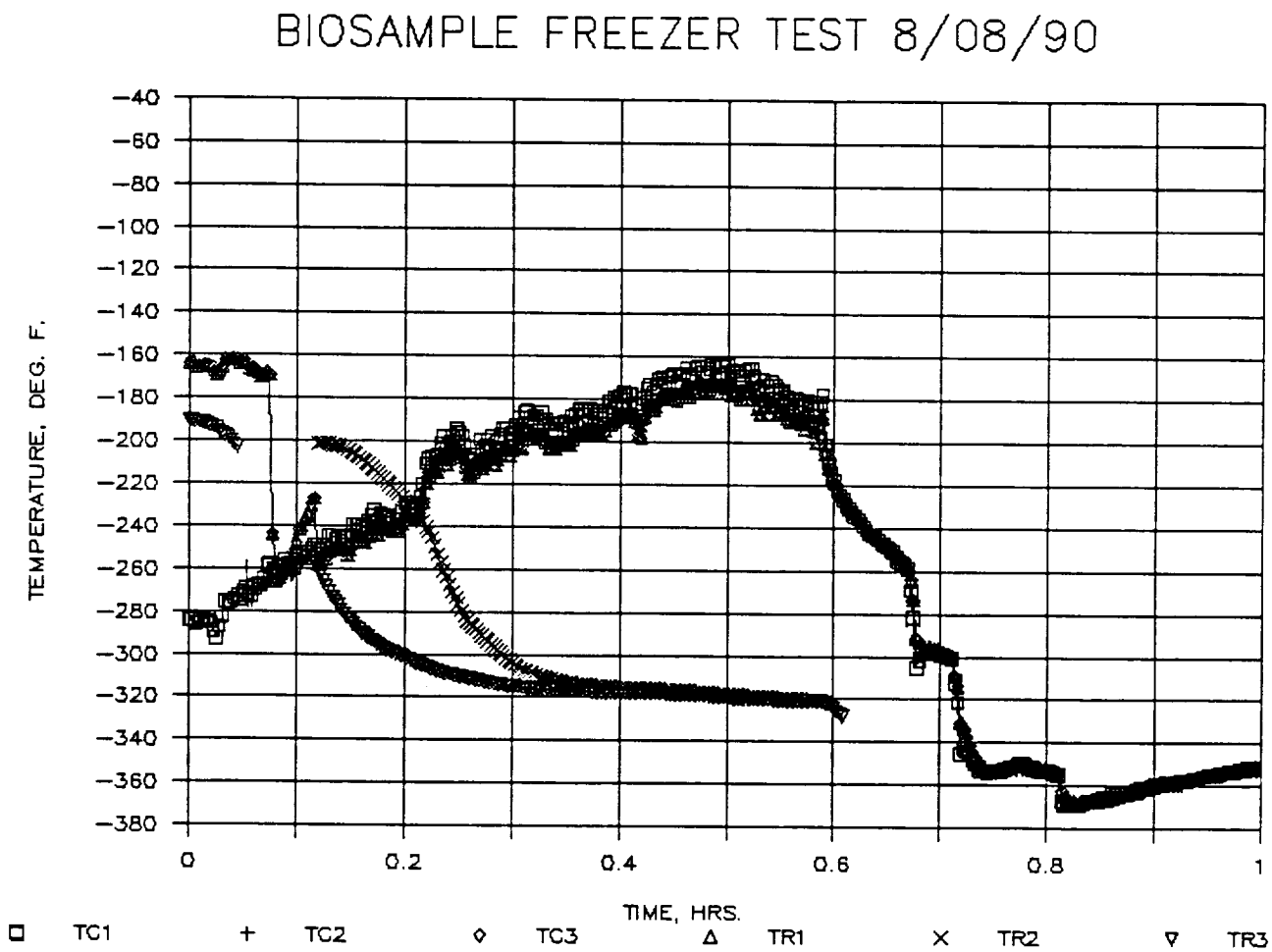

Figure 38. Temperature vs Time for 3 RTDs on Heat Sinks and 3 Thermocouples Inside Freezer on Mylar Blanket during Initial 1 Hour of Biosample Freezer Test on 8/8/90

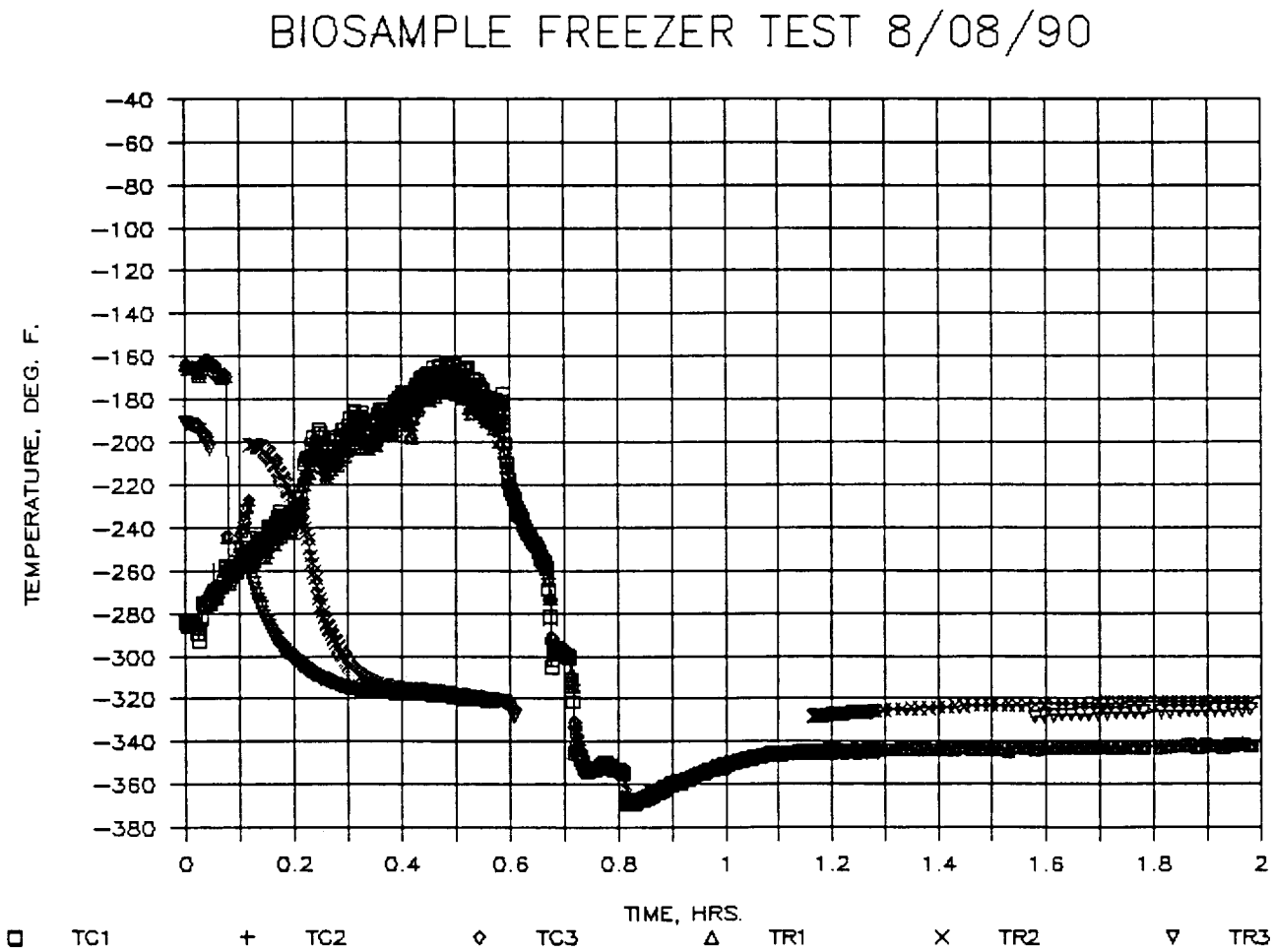

Figure 39. Temperature vs Time for 3 RTDs on Heat Sinks and 3 Thermocouples Inside Freezer on Mylar Blanket during Initial 2 Hours of Biosample Freezer Test on 8/8/90

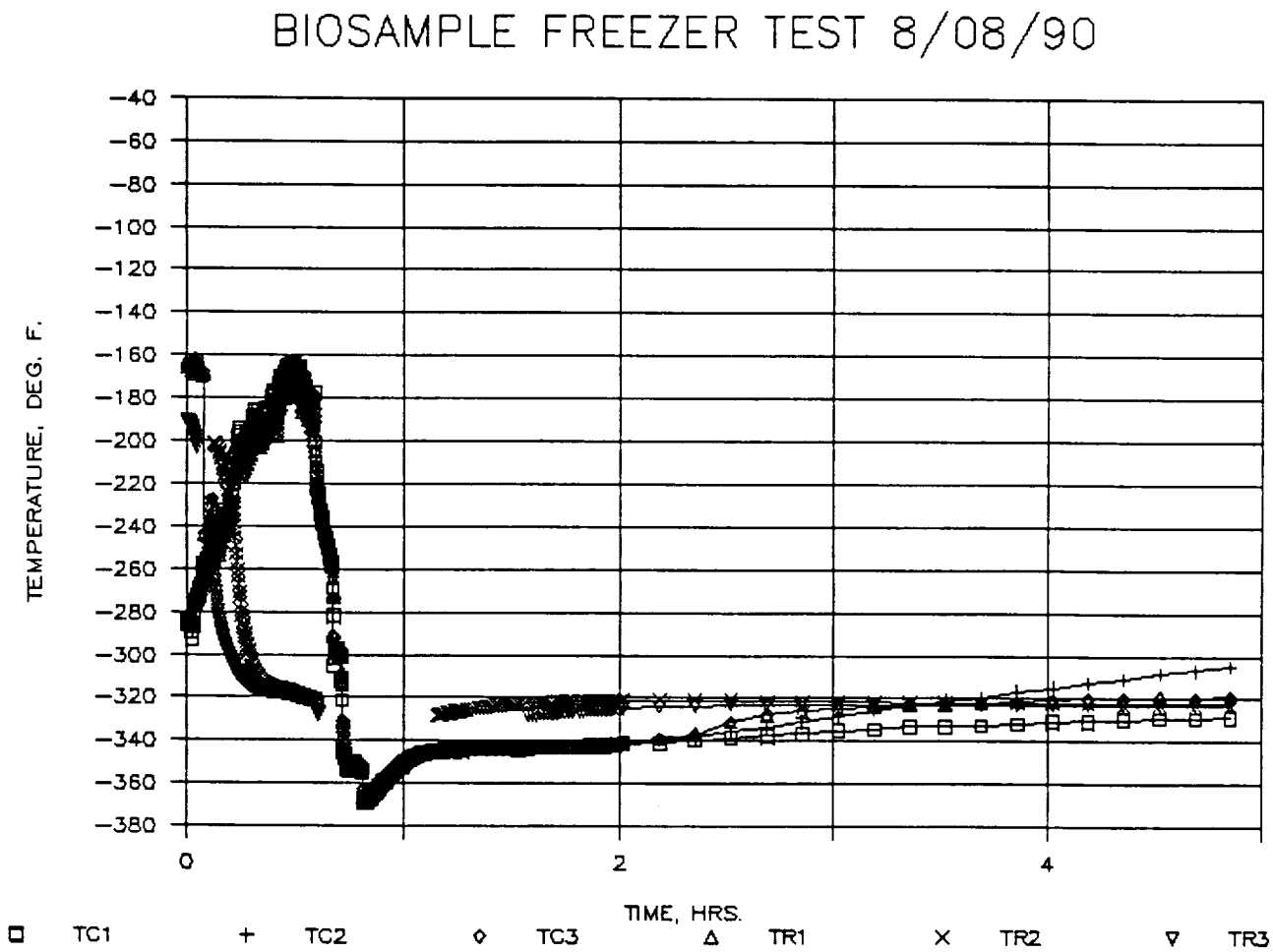

Figure 40. Temperature vs Time for 3 RTDs on Heat Sinks and 3 Thermocouples Inside Freezer on Mylar Blanket during Initial 5 Hours of Biosample Freezer Test on 8/8/90

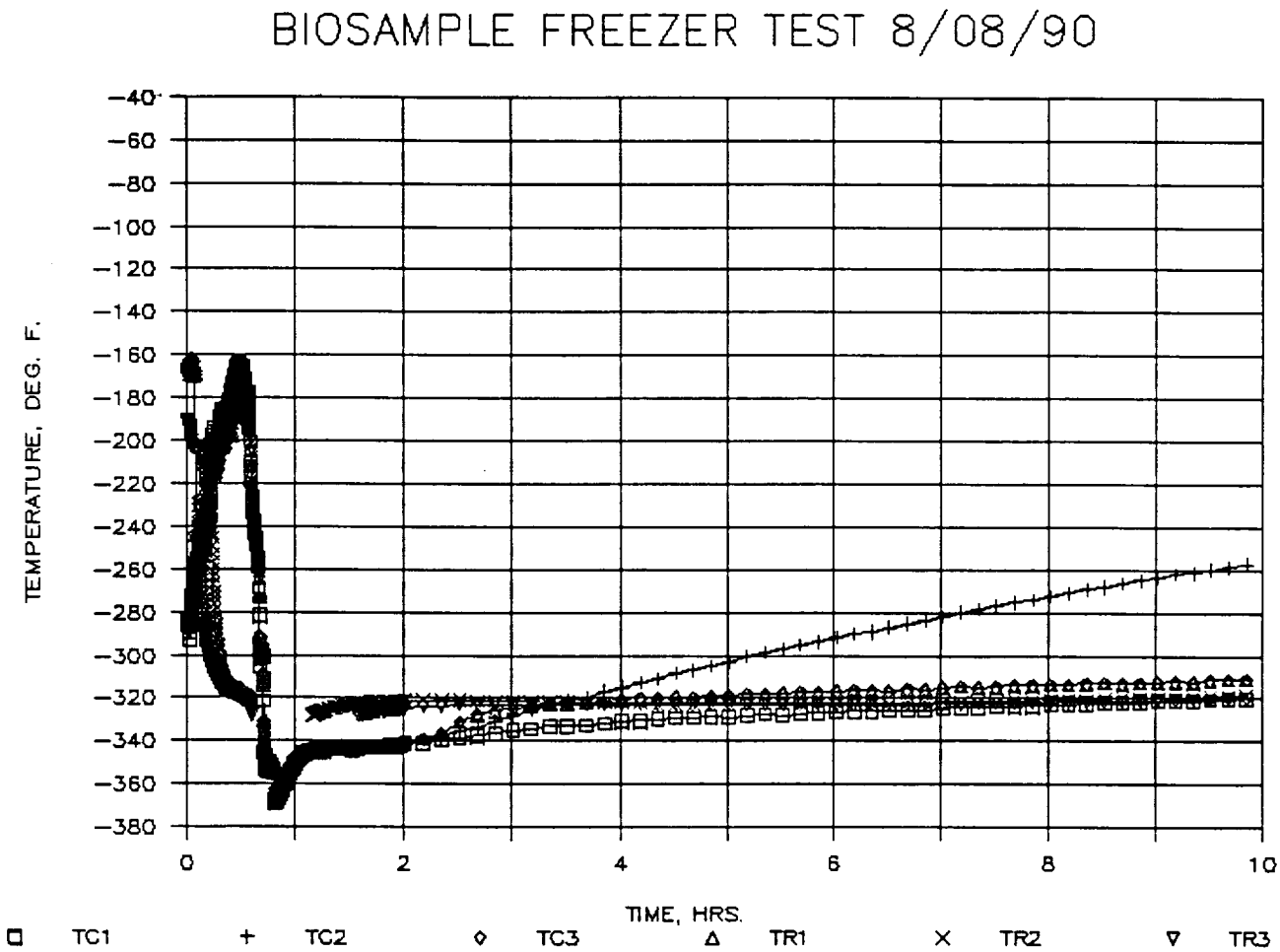

Figure 41. Temperature vs Time for 3 RTDs on Heat Sinks and 3 Thermocouples Inside Freezer on Mylar Blanket during Initial 10 Hours of Biosample Freezer Test on 8/8/90

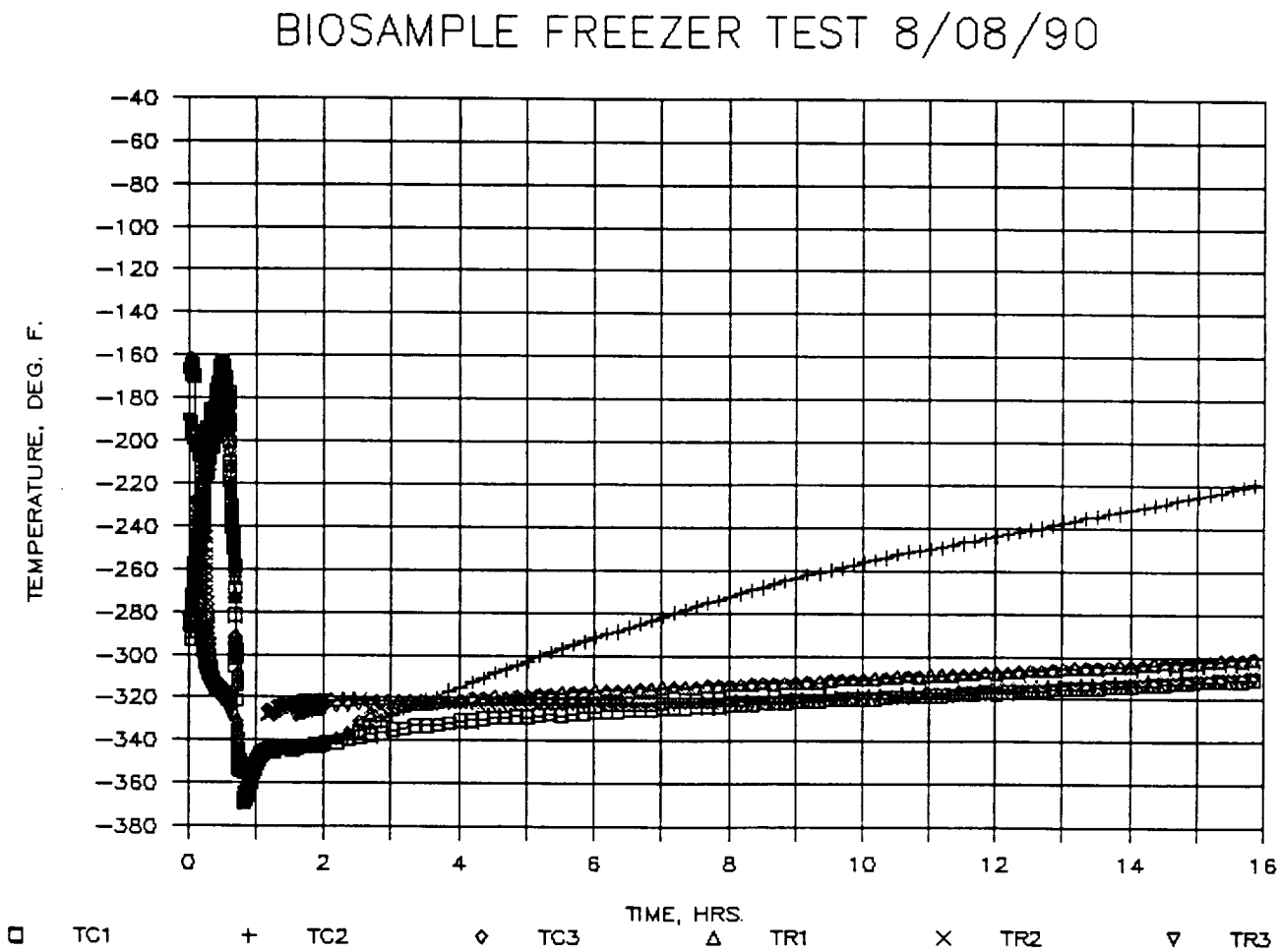

Figure 42. Temperature vs Time for 3 RTDs on Heat Sinks and 3 Thermocouples Inside Freezer on Mylar Blanket during Initial 16 Hours of Biosample Freezer Test on 8/8/90

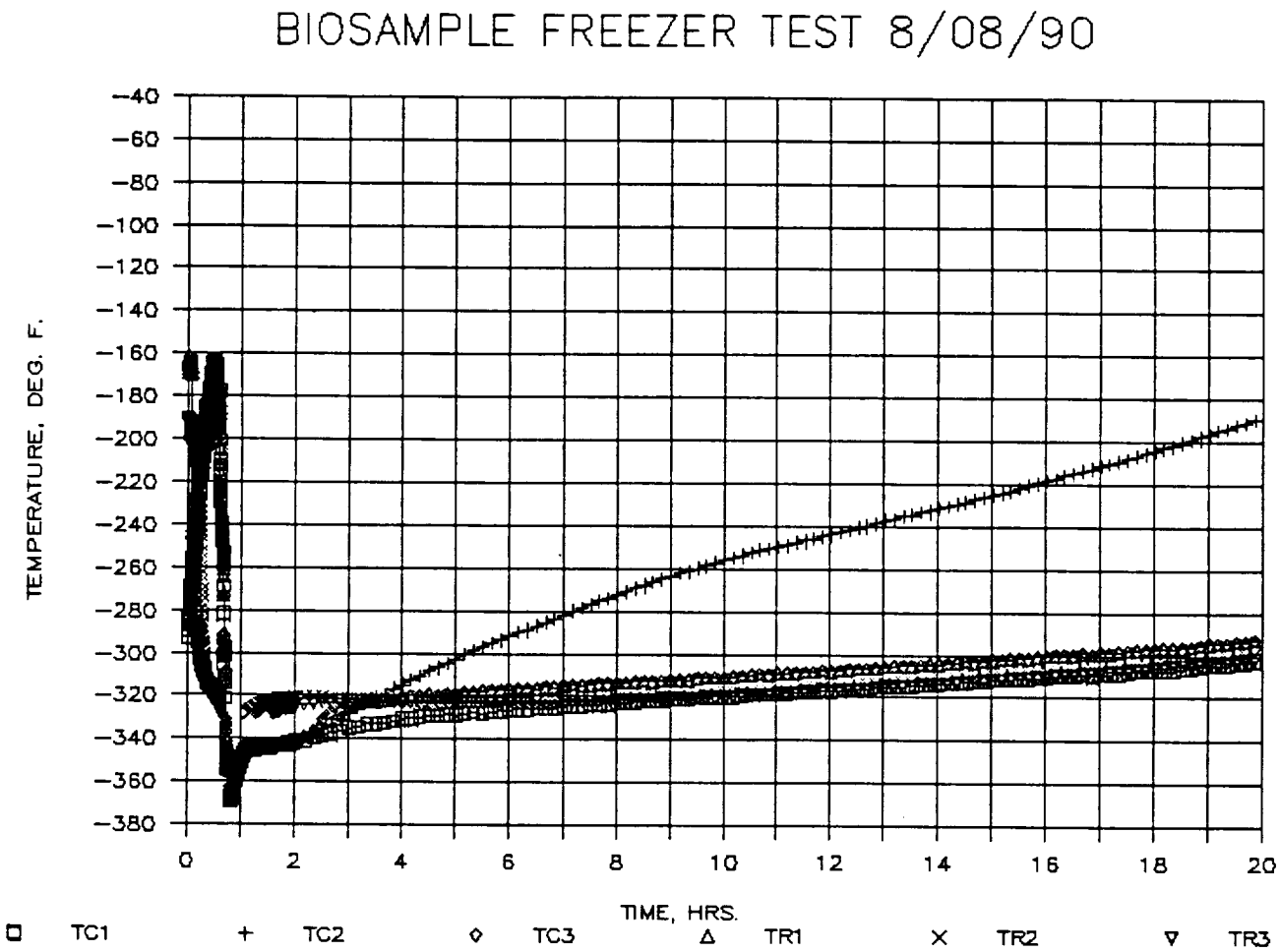

Figure 43. Temperature vs Time for 3 RTDs on Heat Sinks and 3 Thermocouples Inside Freezer on Mylar Blanket during Initial 20 Hours of Biosample Freezer Test on 8/8/90

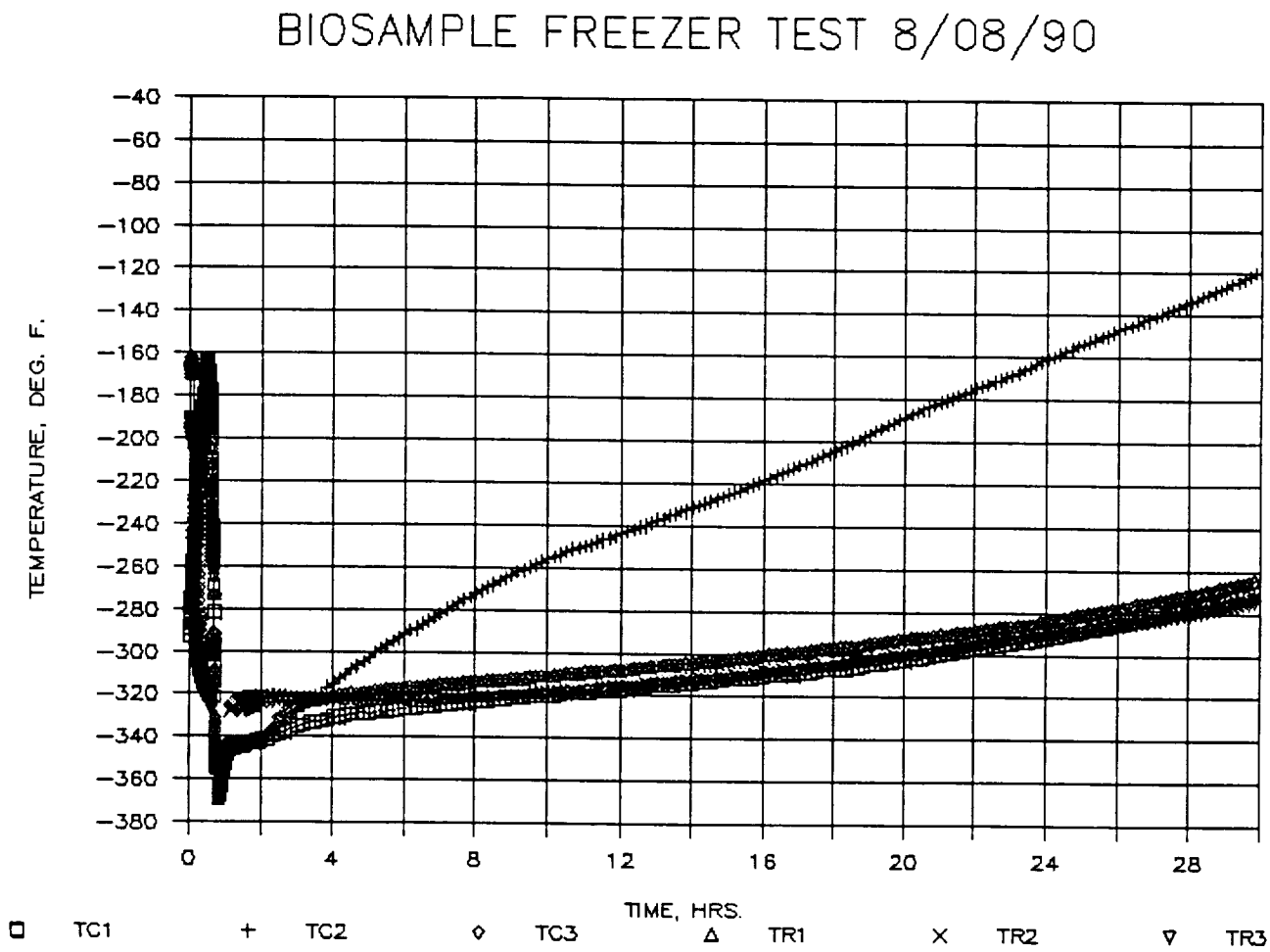

Figure 44. Temperature vs Time for 3 RTDs on Heat Sinks and 3 Thermocouples Inside Freezer on Mylar Blanket during Initial 30 Hours of Biosample Freezer Test on 8/8/90

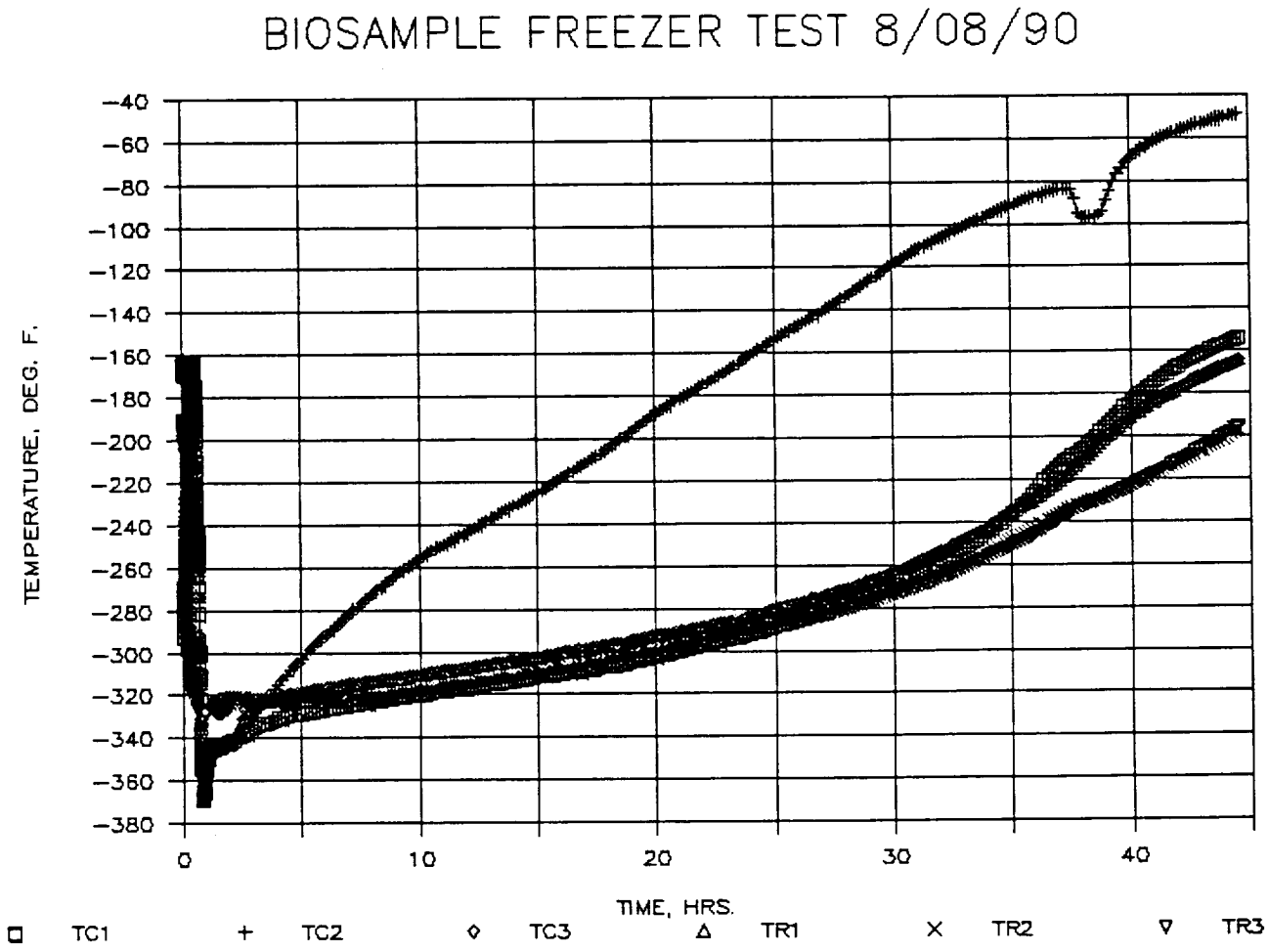

Figure 45. Temperature vs Time for 3 RTDs on Heat Sinks and 3 Thermocouples Inside Freezer on Mylar Blanket during Initial 44 Hours of Biosample Freezer Test on 8/8/90

Excerpt from September 1990 Monthly Progress Report LMSC-HSV PR F312346

PRECEDING PAGE BLANK NOT FILMED

PROGRESS DURING THE CURRENT REPORTING PERIOD

Testing of Biosample Freezer

Table 1 shows a summary of the tests run to date. The last four runs were made since the last progress report was submitted. Two of these tests were for chilldown purposes in preparation for testing on the following days. The other two tests provided useful data. For the test of 8/15/90, the actual heat leak into the inner space of the freezer was determined from the measured temperature rise rate of the aluminum heat sinks, and from the measured solid/liquid nitrogen (i.e., "slush") boiloff rate. The boiloff rate was determined by periodically measuring the weight of the freezer with its contents.

The results were as follows:

Q_{SN2} = 2.63 W

$Q_{AL\ \Delta T}$ = 0.438 W

Total = 3.068 W

The heat leak was calculated from each source as follows:

	Watts	% of Total
Thermocouple Wires	.03	1.1
RTD Lead Wires	.006	0.2
Diaphragm (Stainless Steel Liner)	2.22	79.4
Diaphragm (Epoxy Glass)	0.364	13.0
Fill and Vent Tubes	0.063	2.2
MLI	0.112	4.0
Total	2.795	99.9

This yields a ratio of measured to calculated heat leak of

$$\frac{3.068}{2.795} = 1.10$$

or a 10% difference. This is probably coincidential. Neither the calculations nor the measurement is really expected to be within 10%.

After the test of 8/15/90, a leak was discovered in the inner cylinder-to-vent tube joint on one of the Biosample Freezer halves. This was repaired before the next test. Also, the aluminum heat sinks and RTDs were removed. The inner cylinder was reinstrumented with 12 chromel/alumel thermocouples as shown in Figure 1. Also a chromel/alumel thermocouple material vacuum feedthrough was made up and installed. The pressure gage for the inner cylinder was moved from the vacuum pumping line to the vent port in order to get a more applicable pressure measurement.

Results of the 8/15/90 test are shown in Figures 2 through 12. These plots are shown on progressing time scales so that the temperatures are readable early during the test period.

It is noted that thermocouple 2 rises more rapidly than the others because it is not immersed in the "slush" N_2 but is on top of a mylar layers which were placed inside the freezer to prevent LN_2 from splashing directly on the walls when it enters the freezer from the fill tube. This was done to help reduce or prevent damage due to high temperature gradients. (Also note that the thermocouple locations of Figure 1 do not apply to the test of 8/15/90. These locations apply to the next test only, i.e., 9/7/90). The measurement "TR2" on Figures 2 through 9 is an RTD on one of the heat sinks.

Figure 10 is interesting in that it shows the rise in MLI space pressure at about 14 hours due to release of gas products trapped on the inner cylinder surface during cryopumping. As the "slush" N_2 inside the cylinder boils away, the inner surface warms up and releases these trapped products. Figure 11 shows the pressure over the "slush" N_2 gradually dropping during a period between 5 and 20 hours as the "slush" is pumped away as vapor. Figure 12 shows the weight loss with time which was used to deduce the heat leak rate.

Figures 13 through 25 show the results of the test of 9/7/90. Again the temperature plots are shown progressing with time. See Figure 1 for the 12 thrermocouple locations inside the freezer.

Figure 24 shows the "MLI space" pressure. This pressure did not follow the same pattern of release of cryopumped products as the test of 8/15/90. This may have been due to an insufficient pre-chilldown time. This test will be rerun to see if we can repeat the results of 8/15/90. Also, the measured heat leak was higher on this test, as seen on Figure 25. The weight loss rate was 67.6 g/hr for a heat leak of 3.87 W, which is another reason for repeating this test.

As seen from the analysis results presented earlier, the predominent heat leak is the diaphragm stainless steel liner. We plan to attempt a test without this liner, thus significantly reducing the heat leak.

PRECEDING PAGE BLANK NOT FILMED

Table 1. SUMMARY OF TESTS RUN TO DATE ON BIOSAMPLE FREEZER

Test Date	Heat Sink or "Slush" N_2 Temp. at Start of Test (°F)	Miminum Pressure Obtained (torr)	Test Duration (hr)
5/23/90	-2	1×10^{-3}	5
5/25/90	-6	5×10^{-5}	5
5/29/90	4	6×10^{-4}	27
6/11/90	-52	2×10^{-5}	46
6/15/90	-60	1×10^{-5}	64
6/22/90	-100	1×10^{-5}	66
6/25/90	-150	4×10^{-5}	46
6/28/90	-200	7×10^{-5}	24
6/29/90	-240	3×10^{-5}	48
7/25/90	Room temperature pump-down to check O-ring seal		
7/27/90	-310	**	68
7/30/90	< -328	**	22
7/31/90	< -328	**	23
8/1/90	Data not reduced due to problem with cryopumping air into MLI space		
8/2/90	< -328	**	96
8/7/90	< -328 (-340)*	**	24
8/8/90	< -238 (-370)*	**	44
8/14/90	Chilldown test in preparation for test on 8/15/90		
8/15/90	-345	9×10^{-6}	30
9/6/90	Chilldown test in preparation for test on 9/7/90		
9/7/90	-370	8×10^{-6}	72

* Temperatures in "slush" N_2.

** Data not yet reduced.

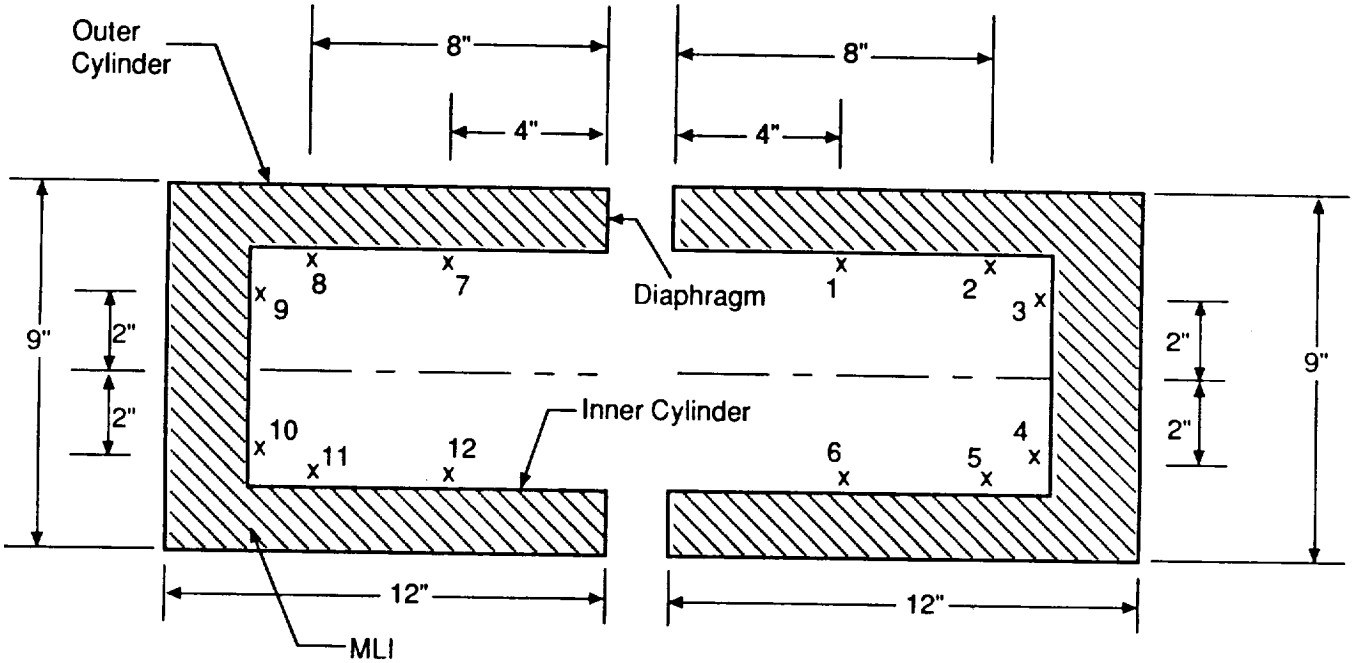

Figure 1. Biosample Freezer Thermocouple Location for Tests Beginning on 9/14/90

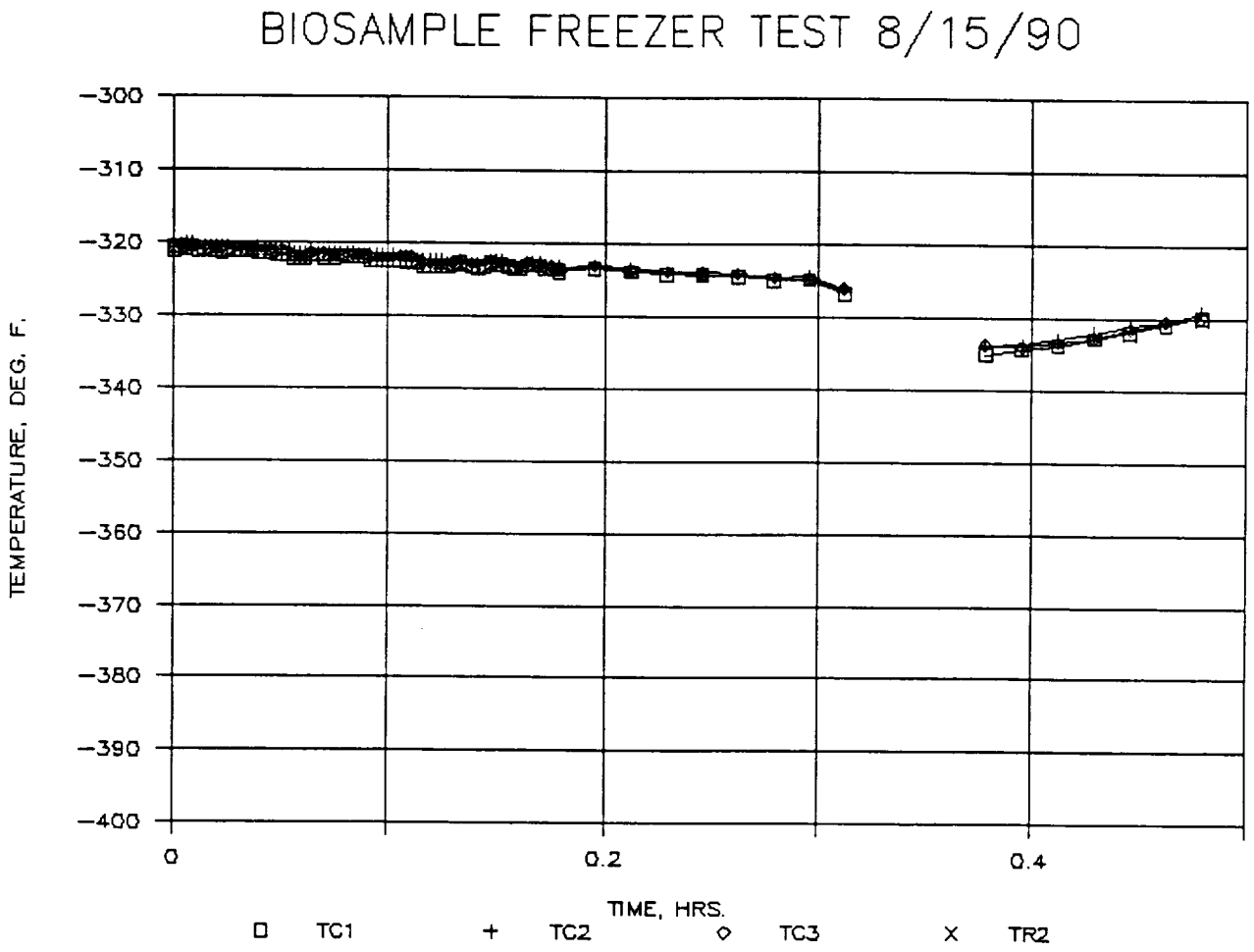

Figure 2. Biosample Freezer Temperatures versus Time for First 0.5 Hours of Test on 8/15/90

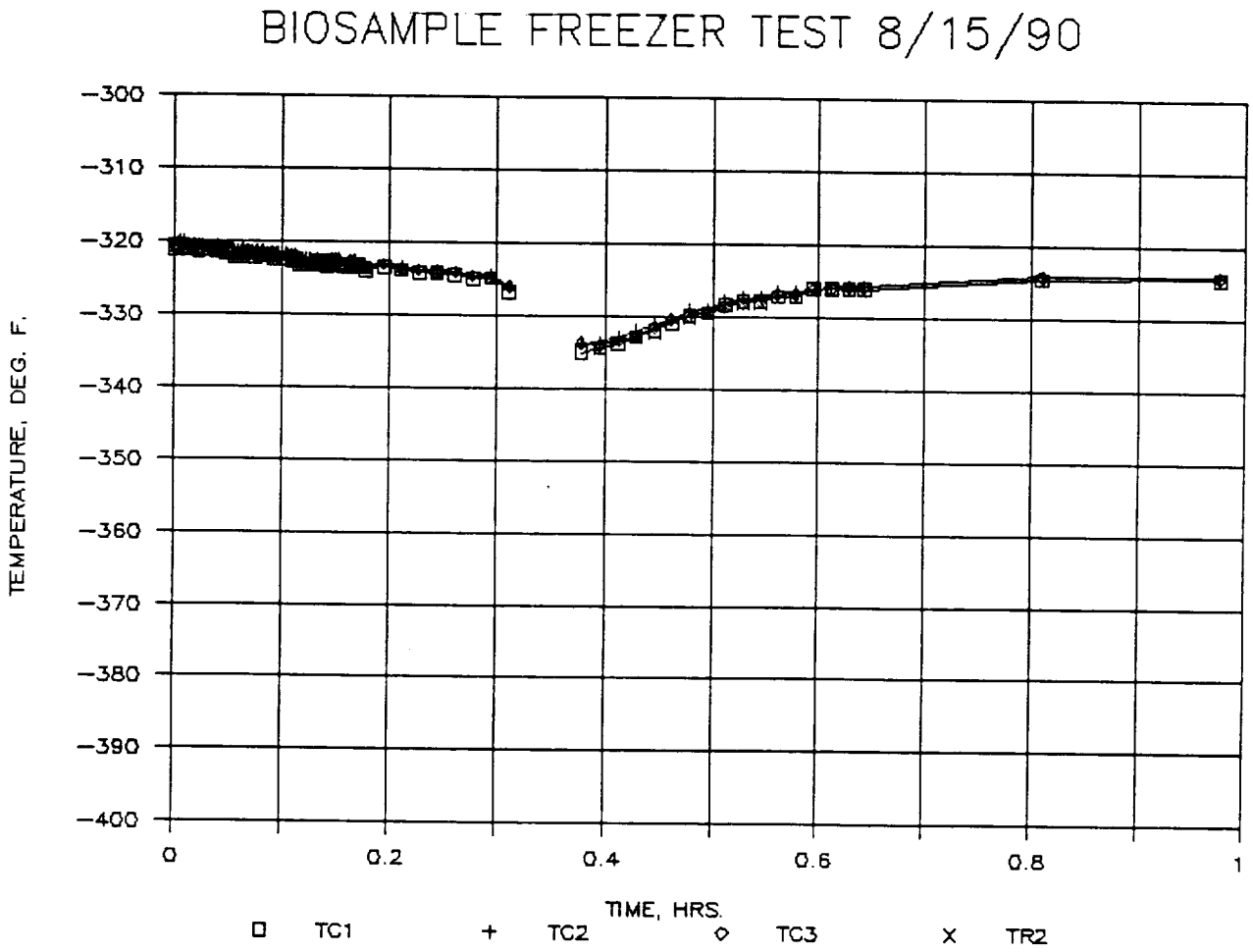

Figure 3. Biosample Freezer Temperatures versus Time for First 1.0 Hour of Test on 8/15/90

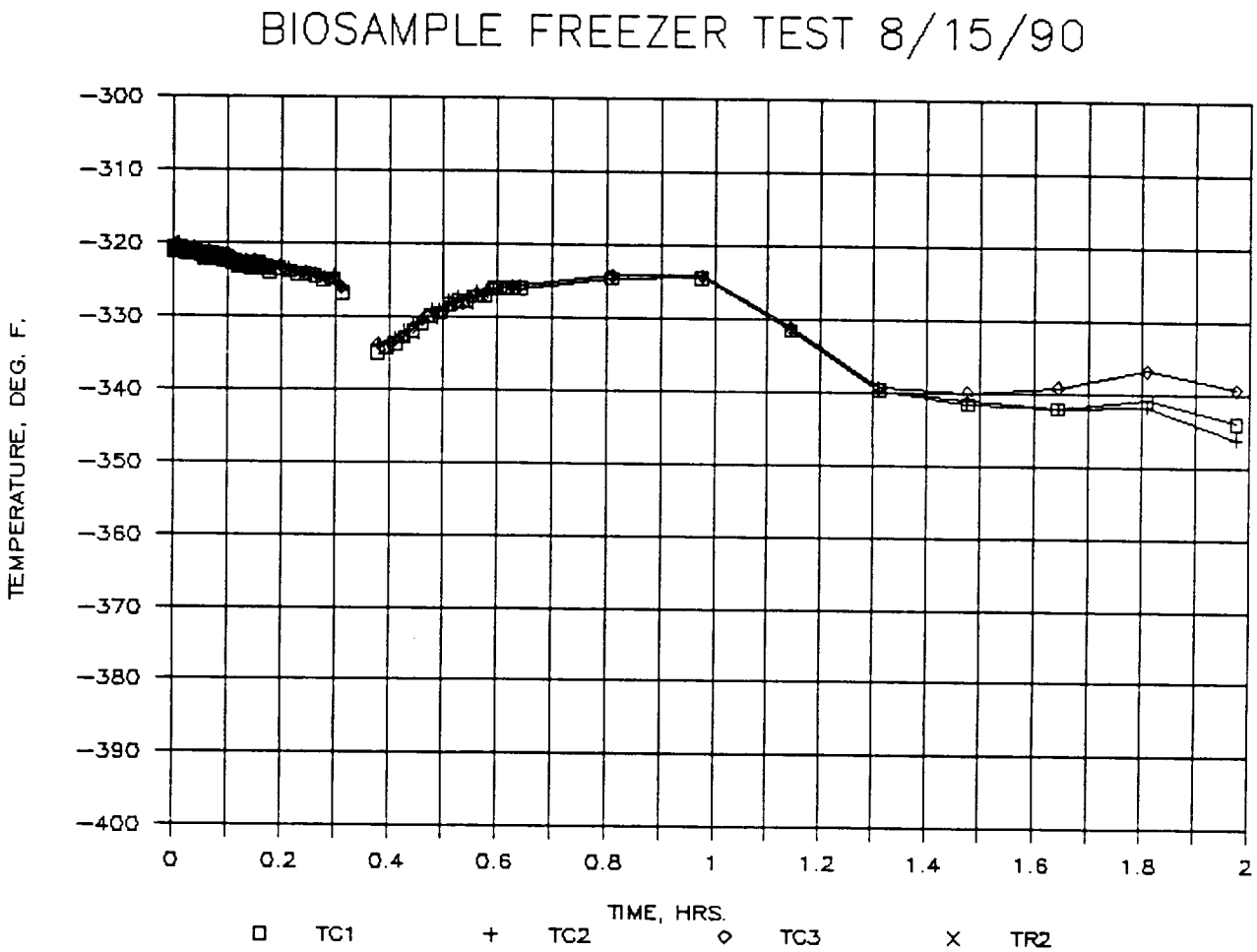

Figure 4. Biosample Freezer Temperatures versus Time for First 2.0 Hours of Test on 8/15/90

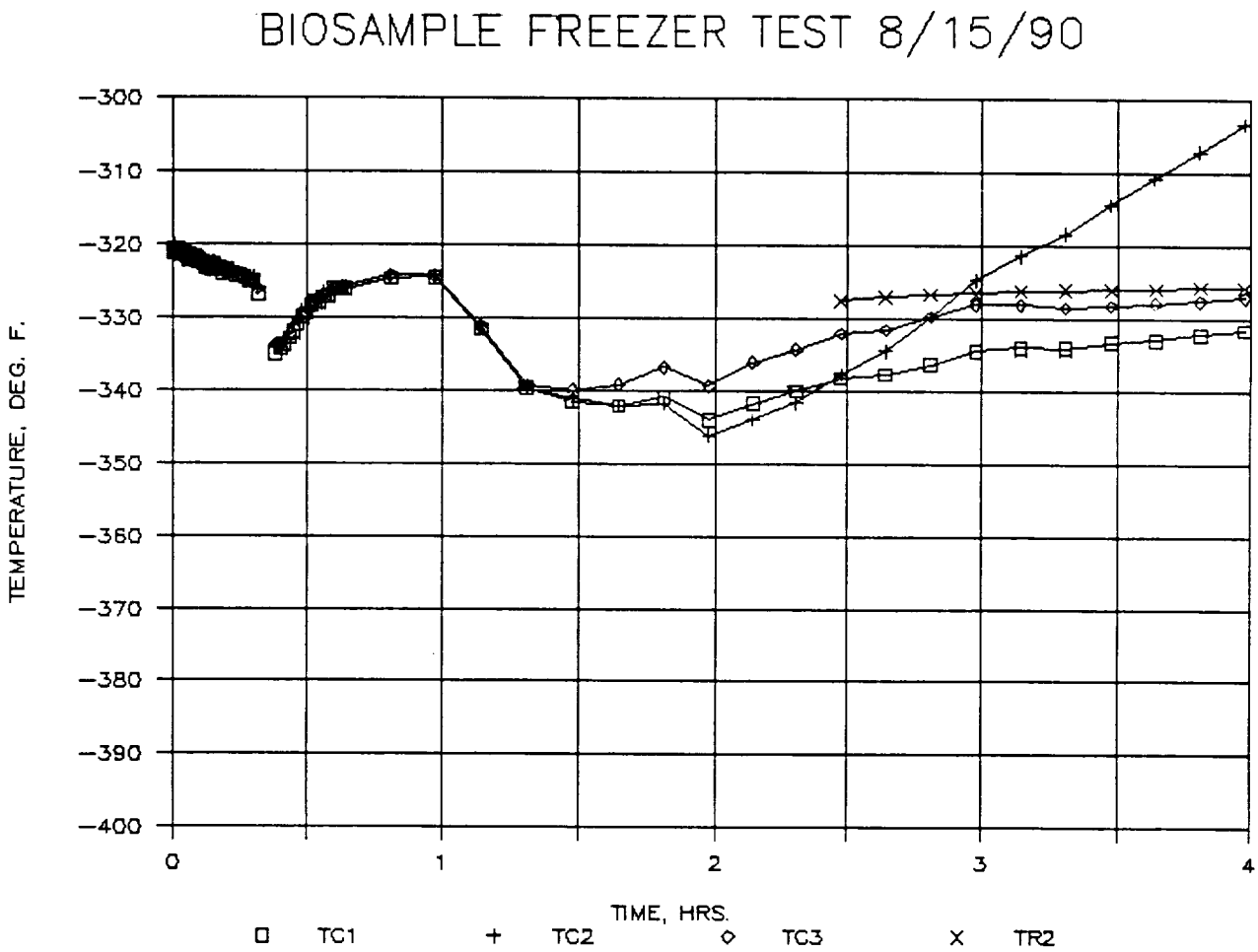

Figure 5. Biosample Freezer Temperatures versus Time for First 4.0 Hours of Test on 8/15/90

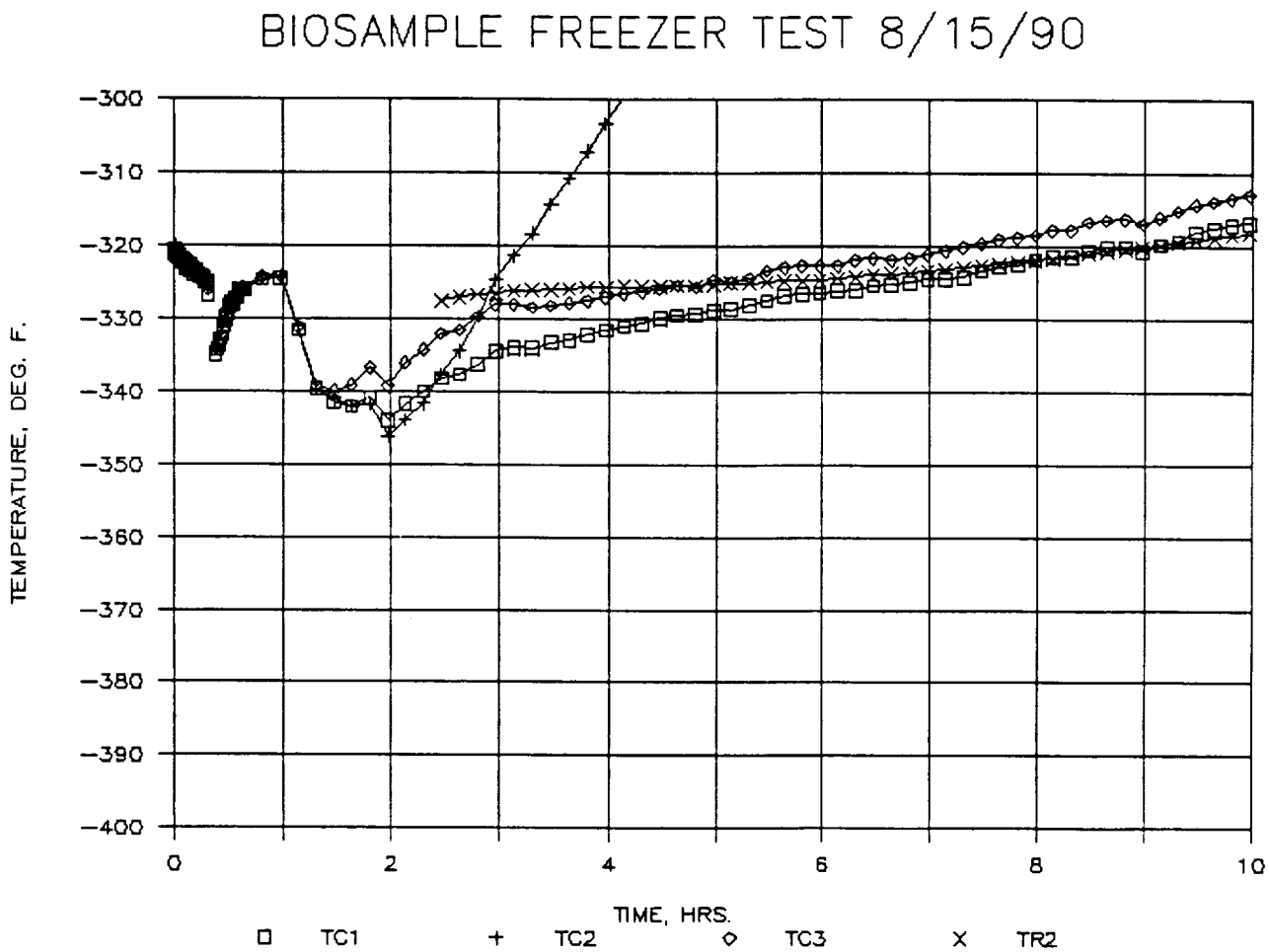

Figure 6. Biosample Freezer Temperatures versus Time for First 10 Hours of Test on 8/15/90

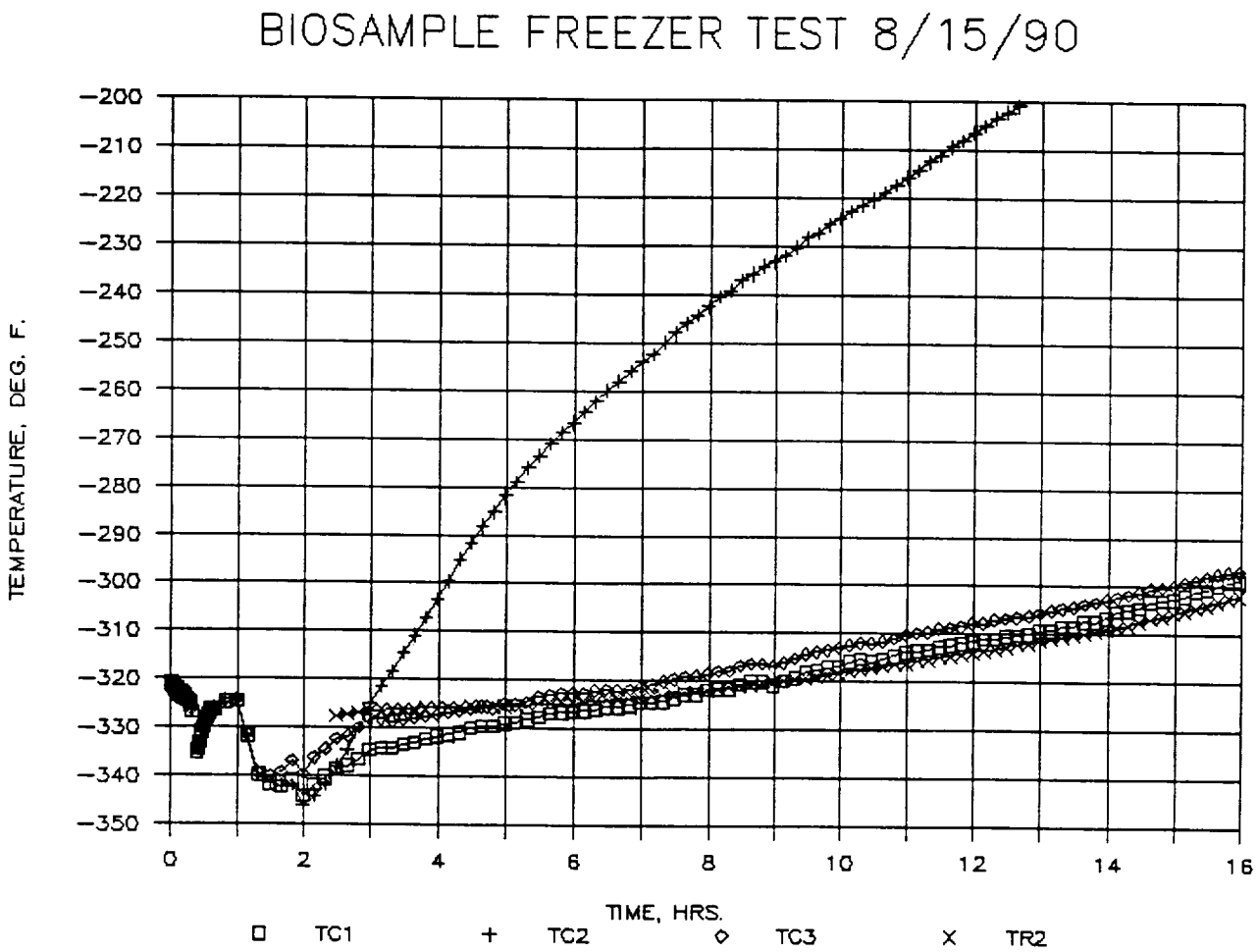

Figure 7. Biosample Freezer Temperatures versus Time for First 16 Hours of Test on 8/15/90

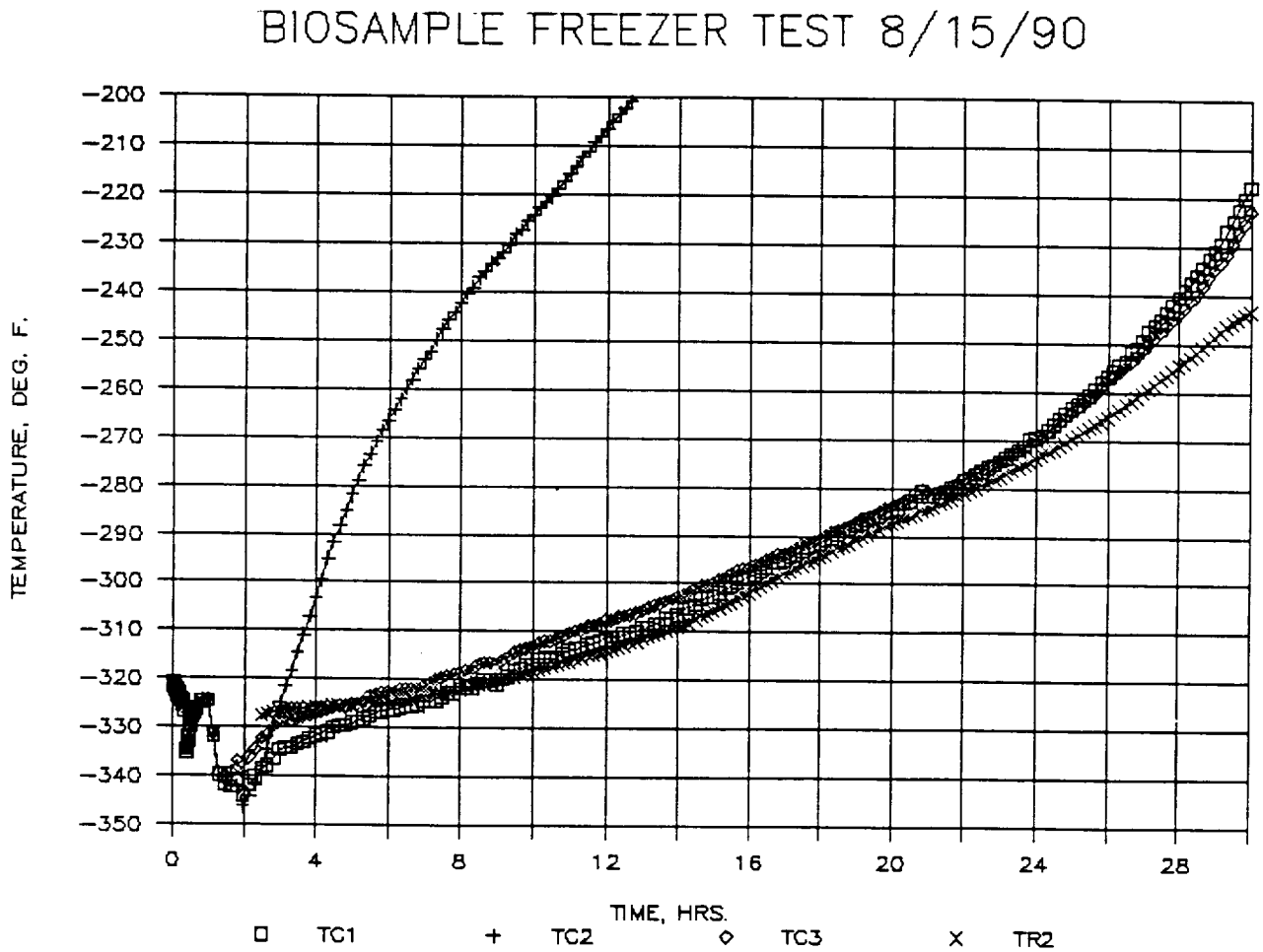

Figure 8. Biosample Freezer Temperatures versus Time for First 30 Hours of Test on 8/15/90

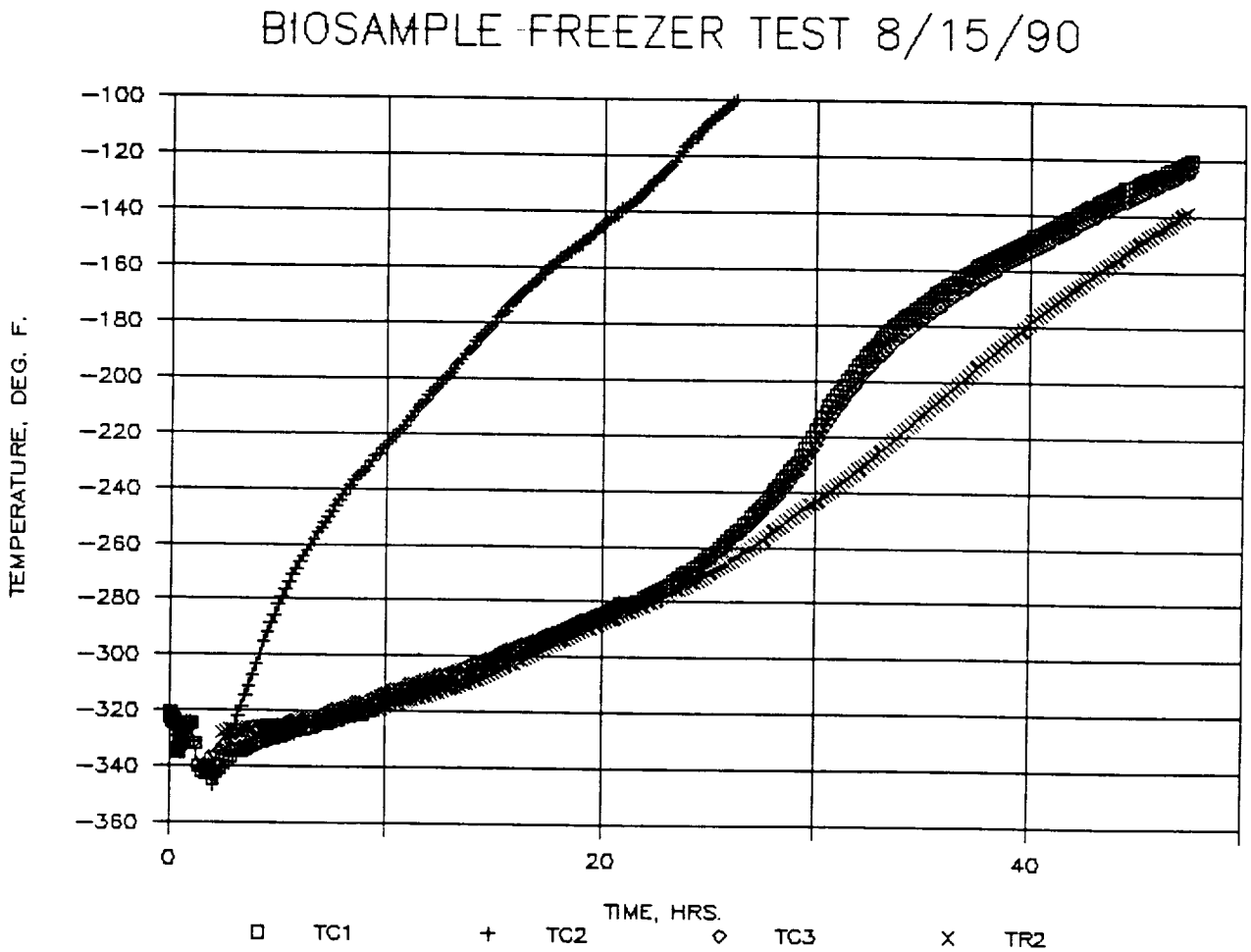

Figure 9. Biosample Freezer Temperatures versus Time for Entire Test Time on 8/15/90

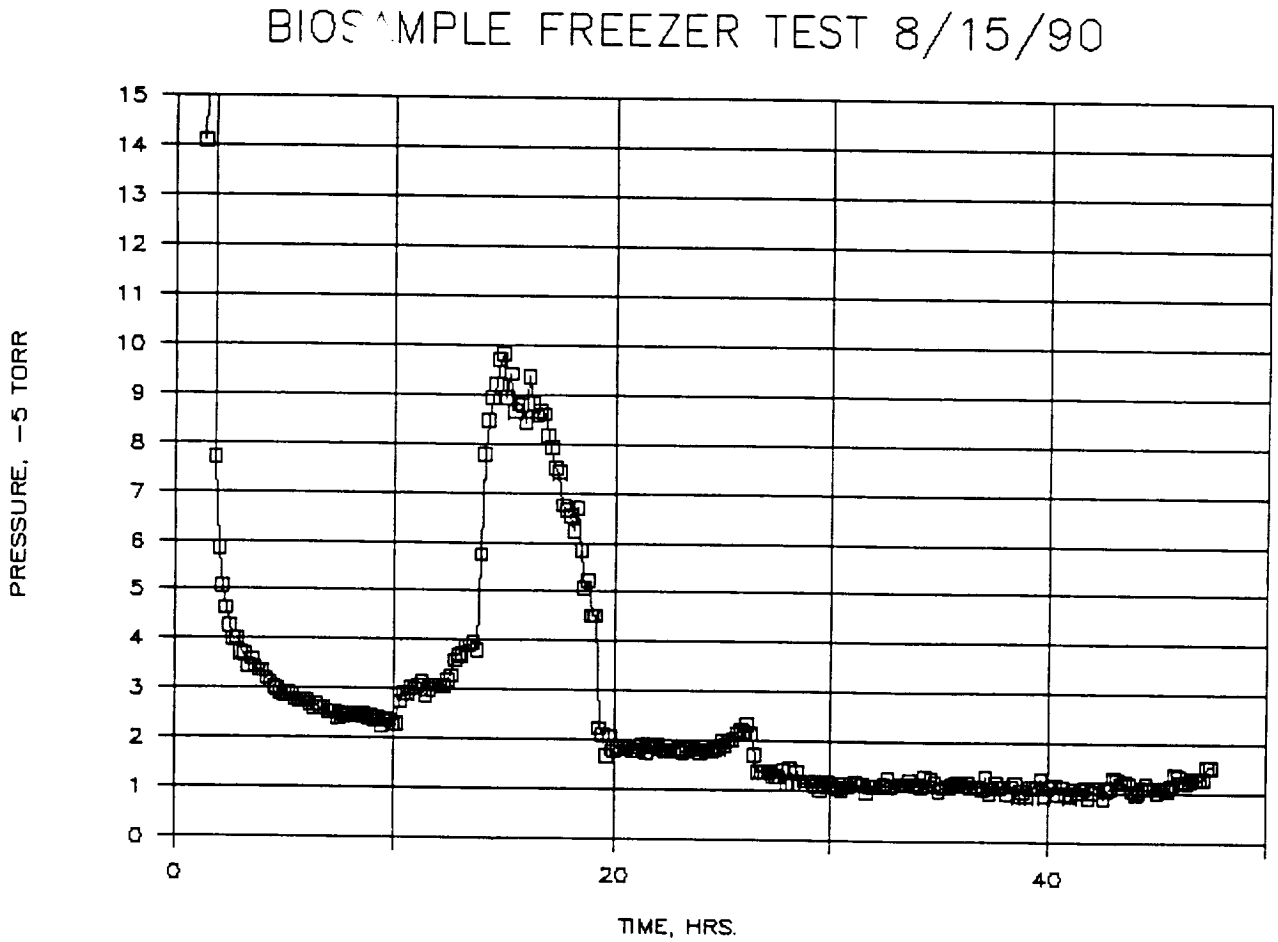

Figure 10. Biosample Freezer Pressure Inside of MLI Space versus Time for Test on 8/15/90

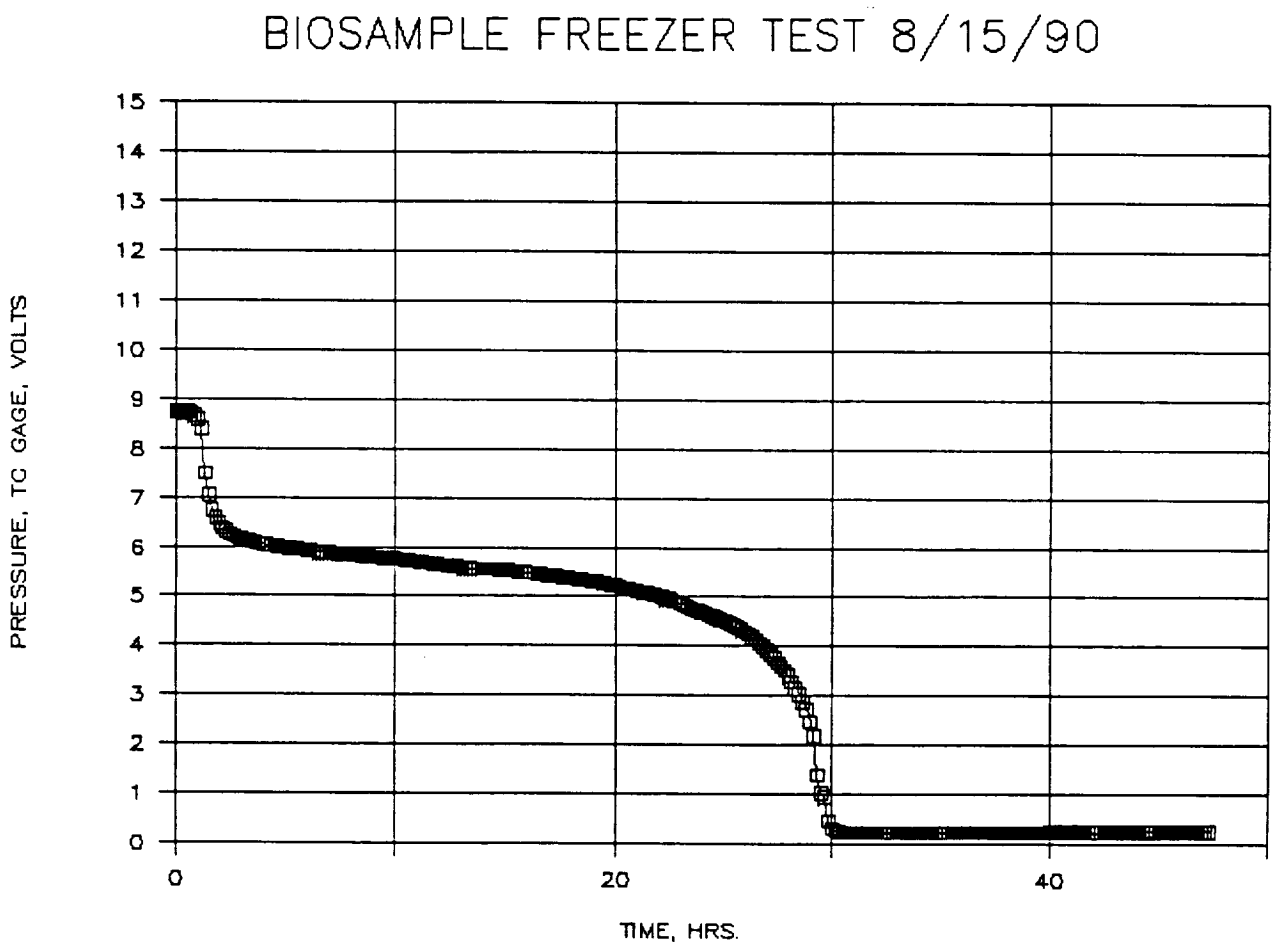

Figure 11. Biosample Freezer Pressure Gage Output in Volts for Inner Cylinder for Test on 8/15/90

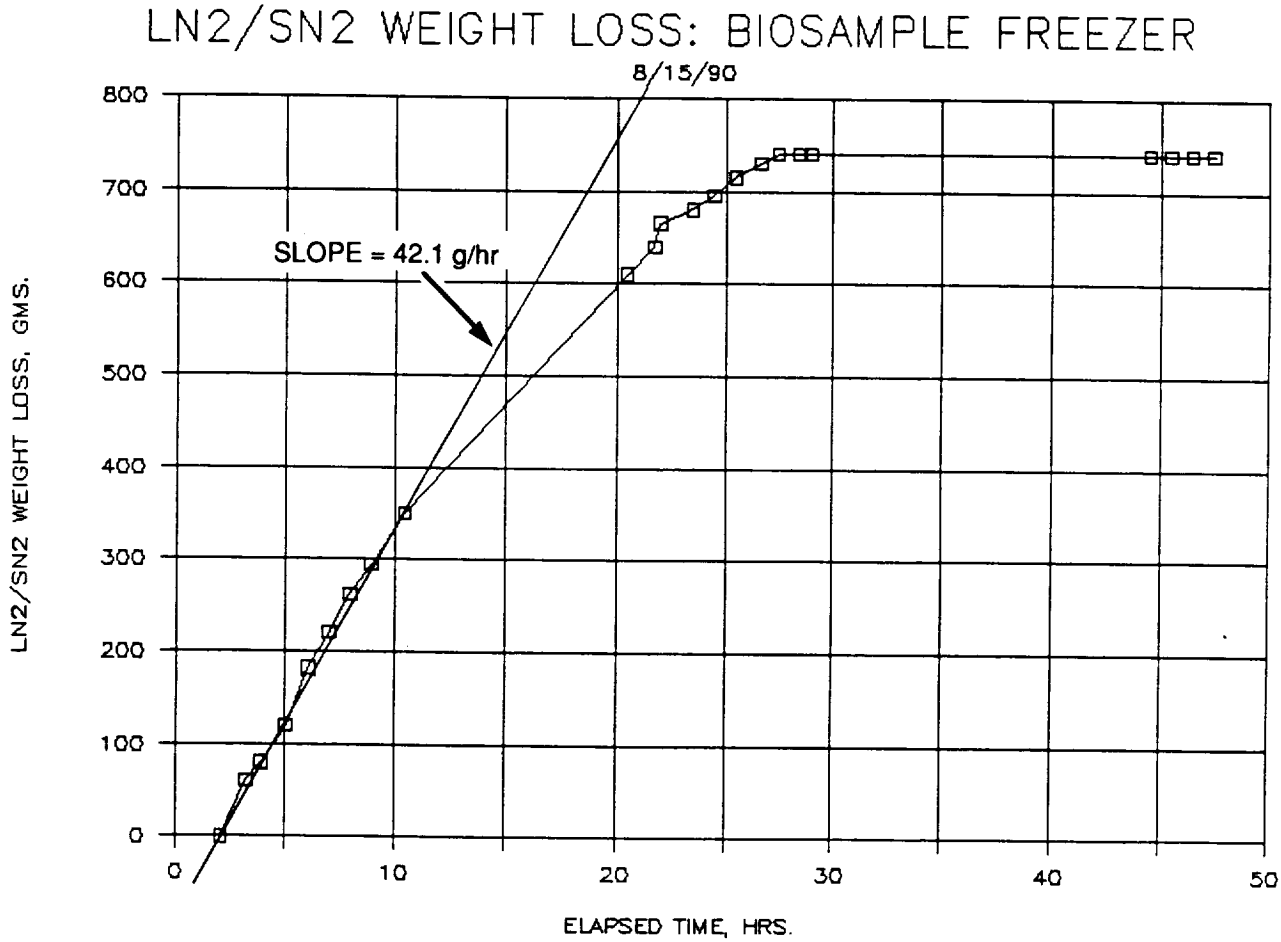

Figure 12. Biosample Freezer Weight Loss versus Time for Test on 8/15/90

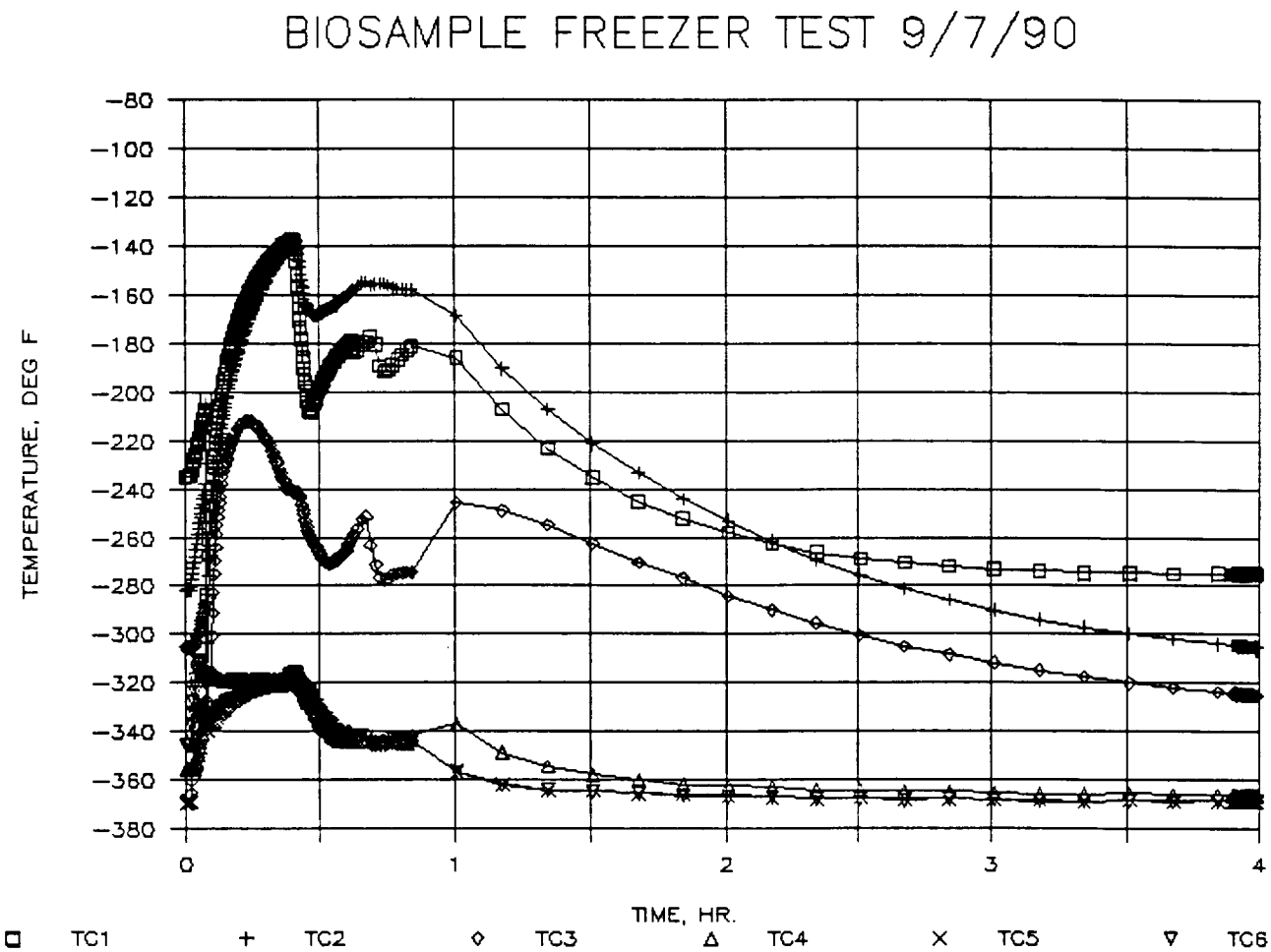

Figure 13. Biosample Freezer Temperatures versus Time for First 4 Hours of Test on 9/7/90 (TC 1-6)

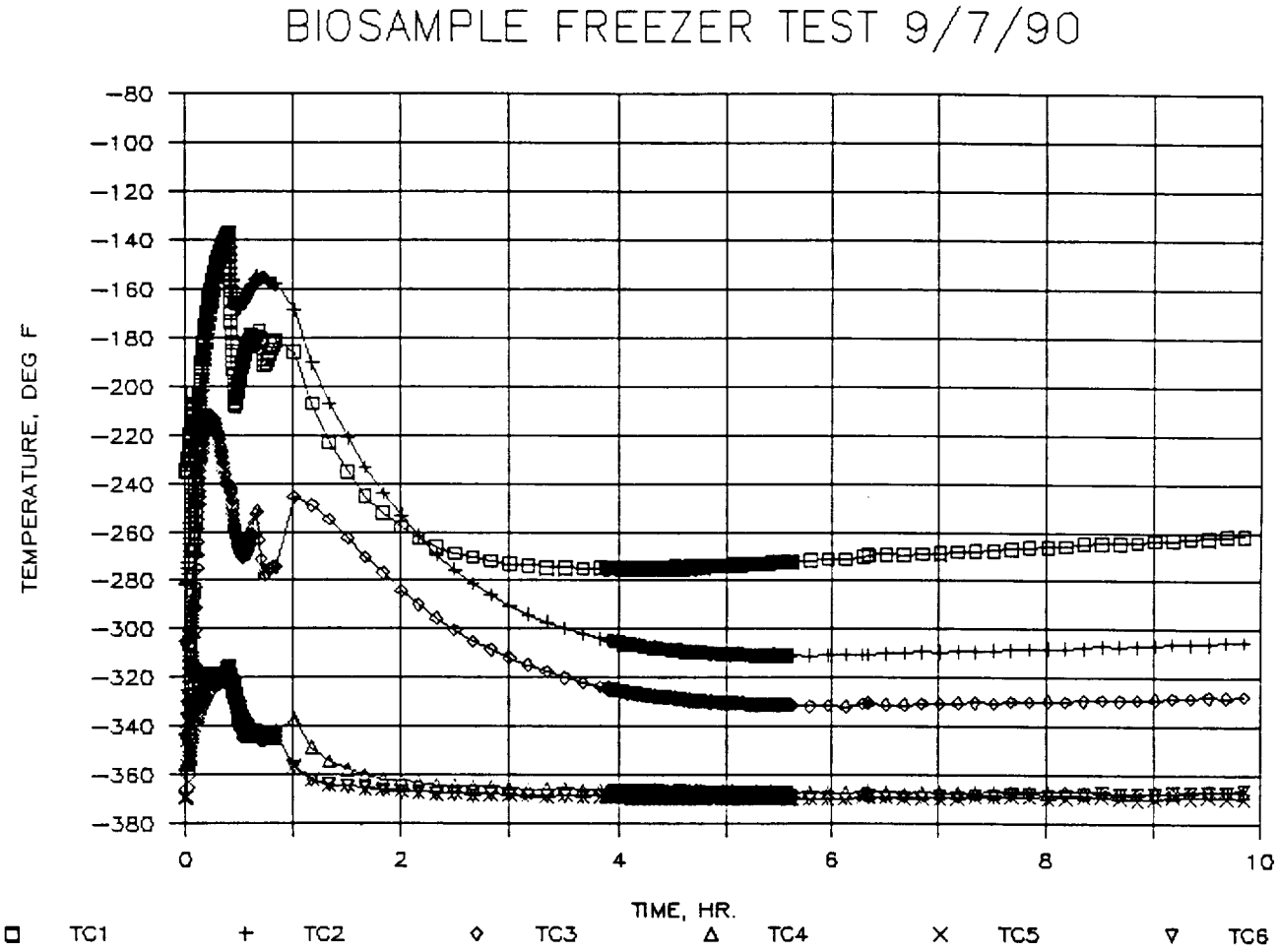

Figure 14. Biosample Freezer Temperatures versus Time for First 10 Hours of Test on 9/7/90 (TC 1-6)

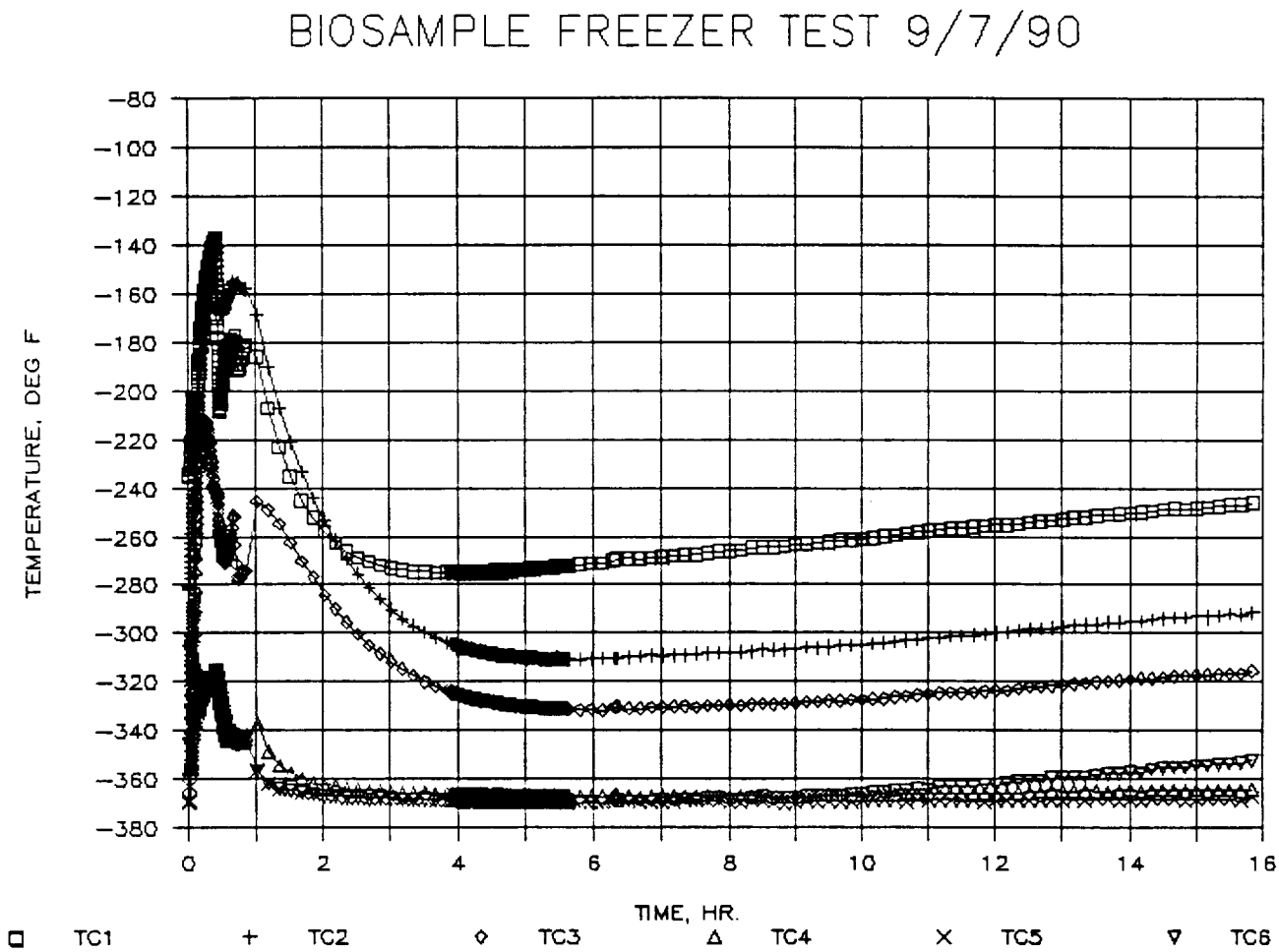

Figure 15. Biosample Freezer Temperatures versus Time for First 16 Hours of Test on 9/7/90 (TC 1-6)

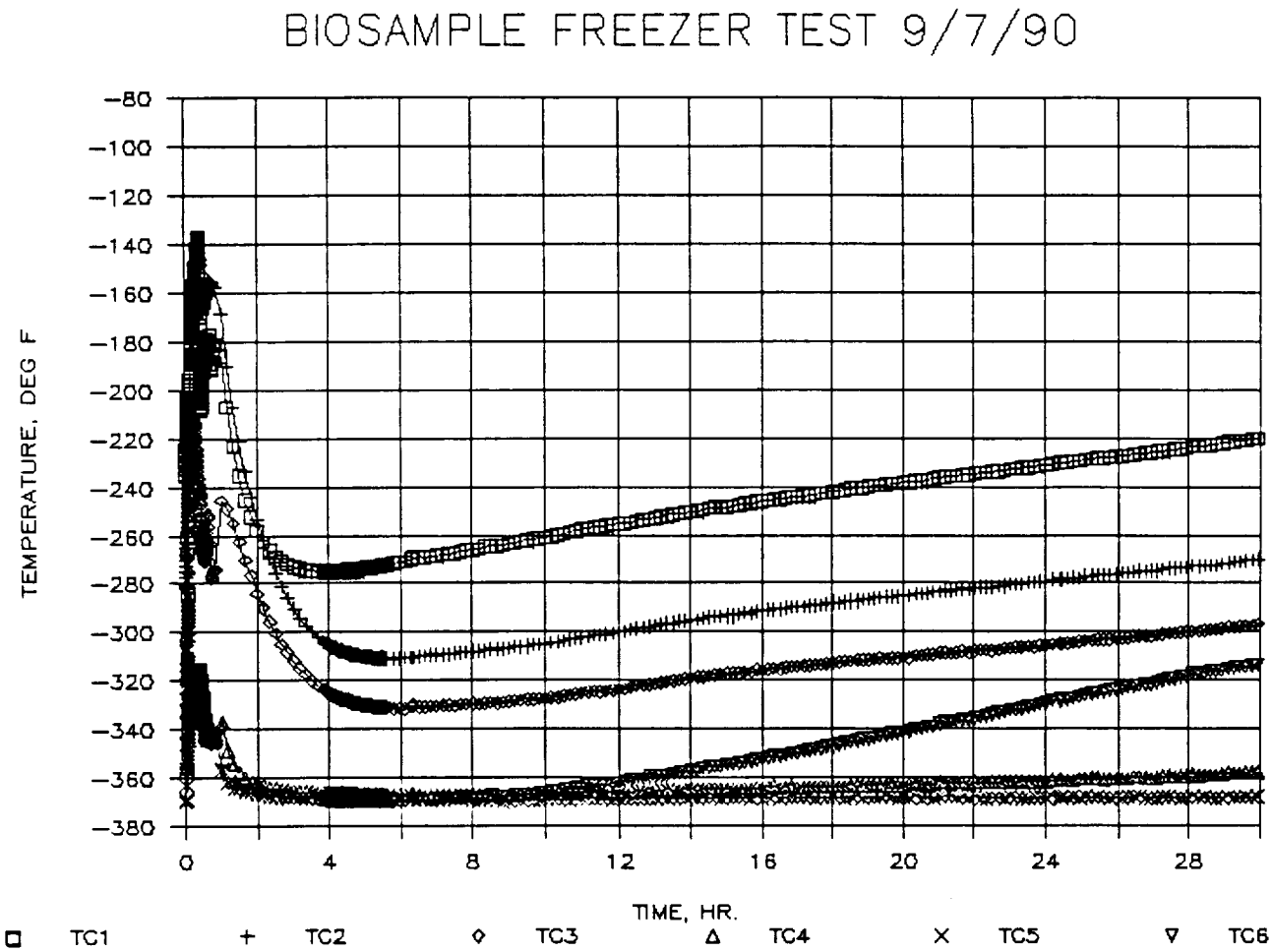

Figure 16. Biosample Freezer Temperatures versus Time for First 29 Hours of Test on 9/7/90 (TC 1-6)

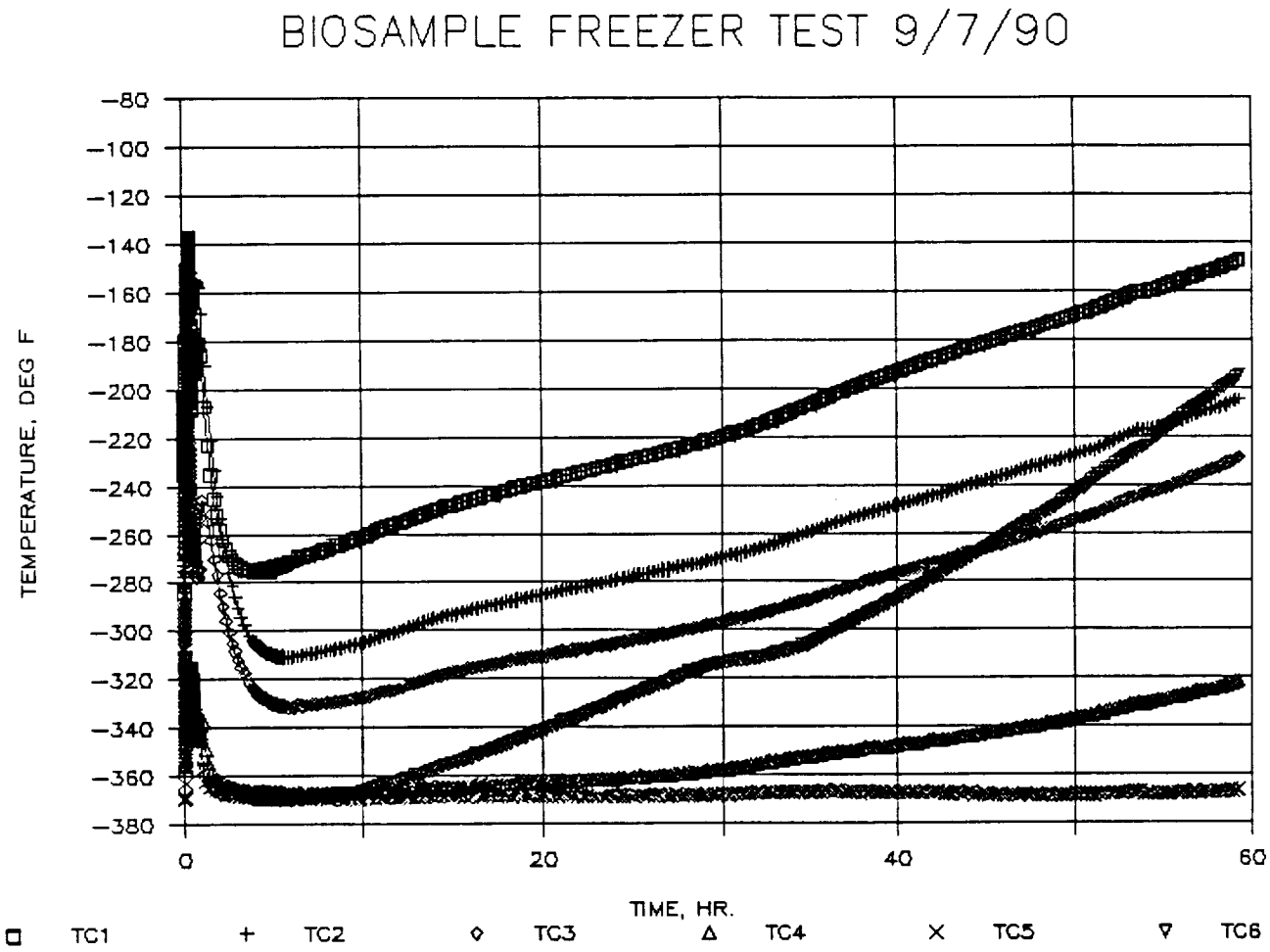

Figure 17. Biosample Freezer Temperatures versus Time for Entire Test Time on 9/7/90 (TC 1-6)

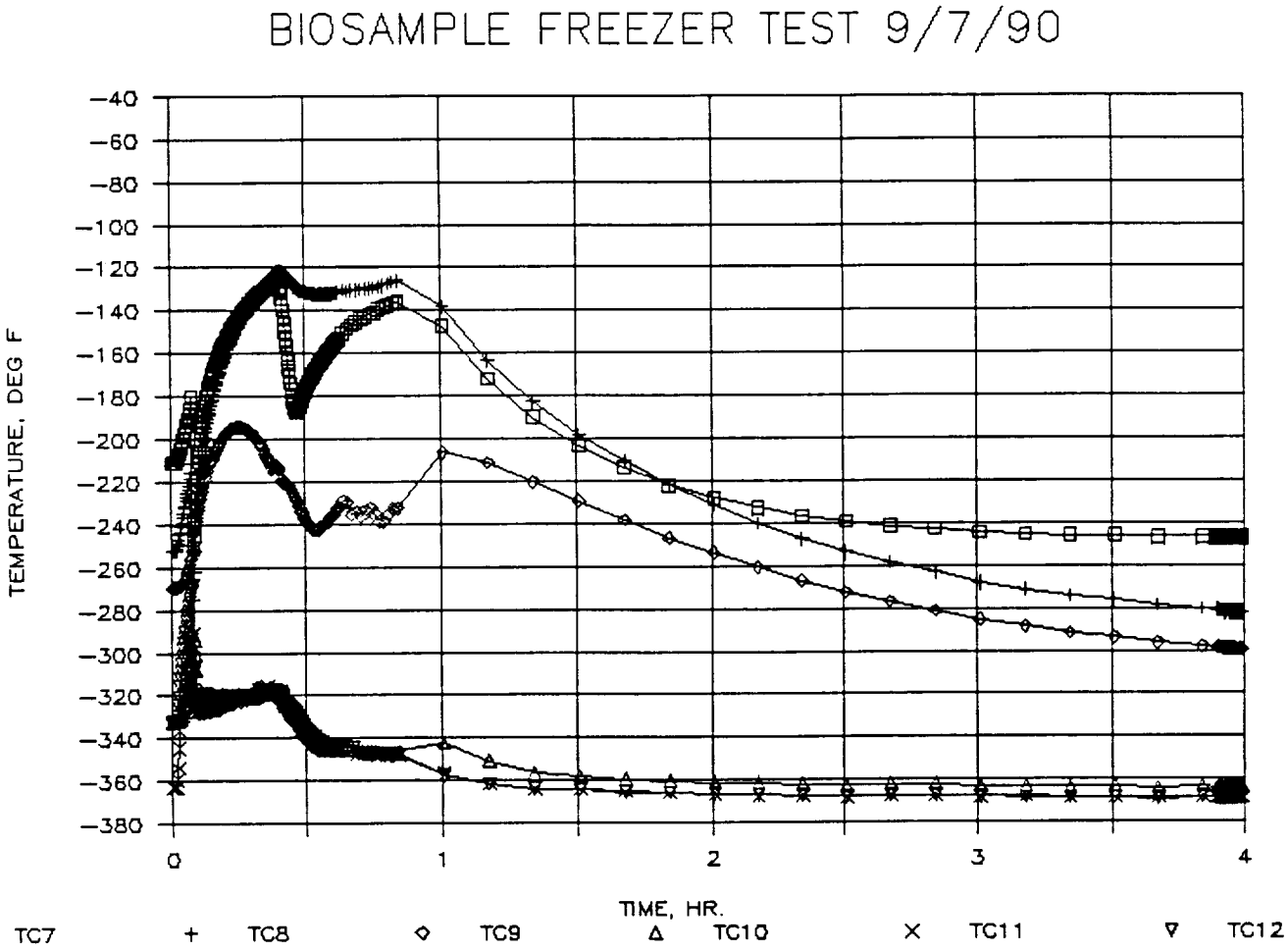

Figure 18. Biosample Freezer Temperatures versus Time for First 4 Hours of Test on 9/7/90 (TC 7-12)

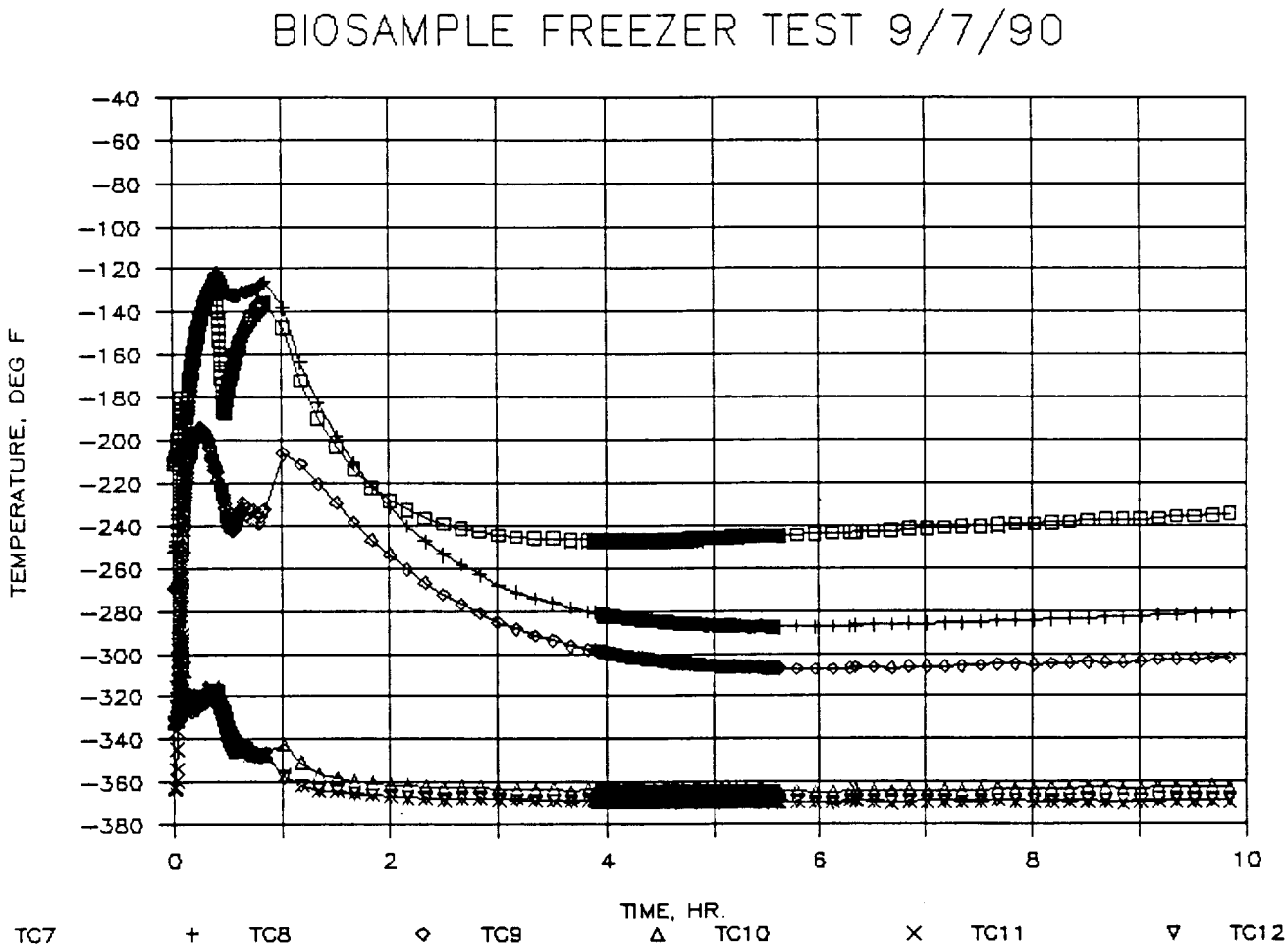

Figure 19. Biosample Freezer Temperatures versus Time for First 10 Hours of Test on 9/7/90 (TC 7-12)

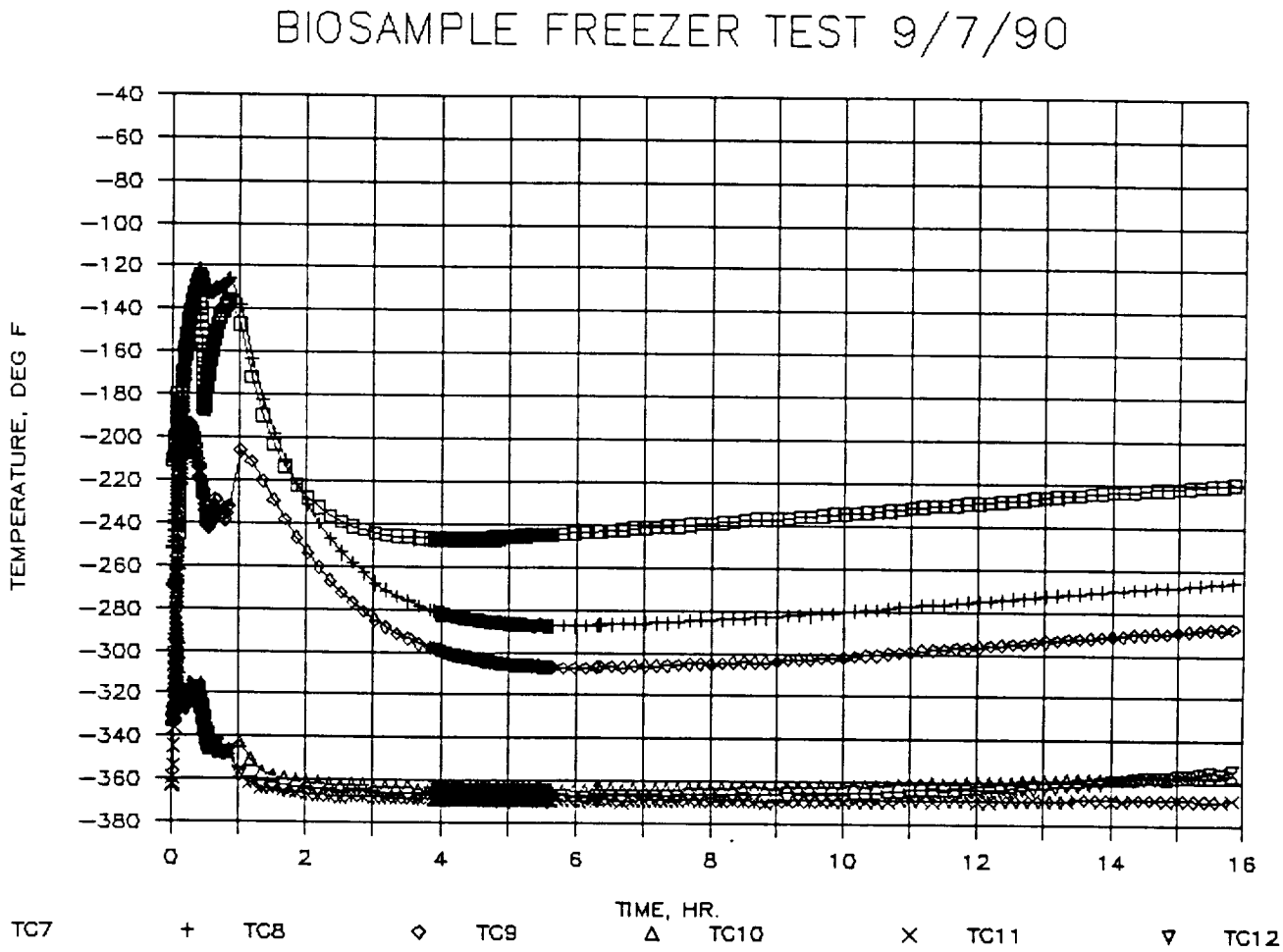

Figure 20. Biosample Freezer Temperatures versus Time for First 16 Hours of Test on 9/7/90 (TC 7-12)

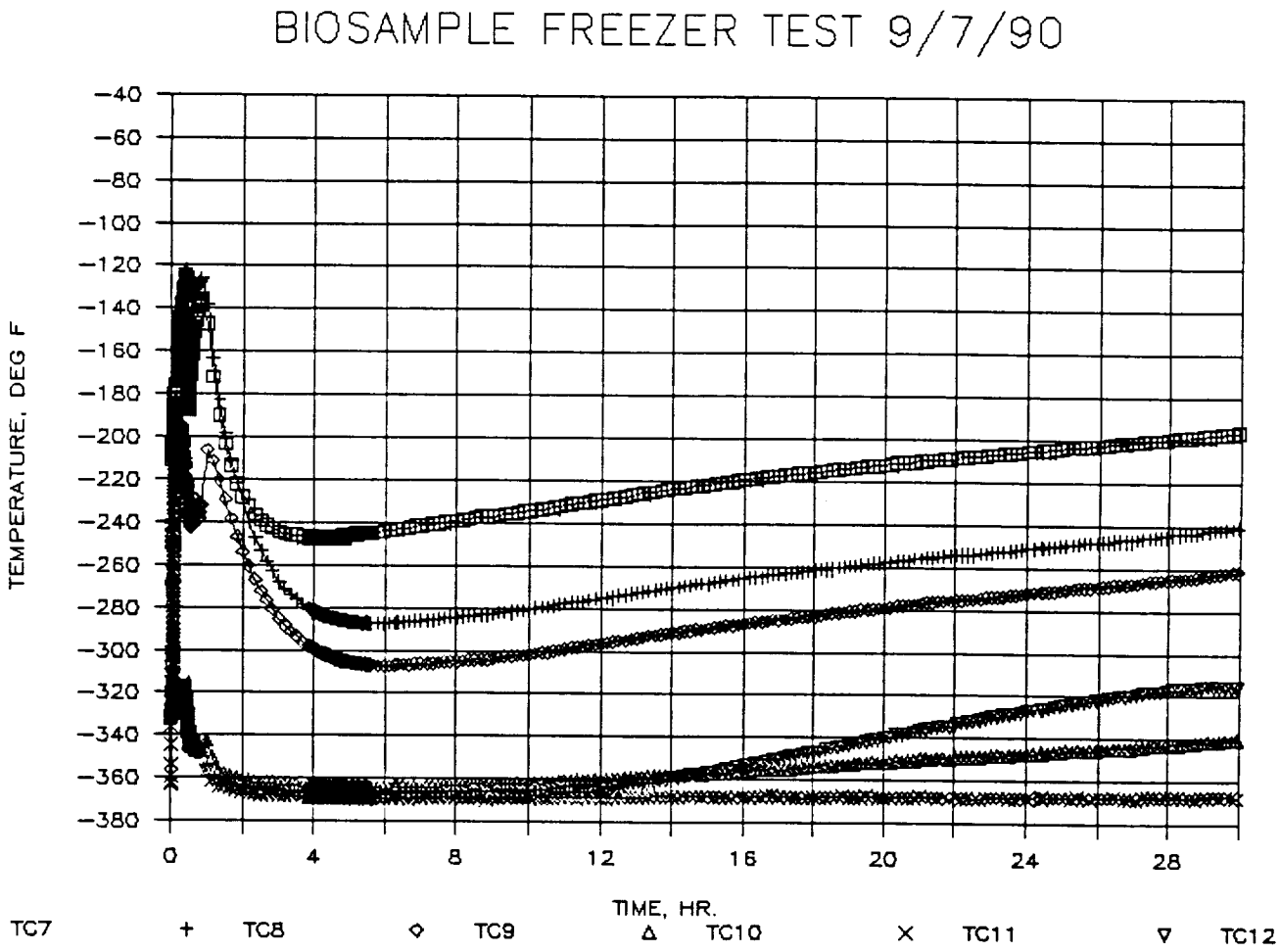

Figure 21. Biosample Freezer Temperatures versus Time for First 29 Hours of Test on 9/7/90 (TC 7-12)

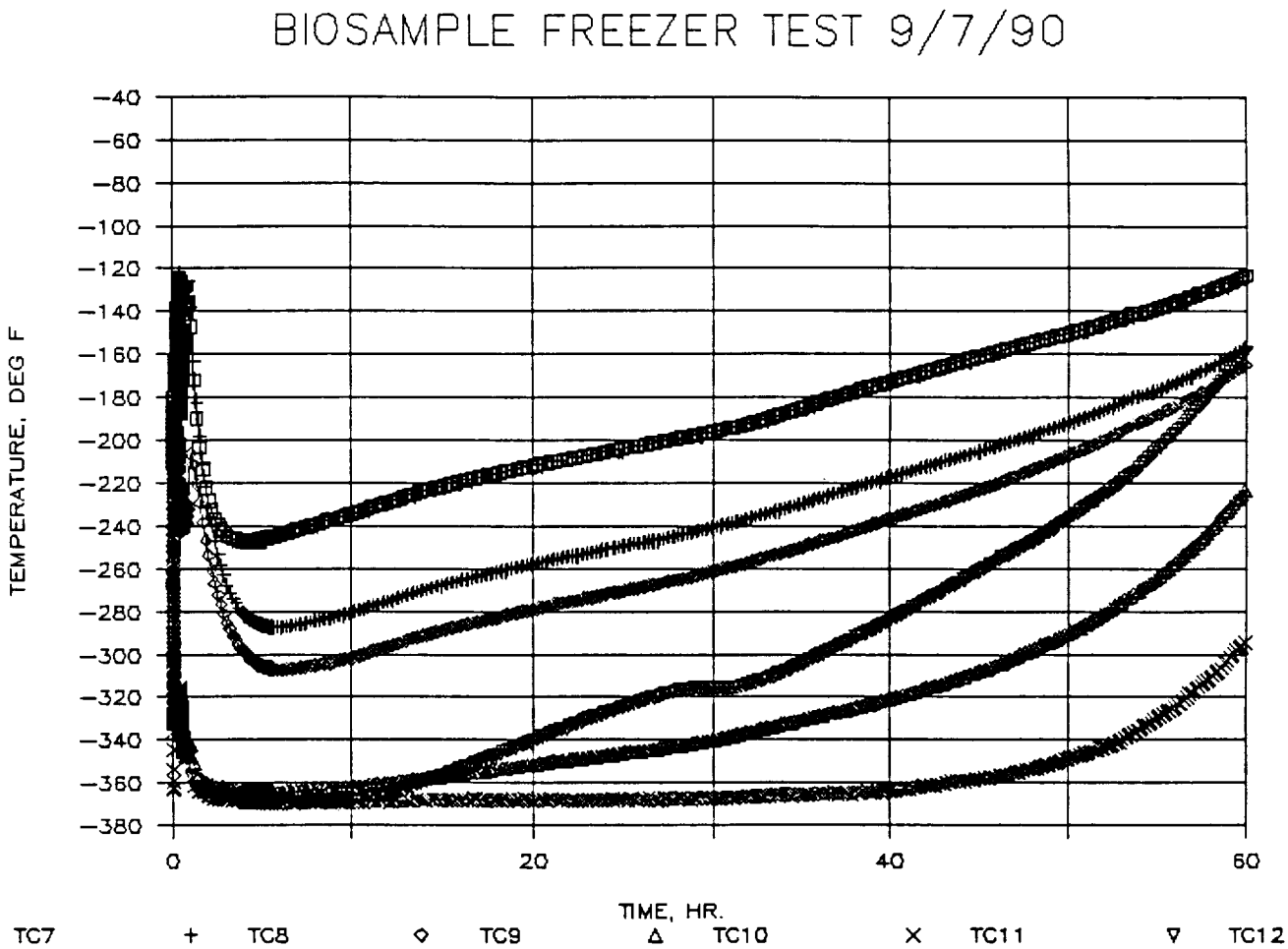

Figure 22. Biosample Freezer Temperatures versus Time for First 60 Hours of Test on 9/7/90 (TC 7-12)

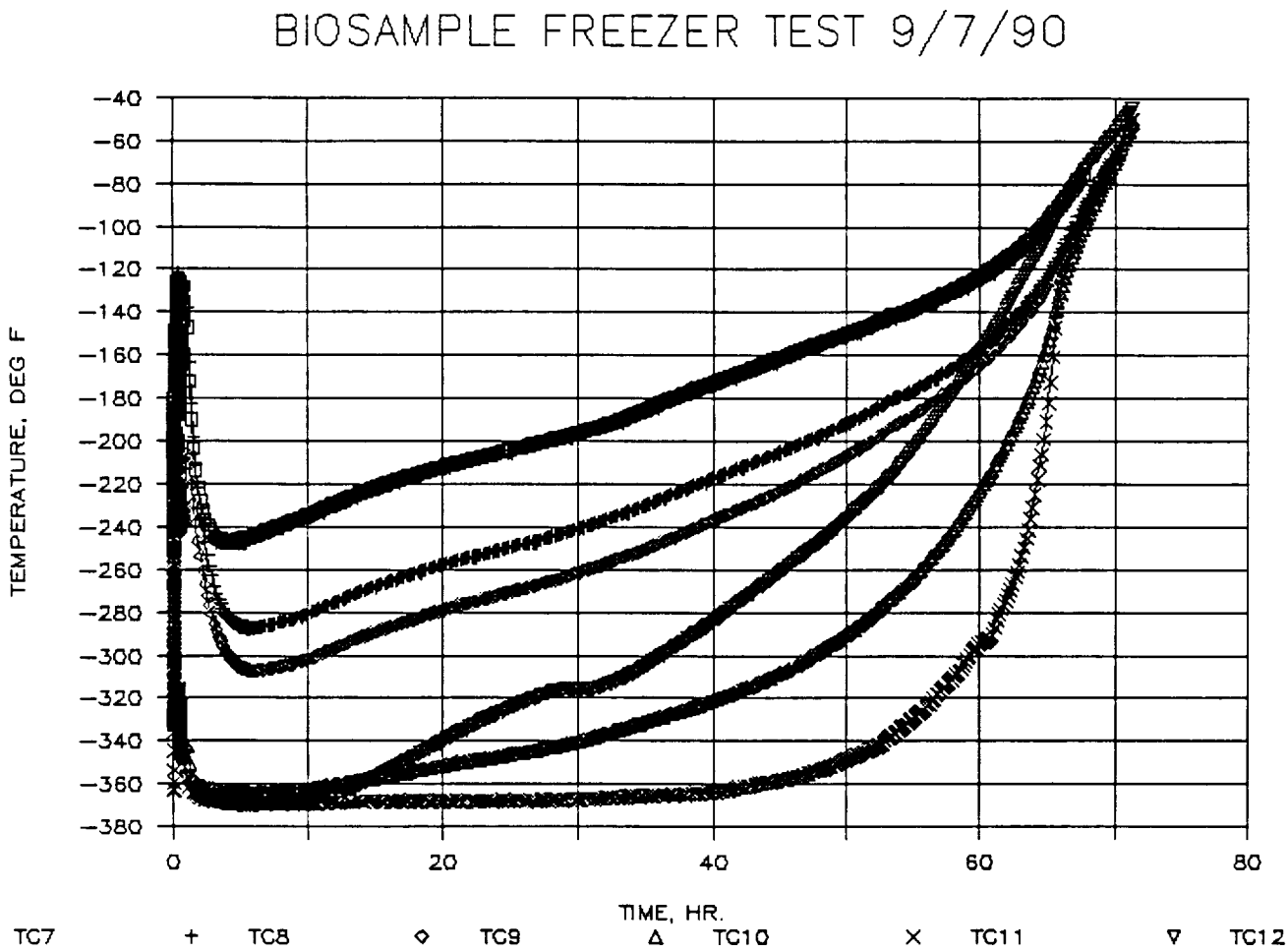

Figure 23. Biosample Freezer Temperatures versus Time for Entire Test Time on 9/7/90 (TC 7-12)

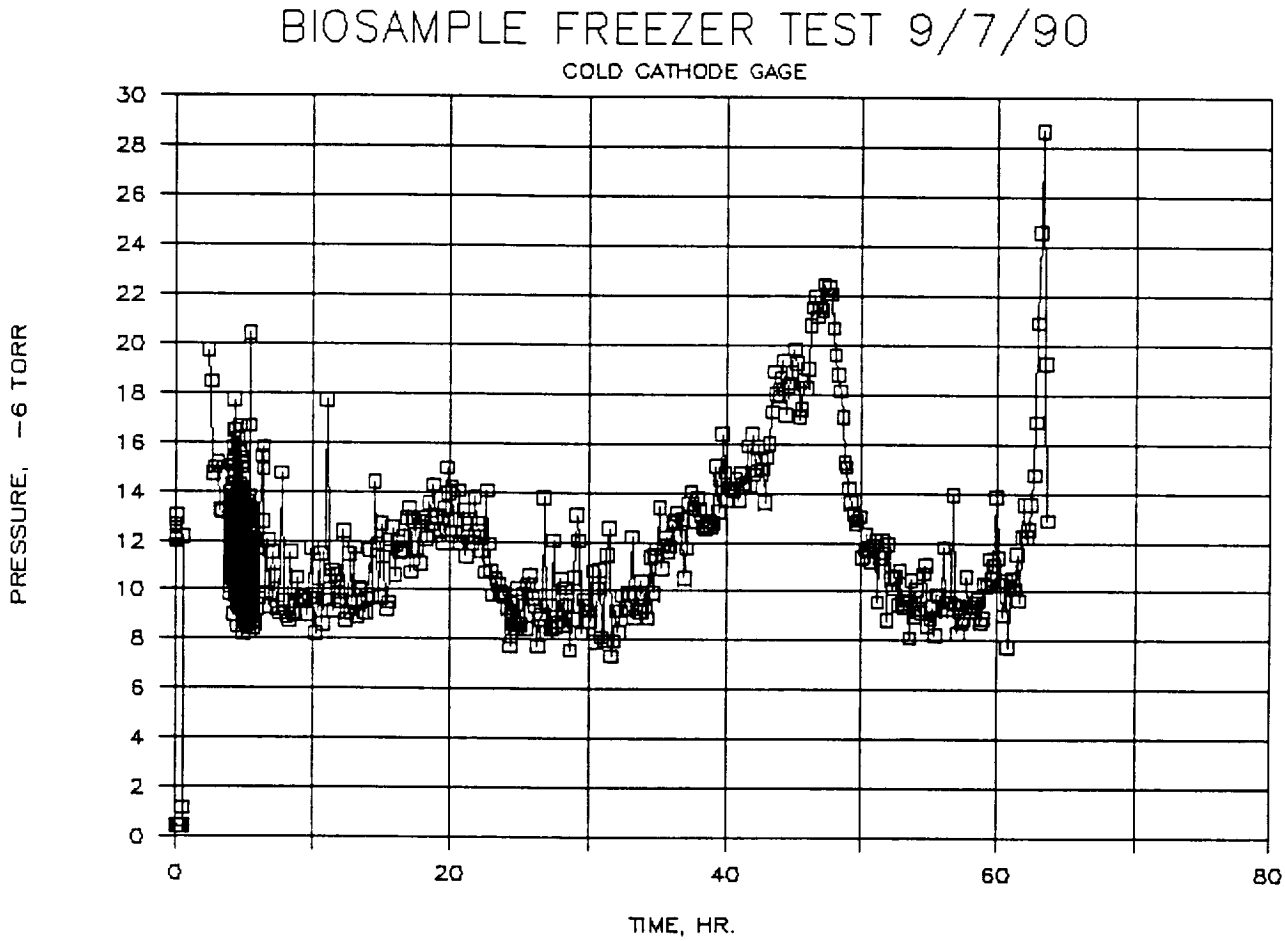

Figure 24. Biosample Freezer Pressure Inside of MLI Space versus Time for Test on 9/7/90

Excerpt from October 1990 Monthly Progress Report LMSC-HSV PR F312367

PRECEDING PAGE BLANK NOT FILMED

PROGRESS DURING THE CURRENT REPORTING PERIOD

Testing of Biosample Freezer

Table 1 shows a summary of tests run to date on the Biosample Freezer. Two tests were made since the last progress report. The purpose of the test of 9/20/90 was to chill down the entire system in preparation for the next test on the following day. The purpose of the test on 9/21/90 was to repeat the test of 9/7/90, since the heat leak on 9/7/90 was higher than that measured during the test of 8/15/90. On 9/21/90 the Mylar blanket inside the inner cylinder was removed to see if that would effect the results.

Figures 1 through 15 show results of the 9/21/90 test. Figure 16 shows the thermocouple locations for this test.

Figures 1 through 6 are for temperatures from thermocouples 1 through 6, and Figures 7 through 12 are for temperatures from thermocouples 7 through 12. These plots are shown in increasing time steps as the test progresses so that the values early in the test can be read. As seen from these plots, there is a large temperature gradient inside the freezer. This is because some of the thermocouples are immersed in the N_2 slush (e.g., 5, 6, 11, and 12) while others are near the diaphragm which is the major source of heat leak (e.g., 1, 2, 7, and 8).

Figures 13 and 14 show pressure measurements for the inner cylinder and MLI space respectively. The MLI space pressure is higher on this test than on the 9/7/90 test. This difference was due to a minute leak in the diaphragm-to-outer-cylinder joint. This leak also caused the inner cylinder pressure to follow the same profile as the pressure in the MLI space, i.e., Figure 13 compared to Figure 14. The two peaks in Figures 13 and 14 are apparently due to release of trapped gases from the inner cylinder surface when the temperature rises enough to stop cryopumping.

Figure 15 shows the freezer weight decrease with time. From the slope of this line, the "slush N_2" boiloff rate is determined and used to calculate the heat leak. For the 9/21/90 test the heat leak was calculated to be 4.11 W as compared to 3.87 W for the 9/7/90 test. This gives a ratio of

$$\frac{4.11}{3.87} = 1.06 \qquad \text{or a 6\% increase.}$$

After completion of the test on 9/21/90 the Biosample Freezer was disassembled. The existing diaphragm with the 0.001 in. thick stainless steel liner was

removed and replaced with an upgraded design. This new diaphragm design consists of a 0.010 in. thick epoxy glass sheet with a 1/4 mil thick double aluminized Mylar liner bonded in place with EA-1210 adhesive. New titanium seals and aluminum inner cylinder diaphragm joint rings were made and bonded in place. This new configuration is now being leak checked and prepared for testing. This testing should resume shortly. Since the stainless steel diaphragm liner is the major heat leak source, the next test results are expected to have a significantly reduced heat leak.

Figure 17 shows the LN_2 fill process during the 9/21/90 test. Figure 18 shows the freezer after removal of the diaphragm, exposing the MLI space, during the upgrading of the unit. Figure 19 shows a sheet of the new diaphragm material before cutting out the diaphragm annular shape.

PRECEDING PAGE BLANK NOT FILMED

Table 1. SUMMARY OF TESTS RUN TO DATE ON BIOSAMPLE FREEZER

Test Date	Heat Sink or "Slush" N_2 Temp. at Start of Test (°F)	Miminum Pressure Obtained (torr)	Test Duration (hr)
5/23/90	-2	1×10^{-3}	5
5/25/90	-6	5×10^{-5}	5
5/29/90	4	6×10^{-4}	27
6/11/90	-52	2×10^{-5}	46
6/15/90	-60	1×10^{-5}	64
6/22/90	-100	1×10^{-5}	66
6/25/90	-150	4×10^{-5}	46
6/28/90	-200	7×10^{-5}	24
6/29/90	-240	3×10^{-5}	48
7/25/90	Room temperature pump-down to check O-ring seal		
7/27/90	-310	**	68
7/30/90	< -328	**	22
7/31/90	< -328	**	23
8/1/90	Data not reduced due to problem with cryopumping air into MLI space		
8/2/90	< -328	**	96
8/7/90	< -328 (-340)*	**	24
8/8/90	< -238 (-370)*	**	44
8/14/90	Chilldown test in preparation for test on 8/15/90		
8/15/90	-345*	9×10^{-6}	30
9/6/90	Chilldown test in preparation for test on 9/7/90		
9/7/90	-370*	8×10^{-6}	72
9/20/90	Chilldown test in preparation for test on 9/21/90		
9/27/90		12×10^{-6}	71

* Temperatures in "slush" N_2.

** Data not yet reduced.

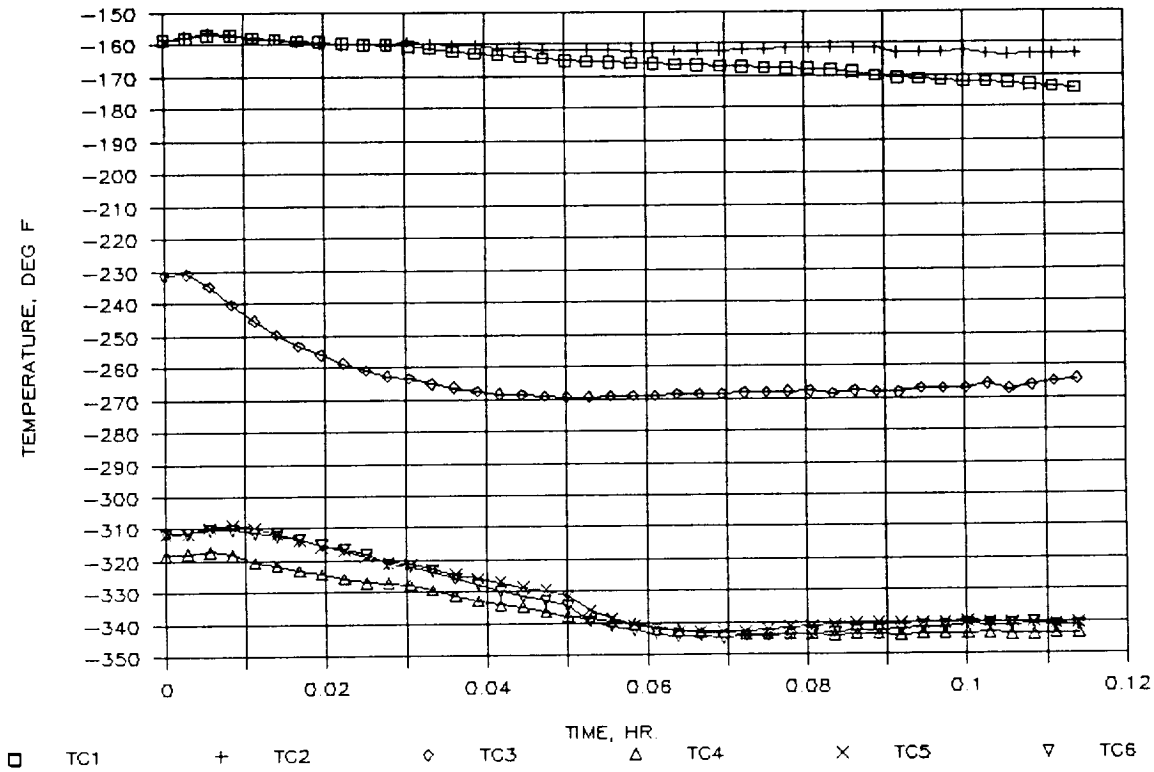

Figure 1. Biosample Freezer Temperature versus Time for first 0.12 Hours of Test on 9/21/90 (TC Nos. 1-6)

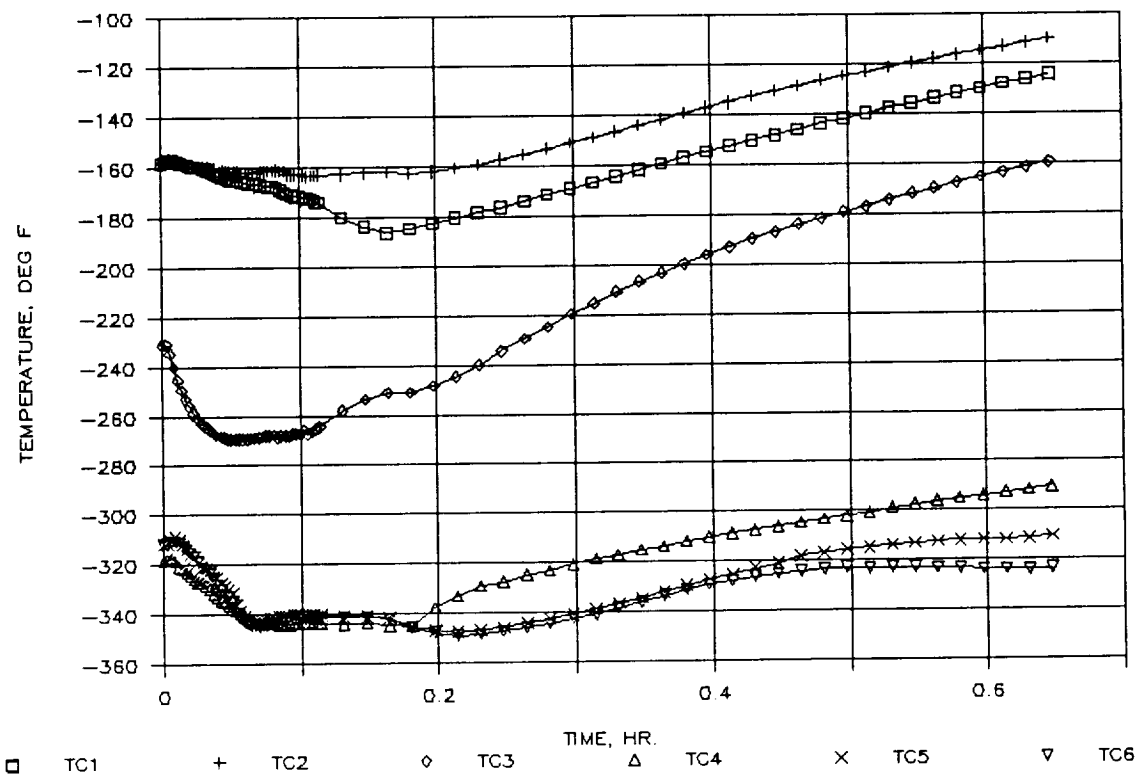

Figure 2. Biosample Freezer Temperature versus Time for first 0.6 Hours of Test on 9/21/90 (TC Nos. 1-6)

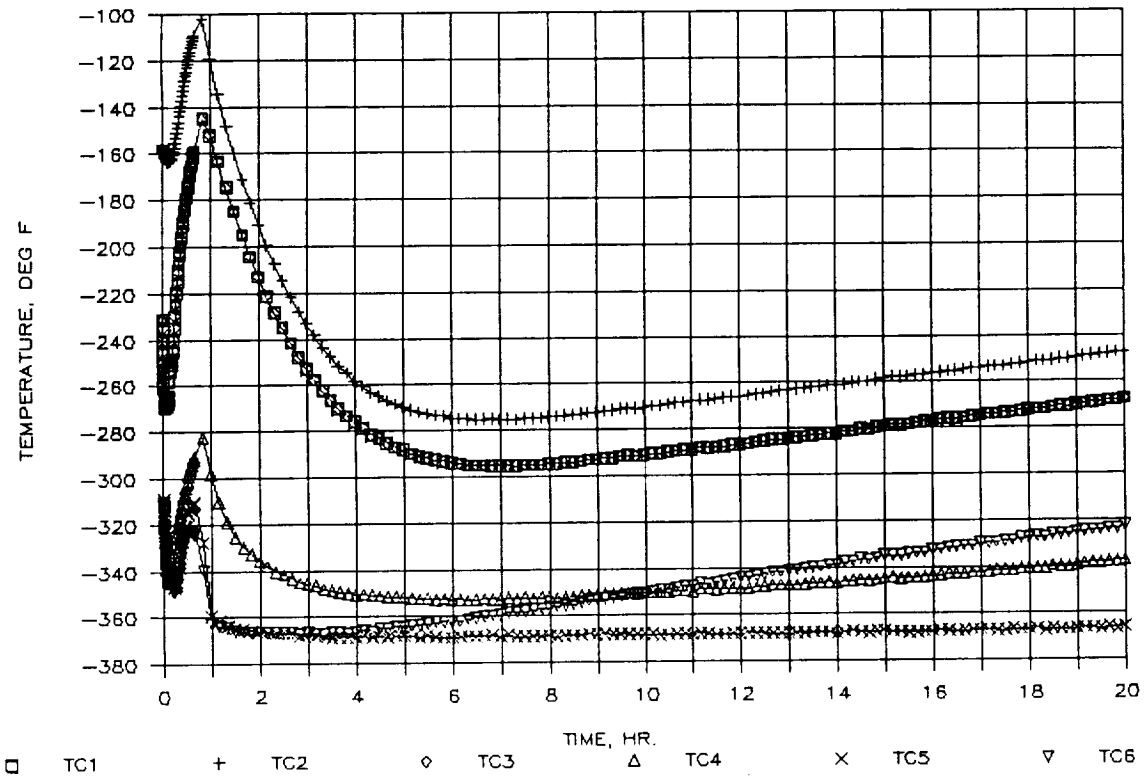

Figure 3. Biosample Freezer Temperature versus Time for first 10 Hours of Test on 9/21/90 (TC Nos. 1-6)

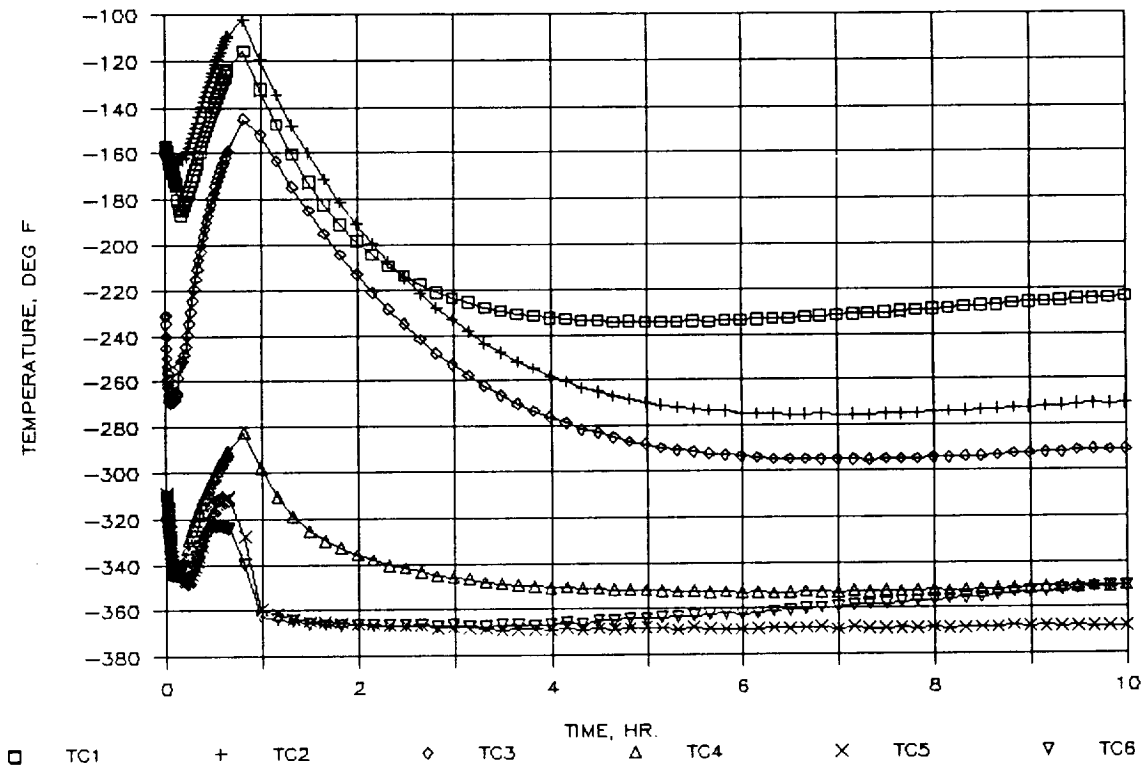

Figure 4. Biosample Freezer Temperature versus Time for first 20 Hours of Test on 9/21/90 (TC Nos. 1-6)

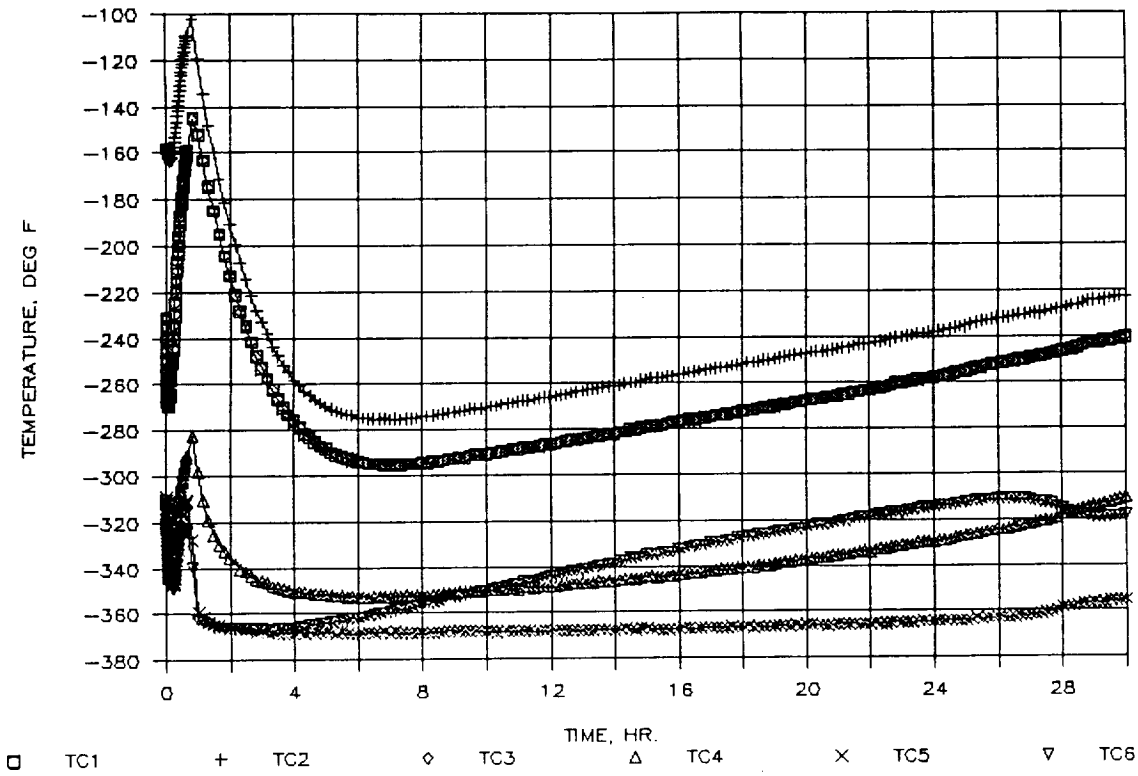

Figure 5. Biosample Freezer Temperature versus Time for first 30 Hours of Test on 9/21/90 (TC Nos. 1-6)

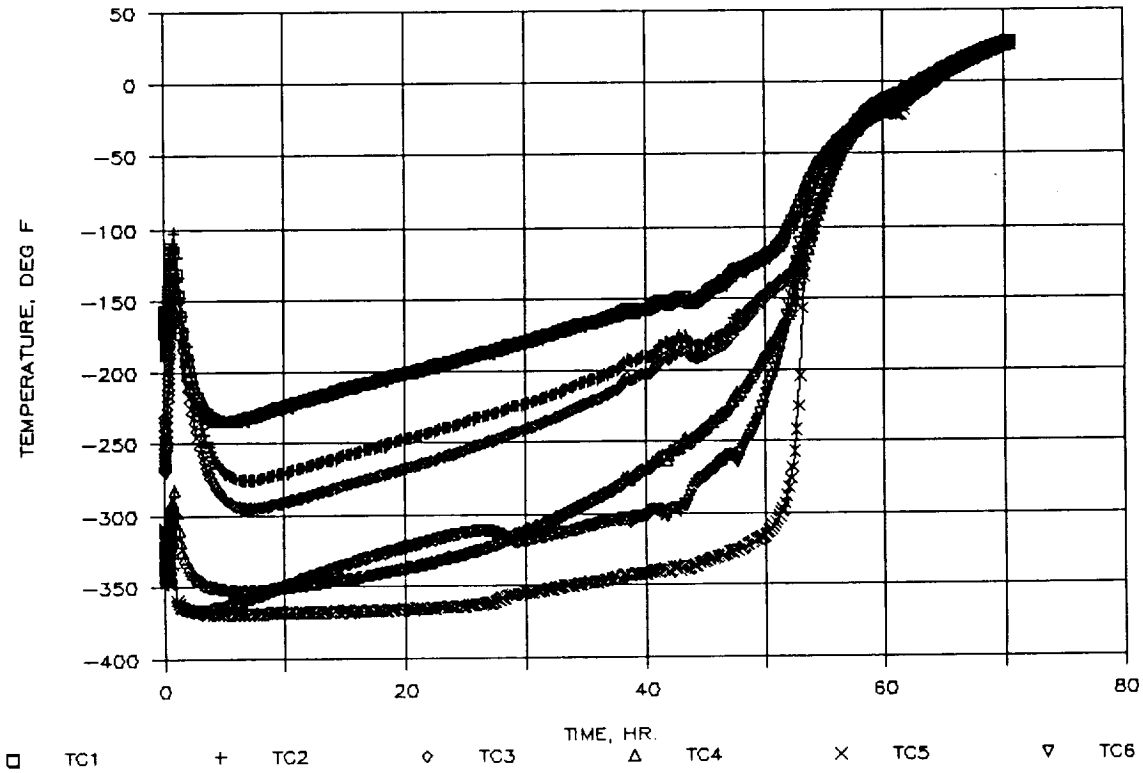

Figure 6. Biosample Freezer Temperature versus Time for first 80 Hours of Test on 9/21/90 (TC Nos. 1-6)

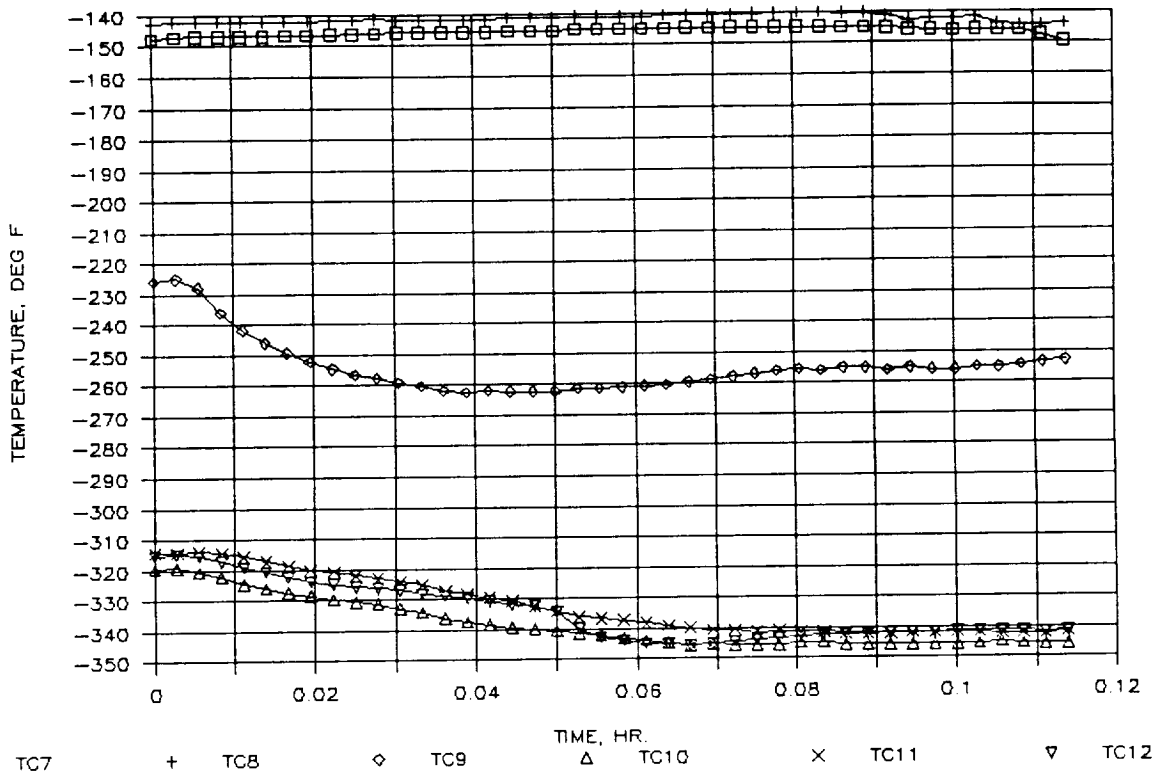

Figure 7. Biosample Freezer Temperature versus Time for first 0.12 Hours of Test on 9/21/90 (TC Nos. 7-12)

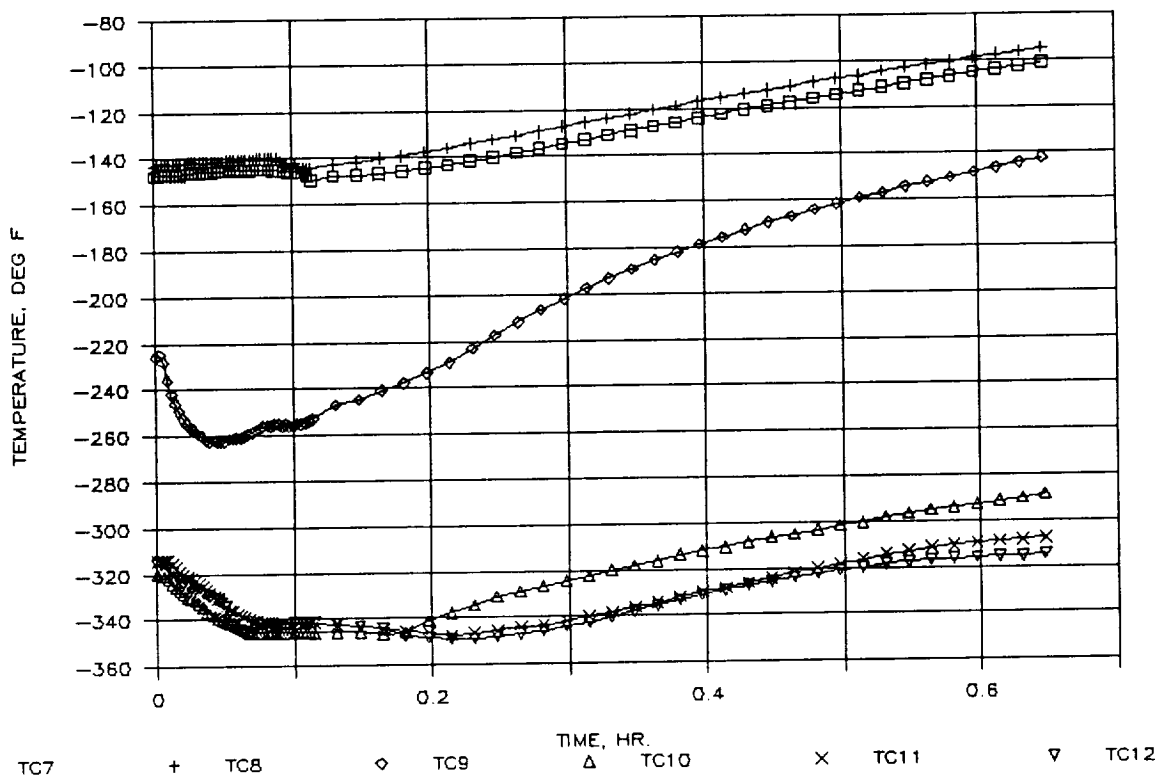

Figure 8. Biosample Freezer Temperature versus Time for first 0.6 Hours of Test on 9/21/90 (TC Nos. 7-12)

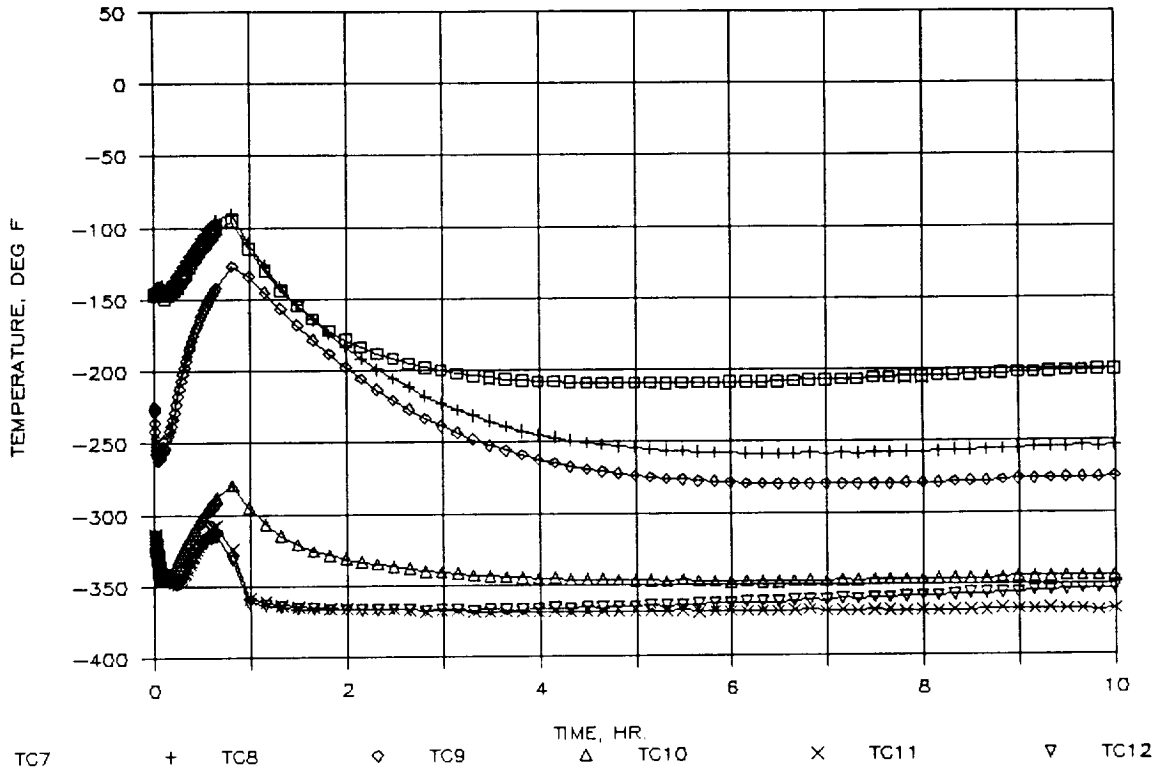

Figure 9. Biosample Freezer Temperature versus Time for first 10 Hours of Test on 9/21/90 (TC Nos. 7-12)

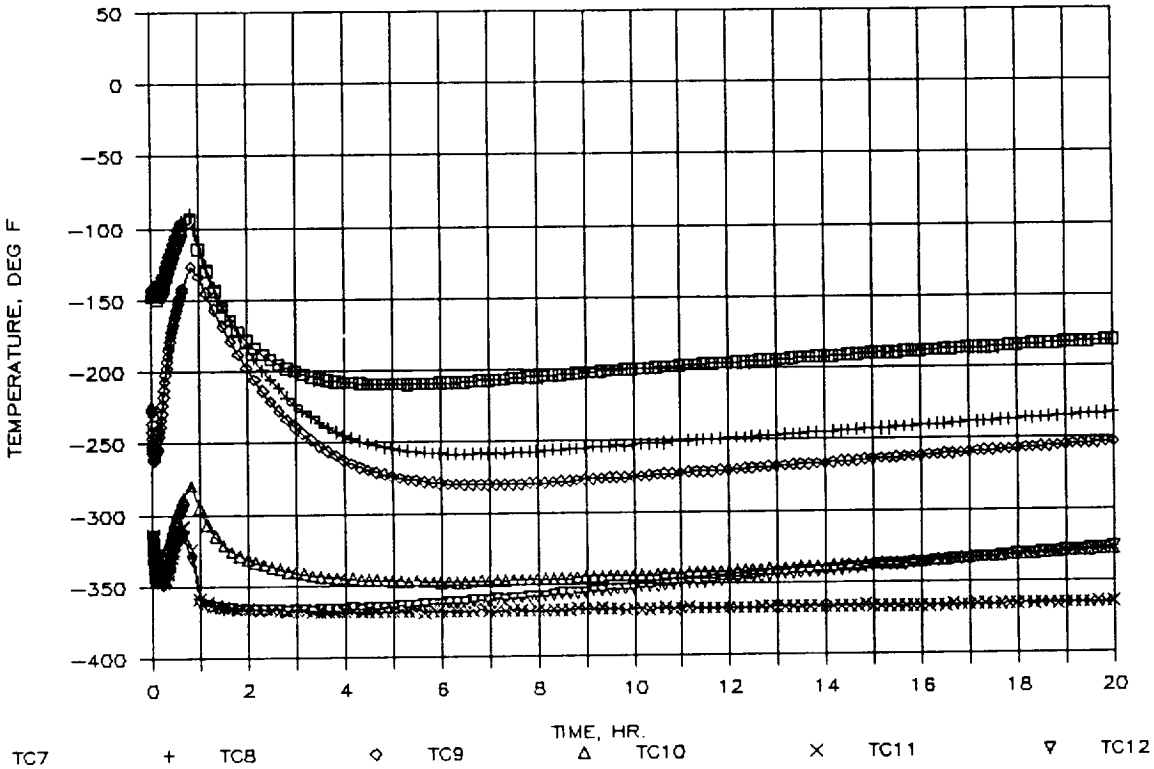

Figure 10. Biosample Freezer Temperature versus Time for first 20 Hours of Test on 9/21/90 (TC Nos. 7-12)

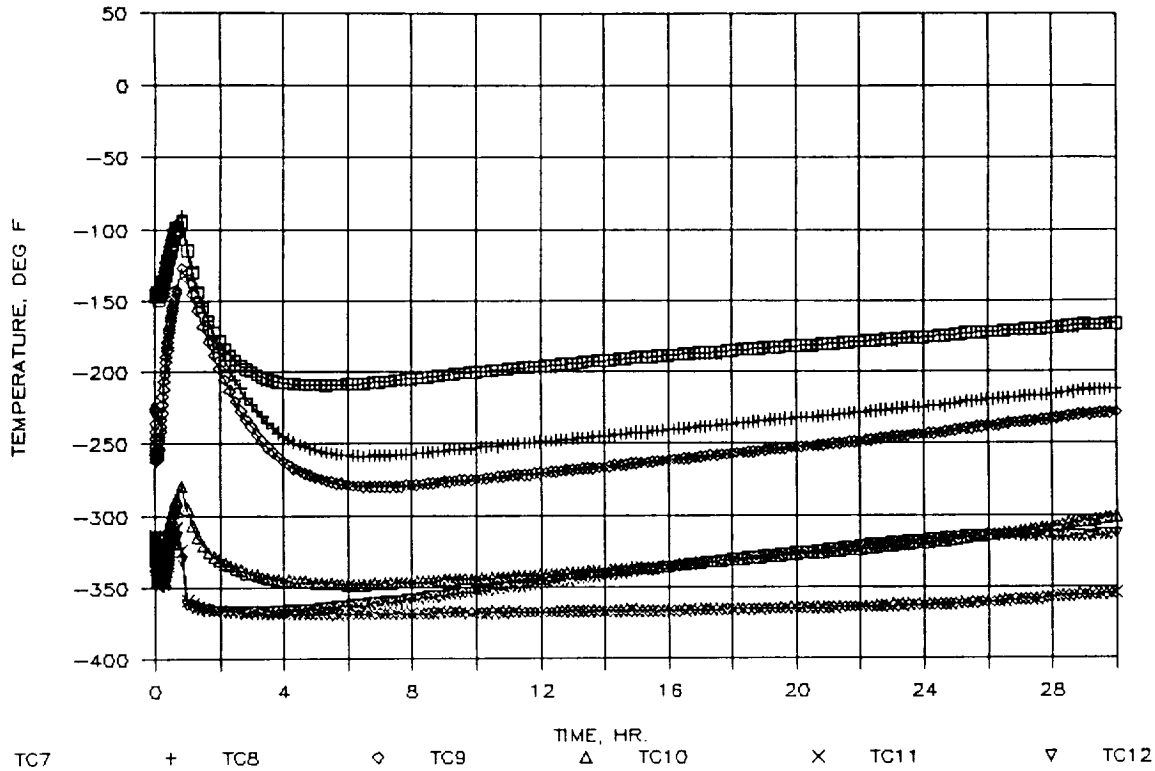

Figure 11. Biosample Freezer Temperature versus Time for first 30 Hours of Test on 9/21/90 (TC Nos. 7-12)

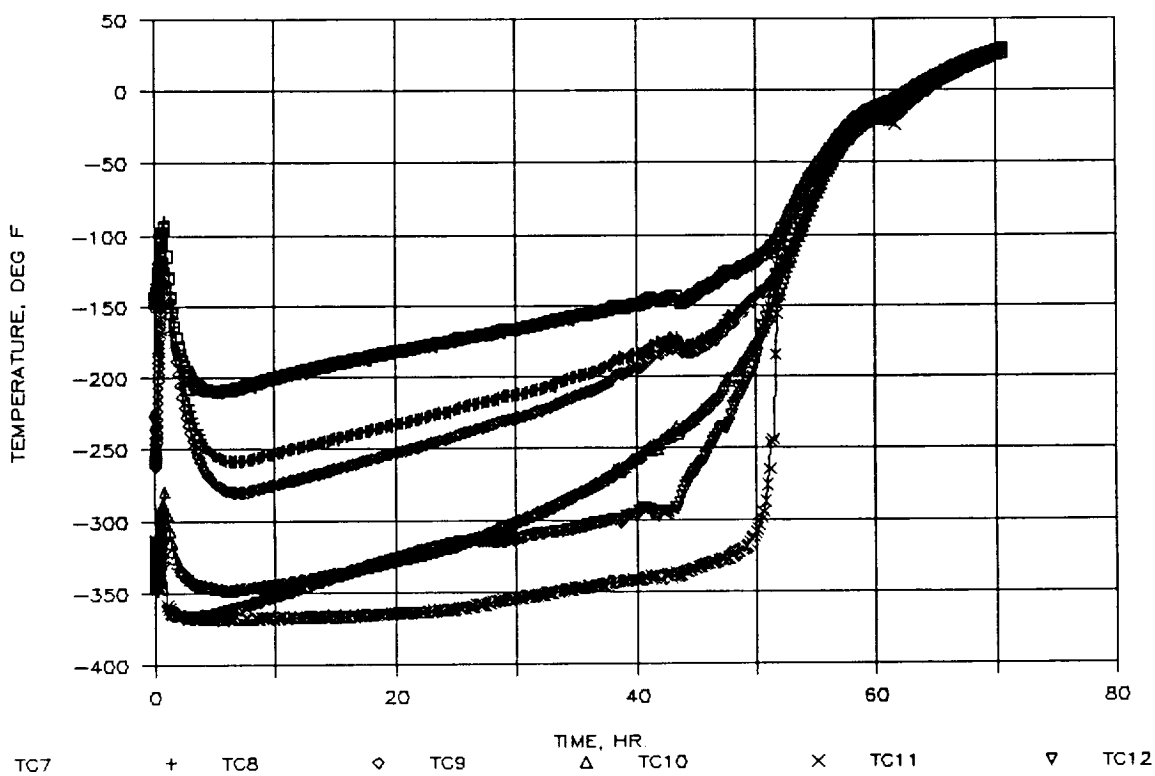

Figure 12. Biosample Freezer Temperature versus Time for first 80 Hours of Test on 9/21/90 (TC Nos. 7-12)

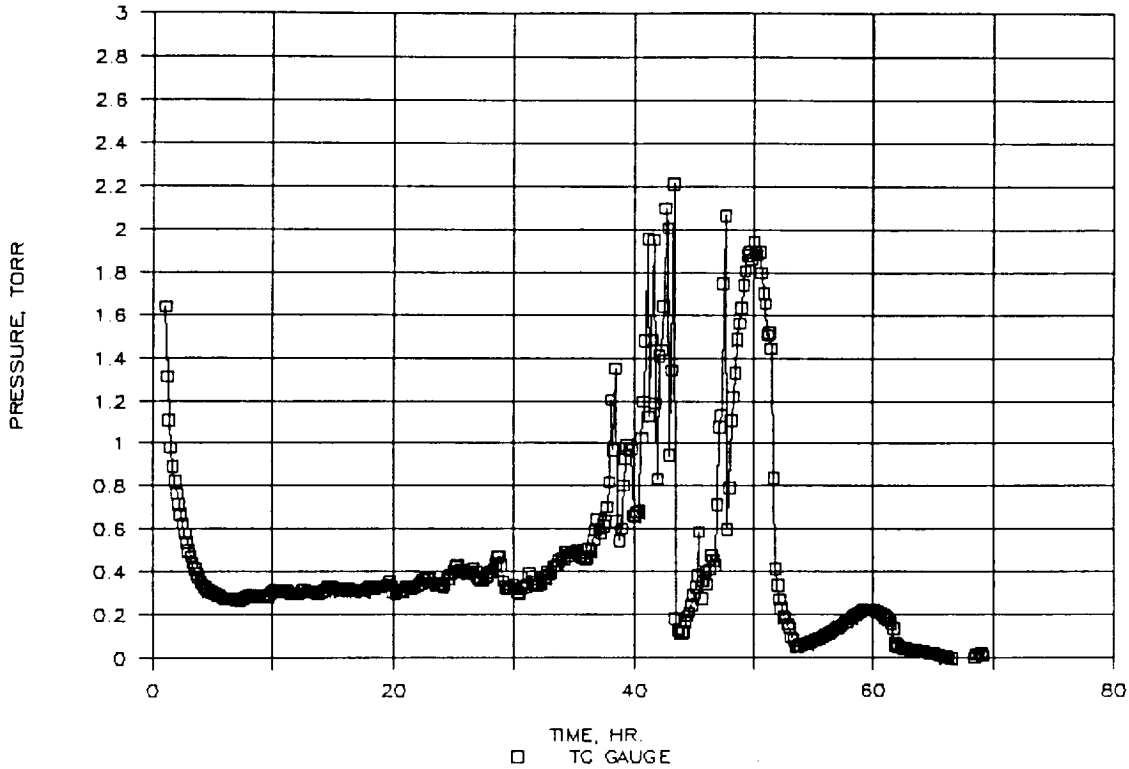

Figure 13. Biosample Freezer Internal Pressure versus Time for Test on 9/21/90

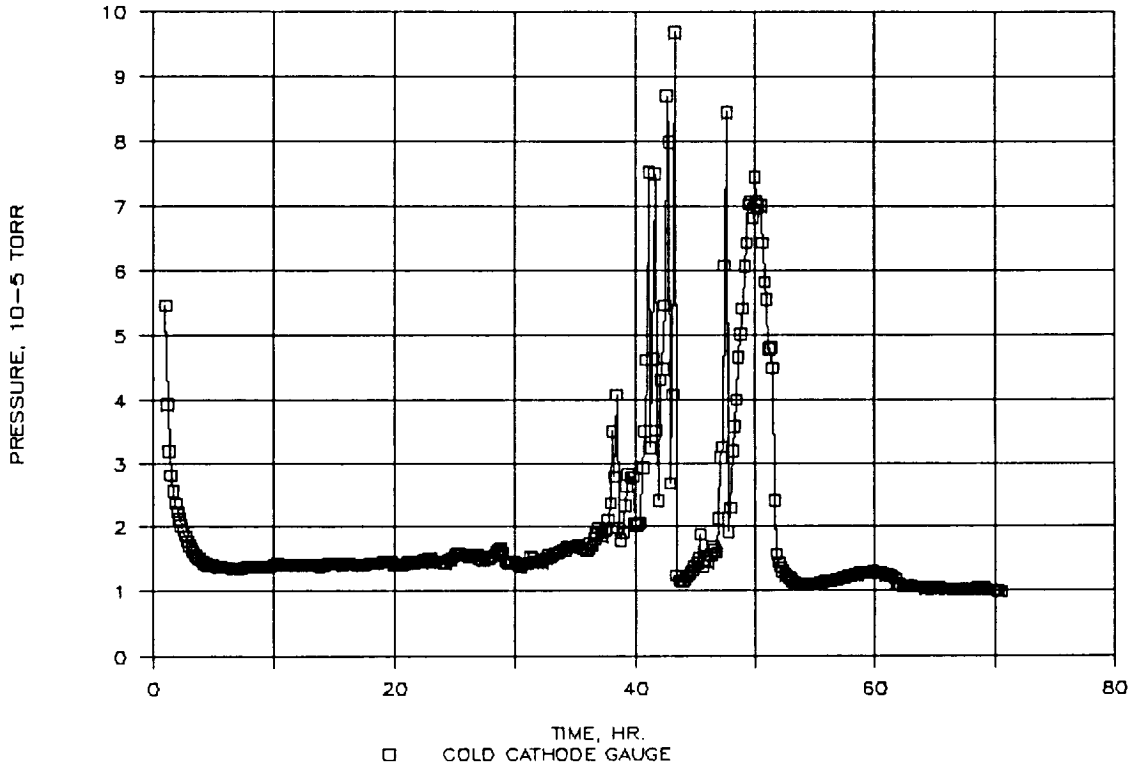

Figure 14. Biosample Freezer MLI Space Pressure versus Time for Test on 9/21/90

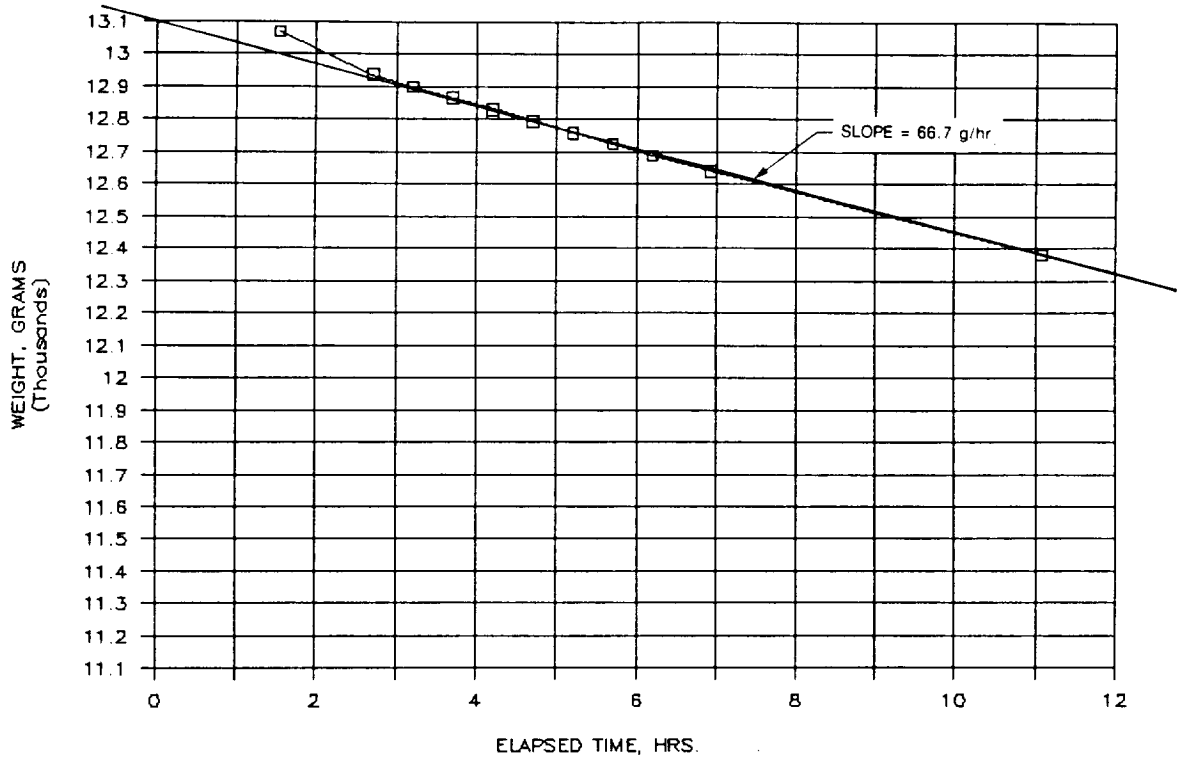

Figure 15. Biosample Freezer Weight versus Time for Test on 9/21/90

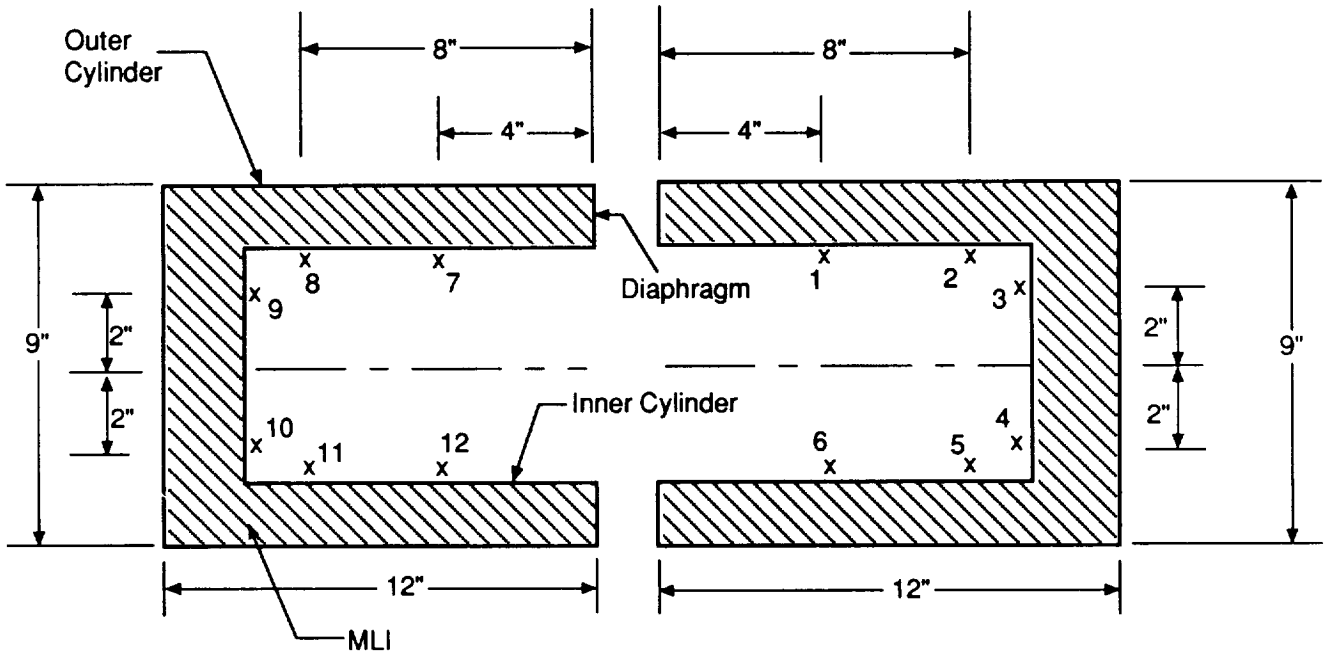

Figure 16. Biosample Freezer Thermocouple Location for Test on 9/21/90

ORIGINAL PAGE
BLACK AND WHITE PHOTOGRAPH

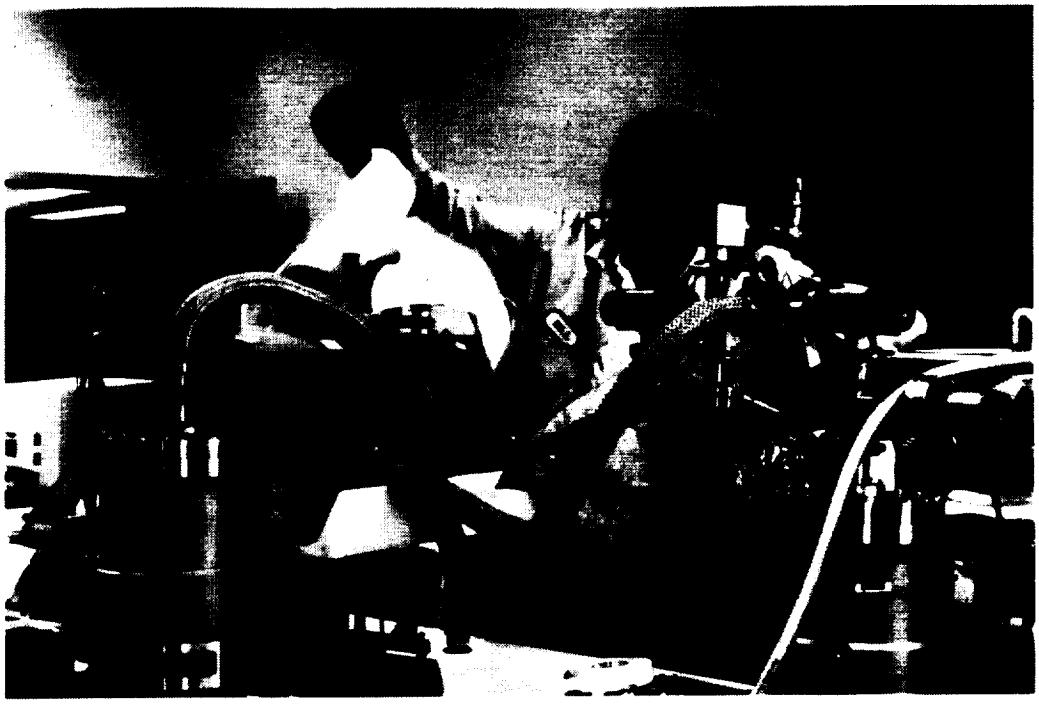

Figure 17. Biosample Freezer Being Charged with LN_2 at Beginning of Test on 9/21/90

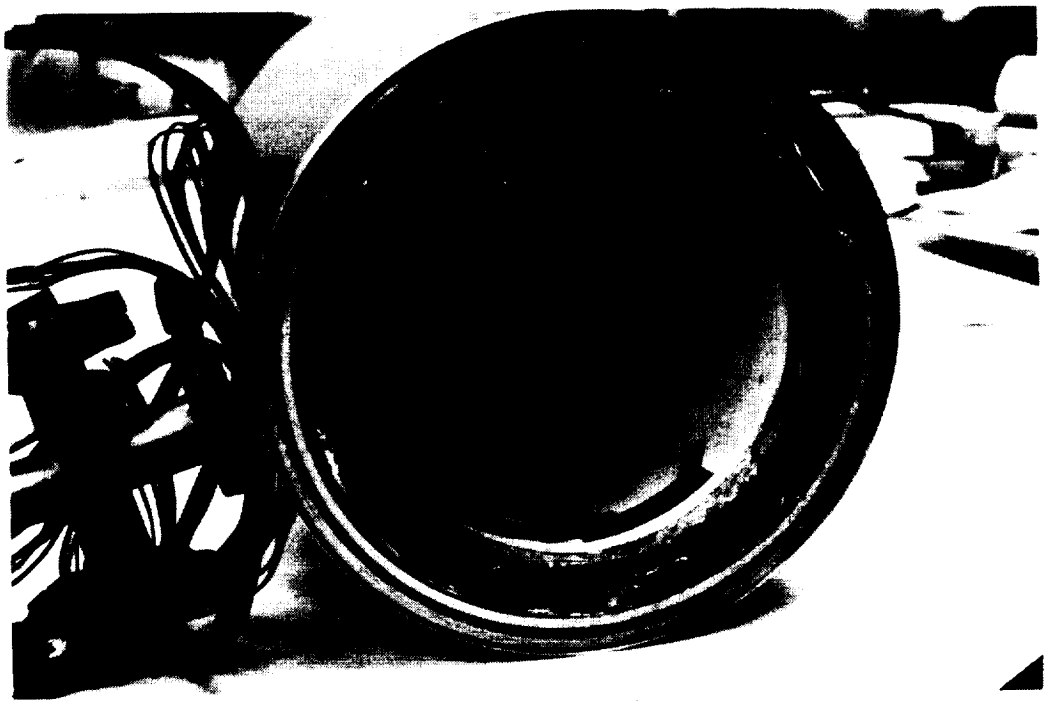

Figure 18. Biosample Freezer During Process of Replacing Stainless Steel Lined Diaphragm with Aluminized Mylar Lined Diaphragm

ORIGINAL PAGE
BLACK AND WHITE PHOTOGRAPH

Figure 19. Diaphragm Material (Epoxy-Glass with 1/4 mil Double Aluminized Mylar Liner)

Excerpt from November 1990 Monthly Progress Report LMSC-HSV PR F312387

PRECEDING PAGE BLANK NOT FILMED

PROGRESS DURING THE CURRENT REPORTING PERIOD

Testing of Biosample Freezer

Table 1 shows a summary of tests run to date on the Biosample Freezer. During this reporting period problems were encountered with the Biosample freezer testing. Three tests were attempted, and all had to be terminated due to vacuum leaks. Leaks were found in the new diaphragm, in the outer ring-to-outer epoxy glass cylinder, and in the fill tube to inner cylinder joint. Apparently these leaks have developed due to thermal cycling to extremely low temperatures. These have all now been repaired. and testing is expected to resume shortly.

PRECEDING PAGE BLANK NOT FILMED

Table 1. SUMMARY OF TESTS RUN TO DATE ON BIOSAMPLE FREEZER

Test Date	Heat Sink or "Slush" N_2 Temp. at Start of Test (°F)	Minimum Pressure Obtained (torr)	Test Duration (hr)
5/23/90	-2	1×10^{-3}	5
5/25/90	-6	5×10^{-5}	5
5/29/90	4	6×10^{-4}	27
6/11/90	-52	2×10^{-5}	46
6/15/90	-60	1×10^{-5}	64
6/22/90	-100	1×10^{-5}	66
6/25/90	-150	4×10^{-5}	46
6/28/90	-200	7×10^{-5}	24
6/29/90	-240	3×10^{-5}	48
7/25/90	Room temperature pump-down to check O-ring seal		
7/27/90	-310	**	68
7/30/90	< -328	**	22
7/31/90	< -328	**	23
8/1/90	Data not reduced due to problem with cryopumping air into MLI space		
8/2/90	< -328	**	96
8/7/90	< -328 (-340)*	**	24
8/8/90	< -328 (-370)*	**	44
8/14/90	Chilldown test in preparation for test on 8/15/90		
8/15/90	-345*	9×10^{-6}	30
9/6/90	Chilldown test in preparation for test on 9/7/90		
9/7/90	-370*	8×10^{-6}	72
9/20/90	Chilldown test in preparation for test on 9/21/90		
9/21/90	-370*	12×10^{-6}	71
10/2/90	Chilldown test (Terminated due to leak; could not get MLI space pressure down.)		
10/29/90	Chilldown test (Terminated due to leak; could not get MLI space pressure down.)		
10/30/90	Chilldown test (Terminated due to leak; could not get MLI space pressure down.)		

* Temperatures in "slush" N_2.

** Data not yet reduced.

LMSC-HSV TR P037989
26 Feb 1993

Excerpt from December 1990 Monthly Progress Report LMSC-HSV PR F312401

PRECEDING PAGE BLANK NOT FILMED

PROGRESS DURING THE CURRENT REPORTING PERIOD

Testing of Biosample Freezer

The problems with vacuum leaks have been solved, and eight successful tests were conducted during this reporting period. The Biosample freezer performance has been considerably improved by changing the diaphragm liner from .001 in. thick stainless steel to .00025 in. thick double aluminized mylar. This was as expected per discussion in several previous months' progress reports. The heat leak was reduced from about 3.8 watts to approximately 1.5 watts.

Table 1 presents a summary of tests run to date. Table 2 presents a summary of the heat leaks before and after the diaphragm liner redesign.

Figures 1 through 5 show weight loss results for the tests run in November. The next monthly progress report will present temperature and pressure data from these tests.

PRECEDING PAGE BLANK NOT FILMED

Table 1. SUMMARY OF TESTS RUN TO DATE ON BIOSAMPLE FREEZER (1 of 2)

Test Date	Heat Sink or "Slush" N_2 Temp. at Start of Test (°F)	Minimum Pressure Obtained (torr)	Test Duration (hr)
5/23/90	-2	1×10^{-3}	5
5/25/90	-6	5×10^{-5}	5
5/29/90	4	6×10^{-4}	27
6/11/90	-52	2×10^{-5}	46
6/15/90	-60	1×10^{-5}	64
6/22/90	-100	1×10^{-5}	66
6/25/90	-150	4×10^{-5}	46
6/28/90	-200	7×10^{-5}	24
6/29/90	-240	3×10^{-5}	48
7/25/90	Room temperature pump-down to check O-ring seal		
7/27/90	-310	**	68
7/30/90	< -328	**	22
7/31/90	< -328	**	23
8/1/90	Data not reduced due to problem with cryopumping air into MLI space		
8/2/90	< -328	**	96
8/7/90	< -328 (-340)*	**	24
8/8/90	< -328 (-370)*	**	44
8/14/90	Chilldown test in preparation for test on 8/15/90		
8/15/90	-345*	9×10^{-6}	30
9/6/90	Chilldown test in preparation for test on 9/7/90		
9/7/90	-370*	8×10^{-6}	72
9/20/90	Chilldown test in preparation for test on 9/21/90		
9/21/90	-370*	12×10^{-6}	71
10/2/90	Chilldown test (Terminated due to leak; could not get MLI space pressure down.)		
10/29/90	Chilldown test (Terminated due to leak; could not get MLI space pressure down.)		
10/30/90	Chilldown test (Terminated due to leak; could not get MLI space pressure down.)		

* Temperatures in "slush" N_2.

** Data not yet reduced.

Table 1. SUMMARY OF TESTS RUN TO DATE ON BIOSAMPLE FREEZER (2 of 2)

Test Date	Heat Sink or "Slush" N_2 Temp. at Start of Test (°F)	Minimum Pressure Obtained (torr)	Test Duration (hr)
11/1/90	Room Temperature	5×10^{-6}	Pressure checkout only
11/2/90	-350*	5×10^{-5} to 1×10^{-4}	2 (MLI space pressure started leaking)
11/6/90	Chilldown after leak repair	(leak)	18
11/14/90	Chilldown after leak repair	6×10^{-6}	
11/15/90	-370*	(2 to 5) x 10^{-6}	92
11/19/90	-360* (Repeat of test on 11/15/90)	4×10^{-6}	20
11/21/90	(Freezer in upright position) -370*	(3 to 5) x 10^{-6}	98
11/26/90	(Freezer in upright position) -370*	(1 to 5) x 10^{-6}	52
11/28/90	(Freezer in upright position) -370* (Test observed by NASA personnel)	(1 to 6) x 10^{-6}	59
11/30/90	(Freezer in upright position) -370*	(1 to 5) x 10^{-6}	91
12/4/90	(Freezer in upright position) -370*	(1 to 6) x 10^{-6}	71
12/7/90	(Freezer in upright position) -370*	(1 to 6) x 10^{-6}	92

* Temperatures in "slush" N_2.

** Data not yet reduced.

Table 2 HEAT LEAKS SUMMARY

Test Date	Heat Leak (Watts)	Remarks
9/7/90	3.07	.001 in. S.S. Diaphragm Liner (Freezer Horizontal)
9/21/90	4.11	.001 in. S.S. Diaphragm Liner (Freezer Horizontal)
11/15/90	1.68	.00025 in. Double Aluminized Mylar Diaphragm Liner (Freezer Horizontal)
11/19/90	1.95	.00025 in. Double Aluminized Mylar Diaphragm Liner (Freezer Horizontal)
11/21/90	1.11	.00025 in. Double Aluminized Mylar Diaphragm Liner (Freezer Upright)
11/26/90	1.03	.00025 in. Double Aluminized Mylar Diaphragm Liner (Freezer Upright)
11/28/90	1.05	.00025 in. Double Aluminized Mylar Diaphragm Liner (Freezer Upright)
11/30/90	1.23	.00025 in. Double Aluminized Mylar Diaphragm Liner (Freezer Upright)

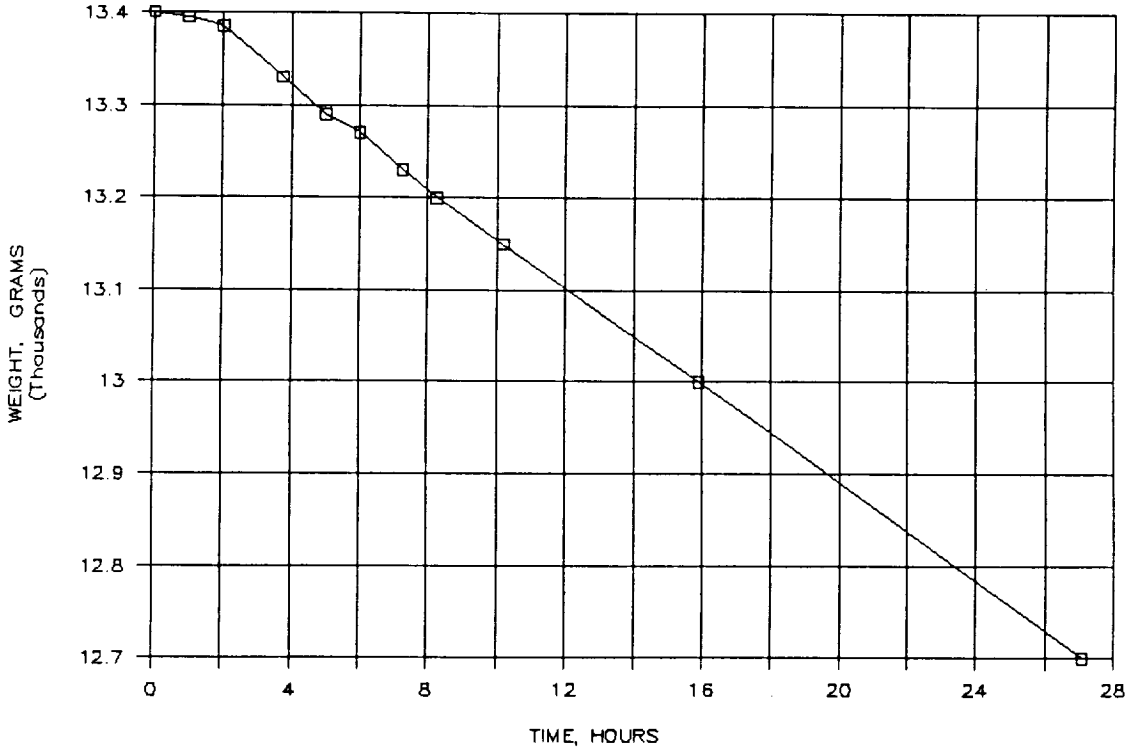

Figure 1. Biosample Freezer Weight versus Time for Test on 15 November 90

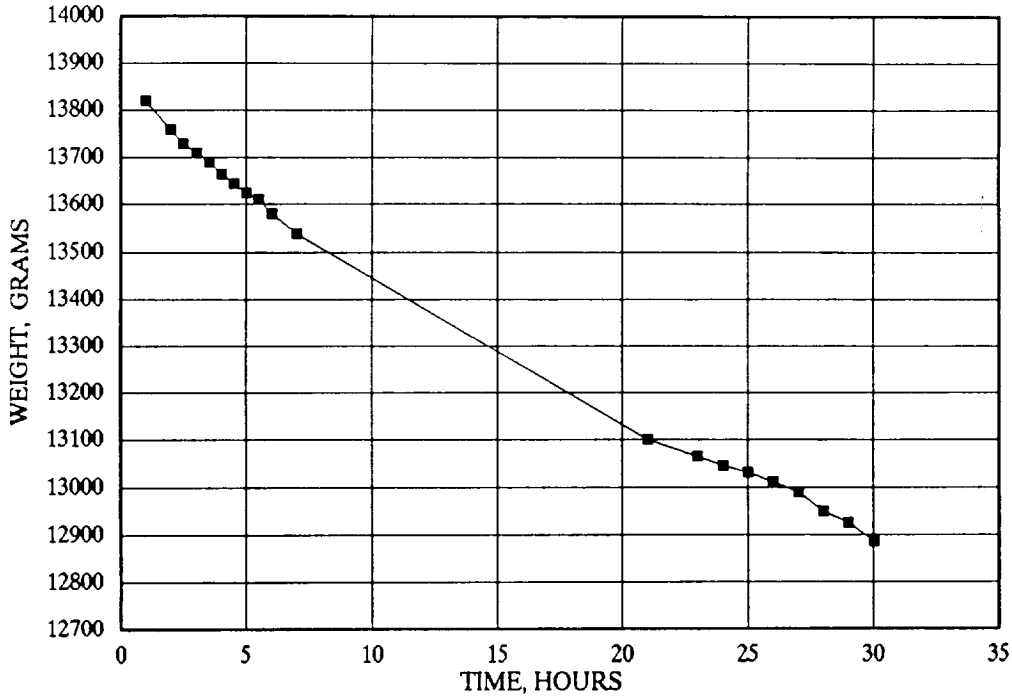

Figure 2. Biosample Freezer Weight versus Time for Test on 19 November 90

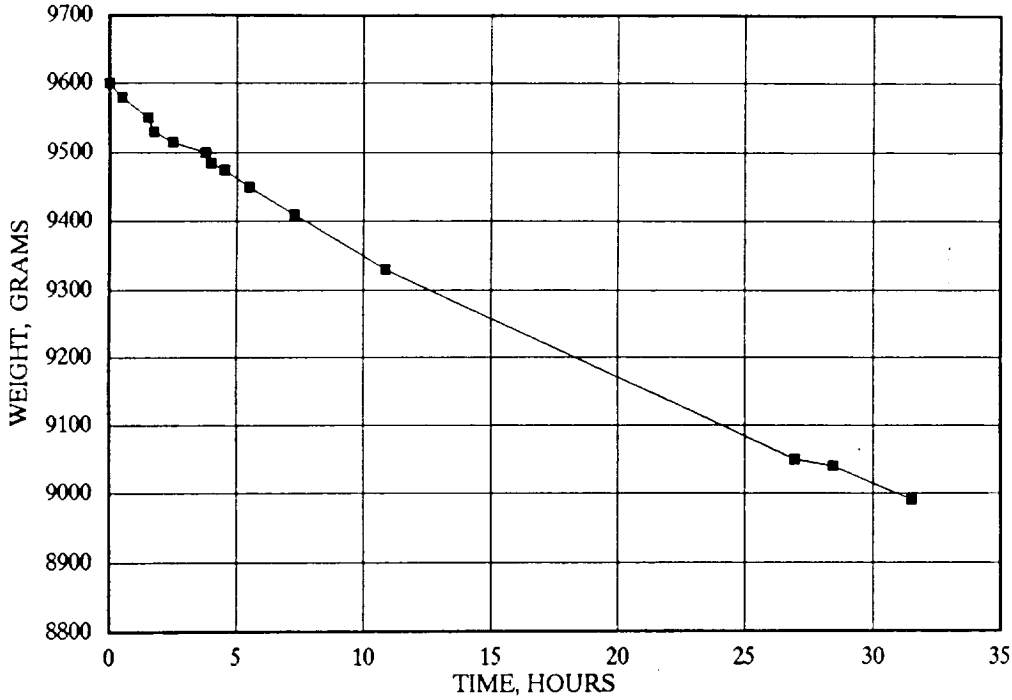

Figure 3. Biosample Freezer Weight versus Time for Test on 21 November 90

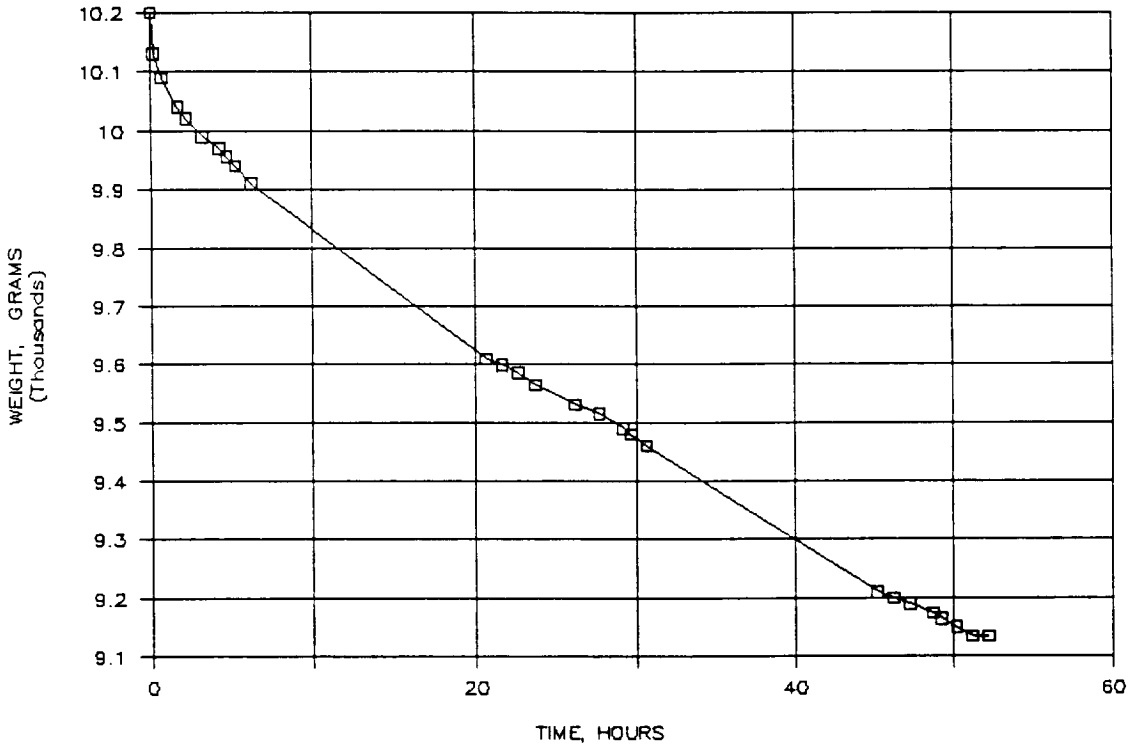

Figure 4. Biosample Freezer Weight versus Time for Test on 26 November 90

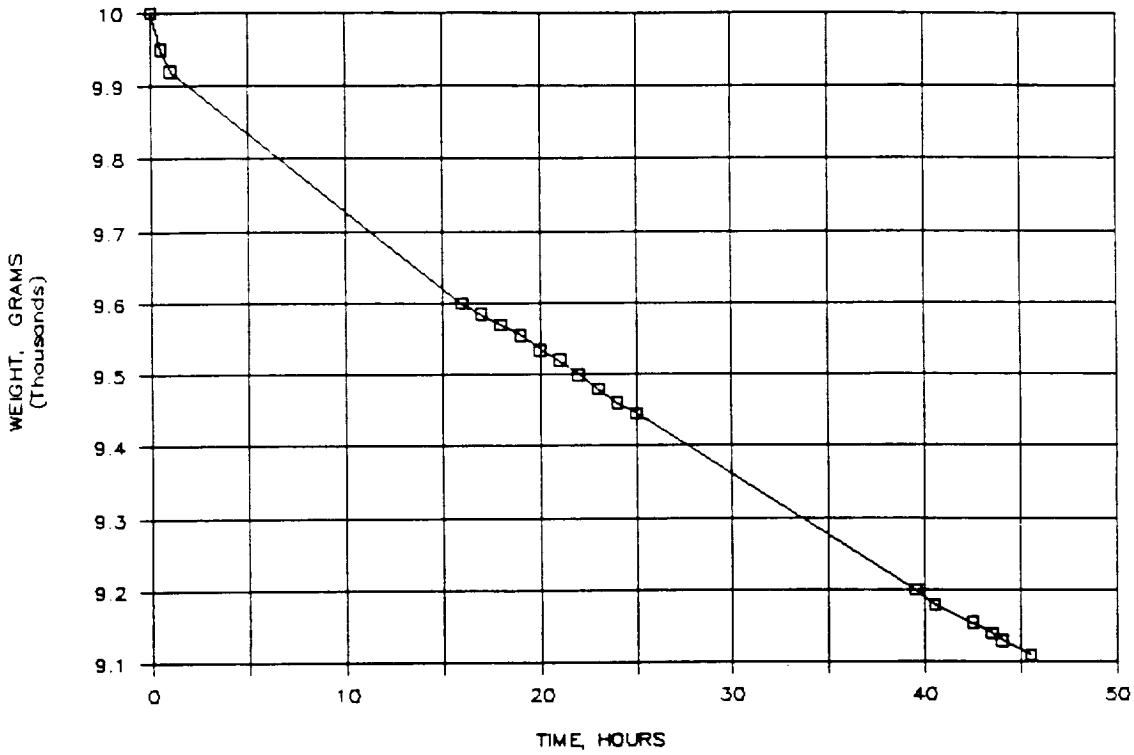

Figure 5. Biosample Freezer Weight versus Time for Test on 28 November 90

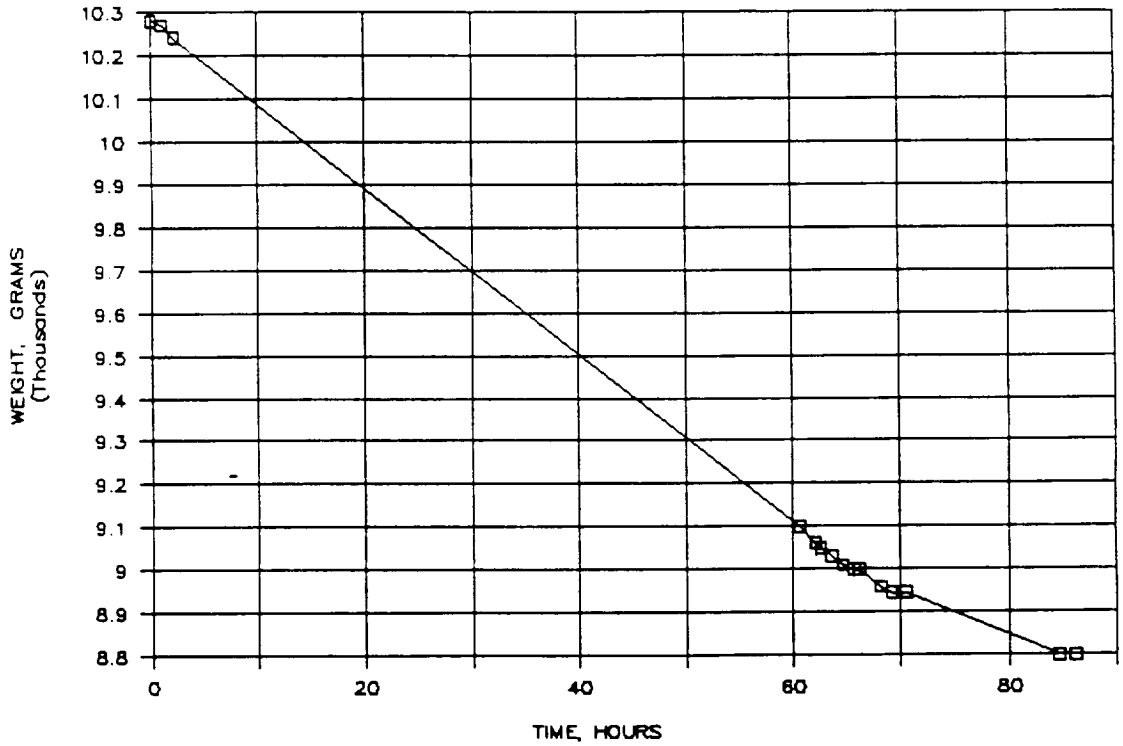

Figure 6. Biosample Freezer Weight versus Time for Test on 30 November 90

LMSC-HSV TR P037989
26 Feb 1993

Excerpt from January 1991 Monthly Progress Report LMSC-HSV PR F312410

PRECEDING PAGE BLANK NOT FILMED

Testing of Biosample Freezer

Table 1 presents a summary of the tests run to date. Table 2 presents a summary of the heat leaks measured during the tests of 7 September 1990 through 12 December 1990.

Figures 14 through 113 show the temperature and pressure results for the test from 15 November 1990 through 12 December 1990. These plots are shown progressing with time so that the temperature scales are readable during the early phases of each test.

Figures 114 through 122 show the plots of weight versus time for each of these tests, from which the heat leak values shown in Table 2 were calculated.

Table 1. Summary of Tests Run to Date on Biosample Freezer (1 of 2)

Test Date	Heat Sink or "Slush" N_2 Temp. at Start of Test (°F)	Minimum Pressure Obtained (torr)	Test Duration (hr)
5/23/90	-2	1×10^{-3}	5
5/25/90	-6	5×10^{-5}	5
5/29/90	4	6×10^{-4}	27
6/11/90	-52	2×10^{-5}	46
6/15/90	-60	1×10^{-5}	64
6/22/90	-100	1×10^{-5}	66
6/25/90	-150	4×10^{-5}	46
6/28/90	-200	7×10^{-5}	24
6/29/90	-240	3×10^{-5}	48
7/25/90	Room temperature pump-down to check O-ring seal		
7/27/90	-310	**	68
7/30/90	< -328	**	22
7/31/90	< -328	**	23
8/1/90	Data not reduced due to problem with cryopumping air into MLI space		
8/2/90	< -328	**	96
8/7/90	< -328 (-340)*	**	24
8/8/90	< -328 (-370)*	**	44
8/14/90	Chilldown test in preparation for test on 8/15/90		
8/15/90	-345*	9×10^{-6}	30
9/6/90	Chilldown test in preparation for test on 9/7/90		
9/7/90	-370*	8×10^{-6}	72
9/20/90	Chilldown test in preparation for test on 9/21/90		
9/21/90	-370*	12×10^{-6}	71
10/2/90	Chilldown test (Terminated due to leak; could not get MLI space pressure down.)		
10/29/90	Chilldown test (Terminated due to leak; could not get MLI space pressure down.)		
10/30/90	Chilldown test (Terminated due to leak; could not get MLI space pressure down.)		

* Temperatures in "slush" N_2.

** Data not yet reduced.

Table 1. Summary of Tests Run to Date on Biosample Freezer (2 of 2)

Test Date	Heat Sink or "Slush" N_2 Temp. at Start of Test (°F)	Minimum Pressure Obtained (torr)	Test Duration (hr)
11/1/90	Room Temperature	5×10^{-6}	Pressure checkout only
11/2/90	-350*	5×10^{-5} to 1×10^{-4}	2 (MLI space pressure started leaking)
11/6/90	Chilldown after leak repair	(leak)	18
11/14/90	Chilldown after leak repair	6×10^{-6}	
11/15/90	-370*	(2 to 5) x 10^{-6}	92
11/19/90	-360* (Repeat of test on 11/15/90)	4×10^{-6}	20
11/21/90	(Freezer in upright position) -370*	(3 to 5) x 10^{-6}	98
11/26/90	(Freezer in upright position) -370*	(1 to 5) x 10^{-6}	52
11/28/90	(Freezer in upright position) -370* (Test observed by NASA personnel)	(1 to 6) x 10^{-6}	59
11/30/90	(Freezer in upright position) -370*	(1 to 5) x 10^{-6}	91
12/4/90	(Freezer in upright position) -370*	(1 to 6) x 10^{-6}	71
12/7/90	(Freezer in upright position) -370*	(1 to 6) x 10^{-6}	92
12/12/90	Freezer in upright position) -370*	(1 to 10) x 10^{-6}	116

* Temperatures in "slush" N_2.

** Data not yet reduced.

Table 2. Heat Leaks Summary

Test Date	Heat Leak (W)	Remarks
9/7/90	3.07	.001 in. S.S. diaphragm liner (freezer horizontal)
9/21/90	4.11	.001 in. S.S. diaphragm liner (freezer horizontal)
11/15/90	1.68	.00025 in. double aluminized Mylar diaphragm liner (freezer horizontal)
11/19/90	1.95	.00025 in. double aluminized Mylar diaphragm liner (freezer horizontal)
11/21/90	1.11	.00025 in. double aluminized Mylar diaphragm liner (freezer upright)
11/26/90	1.03	.00025 in. double aluminized Mylar diaphragm liner (freezer upright)
11/28/90	1.05	.00025 in. double aluminized Mylar diaphragm liner (freezer upright)
11/30/90	1.23	.00025 in. double aluminized Mylar diaphragm liner (freezer upright)
12/4/90	1.01	.00025 in. double aluminized Mylar diaphragm liner (freezer upright)
12/7/90	1.14	.00025 in. double aluminized Mylar diaphragm liner (freezer upright)
12/12/90	1.32	.00025 in. double aluminized Mylar diaphragm liner (freezer upright)

7-12

PRECEDING PAGE BLANK NOT FILMED

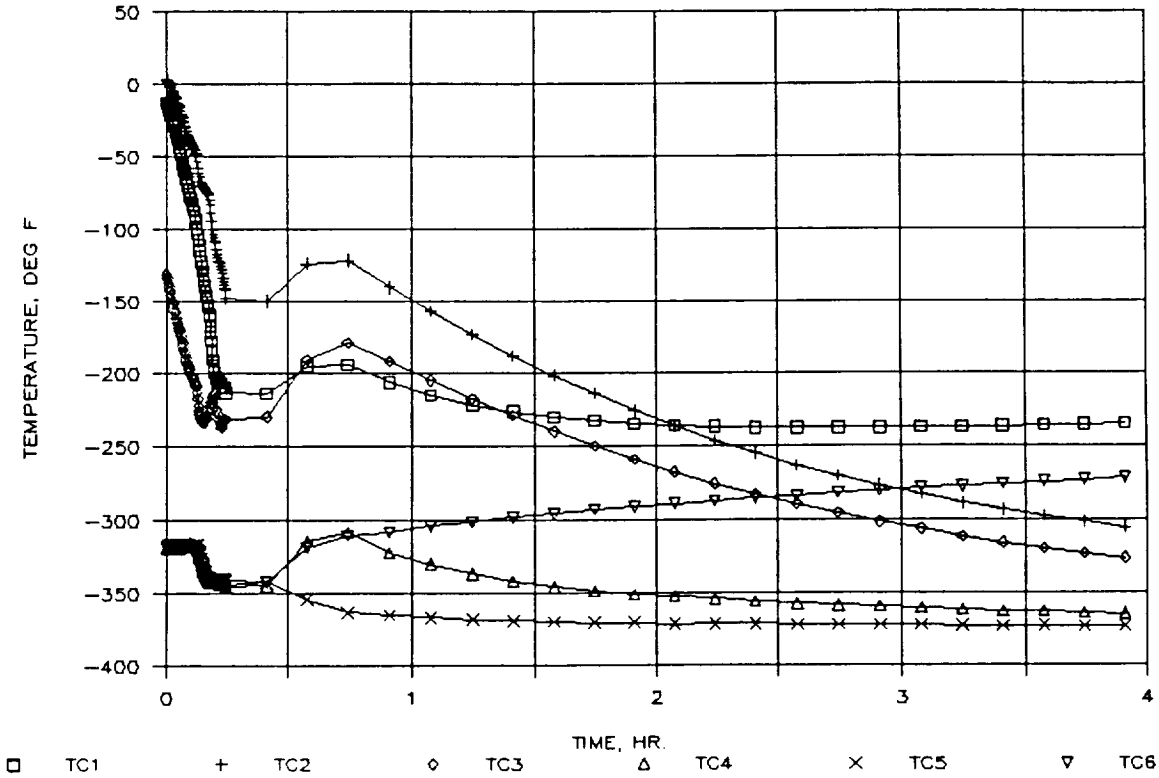

Figure 14. Results of Biosample Freezer Test on 11/15/90, TC1 through TC6, First 4 Hours

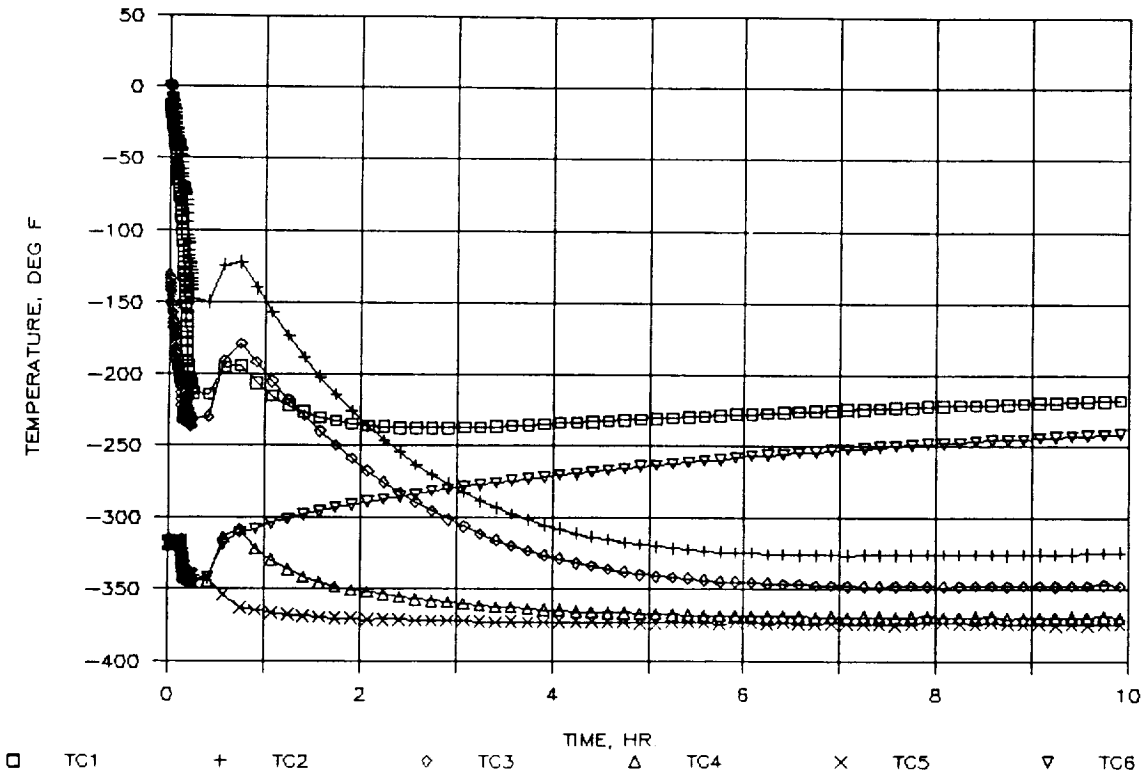

Figure 15. Results of Biosample Freezer Test on 11/15/90, TC1 through TC6, First 10 Hours

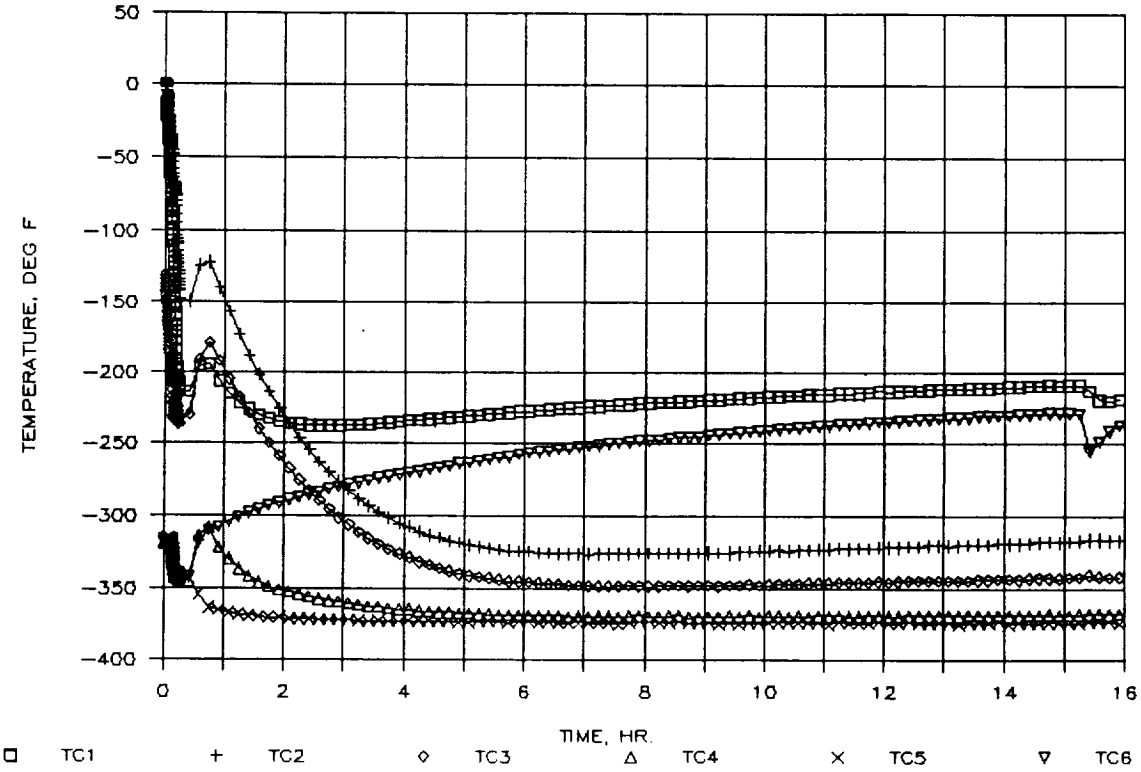

Figure 16. Results of Biosample Freezer Test on 11/15/90, TC1 through TC6, First 16 Hours

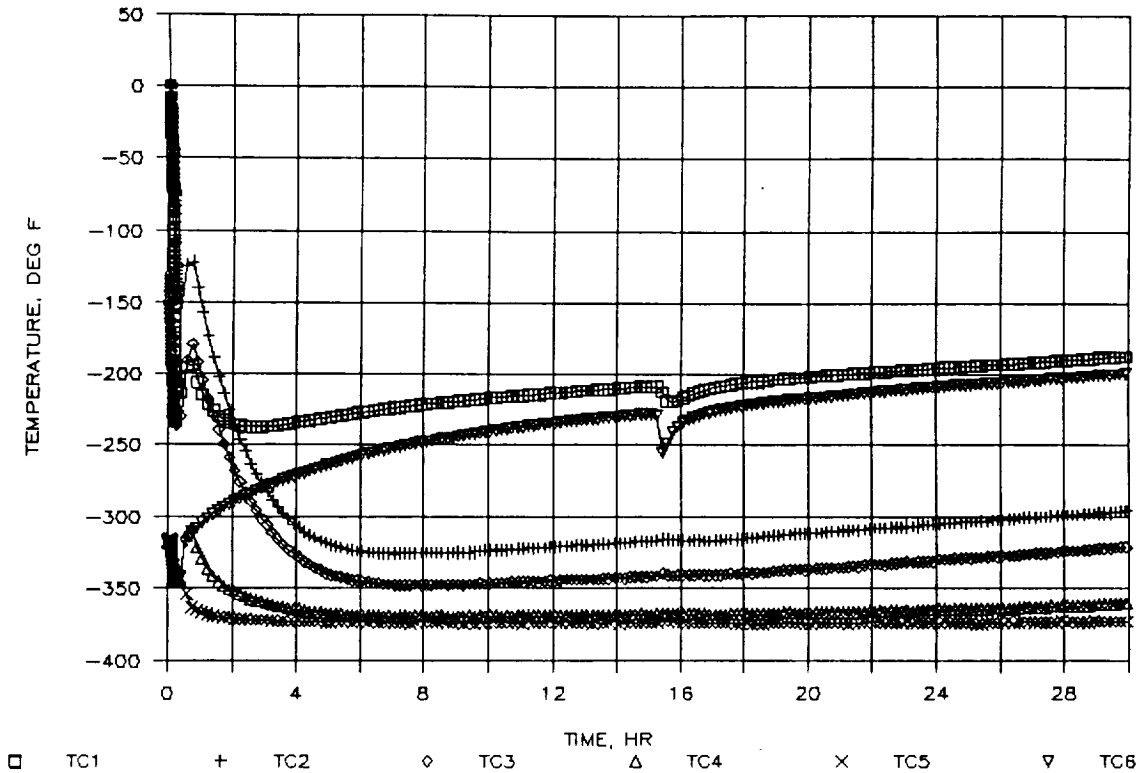

Figure 17. Results of Biosample Freezer Test on 11/15/90, TC1 through TC6, First 30 Hours

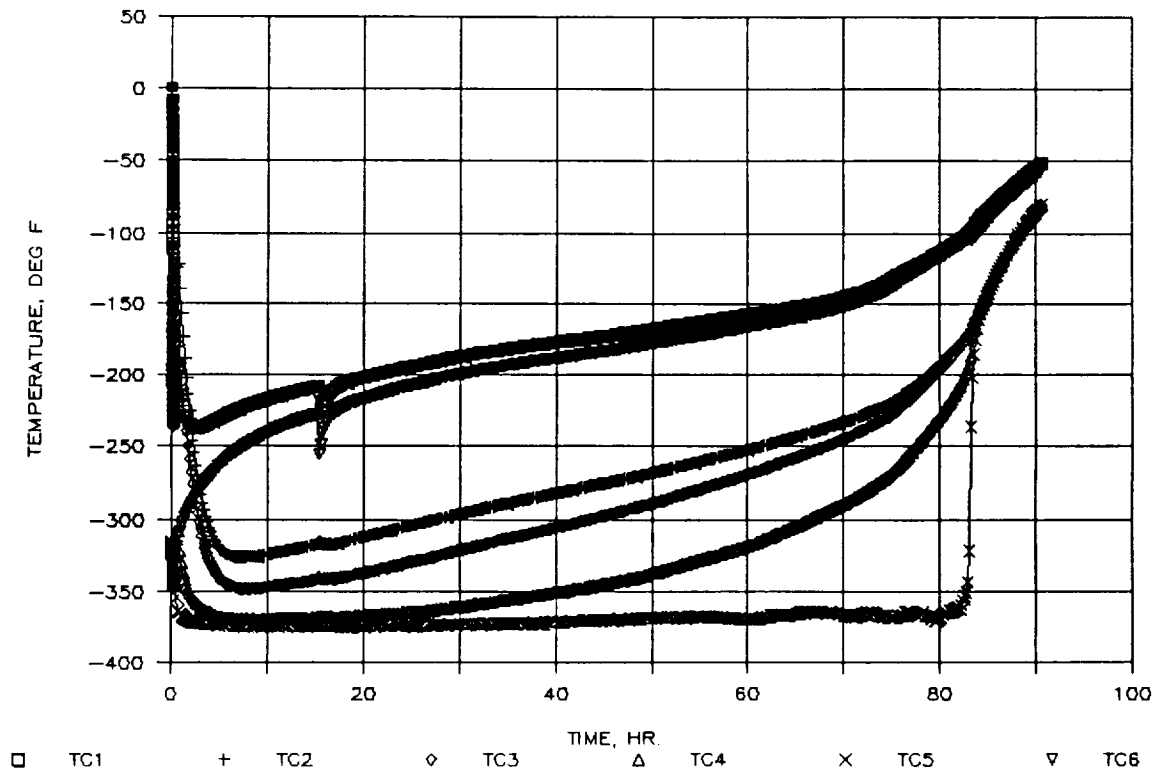

Figure 18. Results of Biosample Freezer Test on 11/15/90, TC1 through TC6, First 90 Hours

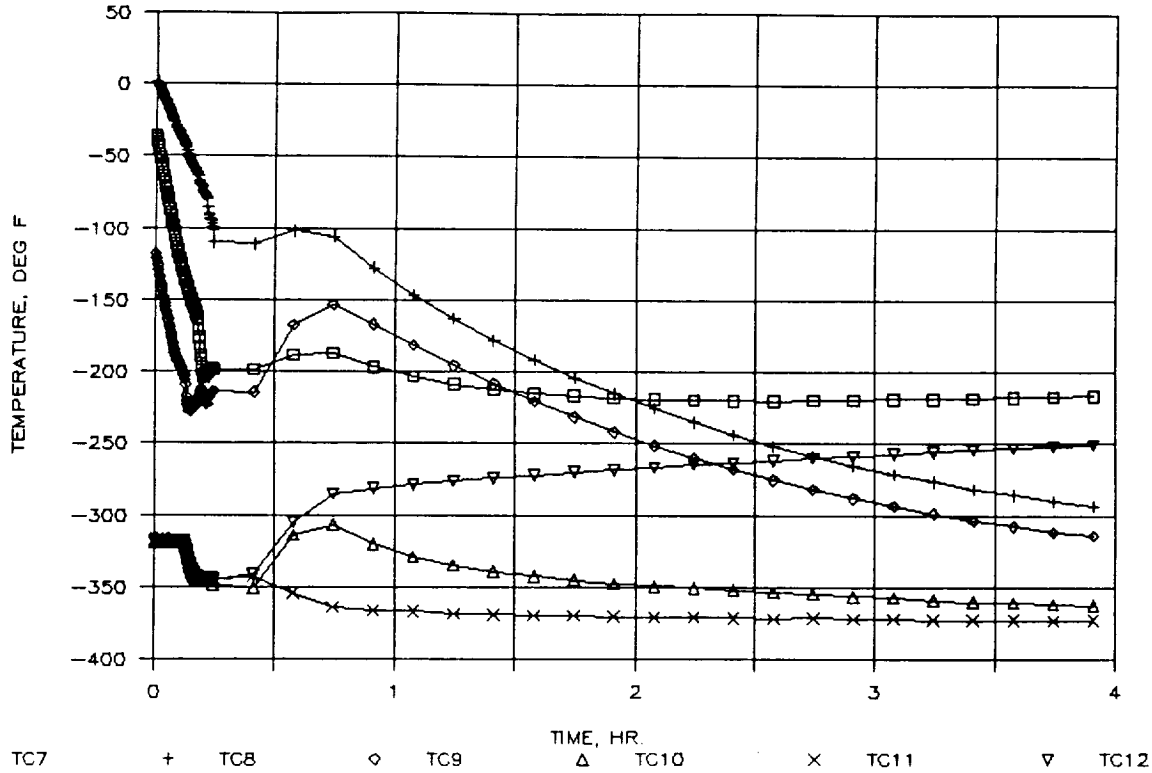

Figure 19. Results of Biosample Freezer Test on 11/15/90, TC7 through TC12, First 4 Hours

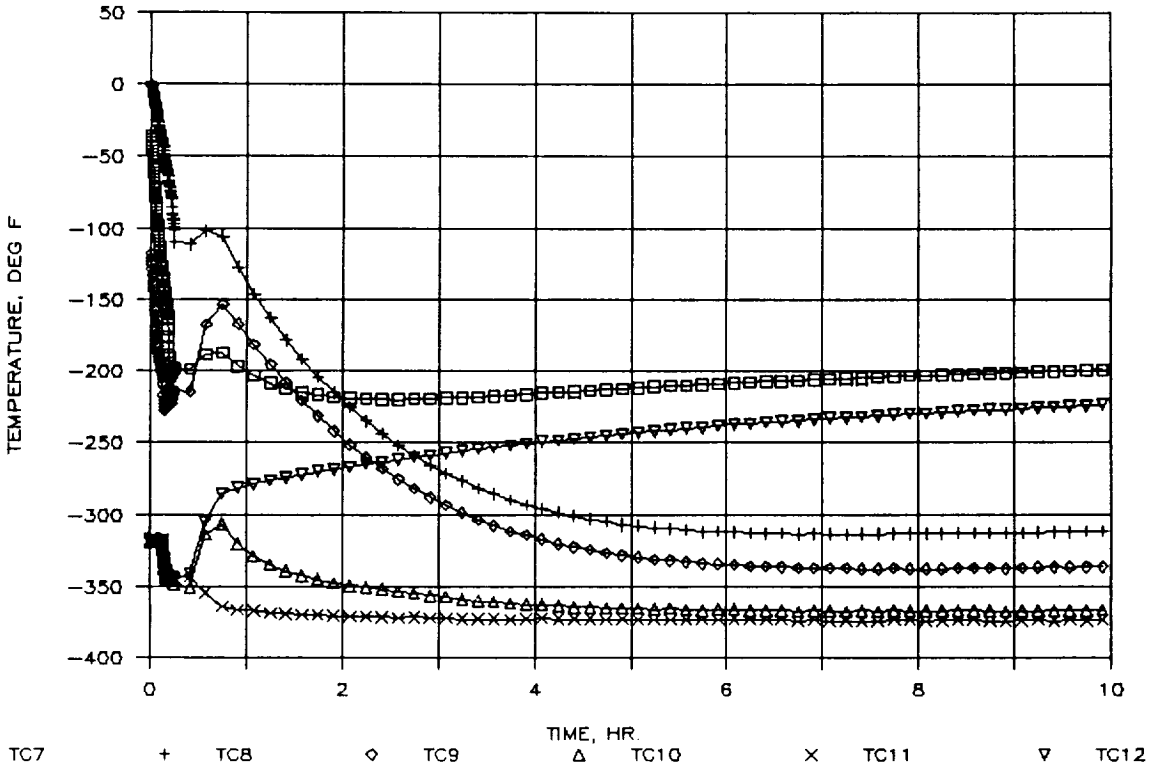

Figure 20. Results of Biosample Freezer Test on 11/15/90, TC7 through TC12, First 10 Hours

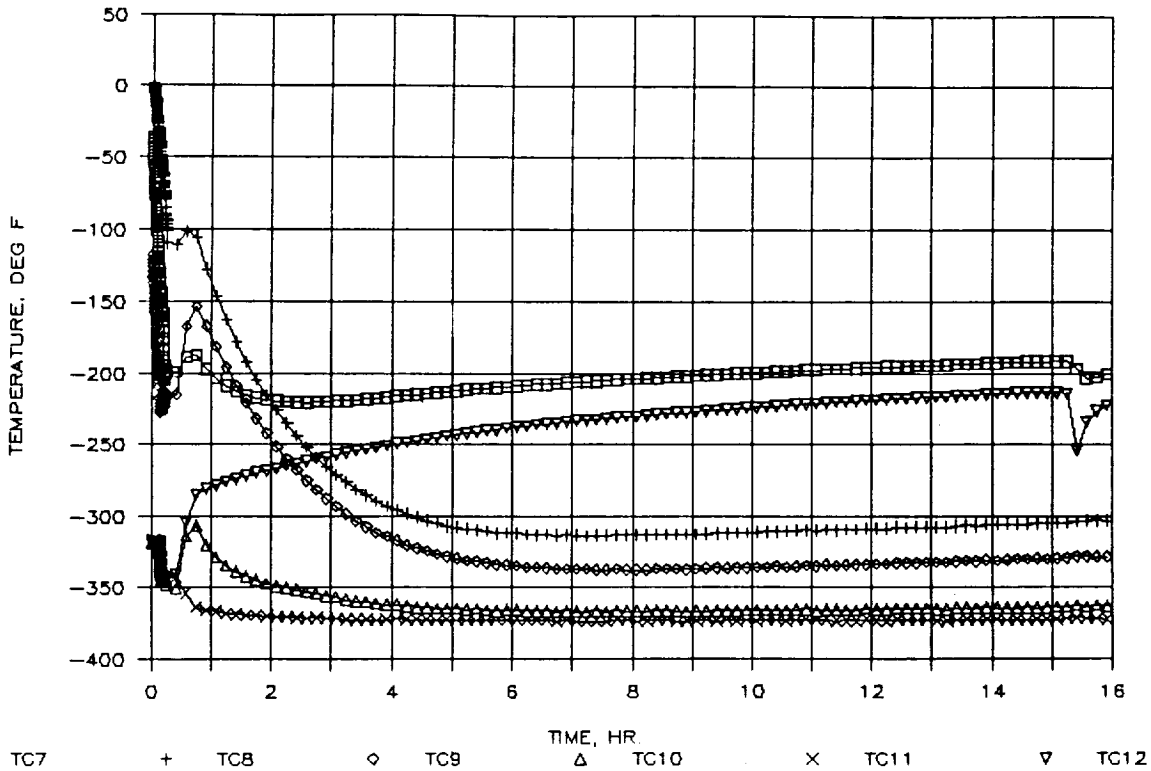

Figure 21. Results of Biosample Freezer Test on 11/15/90, TC7 through TC12, First 16 Hours

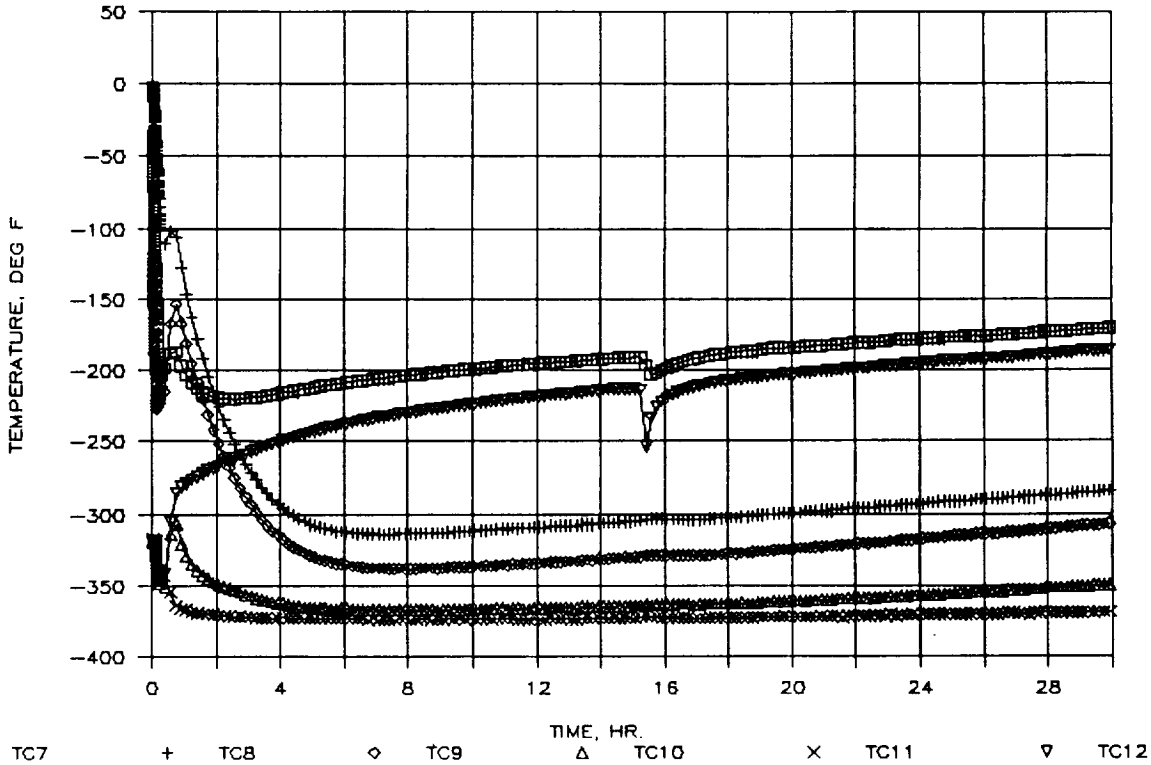

Figure 22. Results of Biosample Freezer Test on 11/15/90, TC7 through TC12, First 30 Hours

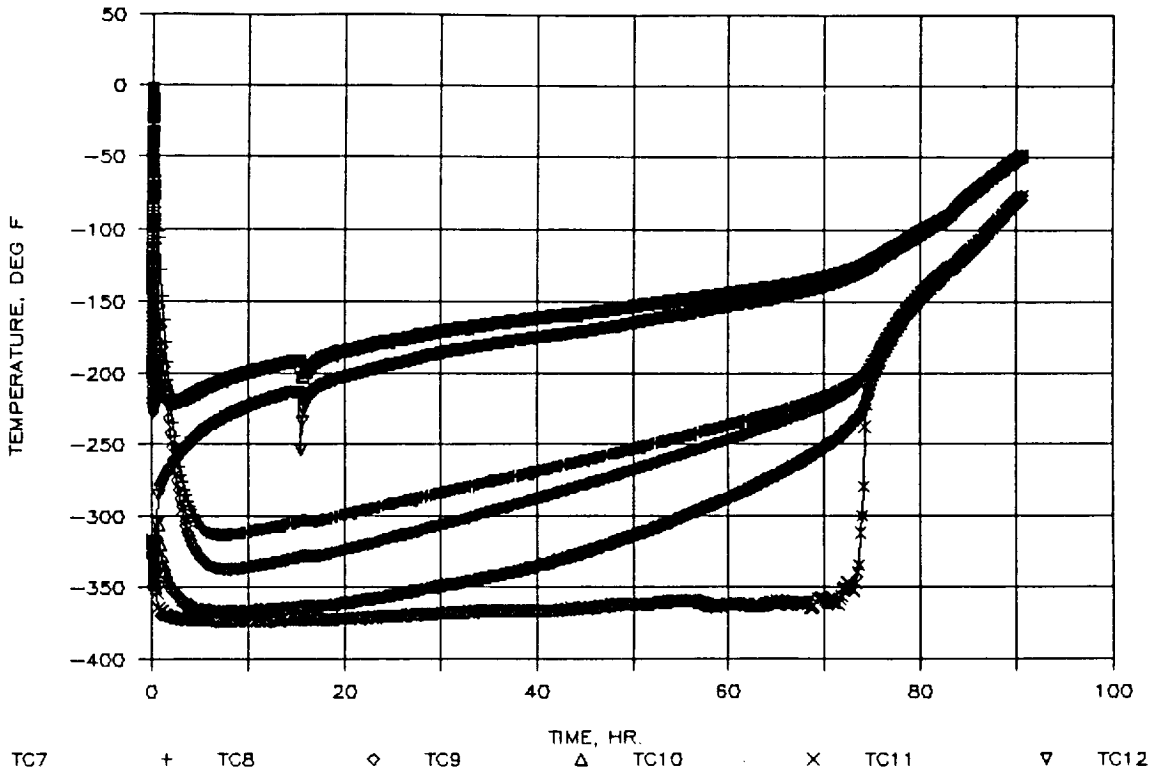

Figure 23. Results of Biosample Freezer Test on 11/15/90, TC7 through TC12, First 92 Hours

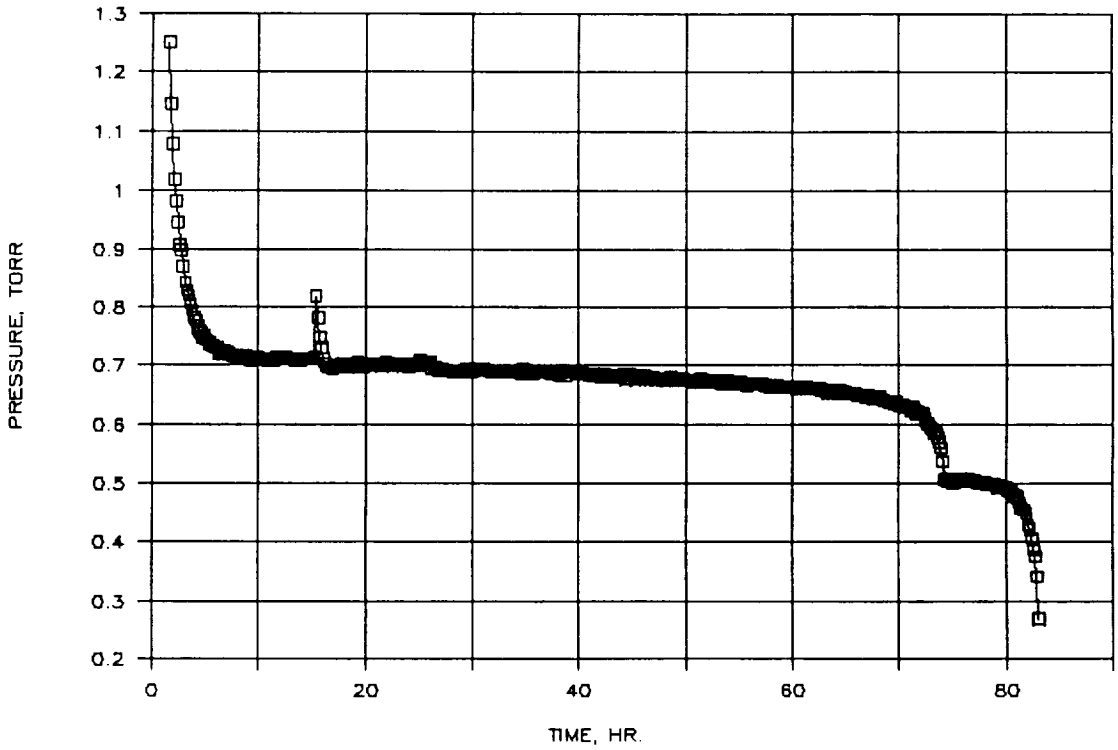

Figure 24. Results of Biosample Freezer Test on 11/15/90, Internal Pressure

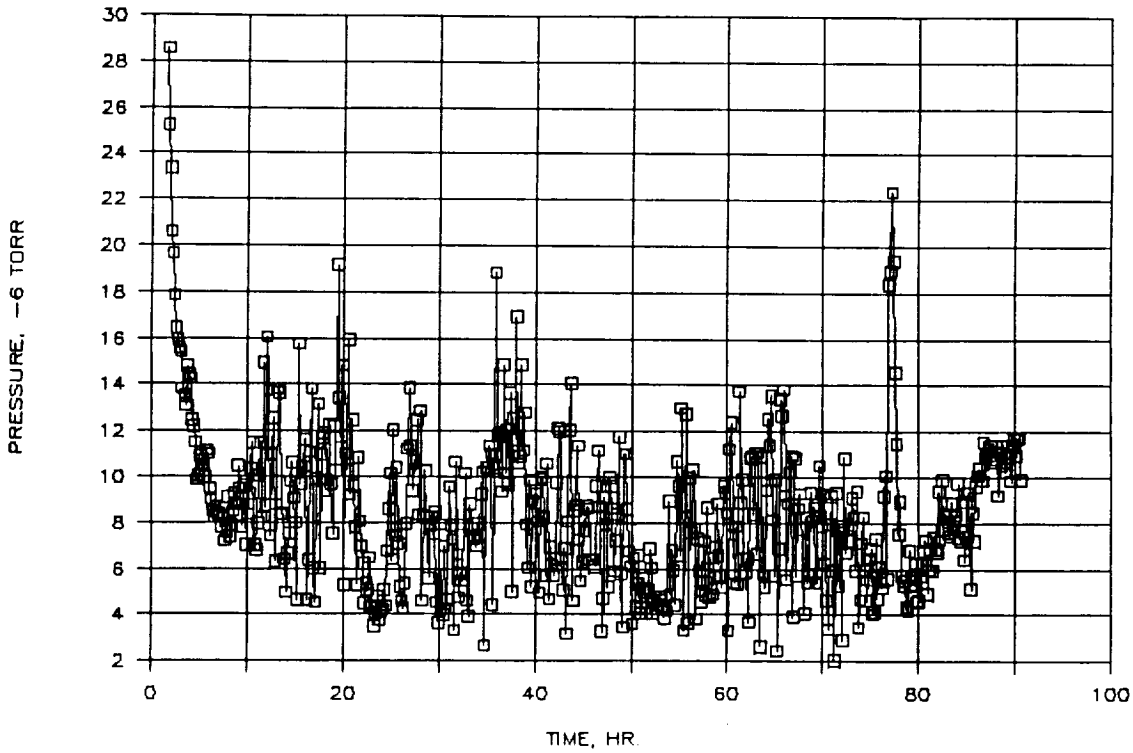

Figure 25. Results of Biosample Freezer Test on 11/15/90, MLI Pressure

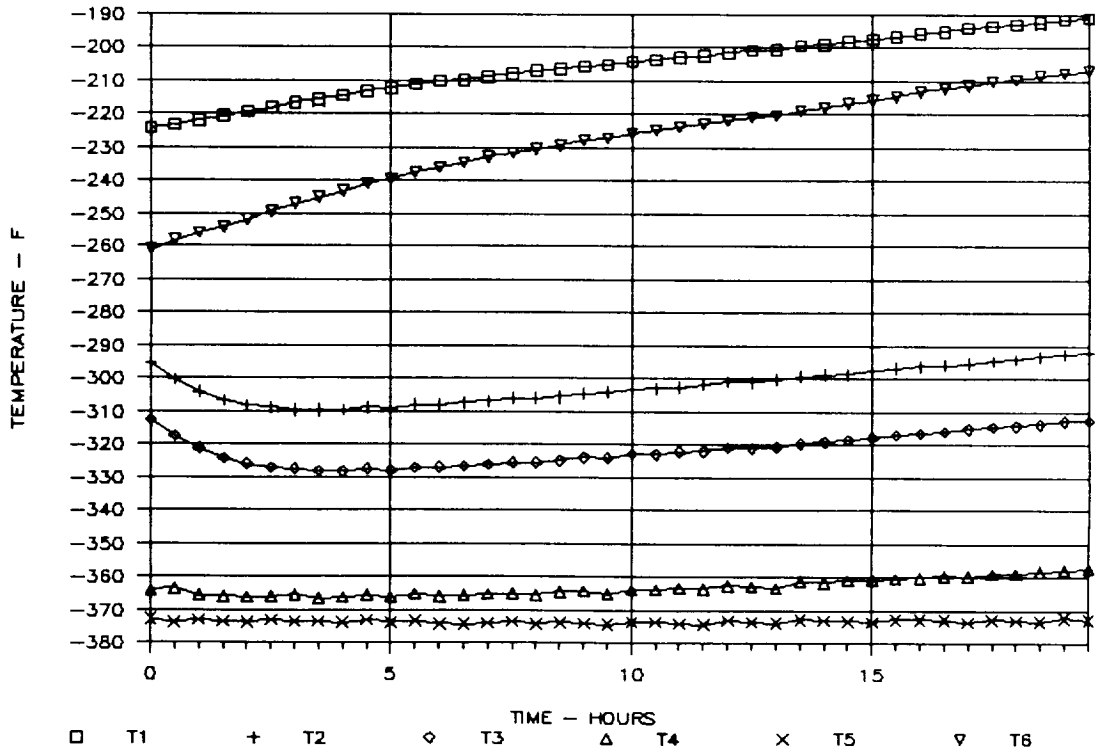

Figure 26. Results of Biosample Freezer Test on 11/19/90, TC1 through TC6, First 20 Hours

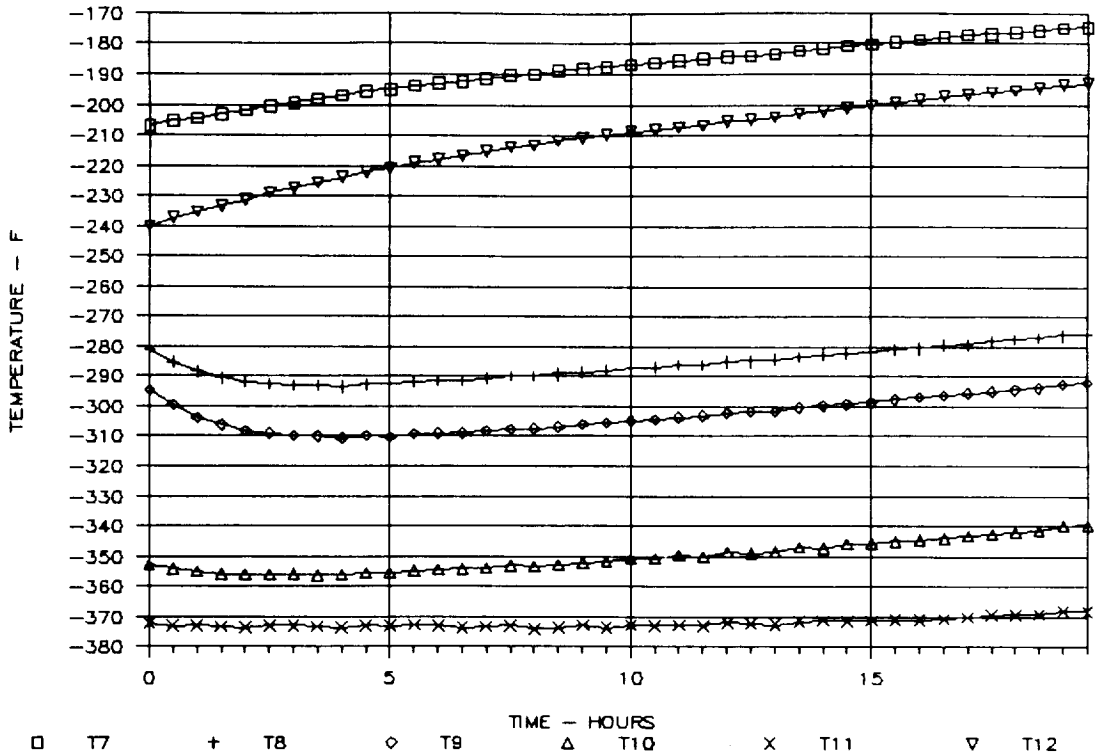

Figure 27. Results of Biosample Freezer Test on 11/19/90, TC7 through TC 12, First 20 Hours

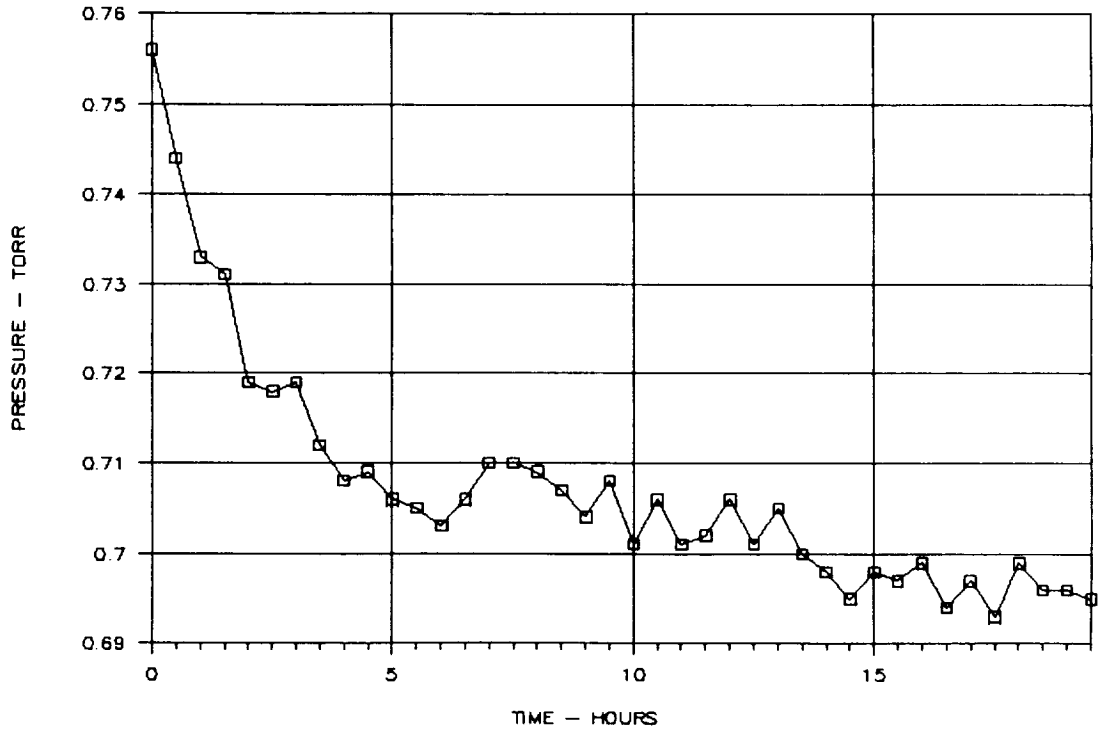

Figure 28. Results of Biosample Freezer Test on 11/19/90, Internal Pressure

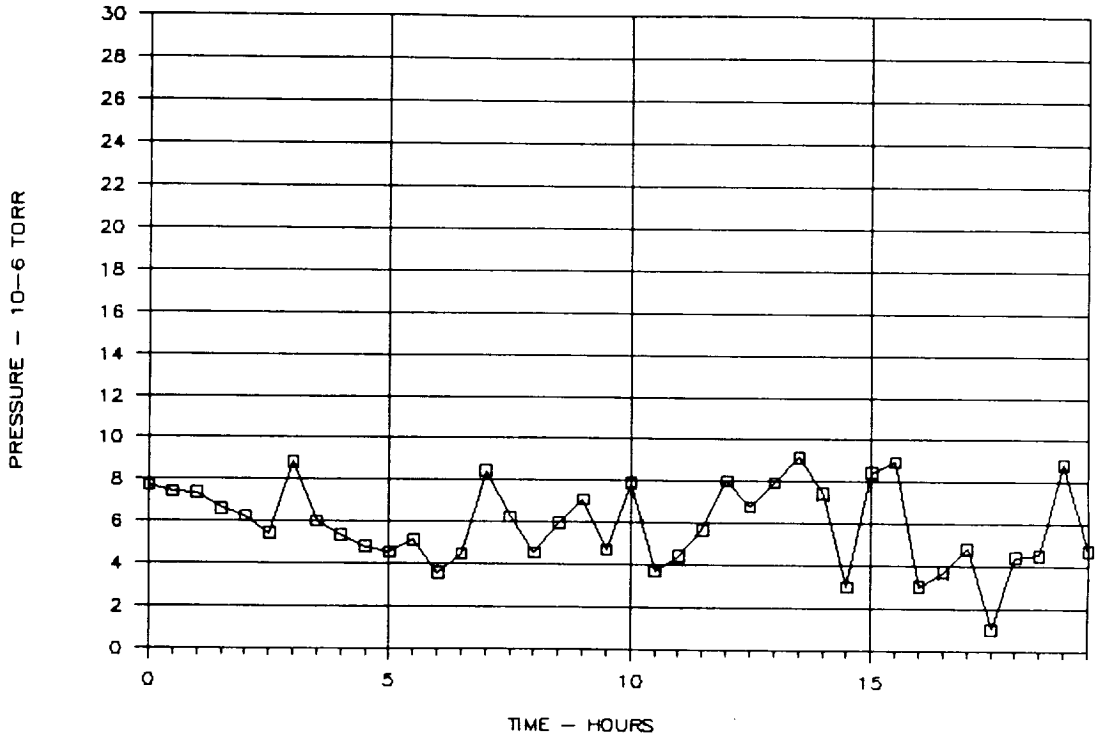

Figure 29. Results of Biosample Freezer Test on 11/19/90, MLI Pressure

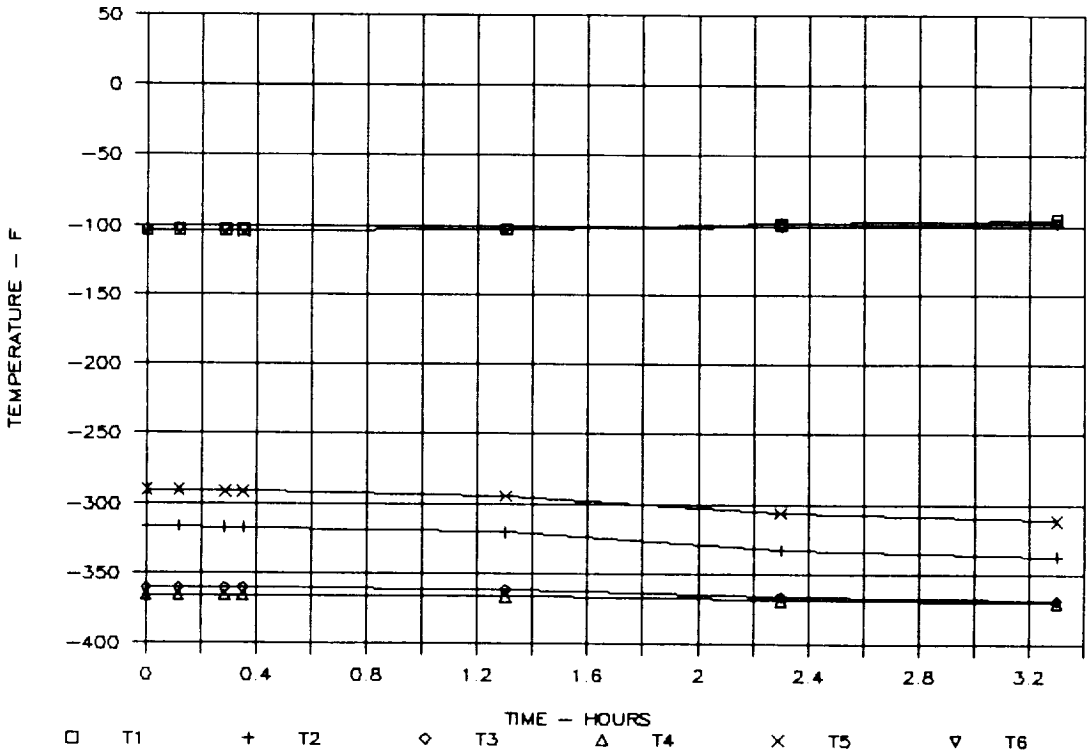

Figure 30. Results of Biosample Freezer Test on 11/21/90, TC1 through TC6, First 4 Hours

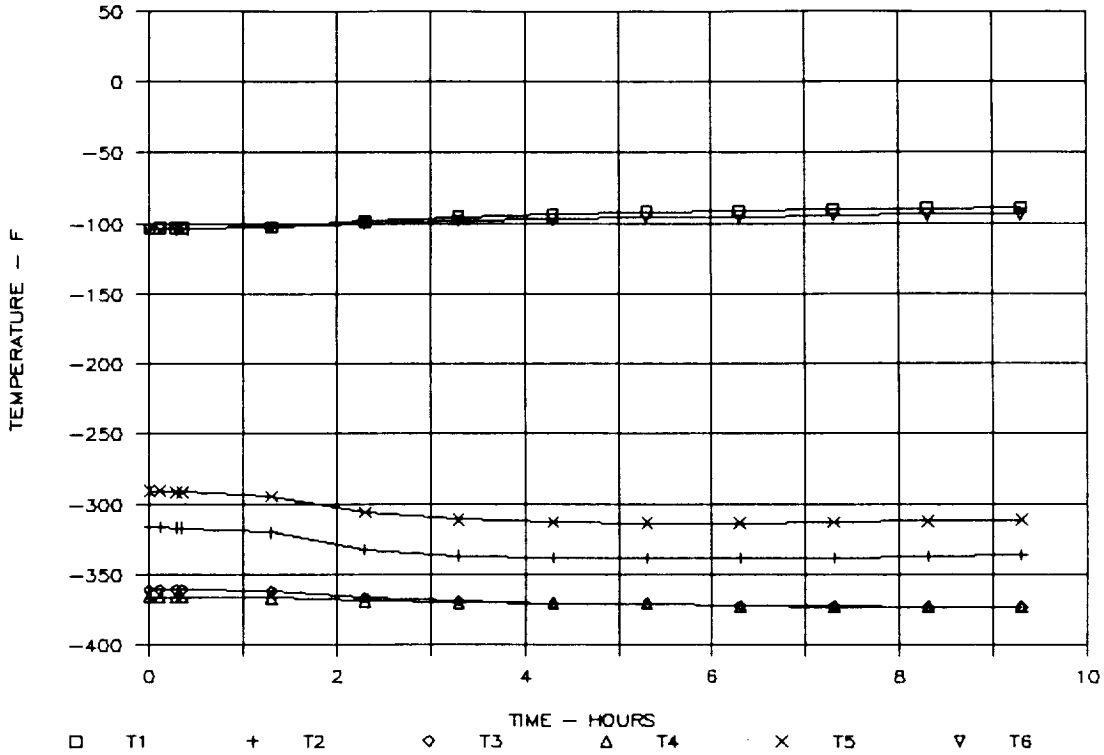

Figure 31. Results of Biosample Freezer Test on 11/21/90, TC1 through TC 6, First 10 Hours

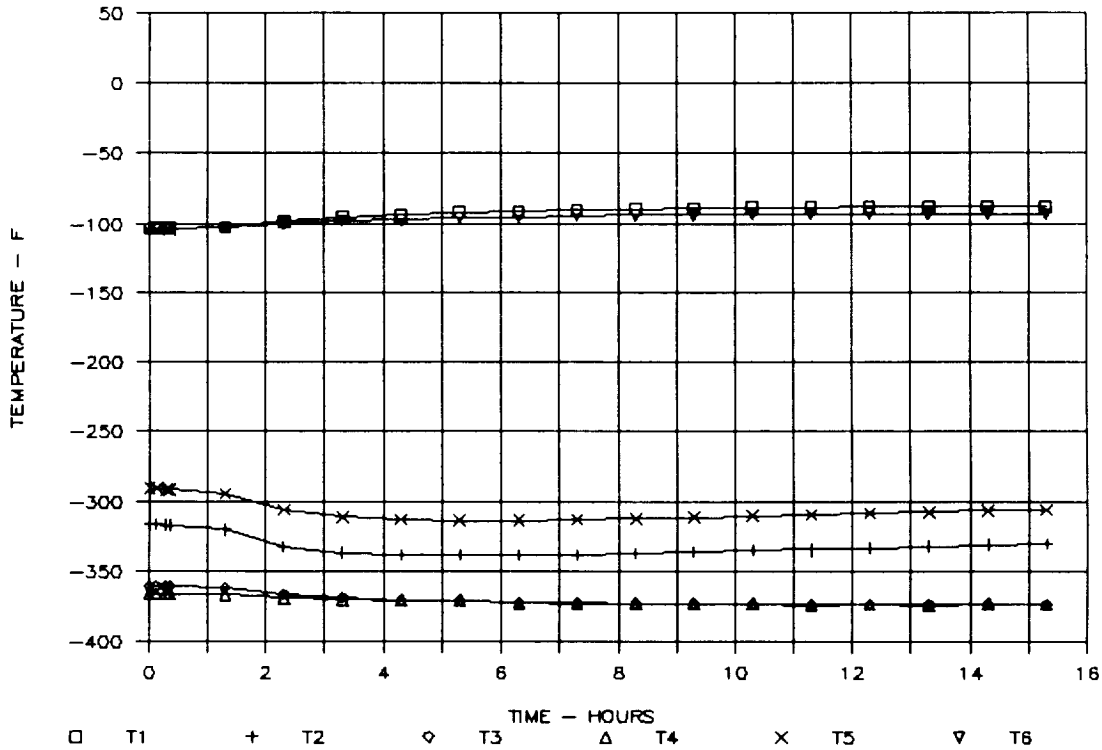

Figure 32. Results of Biosample Freezer Test on 11/21/90, TC1 through TC6, First 16 Hours

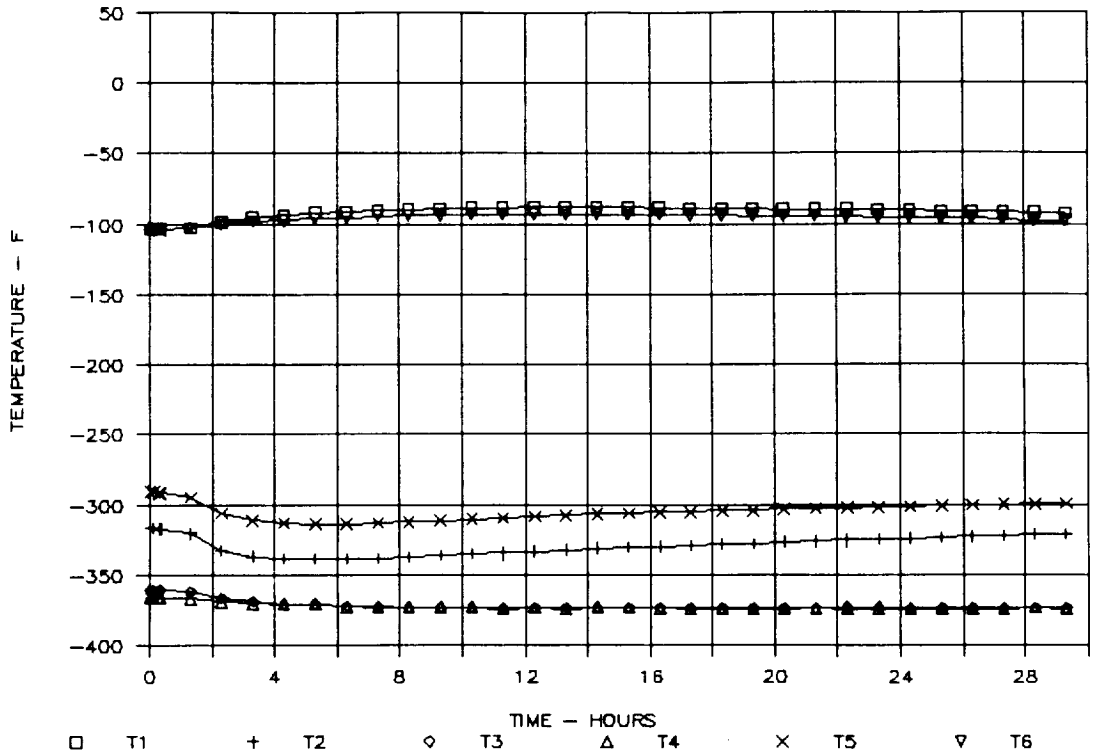

Figure 33. Results of Biosample Freezer Test on 11/21/90, TC1 through TC6, First 30 Hours

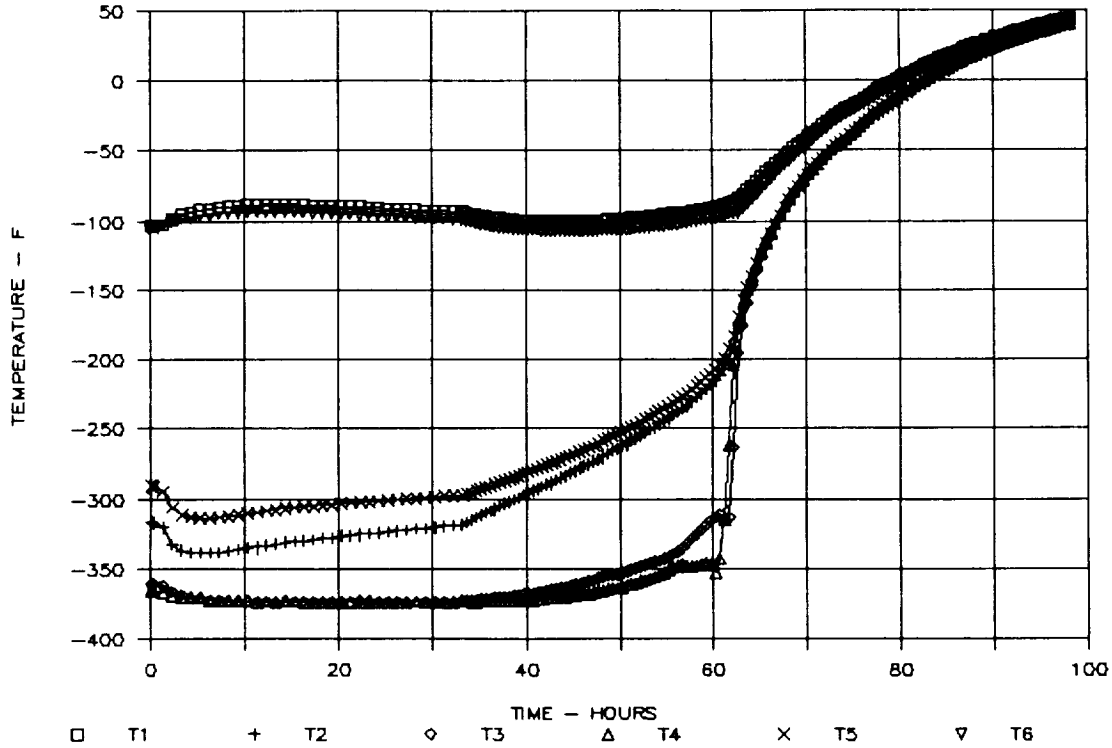

Figure 34. Results of Biosample Freezer Test on 11/21/90, TC1 through TC6, First 98 Hours

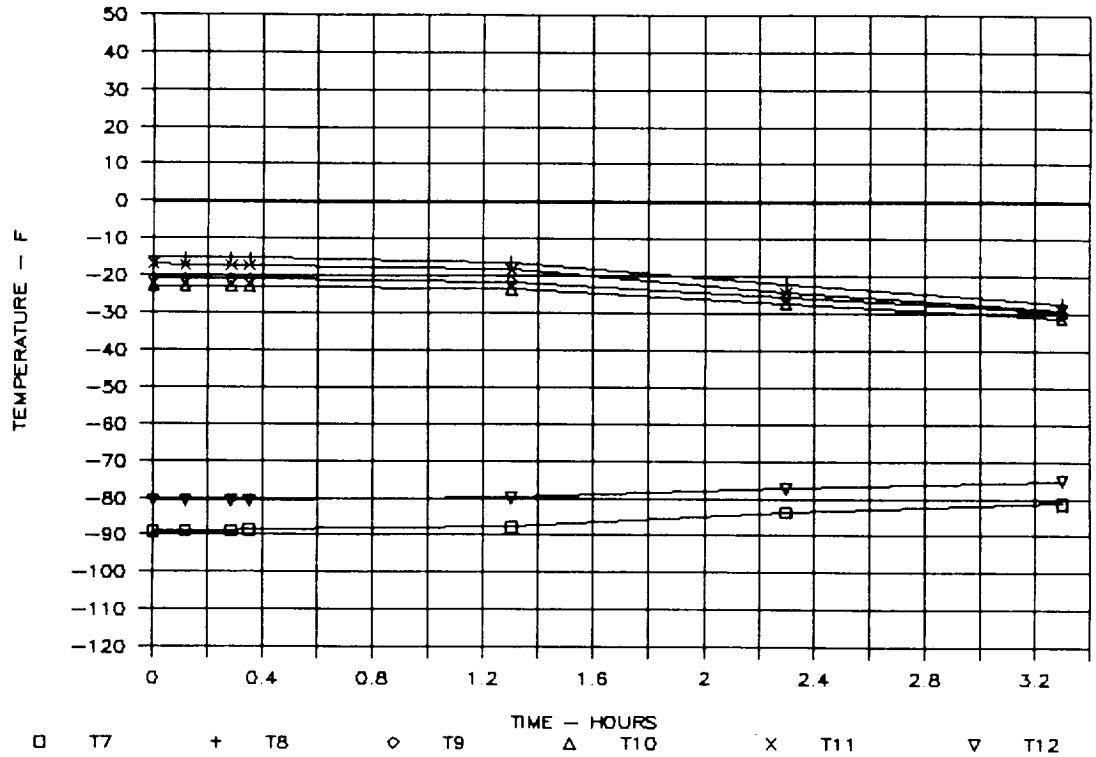

Figure 35. Results of Biosample Freezer Test on 11/21/90, TC7 through TC12, First 4 Hours

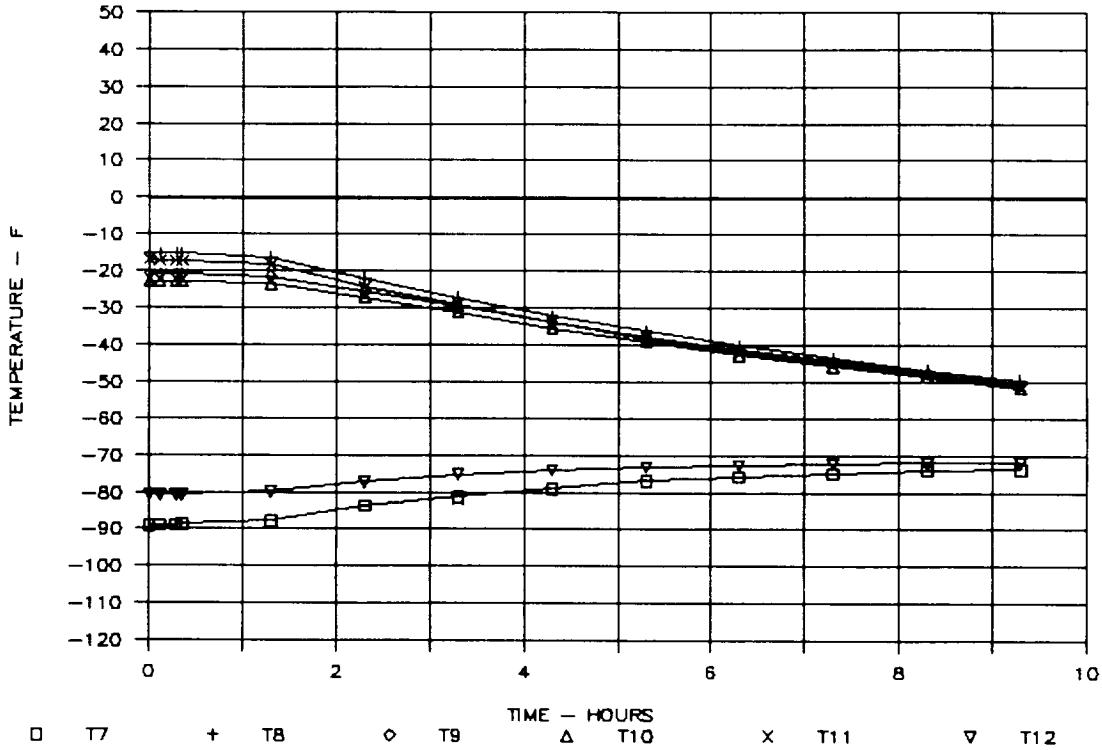

Figure 36. Results of Biosample Freezer Test on 11/21/90, TC7 through TC12, First 10 Hours

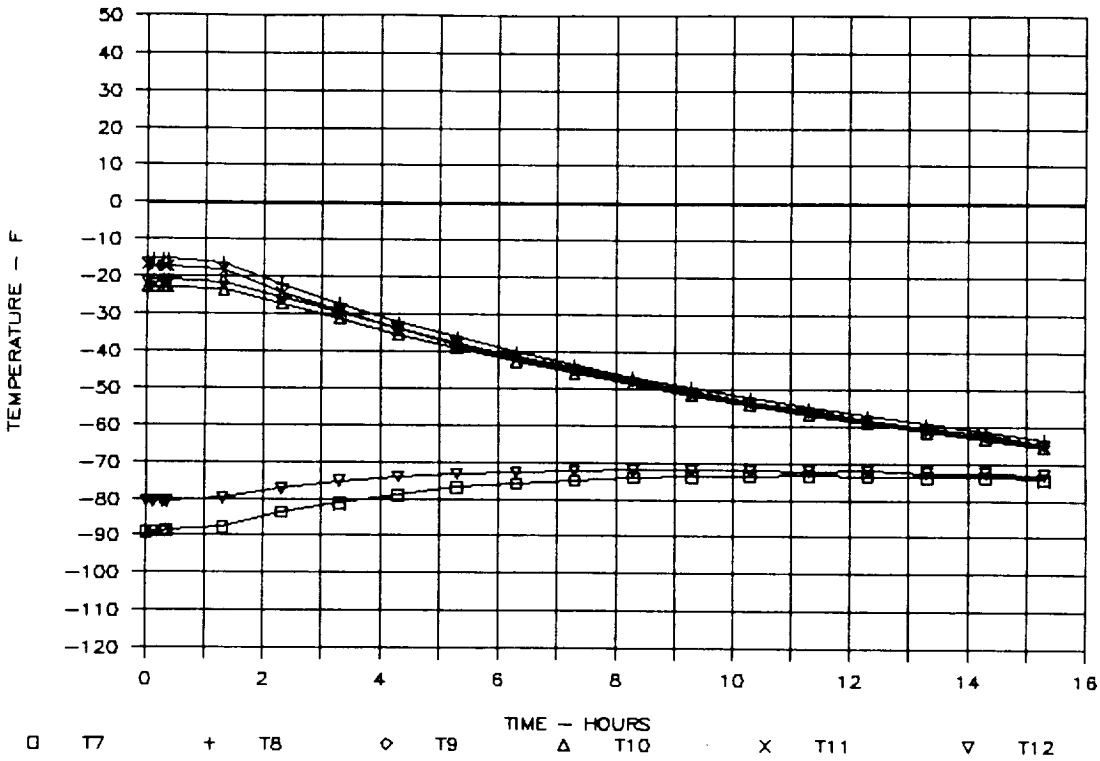

Figure 37. Results of Biosample Freezer Test on 11/21/90, TC7 through TC12, First 16 Hours

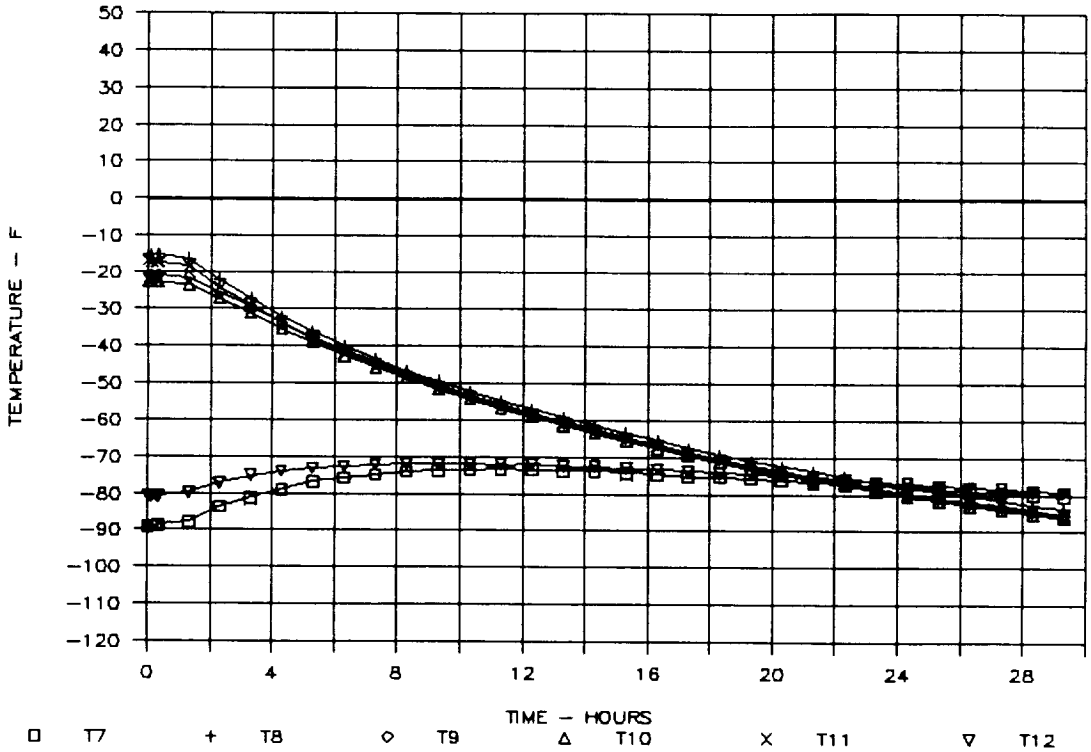

Figure 38. Results of Biosample Freezer Test on 11/21/90, TC7 through TC12, First 30 Hours

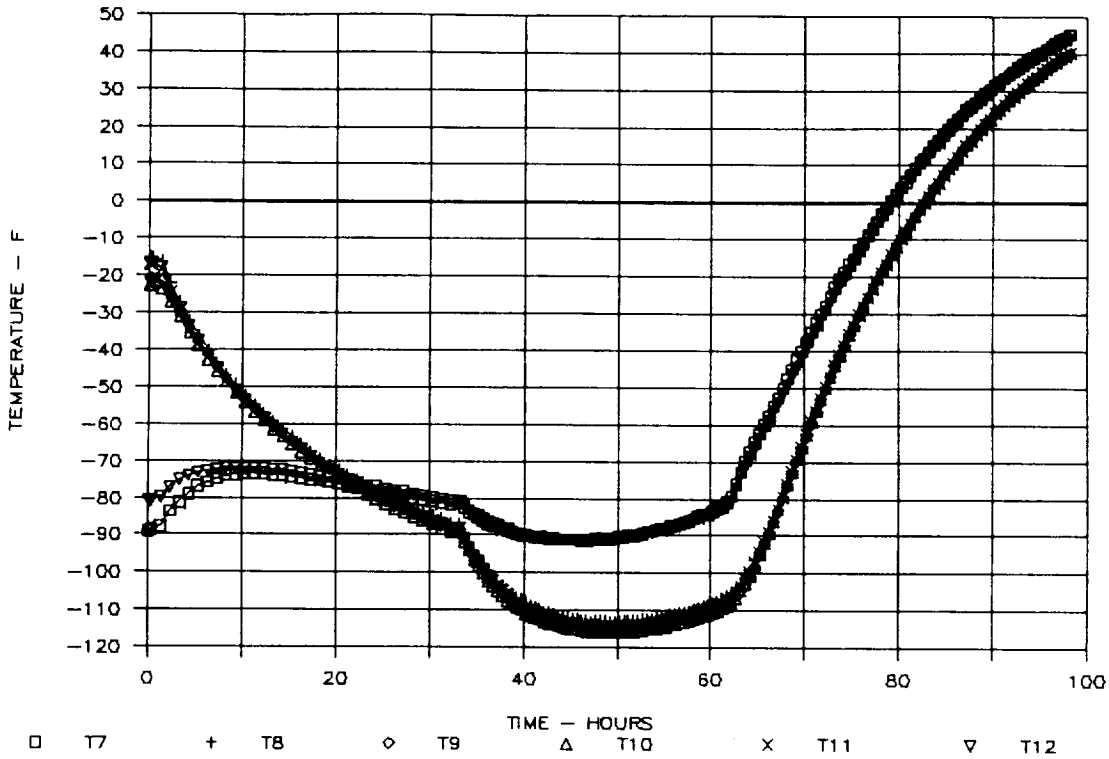

Figure 39. Results of Biosample Freezer Test on 11/21/90, TC7 through TC12, First 98 Hours

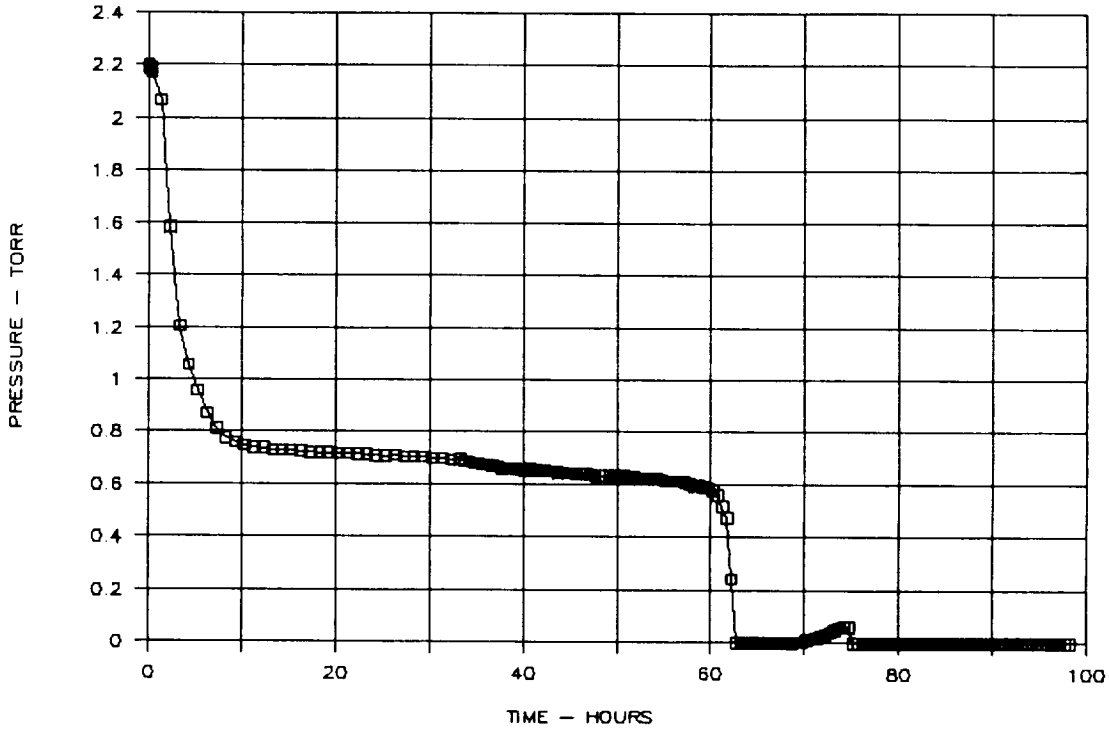

Figure 40. Results of Biosample Freezer Test on 11/21/90, Internal Pressure

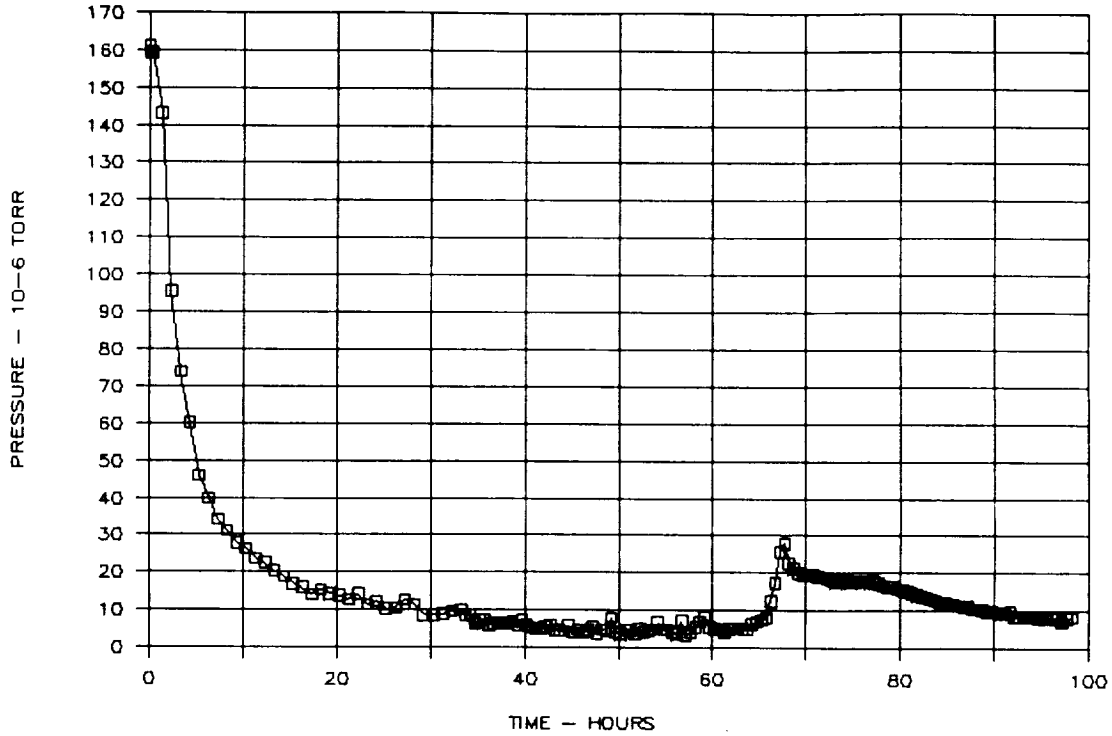

Figure 41. Results of Biosample Freezer Test on 11/21/90, MLI Pressure

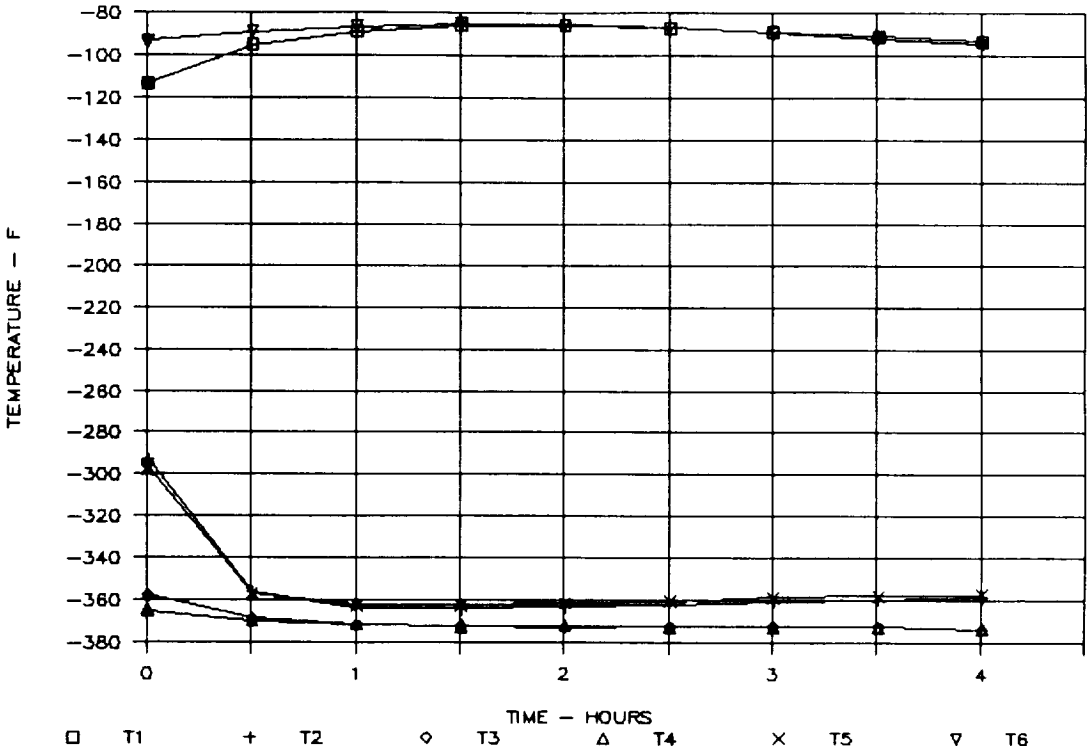

Figure 42. Results of Biosample Freezer Test on 11/26/90, TC1 through TC6, First 4 Hours

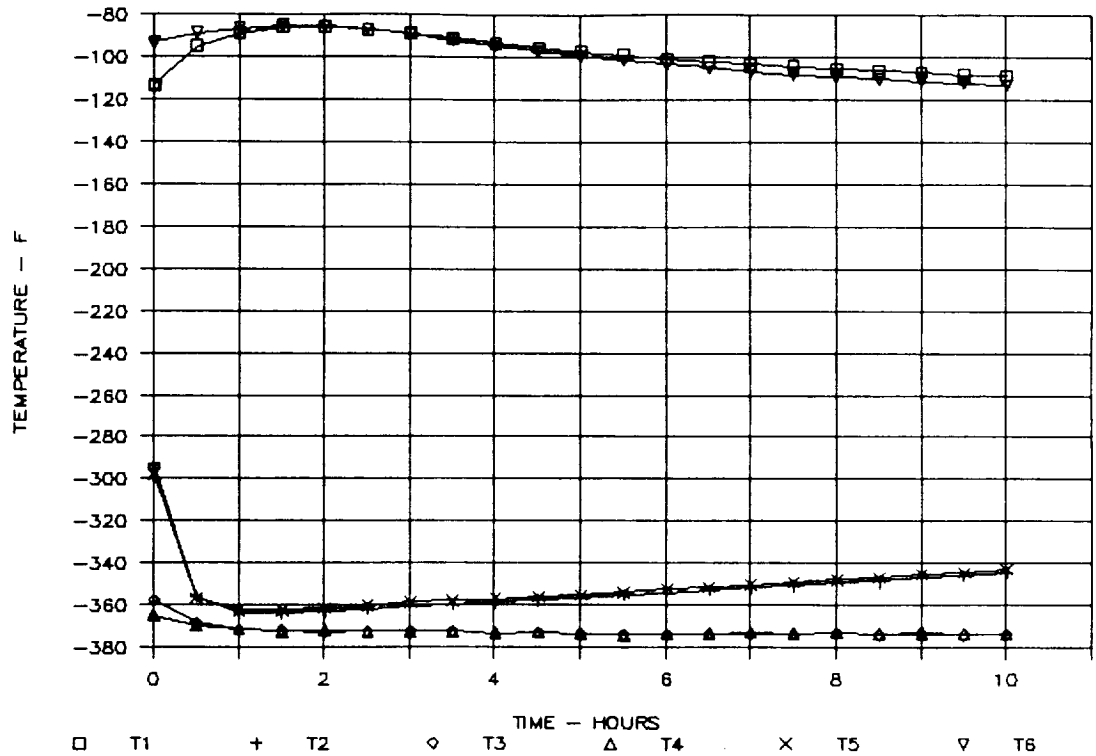

Figure 43. Results of Biosample Freezer Test on 11/26/90, TC1 through TC6, First 10 Hours

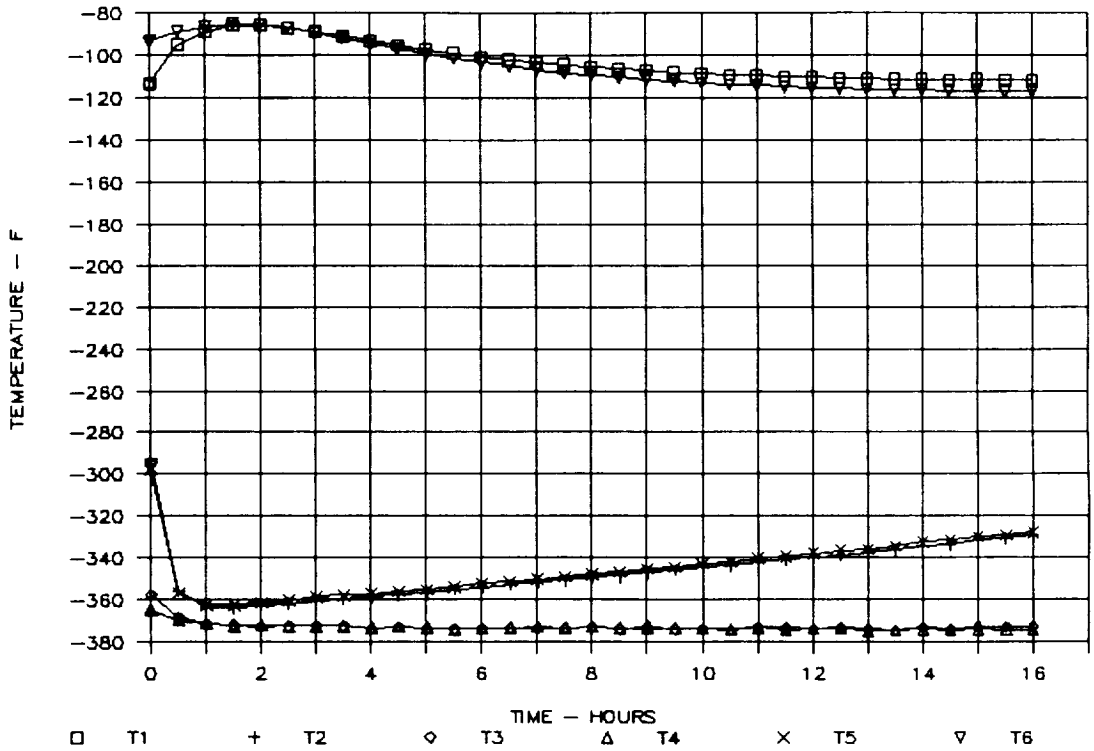

Figure 44. Results of Biosample Freezer Test on 11/26/90, TC1 through TC6, First 16 Hours

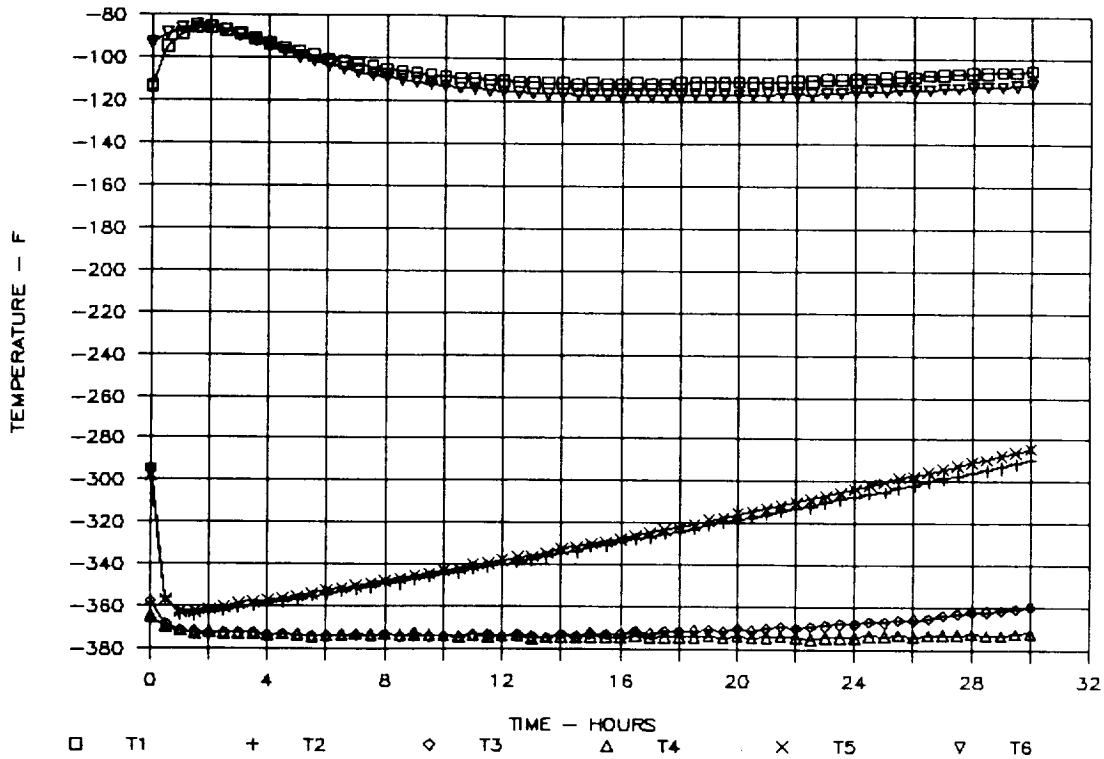

Figure 45. Results of Biosample Freezer Test on 11/26/90, TC1 through TC6, First 30 Hours

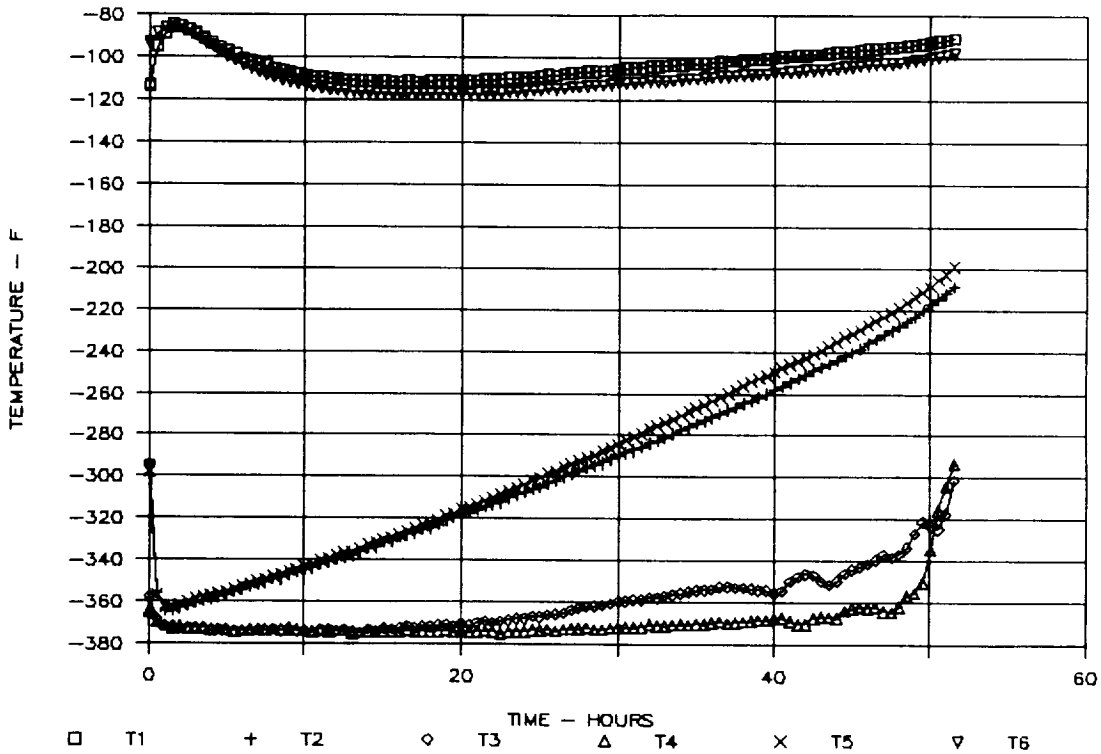

Figure 46. Results of Biosample Freezer Test on 11/26/90, TC1 through TC6, First 52 Hours

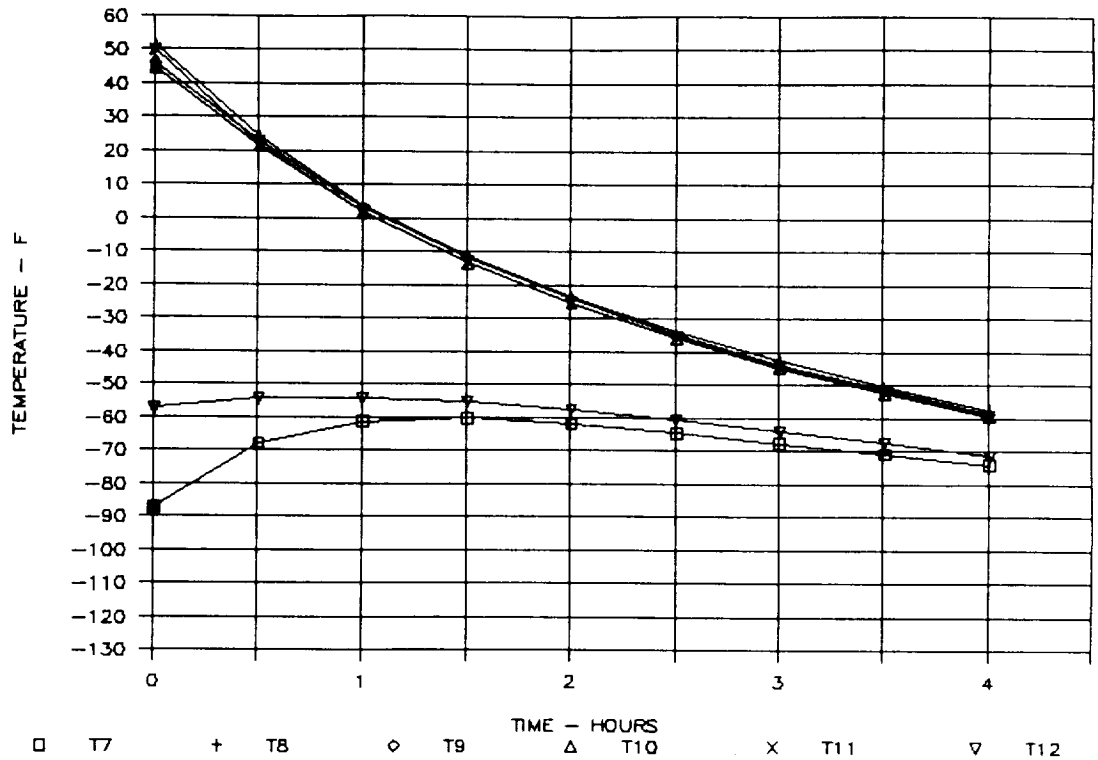

Figure 47. Results of Biosample Freezer Test on 11/26/90, TC7 through TC12, First 4 Hours

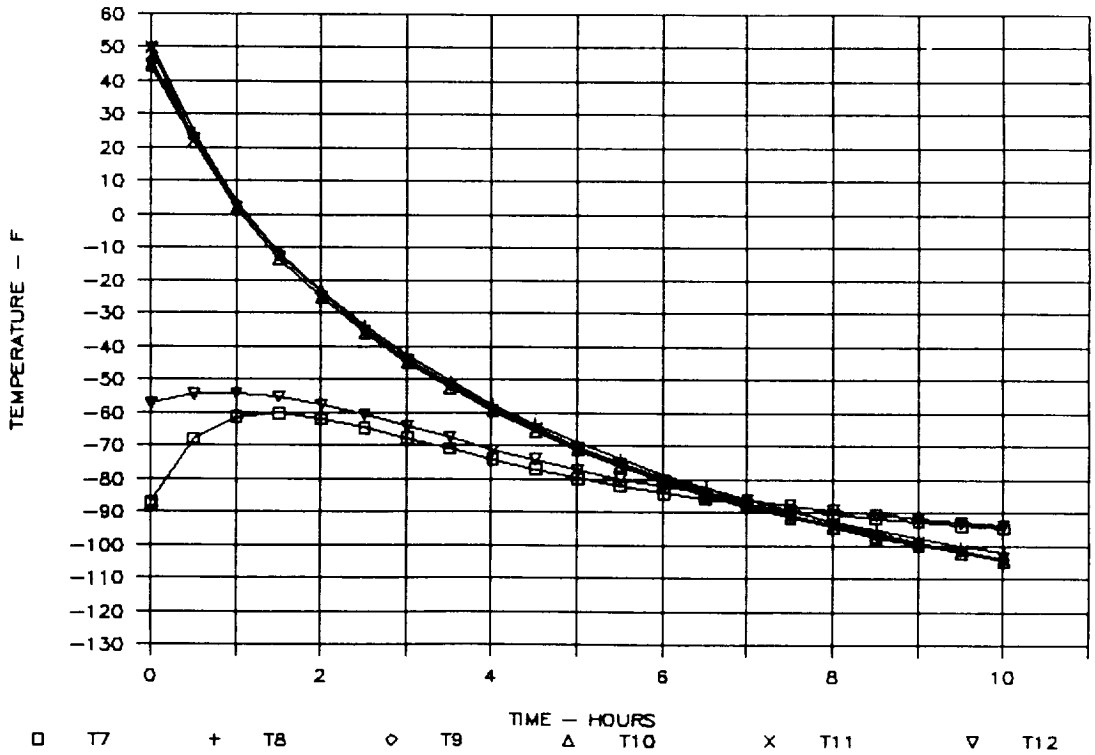

Figure 48. Results of Biosample Freezer Test on 11/26/90, TC7 through TC12, First 10 Hours

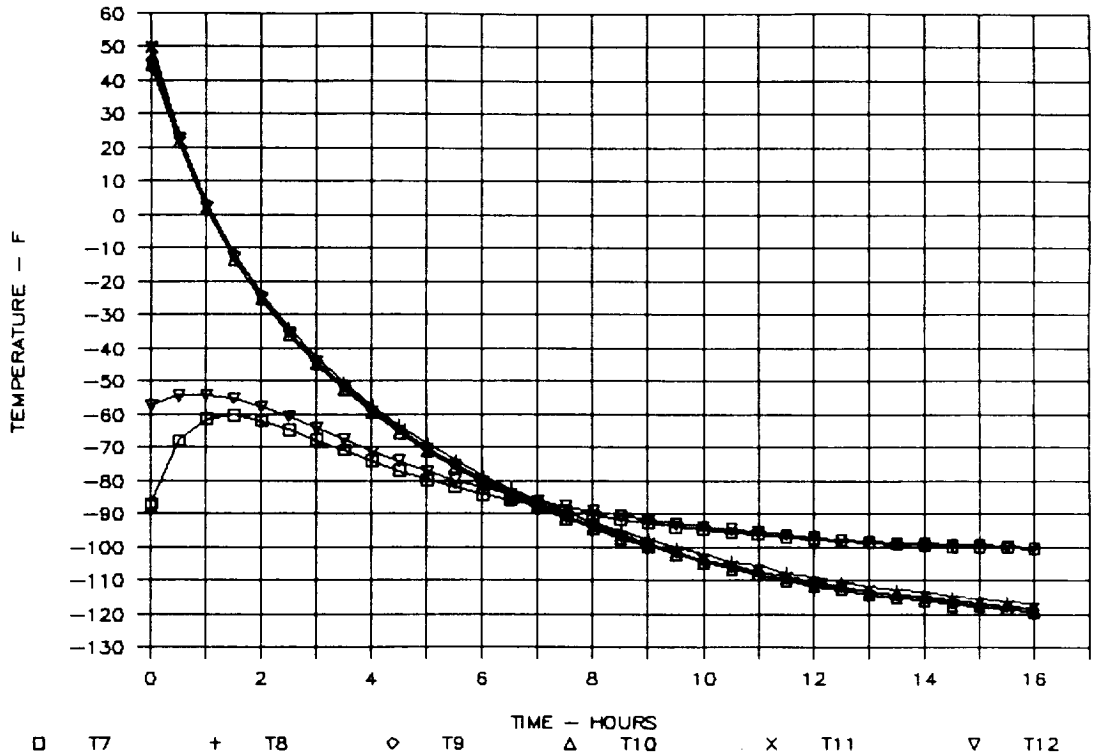

Figure 49. Results of Biosample Freezer Test on 11/26/90, TC7 through TC12, First 16 Hours

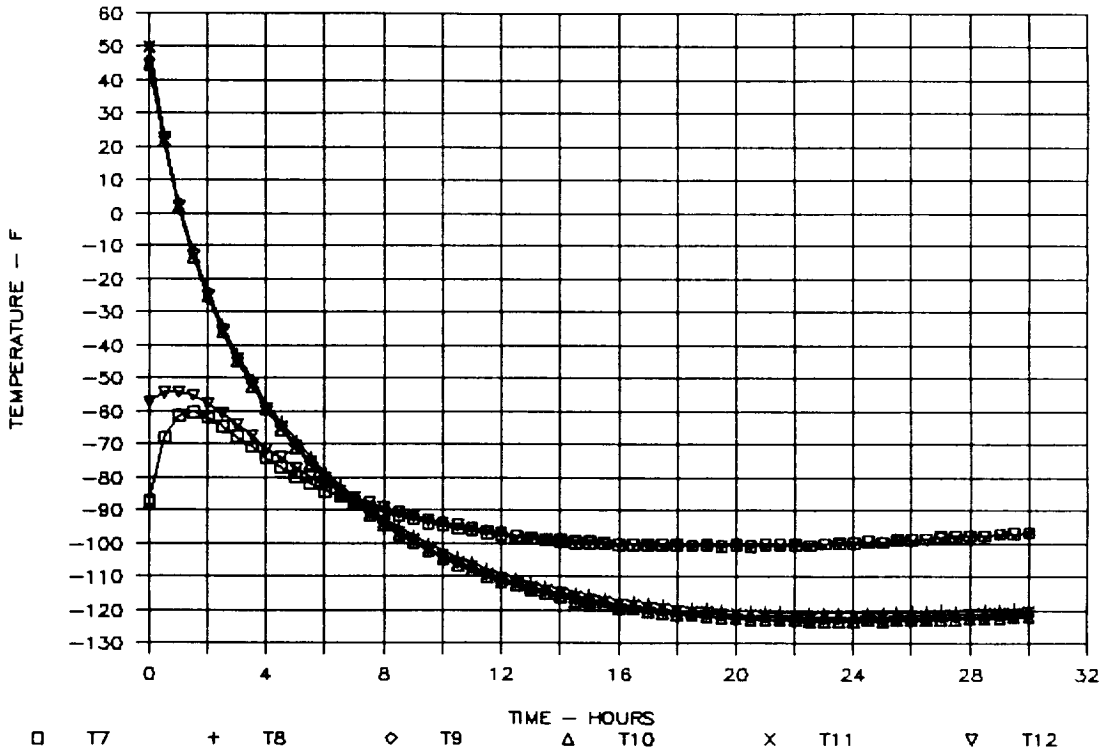

Figure 50. Results of Biosample Freezer Test on 11/26/90, TC7 through TC12, First 30 Hours

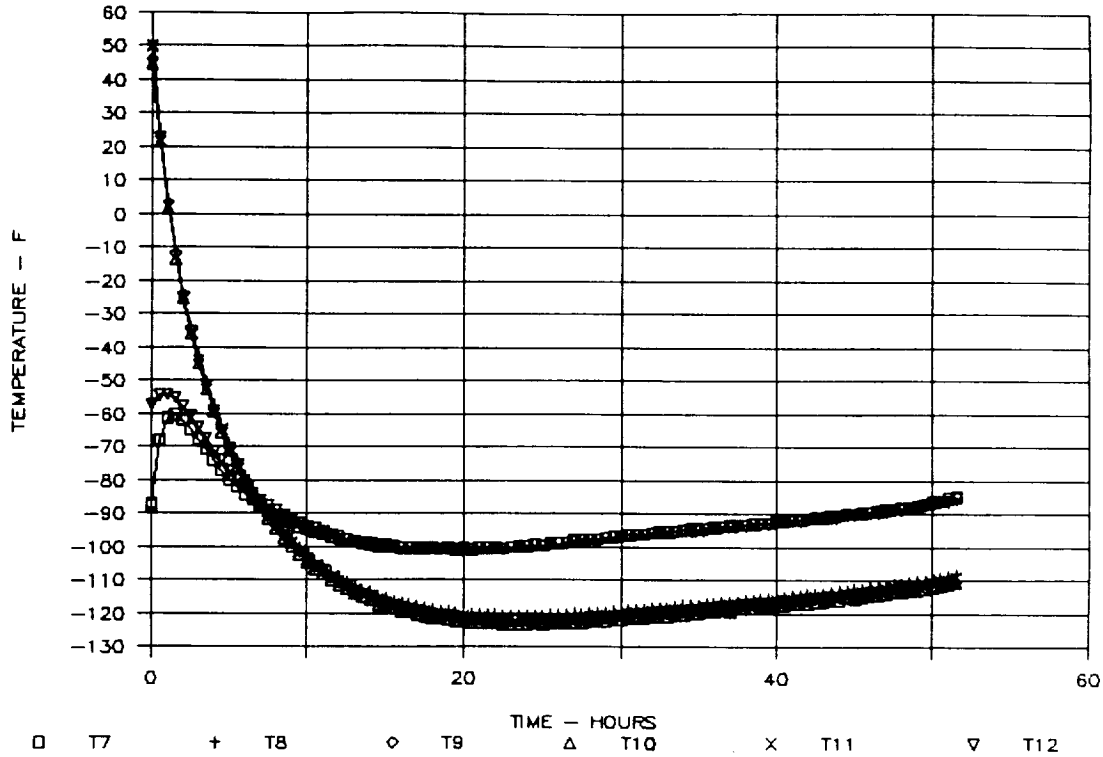

Figure 51. Results of Biosample Freezer Test on 11/26/90, TC7 through TC12, First 52 Hours

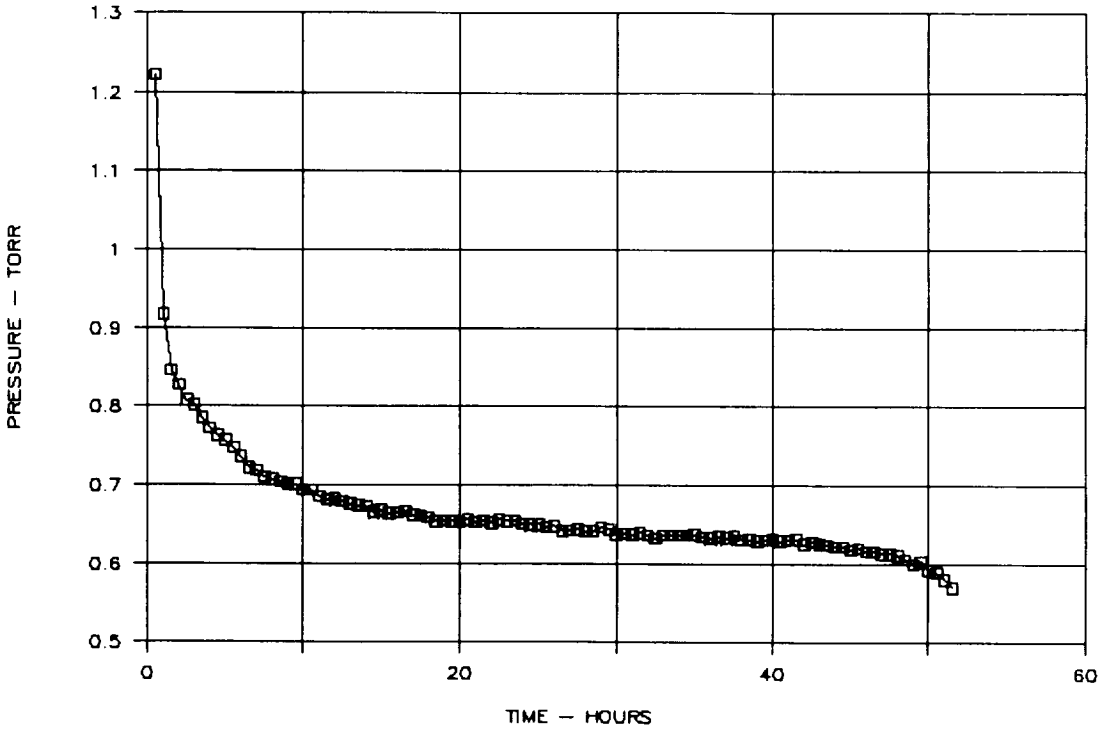

Figure 52. Results of Biosample Freezer Test on 11/26/90, Internal Pressure

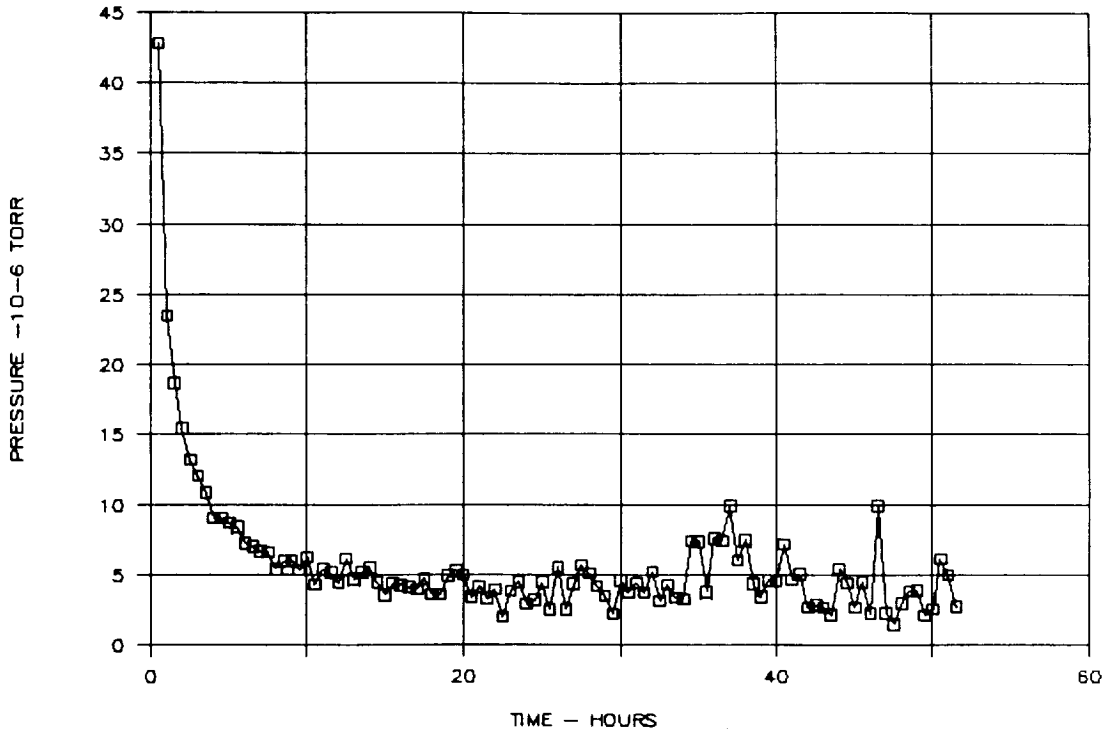

Figure 53. Results of Biosample Freezer Test on 11/26/90, MLI Pressure

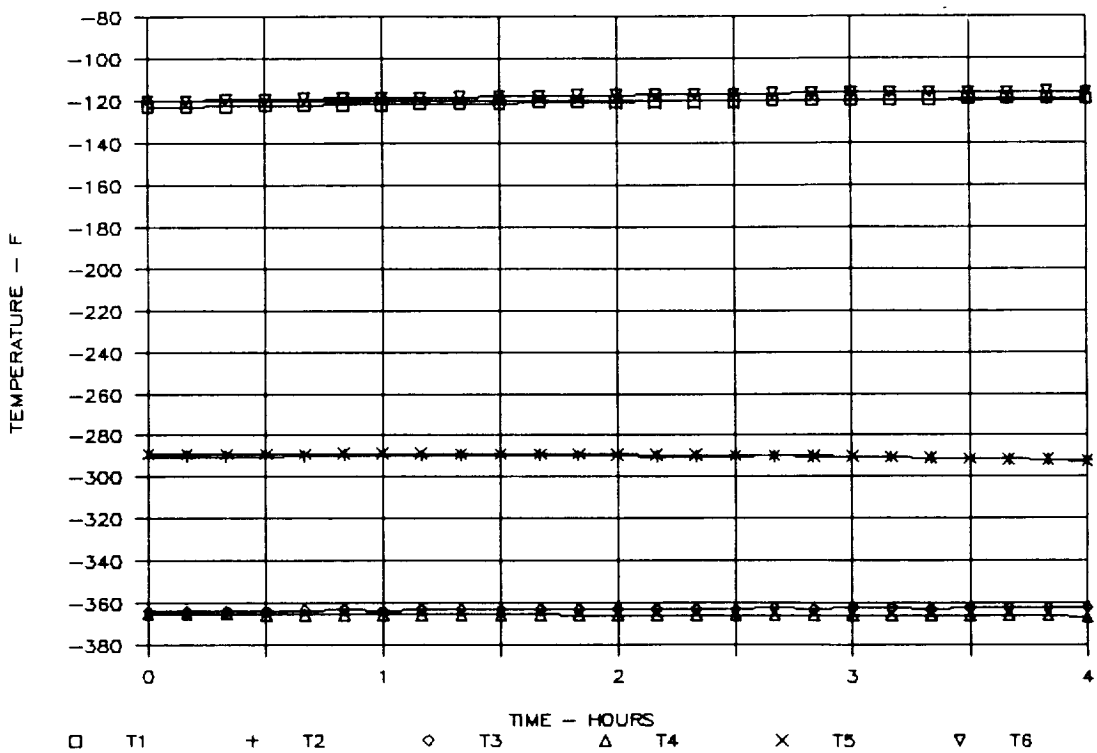

Figure 54. Results of Biosample Freezer Test on 11/28/90, TC1 through TC6, First 4 Hours

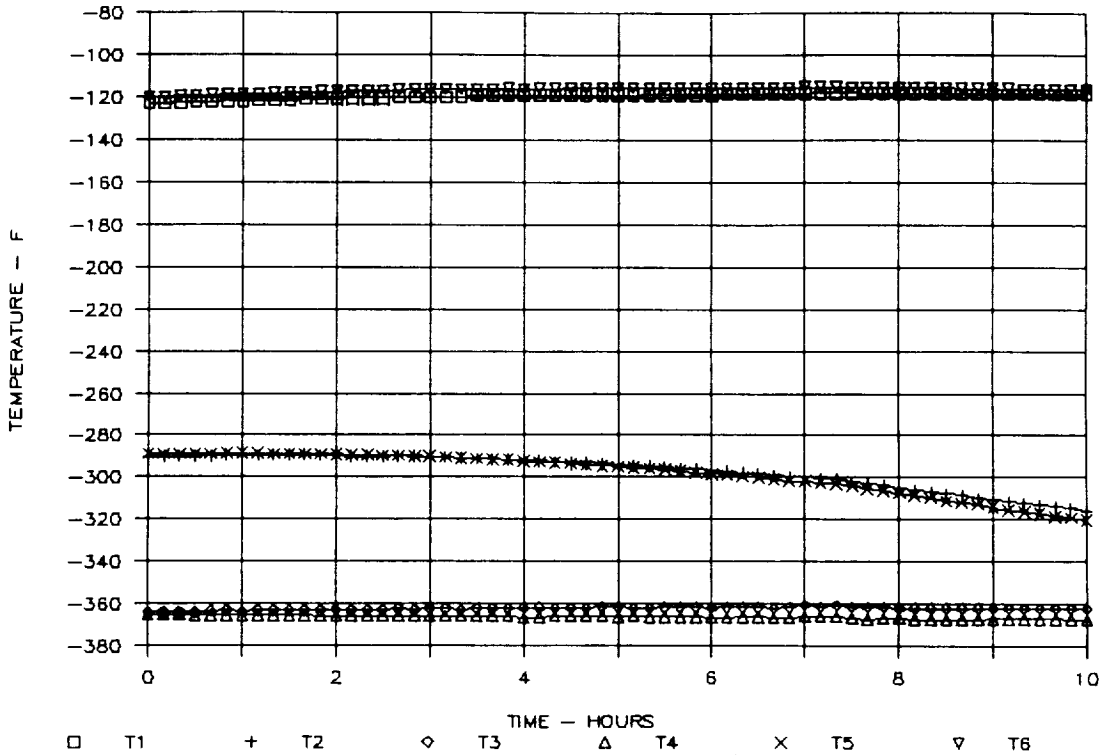

Figure 55. Results of Biosample Freezer Test on 11/28/90, TC1 through TC6, First 10 Hours

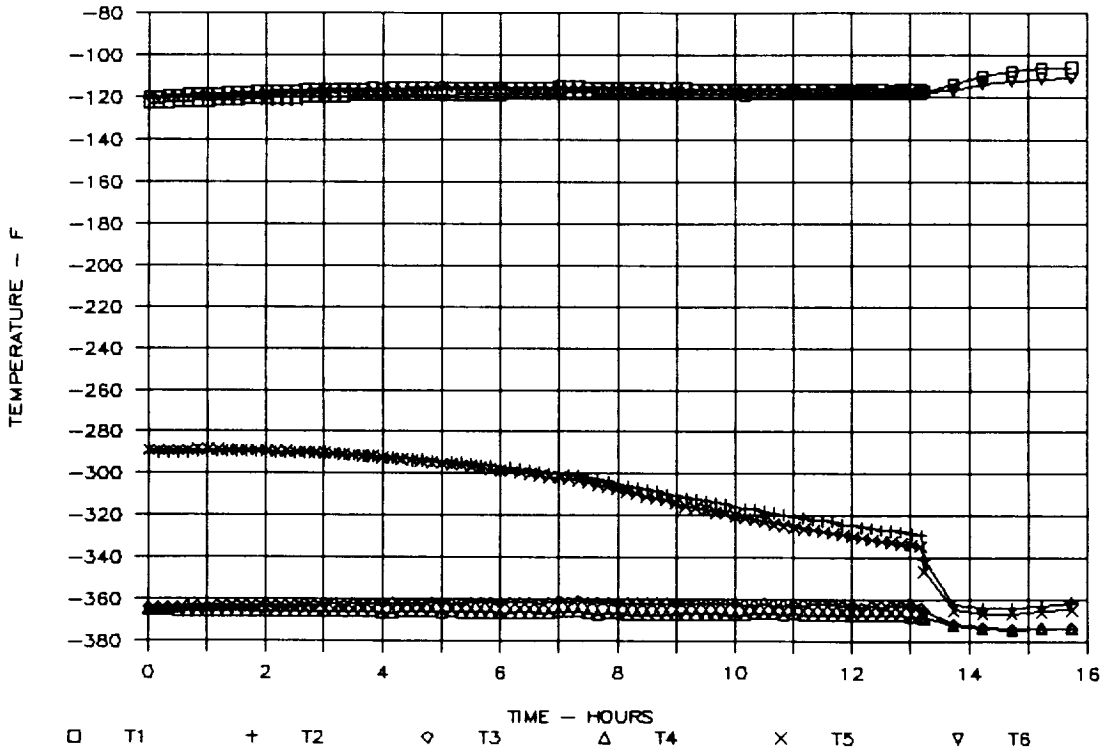

Figure 56. Results of Biosample Freezer Test on 11/28/90, TC1 through TC6, First 16 Hours

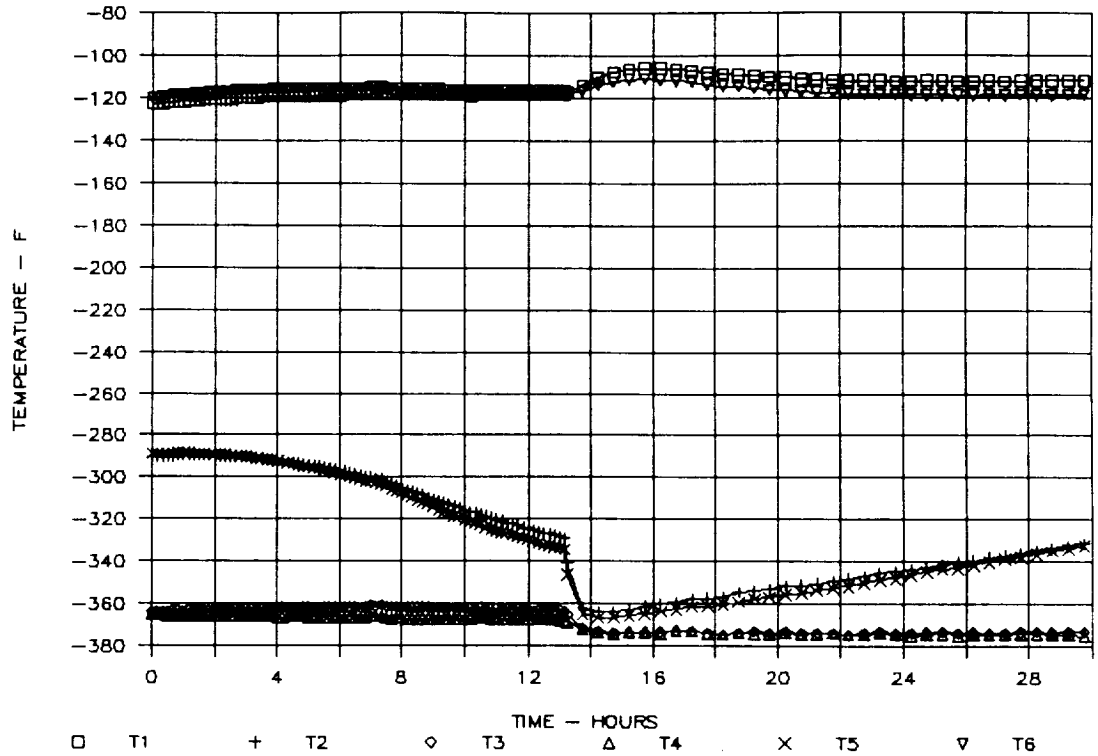

Figure 57. Results of Biosample Freezer Test on 11/28/90, TC1 through TC6, First 30 Hours

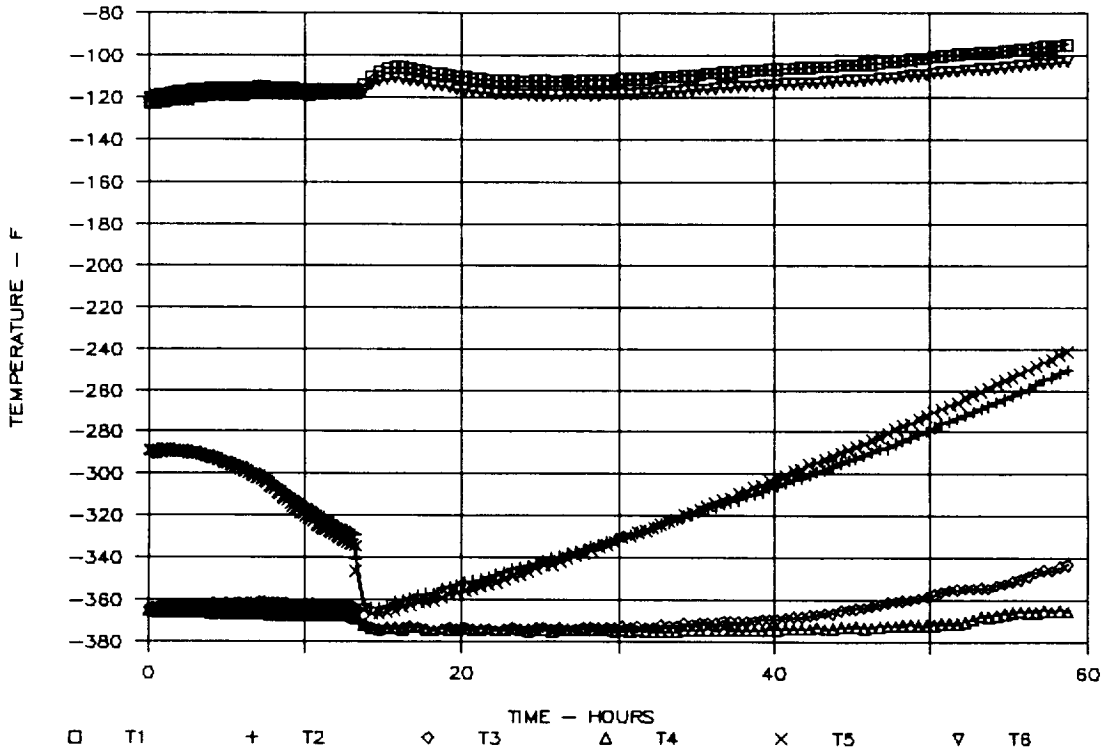

Figure 58. Results of Biosample Freezer Test on 11/28/90, TC1 through TC6, First 59 Hours

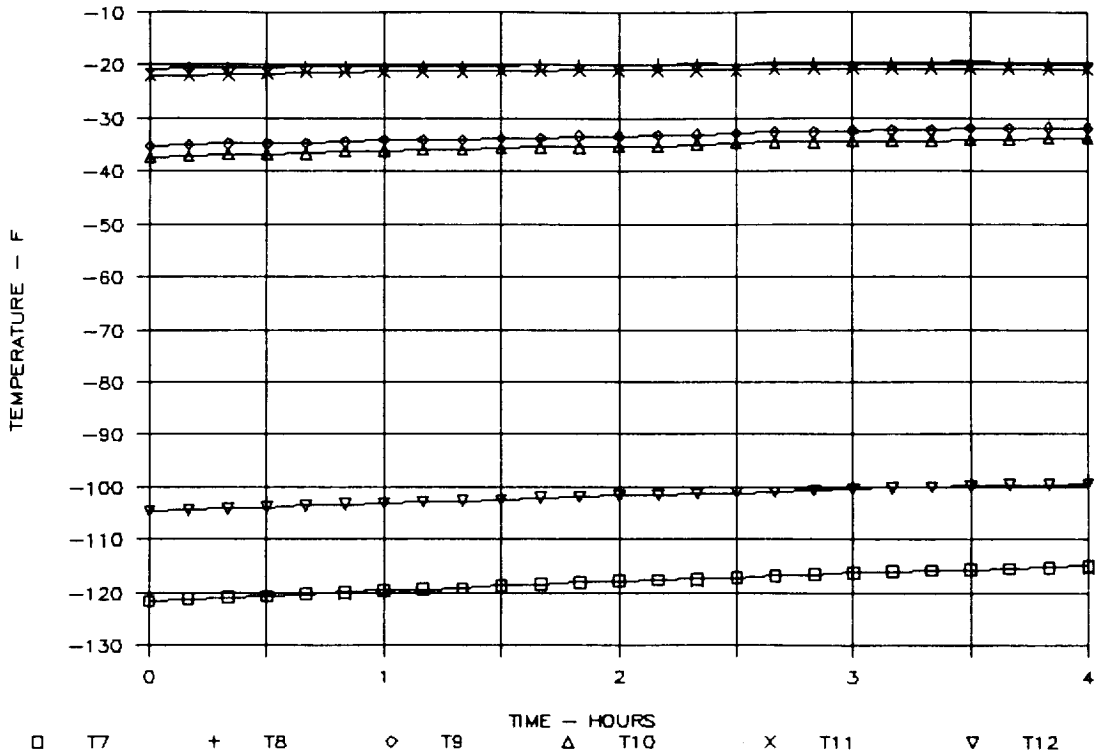

Figure 59. Results of Biosample Freezer Test on 11/28/90, TC7 through TC12, First 4 Hours

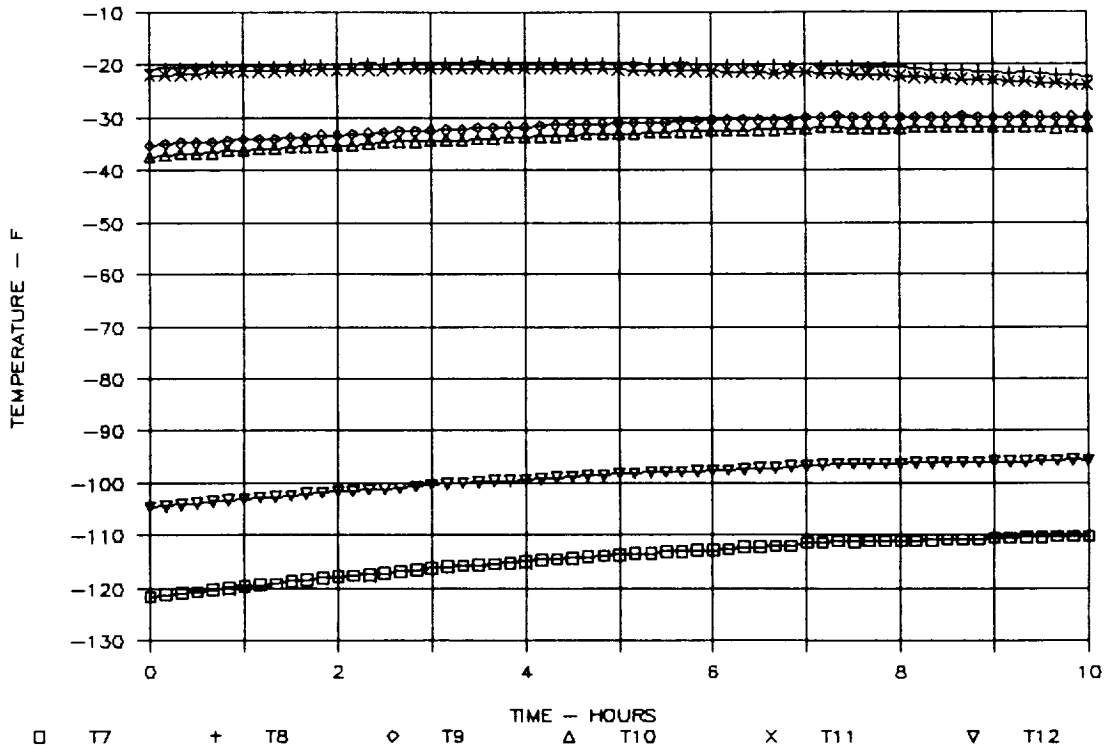

Figure 60. Results of Biosample Freezer Test on 11/28/90, TC7 through TC12, First 10 Hours

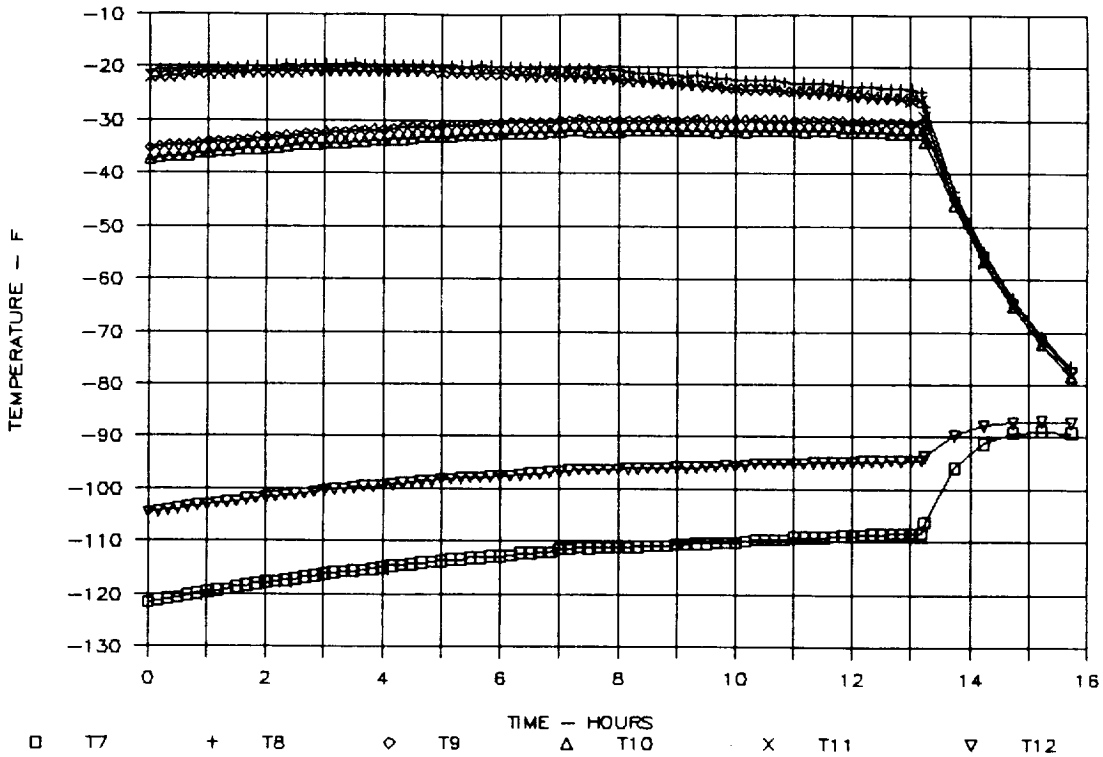

Figure 61. Results of Biosample Freezer Test on 11/28/90, TC7 through TC12, First 16 Hours

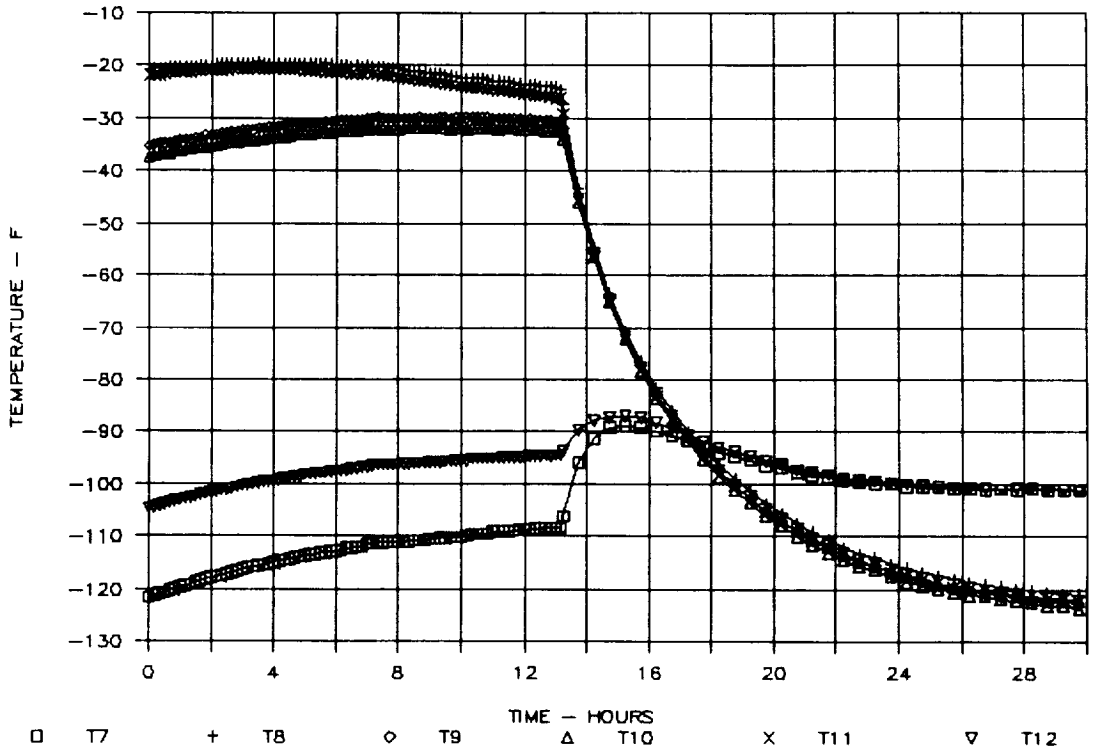

Figure 62. Results of Biosample Freezer Test on 11/28/90, TC7 through TC12, First 30 Hours

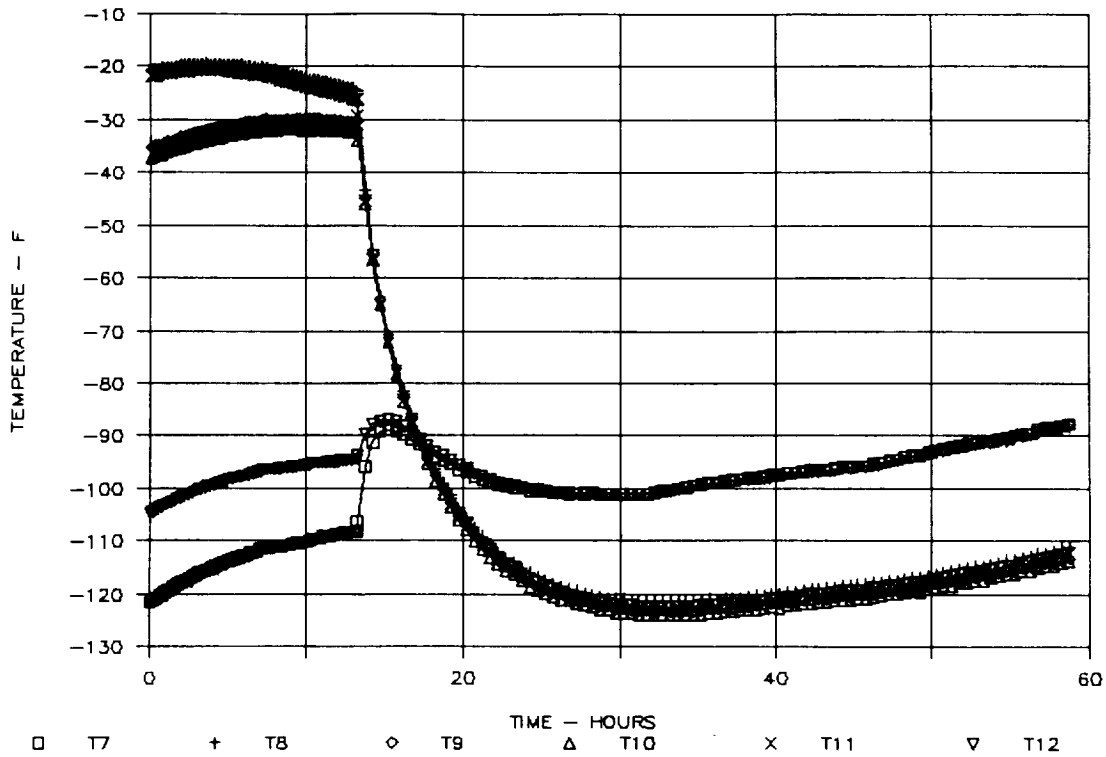

Figure 63. Results of Biosample Freezer Test on 11/28/90, TC7 through TC12, First 59 Hours

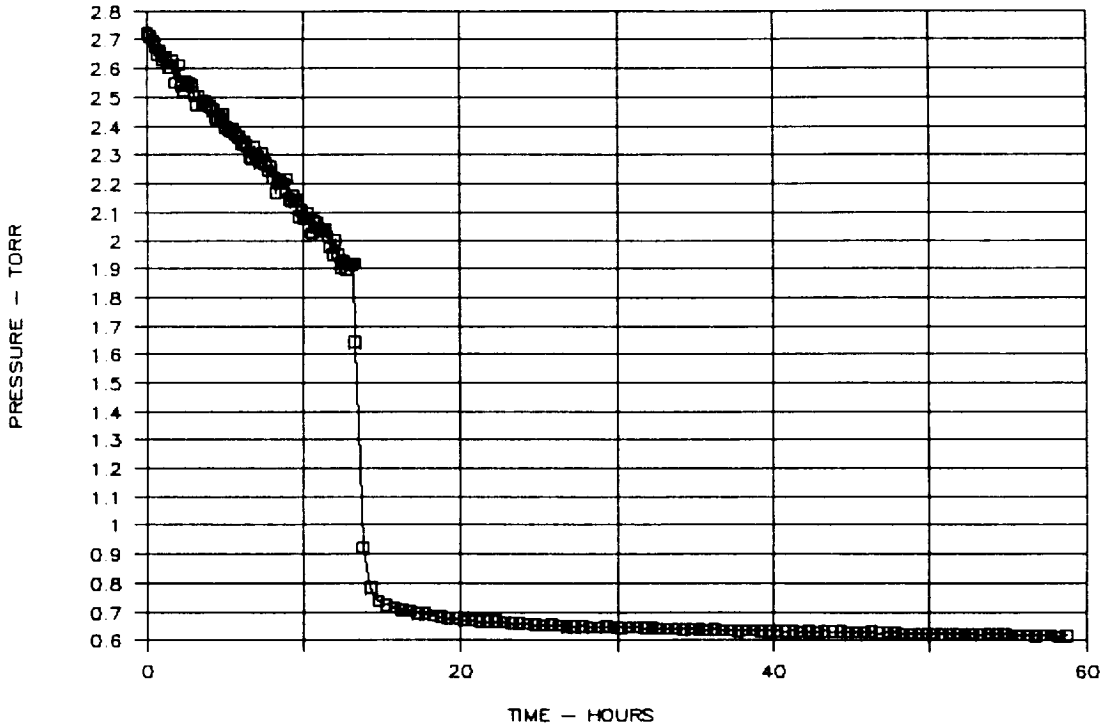

Figure 64. Results of Biosample Freezer Test on 11/28/90, Internal Pressure

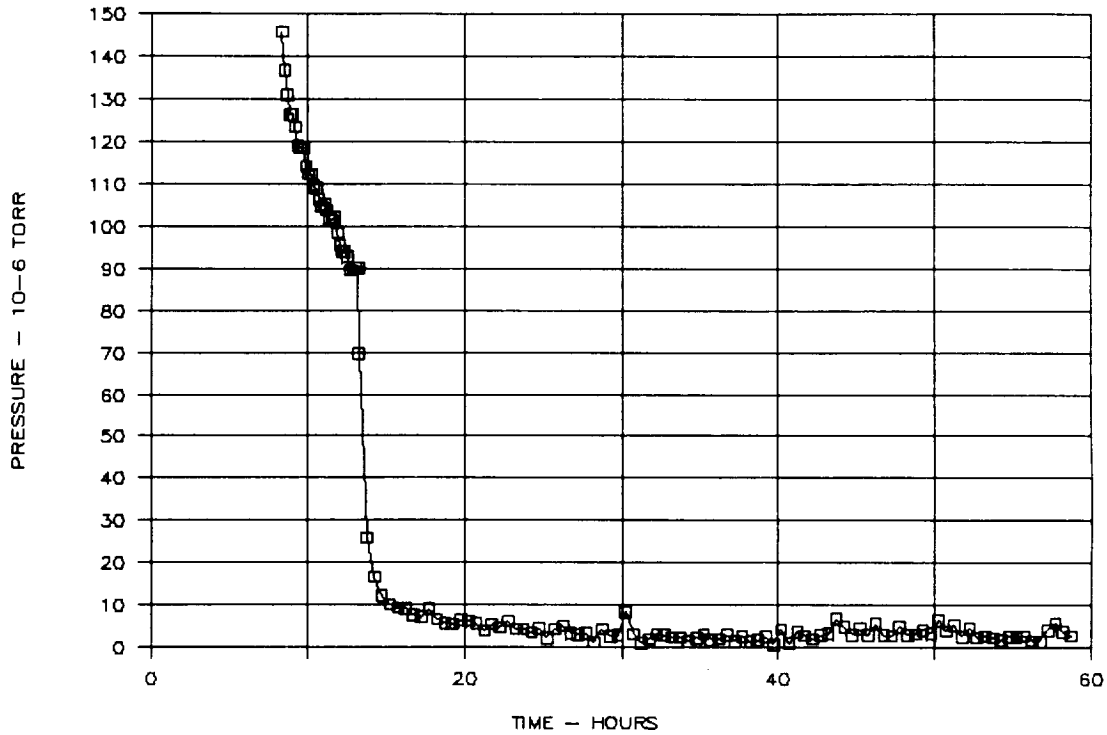

Figure 65. Results of Biosample Freezer Test on 11/28/90, MLI Pressure

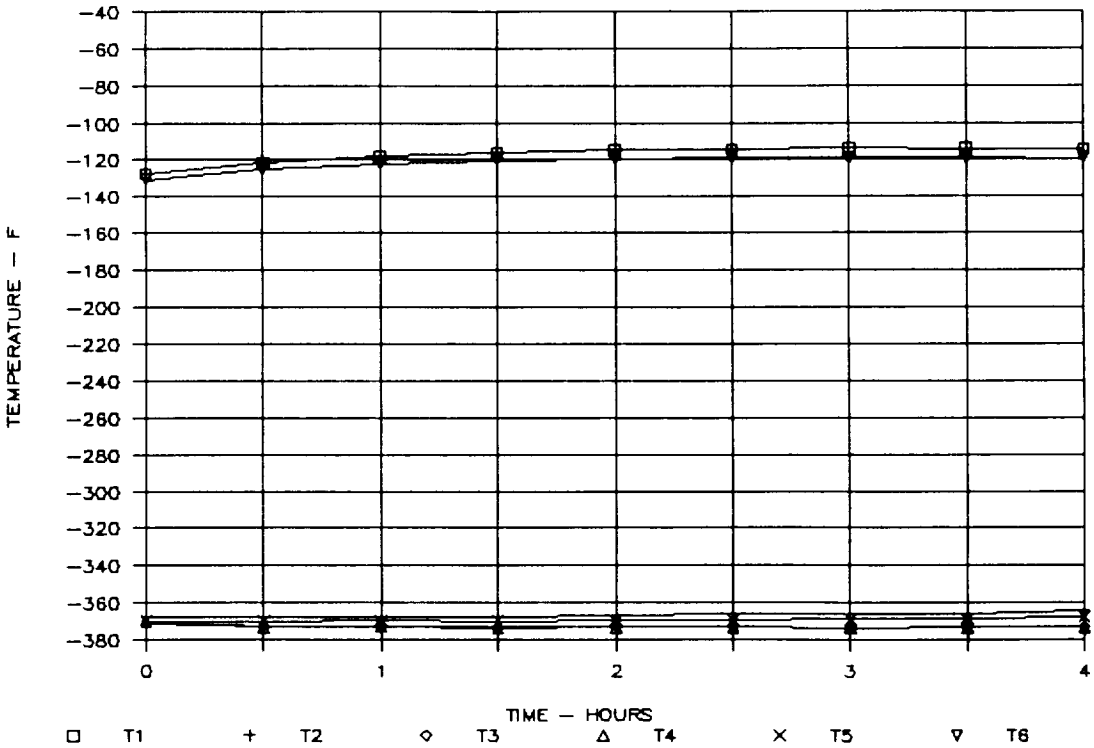

Figure 66. Results of Biosample Freezer Test on 11/30/90, TC1 Through TC6, First 4 Hours

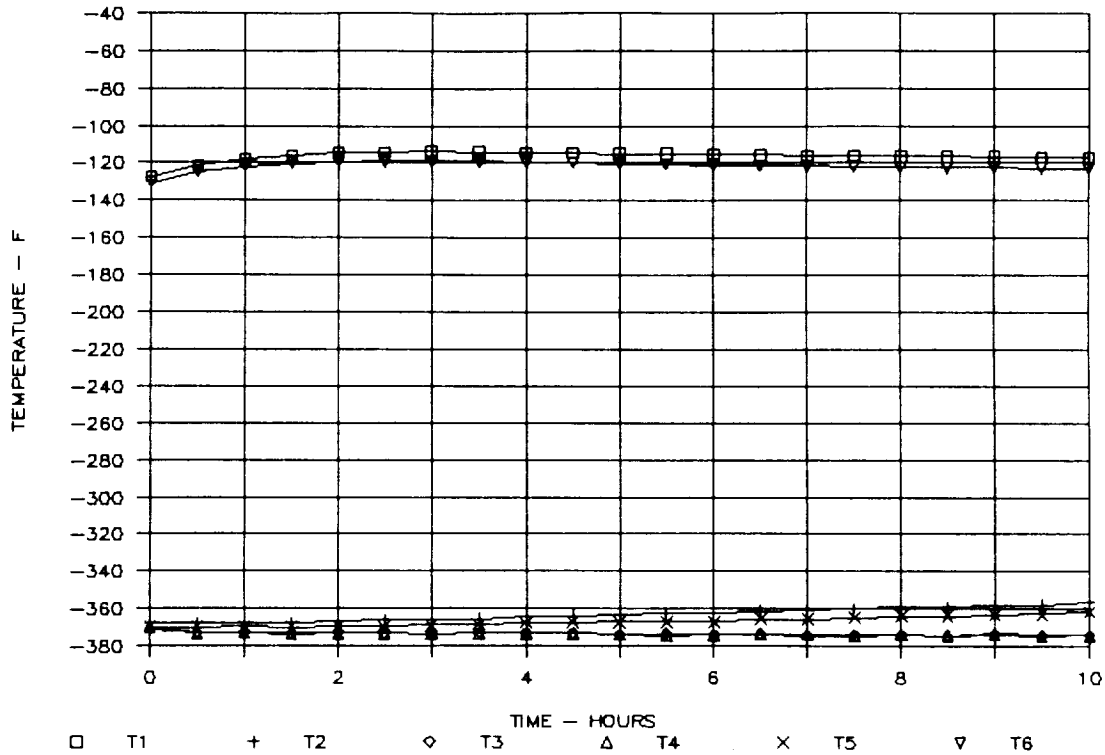

Figure 67. Results of Biosample Freezer Test on 11/30/90, TC1 through TC6, First 10 Hours

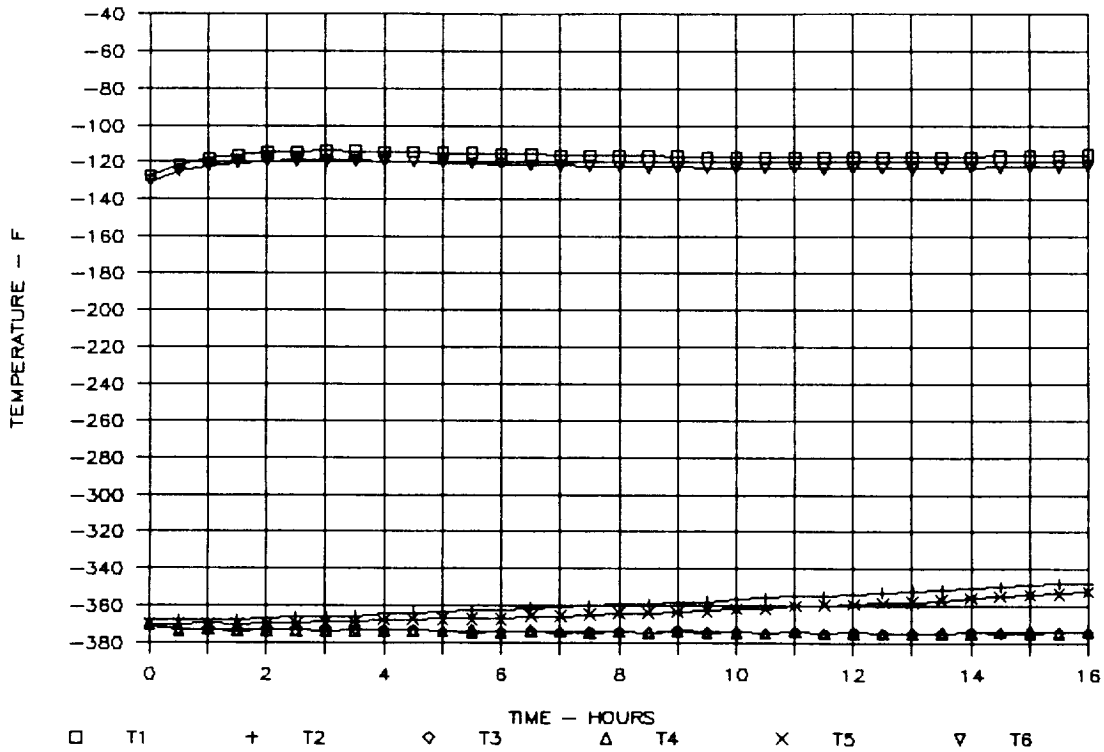

Figure 68. Results of Biosample Freezer Test on 11/30/90, TC1 Through TC6, First 16 Hours

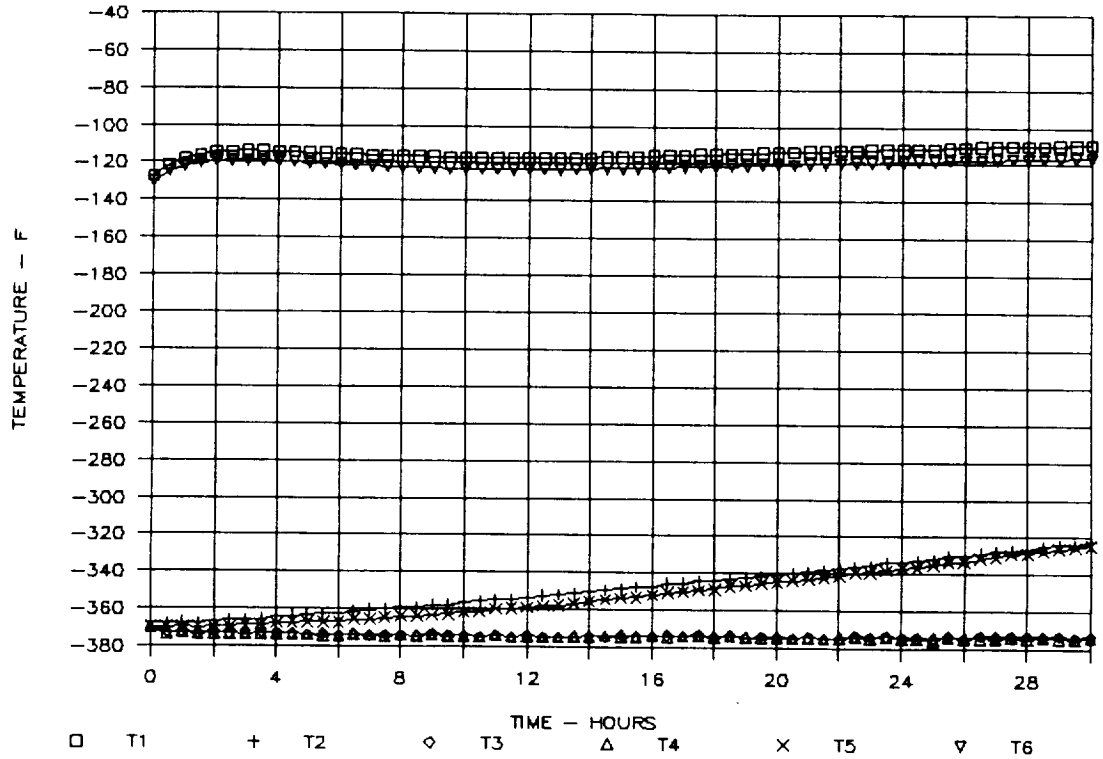

Figure 69. Results of Biosample Freezer Test on 11/30/90, TC1 through TC6, First 30 Hours

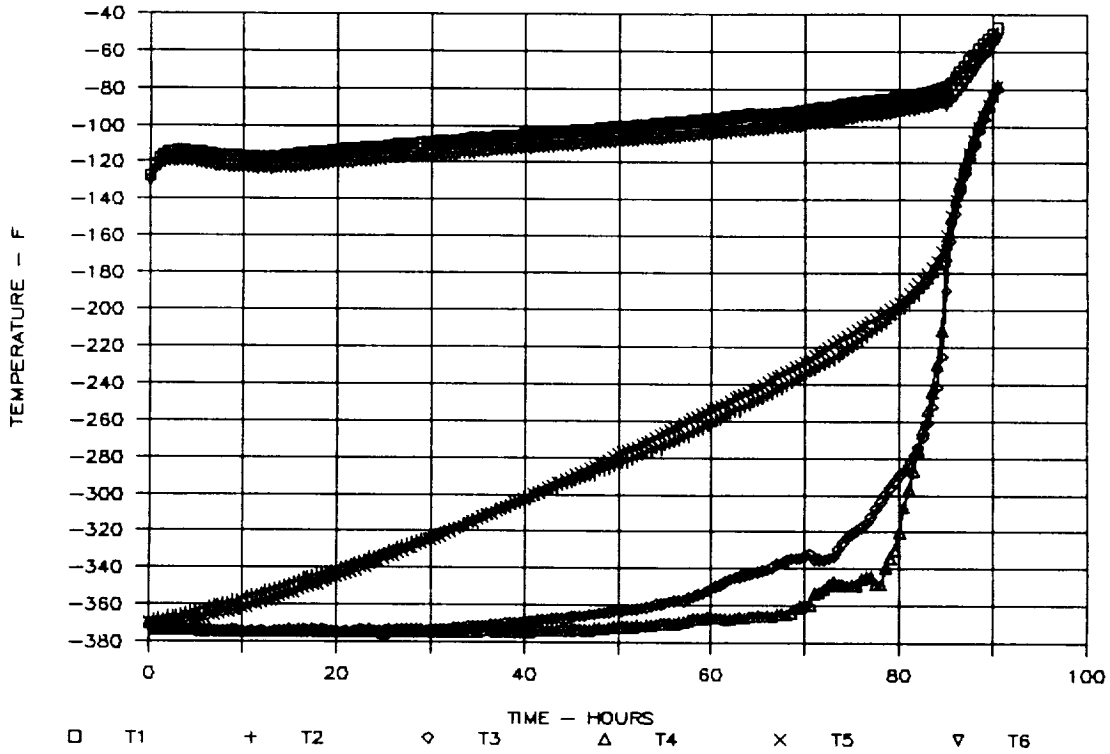

Figure 70. Results of Biosample Freezer Test on 11/30/90, TC1 Through TC6, First 91 Hours

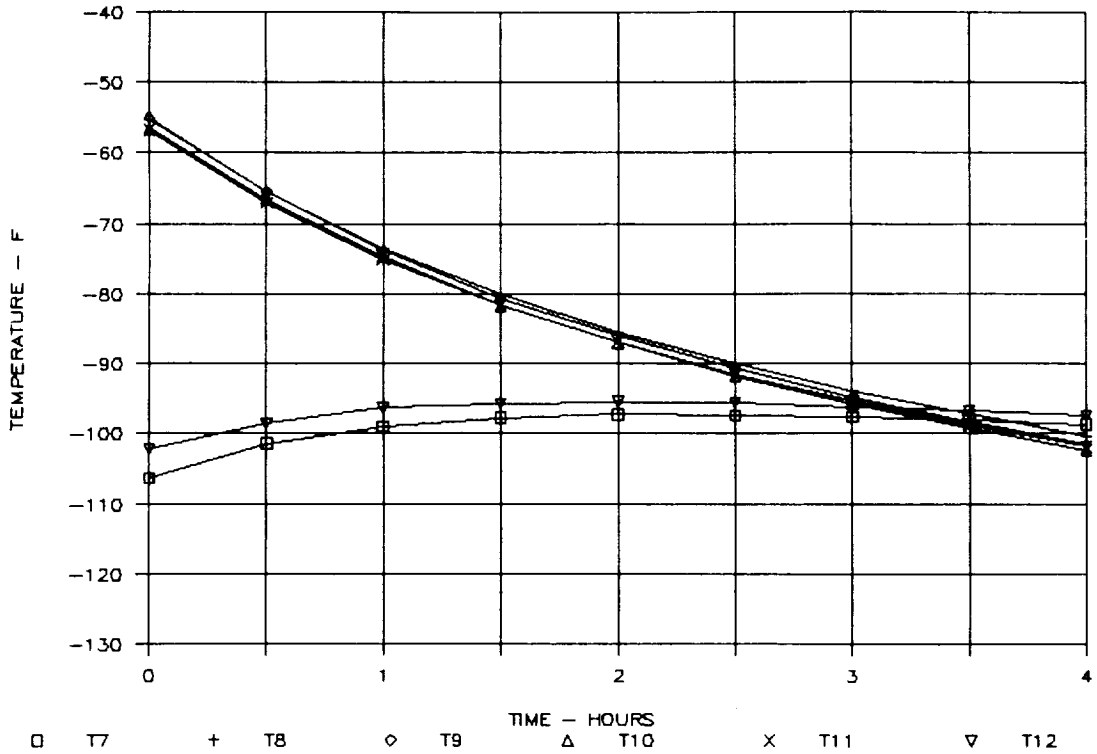

Figure 71. Results of Biosample Freezer Test on 11/30/90, TC7 through TC12, First 4 Hours

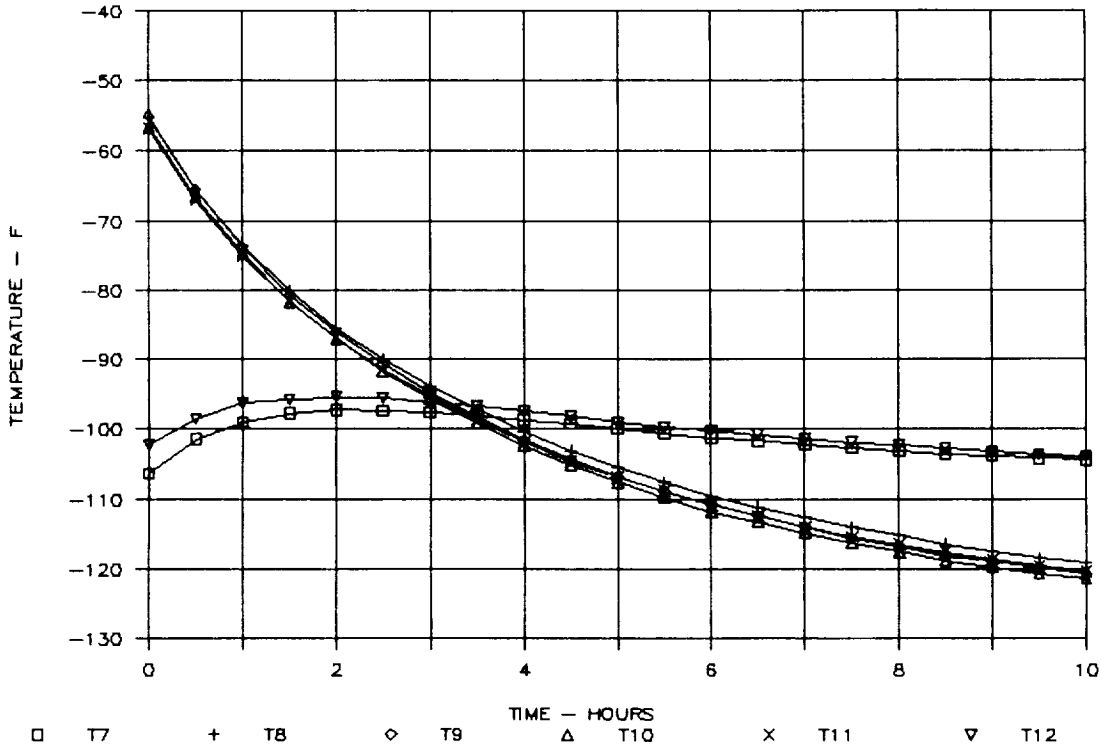

Figure 72. Results of Biosample Freezer Test on 11/30/90, TC7 Through TC12, First 10 Hours

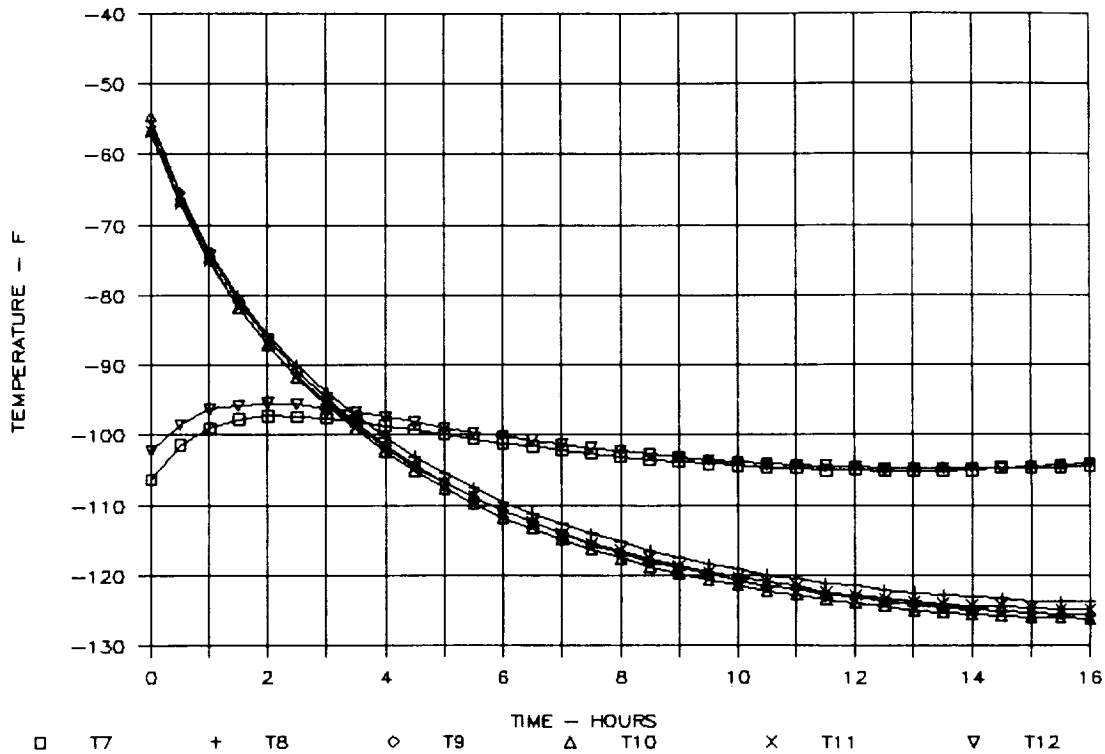

Figure 73. Results of Biosample Freezer Test on 11/30/90, TC7 through TC12, First 16 Hours

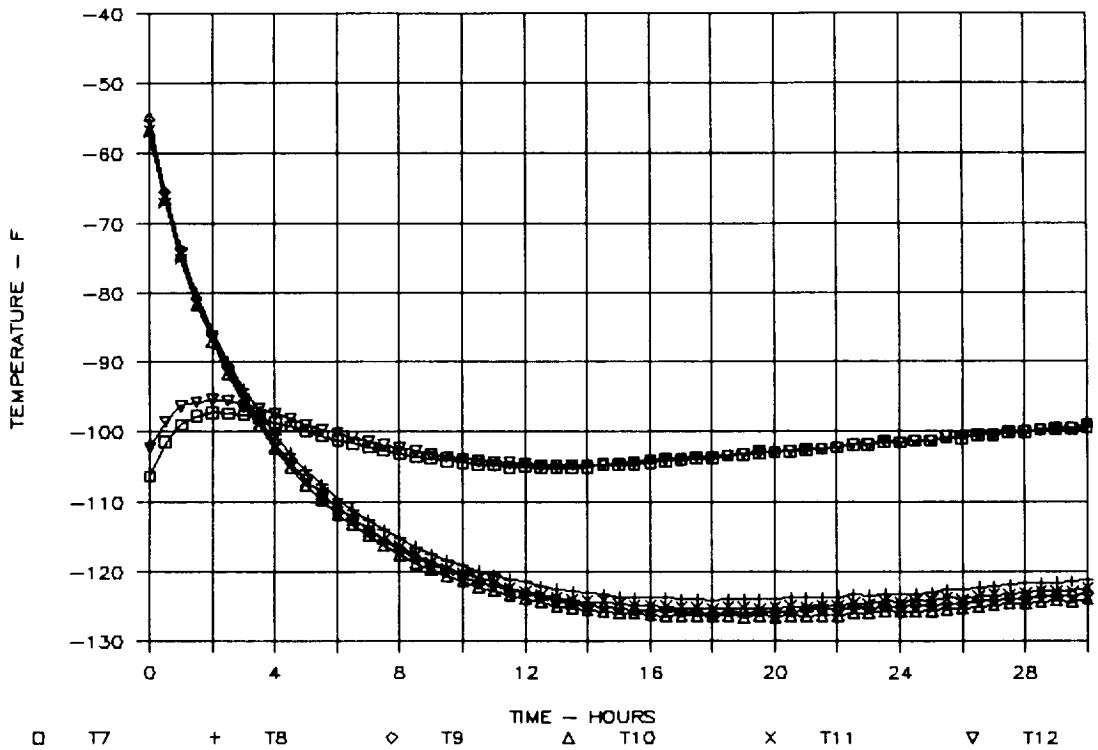

Figure 74. Results of Biosample Freezer Test on 11/30/90, TC7 Through TC12, First 30 Hours

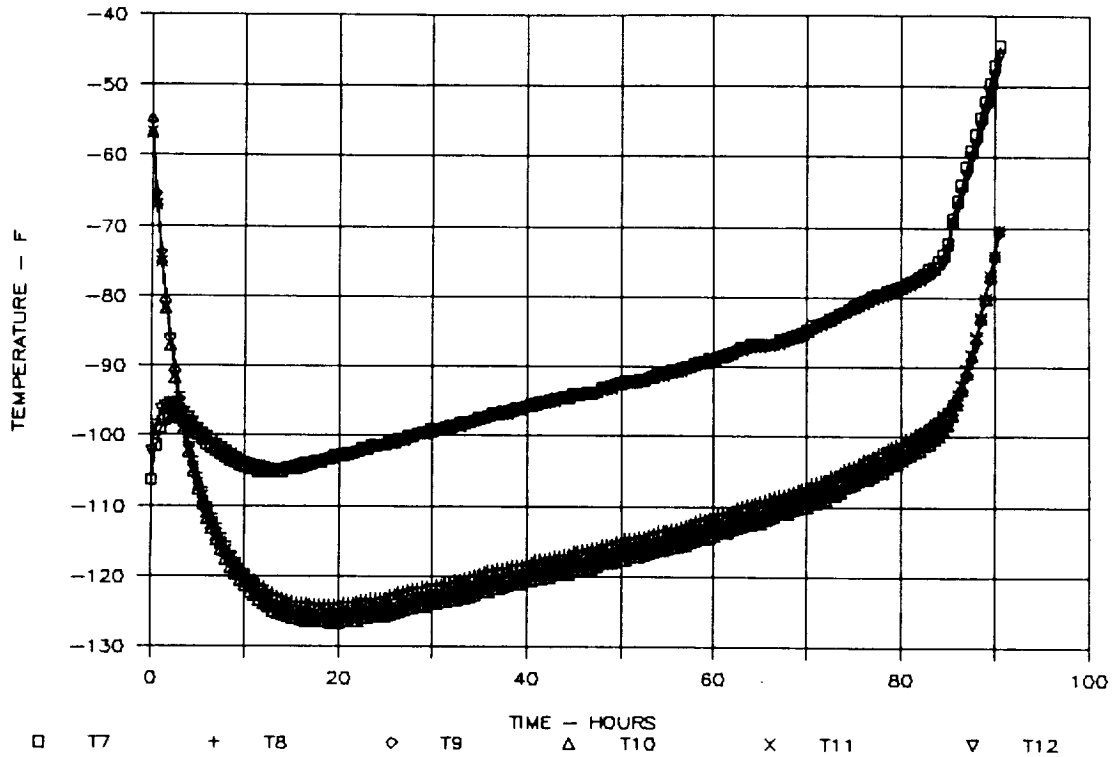

Figure 75. Results of Biosample Freezer Test on 11/30/90, TC7 through TC12, First 91 Hours

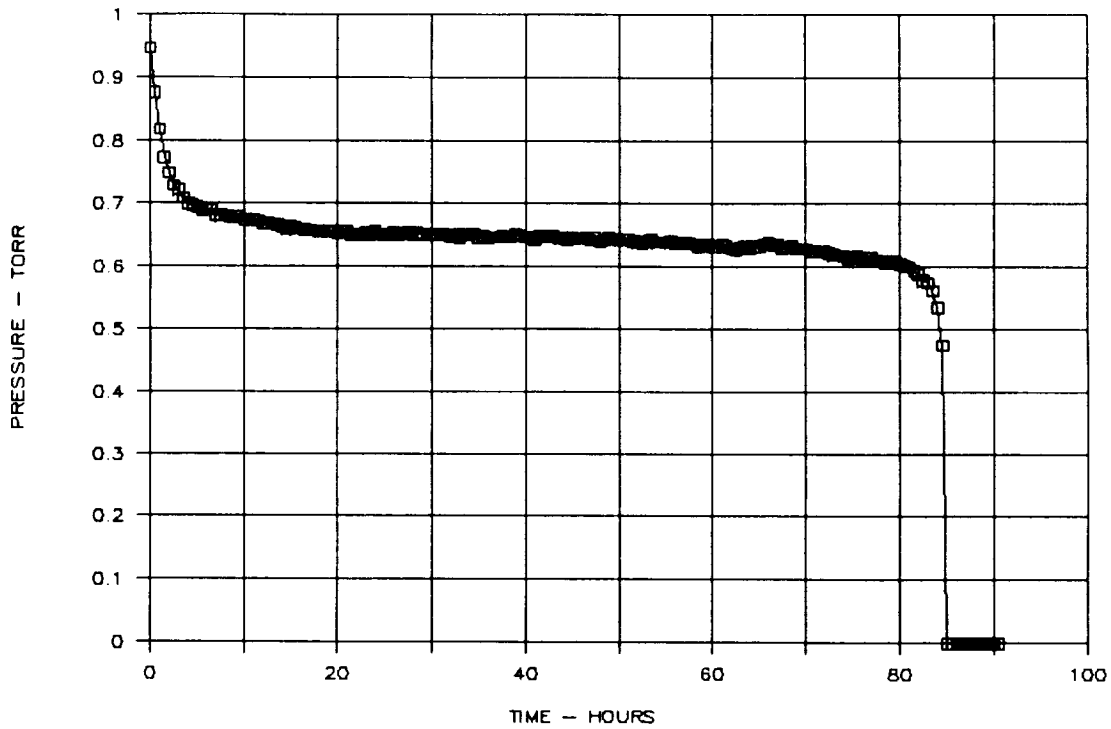

Figure 76. Results of Biosample Freezer Test on 11/30/90, Internal Pressure

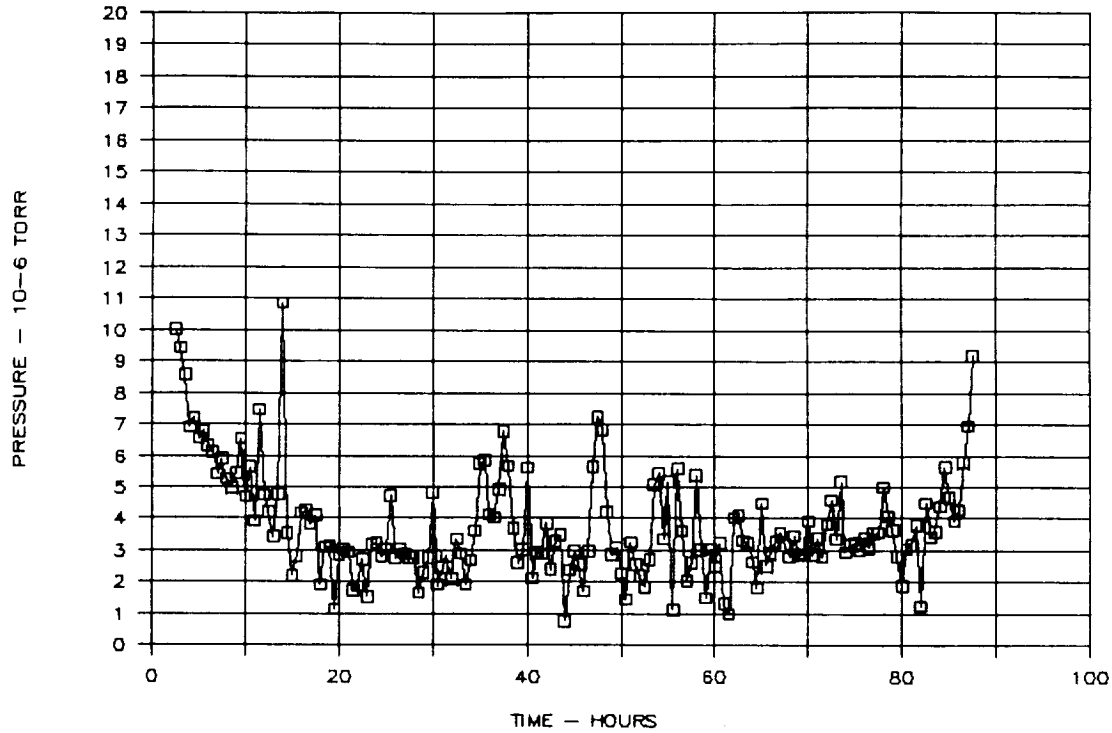

Figure 77. Results of Biosample Freezer Test on 11/30/90, MLI Pressure

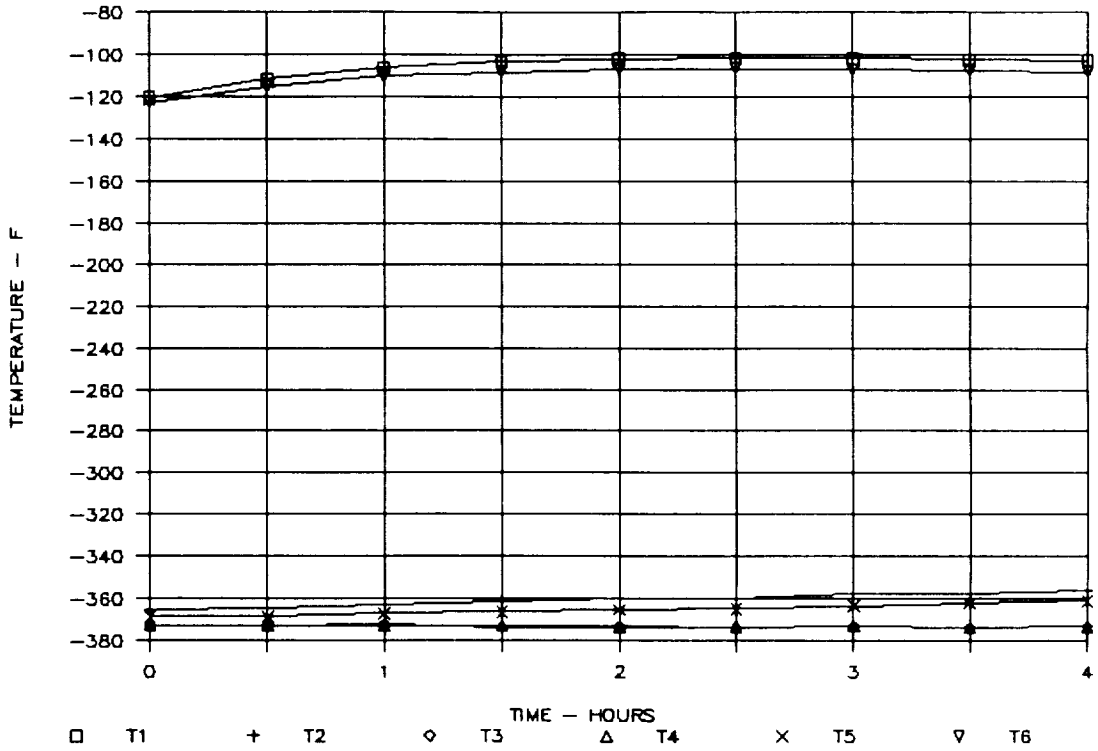

Figure 78. Results of Biosample Freezer Test on 12/4/90, TC1 through TC6, First 4 Hours

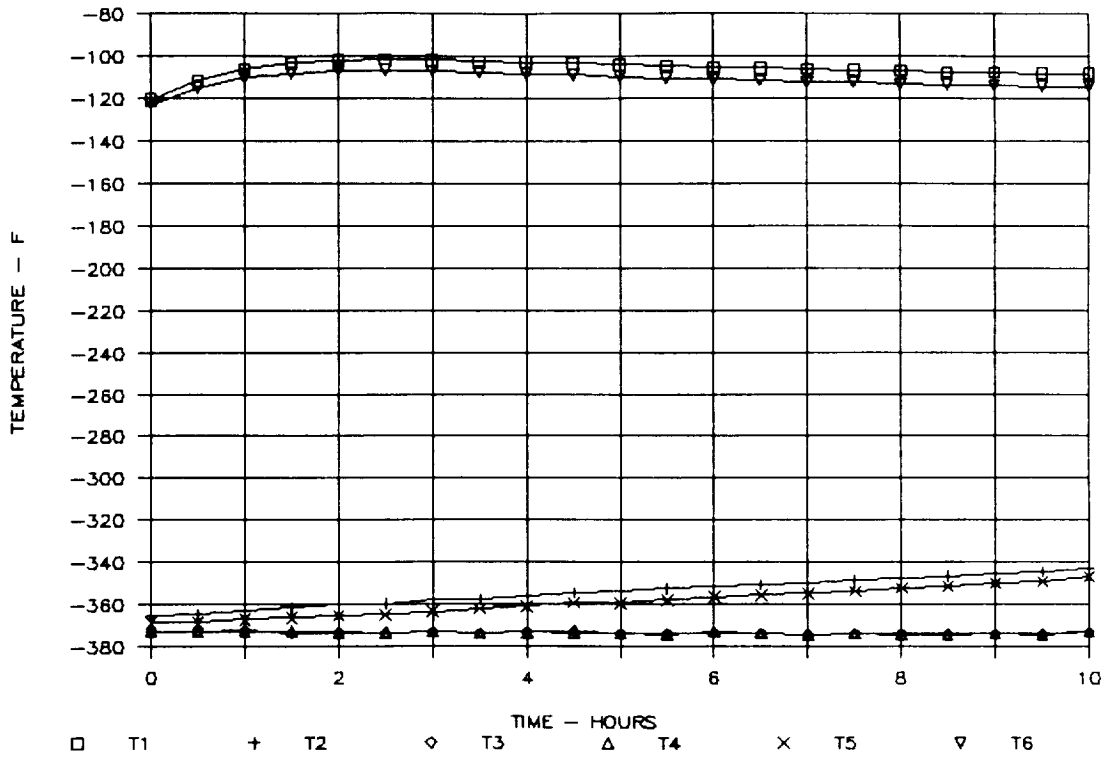

Figure 79. Results of Biosample Freezer Test on 12/4/90, TC1 through TC6, First 10 Hours

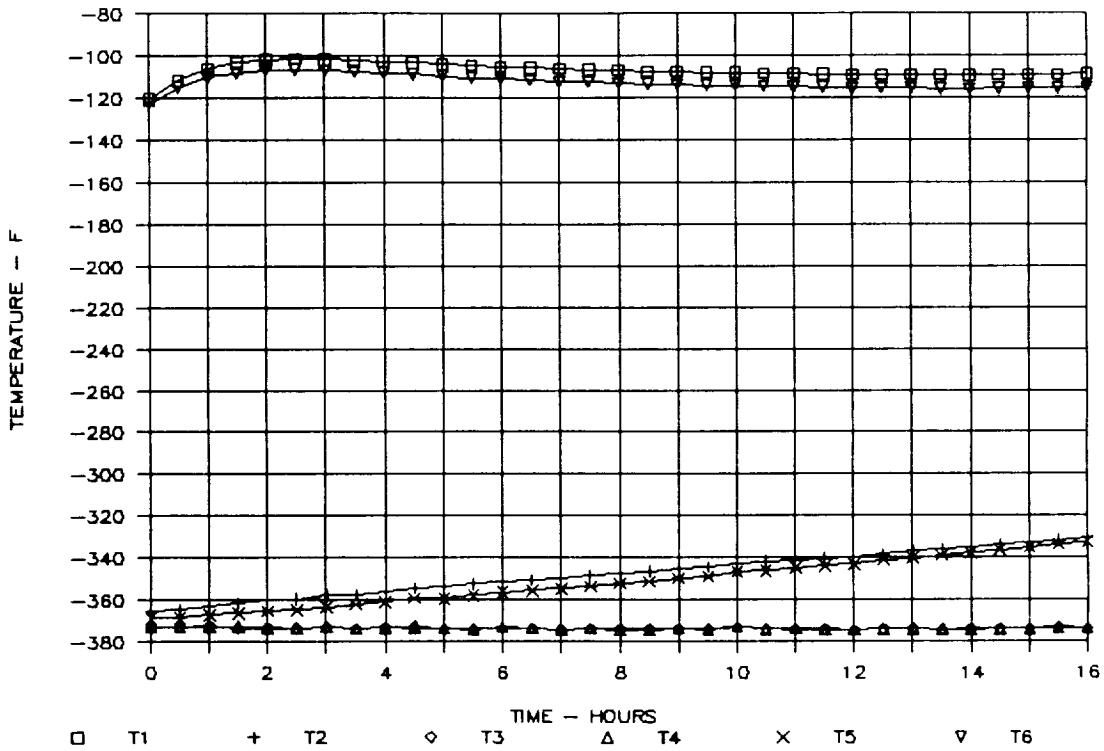

Figure 80. Results of Biosample Freezer Test on 12/4/90, TC1 through TC6, First 16 Hours

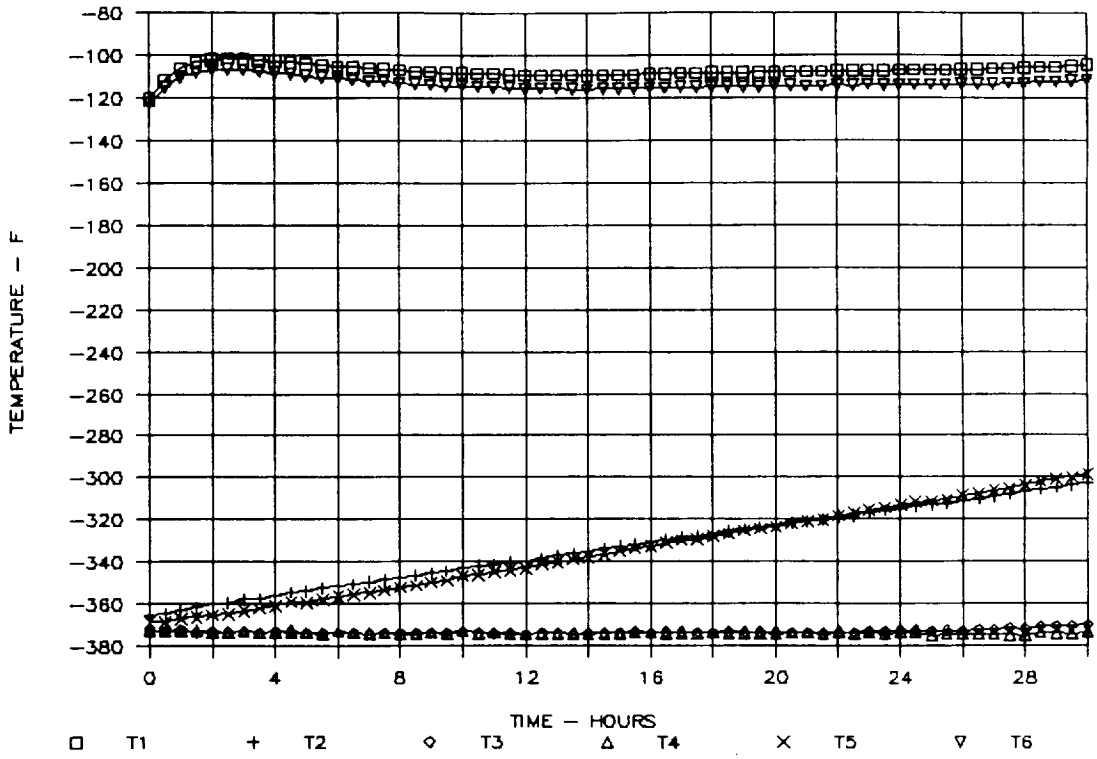

Figure 81. Results of Biosample Freezer Test on 12/4/90, TC1 through TC6, First 30 Hours

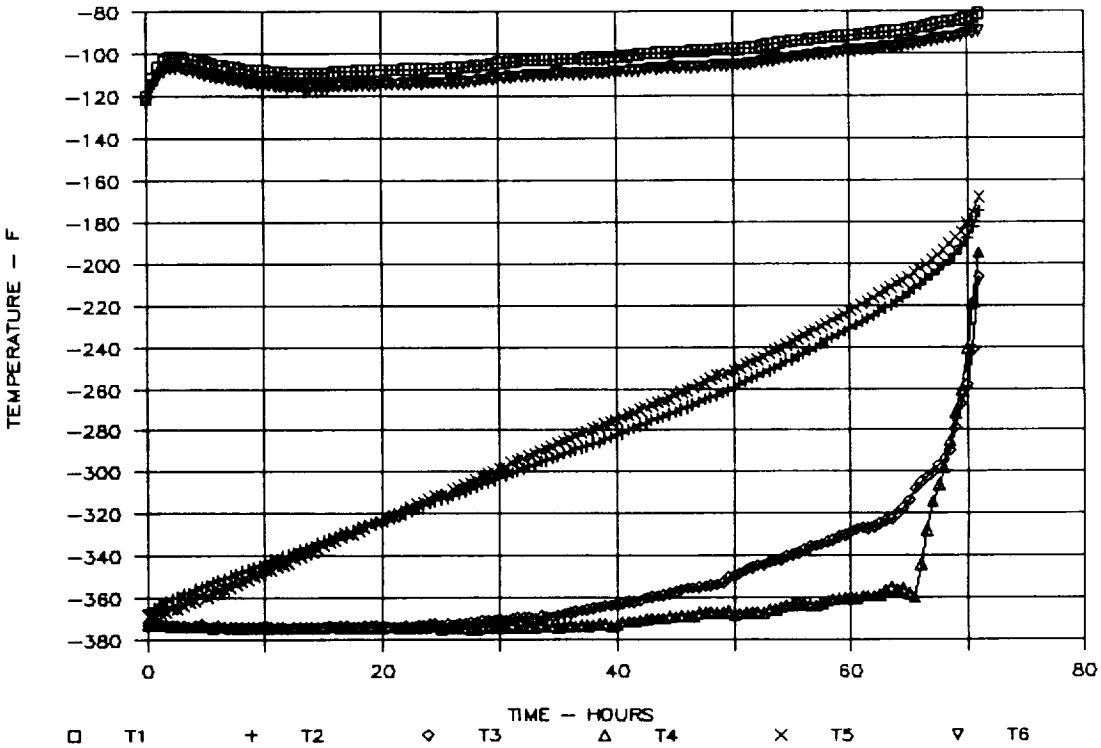

Figure 82. Results of Biosample Freezer Test on 12/4/90, TC1 through TC6, First 71 Hours

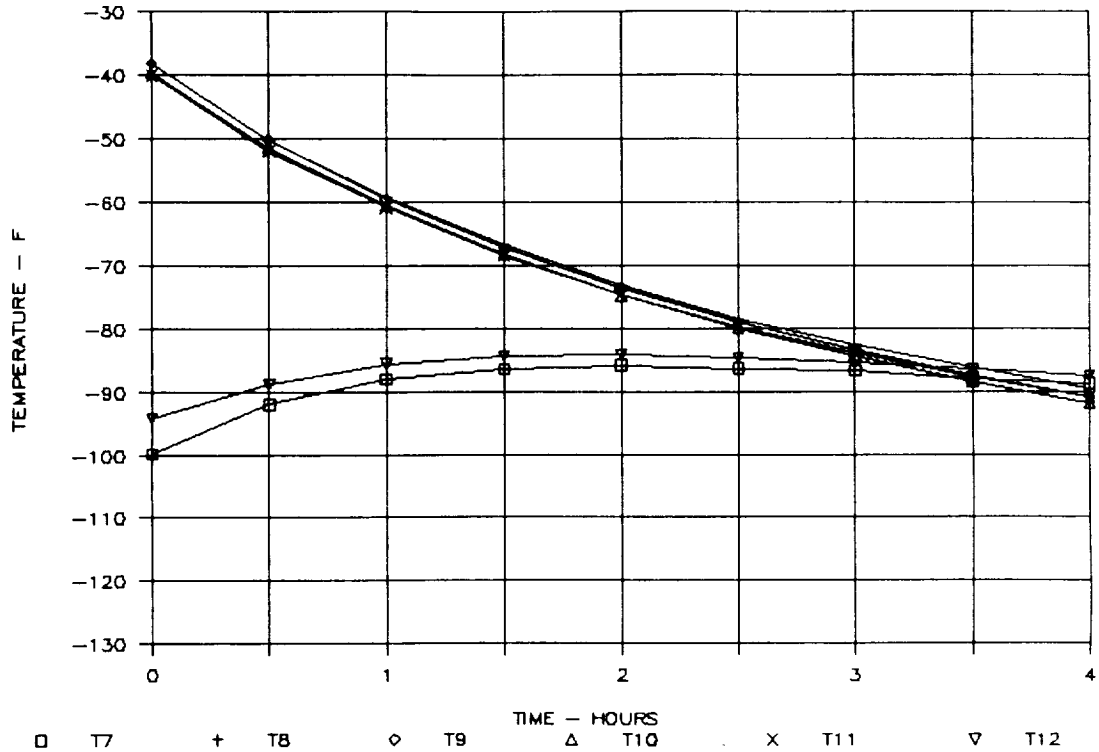

Figure 83. Results of Biosample Freezer Test on 12/4/90, TC7 through TC12, First 4 Hours

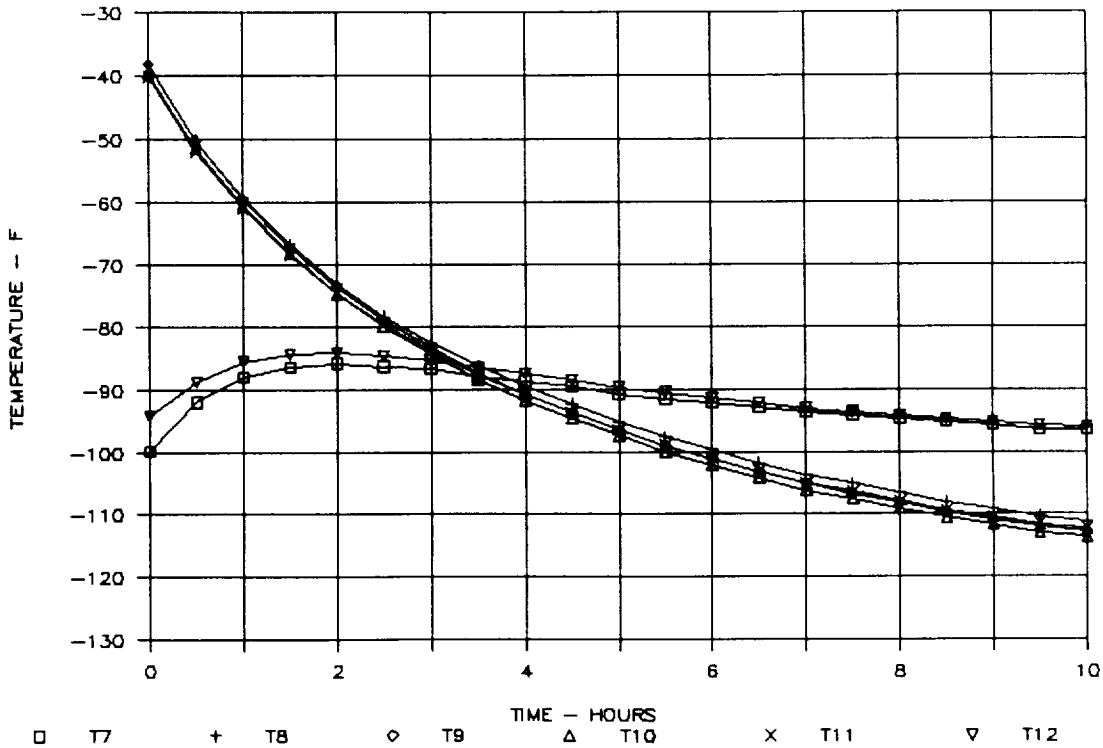

Figure 84. Results of Biosample Freezer Test on 12/4/90, TC7 through TC12, First 10 Hours

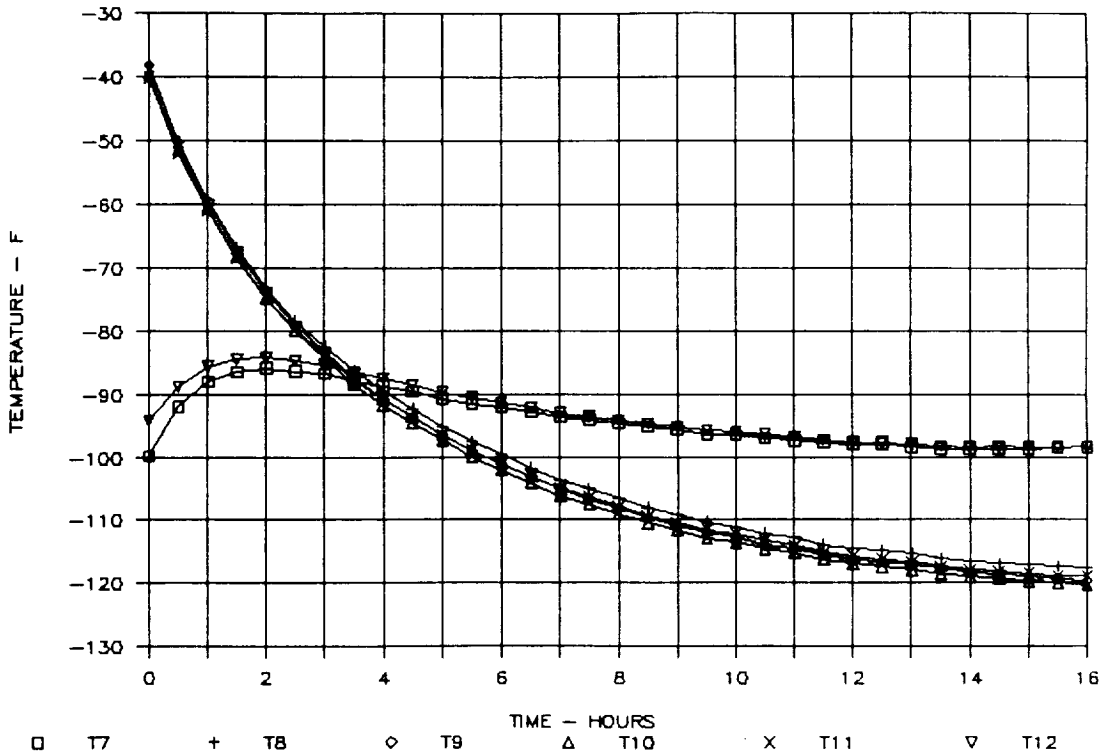

Figure 85. Results of Biosample Freezer Test on 12/4/90, TC7 through TC12, First 16 Hours

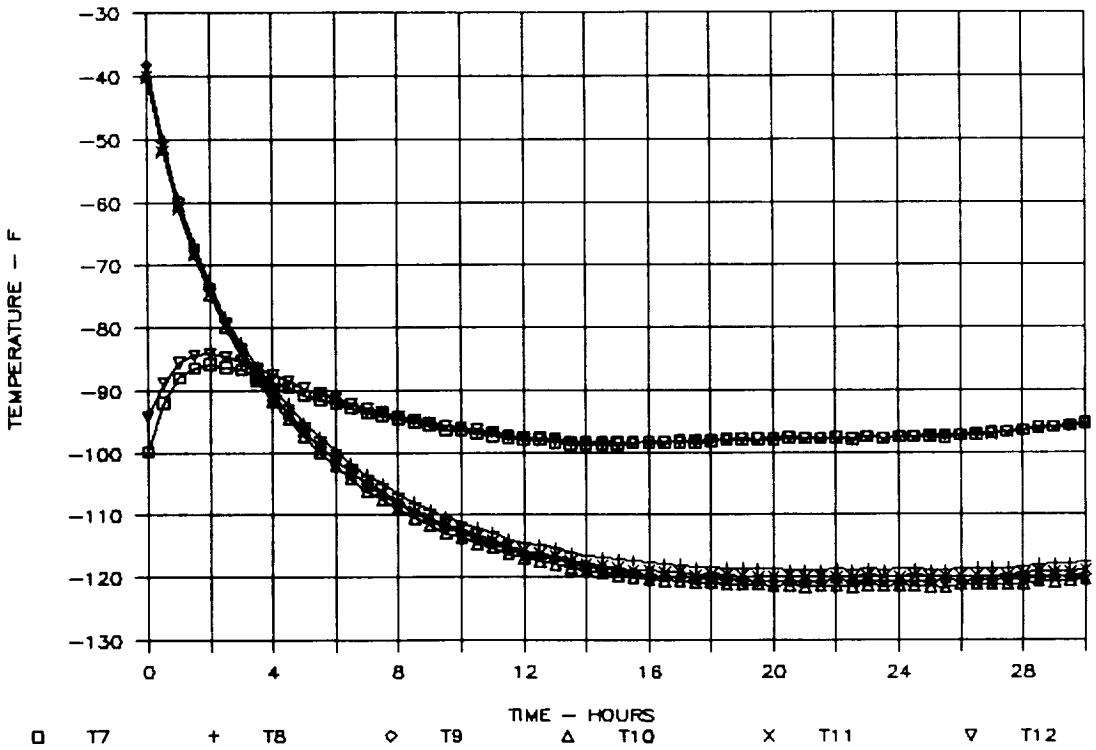

Figure 86. Results of Biosample Freezer Test on 12/4/90, TC7 through TC12, First 30 Hours

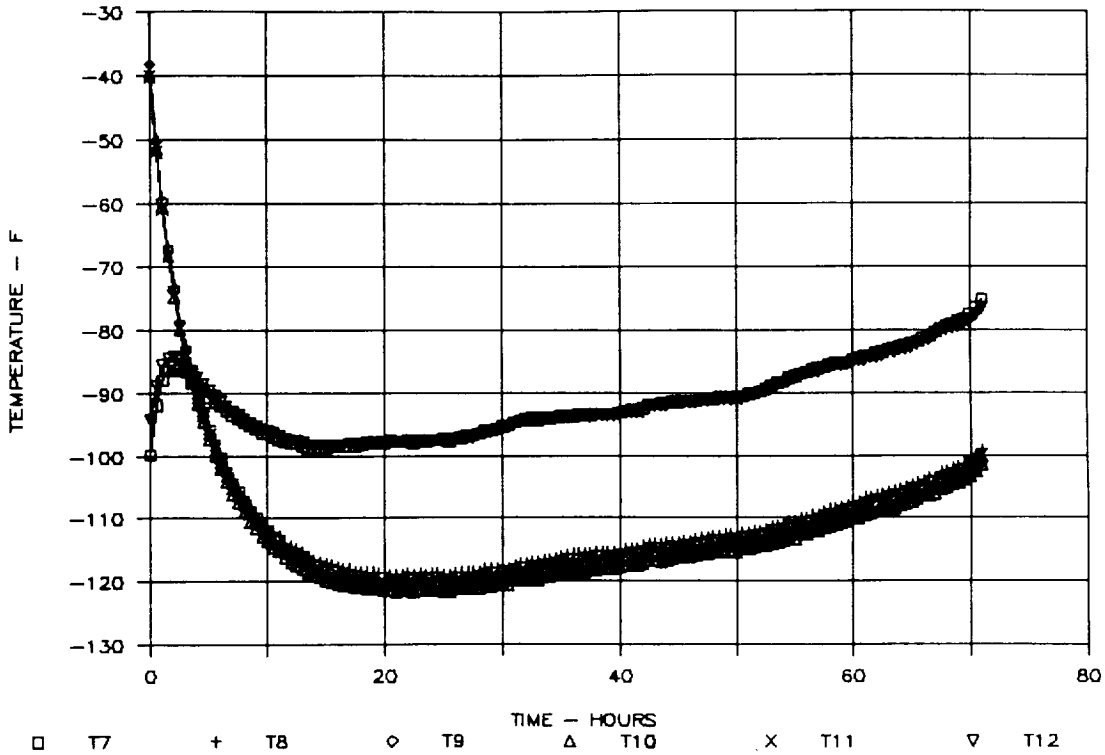

Figure 87. Results of Biosample Freezer Test on 12/4/90, TC7 through TC12, First 71 Hours

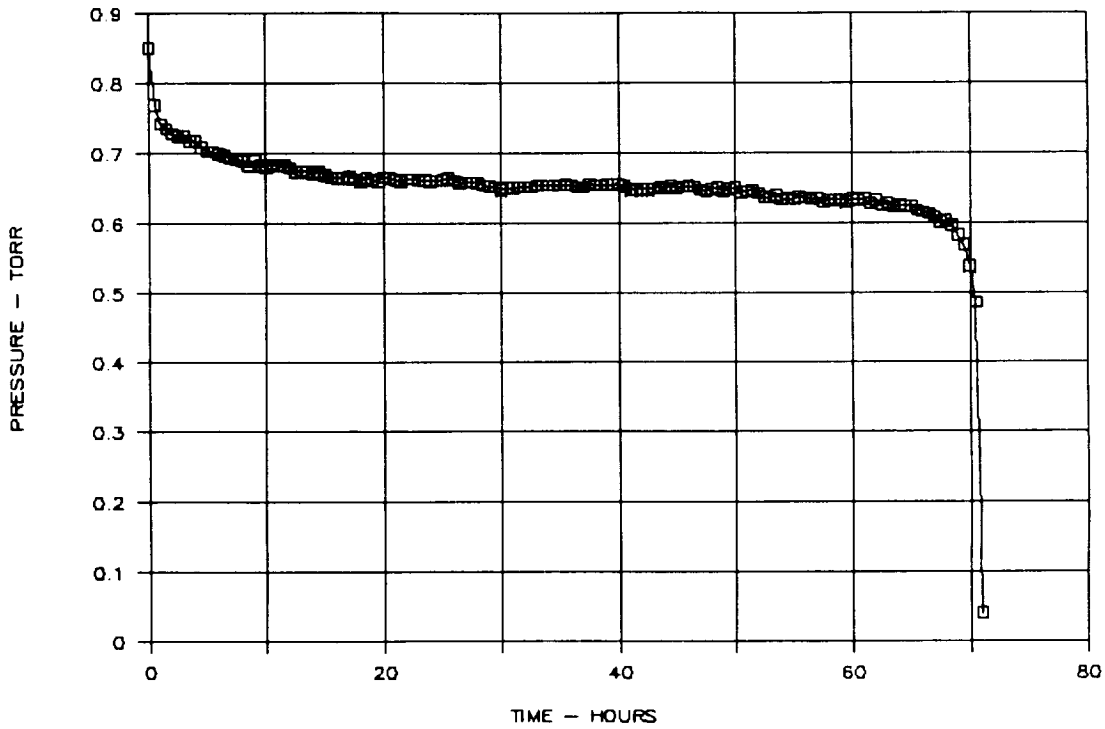

Figure 88. Results of Biosample Freezer Test on 12/4/90, Internal Pressure

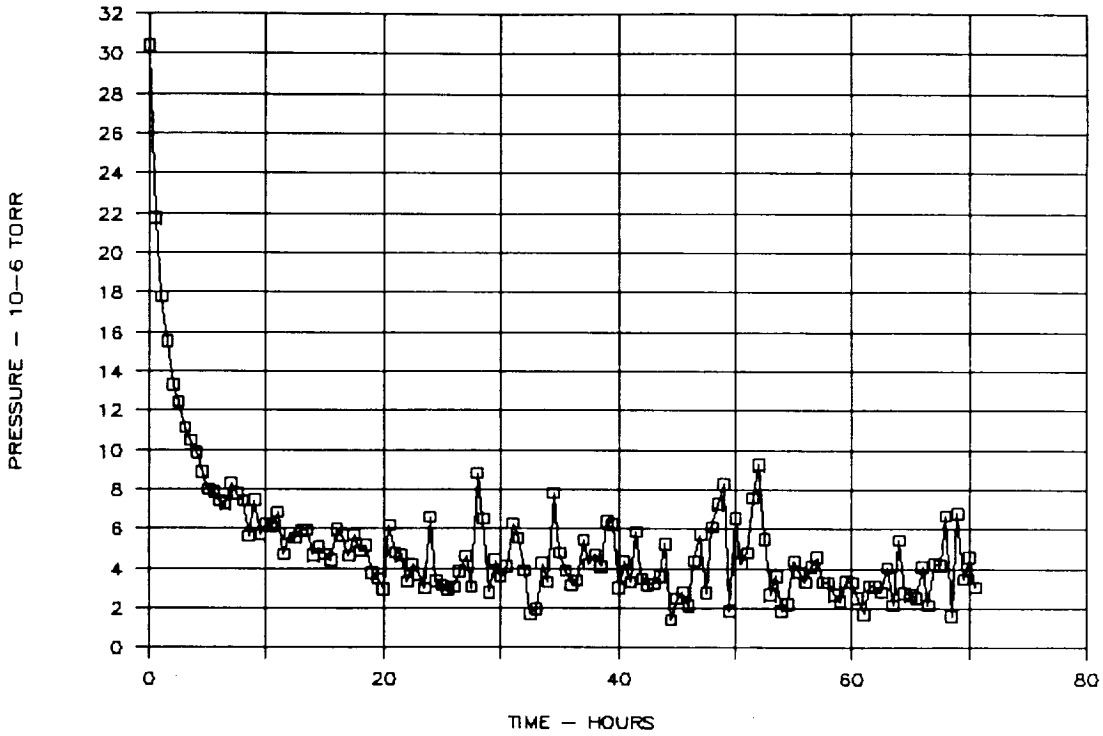

Figure 89. Results of Biosample Freezer Test on 12/4/90, MLI Pressure

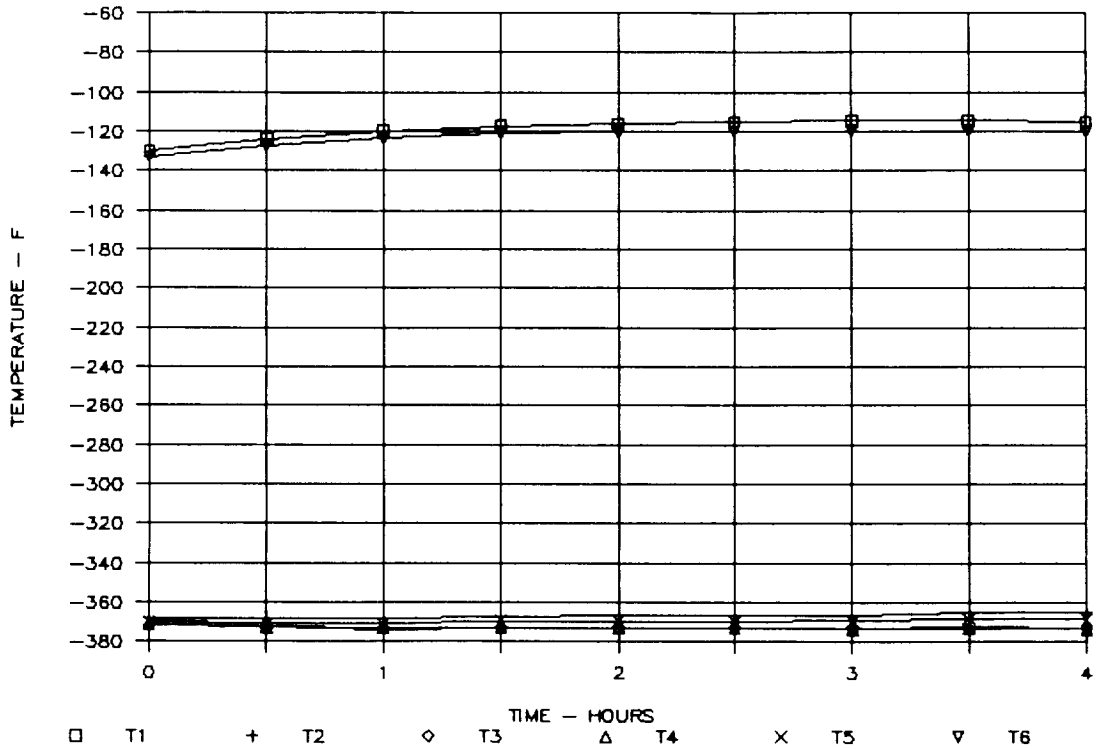

Figure 90. Results of Biosample Freezer Test on 12/7/90, TC1 through TC6, First 4 Hours

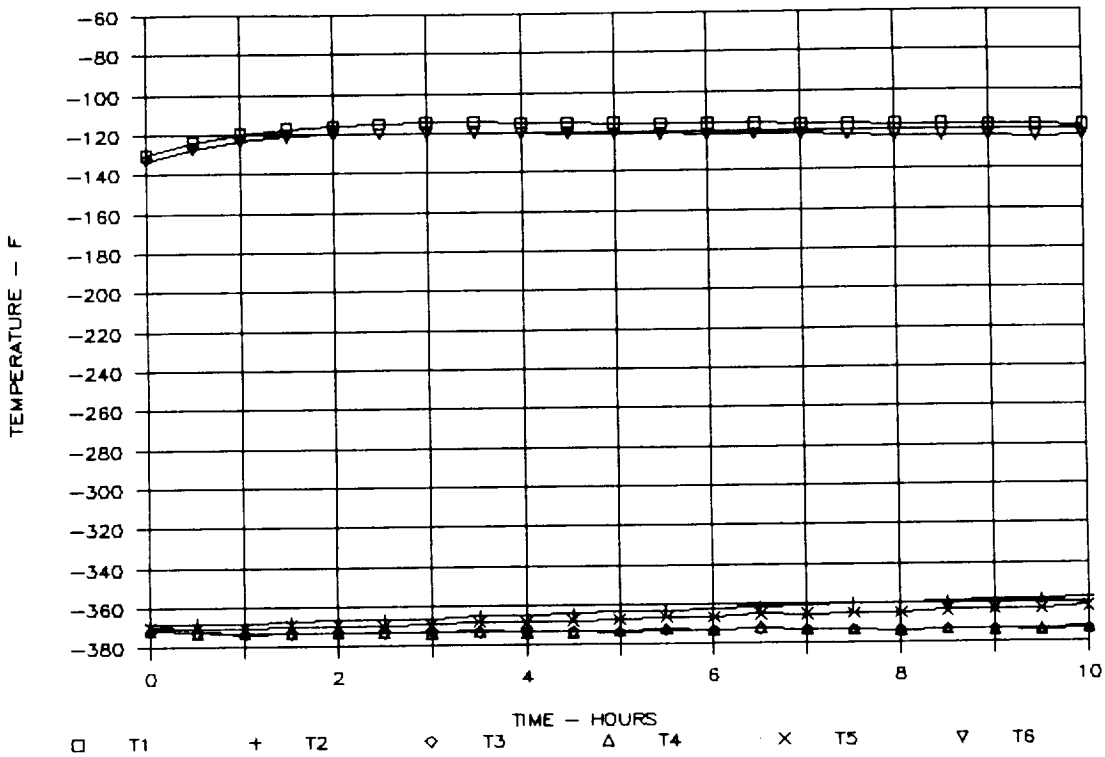

Figure 91. Results of Biosample Freezer Test on 12/7/90, TC1 through TC6, First 10 Hours

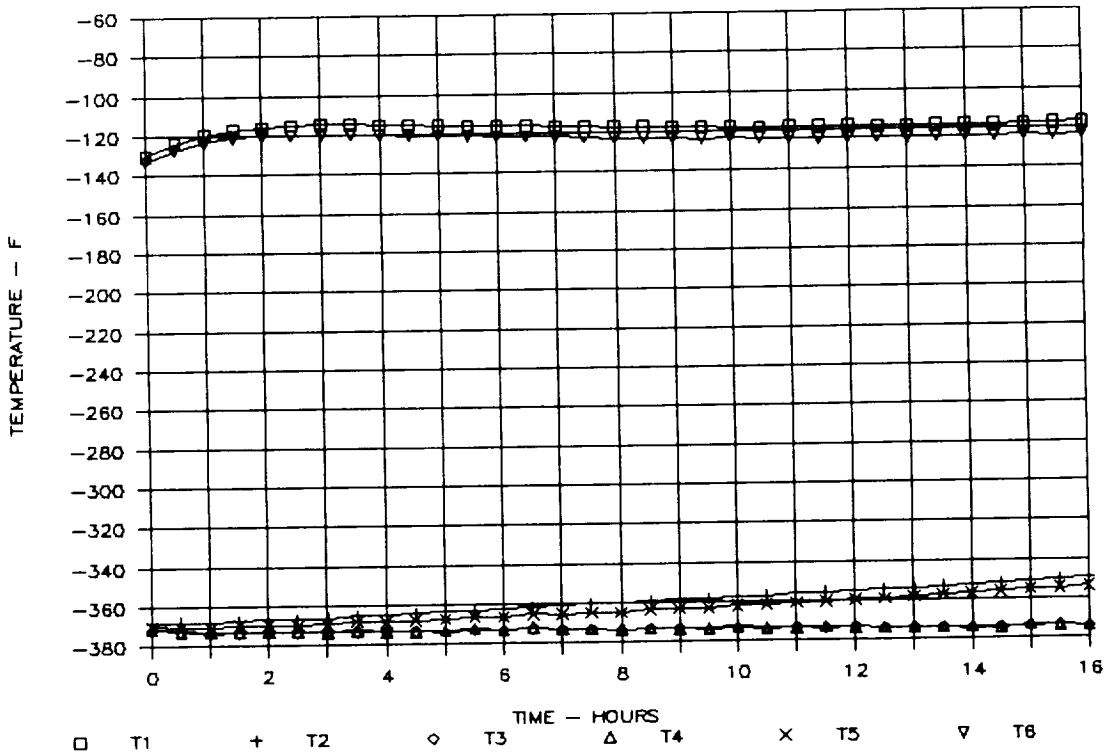

Figure 92. Results of Biosample Freezer Test on 12/7/90, TC1 through TC6, First 16 Hours

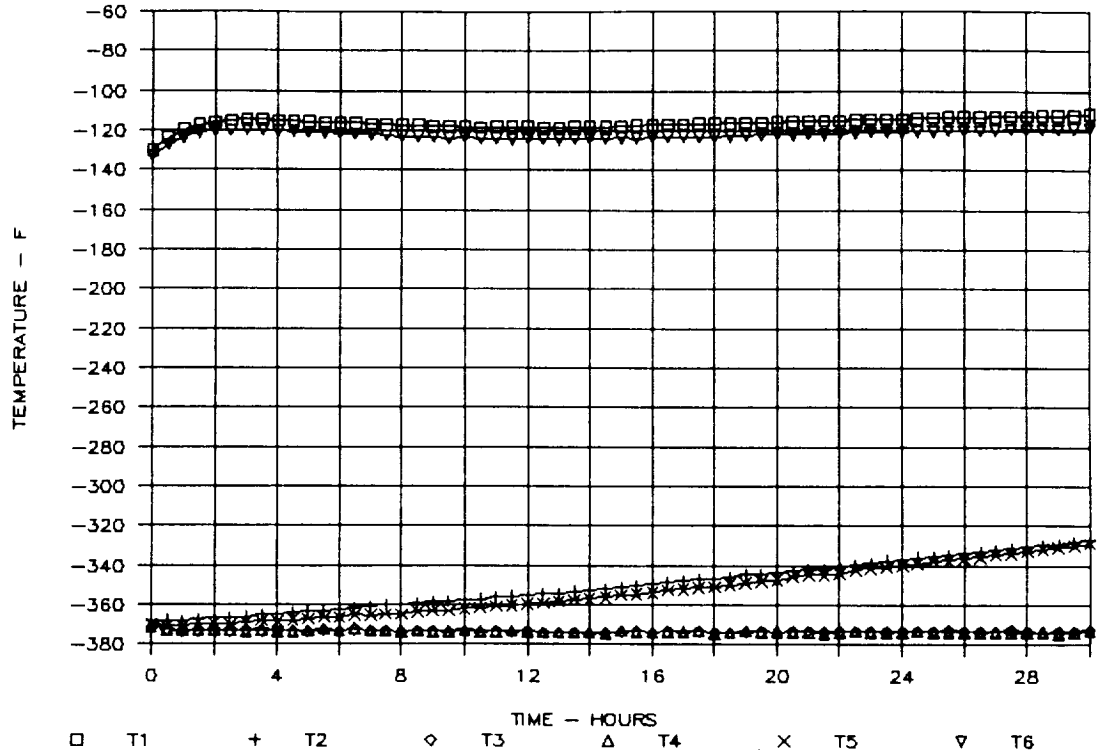

Figure 93. Results of Biosample Freezer Test on 12/7/90, TC1 through TC6, First 30 Hours

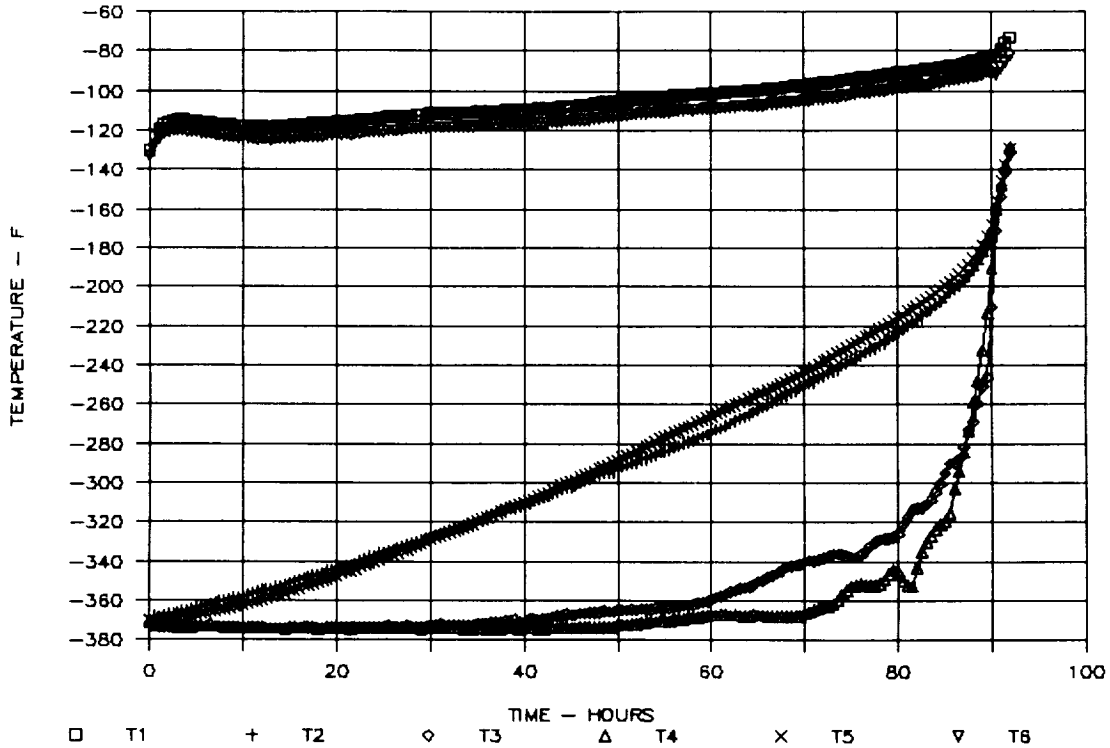

Figure 94. Results of Biosample Freezer Test on 12/7/90, TC1 through TC6, First 92 Hours

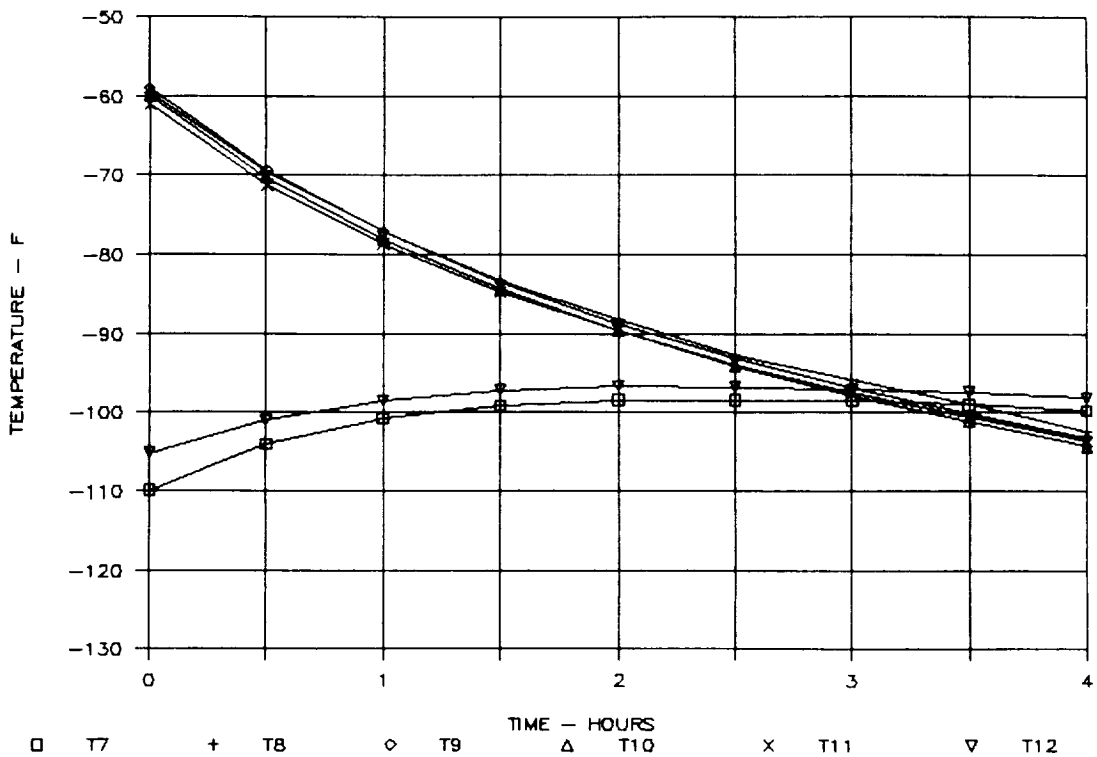

Figure 95. Results of Biosample Freezer Test on 12/7/90, TC7 through TC12, First 4 Hours

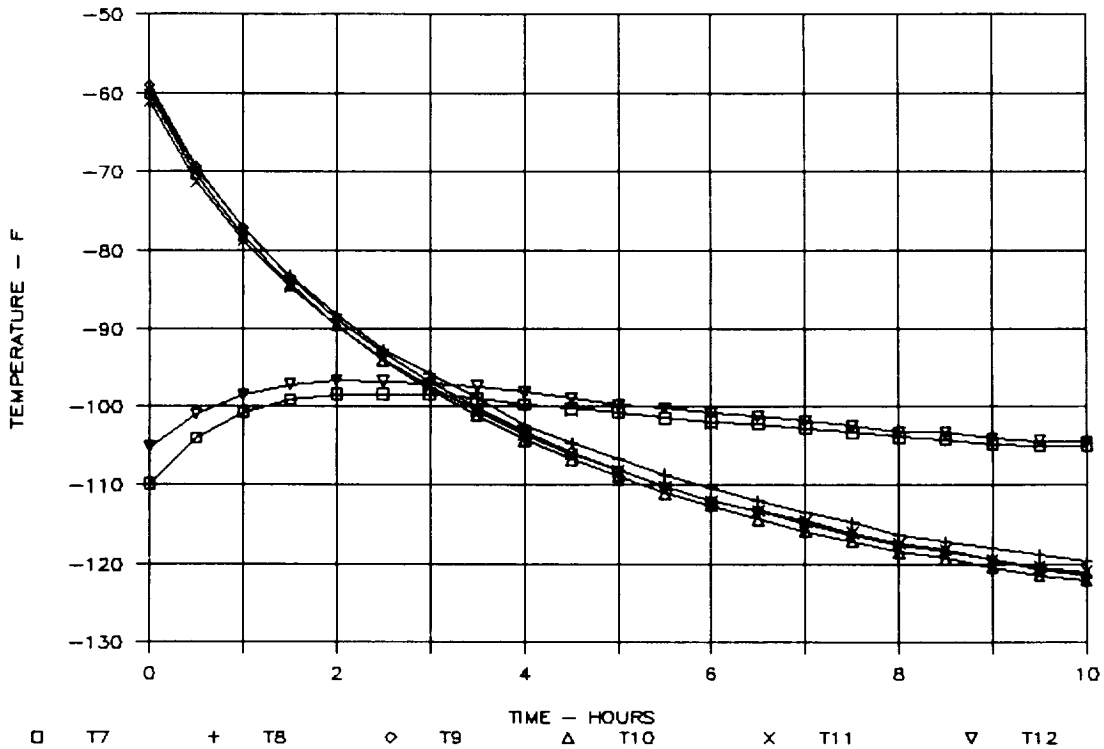

Figure 96. Results of Biosample Freezer Test on 12/7/90, TC7 through TC12, First 10 Hours

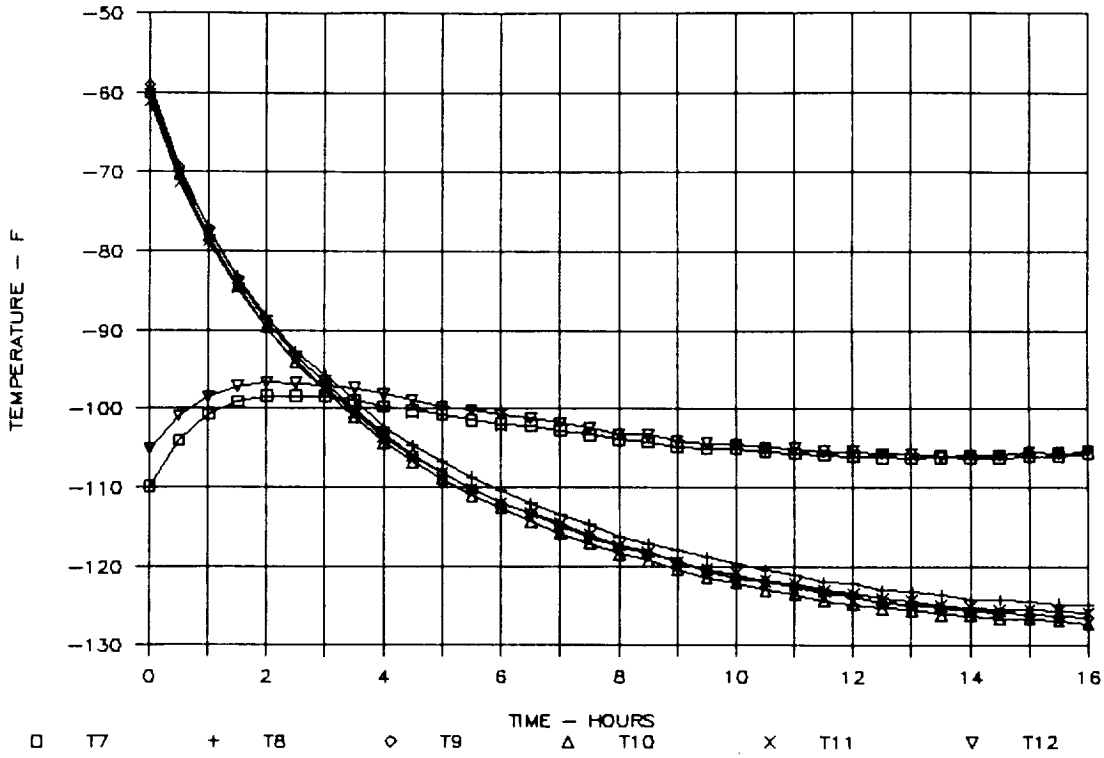

Figure 97. Results of Biosample Freezer Test on 12/7/90, TC7 through TC12, First 16 Hours

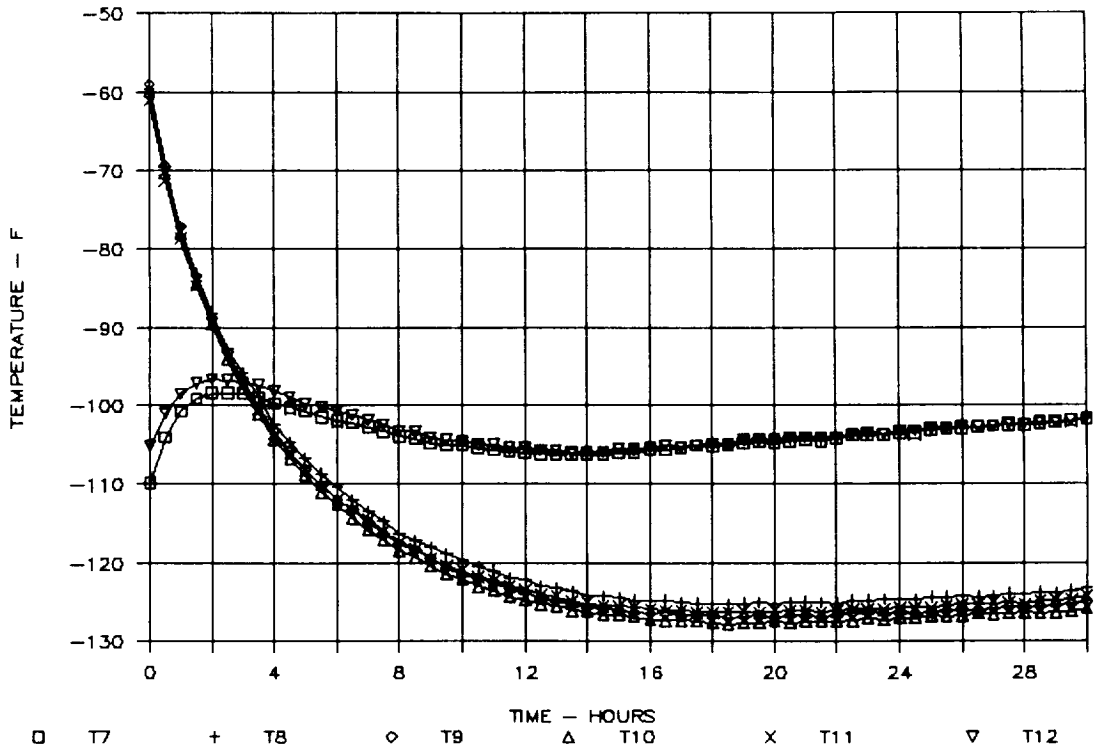

Figure 98. Results of Biosample Freezer Test on 12/7/90, TC7 through TC12, First 30 Hours

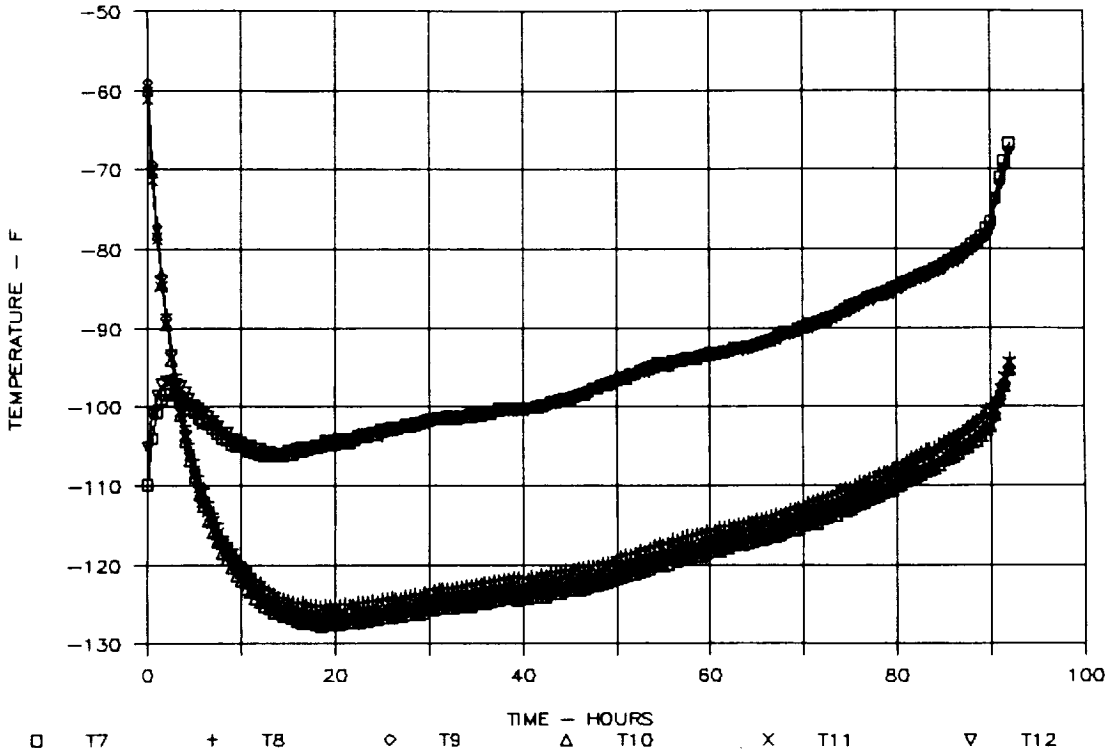

Figure 99. Results of Biosample Freezer Test on 12/7/90, TC7 through TC12, First 92 Hours

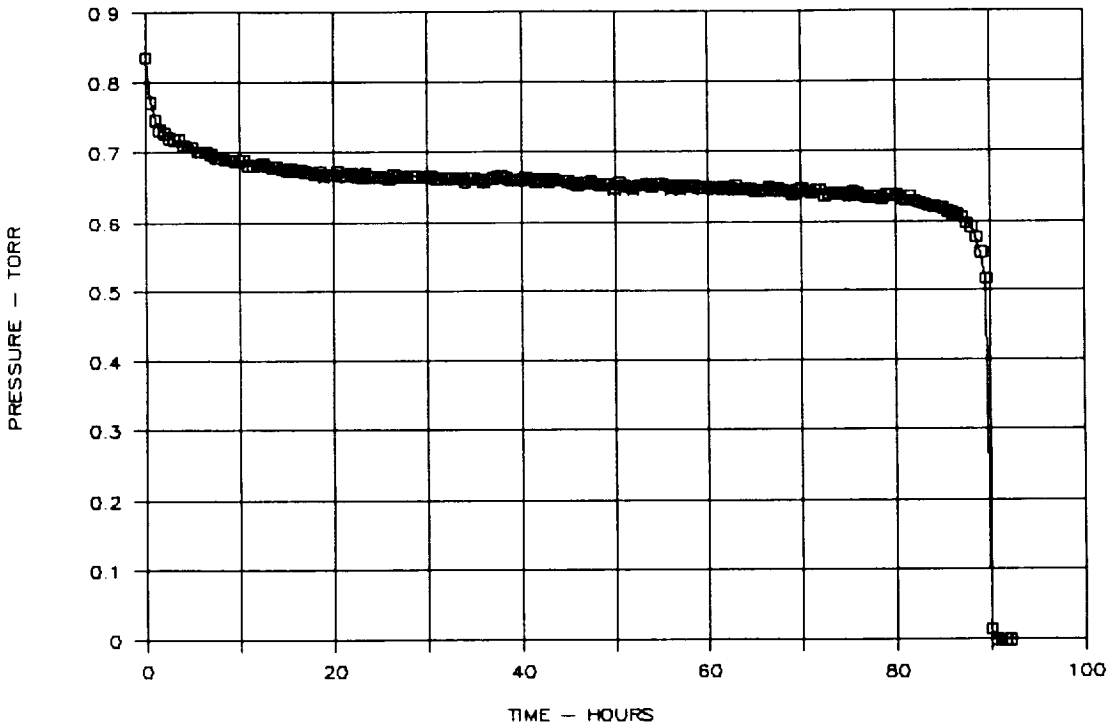

Figure 100. Results of Biosample Freezer Test on 12/7/90, Internal Pressure

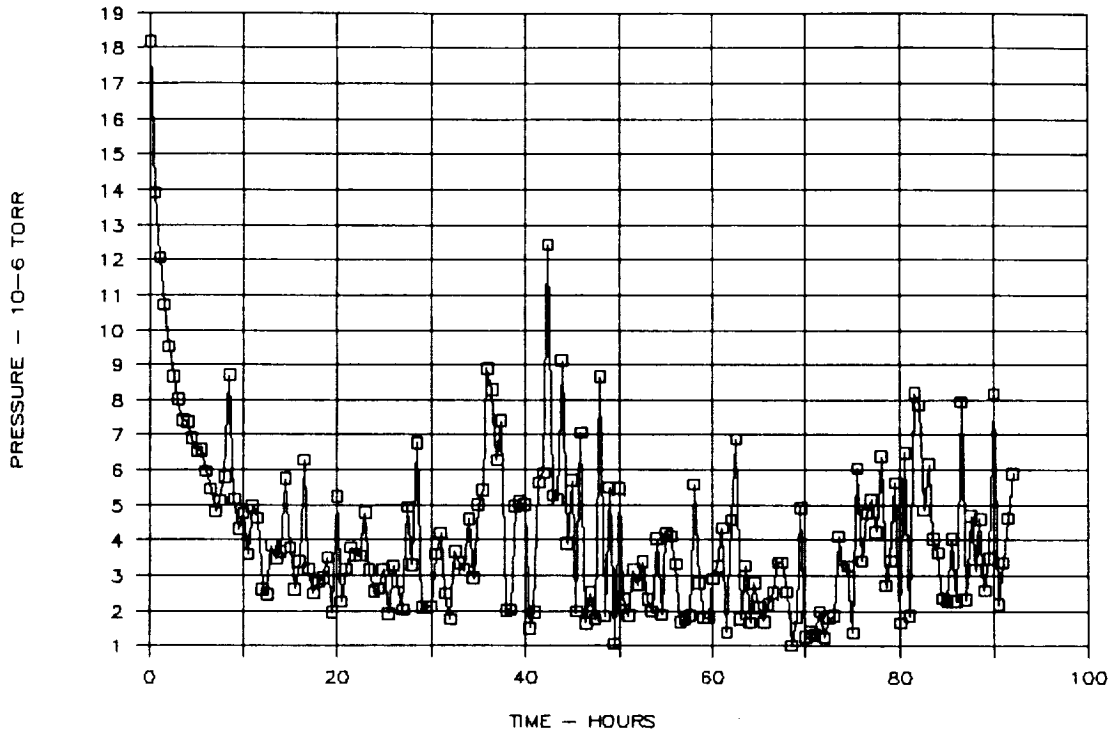

Figure 101. Results of Biosample Freezer Test on 12/7/90, MLI Pressure

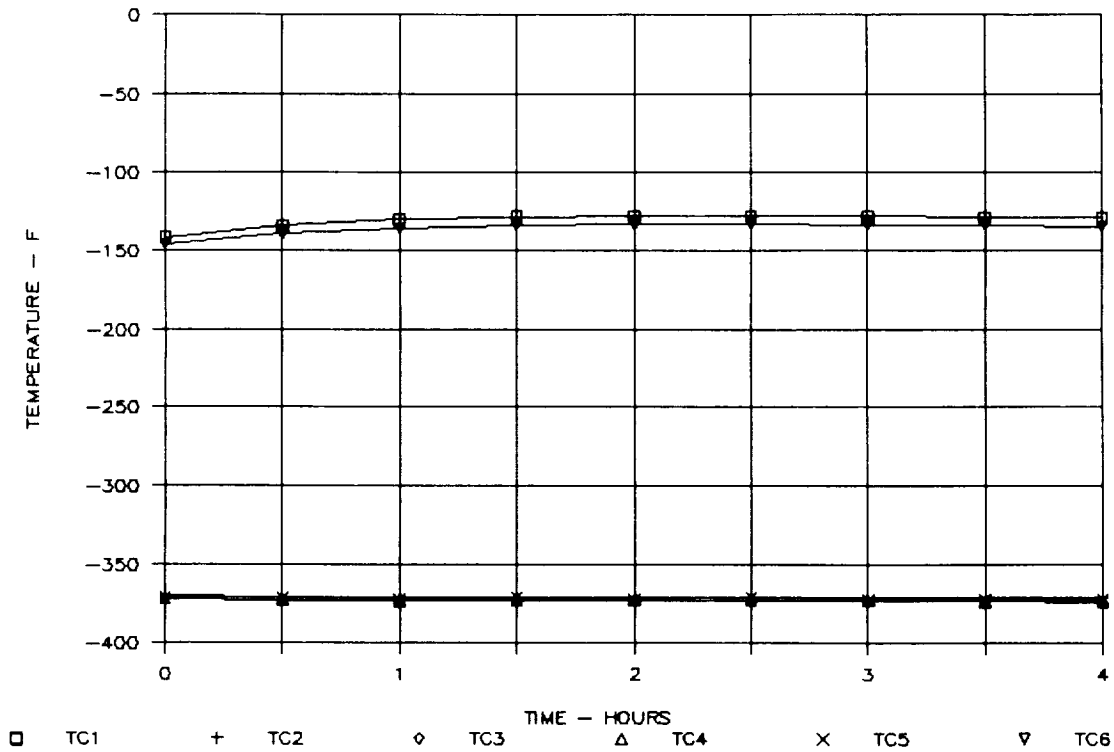

Figure 102. Results of Biosample Freezer Test on 12/12/90, TC1 through TC6, First 4 Hours

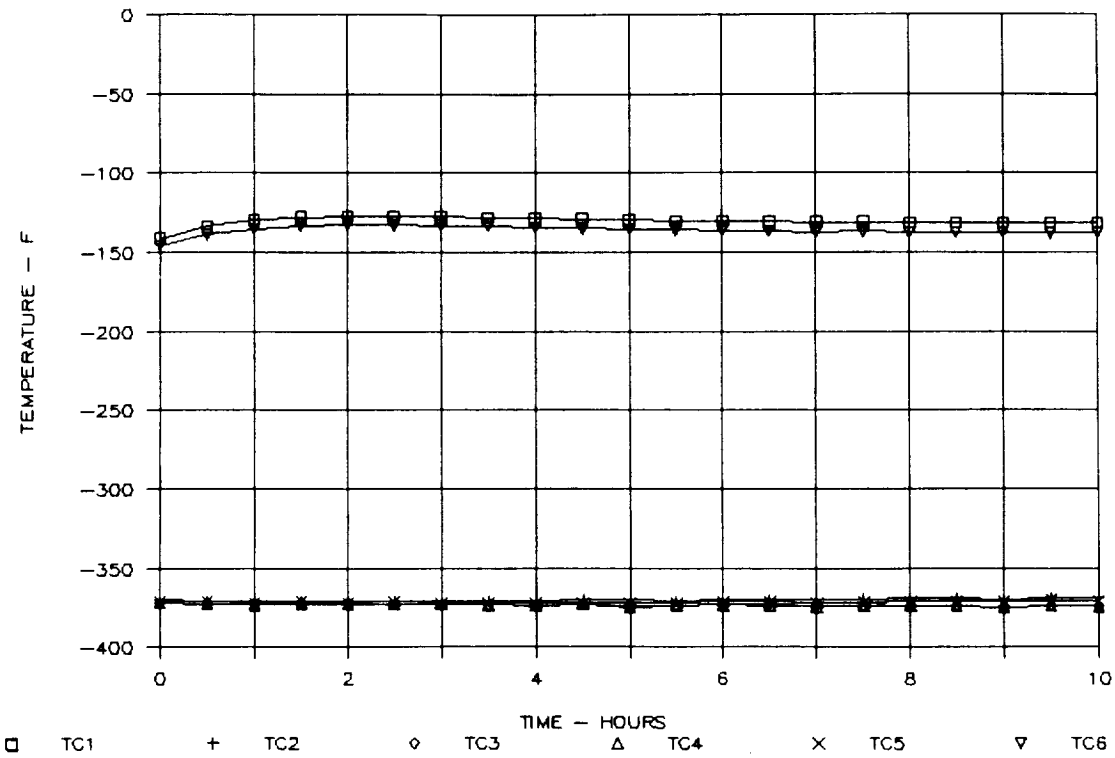

Figure 103. Results of Biosample Freezer Test on 12/12/90, TC1 through TC6, First 10 Hours

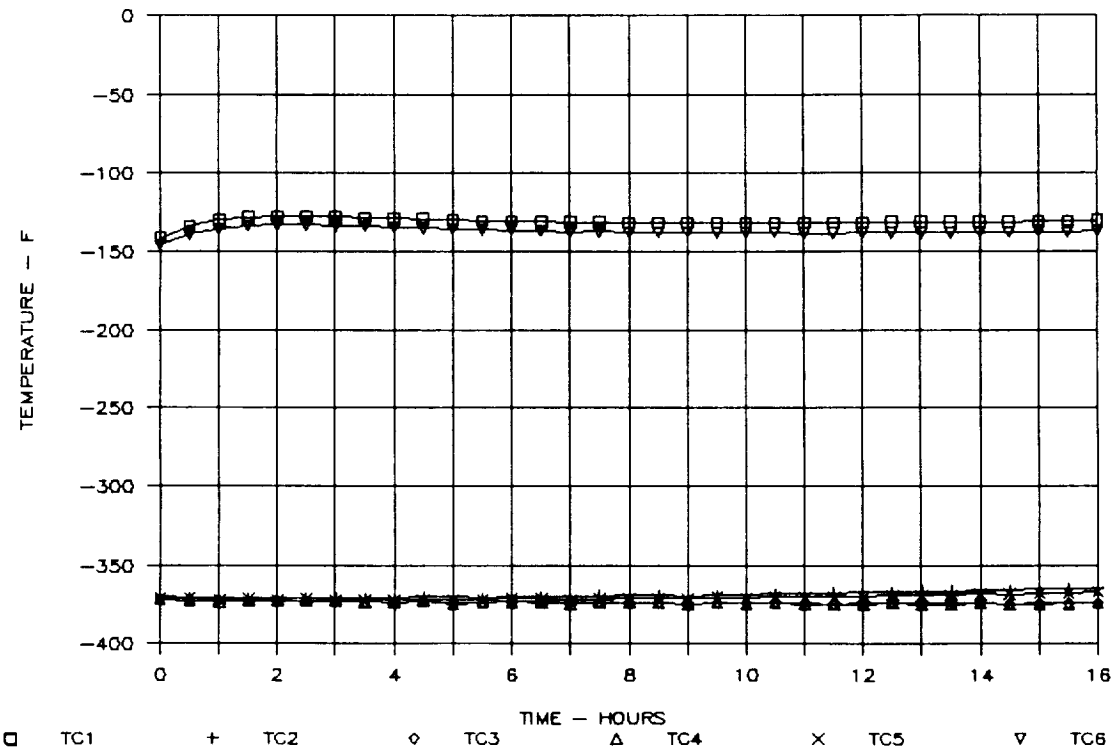

Figure 104. Results of Biosample Freezer Test on 12/12/90, TC1 through TC6, First 16 Hours

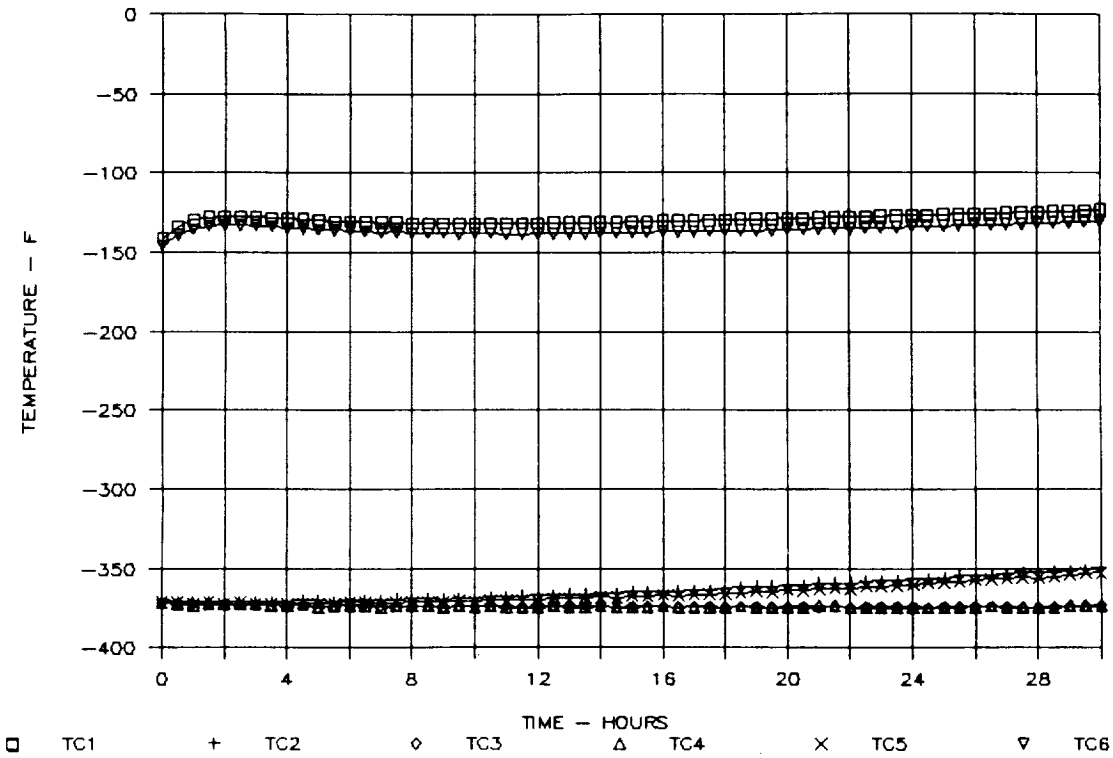

Figure 105. Results of Biosample Freezer Test on 12/12/90, TC1 through TC6, First 30 Hours

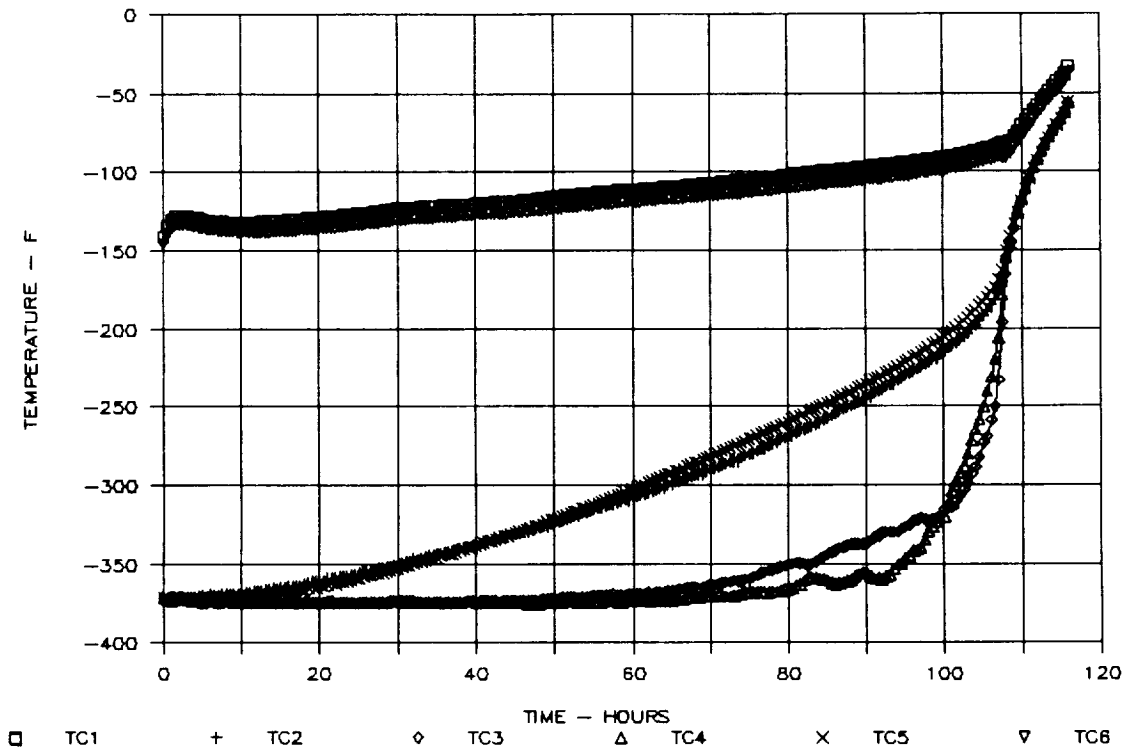

Figure 106. Results of Biosample Freezer Test on 12/12/90, TC1 through TC6, First 116 Hours

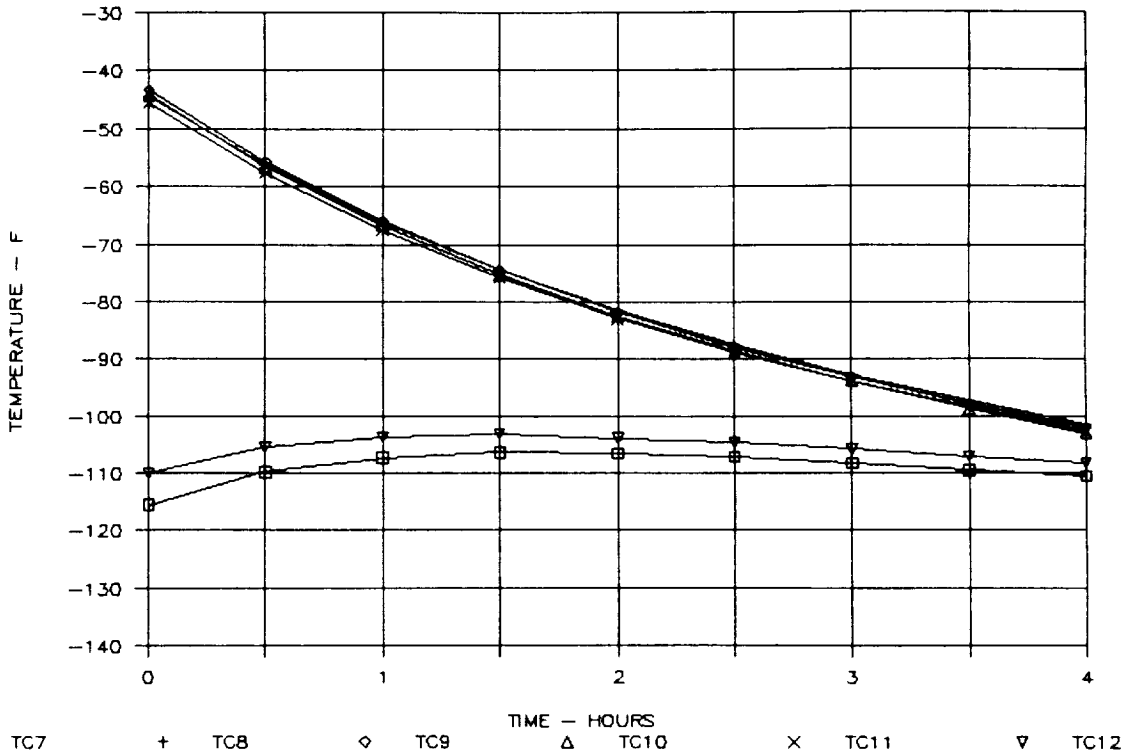

Figure 107. Results of Biosample Freezer Test on 12/12/90, TC7 through TC12, First 4 Hours

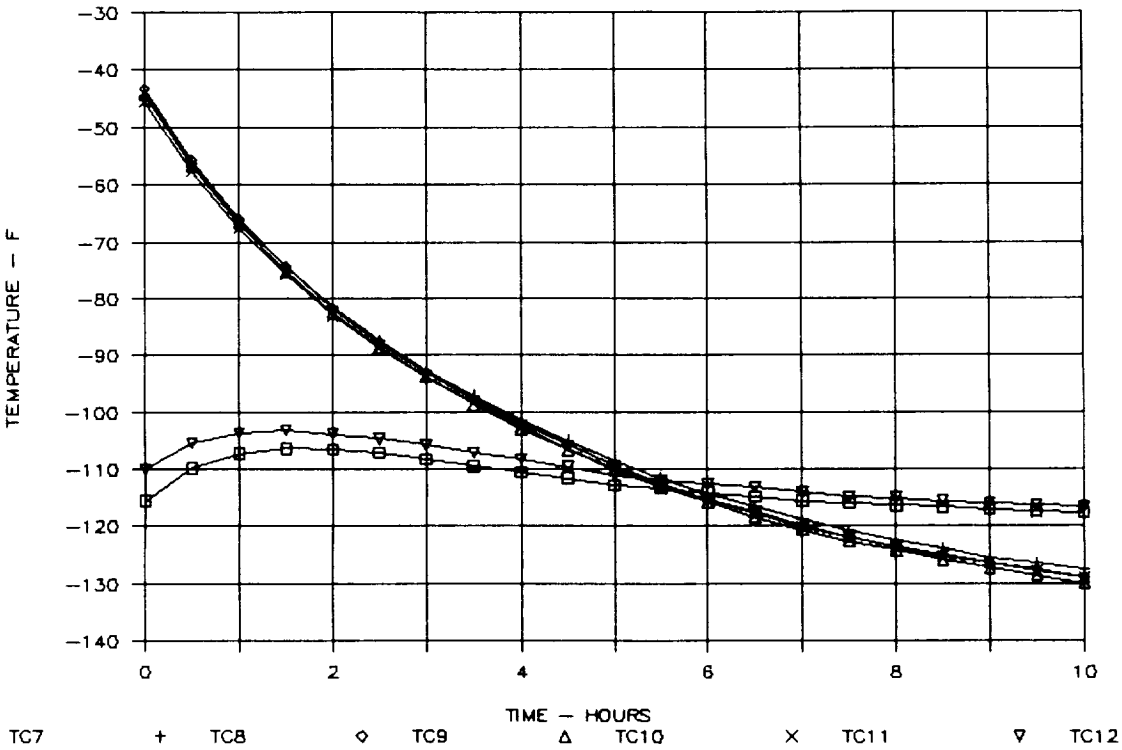

Figure 108. Results of Biosample Freezer Test on 12/12/90, TC7 through TC12, First 10 Hours

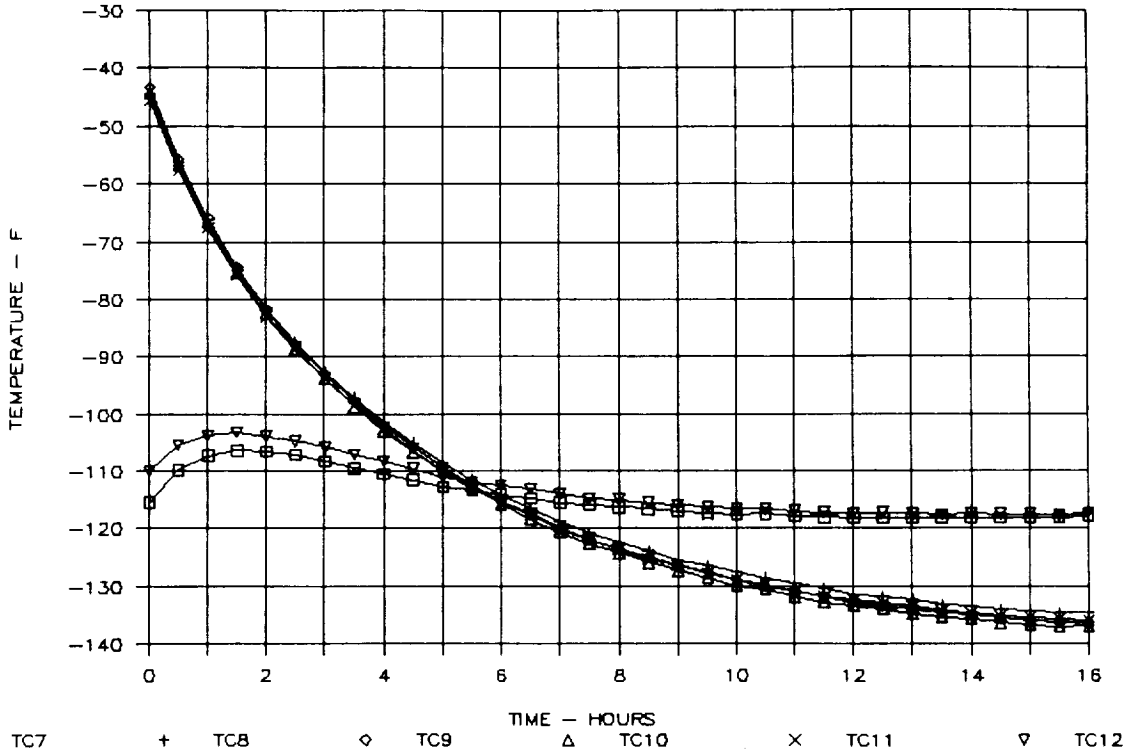

Figure 109. Results of Biosample Freezer Test on 12/12/90, TC7 through TC12, First 16 Hours

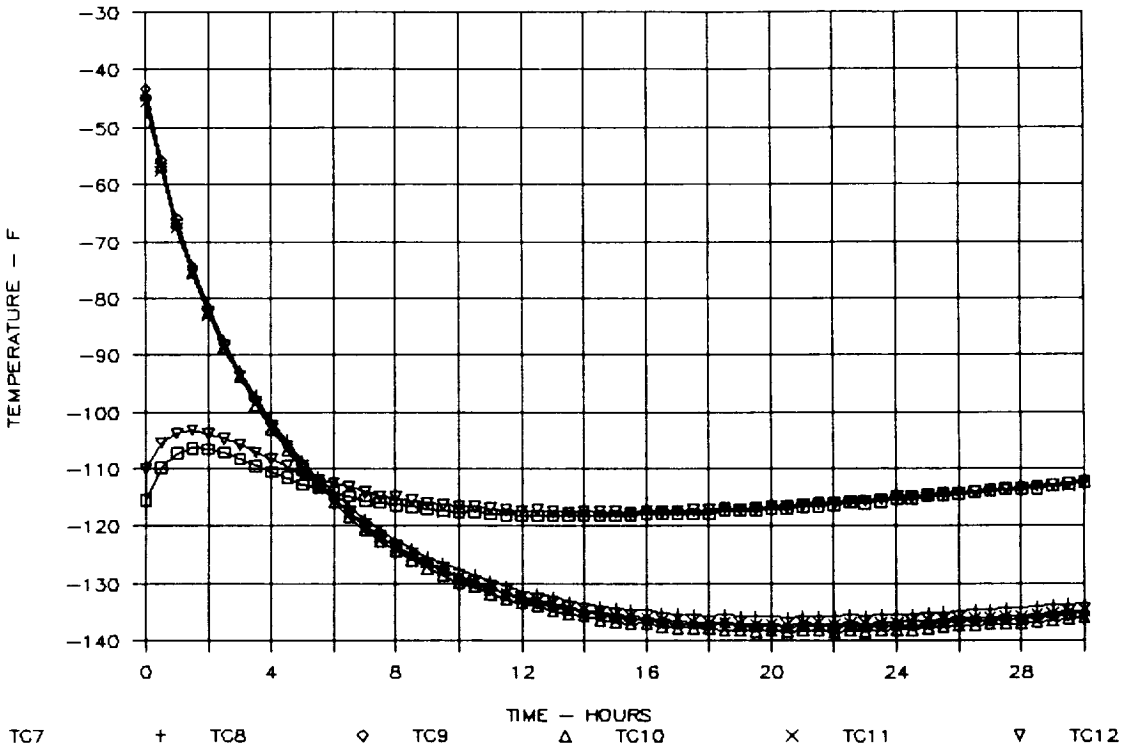

Figure 110. Results of Biosample Freezer Test on 12/12/90, TC7 through TC12, First 30 Hours

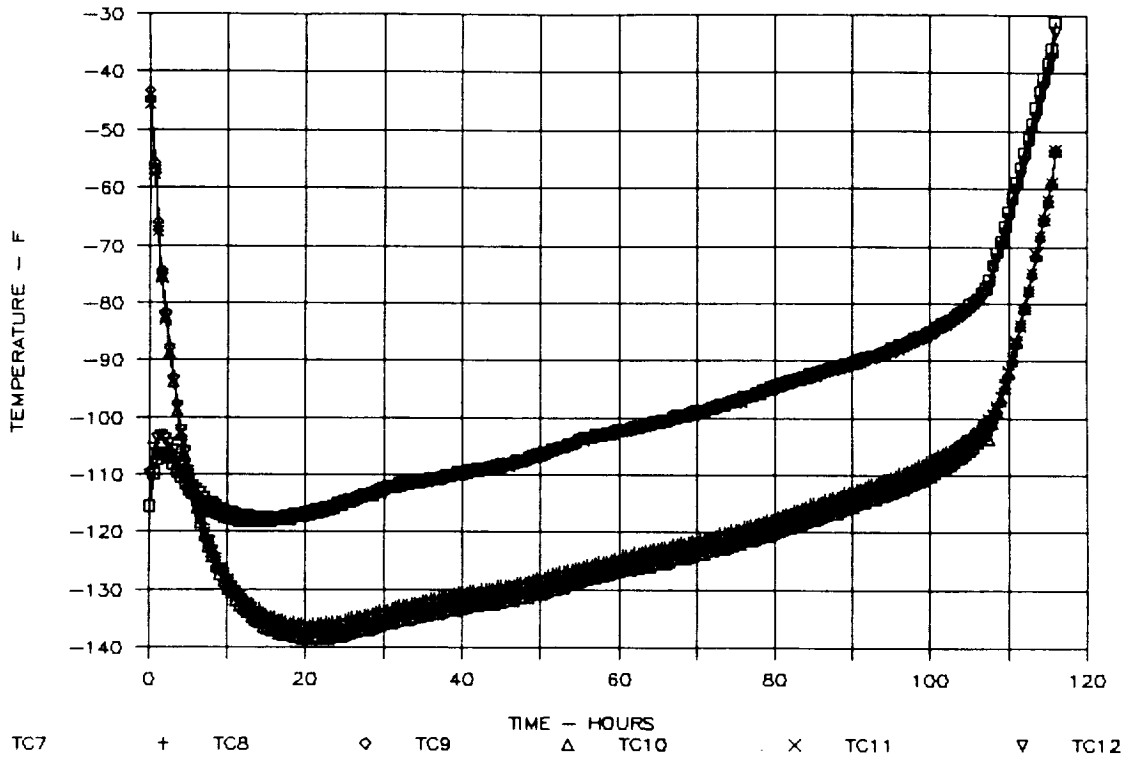

Figure 111. Results of Biosample Freezer Test on 12/12/90, TC7 through TC12, First 116 Hours

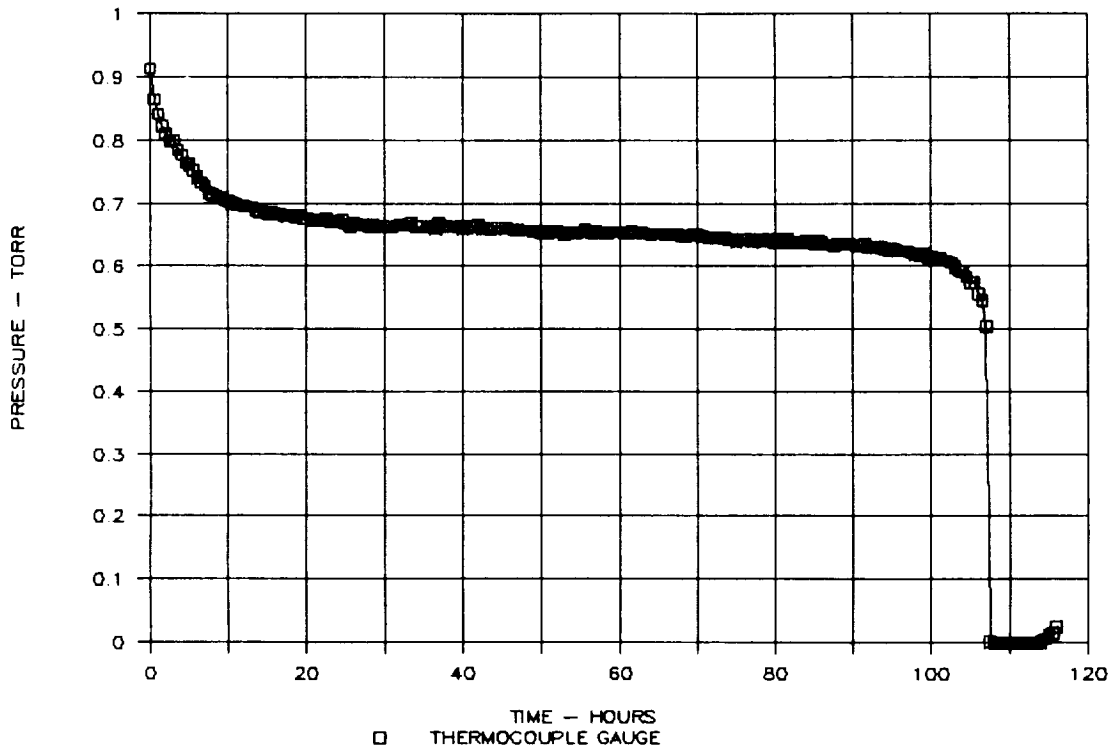

Figure 112. Results of Biosample Freezer Test on 12/12/90, Internal Pressure

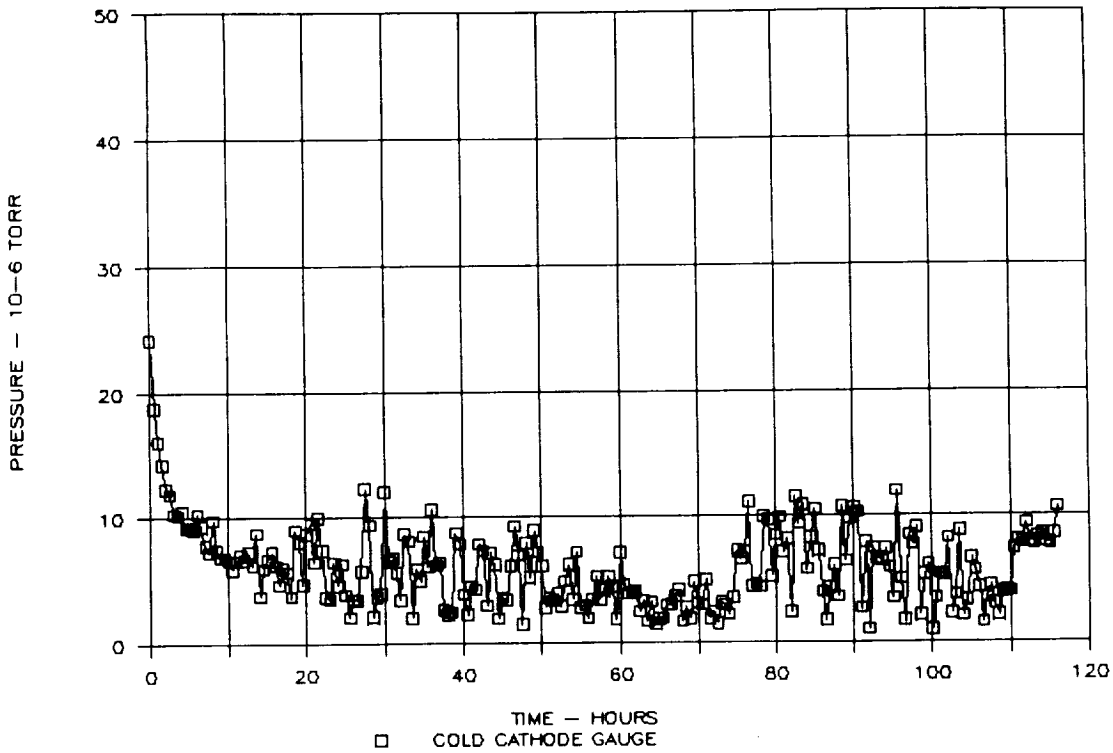

Figure 113. Results of Biosample Freezer Test on 12/12/90, MLI Pressure

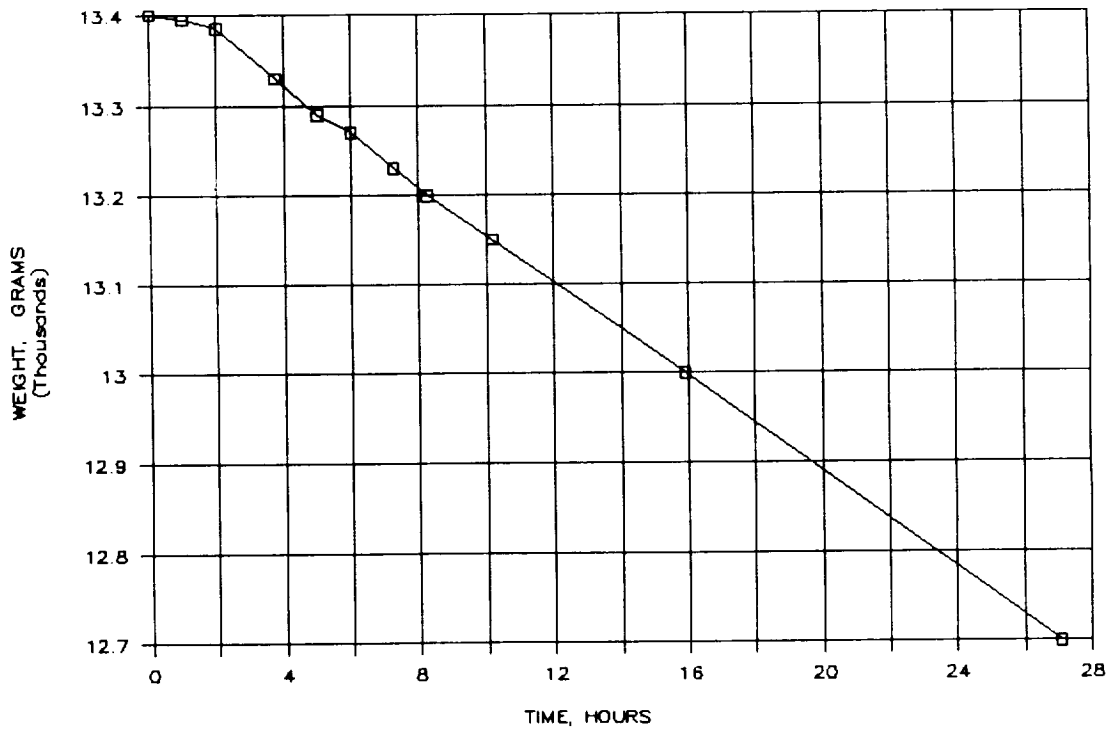

Figure 114. Results of Biosample Freezer Test on 11/15/90, Freezer + LN_2 Weight vs. Time

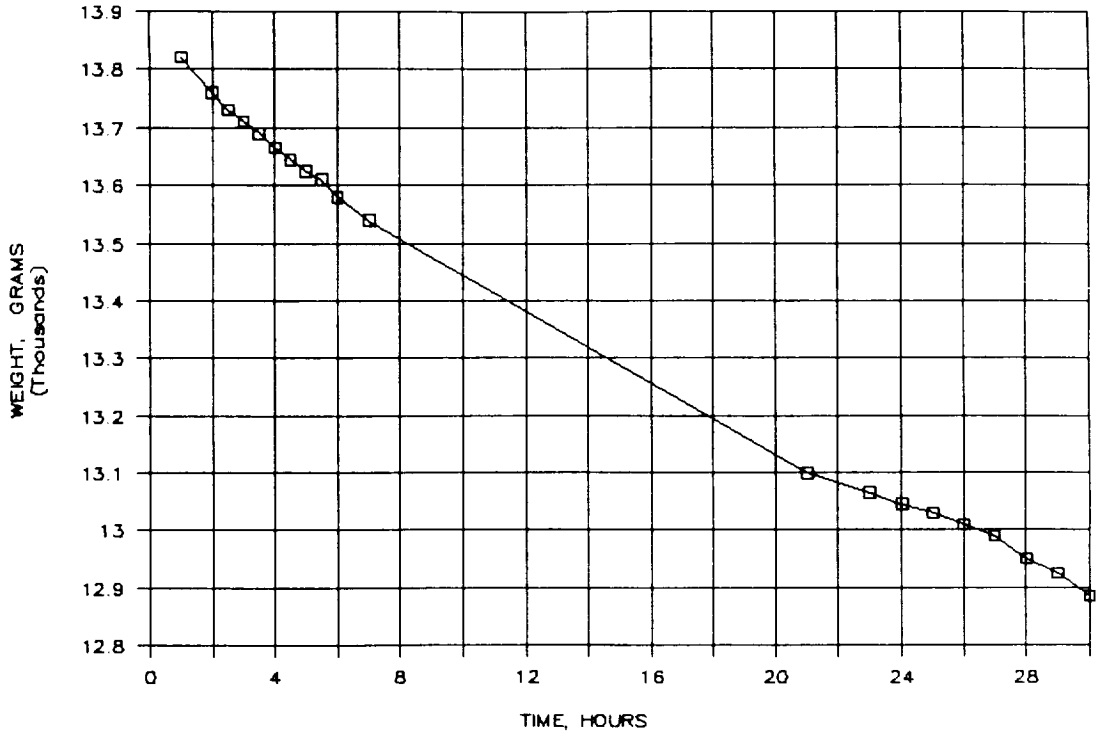

Figure 115. Results of Biosample Freezer Test on 11/19/90, Freezer + LN_2 Weight vs. Time

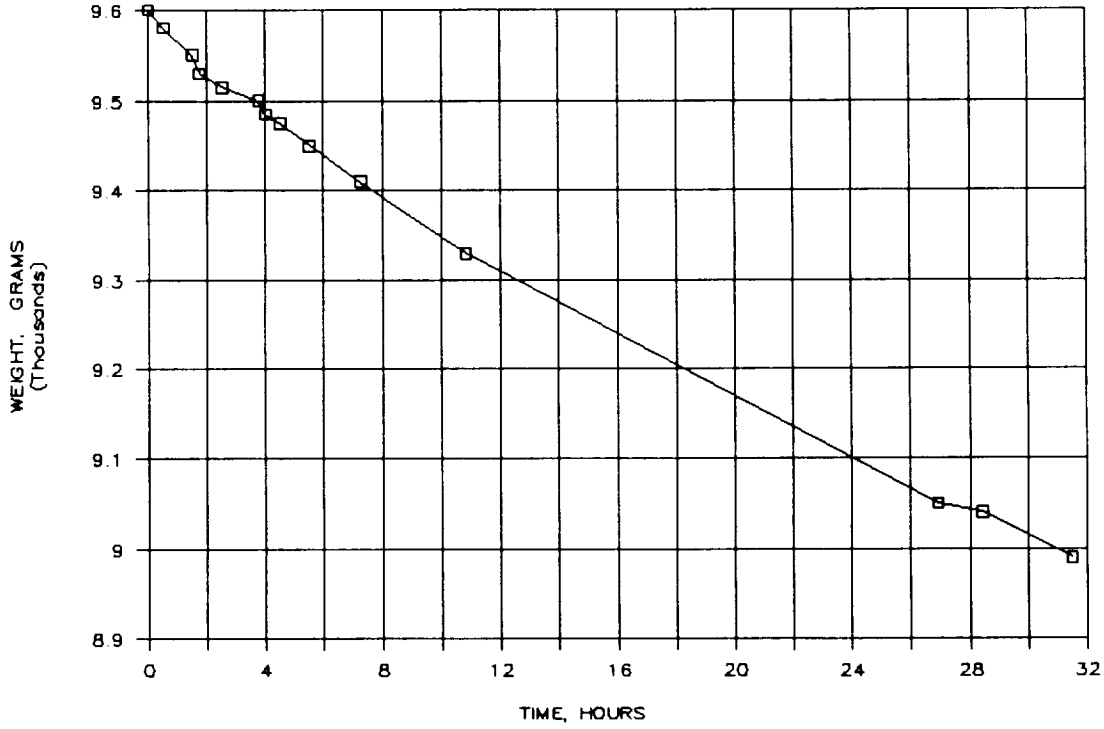

Figure 116. Results of Biosample Freezer Test on 11/21/90, Freezer + LN_2 Weight vs. Time

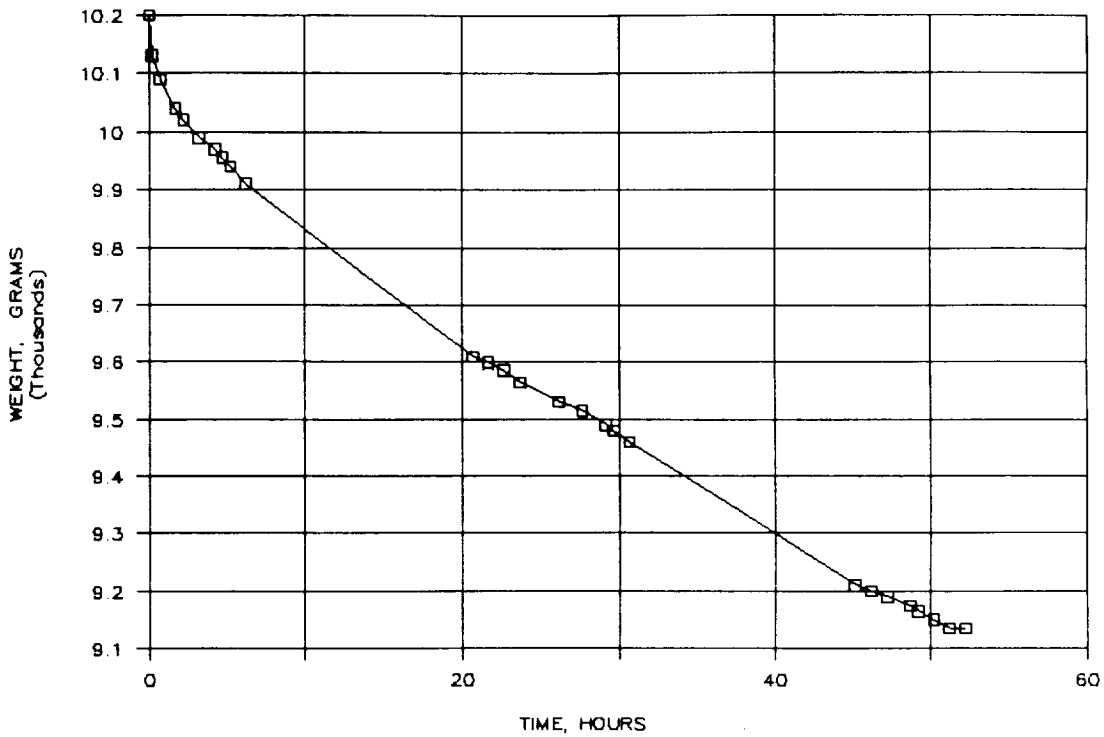

Figure 117. Results of Biosample Freezer Test on 11/26/90, Freezer + LN_2 Weight vs. Time

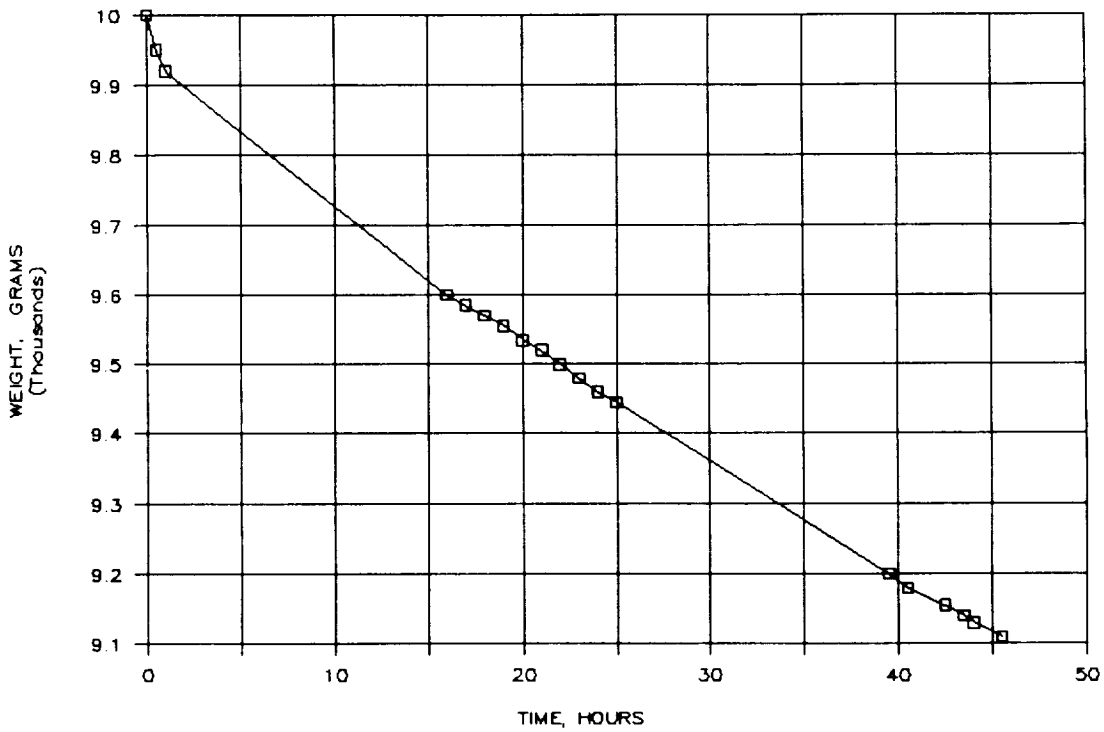

Figure 118. Results of Biosample Freezer Test on 11/28/90, Freezer + LN_2 Weight vs. Time

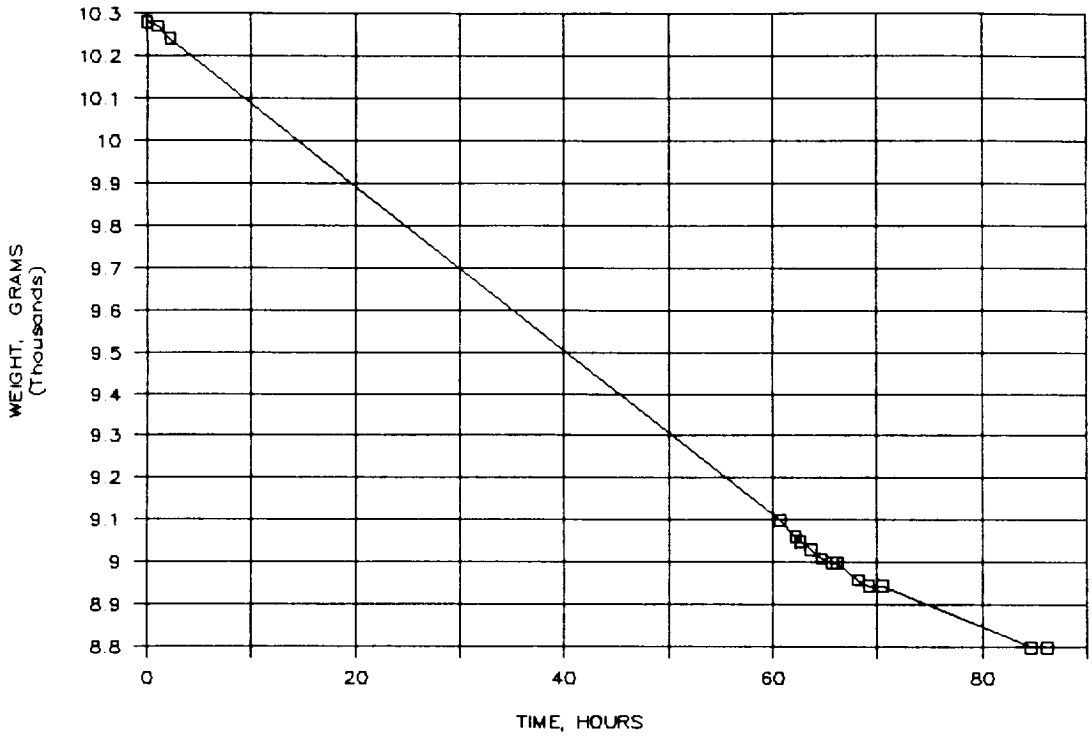

Figure 119. Results of Biosample Freezer Test on 11/30/90, Freezer + LN_2 Weight vs. Time

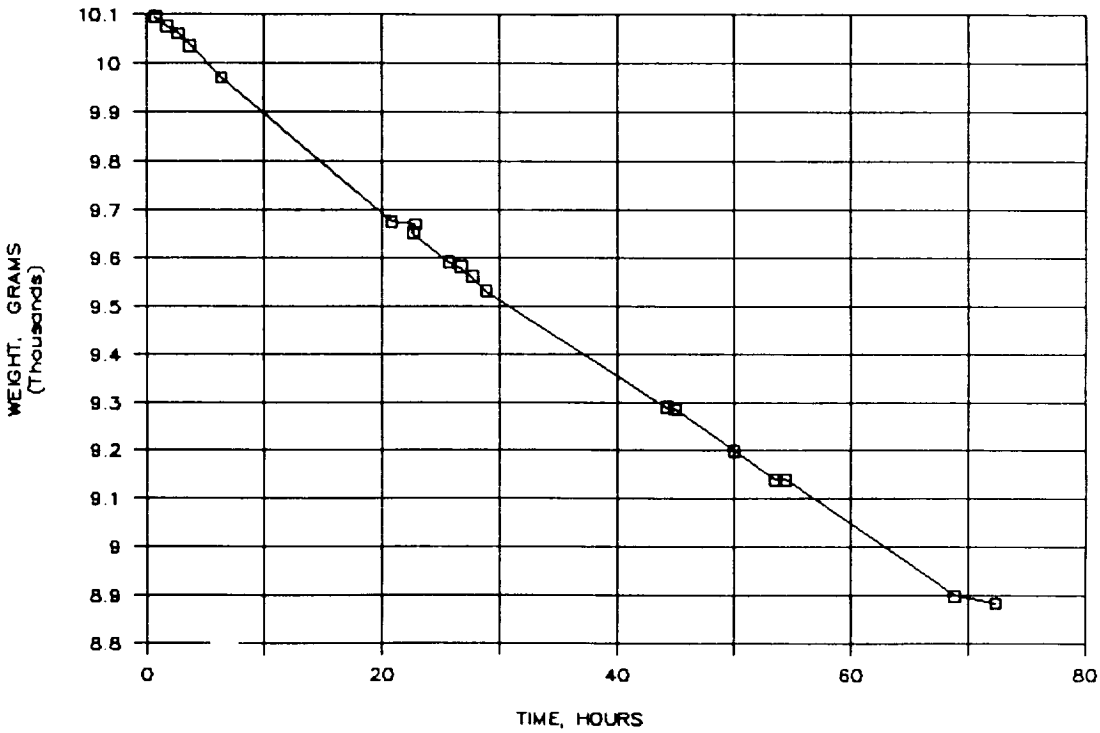

Figure 120. Results of Biosample Freezer Test on 12/4/90, Freezer + LN_2 Weight vs. Time

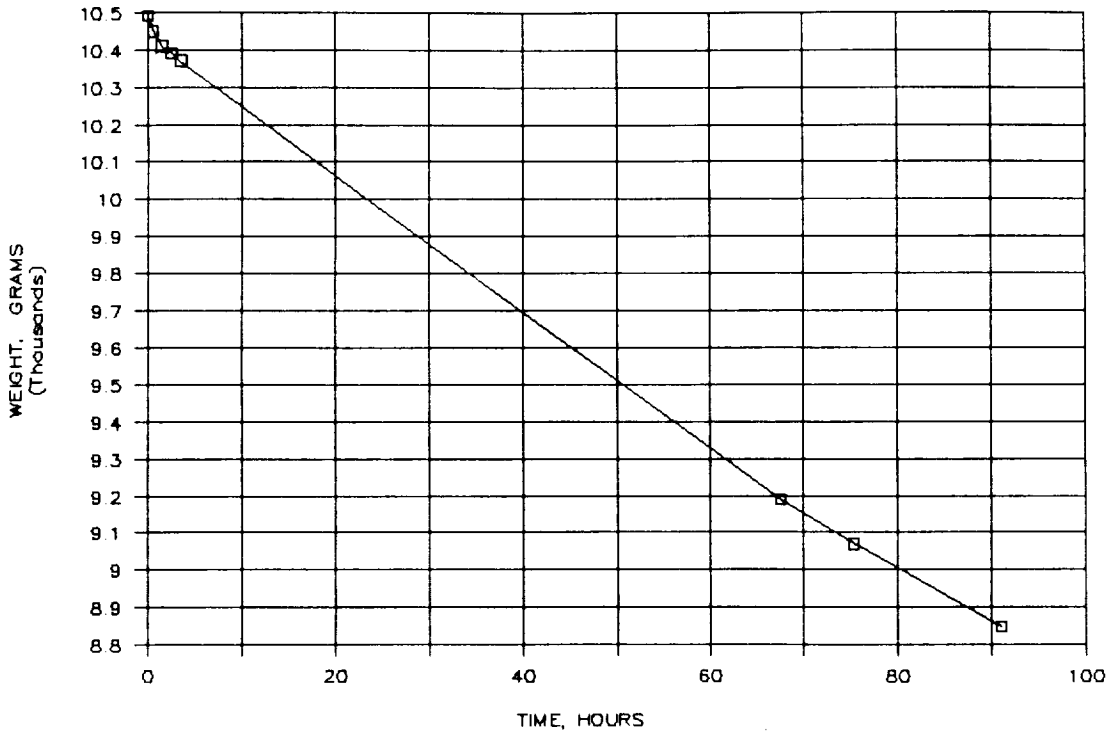

Figure 121. Results of Biosample Freezer Test on 12/7/90, Freezer + LN_2 Weight vs. Time

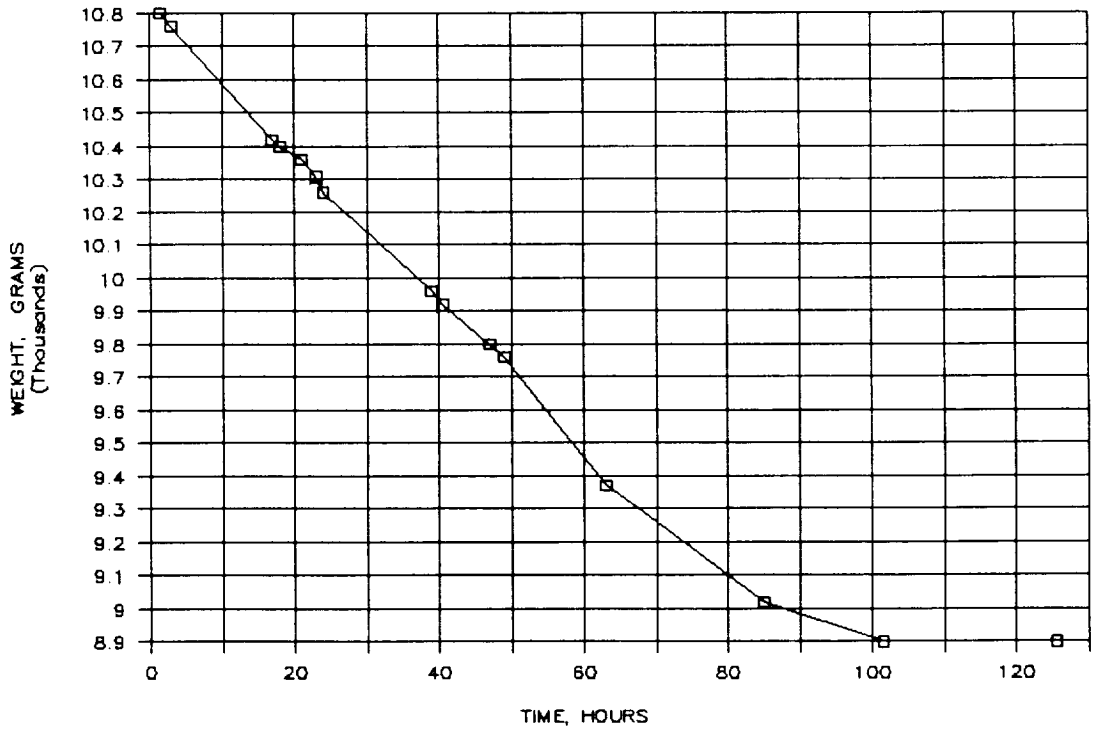

Figure 122. Results of Biosample Freezer Test on 12/12/90, Freezer + LN_2 Weight vs. Time

APPENDIX C

Evaluation and Comparison of Refrigerants for the Vapor Compression Cycles and Comparison Between Single and Cascade Cycles

(Excerpt from November 1985 Monthly Progress Report, LMSC-HEC PR F042708)

PRECEDING PAGE BLANK NOT FILMED

The parameters evaluated are as follows:

- COP — Coefficient of Performance
- Compressor Capacity — cfm/ton
- Mass flow — lb/min-ton

- Evaporator Pressure psia
- Condenser Pressure psia
- Power Factor watts/ton
- Toxicity --

The COP is a measure of the refrigeration effect per unit of work required, and a high COP indicates a low power requirement. The COP estimated for each refrigerant is the cycle COP and not an overall system COP; i.e., power required for fan motors, controls, compressor inefficiencies, etc., are not included. These auxiliary requirements are not considered important for comparison purposes. The compressor capacity is the volumetric flow per ton of refrigeration that the compressor must move. A higher value means a larger displacement compressor which means larger cylinder volumes or increased rotational speeds. The mass flow term indicates the mass flow that must be provided per ton of refrigeration (a ton of refrigeration = 12,000 Btu/hr = 3514 watts). High mass flows could require larger flow passages in transfer lines and heat exchangers. Low evaporator pressures, at the required evaporator temperature usually means high specific volume and larger CFMs for the compressor to move. High condenser pressure is not desirable from a safety consideration, and requires stronger and heavy, less efficient condenser construction. The power factor is related to the COP and is an indication of the cooling effectiveness of the cycle. The toxicity of the refrigerant is of prime importance for long time use in a habitable environment. The toxic limits for none of these refrigerants has been clearly defined for Space Station application.

The toxicity information provided for these refrigerants was taken from Refs. 1, 2, and 3. Reference 1 provides the Underwriter's Laboratory classification as shown in Fig. 1. Reference 2 provides the maximum allowable concentrations shown in Fig. 2. Based on these values the amount of refrigerant allowed was estimated based on the expected volume of the Space Station. For example, assuming a free volume of about 35,000 ft^3 approximately 0.8 lb of Freon 22 can be released without exceeding the maximum allowable concentration (MAC). A preliminary estimate indicates that about one-half pound of R-502 would be required to provide approximately 650 watts of cooling at -20 F with a condenser temperature of 50 F. (R-502 is an azeotrope of R-22 and R-115.) Chemical beds to remove this amount of Freon from the Space Station atmosphere, in less than seven days, could maintain the cabin atmosphere below the MAC even in the case of a total loss of refrigerant. Another concern is the reaction of Freons with other elements in the habitable environment. For example freons react with Lithium Hydroxide (LiOH) and form new compounds dichloroacetelyene (C_2Cl_2) and difloroacetelyene (C_2F_2). These compounds are toxic to humans and affect performance and physical well being of primates in concentrations of 0.1 to 1 ppm. At 7 ppm C_2Cl_2 is 100 percent fatal to monkeys after seven days of exposure (Ref. 3). Although LiOH may not be in the Space Station it is used in the Shuttle ECLS, and could cause a problem when the Shuttle is docked to the Station. In summary the toxicity assessment of heat transfer fluids requires an overall systems evaluation considering the

GROUP	DEFINITION	EXAMPLES
1	Gases or vapors which, in concentrations of the order of ½ to 1 percent for durations of exposure of the order of 5 minutes, are lethal or produce serious injury.	Sulfur Dioxide
2	Gases or vapors which, in concentrations of the order of ½ to 1 percent for durations of exposure of the order of ½ hour, are lethal or produce serious injury.	Ammonia
3	Gases or vapors which, in concentrations of the order of 2 to 2½ percent for durations of exposure of the order of 1 hour, are lethal or produce serious injury.	Methyl formate
4	Gases or vapors which, in concentration of the order of 2 to 2½ percent for durations of exposure of the order of 2 hours, are lethal or produce serious injury.	Methyl chloride
Between 4 & 5	Gases or vapors which appear to classify as somewhat less toxic than Group 4.	Methylene cloride
	Gases or vapors which are much less toxic than group 4, but somewhat more toxic than group 5.	Refrigerant 113
5a	Gases or vapors which are much less toxic than Group 4, but more toxic than Group 6.	Refrigerant 11 Refrigerant 22 Carbon dioxide Refrigerant 500 Refrigerant 502
5b	Gases or vapors which available data indicate would classify as either Group 5a or Group 6.	Ethane Propane Butane
6	Gases or vapors which, in concentrations up to at least about 20 percent by volume for durations of exposure of the order of 2 hours, do not appear to produce injury.	Refrigerant 12 Refrigerant 114

Fig. 1 Underwriter's Laboratories Classification of Comparative Life Hazards of Gases and Vapors

FREON	MAXIMUM ALLOWABLE CONCENTRATION (PPM)	(Mg/M³)	ALLOWABLE MASS** (LBS)	(GMS)
12	100	494.4	1.09	492.6
21	5	21	.0461	20.92
22	100	353.6	.777	352.3
112	100	834.2	1.83	831.2
113	50	383	.841	382
114	100	702.9	1.54	700.38
FE 1301	100	608.8	1.34	606.6
23	100	286.3	.629	285.27
AMMONIA	25	17.4	.038	17.34

**Based on Volume of 35,188 ft^3
* From Reference 2.

Fig. 2 Maximum Allowable Concentration Limits for 7-Day Exposure

interactions of the fluids with the Station systems and any synergistic effects of these interactions. Although this evaluation is beyond the scope of the present analyses, it appears that due to the large volume of the station and the relatively small amount of Freon required, a vapor compressor system, using Freon as a working fluid, could be designed to operate safely in the Space Station.

Thermodynamic Cycle Analysis: The results of the comparative analysis of each of the 10 candidates are shown in Fig. 3. Based on this information the following candidates were eliminated from further consideration.

- R-13 - high condenser pressure and power factor
- R-23 - high condenser pressure and power factor
- R-142b - flammable
- R-503 - high condenser pressure and power factor
  R-504 - high condenser pressure

The effect of lowering the condenser temperature is shown in Fig. 4. This could be done by providing a lower temperature radiator for heat rejection. As shown the power requirements can be reduced by a factor of approximately 2 or better. There is also a reduction in compressor capacity but this is

REFRIGERANT	LATENT HEAT @ -40 F (BUT/LB)	MASS FLOW Lbs/min-ton	COMPRESSOR CAPACITY CFM/TON	EVAPORATOR PRESSURE @ (-40 F) (psia)	CONDENSER PRESSURE @ 50 F (psia)	PRESSURE RATIO	COP	POWER FACTOR WATTS/TON	TOXICITY * RATING
R-12	79.91	3.74	14.51	9.31	61.4	6.6	3.79	927	6
R-13	54.023	6.81	2.88	87.43	365.9	4.18	2.94	1194	6
R-22	100.257	2.63	8.67	15.222	98.727	6.49	3.84	914	5a
R-500	87.74	3.1	12.28	10.95	72.26	6.6	3.87	907	5a
R-502	75.16	3.94	8.23	18.97	111.6	5.9	3.6	975	5a
NH_3	597.6	0.4	9.95	10.41	89.19	8.57	3.73	942	2
R-23	88.565	3.98	2.19	103.07	471.8	4.58	2.76	1277	6
R-142b	95.428	2.67	30.73	3.835	30.26	7.89	4.08	861	5a
R-503	63.737	6.67	2.44	121.45	498.99	4.1	2.52	1394	6
R-504	99.425	2.87	4.71	32.914	185.59	5.64	3.81	992	6

*Toxicity ranking given in Fig. 1.

Fig. 3 Comparison of Refrigerants (-40 F Evaporator, 50 F Condenser Temperatures)

REFRIGERANT	LATENT HEAT @ -40 f (BTU/LB)	COMPRESSOR CAPACITY (CFM/TON)	EVAPORATOR PRESSURE (psia)	CONDENSER PRESSURE (psia)	PRESSURE RATIO	C.O.P.	POWER FACTOR (WATTS/TON)
R-12	79.91	12.24	9.31	26.48	2.84	8.9	395
R-22	100.26	7.45	15.22	42.89	2.82	8.59	409
R-500	87.74	10.4	10.95	31.07	2.99	9.11	386
R-502	75.16	6.6	18.97	50.68	2.67	7.97	441
NH_3	597.6	9.05	10.41	34.27	3.29	8.68	405

Fig. 4 Effects of Lowering Condenser Temperature to 5 F(-40 F Evaporator)

not as significant as the power reduction. Based on this evaluation, R-22 and R-502 are the best choices for these specific applications.

Potential benefits for cascading the cycles were investigated. This is two simple cycles operating in series. Both cycles can use the same or different refrigerants. In this case the same refrigerants were used in both cycles. The cycles selected can be represented on a pressure enthalpy diagram as shown in Sketch 1 below:

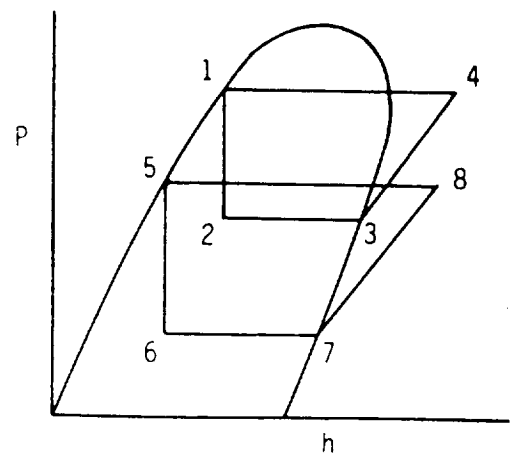

Sketch 1

The temperature differences of 10 F between the 1st stage condensing temperature and the second stage evaporating temperature was selected to allow heat transfer between the two cycles without using a liquid vapor separator. The use of a liquid vapor separator would allow fluid mixing of the first and second stages, eliminating the temperature diffrential between the second stage evaporator and the first stage condenser. This would, however, require development of a zero "g" liquid vapor separator.

The first and second stage characteristics for the selected refrigerants are shown in Fig. 5. The combined system (COP) can be represented as:

$$(COP)_S = \frac{(COP)_1 \, (COP)_2}{(COP)_1 + (COP)_2 + 1}$$

REFRIGERANT	LATENT HEAT @ -5 F (BTU/LB)	COMPRESSOR CAPACITY (CFM/TON)	EVAPORATOR PRESSURE (psia)	CONDENSER PRESSURE (psia)	PRESSURE RATIO	C.O.P.	POWER FACTOR (WATTS/TON)
R-12	69.3	6.22	21.42	61.4	2.87	7.86	447
R-22	94.89	3.81	34.75	98.73	2.84	7.69	456
R-500	83.74	5.28	25.13	72.26	2.87	7.88	446
R-502	70.34	3.62	41.53	111.6	2.69	6.92	507
NH_3	572.6	3.99	26.92	89.19	3.31	7.26	483

LOWER CYCLE (-40 F EVAPORATOR, 5 F CONDENSER)

REFRIGERANT	LATENT HEAT @ -40 F (BTU/LB)	COMPRESSOR CAPACITY (CTM/TON)	EVAPORATOR PRESSURE (psia)	CONDENSER PRESSURE (psia)	PRESSURE RATIO	C.O.P.	POWER FACTOR (WATTS/TON)
R-12	79.91	12.24	9.31	26.483	2.84	8.9	395
R-22	100.257	7.45	15.222	42.888	2.82	8.59	409
R-500	87.74	10.4	10.95	31.07	2.99	9.11	386
R-502	75.16	6.6	18.97	50.68	2.67	7.97	441
NH_3	597.6	9.05	10.41	34.27	3.29	8.68	405

Fig. 5 Comparison of Refrigerants for Cascade Cycle

$(COP)_1$ = 1st stage coefficient of performance

$(COP)_2$ = 2nd stage coefficient of performance.

And the compressor capacity of the second stage is related to the first stage by:

$$C_2 = C_1 \left[1 + \frac{1}{(COP)_1} \right] \frac{v_2}{v_1} \frac{\Delta h_1}{\Delta h_2}$$

Δh - enthalpy change in the evaporator

v - specific volume at the compressor inlet

Subscripts: 1 - 1st stage
2 - 2nd stage.

The combined compressor capacity is the sum of the capacities of the first and second stage compressor capacities. A comparison of the cascade and single cycle characteristics is shown in Fig. 6. As shown there, cascade cycles provides a small reduction in power with an increase in compressor capacity. For these operating conditions, the slight power savings is not sufficient to off set the increase in compressor capacity and the increased complication and weight of the cascade cycle. As will be shown in the following section, as the condenser temperature is increased the cascade cycle becomes more attractive.

Computer Model for Thermodynamic Property Generation and Cycle Calculation: A computer model has been developed to perform single and cascade cycle analysis of a vapor compression refrigeration system. The analysis shows that cascade cycle becomes more beneficial at a higher condenser temperature. The computer model has basically two modules. First, thermodynamic properties are calculated at condenser and evaporator temperatures. Finally, cycle performance parameters are calculated from the state point enthalpies.

The only empirical input of this computer model is the relationship between saturation pressure, P_s, and temperature, T_s. They are related by the following expression (Ref. 4).

$$\ln P_s = A + B/T_s + C \ln T_s + DT_s \qquad (1)$$

where A, B, C, and D are constants to be evaluated from four known state points.

REFRIGERANT	CASCADE CYCLE COMPRESSOR CAPACITY (CTM/TON)	CASCADE CYCLE C.O.P.	CASCADE CYCLE POWER FACTOR WATTS/TON	SINGLE CYCLE COMPRESSOR CAPACITY	SINGLE CYCLE C.O.P.	SINGLE CYCLE POWER FACTOR WATTS/TON
R-12	19.16	3.94	891	14.51	3.79	927
R-22	11.70	3.82	919	8.67	3.84	914
R-500	16.26	3.99	880	12.28	3.87	907
R-502	10.67	3.47	1012	8.23	3.6	975
NH_3	13.50	3.72	944	9.95	3.73	942

Fig. 6 Comparison of Cascade and Single Cycle Characteristics for Vapor Compression Cycles (Evaporator Tempemperature -40 F, Condensing Temperature 50 F)

The enthalpy of evaporation, h_{fg}, is calculated from the Clausius-Clapeyron equation as follows:

$$h_{f_g} = T_s(v_g - v_f)\frac{dp_s}{dp_s} \tag{2}$$

where the specific volume of the vapor, v_g, is calculated from the Van der Waal equation given as:

$$P = \frac{RT}{v_g - b} - \frac{a}{v_g^2} \tag{3}$$

where $a = 27R^2 2T_c^{\ 2}/(64\ P_c)$ (4)

$$b = RT_c/8P_c \tag{5}$$

The specific volume of liquid, v_f, is calculated from a two-degree polynominal given as:

$$v_f = C_o + c_1T + C_2T^2 \tag{6}$$

where C_0, C_1 and C_2 are curve fit constants.

The other thermodynamic relationships used in generating the thermodynamic properties are as follows:

$$h = u + pv \tag{7}$$

$$u = C_v(T - T_{ref}) \tag{8}$$

where $T_{ref} = -40$ F

$$S_2 - S_1 = C_p\ \ell n\ \frac{T_2}{T_1} \tag{9}$$

$$s_{fg} = \frac{h_{fg}}{T_s} \tag{10}$$

$$h_g = h + fg$$

With the help of the above equations, all saturation properties are calculated.

Cycle Performance Calculation: A single stage vapor compression refrigeration cycle is shown in the Sketch 2.

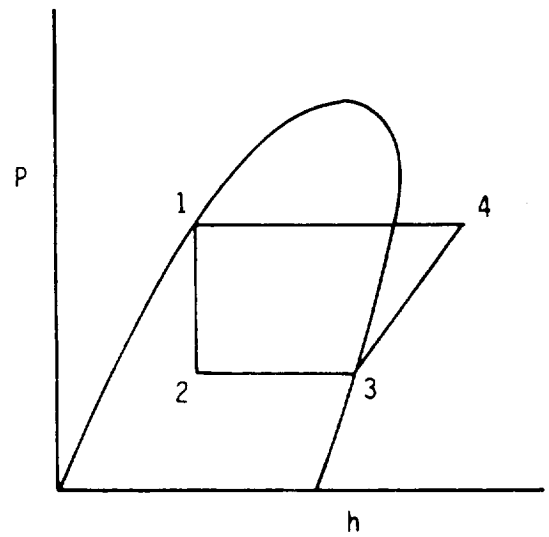

Sketch 2

$$COP = \frac{h_3 - h_2}{h_4 - h_3} = \frac{\text{Accomplished Cooling}}{\text{Compressor Work}}$$

$$\text{Compressor Capacity} = \frac{v_3 \times \text{Cooling Load}}{(h_3 - h_2)}$$

$$\text{Mass flow of refrigerant} = \frac{\text{Cooling Load}}{h_3 - h_2}$$

Pressure ratio = P_1/P_2

$$\text{Power factor} = \frac{\text{Cooling Load}}{\text{COP}}$$

A schematic of the cascade cycle and its representation in a pressure-enthalpy diagram is shown below as Sketch 3.

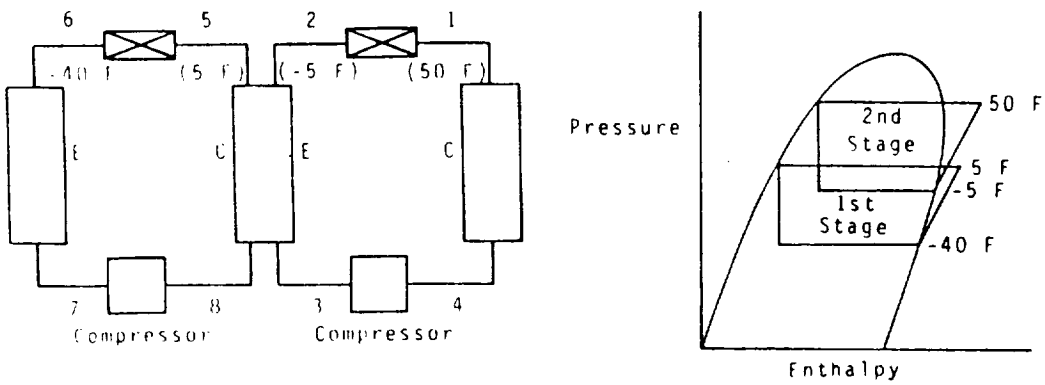

Sketch 3

$$\text{COP of the system} = \frac{h_7 - h_6}{h_8 - h_7 + \frac{h_8 - h_5}{h_3 - h_2}(h_4 - h_3)}$$

A comparison of the performance between single stage and cascade vapor compression cycle using R-12 as refrigerant is given in Figs. 7 and 8.

Evaporator Temperature =-40°F
Refrigerant - R-12

Ratio of COP	Condenser Temperature (°F)	Single Stage	Cascade Cycle Interfacing Heat Exchanger ΔT ΔT=5°F	ΔT=10°F	ΔT=15°F
COP		3.8744	5.0461	4.765	4.512
$\frac{(COP)}{(COP)\ \text{single stage}}$	50	1	1.302	1.230	1.165
COP		3.381	4.648	4.411	4.196
$\frac{(COP)}{(COP)\ \text{single stage}}$	60	1	1.375	1.305	1.241
COP		2.96	4.32	4.12	3.934
$\frac{(COP)}{(COP)\ \text{single stage}}$	70	1	1.459	1.392	1.329
COP		2.619	4.05	3.886	3.727
$\frac{(COP)}{(COP)\ \text{single stage}}$	80	1	1.546	1.484	1.423
COP		2.314	3.833	3.682	3.541
$\frac{(COP)}{(COP)\ \text{single stage}}$	90	1	1.656	1.591	1.530

Fig. 7 Comparison of Cycle Performance Parameters Between Single Stage and Cascade Vapor Compression Cycle

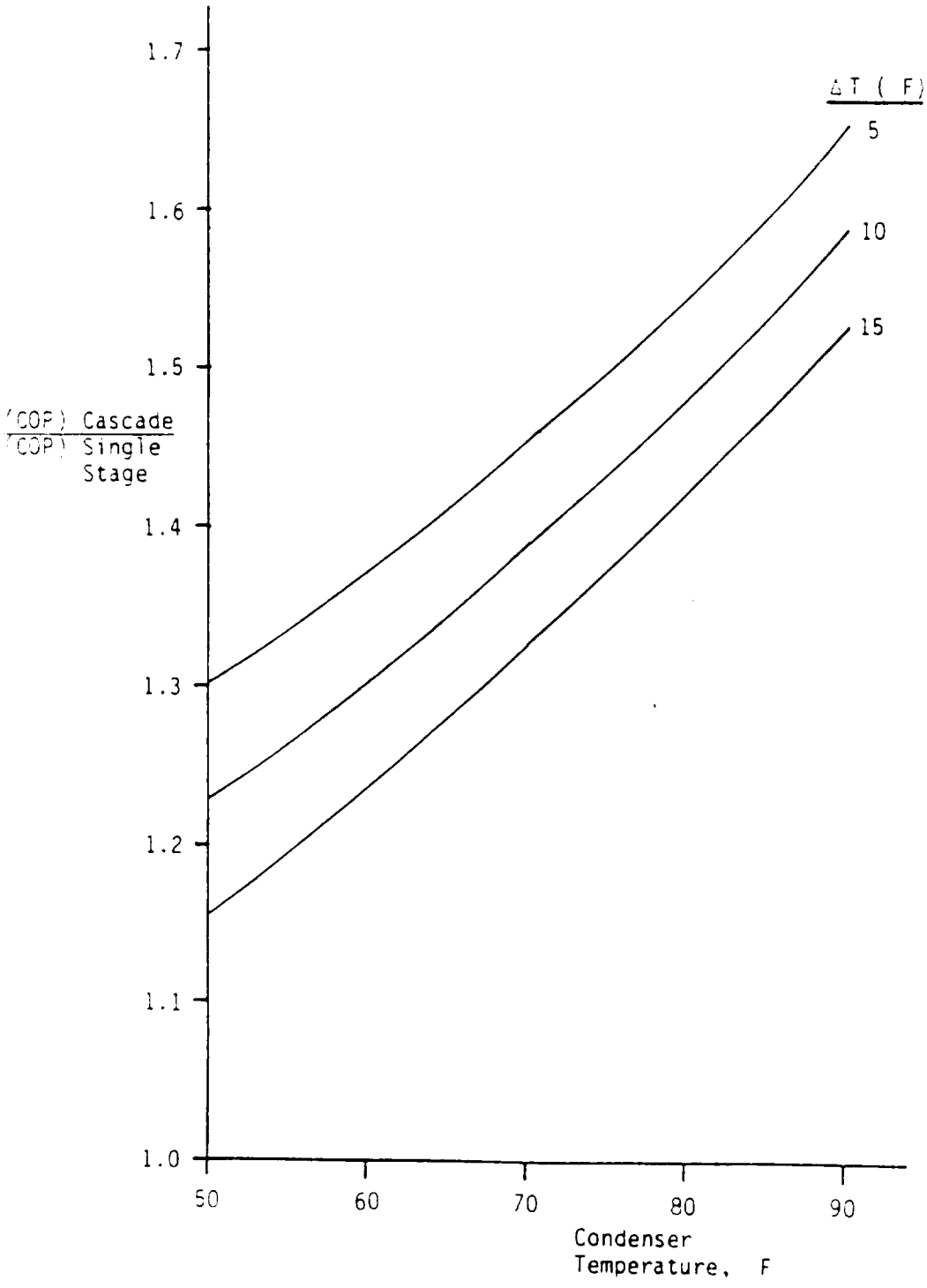

Fig. 8 Comparison of Cycle Performance Parameter at Different Condenser Temperature

References

1. Thermodynamic Properties of Refrigerants, American Society of Heating, Refrigerating and Air Conditioning Engineers, 1969.

2. Flammability, Odor, and Off-Gassing Requirements and Test Procedures For Materials in Environments that Support Combustion, NHB 8060.1B, Appendix D, September 1981.

3. Proceedings of the Fifth Annual Conference on Atmospheric Contamination in Continued Spaces, 16-18 September 1969, Paper N020; page 289.

4. Van Wylen, Gordon J., and Sonntag, Richard E. Fundamentals of Classical Thermodynamics, Second Edition, Wiley & Sons, 1976.

APPENDIX D

Bibliography (Excerpt from LMSC-HEC PR F225603)

BIBLIOGRAPHY

1. Albers, James A., and Robert P. Macosko, "Experimental Pressure-Drop Investigation of Nonwetting, Condesing Flow of Mercury Vapor in a Constant Diameter Tube in 1-g and Zero-Gravity Environments," NASA-N6.-24561, Lewis Research Center, Cleveland, Ohio, June 1965.

2. Azer, Naim Z., Leopoldo V. Abs, Hassan M. Soliman, "Local Heat Transfer Coefficients During Annular Flow Condensation," ASHRAE Annual Meeting, Nassau, Bahamas, June 1972.

3. Bae, Soonhoon, John S. Maulbetsch, and Warren M. Rohsenow, "Refrigerant Forced Convection Condensation Inside Horizontal Tubes," DSR 79760-59, Engineering Projects Laboratory, MIT, November 1968.

4. Berner, F., H. Oesch, and K. Goetz, "Development of a Reverse-Rankine Cycle Heat Pump for Space Use: Design and Testing of the Engineering Model of the Vapor Compressor," Swiss Federal Aircraft Factory, Emmen, Switzerland, September 1981.

5. Berner, Felix, "Initial Development of a Vapor Compressor for a Heat Pump to be Used in Spacecraft," Swiss Federal Aircraft Factory, Emmen, Switzerland, December 1977.

5. Berner, F., and C.J. Savage, "Development of a Vapor Compression Heat Pump for Space Use," ESA, American Institute of Aeronautics and Astronautics, 16th Thermophysics Conference, Palo Alto, Calif., June 1981.

6. Berner, F., and C.J. Savage, "Development of a Vapor Compression Heat Pump for Space Use," AIAA 16th Thermophysics Conference, Palo Alto, Calif., June 1981.

7. Berner, F., H. Oesch, K. Goetz, and C.J. Savage, "The Mechanical Design of a Vapor Compressor for a Heat Pump to be Used in Space," Swiss Federal Aircraft Factory, Emmen, Switzerland; ESA, The Netherlands.

8. Cavallini, A., S. Frizzerin, and L. Rossetto, "Condensation of Refrigerants Inside Annuli," Instituto di Fisica Tecnica, Universita di Padua, Italy.

9. Chen, John C., "Correlation for Boiling Heat Transfer to Saturated Fluids in Convective Flow," Brookhaven National Laboratory, Upton, N.Y., July 1966.

10. Feldmanis, C.J., "Performance of Boiling and Condesning Equipment Under Simulated Outer Space Conditions," ASD-TDR-68-862, Air Force Systems Command, Wright-Patterson Air Force Base, Ohio, November 1963.

11. Feldmanis, Carl J., "Pressure and Temperature Changes in Closed Loop Forced Convection Boiling and Condensing Under Zero Gravity Conditions," Air Force Flight Dynamics Laboratory, Institute of Environmental Sciences, 1966, and Annual Technical Meeting Proceedings, 1966.

12. Jaster, H., and P.G. Kosky, "Condensation Heat Transfer in a Mixed Flow Regime," General Electric Company, Schenectady, N.Y., April 1975.

13. Keshock, Edward, Gordon Spencer, and James L. Williams, "A Photographic Study of Flow Condensation in 1-g and Zero-Gravity Environments."

14. Namkoong, David, Henry B. Block, Robert P. Macosko, Clifford C. Crabs, "Photographic Study of Condensing Mercury FLow in 0- and 1-g Environments," NASA-N67-28739, Lewis Research Center, Cleveland, Ohio, June 1967.

15. Shah, M.M., "A General Correlation for Heat Transfer During Film Condensation Inside Pipes," Port Jefferson Station, N.Y., August 1978.

16. Shah, Mirza M., "A New Correlation for Heat Transfer During Boiling Flow Through Pipes," Gilbert/Commonwealth, Jackson, Miss.

17. Soliman, M., J.R. Schuster, and P.J. Berenson, "A General Heat Transfer Correlation for Annular Flow Condensation," Ai Research Manufacturing Company, Los Angeles, Calif., May 1968.

18. Soliman, Moustafa, and Paul J. Berenson, "Flow Stability and Gravitational Effects in Condenser Tubes," Ai Research Manufacturing Company, Los Angeles, Calif.

19. Traviss, D.P., W.M. Rohsenow, and A.B. Baron, " Forced Convection Condensation Inside Tubes: A Heat Transfer Equation for Condenser Design," 2272RP-63, Department of Mechanical Engineering, MIT.

20. Williams, J.L., E.G. Kesnock, C.L. Wiggins, "Development of a Direct Condensing Radiator for Use in a Spacecraft Vapor Compression Refrigeration System," ASME Presentation at the Intersociety Conference on Environmental Systems, San Diego, Calif., July 1973.

(PATENTS)

Inventor: Schwemin, Arnold J., Oakland, Calif.
Invention: Closed-Cycle Gas Engine
Patent No.: 3,478,511
Patented: 18 November 1969
Serial No.: 653,119

Inventors: Yutaka Momose, Toyata; Kazuaki Nakamura, Kariya, Japan
Invention: Stirling Cycle Refrigerator
Patent No.: 4,282,716
Patented: 11 August 1981

Inventor: Don B. Kantz, Ferndale, Mich.
Invention: Separator Apparatus for Differential High Pressure Systems of a Stirling Engine
Patent No.: 4,080,788
Patented: 28 March 1978

APPENDIX E

Description of Various Compressor Types for Application to Space Station Refrigeration (Excerpt from LMSC-Hsv PR F312427, 15 February 1991 Progress Report

PROGRESS DURING THE CURRENT REPORTING PERIOD

Comparison of Various Compressor Types and their Potential Application to Space Station Refrigeration

A study is being performed to compare various generic types of existing compressor designs. Specifically, the purposes of this study are to answer the following questions.

- What are the various candidate types of compressors?
- How does each type work?
- What are the advantages/disadvantages of each type?
- What is their relative merit for Space Station refrigeration application?

As shown in *Figure 1*, compressors can be divided into two broad groups, intermittent and continuous. The intermittent, or positive displacement, mode of compression is cyclic in nature, in

ORIGINAL PAGE IS
OF POOR QUALITY

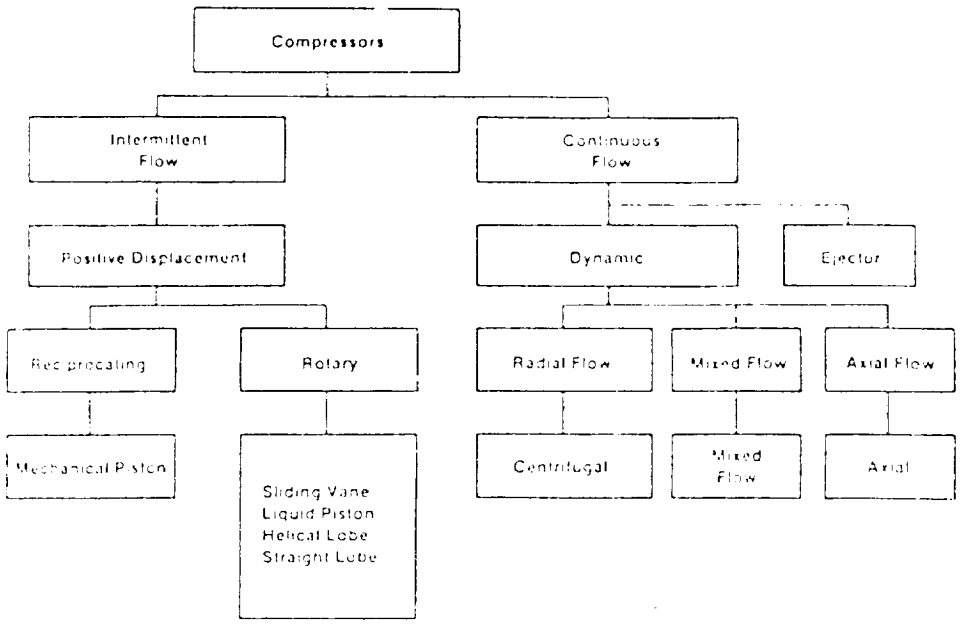

Figure 1. Compressor Types

that a specific volume of gas is ingested, compressed, and discharged before the cycle is repeated. There are two distinct types of intermittent flow compressors, reciprocating and rotary. As their name implies, continuous compressors deliver a continuous stream of compressed gas. There are also two types of continuous-mode compressors, dynamic and ejector.

Drivers are usually electric motors, except for portable equipment which use internal combustion engines. Also, on small reciprocating compressors, unique, linear motors with spring-loaded pistons and electromagnets and coils are effective.

Positive displacement compressors are more suitable for high compression ratio and low volume applications, especially the reciprocating type, which can attain compression ratios up to 20 in a single stage and greater than 200 in multistage designs. The continuous flow dynamic types are more suitable for high volume and low compression ratio; however, multistage models can attain compression ratios equivalent to single stage reciprocating type (see *Figure 2*). Once specific compression/volume requirements are established, *Figure 2* can be used for initial compressor selection. When all system and special requirements are known, *Table 1* can be helpful in final selection.

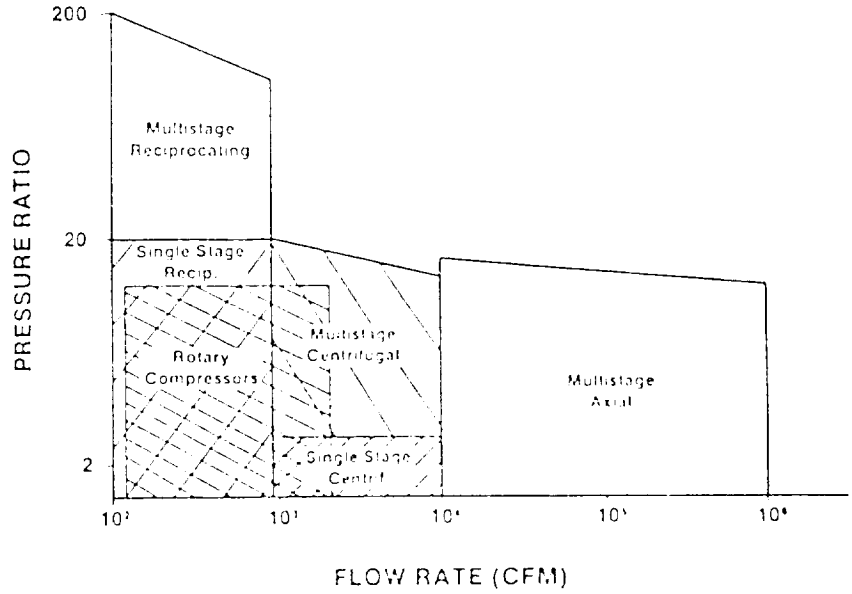

Figure 2. Typical Application Ranges of Compressor Types

Intermittent Mode Compressors

Reciprocating Compressors

These are the most widely used compressors and are generally for lower flow rate applications. They are well suited for high pressure service, being one of the most efficient of all compressors at compression ratios above 1.5:1. Reciprocating compressors are single or double acting depending upon whether compression takes place on one or both sides of the piston. *Figures 3, 4,* and *5* show typical single stage and multistage reciprocating compressor arrangements. Normally, reciprocating compressors utilize oil lubrication between the piston and inner cylinder wall. This serves two purposes: 1) to reduce friction and wear and 2) to help create a seal and reduce "blow by" of the gas as it is being compressed. However, crosshead type reciprocating compressors are designed to run oil-free. In the crosshead design, the connecting rod is divided into two sections. The section which is connected to the piston is mounted in two guide bearings which eliminate side loads from the piston and inner cylinder walls (see *Figure 5*). With this arrangement, self lubricating or dry lubricated materials such as PTFE composites can be used. These designs are utilized for application where high purity gases are being compressed, or in cases where the gases may be highly reactive or otherwise incompatible with oil lubrication. These have been designed for numerous industrial applications and yield both long life and high pressures.

Essentially all reciprocating compressors use intake and exhaust valves of some type.

A third variation of the reciprocating type compressor is shown in *Figure 6*. This approach is very well suited to oil-free, or dry-lubricated applications because it has essentially zero side loads without the need for the crosshead linkage as described above. In this design, a linear motor is used to move the piston back and forth. It is unique in that it moves the coil rather than the

Table 1. Compressor Selection Guidelines (1)

System Characteristic	Generally Suitable	Conditionally Suitable	Requires Add. Investment	Usually Unsuitable
Liquid carryover into compressor likely	Liquid ring, helical screw	Centrifugal, axial	Reciprocating, sliding vane, high-speed centrifugal	
Solids carry over into compressor is likely	Liquid ring	Helical screw, centrifugal, axial	Reciprocating, sliding vane, high-speed centrifugal	
Intolerant to lube oil	Nonlubricated reciprocating	Centrifugal, axial, liquid ring	Helical screw	Lubed reciprocating, sliding vane
Fouling tendency of gas	Helical screw	Centrifugal		Lubed reciprocating, high-speed centrifugal, axial
Special Requirement	**1st Choice**	**2nd Choice**	**3rd Choice**	**4th Choice**
High efficiency[2]	Reciprocating, sliding vane, scroll	Axial, helical screw	Centrifugal	Liquid ring
Low maintenance costs	Centrifugal, axial	Helical screw, liquid ring	Reciprocating (lubed)	Sliding vane, reciprocating (non-lubed)
Very low flow	Low flow - high head centrifugal	Diaphragm		

1. From *Compressors and Expanders, Selection and Application for the Process Industry*, Marcel Debber, Inc.

2. Volumetric efficiency of a reciprocation compressor may be expressed as

$$Vol_{(eff)} = \frac{\text{Mass of gas actually compressed and delivered}}{\text{Mass of gas occupying the piston displacement at inlet pressure and temperature}}$$

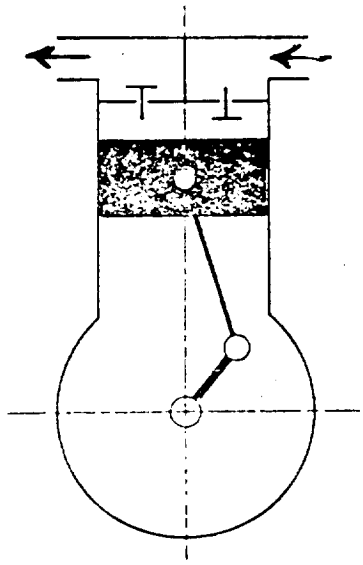

Figure 3. Trunk Type Reciprocating Compressor, Lubricated

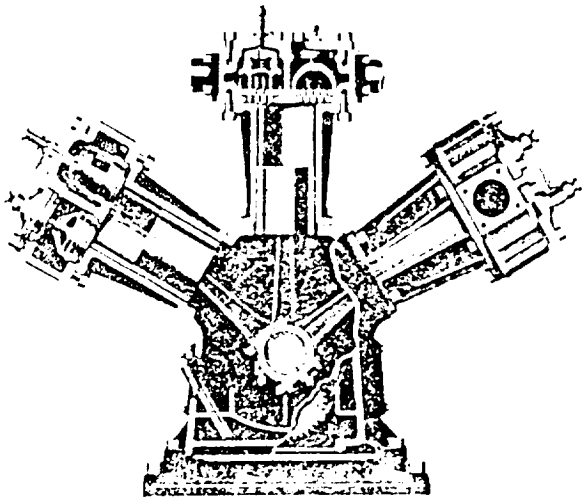

Figure 4. Three Stage Single -Acting Reciprocating Compressor, Trunk Type (Courtesy of Ingersoll-Rand)

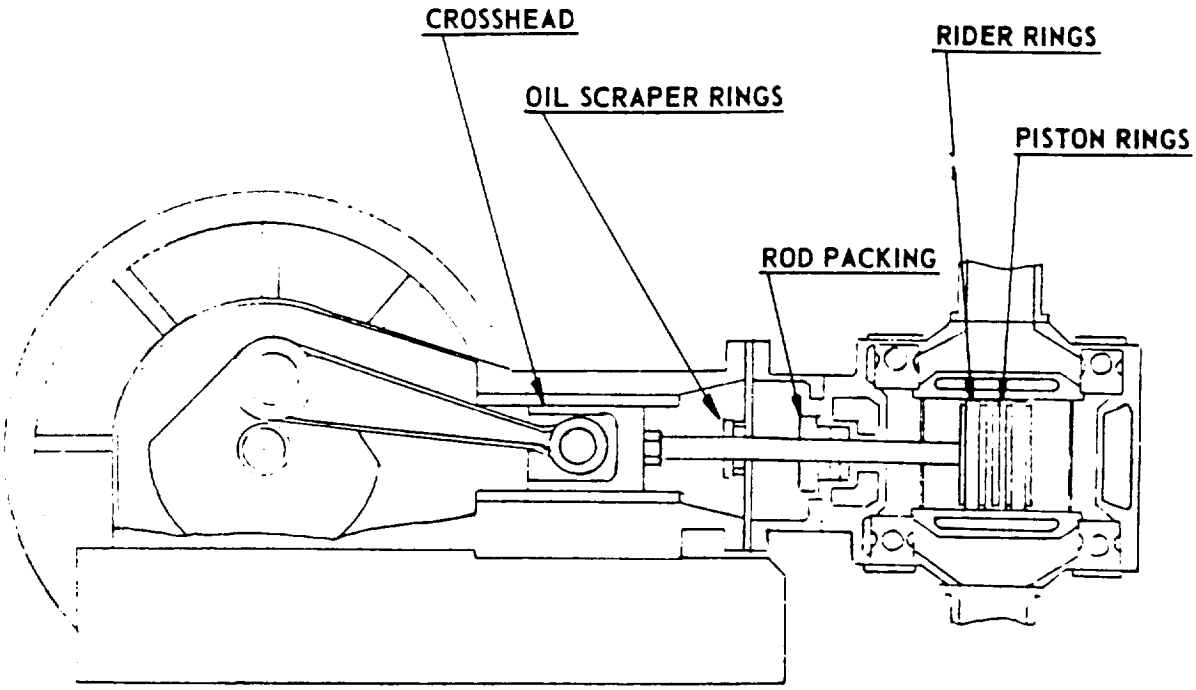

Figure 5. Reciprocating Compressor, Nonlubricated, Crosshead Type

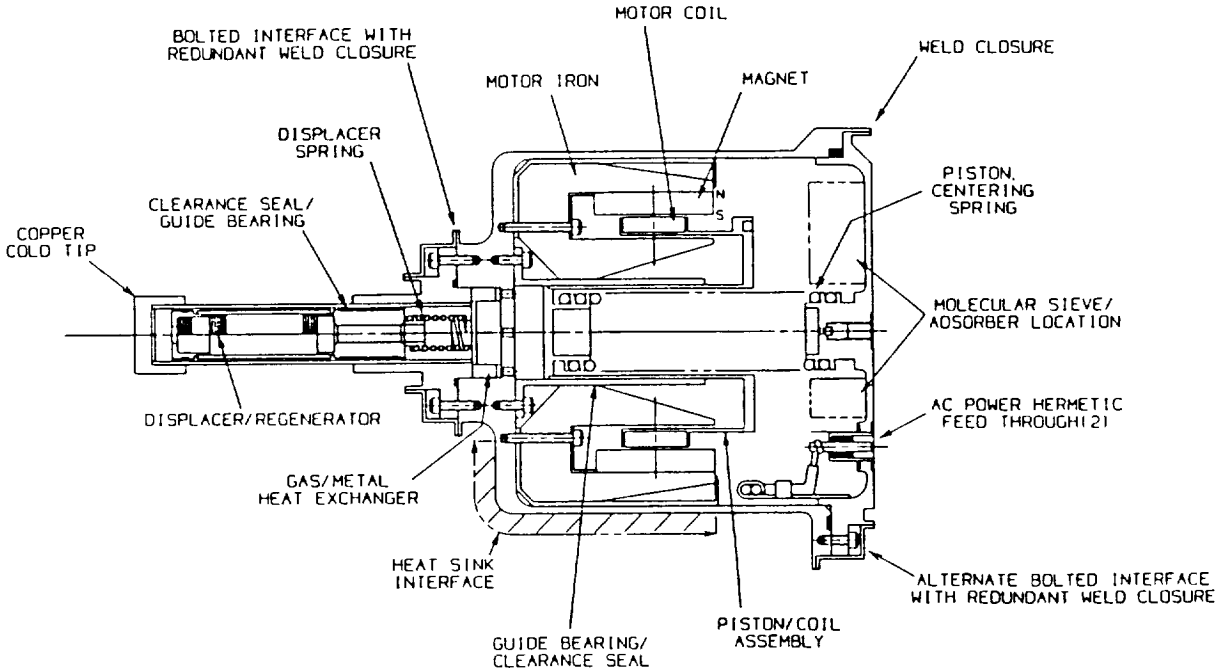

Figure 6. Integral Reciprocating Compressor/Linear Drive Configuration Currently Used in Stirling Refrigeration Devices (from Magnavox, Mowah, NJ)

magnet, which reduces or eliminates the torque on the moving parts, allowing extremely high tolerances and low wear on the moving parts. This design is now in high quantity mass production application.

Rotary Compressors

The several configurations of rotary positive displacement compressors have the following common features.

1. They impart energy to the gas with an input shaft moving a single or multiple rotating element.
2. They compress in an intermittent mode.
3. They do not normally use inlet and discharge valves.

The helical and spiral lobe compressors use two intermeshing helical or spiral lobes to compress gas between the lobes and the rotor chamber of the casing (see *Figure* 7).

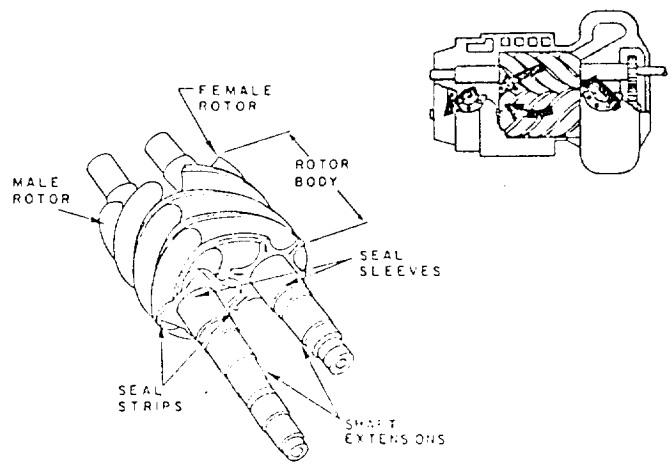

Figure 7. Helical Compressor Rotors

The helical lobe (or screw) compressors can be either dry, using timing gears, or oil-flooded. The flooding provides cooling, lubrication, and sealing between parts. The male rotor drives the female through the oil film. The flooded version is less complex than the dry version because of elimination of timing gears. It also provides a higher volumetric and overall efficiency because the oil acts as a seal for internal clearances.

The lobe compressor is a clearance type design using timing gears and requiring no lubrication in the compression chamber. A stage consists of a male and a female rotor each with either one or two lobes extending from a center hub section (see *Figure 8*). Compression occurs between the rotors and around their perimeter as the entrapped gas volume is carried from the inlet to the outlet. Compression is achieved by the intermeshing and trapping of gas between the male and female rotors, with the volume of gas being progressively reduced as it is moved from the inlet to the outlet port.

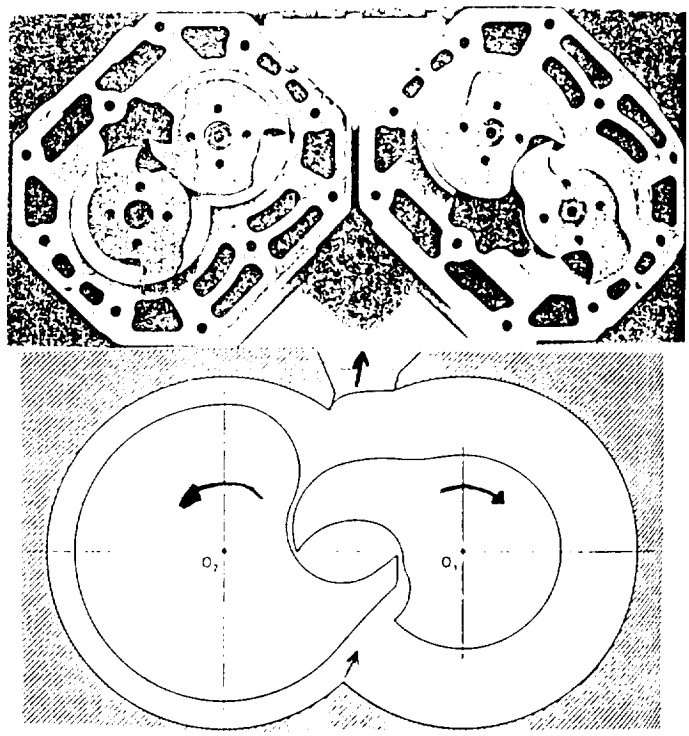

Figure 8. Two-Lobe and Single-Lobe Rotors for Rotary, Positive Displacement Compressors

The straight-lobe (or roots) compressor is similar to the helical-lobe but with two untwisted or straight lobe rotors which intermesh as they rotate (*Figure 9*). All versions use timing gears to phase the rotors. Compression is only by backflow from the discharge port and is low, up to 15 psi output in the first stage.

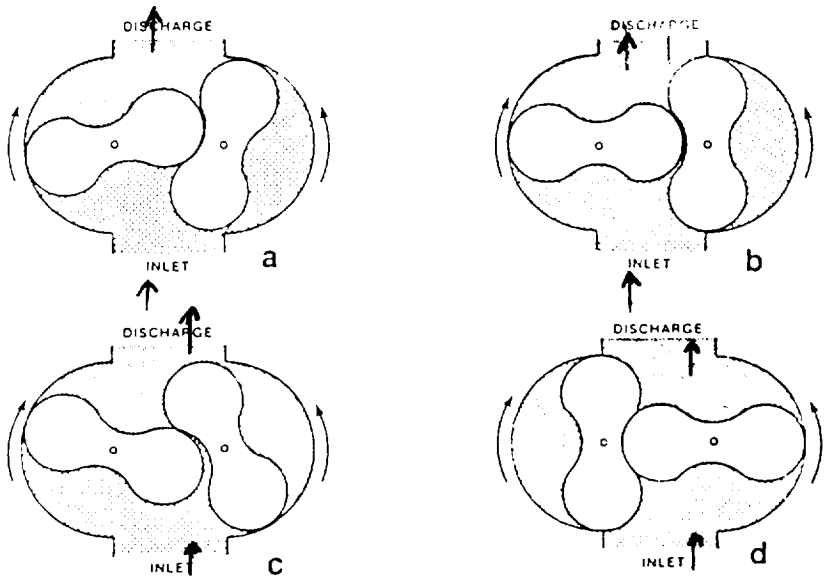

Figure 9. Operating Cycle of a Straight Lobe Rotary Compressor (Modified Courtesy of Ingersoll-Rand)

Figure 9. Operating Cycle of a Straight Lobe Rotary Compressor (Modified Courtesy of Ingersoll-Rand)

The sliding-vane, oil injected compressor uses an eccentrically mounted single rotating element with vanes which are free to move in and out as the rotor rotates (see *Figure 10*). Gas is trapped, moved, and compressed as the vane pair moves circumferentially to the discharge post. Cooling and efficiency depend on injection of liberal quantities of lubricating oil.

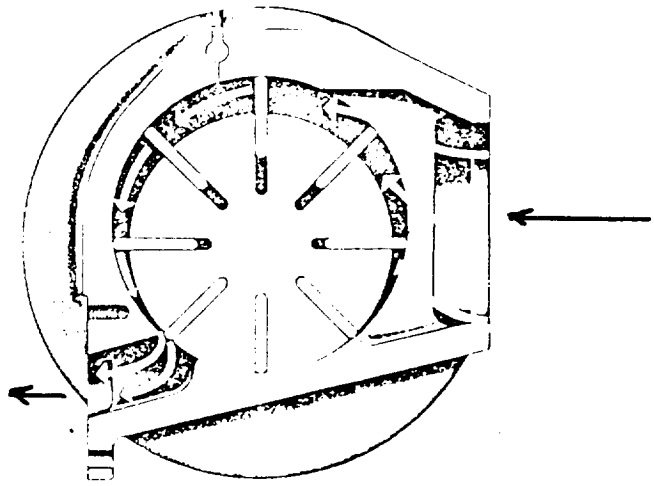

Figure 10. An Oil-Flooded, Sliding Vane Rotary Compressor

The liquid piston compressor (or liquid ring pump) uses a single rotor which consists of a set of forward curved fixed vanes (see *Figure 11*). The inner area of the rotor contains sealed openings rotating about a stationary hollow inner core containing the inlet and discharge ports. The rotor, carrying liquid at the tips of the vanes, turns in an eccentric cylinder which moves in and out as the rotor turns, forming a liquid piston. Port openings are located to allow gas to enter as the liquid moves away from center and to be compressed and discharged as rotation progresses.

Scroll compressors are rotary positive displacement compressors whose gas passages are in various stages of compression at all times, resulting in nearly continuous suction and discharge. Compression is by interaction of a stationary spiral and an orbiting (not rotating) spiral (see *Figure 12*). Gas enters the outer openings and discharges at the center port as one of the spirals orbits. The scroll is inherently more efficient than the piston compressor due to 1) separation and resultant reduced heat transfer between suction and discharge gases, 2) no need for dynamic suction and discharge valves, and 3) smoother rotary motion with less vibration and noise. In addition, there are no seals to wear and cause gas leakage. However, only recently has computer controlled advanced manufacturing technology overcome complex part geometries and precise tolerance requirements for cost competitiveness. Oil lubrication is normally required.

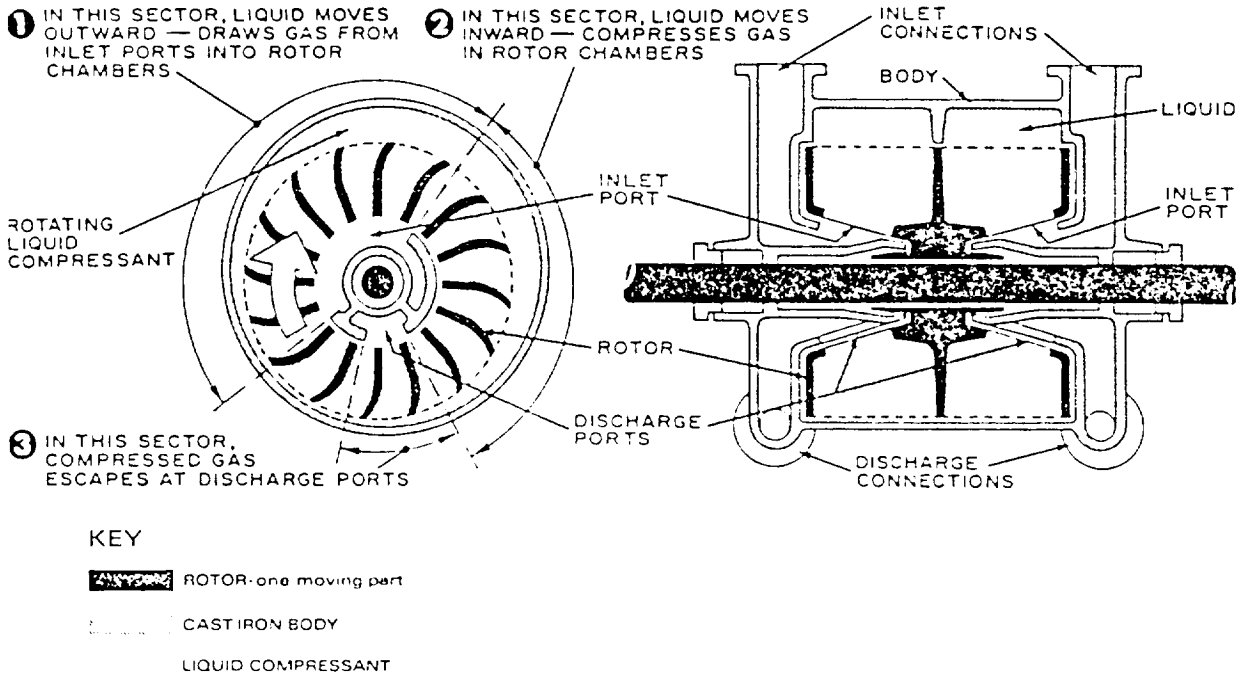

Figure 11. A Sectional and End View of a Liquid Piston Compressor (Courtesy of Nash Engineering Co.)

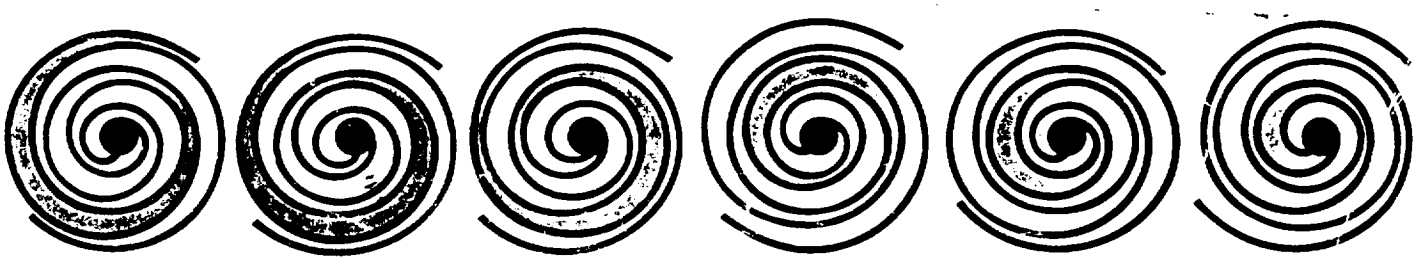

Figure 12. Scroll Compressor Cycle

Diaphragm compressors supply pressures intermediate to rotary and piston positive displacement pumps. They require no oil lubrication in the compression chamber and are applicable where low flow rates and cool, clean, oil-free compression are desired. Energy is imparted by a diaphragm which alternately pulls in, compresses, and discharges air. *Figure 13* shows the assembly and air flow of a typical diaphragm compressor by Gast Manufacturing Corp.

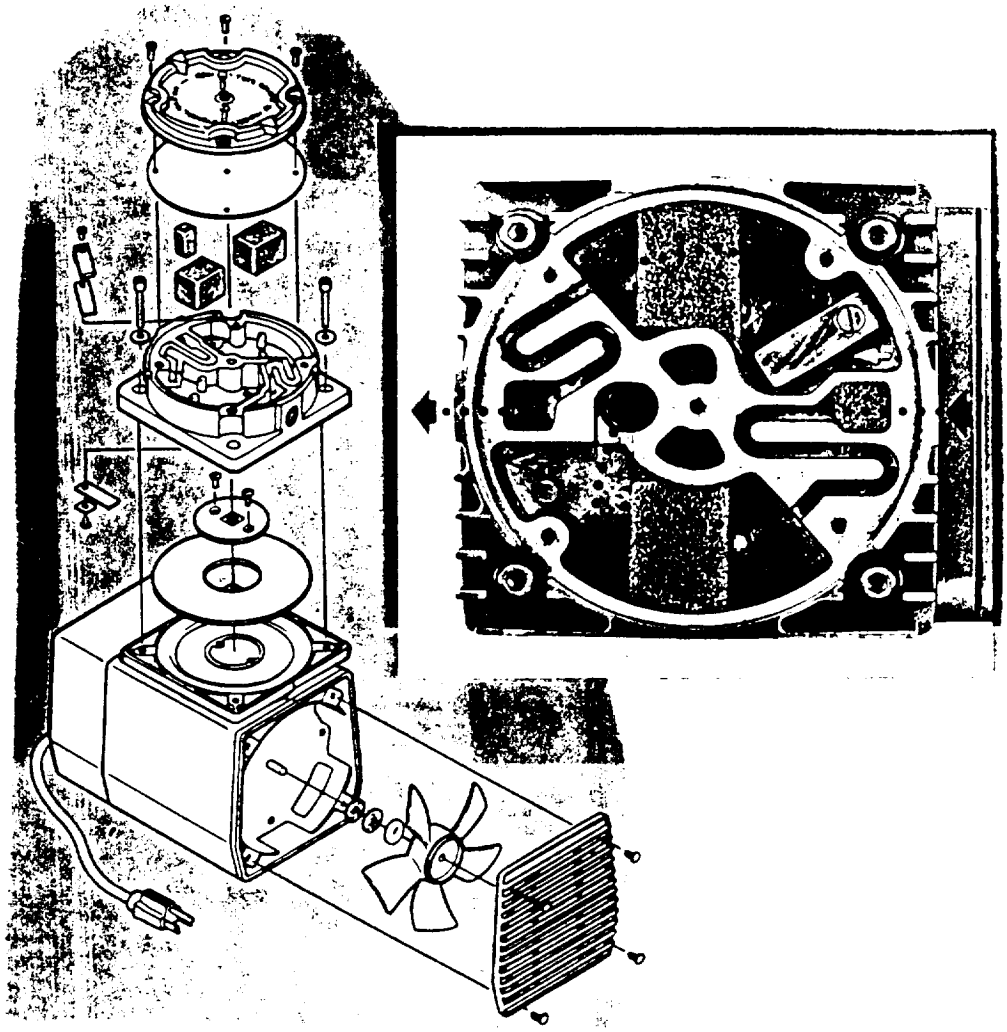

Figure 13. Diaphragm Compressor Assembly and Air Flow

Continuous Mode Compressors

Continuous mode compressors are of two types, ejector and dynamic. Ejectors have no moving parts and are operated by a motive gas, usually air or steam, which is mixed with the suction gas (see *Figure 14*). They are used mainly as vacuum pumps.

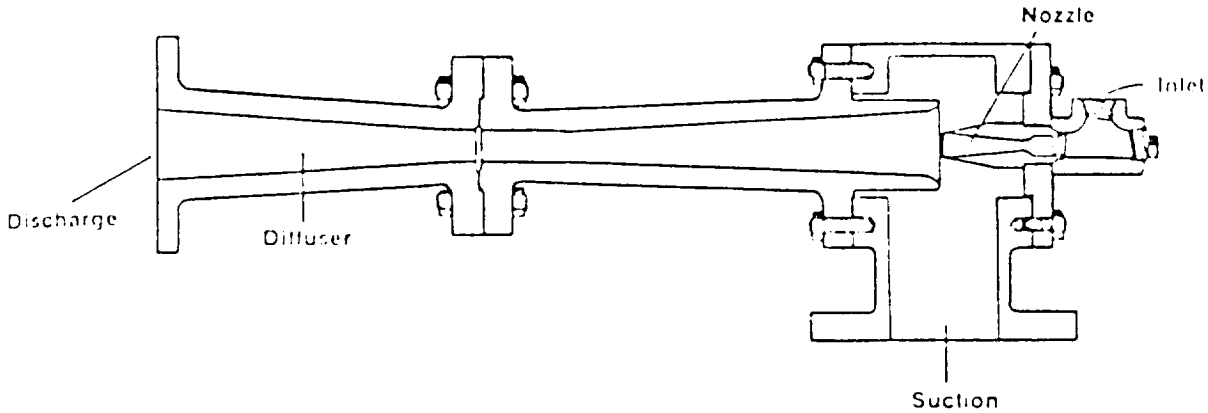

Figure 14. Cross Section of an Ejector (Courtesy of Graham Manufacturing Co., Inc.)

Dynamic compressors transfer energy from a moving set of blades to the gas. They are further classified as radial, axial, and mixed flow and have the following characteristics.

- The radial, or centrifugal, compressor uses an impeller consisting of radial or backward-leaning blades on a front and rear shroud. Gas is moved between the rotating blades near the shaft and radially outward, discharging into the stationary diffuser (see *Figure 15*). Part of the imparted energy converts to pressure along the blade path while the balance is velocity at the impeller tip, where it is slowed in the diffuser and converted to pressure.
- Axial compressors are characterized by the axial direction of flow and are basically smaller and significantly more efficient than centrifugal compressors. The rotor consists of multiple rows of unshrouded blades alternating with stationary blades. A pair of rotating and stationary blades defines a stage (see *Figure 16*).
- Mixed flow compressors are relatively uncommon except in pipeline booster service. The energy transfer is the same as for the centrifugal compressor except that the flow path has both axial and radial components as can be seen from comparison of centrifugal and mixed flow impeller shapes (see *Figure 17*).

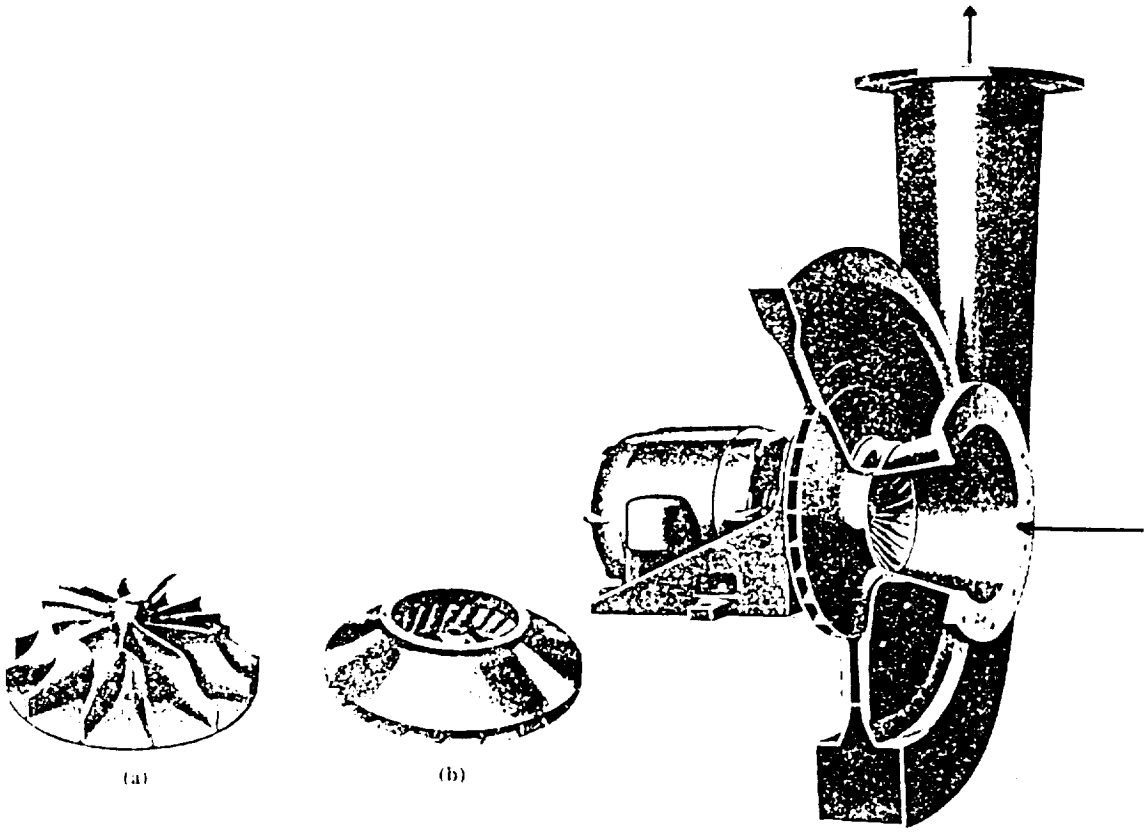

Figure 15. Cutaway View of a Single-Stage, Single Inlet Centrifugal Compressor with Closed-Type Impeller

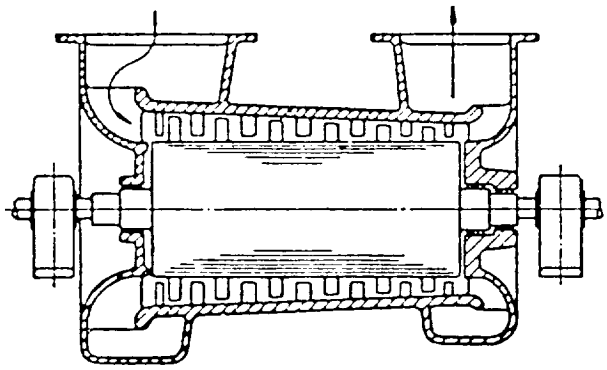

Figure 16. Multistage Single-Flow Axial Compressor

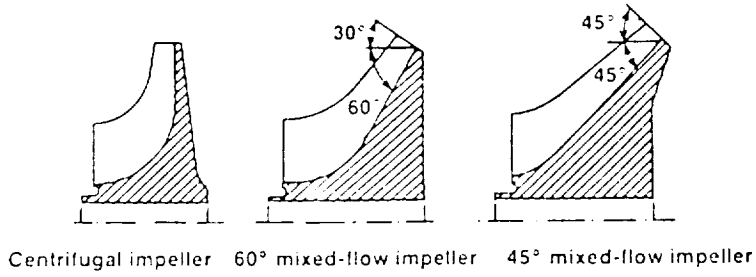

Figure 17. Comparison of Radial and Mixed Flow Compressor Impellers

COMPRESSOR SOURCES

Table 2 lists available compressor sources.

BIBLIOGRAPHY

1. Brown, Royce N. *Compressors, Selection & Sizing*. Houston, TX: Gulf Publishing Company, Book Division.
2. Rollins, John P., Editor. *Compressed Air and Gas Handbook*. Englewood Cliffs, NJ: Prentice Hall, Fifth Edition.
3. *Air Compressors, Rotary Vane, Piston, Diaphragm, Roc-R*. Gast Manufacturing Corp. P.O. Box 97, Benton Harbor, MI 49022, Tel: 616-926-6171.
4. "Compressors and Expanders, Selection and Application for the Process Industry." *Encyclopedia of Chemical Processing and Design,* Volume 10.
5. *Positive Displacement Compressors*. American Society of Heating, Refrigerating and Air Conditioning Engineers, Semi-Annual Meeting, Jan 30 - Feb 2, 1967. American Society of Heating, Refrigerating and Air-Conditioning Engineers, Inc., 345 East 47th St., NY, NY 10017.

Note: The above sources are not referred to within this report. Descriptions of compressor types and modes are similar, regardless of source.

Table 2. Compressor Sources

No.	Source	Recipro.	Rotary	Dynamic	Other
1	Ingersol-Rand, Woodcliff Lake, NJ 07657	x	x	x	
2	Worthington Operation, Dresser Industries Inc., Buffalo, NY 14240				
3	Joy Manufacturing Co., Ind. Compressor Group, Pittsburgh, PA 15219	x	x	x	
4	Gardner-Denver Industrial Machinery Div., Quincy, IL 62301	x	x		
5	Compair Kellog, Inc., Kingston, NH 03848-0159	x	x		
6	U.S. Air Compressor, Minneapolis, MN 55407	x			
7	Pneumotive, Monroe, LA 71203	x	x		
8	Gast Manufacturing Corp., Benton Harbor, MI 49022	x	x		Diaphragm
9	Rix Industries, Oakland, CA 94608	x			
10	Atlas Copco Industrial Compressors, Inc	x	x	x	
11	American Compressors, Charlotte, NC 28217	x	x	x	
12	LeRoi Division, Dresser Industries, Inc., Sidney, OH 45365	x	x		
13	Thomas Industries, Sheboygan, WI 53082-0029	x			Diaphragm
14	Dresser Clark Division, Dresser Industries, Inc., Olean, NY 14760	x		x	
15	Nash Engineering Co., Norwalk, CT 06856	x			
16	Graham Manufacturing Co., Inc., Batavia, NY 14020		x		Ejector
17	Copeland Corp., Wapakonita & West Union, OH	x			Scroll